Universidad Autónoma de Madrid
Facultad de Medicina
Departamento de Bioquímica
Programa de Doctorado en Biociencias Moleculares

DOCTORAL THESIS

Histone Deacetylase 6 at Crossroads of Infection and Innate Immunity

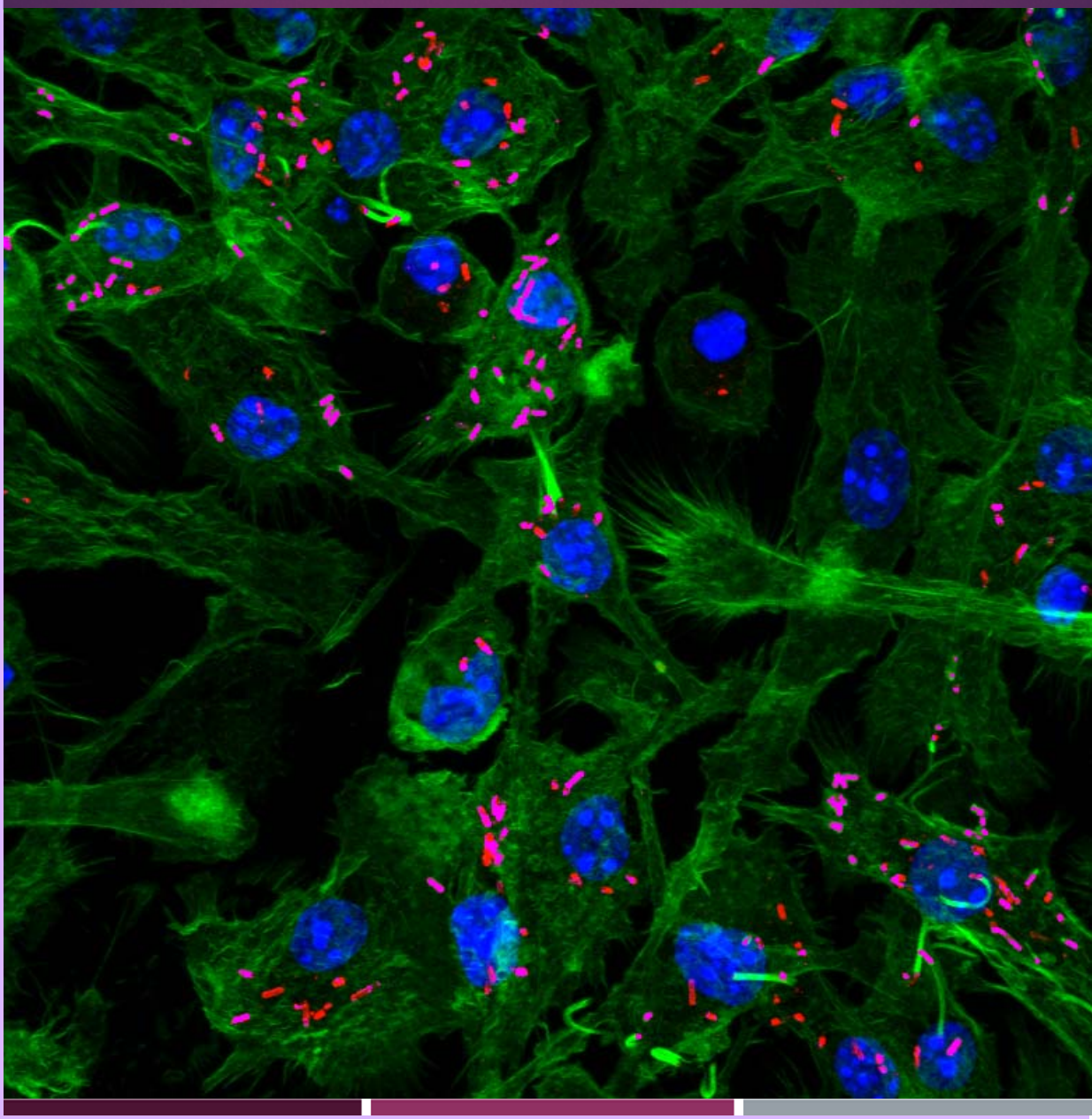

Olga Moreno Gonzalo

Madrid, 2018

Universidad Autónoma de Madrid

Facultad de Medicina

Departamento de Bioquímica

Programa de doctorado en Biociencias Moleculares

Histone Deacetylase 6 at Crossroads of Infection and Innate Immunity

Doctoral Thesis

Olga Moreno Gonzalo

Madrid, 2018

Departamento de Bioquímica

Facultad de Medicina

Universidad Autónoma de Madrid

Programa de Doctorado en Biociencias Moleculares

Histone Deacetylase 6 at Crossroads of Infection and Innate Immunity

Memoria presentada por la licenciada en Biotecnología:

Olga Moreno Gonzalo

Para optar al título de Doctor por la Universidad Autónoma de Madrid

Doctorado en Biociencias Moleculares

Director de tesis:

Dr. Francisco Sánchez-Madrid

Doctor en Ciencias Biológicas y Catedrático de Inmunología de la Universidad Autónoma de Madrid

Este trabajo se realizó en el Hospital Universitario de la Princesa (HUP) y en el Centro Nacional de Investigaciones Cardiovasculares (CNIC)

Madrid, 2018

Francisco Sánchez Madrid, Doctor en Ciencias Biológicas y Catedrático de Inmunología de la Universidad Autónoma de Madrid,

CERTIFICA:

Que Olga Moreno Gonzalo, Licenciada en Biotecnología por la Universidad Francisco de Vitoria, ha realizado bajo su dirección el trabajo de investigación correspondiente a su Tesis Doctoral con el título:

Histone Deacetylase 6 at Crossroads of Infection and Innate Immunity

Revisado este trabajo, el que suscribe lo considera satisfactorio y autoriza su presentación para ser evaluado por el tribunal correspondiente.

Y para que así conste y a los efectos oportunos, firma el presente certificado en Madrid a 12 de marzo de 2018.

Fdo.: Prof. Francisco Sánchez-Madrid

This work has been performed at the Prof. Francisco Sánchez-Madrid's laboratory in the Hospital Universitario de la Princesa (HUP) and Centro Nacional de Investigaciones Cardiovasculares (CNIC) in Madrid. This study was funded by grants SAF2014-55579-R from the Spanish Ministry of Economy and Competitiveness, INDISNET-S2011/ BMD-2332 from the Comunidad de Madrid, CIBERCARDIOVASCULAR and grant PIE13/00041 from the Instituto de Salud Carlos III (Fondo de Investigación Sanitaria del Instituto de Salud Carlos III with co-funding from the Fondo Europeo de Desarrollo Regional; FEDER), and ERC-2011-AdG 294340- GENTRIS and COST-Action BM1202 from the European Comission to Francisco Sánchez-Madrid.

The Centro Nacional de Investigaciones Cardiovasculares (CNIC) is supported by the Spanish Ministry of Economy and Competitiveness (MINECO) and the Pro-CNIC Foundation and is a Severo Ochoa Center of Excellence (MINECO award SEV-2015-0505).

Olga Moreno was supported by a PhD fellowship from the Spanish Ministry of Education (FPU Program, FPU12/00733).

We thank Dr. M. Gómez for assitance with English editing and for critical reading of this PhD thesis.

A mis padres,

a Maryan

y a David

The important thing is not to stop questioning.
Curiosity has its own reason for existing.

(Lo importante es no dejar de hacerse preguntas.
La curiosidad tiene su propia razón de existir)

Albert Einstein
(1879-1955)

Agradecimientos

AGRADECIMIENTOS

En primer lugar, me gustaría dar las gracias a Paco, quién me dio la oportunidad de investigar en su laboratorio y realizar una tesis doctoral bajo su paraguas. Gracias a su confianza y a su pragmatismo, el trabajo recogido en esta tesis doctoral ha podido desarrollarse y publicarse. Además, me ha dado la libertad de pensar y hacer la tesis doctoral en el tema que más me apasiona, la interacción de patógenos con el sistema inmune. Dicha libertad me ha enseñado la mejor lección para la tesis y para la vida, que es la toma de decisiones continua para escribir una historia con sentido y la autonomía para conseguirla. Muchas gracias por recordame que siguiera el camino cuando nuevos senderos aparecían y por tu optimismo incansable. También por animarme a intentarlo y a pelearlo todo, porque lo que no se intenta nunca se consigue. No hay mejor regalo que éste.

También tengo que agradecer a mis compañeros de laboratorio el gran apoyo científico y personal que me han dado durante estos seis años.

Gracias a Mª Laura, por ser una excelente científica y una gran amiga. Por todo el tiempo que has dedicado a enseñarme, a discutir resultados, por tus consejos, por tus ánimos, etc. Haberte tenido como compañera de escritorio ha sido una gran suerte. Desde el principio hemos congeniado, nos hemos apoyado en nuestras tesis y en los problemas de la vida. Tu gran capacidad de esfuerzo y tu voluntad de hierro me han inspirado para querer ser tan buena como tú. Gracias por sacar la parte positiva de todo y por los buenos momentos de libertad y diversión que hemos vivido juntas.

Gracias a Marta, por ser tan sincera, tan trabajadora y una gran amiga. Nunca podré agradecerte todo lo que me has enseñado, no sólo de técnicas de laboratorio, sino de la vida en general. Eres la persona más pragmática en la experimentación del laboratorio y tus consejos siempre son buenas ideas, que además ahorran tiempo, dinero y esfuerzo. Gracias por tu apoyo, tus ánimos han sido fundamentales para levantarme de nuevo cuando tropezaba. Nos has enseñado a relativizar los problemas y a ser mas *zen* en el trabajo. Eres el pilar fundamental de este laboratorio.

Gracias a Ana (ARG), una gran psicóloga y amiga. Gracias por ser tan buena persona, por tu apoyo y tu optimismo. Tenerte de compañera de *bench* ha sido un placer, sabes compartir y dar buenos consejos. Eres la humanista y la pacifista del grupo y sabes escuchar como nadie. Tus habilidades artísticas y tu capacidad para poner a punto protocolos nos han sorprendido a todos.

Gracias a Noelia por su apoyo y su gran capacidad de trabajo. Nunca podré agradecerte tu enorme esfuerzo con los *western blots* tan perfectos que hiciste. Gracias a ellos conseguimos publicar el

artículo. Muchas gracias por ayudarme con los experimentos y por tus críticas tan constructivas para mejorarlo.

Gracias a Danay, la persona más trabajadora que he conocido. Muchas gracias por ayudarme cuando estaba tan perdida. Gracias por haberme enseñado que no hay que temer al ratón, que por tamaño ganamos. Gracias por haberme transmitido tus conocimientos de citometría y de experimientación animal. Gracias por proponerme ideas, discutirlas y por tu sinceridad. También por enseñarme a trabajar con cantidades ingentes de ratones, tubos, marcajes, etc y que además saliera todo bien.

Gracias a Irene por tu ayuda con la biología molecular. Muchas gracias por estar siempre dispuesta a echar una mano y por tu riguroso orden del material. También por tu ayuda con todos los problemas ofimáticos y con la documentación de la tesis doctoral. Si no hubiera sido por ti, todavía estaría haciendo los informes de evaluación del doctorando.

Gracias a Lola por su optimismo, su alegría y su dulzura. Gracias por tus consejos cuando algún experimento se me atascaba. Es un placer hablar contigo no sólo de ciencia, sino de temas políticos, sociales, etc. También sobre viajes y gastronomía.

Gracias a Dani por su alegría y su buen humor. Tener de compañero de *bench* ha sido una experiencia divetida y enriquecedora. Sabes compartir e irradias felicidad. Nunca olvidaré tus bailes entre experimentos y tus consejos sobre ciencia y salud. Sin duda mejoras el ambiente del laboratorio entero.

Gracias a Hortensia por enseñarme tantas cosas cuando llegué a al Hospital de la Princesa. Muchas gracias por tu paciencia y por tratarme tan dulcemente cuando metía la pata en los experimentos. Tu me transmitiste la curiosidad por las células dendríticas.

Gracias a Eugenio por sus ideas y por sus consejos. Muchas gracias por ayudarme con los documentos de la tesis y por tus ánimos cuando las cosas no salían.

Gracias a Raquel por su dulzura. Muchas gracias por tus ánimos y tus consejos.

Gracias a Nieves por su entereza. Cuando vinistes al laboratorio pensaba que eras mayor por tu madurez. Eres optimista, generosa y trabajadora. Gracias por animarme.

Gracias a Noa por tu ayuda al principio de mi tesis en el Hospital de la Princesa. Gracias por enseñarme a hacer *western blots* y *strippings*.

Gracias a las nuevas incorporaciones del laboratorio, Ana y César.

Gracias a Ángeles Ursa y Alicia Vara por su ayuda al cominzo de mi tesis doctoral con técnicas de laboratorio de las cuales llevan siendo expertas más de treinta años.

Gracias a Manolo Gómez y Miguel Vicente por haber corregido este trabajo con el mejor rigor científico y por sus correcciones de inglés.

Gracias a todos los miembros, presentes y pasados, del laboratorio. A Vera, Carolina, Fran, Gloria, Mittelbrunn, Giulia, Norman, etc. Ha sido un placer haber trabajado con vosotros y compartir las largas horas de experimentación con gente tan diversa me ha enriquecido científica y personalmente.

Gracias a los grupos de investigación vecinos y colaboradores. A los grupos de David Sancho, de Guadalupe Sabio, de Almudena Ramiro, de Pilar Martín y de Jacob Bentzon en el CNIC. Muchas gracias por compartir reactivos, protocolos y trucos y por generar el buen ambiente colaborador que tenemos en la segunda planta del CNIC. Gracias a Helena Izquierdo y a Michel, por vuestros consejos científicos y por vuestra amistad. También por las meriendas y reuniones de pasillo donde nos animábamos unos a otros. Gracias a Salva, María, Carlos, Paula, Sofía, Paola y demás componentes por vuestra ayuda con la inmunidad innata. Muchas gracias a Toñi y Guadalupe por vuestros consejos sobre la ruta de mTOR y de *western blots*. Gracias a Carlos, Esmeralda, Paula, Leti y Rocío por vuestras aportaciones sobre la estética de esta tesis. También por vuestro apoyo y compañía durante la última etapa de mi tesis.

Gracias al soporte técnico y científico de las unidades del CNIC de Proteómica, Celómica, Microscopía, Cultivos Celulares, Animalario, Control Microbiológico, Informática, Esterilización y Medios. A Emilio y a Inma de Proteómica por haber sido unos colaboradores tan trabajadores, por vuestras ideas y aportaciones. A Jesús Vázquez, me ha hecho mucha ilusión poder colaborar con el profesor de proteómica que tanto me enseñó. A Mariano, Raquel, Ligos y Elena de Celómica por su contínua ayuda con los citómetros y sorters. A Antonio, Elvira, Verónica y Helio de Microscopía por ayudarme con los microscopios y por enseñarme a cuantificar imágenes. A Yoli, Ana y todas las chicas de Cultivos que con su trabajo hacen posible que nuestras células crezcan limpias y sanas. A los técnicos de Animalario, en especial a Eli y a Juanjo, por haber cuidado y gestionado nuestras líneas de ratones. A la unidad de Esterilización y Medios por haber generado miles de plascas de BHI y LB para los experimentos de colonias de esta tesis. A Esther Pariente por haberme prestado su lugar de trabajo para experimentar con *Listeria*. Muchas gracias por haberme animado tanto, por tu positividad y las horas tan divertidas que hemos pasado juntas en el sótano de la planta -3 del CNIC. Gracias a Almudena Fernández, Antonio Quesada y Laura Grau por resolver nuestros trámites en el CNIC y Mª Ángeles Vallejo por resolverlos en la Princesa. Gracias a Alicia, Juan Carlos, Eduardo y Luís por resolver todos los problemas informáticos que he tenido durante la tesis. Gracias a Simon Barlett por las correcciones de inglés del artículo.

A los grupos de Miguel Vicente, María Navarro, Ana Urzainqui, Antonio Martínez, Isidoro González, Susana Cadenas y Mª José Calzada del Hospital de la Princesa. Al grupo de Esteban Veiga, quien me

acogío en su laboratorio para infectar con *Listeria*. Gracias Esteban, Arantxa, Guille y Mónica por ayudarme en los primeros experimentos de infección y por vuestras aportaciones en este trabajo.

Gracias a mi tutor de tesis Víctor Calvo, por haberme rellenado inumerables informes y evaluaciones tan rápidamente y tan bien. También me ha gustado mucho colaborar contigo y otros profesores del Departamento de Bioquímica en la docencia de las prácticas de laboratorio de la carrera de medicina.

Gracias a mis profesores de la infancia María Quiroga, Loli Lucas y Antonio Pesado que despertaron en mi la curiosidad por la ciencia. Gracias a mis profesores de instituto Juana Franco, Encarna Gómez y Amador González que dieron las primeras lecciones de ciencias que tanto me marcaron. Gracias a los profesores de la carrera de biotecnología que hicieron que la ciencia me apasionase, en especial a Cruz Santos, Maite Iglesias, José Arencibia, Julián Romero, Juan Carlos Ramírez y Gemma Rodriguez-Tarduchy.

Gracias a mis mejores amigas, Bea, Alba, Ana, Mª Ángeles y Mª Carmen. Gracias a todos mis amigos y amigas de Mérida, Madrid y Zaragoza.

Sobre todo, quiero dar las gracias a mi famia, los Moreno y los Gonzalo, quienes me han apoyado tanto para que esta tesis fuera posible. También a mi nueva familia, los Funes y los Sebastían, quienes me han acogido como a una de su clan y me han animado con el doctorado.

Gracias a mis padres por entender que cuando viajaba poco a casa era porque estaba trabajando en esta tesis. Papá, siento mucho haber tirado del cable del ordenador cuando era pequeña. Se borró la mitad de la discusión de tu tesis y esa parte es la que más cuesta escribir. También siento haberte desorganizado las 600 diapositivas de histologías de tu tesis. Por no hablar de cuando até los cordones de ambos zapatos al director de tu tesis y casí se lesiona. Todavía no sé como fuiste capaz de hacer una tesis doctoral con una niña tan pequeña saboteando tu trabajo. Gracias Mamá por llamarme muchos días a las 7.30 de la tarde para decirme que soltara las pipetas y me fuera a casa a descansar. Eso ha ayudado a mejorar mi productividad y a recordar que en casa tenía una hermana y un novio.

Gracias a mi hermana Maryan, por su gran confianza en mí, por animarme a seguir intentándolo y por tu sinceridad cuando no hago bien las cosas. Eso me hace ser mejor persona. Sin nuestras charlas de hermanas esta tesis nunca hubiera visto la luz.

Y por último, y no menos importante, a David. Mi amor, mi amigo, mi compañero, mi confidente, mi *personal coach*, mi psicólogo, mi chófer, mi todo. Eres la persona que más me ha apoyado. Tu amor ha hecho posible aguantar una casa tan vacía cuando la tesis y los papers lo requerían. Gracias por tu paciencia infinita y por tu optimismo contagioso. Sigue recordándome cada día lo que verdaderamente importa, que a veces se me olvida.

Summary

SUMMARY

Recent evidence on Histone deacetyase 6 (HDAC6) function underlines its role as a key protein in the innate immune response to viral infection. However, whether HDAC6 regulates innate immunity during bacterial infection remains unexplored. To assess the role of HDAC6 in the regulation of defence mechanisms against intracellular bacteria, we used the *Listeria monocytogenes* (*Lm*) infection model. Here we describe that in the absence of HDAC6 Granulocyte/Macrophage colony stimulating factor-derived dendritic cells (GM-CSF DCs) display higher intracellular bacterial titres than their *wild type (wt)* counterparts. The impaired bacterial clearance appears to be caused by a defect in autophagy. This correlates with an increase in the accumulation of the autophagy marker p62 in *Hdac6*$^{-/-}$ DCs, due to a defective phagosome-lysosome fusion. We also identify higher levels of acetylated cortactin co-localizing with intracellular bacteria in *Hdac6*$^{-/-}$ DCs compared to *wt*, suggesting that this Post-translational modification (PTM) in cortactin could delay the phagosome-lysosome fusion.

Additionally, a lower expression of interferon-related genes and pro-inflammatory cytokines is detected in *Hdac6*$^{-/-}$ DCs after *Lm* infection. This observation is in accordance with lower nitrite production and inducible nitric oxide synthase (iNOS) induction during bacterial infection in *Hdac6*$^{-/-}$ DCs. Likewise, phosphorylation of Mitogen-activated protein kinase (MAPK) and mammalian target of rapamycin (mTOR) signalling pathways is reduced in *Hdac6*$^{-/-}$ DCs in response to *Lm*, suggesting an altered Toll-like receptor (TLR) signalling. A defective pro-inflammatory cytokine production in response to *Lm* and various TLR agonists is detected in both *Hdac6*$^{-/-}$ GM-CSF-derived and FMS-like tyrosine kinase 3 (FLT3L)-derived dendritic cells.

Interestingly, our data reveal the molecular association of HDAC6 with the TLR-adaptor protein Myeloid differentiation primary response gene 88 (MyD88), and how the absence of HDAC6 seems to diminish Nuclear factor κB (NF-κB) induction after TLR stimuli. Moreover, *Hdac6*$^{-/-}$ mice display low serum levels of the inflammatory cytokine IL-6 and correspondingly an increased survival to a systemic infection with a lethal dose of *Lm*. These data underline the important function of HDAC6 in DCs, not only in the control of bacterial burden through degradation by autophagy, but also in the proper activation of TLR signalling. These results thus underscore an important regulatory role for HDAC6 in almost every step of DC functions against intracellular bacterial infection, highlithing HDAC6 as a new player of innate immune responses.

Resumen

RESUMEN

Las evidencias recientes sobre la función de la Histona desacetyase 6 (HDAC6) ponen de manifiesto su implicación como proteína esencial en la respuesta inmune innata durante la infección viral. Sin embargo, la función de HDAC6 en la inmunidad innata durante la infección bacteriana es desconocida. Para estudiar el papel de HDAC6 en la regulación de los mecanismos de defensa contra bacterias intracelulares, se usó el modelo de infección de *Listeria monocytogenes* (*Lm*). Aquí se describe como la ausencia de HDAC6 en las células dendríticas diferenciadas con el factor estimulador colonias de granulocito/macrófago (GM-CSG DCs) causa un incremento en la carga de la bacteria intracelular comparado con la silvestre *(wt)*. La deficiente eliminación bacteriana parece estar causada por un defecto en la autofagia. Este dato concuerda con un incremento en la acumulación del marcador de autofagia p62 en las *Hdac6*$^{-/-}$ DCs, que es debido a un defecto en la fusión del fagosoma con el lisosoma. También se han identificado niveles más altos de cortactina acetilada co-localizando con bacterias intracelulares en *Hdac6*$^{-/-}$ DCs, lo que sugiere que esta modificación post-traduccional (PTM) en la cortactina podría estar retrasando la fusión fago-lisosomal.

Además, se han identificado menores niveles de expresión de genes relacionados con interferón y citoquinas pro-inflammatorias en las *Hdac6*$^{-/-}$ DCs después de la infección con *Lm*. Esta observación concuerda con una menor producción de nitrito e inducción de la sintetasa de óxido nítrico inducible (iNOS) durante la infección en las *Hdac6*$^{-/-}$ DCs. Así mismo, las *Hdac6*$^{-/-}$ DCs muestran una menor fosforilación de las rutas de señalización de proteínas quinasas activadas por mitógenos (MAPK) y de la diana de mamíferos de rapamicina (mTOR) en respuesta a la infección por *Lm*, sugiriendo una alteración en la señalización de la ruta de receptores tipo Toll (TLR). Tanto las DCs derivadas de GM-CSF como las de la tirosina quinasa 3 de tipo FSM (FLT3L) tienen un defecto en la producción de citoquinas pro-inflamatorias en respuesta a *Lm* y a varios agonistas de TLR.

Se ha demostrado la asociación molecular de HDAC6 con la molécula adaptadora de TLR, el gen 88 de respuesta primaria a diferenciación mieloide (MyD88), y como la ausencia de HDAC6 disminuye la inducción del factor nuclear κB (NF-κB) despúes del estímulo de los TLRs. Adicionalmente, los ratones *Hdac6*$^{-/-}$ muestran menores niveles séricos de la citoquina pro-inflamatoria IL-6, relacionado con una mayor supervivencia a la infección sistémica por la dosis letal de *Lm*. Estos datos remarcan la importante función de HDAC6 en las DCs, no solo por el control de la carga bacteriana por la degradación autofágica, sino también por la adecuada activación de la señalización de los TLRs.

Index

INDEX

Abbreviations

LIST OF ABBREVIATIONS

3-MA: 3-MethylAdenine
5´pppRNA: 5´triphospathe RNA
aa: amino acid
ACK: Ammonium Chloride Potassium
ActA: Actin Assembly-inducing protein
AHR: Aryl Hydrocarbon Receptor
AKR1C13: Aldo-keto reductase family 1 member C13 or RECON
AKT: Protein Kinase B or AKT (PKB/AKT)
AP-1: Activator Protein-1
APC: Allophycocyanin
APC: Antigen presenting cell
ARP2/3 complex: Actin Related Protein (subunits 2 and 3) complex
ATCC: American Type Culture Collection
ATG: AuTophaGy-related gene
AU: Arbitrary Units
Baf: Bafilomycin A1
BAHD1: Bromo Adjascent Homology Domain-containing 1 protein
BHI: Brain Heart Infusion
BMDCs: Bone Marrow-derived Dendritic Cells
BMDMs: Bone Marrow-Derived Macrophages
BNIP3L/NIX: mitophagy-inducing proteins, BCL2/adenovirus E1B 19-kDa interacting protein 3-like (BNIP3L)/Nyctalopin
BSA: Bovine Serum Albumin
BUZ domain: Binding-of-Ubiquitin Zing finger domain of HDAC6
CD: Cluster differentiation
cDC: conventional DC
c-di-AMP: cyclic di-AMP
CDN: Cyclic DiNucleotide
CFUs: Colony-Forming Units
cGAMP: cyclic Guanosine monophosphate (GMP)–Adenosine MonoPhosphate (AMP)
cGAS: cyclic GMP-AMP synthase
CK2: Casein Kinase II
CMA: Chaperone-Mediated Autophagy
CpG: Cytosine-phosphate-Guanine oligodeoxynucleotide
A3G: apolipoprotein B m-RNA-editing enzyme-catalytic, polypeptide-like 3G
CXCL5/10: Cysteine-X-Cysteine motif chemokine Ligand 5/10
CXCR1: Cysteine-X-Cysteine motif chemokine Receptor 1
CYLD: Deubiquitinating enzyme
DAPI: 4',6-diamidino-2-phenylindole
DCs: Dendritic Cells
DD: double deacetylase domain mutant of HDAC6 (H216A/H611A)
DD1: Deacetylase domain 1 of HDAC6
DD2: Deacetylase domain 2 of HDAC6
DMB: Dynein Motor binding domain
DMEM: Dulbecco´s Modified Eagle Medium
DMSO: Dimethyl Sulfoxide
dpi: days post-infection
DPI: Diphenyleneiodonium Chloride
DSS: Dextran Sodium Sulphate
***E. coli*:** *Escherichia coli*
EDTA: Ethylenediaminetetraacetic acid
eGFP: enhanced Green Fluorescent Protein
EGFR: Epidermal Growth Factor Receptor
EGTA: Ethylene glycol bis-(β-aminoethyl ether)-N,N'-tetraacetic acid
ELISA: Enzyme-Linked ImmunoSorbent Assay
ER: Endoplasmic Reticulum
ERK: Extracellular signal-Regulated Kinase
FC: Flow Cytometry
FCGR1A: high affinity immunoglobulin gamma Fc receptor I or CD64
FITC: Fluorescein Isothiocyanate
FLT3L: Fms-related tyrosine kinase 3 ligand
Foxp3: Forkhead box P3
GAPDH: Glyceraldehyde-3-phosphate dehydrogenase
GM: geometric mean
GM-CSF: Granulocyte/Macrophage Colony-Stimulating Factor
gp120: envelope glycoprotein 120 of HIV
GRK2: G protein-coupled Receptor Kinase 2

GSK3β: Glycogen Synthase Kinase 3 beta
HA: influenza HemmAgglutinin protein
HATs: Histone Acetyl Transferases
Hda1: yeast histone DeAcetylase 1
HDAC6: Histone Deacetylase 6
HDAC6i: HDAC6 inhibitors
***Hdac6^{tg}*:** Overexpressing HDAC6 mice
HDACi: Histone Deacetylase inhibitors
HDACs: Histone Deacetylases
HIV-1: Human Immunodeficiency Virus type-1
HKLM: Heat killed *Listeria monocytogenes*
HKST: Heat killed *Salmonella* Typhimurium
hpi: hours post-infection
HRP: Horseradish Peroxidase
Hsc70: Heat Shock Cognate 70
HSF1: Heat Shock Transcription Factor 1
HSP70/90: Heat Shock Proteins 70/90
Hx: Highly Cross-adsorved
IAV: Influenza A virus
IF: ImmunoFluorescence
IFIT3: IFN-Induced protein with Tetratricopeptide repeats 3
IFNAR-I: IFN-α/β Receptor
IFN-α/β/ɣ: Interferon α/β/ɣ
Ig: Immunoglobulin
IKK: IκB Kinase
IL: Interleukin
Inl: Internalin
iNOS: inducible Nitric Oxide Synthase
IP: ImmunoPrecipitation
IRAK: Interleukin-1 Receptor-Associated Kinase
IRF3: Interferon Regulatory Factor 3
IS: Immune Synapse
ISG-15: Interferon-Stimulated Gene 15
JNK: c-Jun N-terminal Kinase
K63/48 polyUb: K63/48 poly-ubiquitin chains
kDa: KiloDalton
LAMP-1/2: Lysosome Associate Membrane Protein 1/2
LC3b: Microtubule-associated protein Light-Chain 3 b
LFA-1: Lymphocyte Function-associated Antigen 1
LIR: LC3-Intercating region of LC3
LLO: Listeriolysin O
***Lm:** Listeria monocytogenes*
LntA: *Lm* virulence factor Nuclear-Targeted protein A
LPS: Lipopolysaccharide
Lys or K: Lysine
mAb: Monoclonal Antibody
MAL: MyD88-Adapter-Like
MAPK: Mitogen-Activated Protein Kinases
MAVS: Mitochondrial Anti-Viral-Signalling Protein
M-CSF: Macrophage Colony-Stimulating Factor
mDia1/2: diaphanous-related formin 1/2
Mdp3: Microtubule-associated protein 7 (MAP7) Domain-containing Protein 3
MEFs: Mouse Embryonic Fibroblasts
MEK: Mitogen-activated protein kinase kinase, MAP2K
MHC-I/II: Major histocompatibility complex class I/II
miRNA: microRNA
MMP2: Matrix MetalloProtease 2
moDCs: monocyte-derived Dendritic Cells
MOI: Multiplicity Of Infection
mRNA: messenger RNA
MT: Microtubule
MTOC: MT Organizing-Centre
mTORC1: mammalian Target Of Rapamycin Complex 1
MVP: Major Vault Protein
Mx1: Myxovirus resistance 1
MyD88: Myeloid Differentiation primary response Gene 88
NADH: reduced Nicotinamide Adenine Dinucleotide
NADPH oxidase/NOX2: Nicotinamide Adenine Dinucleotide Phosphate oxidase
NBR1: Neighbor of BRCA1 gene 1 protein
NDP52: nuclear dot protein 52 kDa
NEMO: NF-κB Essential MOdulator
NES: Nuclear Import Signal
NFκB: Nuclear Factor kappa B

NH_4Cl: ammonium chloride
NI: Non-Infected
NLR: NOD-like Receptor
NLRP3: NLR family Pyrin domain-containig 3
NLS: Nuclear Localization Signal
NO: Nitric Oxide
NOD: Nucleotide-binding Oligomerization Domain
NOS: Nitric Oxide Species
OVA: Ovalbumin
P97/VCP: p97/Valosin-Containing Protein
pAb: Polyclonal Antibody
Pam2GSK4: palmitoyl-2 cisteine-serine-(lysine)4
Pam3GSK4: palmitoyl-3 cisteine-serine-(lysine)4
PAMPs: Pathogen-Associated Molecular Patterns
PBMC: Peripheral Blood Mononuclear Cells
PBS: Phosphate Buffered Saline
PCR: Polymerase Chain Reaction
PE: phosphatidylethanolamine
PE: Phycoerythrin
PeCy7: PE-Cy7
PerCP: Peridinin-chlorophyll Protein Complex
PI3K: Phosphatidyl Inositol 3-Kinase
PKC: Protein Kinase C
PLC: Phospholipase C
Poly(I:C): Poly(inosinic:cytidylic acid)
PrxI/II: Peroxiredoxin I/II
PTMs: Post-Translational Modifications
PVDF: Polymer of ViNylidene Fluoride
RAF: Mitogen-activated protein kinase kinase Kinase, MAP3K
***Rag1*$^{-/-}$:** Recombination-activating gene 1 mice
RanBPM: Ran-Binding Protein M
RAS: Rapidly Accelerated Fibrosarcoma
RD: Repressor domain of RIG-I
RFP: Red Fluorescent Protein
RIG-I: Retinoic acid Inducible Gene-I
RNS: Reactive Nitrogen Species
ROS: Reactive Oxigen Species
Rpd3: yeast Reduced postassium dependency-3
RPMI: Roswell Park Memorial Institute-1640
RT-qPCR: Reverse Transcription-quantitative Polymerase Chain Reaction
***S. aureus*:** *Staphilococcus aureus*
***S.* Thyphimuruim:** *Salmonella enterica* serovar Thyphimuruim
S: Supernatant
S+P: Supernatant + Pellet
SCID: Severe Combined ImmunoDeficient mice
SCV: *Salmonella*-Containig Vacuole
SE14: cytoplasmic anchoring motif of HDCA6
SEAP: Secreted Embrionic Alkaline Phosphatase
SEM: Standard Deviation of the Mean
Ser: Serine
SeV: Sendai Virus
shRNA: small hairpin RNA
Sir2: yeast silent information regulator 2
Sirt: Sirtuin
SLAPs: Spacious *Lm*-contaning Phagosome
SQSTM1/p62: Sequestosome 1/p62
STING: STimulator of INterferon Genes
SUMO: Small Ubiquitin-like Modifier
TAB1/2/3: TAK1-Binfing Proteins 1/2/3
TAK1/2/4: TGF-β Activated Kinase 1/2/4
Tat: Transactivation ptotein of HIV-1
TBS: Tris-Buffered Saline
TCR: T Cell Receptor
TEMs: Thyoglycollate-Elicitated Macrophages
TF: Transcription Factor
TG: Thioglycollate
TGF-β: Transforming Growth Factor-β
Thr: Threonine
Tip-DC: TNF/Inducible NO synthase-Producing DC
TIRAP: Toll/Interleukin-1 Receptor domain containing Adaptor Protein
TLR: Toll-Like Receptor
TNF-α: Tumor Necrosis Factor-α
TRAF6: TNF receptor-associated factor 6
Treg: Regulatory T cell
TRIF: TIR(Toll/interleukin-1 receptor)-domain-containig adapter-inducing IFN-β

TSA: Tubastatin A
TTTP/p25: Tubulin Polimerization Promoting protein 1/p25
Ub: Ubiquitin
UBA: Ubiquitin-Associated Domain
UBD: Ubiquitin-Binding Domain
UPEC: Uropathogenic *Escherichia coli*
UPR: Unfolded Protein Response
UPS: Ubiquitin-Proteasome System
Vif: Viral Infectivity Factor
VSV: Vesicular Stomatitis Virus
WASP: Wiskott Aldrich Syndrome Protein
WB: Western Blot
***wt*:** wild-type
Ywhaz: (tyrosine 3-monooxygenase/tryptophan 5-monooxygenase activation protein, ζ)
β2-M: β2-Microglobulin

Introduction

1. INTRODUCTION

The immune response is carried out by a higly specialized system and is constituted by cells and molecules that work in a coordinated and cooperative manner to react against pathogens and external threats to protect the body. The "innate immunity", constitutes the first line of defence against pathogens, acting very fast to counteract pathogens during the earliest phase of infection. Mechanisms involved in the recognition of microbes or damaged tissues and the subsequent reaction are repeated patterns common to groups of related pathogens. On the other hand, the "adaptive immune response" is highly effective and specific to fight against particular microbes. The most important hallmark of adaptive immunity is "immunological memory", essential to respond in a faster way and to generate a pool of memory cells that protect the body against reinfections. Innate and adaptive immune responses constitute a very precise integrated system of defence. In this regard, soluble factors delivered by innate immune responses to pathogens influence in the function of adaptive immune responses. Conversely, adaptive immune responses can focus the activity of innate immunity to be more effective to combat microbe insults.

The interest of this work is focused in the understanding of immunological mechanisms involved in the role played by HDAC6 in host cell defence against infection by the intracellular bacterium *Listeria monocytogenes*.

1. Histone deacetylase 6 (HDAC6)

1.1. Histone Deacetylase family (HDACs)

Histone deacetylases (HDACs) belong to a protein family with a mainly nuclear localization, which play an important role in the regulation of gene expression together with other histone modifier proteins such as acetyltransferases (HATs), methylases or methyltransferases [118,51]. Histone acetylation (mediated by HATs) is a versatile process that relax the chromatin structure, increasing gene transcription, whereas histone deacetylation, (carried out by HDACs), compacts the chromatin structure, inducing genetic silencing. HDAC family is composed by proteins that at least contain one deacetylase catalytic domain responsible for the removal of acetyl groups from target proteins [51]. There are 18 mammalian HDACs that are classified into four main groups according to their homology to yeast HDACs (**Figure 1.1**). Class I HDACs are orthologues of yeast reduced potassium dependency-3 (Rpd3) and comprise HDAC1, HDAC2, HDAC3 and HDAC8, which remain mainly localized in the nucleus. Class II HDACs are related to yeast Hda1 and according to their sequence homogy and domain structure, are subdivided into class IIa (HDAC4, HDAC5, HDAC7 and HDAC9) and class IIb (HDAC6 and HDAC10) [264]. Class III HDACs belong to the family of deacetylases called silent information regulator

2-like (Sir2) and include seven sirtuins (Sirt-1 to 7). The class IV HDAC group is formed by HDAC11, which shares conserved catalytic core domains with Classes I and II HDACs, but shows a different structure [21]. HDAC3, Class IIa and IIb HDACs are able to interchange their cellular localization between nucleus and cytoplasm depending on several cellular signals. However, Sirt-1, 6 and 7 are mainly found in the nucleus, while Sirt-3, 4 and 5 are localized at mitochondria.

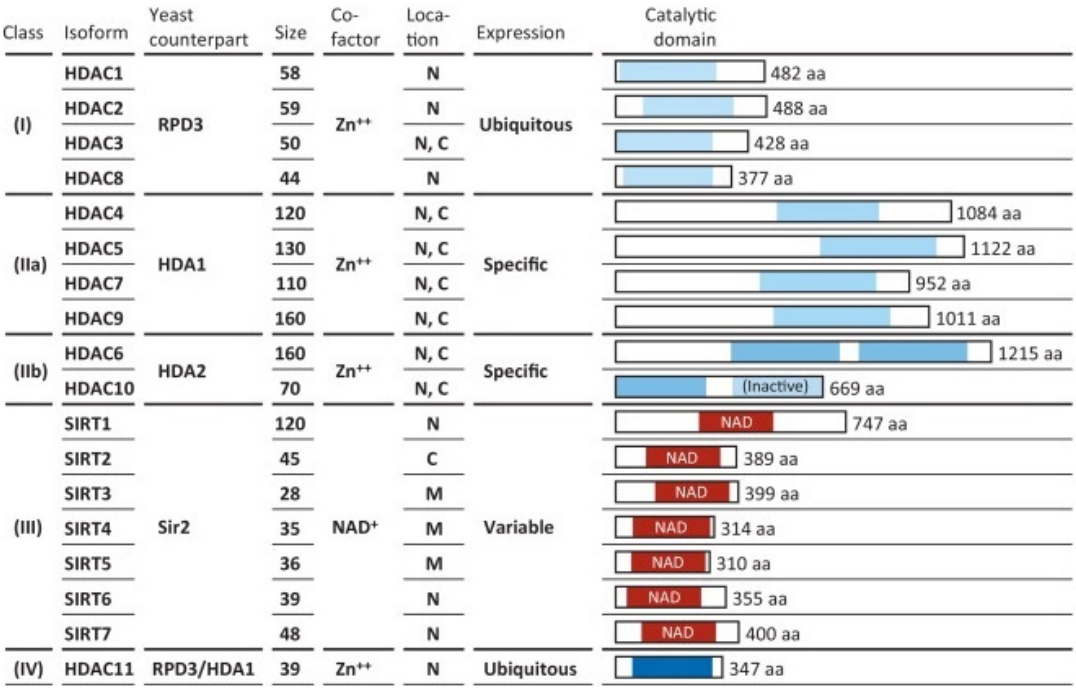

Figure 1.1. HDACs family. Classification of the 18 mammalian HDACs which are classified into four groups based on sequence similarity to the catalytic domain of yeast prototypes. Class I HDACs include the yeast Rpd3 homologs, HDAC 1, 2, 3 and 8. Class II HDACs encompass the yeast HDAC1/2 homologs, HDAC 4, 5, 6, 7, 9 and 10. They are further subclassified as IIa (HDAC 4, 5, 7 and 9) and IIb (HDAC 6 and 10). Class III HDACs (namely sirtuins) are composed by the yeast Sir2 orthologs SIRT 1, 2, 3, 4, 5, 6 and 7. HDAC11 belongs to the Class V HDACs, which has sequence similarity to both Rpd3 and Hda1. The subcellular localization is indicated as N: nuclear, M: mitochondrial and C: cytosolic. Sizes correspond to protein molecular weight and are expressed in kDa. From Shirakawa *et al* 2013 [223].

The common characteristic of HDACs is that they use zinc (Zn^{2+}) like enzymatic co-factors, belonging to the zinc-depending deacetylases groups [21]. This feature distinguishes them from sirtuins or NADH-depending deacetylases [213,246]. HDACs are ubiquitous and pleiotropic proteins that can be found in all cell types, although Class II HDACs are enriched in specific tissues. All of them are expressed in all mammalian cells and are distributed in different compartments such as nucleus, cytosol and mitochondria [51]. HDACs controls gene expression and are involved in many biological processes such as cell growth, proliferation and differentiation, cytotoxicity and apoptosis [51].

1.2. HDAC6 Structure

HDAC6 was the first characterized HDAC to be in the cytoplasm in an active form [91]. HDAC6 has a molecular weight of 130 KDa. This protein has two functional deacetylase domains (DD1 and DD2),

which are involved in the removal of acetyl groups from target proteins such as tubulin, cortactin and Heat Shock Protein 90 (HSP90) [91,268,269,273] (**Figure 1.2**). Although both domains are functional, DD1 has a weak enzymatic activity and shows substrate specificity for C-terminal acetyl lysine residues, whereas DD2 displays broad substrate spectrum [78,156]. It also possesses the SE14 domain, built with 8 consecutive repeats of a tetradecapeptide, essential for its cytosolic retention and for interaction with Tau [20]. Moreover, its N terminal nuclear export signal (NES) is stronger than its nuclear localization signal (NLS), leading to a predominant presence of HDAC6 in the cytosol. Both signals control the cytoplasmic-nuclear shuttling process of HDAC6.

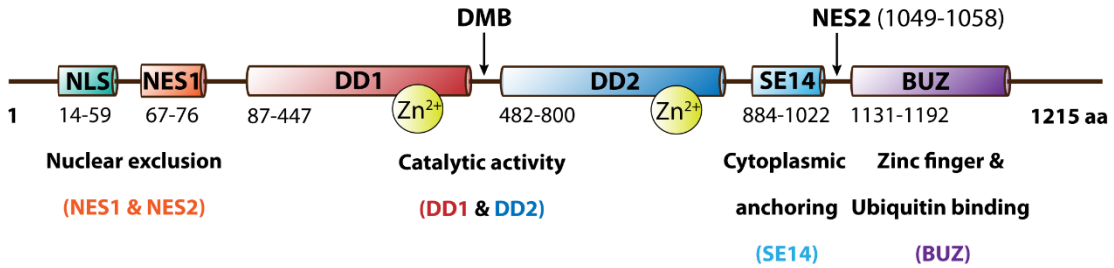

Figure 1.2. HDAC6 structure. HDAC6 protein is composed by the following domains. NLS: Nuclear localization signal, NES 1 and 2: Nuclear export signals 1 and 2, DD1 and DD2: functional deacetylase domains 1 and 2, DMB: dynein motor binding domain, SE14: cytoplasmic anchoring motifs, BUZ: Binder of Ubiquitin Zing finger domain. The corresponding amino acid (aa) sequence is showed below each domain by a range of numbers. Adapted from Li *et al* 2013 and Ageta-Ishihara *et al* 2013 [134,2].

To carry out its nuclear function, HDACs deacetylate histones modifying the packaging of the genetic material, however, HDAC6 also has a C-terminal zinc-finger ubiquitin-binding protein domain (ZnF-UBP) namely BUZ domain, that mediates the direct binding to DNA, regulating gene transcription. Besides, the ZnF-UBP domain is composed by a conserved cysteines and histidines repeat, also present in a group of proteins called ubiquitin-specific proteases, which allows HDAC6 to interact with mono- and poly-ubiquitinated chains, present in ubiquitinated proteins and in ubiquitin-interacting proteins [183,179,180]. This feature highlights the wide magnitude of the HDAC6 interactome, where a large variety of molecules can bind to HDAC6 dependently or independently of its catalytic function [244]. For this reason, HDAC6 is considered a crucial protein to link two cell signalling systems, mediated by acetylation and ubiquitination [244,31,216].

1.3. General functions of HDAC6

Due to the predominantly cytosolic localization of HDAC6, this enzyme is able to regulate several important biological processes such as immune response, lymphocyte activation, immune synapse organization, cell adhesion, migration, proliferation, survival, and differentiation through both deacetylase- and ubiquitin-dependent mechanisms [244,134,31,216]. HDAC6 is also involved in various pathological disorders, including autoimmunity and inflammation (autoimmune and Dextran

sodium sulphate (DSS)-induced colitis, autoimmune arthritis, and encephalomyelitis) viral infections (Human Immunodeficiency Virus (HIV), influenza A virus (IAV), Sendai virus (SeV)), neurodegenerative diseases (Parkinson and Alzheimer) and tumour progression and metastasis (solid and haematological tumours) [75]. The role of HDAC6 in relevant physiological processes is summarized in the following chart (**Figure 1.3**).

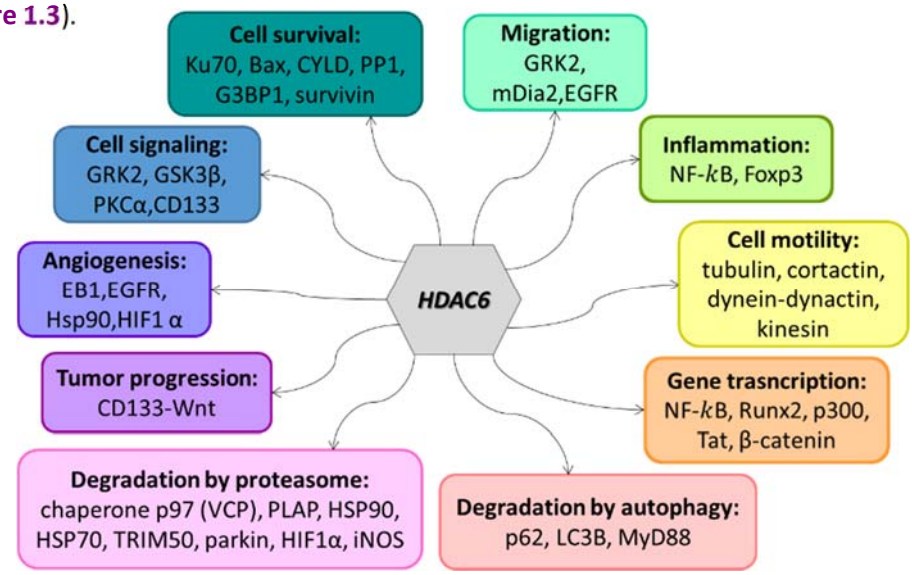

Figure 1.3. Functions of HDAC6 in physiological processes. Cellular functions are indicated in boxes, where HDAC6-interacting proteins implicated in particular cellular functions are listed.

1.3.1. Deacetylase-dependent functions

The first characterized HDAC6 substrate was tubulin, which is acetylated at lysine 40 (Lys^{40}) [91,184] [151]. HDAC6 enzymatic inhibition or downregulation results in tubulin acetylation, which enhances the stability of microtubule (MT) network and the binding of the two principal molecular motors of the cell, kinesin-1 and dynein, responsible for the anterograde and retrograde transport, respectively [7,115,272]. HDAC6 also binds to the dynein-activator complex, called dynactin. HDAC6 function is necessary to transport of misfolded protein aggregates (aggresomes) to proteasomes or lysosomes for degradation, avoiding cell toxicity [115,272,107,98,32].

One of the best characterized HDAC6 substrates is cortactin, a filamentous (F)-actin binding protein, which promotes actin polymerization and microfilament branching. Acetylated cortactin has diminished F-actin binding, influencing actin-mediated cellular processes such as endocytosis, migration, chemotaxis, adhesion or intracellular transport [268,140]. Besides, HDAC6 is able to regulate in a coordinate manner the intersection between microtubule cytoskeleton and actin filaments by the interaction with mediator proteins called formin homology proteins, mDia1 and mDia2 [56,19]. Other mediator proteins are septins, which are cytoskeletal guanosine triphosphatase proteins involved in providing a physical scaffold for HDAC6 to achieve MT deacetylation [2]. For these reasons, HDAC6 is considered as a crucial regulator of cell motility, able to connect both actin and

tubulin cytoskeletons. In fact, HDAC6 deregulation has been described in many tumours due to its implication in cytoskeleton, not only in cell progression, but also in angiogenesis and metastasis [91,184,3,76,103,136].

HDAC6 deacetylates HSP90 changing its activity, which is implicated in the regulation of many fundamental cell processes. HSP90 acetylation at Lys^{294} favours its dissociation from its co-chaperone p23, promoting the instability of many HSP90-interacting proteins involved in cell growth and survival [202,110,13,116]. New HDAC6 substrates have been characterized in last years and are summarized in **Table 1.1**.

Table 1.1. List of HDAC6 substrates. The table shows new non-histone HDAC6 client proteins, lysine residue susceptible of acetylation, related function and references.

Substrates	Deacetylated residues	Related function	References
α-tubulin	K^{40}	IS formation, virus infection, cell migration and chemotaxis	[91,151,220,243,36]
Cortactin	$K^{87/124/161/189/198/235/272/309/319}$	Regulation of actin filaments, cell motility, fusion of vesicles	[268,127]
HSP90	K^{294}	kinase activation and macropinocytosis	[116,110]
Tat	K^{48}	Suppression of HIV transactivation	[92]
RIG-I	K^{858} and K^{909}	Viral RNA recognition	[49,137]
Ku70	$K^{539/542}$	Suppression of apoptosis	[232]
β-catenin	K^{49}	Gene transcription activation	[271,135,145]
Peroxiredoxin-1 and 2	PrxI (K^{197}) PrxII (K^{196})	Redox regulation	[187]
Survivin	K^{129}	Anti-apoptotic function	[207]
MYH9	-	Actin-binding regulation	[267]
HSC70	-	Protein folding	[267]
DNAJA1	-	Protein folding	[267]
HSPA5	K^{447}	Suppression of breast cancer metastasis	[45]
HMGN2	K^{2}	Gene transcription and breast cancer growth	[153]
Sam68	-	Alternative splicing	[167]
14-3-3ζ	$K^{49/120}$	Suppression of growth and survival signalling	[159]
Tau	-	Neurodegeneration	[39,155,133]
Microtubule-associated protein 1 light-chain 3 (LC3b)	-	Autophagy	[138]

1.3.2. Ubiquitin-dependent functions

Through its BUZ domain, HDAC6 interacts with mono- and poly-ubiquitin chains, with a preferential binding for K63-linked ubiquitin chains [179,180]. For this reason, this protein participates in the formation of aggresomes, which transiently store toxic misfolded proteins (ubiquitinated protein aggregates). Besides, HDAC6 participates in the retrograde transport of aggregates along MT to be degraded by the primary quality control mechanism of the cell, the Ubiquitin-Proteasome System (UPS) [98,256,30,32]. HDAC6 also mediates the stability of ubiquitinated aggregates through its molecular association with the USP chaperone p97/valosin-containing protein (p97/VCP) and HSP90 [32,58]. Ubiquitinated protein aggregates are subsequently disrupted by p97/VCP machinery from

HDAC6 to deliver them to the proteasome for degradation, which promotes HDAC6 recycling [29]. In some situations, proteasomes are disrupted or overloaded, and aggresomes can be cleared by autophagy in a specific process called aggrephagy [98,58,186]. In this regard, HDAC6 is responsible for the dynein-mediated centripetal transport through MT of altered organelles and protein aggregates, concentrating them in perinuclear regions near the Microtubule Organizing Center (MTOC), where lysosomes are usually located [259,112,99]. Tubulin acetylation at Lys^{40} increases the recruitment and mobility of dynein through MT, enhancing the transport [59,203]. Therefore, HDAC6 has an important role in ubiquitin-selective quality-control autophagy, controlling the actin and tubulin networks [127]. Selective autophagy exclusively eliminates specific cellular components, as organelles like mitochondria (mitophagy) or unfolded protein aggregates (aggrephagy) [127,268,129,74,231]. Although HDAC6 is not required for autophagy induction, its deacetylase activity over cortactin is involved in autophagosome maturation. Deacetylation of cortactin induces the local assembly of actin microfilaments necessary for autophagosome fusion with the lysosome [127]. However, this is not dispensable for starvation-induced autophagy. SQSTM1/p62 interacts with HDAC6 and recruits F-actin filaments near HDAC6, promoting their deacetylation and the subsequent autophagosome-lysosome fusion [262]. Interestingly, the ubiquitin-like interferon (IFN)-stimulated gene 15 (ISG15) is able to interact with the BUZ domain of HDAC6 due to the structural similarity between K63-polyUb and ISG15 post-translational modifications (PTMs), labelling proteins for autophagic degradation [166].

HDAC6 forms a complex with HSP90, p97/VCP and heat shock transcription factor 1 (HSF1), which is disrupted in the presence of misfolded proteins due to the binding of HDAC6 to ubiquitinated aggregates. Available HSF1 activates the heat shock response and aggregates are degraded in the proteasome, highligthting the HDAC6 ability to sense cellular stress [32,107]. The roles of HDAC6 in aggresome formation, aggrephagy, autophagy, mitophagy and Heat Shock response are schemmaticaly illustrated in **Figure 1.4**.

On the other hand, the lack of HDAC6 impairs mitofusin 1 deacetylation, which blocks the mitochondrial fusion induced by glucose deprivation, causing an excess of reactive oxygen species (ROS) responsible of cellular oxidative damage [126,11]. It has been reported other role of HDAC6 in the mitochondria by its interaction with parkin and HSP70, regulating the homeostasis of this organelle through the control of mitophagy [128,104]. Hence, HDAC6 is an essential player of cell homeostasis because of its regulation not only of the cross-talk between the two main cellular degradation systems, the autophagy and the proteasome, but also of mitochondrial metabolic balance [98,57,186,72,104].

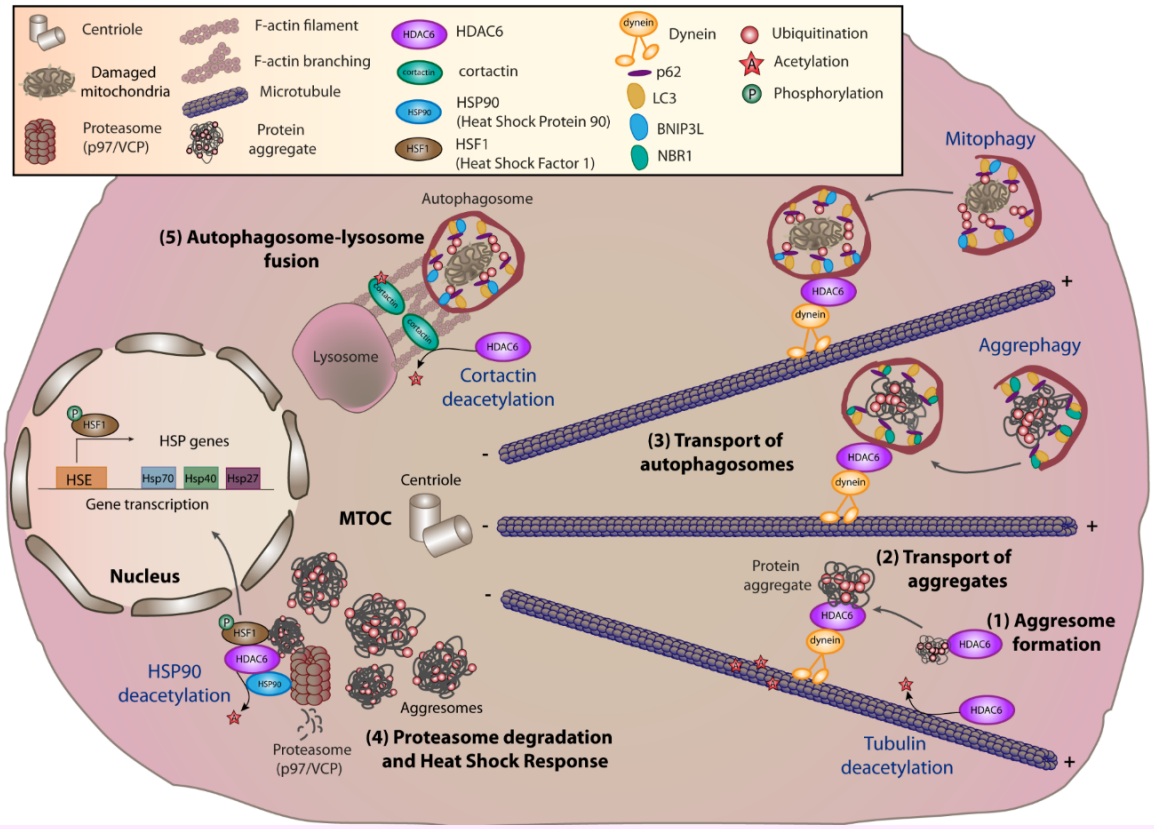

Figure 1.4. HDAC6 controls the principal clearance mechanisms of the cell. HDAC6 is involved in the regulation of aggresomes, proteasomes, Heat Shock response (HSR), and selective autophagy through the control of actin and tubulin networks and HSP90. **(1)** HDAC6 BUZ domain binds ubiquitinated protein aggregates and promotes aggresome formation to avoid cell toxicity. **(2)** HDAC6 is able to transport aggresomes through the MT due to its binding to the molecular motor dynein. Aggresomes are concentrated near the MTOC, where proteasomes are located. **(3)** HDAC6 binds to autophagosome-contained ubiquitinated substrates (protein aggregates and damaged mitochondria) and is implicated in their dynein-mediated transport to MTOC areas, where lysosomes are accumulated. Autophagy receptors p62 and NBR1 recognize protein aggregates and BNIP3L/NIX receptors detect damaged mitochondria by theirs UBA domains, whereas their LIR domains bind to the membrane autophagosome marker LC3. Acetylation of MT enhances dynein transport. **(4)** HDAC6 transfers aggresomes to the proteasome to be degraded and deacetylates HSP90 to start an HSR. Phosphorylation of HSF1 leads its nuclear import to initiate the transcription of HSP genes (HSP70, 40 and 27) **(5)** HDAC6 recruits cortactin to ubiquitinated substrates, whereas p62 assembles F-actin. HDAC6 deacetylates cortactin, promoting actin filament polymerization and branching and the subsequent autophagosome-lysosome fusion. Cortactin acetylation impairs this fusion. Adapted from Banreti *et al* 2013 and Richter-Landsberg *et al* 2013 [16,206].

1.4. Regulation of HDAC6

There is growing evidence regarding the regulation of the HDAC6 activity that encompasses post-translational modifications (PTMs), such as phosphorylation and acetylation, and RNA silencing by microRNAs. These mechanisms are able to control the levels of both cytoplasmic and nuclear HDAC6.

1.4.1. Phosphorylation

Phosphorylation has been broadly observed to improve the deacetylase activity of HDAC6. For instance, phosphorylation at serine 22 (Ser^{22}) of HDAC6 by the glycogen synthase kinase 3 (GSK3β)

enhances its enzymatic activity, regulating mitochondrial transport in hippocampal neurons [47]. Similar results have been detected at Ser^{1035} of HDAC6 by the activation of epidermal growth factor receptor (EGFR)-RAS-RAF-MEK-ERK signalling axis *in vivo*, whereas ERK-1 is able to phosphorylate HDAC6 at threonine 1031 (Thr^{1031}) and Ser^{1035} for the regulation of cell motility *in vitro* [254]. Casein kinase II (CK2) phosphorylates HDAC6 at Ser^{458}, enhancing its activity during the formation and the clearance of aggresomes [251]. HDAC6 is also phosphorylated at unknown residues by G protein-coupled receptor kinase 2 (GRK2) [119], Aurora A kinase [196], and protein kinase C isoform ζ (PKCζ) [61]. Moreover, SeV entry activates PKCα activity, which phosphorylates HDAC6, promoting the deacetylation and nuclear translocation of β-catenin to induce antiviral response [271].

1.4.2. Acetylation

HDAC6 can be modified by acetylation, affecting its deacetylase activity. Currently, it remains unknown whether HDAC6 is able to acetylate itself. Acetyltransferase p300 is responsible for HDAC6 acetylation at Lys^{16}, imparing its tubulin deacetylation and Sp1 transcriptional activities [84]. Acetylation of HDAC6 changes its subcellular localization because this PTM breaks the interaction between HDAC6 and importin-α, promoting the cytosolic retention of HDAC6 and the subsequent inability to deacetylate histones [141].

1.4.3. Regulators

It has been reported that several regulators interact with HDAC6 to directly inhibit its deacetylase activity. For example, tubulin polymerization-promoting protein-1 (TPPP/p25) binds to HDAC6, inhibiting its deacetylase activity on tubulin and β-catenin [238,215]. Paxillin also inhibits HDAC6 tubulin deacetylation, regulating Golgi structure and polarized migration [54]. The deubiquitinating enzyme CYLD negatively regulates HDAC6 activity on tubulin, which affects cell-cycle progression [253]. However, inactivation of HDAC6 by CYLD promotes ciliogenesis [265]. Mdp3 blocks HDAC6 function, promoting the acetylation of tubulin and the subsequent stabilization of microtubules [235]. The microtubule-associated protein tau inhibits HDAC6 deacetylase function [190]. Ran-binding protein M (RanBPM) interacts with HDAC6, imparing its deacetylase function, which favours aggresome formation [212]. On the contrary, absence of p62 causes an enhanced deacetylase activity of HDAC6 on tubulin and cortactin, necessary for the engulfment of aggresomes into autophagosomes [262].

1.4.4. microRNA

Numerous microRNAs regulate HDAC6 expresion and function, such as miRNA-22 [90,147], miRNA-26a [130], miRNA-221 [9], miRNA-433 [224,250,147] and miRNA-548m [143].

1.5. HDAC6 functions in the immune system

1.5.1. Role of HDAC6 in adaptive immunity

The regulation of tubulin cytoskeleton by HDAC6 is important in the cognate immune synapse (IS) between a T helper cell and an antigen presenting cell (APC) [220]. Acetylated microtubules are concentrated at the T cell contact area with APCs, surrounding CD3 and lymphocyte function-associated antigen 1 (LFA-1) clusters. After antigen-specific engagement of T cell receptor (TCR), a transient deacetylation of microtubules is induced at early times, followed by their subsequent acetylation at late times. Early deacetylation is carried out by HDAC6, which specifically translocates and concentrates to APC-T cell contact sites. Moreover, overexpression of HDAC6 disorganizes CD3 and LFA-1 clusters, translocation of microtubule organizing centre (MTOC), and IL-2 secretion, all necessary for a proper IS. However, overexpression of HDAC6-DD mutant does not exert the same effect and Trichostatin A (TSA) treatment reverts the effect, indicating the enzymatic contribution of HDAC6 during IS formation.

HDAC6 is also important for the chemotactic migration of the lymphocyte [36]. There is dynamic subcellular location of HDAC6 in the leading edge of lamellipodium and in the rear edge of uropod on migrating T cells. HDAC6 overexpression increases chemokine-mediated T cell migration and transendotelial migration under shear flow, whereas HDAC6 silencing diminishes T cell chemotactic capacity. The use of specific chemical inhibitors of HDAC6 and enzymatic activity mutants reveals that HDAC6 regulation of lymphocyte chemotactic migration is not mediated by its catalytic activity, but by an scaffold role.

HDAC6 plays a role in cytotoxic $CD8^+$ T lymphocytes during DNA virus infection [176]. *In vivo* immunization studies reveal a defective cytotoxic response in HDAC6 *knockout* mice. $CD8^+$ T lymphocyte adoptive transfer into Recombination-activating gene 1 ($Rag1^{-/-}$) recipient mice demonstrates the specific impairment of cytotoxic response against vaccinia virus infection. The altered dynamics of lytic granules of HDAC6 deficient $CD8^+$ T lymphocytes is due to the lack of binding of HDAC6 to kinesin-1-dynactin, involved not only in the altered terminal transport of these granules to the synapse but also in their defective exocytosis [176].

HDAC6 exerts a role in the adaptive response of $CD4^+$ T cells in different autoimmune and inflammatory disorders such as colitis and cardiac-allograft rejection by the enhanced transcription of Foxp3 [52]. HDAC6 deficient $CD4^+$ T cells express higher levels of the transcription factor Foxp3, deregulating the balance between pro- and anti- inflammation in favour of regulatory T cells, promoting a protective role during DSS-induced and autoimmune models of colitis and fully MHC-incompatible cardiac allograft rejection [52]. Accordingly, mice treated with HDACi show acetylated

Foxp3, which increases its DNA-binding capacity, enhancing Treg differentiation [18]. HDAC9-deficient mice display HSP70 acetylation, which prevents its degradation by proteasome and results in its accumulation, enhancing HSP70-Foxp3 interaction that stabilizes Foxp3 [53]. Both observations could be also extended to HDAC6-deficient mice. Interestinglly, HSP90 acetylation impairs its binding to Aryl Hydrocarbon Receptor (AHR), which affects the AHR ability to recognize ligands and the subsequent activation of AHR signalling [110]. Activation of AHR signalling pathways, enhances *in vitro* Th17 polarization [62]. Hence, Th17 response might be decreased in HDAC6 absence.

1.5.2. Role of HDAC6 during viral infections

Through acetylation, HDAC6 controls microtubule stability and consequently the kinesin and dynein-dependent transport of various cargoes. Cargo movement mechanisms are co-opted by different types of pathogens, including viruses and intracellular bacteria. Thus, HDAC6 becomes a crucial intermediary involved in viral fusion, entry, nuclear shuttling, replication, assembly and egress [249,165,93]. Likewise, HDAC6 controls the mechanisms involved in the elimination of these pathogens. For example, HDAC6 is involved in $CD4^+$ T lymphocytes function during the human immunodeficiency virus (HIV) infection [243]. The binding of the viral envelope glycoprotein gp120 to permissive $CD4^+$ T cells increases acetylated tubulin. HDAC6 overexpression inhibits tubulin acetylation, preventing viral envelop-mediated cellular fusion and infection, without affecting the expression and co-distribution of viral receptors. Consequently, the diminished enzymatic activity of HDAC6 favours HIV-1 infection and syncytia formation [243]. However, the activity of this protein in the case of influenza A virus (IAV) seems to play a dual role. On one hand, it has been described that viral capsids mimic unfolded-protein aggregates to take advantage of the host cell aggresome formation to disassemble and successfully eliminate viral capsids to continue the infection [15]. On the other hand, it has been observed that microtubules deacetylated by HDAC6 hamper the viral cycle, preventing trafficking of viral components through the cytoskeleton, which is necessary for viral assemble sites in the host plasma membrane and their posterior spreading to neighbouring cells [93]. Besides, caspase-3 cleaves HDAC6 in IAV-infected cells, removing its BUZ domain, although the consequence in IAV infection remains unknown [94].

Other HDAC6 substrates different from cytoskeletal proteins participate in viral pathogenesis like the HIV-1 transactivator of transcription protein (Tat) and the Retinoic acid Inducible Gene-I (RIG-I) [49,137,92,226]. HDAC6 regulates HIV viral replication by the deacetylation of Tat at transcriptional level, imparing the binding of Tat to cyclin T1, which inhibits viral transactivation [92,226]. In addition, HDAC6/"apolipoprotein B m-RNA-editing enzyme-catalytic, polypeptide-like 3G" (A3G) complex interacts with Viral infectivity factor (Vif) for its autophagic degradation, inhibiting HIV-1 spreading

[245]. Recognition of 5´ppp-dsRNA by RIG-I induces its self-oligomerization via repressor domain (RD) of two RIG-I molecules, initiating a conformational change. RIG-I specific deacetylation at residues K^{858} and K^{909} by HDAC6 induces RIG-I "signalling on" conformation, an essential step to engage Mitochondrial anti-viral-signalling protein (MAVS) and to activate the anti-viral response through Interferon responding factor 3 (IRF-3)-Interferon-β (IFN-β) axis [137,49] (**Figure 1.5**). Protein kinase C-α (PKC-α) is activated by calcium changes, phosphorylating HDAC6 during SeV infection [271]. This PTM enhances HDAC6 enzymatic activity and thereby, mediating deacetylation of β-catenin, which works as co-activator of IRF-3 transcription [271] (**Figure 1.5**)

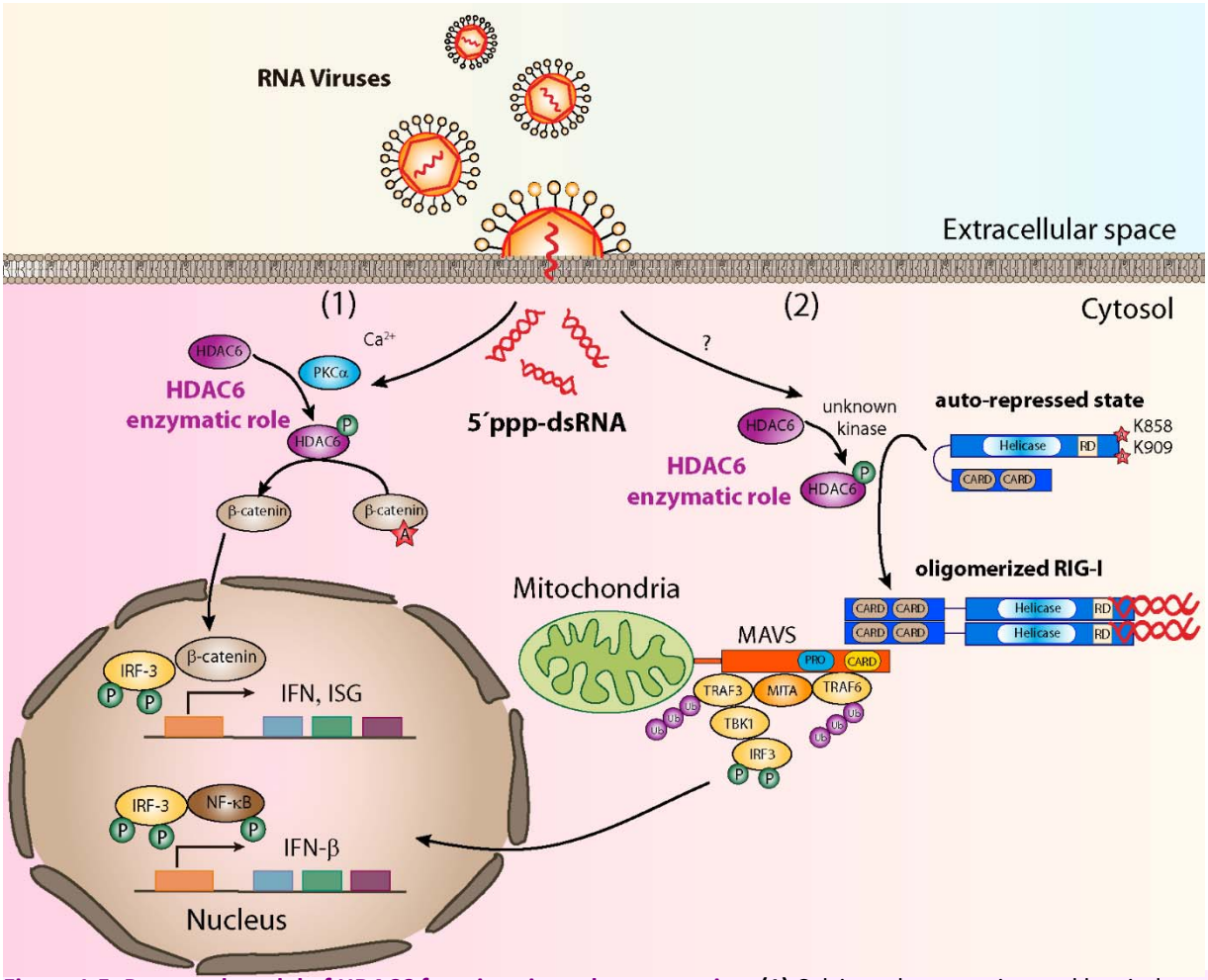

Figure 1.5. Proposed model of HDAC6 functions in pathogen sensing. **(1)** Calcium changes triggered by viral entry activates PKCα, which phosphorylates HDAC6, increasing its deacetylase activity on β-catenin. This protein is imported in the nucleus together with IRF-3 to activate the interferon response. **(2)** After RNA viral infection, 5´ppp-dsRNA alerts to an unknown kinase, which activates HDAC6 by phosphorylation. HDAC6 deacetylates K^{858} and K^{909} residues of RIG-I, promoting its dimerization and binding of 5´ppp-dsRNA, which is necessary for the activation of MAVS signalling pathway. Then, IRF-3 and Nuclear factor-κB (NF-κB) initiate the interferon-β genetic transcription to alert the anti-viral host response. Adapted from Zheng *et al* 2017 [270].

Protein kinase C-β (PKC-β) is also able to phosphorylate HDAC6 and enhaces its enzymatic function over β-catenin, promoting the transcriptional activation of IRF-3 and the subsequent production of type-I IFN in response to Toll-like receptors 3 and 4 (TLR-3 and 4) agonists [46].HDAC6, through its BUZ

domain, directly associates with ubiquitinated NOD-like receptor (NLR) family, pyrin domain-containing 3 (NLRP3), down-regulating the activation of NLRP3 inflammasome independently of deacetylase activity [95]. Finally, the observation that HDAC6-deficient mice are more susceptible to RNA virus infections is in accordance with the observed increased resistance of overexpressing-*Hdac6*^{tg} mice to avian H5N1 virus, highlighting the role of HDAC6 as a new regulator of the innate immune defence [249,93,165].

1.5.3. Role of HDAC6 during bacterial infections and TLR-activation

Recent evidence supports a role of HDAC6 in bacterial infections. Hence, bladder-infiltrating neutrophils of HDAC6-deficient mice during uropathogenic *Escherichia coli* (UPEC) infection display higher bacteria titres [132]. Recently, new molecular mechanisms have been characterized to be involved in inflammatory processes caused by bacterial TLR-agonists such as LPS, suggesting a wider implication of HDAC6 in innate immunity [171,261,46]. HDAC6-deficient mice are protected from LPS-induced septic shock compared to *wild-type* mice, due to a defective pro-inflammatory response in the absence of HDAC6 [46]. Inhibition of HDAC6 expression and HDAC6-deficiency cells reduce pro-inflammatory cytokines after TLR-stimulation, although it is not clear whether deacetylase activity is directly involved in all cases [171,261,46,137,49]. However, it has been observed that HDAC6 hampers the formation of MyD88-TRAF6 signalling complex, suppressing TLR-4 mediated activation [97]. Tat protein in primary mouse astrocytes induces a severe neuroinflammation, and the silencing of HDAC6 reduces levels of chemokines, cytokines and adhesion molecules, diminishing the activation of NF-κB and AP-1 Transcription Factors (TF) responsible of pro-inflammatory response [226]. Therefore, increased expression of HDAC6 protein after TLRs activation and viral infections could serve as a protective cellular strategy to deacetylate microtubules and actin networks for avoiding microbial spreading [249,226].

2. Listeria monocytogenes

Lm was identified in Cambridge in 1926 as a lethal disease which displayed a pronounced monocytosis, an increased number of monocytes in circulating blood, in rabbits and guinea pigs caused by a *Gram*-positive bacterium referred to as *Bacterium monocytogenes* [163]. Another report in South Africa described also a *Gram*-positive bacterium responsible of Tiger River Disease in wild gerbils. Prominent necrotic lesions in liver were described and the microorganism was called *Listerella hepatolytica*, in honour to the surgeon Joseph Lister. New studies concluded both pathogens were the same, and the final name was designated as *Listeria monocytogenes*.

The genus *Listeria* contains 17 species which are able to grow at low temperatures and are very resistant to environmental stresses, such as low pH and hight salt concentrations, remarking the

concerns for the food industry [181]. Besides, *Listeria* spp. thrives in a huge range of environments, can survive in water, soil and detritus and is able to infect mammalian hosts due to a particular adaptability to cross several host barriers, mediated by a vast number of regulatory factors. *Lm* is a non-spore-forming facultative anaerobic rod-shaped bacterium, which can be flagellated under 30°C. The systematic sequencing of the bacterial genome of *Lm* has revealed a genome size of 2,944528 base pairs coding for 2,853 proteins [161,73]. However, the most important virulence factors of this pathogen has been characterized using biochemical and molecular genetic tools. Besides, murine listeriosis has been widely used as a forefront model for the study of host-pathogen interaction and innate and adaptive immune responses to intracellular bacterial infection over the past 20 years [185,80,175,242].

2.1. *Listeria monocytogenes* pathogenesis

Although *Lm* was first reported to infect rabbits and gerbils, this bacterium has an unusually broad host range, infecting almost every mammals, including humans [33]. This intracellular *Gram*-positive bacterium causes listeriosis, a self-limiting gastroenteritis in healthy individuals, but can cause severe and systemic infection in immunocompromised individuals, the elderly, pregnant women and new-borns due to its ability to cross the blood-brain barrier and placenta [185,214]. Immunocompromised individuals suffer septicaemia and meningitis, pregnant women in third trimester develop chorioamnionitis and infectious of the foetus which can lead to septic abortion [12]. Humans are exposed to the infection of this bacterium by ingesting contaminated food, usually unpasteurized or incompletely cooked meats [214]. Although *Lm* is considered a food-borne intracellular bacteria that causes a moderately low number of infections per year (listeriosis to 23.150 people worldwide in 2010), the mortality among infected individuals is strikingly high (30%) being responsible of approximately 6,900 deaths every year [50].

2.2. Infective cycle of *Listeria monocytogenes*

2.2.1. Bacterial entry

Despite most studies have used intravenous or intraperitoneal inoculation of *L. monocytogenes*, the natural route of infection is through the gastrointestinal tract [125]. *Lm* can replicate in the cytosol of several host cell types such as epithelial cells and macrophages [194]. The efficiency of bacteria uptake can vary depending of cellular type, e.g. macrophages and other phagocytic cells internalize up to 20 bacteria per cell, whereas fibroblast cell lines internalize less than one bacterium [33]. *Lm* co-opts the cellular receptor-mediated endocytosis machinery to entry into non-phagocytic cells, while *Lm* entry in phagocytic cells is actively mediated by immunoglobulin receptor-mediated engulfment of opsonized bacteria [43]. After the ingestion of this pathogen, intestinal epithelial cells are infected by

the interaction of the surface bacterial protein internalin A (InlA) with the extracellular domain of the epithelial E-cadherin of the host cell through a zipper-like mechanism [69,188]. The ability of this bacterium to infect intestinal epithelial cells is quite variable among mammals [111]. For example, mice have a limited susceptibility to intestinal infection due to a single amino-acid difference between human and mouse E-cadherin [124]. Upon this interaction, *Lm* is able to traverse the epithelial cell layer and disseminate in the bloodstream towards other organs. This bacterium has tropism in particular for spleen and liver, where not only is internalized by splenic and hepatic macrophages, but also by hepatocytes using the bacterial protein internalin B (InlB) to interact with the hepatocyte growth factor receptor (HGFR), mediating the internalization via Phosphatidyl Inositol 3-phosphate (PI3)-kinase activation [42,221]. Hence, internalins A and B are considered strategic tools of *Lm* for adhesion and invasion of host cells, increasing the level of bacteria internalization by non-professional phagocytic cells. The family of internalins is composed of 25 members, can be anchored to the cell wall, associated or secreted for regulating a vast number of virulence-related function [22]. InlC seems to affect the rigidity of the cytoskeleton and innate immune signalling, InlP is implicated in placental invasion and InlJ has unknown function and is only expressed *in vivo* [201,211,68]. In addition to InlA and B, both fibroblasts and monocytes use the high affinity immunoglobulin gamma Fc receptor I (FCGR1A or CD64) as *Lm* entry receptor without the opsonisation step [189].

2.2.2. Bacterial tools to evade the autophagy system

From the first hours of infection, professional phagocytic cells trap bacteria in the blood and target organs, spleen and liver, exerting a degree of control on bacterial growth [236]. Liver macrophages and hepatocytes are the preferential hosts for *Lm*, although other cell types are also infected such as epithelial cells and other phagocytic cells. Upon entry, bacterium is internalized inside a phagocytic vacuole and *Lm* is eliminated by fusion of the phagosome with lysosomes. Interestingly, phagosome-contained bacteria are also eliminated by the action of reactive oxygen species (ROS) and nitric oxide (NO), respectively produced by NADPH oxidase 2 (NOX2) and inducible NO synthase (iNOS) [144] [222] (**Figure 1.6**). However, the majority of bacteria escape from the phagosome into the cytoplasm through the action of the cholesterol dependent family of cytolysine listeriolysin O (LLO) and two other phospholipases C (PLCs), a phosphatidylinositol-specific PLC (PlcA) and a broad spectrum one (PlcB), which causes vacuolar rupture [17,71,148,35,23]. In HeLa cell line, escape from the vacuole is exclusively mediated by both phospholypases [148].

Lm is able to replicate in spacious *Lm*-containing phagosomes (SLAPs) in some macrophages [23]. The formation of SLAPs depends on microtubule associated protein light-chain 3 (LC3)-mediated phagocytosis combined with intermediate levels of LLO expression, which dampen the phagosome acidification, resulting in *Lm* proliferation without phagosomal rupture [120]. ActA is also an essential

bacterial protein to evade the cell host autophagy. In this regard, Δ*actA* bacteria is ubiquitinated and subsequently recognized by ubiquitin-binding receptors p62 and nuclear dot protein 52 (NDP52) and incorporated in $LC3^{+}$-compartments [266,160]. Indeed, cellular factors that alter ActA localization on the bacterial surface could dampen cell-to-cell spreading of *Lm*, such as the case of type I IFN receptor 1 (IFNAR1)-deficient mice, which display lower bacterial burden [63,8,230,182]. Cell host Major Vault protein (MVP) is hijacked by bacterial InlK to avoid ubiquitination and the subsequent autophagy [60].

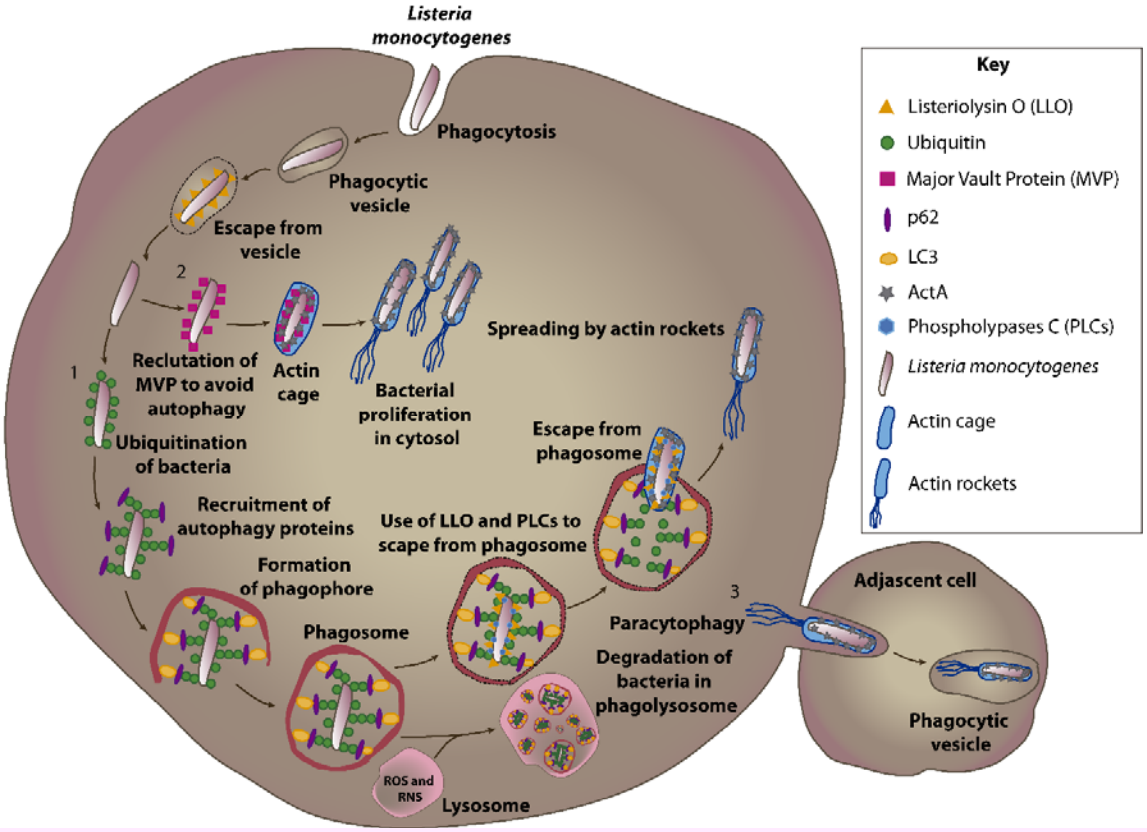

Figure 1.6. Overview of infective cycle of *Lm* in a phagocytic cell. *Lm* enters the cell by membrane vesicle phagocytosis. Using LLO is able to escape from the vesicle to the cytoplasm. **1.** Once in the cytosol, bacteria are rapidly ubiquitinated and consequently recognized by autophagy proteins, such as LC3, p62, ATG family. These proteins are required to initiate the phagophore formation, a double-membrane vesicle where ubiquitinated bacteria are engulfed. Inside phagosome, the action of ROS, Reactive Nitrogen Species (RNS) and lytic enzymes of the lysosome contribute to bacterial degradation in a continuous process of phagosome-lysosome pH acidification. However, a percentage of bacteria can avoid this process by the expression of LLO and two phospholypases C (PlcA and B), which are activated with the lower pH, allowing *Lm* to form a pore in the phagosome membrane to evade its degradation. By the use of ActA, *Lm* travels through the cytosol polymerizing cellular actin, drawing characteristic acting comets. **2.** Besides, this bacterium can avoid the autophagy by another mechanism, expressing InlK, which recruit the mammalian MVP to block bacteria ubiquitination. The use of ActA protein is also responsible of the formation of actin cage, to avoid autophagy. Once in the cytosol, *Lm* proliferates due to permissive environmental conditions. **3.** Moreover, actin-polymerizing bacteria are able to infect neighbouring cells without leaving the cytoplasm, making long actin rockets in a process named paracytophagy.

2.2.3. *Lm*-induced cellular changes

In the cytoplasm, *Lm* replicates in a more benign and nutrient-rich environment and is able to infect neighbouring cells [193,28,178]. *Lm* is able to replicate and survive in cell host cytosol without causing

cell death because of its unique intracellular lifestyle. This hallmark is due to additional functions of LLO, different from its pore-forming activity, which cause multiple changes in organelle morphology and function before LLO plasma membrane entry and after its cellular internalization [83] (**Figure 1.7**). LLO causes a non-cannonical mitochondrial fission, independent of dynamin-related protein 1 (DRP1) and accompained by smaller and rounded mitochondria, which seems to enhance bacterial division [227-229]. Upon infection, this cytolysin induces Endoplasmic Reticulum (ER) stress and Unfolded Protein Response (UPR), responsible for upregulating chaperones, blocking translation into the ER and increasing ER folding capacity [192]. Animals with a defective UPR succumb to *Lm* infection [106]. Finally, LLO alters lysosomal membrane permeability and homeostasis, causing a release of cathepsins into cytosol [146].

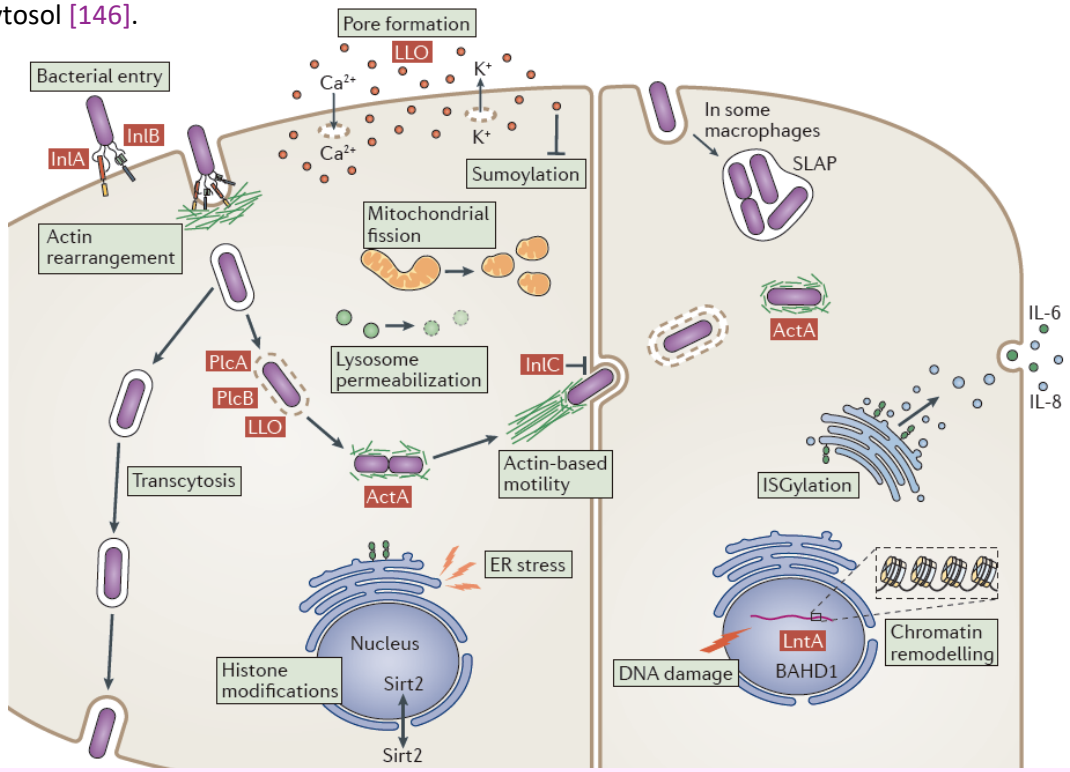

Figure 1.7. *Lm* infective cycle in a non-phagocytic cell and in some macrophages. *Lm* enters epithelial cells throught receptor-mediated endocytosis and the majority of bacteria scape from the vacuole. By trancytosis, vacuole-contained *Lm* can pass across the cell in globet cells, whereas *Lm* can replicate in spacious *Lm*-containing phagosomes (SLAPs) in some macrophages. Potent virulent factors as LLO, PlcA and PlcB are involved in vacuolar escape. Upon vacuolar escape, *Lm* is able to polymerize actin by using the actin-assembly-inducing protein ActA, enhancing the spreading to neighbour cells. The pore-forming activity of LLO triggers numerous changes in host cell, such as histone modifications, desumoylation, mitochondrial fission, ER stress and lysosomal permeabilization. Host gene expression is controlled by LntA of *Lm*, which interacts with BAHD1 complex to derepress ISGs. This provokes Sirt2 shuttle into the nucleus to deacetylate histone 3 at K^{18}, that changes chromatin packing and the subsequent gene expression and DNA damage. The host cell fights against infection by upregulating antibacterial effectors, such as ISG15 and its covalent incorporation to ER and Golgi proteins (a process namely ISGylation), which modulates cytokine secretion. From Radoshevich *et al* 2018 [198].

However, the host cell fights against infection by upregulating IFNs, cytokines and antibacterial effectors, such as IFN-stimulated genes (ISGs) [189]. In this regard, an ubiquitin-like protein, called IFN-stimulated gene 15 (ISG15), is induced during *Lm* infection and its covalent incorporation to newly-

synthesized proteins of ER and Golgi (namely ISGylation), increases cytokine secretion to counteract infection [200]. *Lm* dampens sumoylation of host cell proteins by degradation of Small ubiquitin-like modifier (SUMO)-conjugating enzyme UBC9 required for this kind of PTM [204,96]. *Lm* is able to mimic receptor-mediated endocytosis engagement, promoting the phosphorylation and ubiquitination of the cytosolic domain of receptors E-cadherin and Met and their subsequent internalization, co-opting the clathrin machinery of the host cell [248,26]. *Lm* also promotes changes in histone PTMs, which modifies the chromatin packaging and the subsequent access of transcription factors [81,82]. For instance, cell host sirtuin-2 is shuttled to the nucleus to deacetylase histone 3 at K^{18} [67]. A nucleomodulin-type of bacterial virulence factor namely nuclear-targeted protein A (LntA), controls host gene expression throught its interaction with the bromo adjacent homology domain-containing 1 protein (BAHD1) complex to derepress ISGs [122,123].

3.2.4. Intracellular and extracelular motility

Wiskott Aldrich Syndrome protein (WASP) is a nucleation promoting factor that interacts with the actin-related protein 2/3 (ARP2/3) complex to induce actin polimeryzation on host cell. *Lm* contains a surface-anchored protein, called actin-assembly inducing protein (ActA), which mimicks WASP to enable bacterial propulsion to neighbouring cells through the directional assembly of actin filaments (actin rockets) [113,121,37,28,225]. The canonical ARP2/3 complex is formed by 7 subunits: ARP2 and 3 and ARPC1-5, and *Lm* co-opt different combinations of these subunits depending on the type of actin polymerization or branching required in every step, such as bacterial entry or actin comet tail formation [117]. However, *Lm*-containing vacuoles can pass across the cell cytoplasm in globet cells by trancytosis, acting as a vacuolar bacterium for avoiding cytosolic immune detection [174]. *Lm* can also spread from cell to cell elongating filopods to adjacent cells without exiting the intracellular compartment by a process called paracytophagy, which exploits host cell efferocytosis for evading immune detection [157]. LLO induces membrane damage in actin protrusions, exposing phosphatidylserine, which is usually found in the inner membrane of the host cells, therefore adjacent macrophages capture protrusion-containing *Lm* [44].

3.2.5. Cellular immune response to infection

During food-borne infection, the majority of *Lm* is extracellularly attached to the surface of activated monocytes, although these cells are not a proliferation niche for bacteria [100]. However, monocytes increase CD64 expression during their transition to macrophages, which *Lm* uses as an entry receptor, thereby allowing intracellular bacteria to spread to the liver and spleen [101,41]. Resident Kupffer cells phagocytose *Lm* in the liver and the posterior necroptosis of these macrophages generates specific inflammatory mediators that activate liver repair processes, the mobilization of bone-marrow-derived

monocytes and awake the immune system [25]. Nevertheless, the early control of *Lm* burden largely depends on the innate immune response occurring in the spleen, which relies on two main cell populations of dendritic cells (DCs). On one hand, a subset of monocyte-derived DCs namely TNF/iNOS–producing DCs (Tip-DCs) has the ability to produce TNF-α and NO [219,236]. On other hand, CD8α$^+$splenic conventional DCs (cDCs) are responsible for the final resolution of *Lm* infection through the presentation of bacterial-derived antigens to specific CD8$^+$T cells to induce cytotoxicity [86,65,102]. Moreover, it has been reported that CD8α$^+$ cDCs are the first splenic population responsible for the phagocytosis of bacteria *in vivo* [170]. However, the host cell of cytosolic *Lm* is able to develop a specific CD8$^+$T cell response, which is crucial for the control of infection [40,154,79,10]. It has been reported that mutant LLO *Lm* strains are unable to develop CD8$^+$ T cell adaptive response and, accordingly, CD8$^+$ T cell memory against this pathogen [154,79,10].

3.2.6. Innate immune sensing of *Lm*

The response of dendritic cells (DC) to live *Lm* is mediated by Toll-like receptors (TLRs), nucleotide-binding oligomerization domain (NODs)-like receptors (NLRs), and other cytosolic receptors and involves two signalling pathways: TLR-dependent and independent signalling [198,199]. *Lm* pathogen-associated molecular patterns (PAMPs) are sensed on the cellular surface by TLRs 1, 2 and 6, whereas phagosomal-contained bacteria activate endosomal TLRs 2, 3, 7, 8 and 9. TLR-3 mediates TRIF-dependent signalling pathways and the rest of TLRs mediates a MyD88-dependent response. Both cellular pathways activate NF-κB signalling for the initiation of anti-bacterial host response. After phagosomal escape, *Lm* activates the inflammasome and cyclic GMP-AMP synthase (cGAS), which produces a host-specific cyclic dinucleotide (CDN) called cGAMP, that also activates the sensor stimulator of interferon (IFN) genes (STING) [237]. Passive release or active secretion by *Lm* of the bacterial 5´triphosphate RNA (5´-pppRNA) is sensed by retinoic acid-inducible gene I protein (RIG-I), which triggers the mitochondrial and peroxisomal forms of anti-viral-signalling protein (MAVs) [1,77]. These synergic pathways upregulate IFNs, cytokines and anti-bacterial effectors such as IFN-stimulated genes (ISGs). At early stage of infection, bacterial DNA is sensed by the cytosolic surveillance pathway, that includes STING, the serine/threonine-protein kinase TBK1 and the IFN regulatory factors (IRFs) 3 and 7 [4,199]. This pathway induces the expression of ubiquitin-like protein ISG15, independently of IFN, and the conjugation of ISG15 to newly synthetized Endoplasmic Reticulum (ER) and Golgi proteins as a cellular mechanism for tagging proteins after infection [200]. Besides, *Lm* secretes a small dinucleotide namely cyclic di-AMP (c-di-AMP) that directly triggers STING pathway, leading to IFNβ production and activation of downstream signals that control the transcription of IFN target genes essential for antiviral and antibacterial responses [255,89,4,257]. However, the activation of innate immune pathways by c-di-AMP negatively activates T cell-mediated responses, reducing the clearance

of *Lm* after a reinfection [4]. Additionally, the liver enzyme called aldo-keto reductase family 1 member C13 (AKR1C13 or RECON) binds to c-di-AMP with higher affinity than STING. STING affinity for host CDNs is stronger than for c-di-AMP, balancing the signalling pathways triggered by c-di-AMP on favour of RECON [152]. Although TLR-1 and 2 and NOD1 are activated by *Lm* PAMPs to stimulate NF-κB signalling, RECON negatively regulates this pathway [152]. However, after bacterial CDN-RICON binding, the enzyme is inactivated, recovering the NF-κB signalling and Nitric Oxide (NO) production [152]. The complete molecular innate immune response to *Lm* is summarized in **Figure 1.8**.

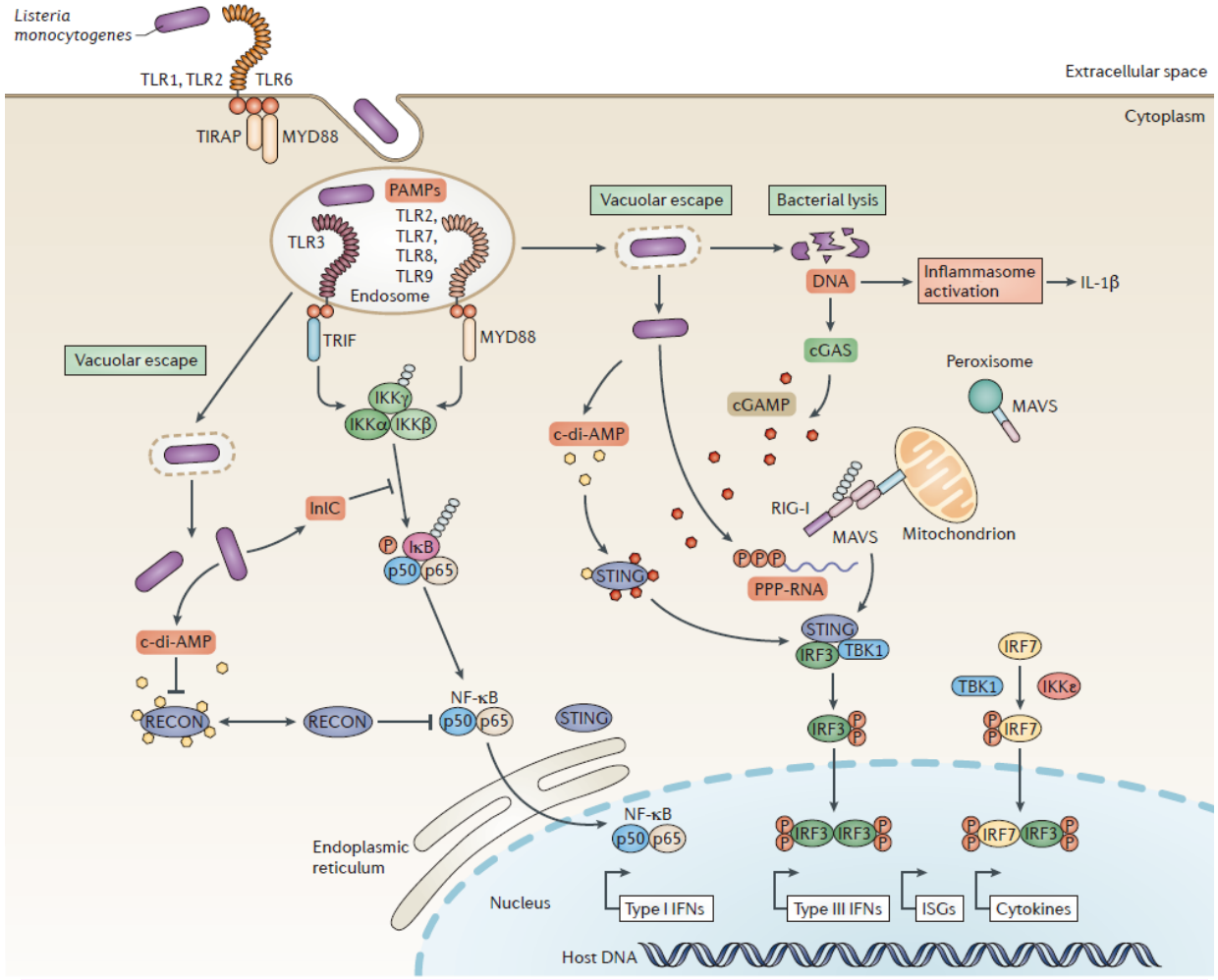

Figure 1.8. Innate immune sensing of *Lm*. *Lm* is sensed by TLRs 1, 2 and 6 in the plasma membrane and by TLRs 2,3,7,8, and 9 in endosomes, triggering the TLR-signalling pathway and the nuclear import of NF-κB to induce genetic transcription of IFNs, cytokines and ISGs. Upon vacuolar escape of *Lm*, the cytosolic surveillance pathway is activated by bacterial DNA, 5´pppRNA and c-di-AMP, inducing STING, TBK1, RIG-I, mitochondrial and peroxisomal MAVs, IRFs 3 and 7 and RECON. From Radoshevich *et al* 2018 [198].

Although, the function of HDAC6 has been described in autoimmune, inflammatory and viral disease models, there is not much information about its role in the regulation of innate immunity during the infectious processes by non-viral pathogens, such as bacteria and protozoan. For this reason, this doctoral thesis is focused in the study of the role of HDAC6 in the innate immune host defence against *Listeria monocytogenes* infection and tentative molecular mechanisms involved.

Objectives

2. OBJECTIVES

The general objective of this thesis aims to investigate the functions of HDAC6 during the innate immune response to the intracellular bacteria *Listeria monocytogenes (Lm)*. The specific objectives are the following:

1. **Analysis of HDAC6 contribution to cellular mechanisms that eliminate intracellular bacteria by phagocytic cells**
   - 1.1. Effect of HDAC6 absence in the intracellular pathogen clearance of dendritic cells
   - 1.2. Measurement of *Lm* load in HDAC6-deficient myeloid cells
   - 1.3. Determination of *in vivo* bacterial burden
   - 1.4. Evaluation of cellular clearance mechanisms of *Lm*
   - 1.5. Consequence of the lack of HDAC6 in the autophagy of *Lm*
   - 1.6. Effect of HDAC6 absence in the accumulation of autophagy marker p62
   - 1.7. Mechanism by which HDAC6 regulates autophagy of *Lm*

2. **Study of the role of HDAC6 in the activation of dendritic cell functions by bacterial infection and stimulation of TLRs**
   - 2.1. Determination of pro-inflammatory gene expression
   - 2.2. Effect of HDAC6 in pro-inflammatory cytokine secretion after *Lm* infection
   - 2.3. Influence of HDAC6 in the microbicidal activity of iNOS
   - 2.4. Study of the expression of MHC co-stimulatory molecules on the membrane
   - 2.5. Function of HDAC6 in the activation of MAPK- and mTOR-signalling pathways
   - 2.6. Pro-inflammatory cytokine secretion after stimulation with TLR agonists
   - 2.7. Consequence of HDAC6 defect in the activation of TLR-signalling pathway
   - 2.8. Evaluation of the HDAC6 role in the *in vivo* TLR-dependent inflammatory response

Materials and Methods

3. MATERIALS AND METHODS

1. Ethical Statement

1.1. Mice procedures

Mice were housed under specific pathogen-free conditions at the Centro Nacional de Investigaciones Cardiovasculares Carlos III (CNIC), and experiments were approved by the CNIC Ethical Committee for Animal Welfare and by the Spanish Ministry of Agriculture, Food, and the Environment. Animal care and animal procedures license were reviewed and approved by the local Ethics Committee for Basic research at the CNIC Ethical Committee for Animal Welfare and the Órgano Encargado del Bienestar Animal (OEBA) del Gabinete Veterinario de la Universidad Autónoma de Madrid (UAM). This committee approved the document with an associated identification number PROEX 158/15 (CNIC 04/15).

1.2. Human samples

Buffy coats of healthy donors were received from the Blood Transfusion Center of Comunidad de Madrid, and all donors signed their consent for the use of samples for research purposes. All the procedures using primary human cells were approved by the Ethics Committee of the Hospital Universitario de la Princesa (HUP).

2. Mice

Hdac6$^{-/-}$ mice were generated through targeting of exons from 10 to 13 by inserting a neomycin (Neo) and zeocin (Zeo) cassette, resulting in the disruption of the first catalytic domain of HDAC6 [70]. These mice were intercrossed on a C57BL/6 background to generate sex and age matched wild-type (*wt*) and knockout (KO). Mice used in this work were generously donated by Dr. Tso-Pang Yao (Department of Pharmacology and Cancer Biology, Duke University, Durham, North Carolina, USA) in a mixed background Sv129-C57BL/6. After that, mice were inter-crossed on a C57BL/6 background 8 times more to ensure a purer C57BL/6 background. F8 inter-crossed on C57BL/6 background ensures over 90% of the latter background.

3. Genotyping of mice

In order to genotype these mice and check the homozygosity of the deletion of the first catalytic domain of HDAC6, a PCR was performance with the two pairs of primers of the **Table 3.1**.

Table 3.1. Genotyping primers. Table of primers used to genotype mice disclosed by gene name, sequence 5´-3´ and size of the amplification product. (bp: base pair).

Gene	Sequence (5´-3´)	Amplification product
Int-9	CTGGTTCGTCTGAAG	350 bp
Exo-10	GTGGACCAGTTAGAAGCC	
Zeo-1	CCATGACCGAGATCGGCGAGC	250 bp
Zeo-3	CGTGAATTCCGATCATATTCAAT	

The pair of primers Int-9/Exo-10 amplifies the *wt* allele (350 bp), whereas the pair of primers Zeo-1/Zeo-3 amplifies the knockout allele (250 bp). These two pairs of primers were employed in PCR reactions using the genomic DNA from mouse tails as template DNA. Genomic DNA was obtained from mouse tails using the protocol of the reactive REDExtractc-N-Amp tissue PCR kit (Sigma). As controls, genomic DNA from *wt*, heterozygous and homozygous mice were used. The amplification protocol is showed in the **Table 3.2**.

Table 3.2. PCR amplification protocol. Table of PCR cycles for genotyping mice disclosed by phase, temperature, time and number of cycles.

Phase	Temperature (°C)	Time (min, s)	Cycles
1	95	3 min	1x
2	95	30 s	30x
	55	30 s	
	72	1 min	
3	72	10 min	1x

4. Bacteria strains

4.1. *Listeria monocytogenes* strains

We used the *Listeria monocytogenes* EGD (BUG 600) strain, provided by Dr. Esteban Veiga (Centro Nacional de Biotecnología, CNB, Madrid). Red Fluorecent Protein-expressing *Listeria monocytogenes* (RFP-*Lm*) was provided by Dr Carlos Ardavín´s laboratory (Centro Nacional de Biotecnología, CNB, Madrid). BUG600 strain was grown in Brain Herat Infusion (BHI) broth.

4.2. *Salmonella enterica* strain

Salmonella enterica serovar Thyphimurium strain SL1344 was provided by Dr. J. Garaude (Centro Nacional de Investigaciones Cardiovasculares, CNIC, Madrid). SL1344 strain was grown in Luria-Bertani (LB) broth supplemented with 50 µg/ml streptomycin (Sigma).

4.3. *Staphylococcus aureus* strain

Staphylococcus aureus 132 (*S. aureus*) was purchased from Invitrogen. *S. aureus* strain was grown in BHI broth.

4.4. *Escherichia coli* K12 strain

Escherichia coli K12 strain DH5α (*E. coli*) was purchased from Invitrogen. DH5α strain was grown in LB broth supplemented with 50 µg/ml streptomycin (Sigma).

For phagocytosis experiments, *Lm* and S. aureus were grown overnight in BHI broth and *E. coli* and *S.* Thyphimurium in LB broth with shaking, diluted 1/50, and grown until log-phase (optical density 0.8-1.2 at 600 nm) without shaking. Bacteria were washed with phosphate-buffered saline (PBS) to remove LB and BHI salts before addition to cells.

5. Cell culture

5.1. HEK293T cell line

The HEK293T cell line came from human embryonic kidney transformed with the large T antigen of SV40. The HEK293T cell line (ATCC) was cultured in Dulbecco´s Modified Eagle medium (MEM) (Sigma) containing 10% FBS (Invitrogen), 2 mM L-glutamine, 100 mg/ml penicillin and 100 mg/ml streptomycin.

5.2. HEK Blue hTLR2 cell line

HEK Blue hTLR2 cell line (Invivogen), the HEK293 cell line expressing human TLR2, CD14 and NF-κB-SEAP (secreted embryonic alkaline phosphatase) reporter gene was cultured in DMEM medium (Sigma) containing 10% FBS (Invitrogen), 2 mM L-glutamine, 100 µg/ml Normocin (Invivogen) and 1X HEK-Blue Selection (Invitrogen).

6. Generation of Bone Marrow-Derived Dendritic Cells (GM-CSF) and Macrophages (M-CSF)

Mouse primary bone marrow-derived dendritic cells (BMDCs) and macrophages (BMDMs) were obtained from bone marrow cell suspensions after culture on non-treated 150-mm Petri dishes in complete Roswell Park memorail institute-1640 medium (RPMI 1640) supplemented with 10% FBS, 2 mM L-glutamine, 100 mg/ml penicillin, 100 mg/ml streptomycin, 50 mM 2-ME, and 20 ng/ml granulocyte-macrophage colony-stimulating factor (GM-CSF, PeproTech, London, U.K.) for BMDCs and macrophage colony-stimulating factor (30% mycoplasma-free L929 cell supernatant, NCBI Biosample accession number SAMN00155972) for BMDMs. BMDCs were collected at day 9 and BMDCs were characterized as $CD11c^{+}MHC\text{-}II^{+}Gr\text{-}1^{-}$ cells by flow cytometry. BMDMs were collected at day 6 and BMDMs were characterized as $CD11b^{+}F4/80^{+}$ or $CD11b^{+}CD64^{+}$ cells.

7. Generation of Bone Marrow-Derived Dendritic Cells (FLT3L)

Bone marrow cell suspensions were culture on treated 6 well plates in complete RPMI 1640 supplemented with 10% FBS, 2 mM L-glutamine, 100 mg/ml penicillin, 100 mg/ml streptomycin, 50 mM 2-ME, and 150 ng/ml Fms-related tyrosine kinase 3 ligand dendritic cells (FLT3L, PeproTech, London, U.K.). After 9-11 days of differentiation cells were collected to be characterized by flow cytometry as $CD11c^{+}B220^{-}CD11b^{+}CD24^{-}$ (60% of the culture) and $CD11c^{+}B220^{-}CD11b^{+}CD24^{+}$(40%).

8. Obtainment of Thioglycollate-Elicited Macrophages (TEMs)

Mice received peritoneal injections with 1ml 4% thioglycollate (TG). The peritoneal exudate was collected after 4 days and cultured in complete RPMI 1640 supplemented with 10% FBS, 2 mM L-glutamine, 100 mg/ml penicillin, 100 mg/ml streptomycin, and 50 mM 2-ME. To enrich the culture for macrophages, non-adherent cells were eliminated after a few hours by washing five times with warm PBS and gentle swirling. These cells expressed CD64 macrophage marker in more than 90% after this enrichment.

9. Obtainment of human monocyte-derived Dendritic Cells (moDCs)

Peripheral blood mononuclear cells (PBMCs) from Buffy coats of healthy donors were isolated using Biocoll separating solution (Millipore) by centrifugation at 700 g 30 min at RT. Monocytes were purified from peripheral blood mononuclear cells (PBMCs) by an adhesion step at 37°C in incomplete RPMI 1640 medium during 1 h. Non-adherent cells were removed and adherent monocytes were washed three times with warm 1x PBS to remove residual PBMCs. Monocytes were cultured in complete RPMI 1640 supplemented with 10% FBS, 2 mM L-glutamine, 100 mg/ml penicillin, 100 mg/ml streptomycin, 500 U/ml IL-4 (R&D) and 500 U/ml GM-CSF (Immunotools) for 6 days. Fresh medium and cytokines were added every 48 h to differentiate monocytes to immature human dendritic cells. Cells were characterized by flow cytometry as $HLA\text{-}DR^{+}CD3^{-}DC\text{-}SIGN^{+}CD14^{-}CD11c^{+}$. Activation of dendritic cells was induced with Pam2GSK4, Pam3GSK4 and HKLM for 30 min (Invivogen).

10. *In vitro Lm*-infection of BMDCs, BMDMs and TEMs

Cells were incubated with *Lm* and assessed for survival to gentamicin exposure [247]. Detailed, cells were infected with *Lm* at a multiplicity of infection (MOI) of 10 for 30 min at 37°C and 5% CO_2. *Lm* is a facultative pathogen able to growth in culture medium. To prevent extracellular replication, the aminoglycoside antibiotic gentamicin was added to the medium after bacterial internalization. This antibiotic is bactericidal for extracellular bacteria at high concentrations and does not have any significant effect in intracellular ones during the first 8 hpi [247]. Hence, to determine the number of bacteria entering the cells, extracellular bacteria were killed by treatment with 100 µg/ml gentamicin

(Sigma-Aldrich, St. Louis, MO) for an additional 30 min at 37°C. Then, infected cells were washed with PBS three times and lysed with 0.05% Triton X-100 (Sigma-Aldrich, St. Louis, MO) in distilled water. Serial dilutions were seeded on brain-heart infusion (BHI) agar plates and colony-forming units (CFUs) were counted after 36-48 h. Quantification method of intracellular live bacteria is represented in the the following scheme (**Figure 3.1**).

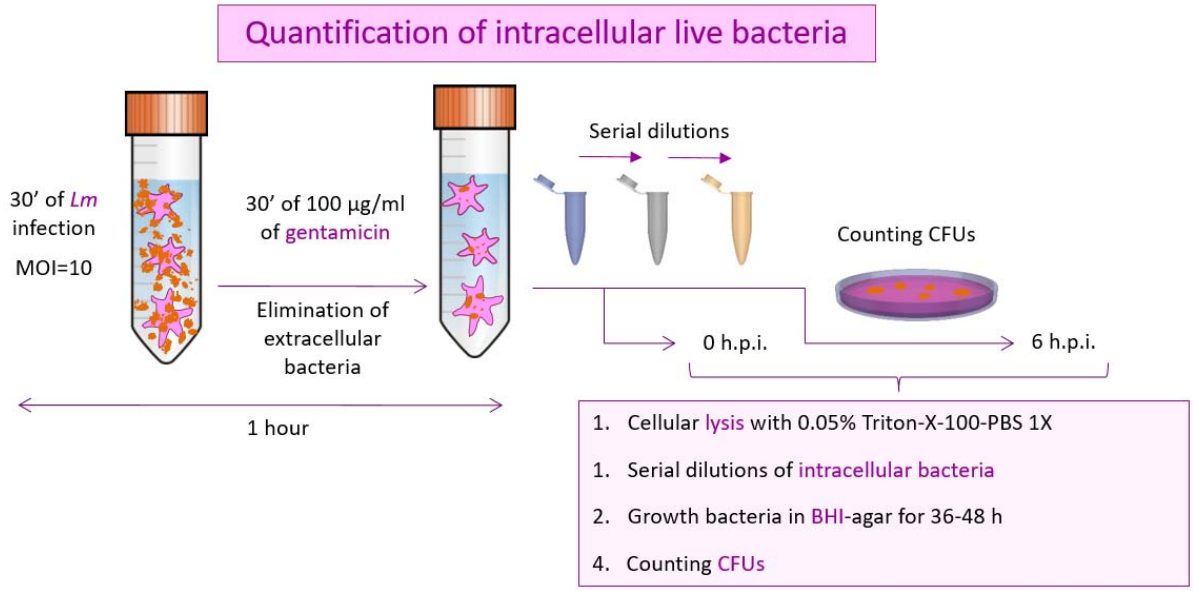

Figure 3.1. Quantification of intracellular live bacteria in myeloid cells. Myeloid cells are infected with *Lm* using a MOI of 10 during 30 min, followed by the addition of gentamicin during other 30 min. Cells are washed with PBS to eliminate the antibiotic and lysed with detergent at diferent experimental points (e.g. 0 and 6 hpi). Serial dilutions and not diluited sample are grown in BHI-agar plates for 36-38 h. At this time colony-foming units (CFUs) can be counted.

11. *In vivo Lm* systemic infections

Hdac6$^{+/+}$ and *Hdac6*$^{-/-}$ mice were intravenously injected with *Listeria monocytogenes* EGD (125,000 CFUs/mouse resuspended in 200 µl of PBS 1x) using a 29-gauge needle. For survival experiments mice were monitored twice a day in order to detect casualties during 15 days of infection.

After 12, 24, 48 and 72 hpi, mice were perfused with 1X PBS to clean blood from organs and spleens and livers were weighted. To determine bacterial load, spleens and livers were digested with 0.1 mg/ml type IV collagenase and 0.5 mg/ml DNAse I (Roche, Mannheim, Germany) for 30 min at 37°C. After digestion, organs were homogenized in 70 µm filters and red blood cells were lysed with ammonium chloride potassium lysis buffer (ACK, Sigma). Splenic cell suspensions were resuspended in PBS and cells were counted. Serial dilutions were grown on BHI agar plates. CFUs were counted after 36-48 h of incubation at 37°C. CFUs were calculated by cell number and by gram per organ. The model of quantification of intracelular bacteria in mouse target organs is illustrated in **Figure 3.2**.

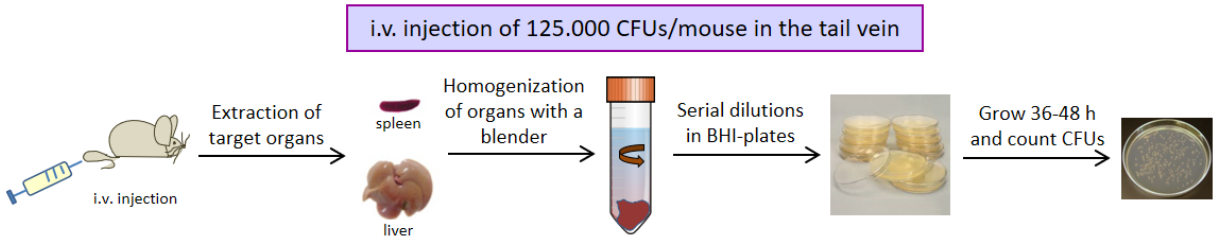

Figure 3.2. Quantification of intracellular live bacteria in mouse target organs. Mice are infected with *Lm* by intravenous injection of 125.000 CFUs/mouse. Organs are extracted and homogenizated using enzymatic digestion in combination with mechanical force on 70 µm with the piston of a siringe. Cell suspensions are lysed with detergent and serial dilutions are perfomed. Serial dilutions and not diluited sample are grown in BHI-agar plates for 36-38 hours. At this time Colony-foming units (CFUs) can be counted.

12. Antibodies and reagents

Rapamycin, bafilomycin A1, 3-MA, cloroquine, NH_4Cl, 1400W and DPI were from Sigma-Aldrich and are illustrated in **Table 3.3**.

Table 3.3. Table of Autophagy inhibitors. Table of inhibitors used in experimental procedures. Concentration and function of experimental use are indicated.

Inhibitors	Concentraiton	Function
1400W dihydrochloride	10 µM	Specific inhibitor of inducible nitic oxide synthase (iNOS)
3-methyladenine (3-MA)	0,5 mM	Inhibitor of the formation of phagosome by inhibition of classs III phosphatidylinositol-3 phosphate (PI3P)
Bafilomycin A1	20 nM	Inhibits vacuolar H+ATPase dampening the fusion of autophagosome with lysosome
Cloroquine diphosphate	50 µM	Cystein proteases inhibitor which impairs acidification of lysosome and late endosomes
Diphenyleneiodonium chloride (DPI)	5 µM	Inhibitor of the NADPH oxidase
NH_4Cl	50 mM	Inhibit the acidification of lysosome and late endosomes
Rapamycin	4 µM	Inhibitor of mTOR. Increase autophagy flux

Poly-L-lysine (PLL) was purchased from Sigma. Phalloidin-Alexa488 and 647 were from BD Biosciences. Zenon Alexa Fluor 488 rabbit IgG labelling kit, DAPI and Prolong Gold anti-fade mounting medium were from Thermofisher Scientific. Anti-human CD3 antibody (T3b hybridoma) was grown in Dr. F. Sánchez-Madrid laboratory (Hospital Universitario de la Princesa, HUP, Madrid) [158].

TLR agonists used for the activation of DCs are listed in **Table 3.4**, indicating their specific TLR activation, the used concentration and the brand.

Table 3.4. TLR agonists. Table of TLR agonists used in experimental procedures disclosed by target TLR, concentration and brand.

Agonist	TLR activation	Concetration	Brand
Lm	various	MOI=10	EGD strain
Heat killed *Lm* (HKLM)	various	MOI=50	InvivoGen
Heat killed *S.* Thyphimurium (HKST)	various	MOI=50	InvivoGen
Palmitoyl-2-cysteine-serine-(lysine)-4 (Pam2GSK4)	TLR-2/6	10 µg/ml	InvivoGen
Palmitoyl-3-cysteine-serine-(lysine)-4 (Pam3GSK4)	TLR-1/2	10 µg/ml	InvivoGen
Polyinosinic-polycytidylic acid (Poly(I:C)) HMW	TLR-3	20 µg/ml	InvivoGen
Lipopolysaccharide (LPS)	TLR-4	1 mg/ml	Sigma-Aldrich
Flagellin	TLR-5	100 µg/ml	InvivoGen
Imiquimod	TLR-7	1 mg/ml	InvivoGen

13. Gene overexpression and silencing

HEK293 cells were co-transfected with plasmids encoding human MyD88 fused to the influenza hemmagglutinin (HA)-tag (Addgene plasmid #12287) together with plasmids encoding *HDAC6-WT* or double mutant deacetylase domain DD (mutated human HDAC6-H216A/H611A) fused to the enhanced Green Fluorescent protein (eGFP) tag (*HDAC6-WT* and *HDAC6-DD* previously described [220]). When indicated, cells were co-transfected with the appropriate small harping RNA plasmid pLVX-IRES-ZsGreen1, where *shHDAC6*-2049 (TRCN0000004842) was cloned between BamH1 and EcoR1 sites. Cells were transfected using Lipofectamine 2000 (Invitrogen). Experiments were performed 24 h after transfection.

14. RNA isolation

RNA from mouse GM-CSF- derived DCs was isolated with the QIAGEN RNeasy Kit (Qiagen). Residual DNA contamination was removed with the Turbo DNA-free Kit (Ambion). RNA purity and concentration was analysed in a Nanodrop-1000 Spectrophotometer /Thermo Scientific). RNA integrity was assessed by etidium bromide labelling on a 1.5% agarose gel.

15. Reverse transcription and quantitative real-time-PCR

Total RNA (1-2 µg) was reverse transcribed to cDNA with a Reverse Trancription Kit (Applied Biosystems). Quantitative PCR was then performed in an AB7900-384 thermocycler (Applied Biosystem) using SYBR Green master mix (Applied Biosystems, Warrington, UK) as the reporter. PCR reactions were performed by triplicate in 10 µl volumes in 384-well plates. Expression levels of target genes were normalized to the expression of housekeeping genes β-actin, glyceraldehyde-3-phosphate dehydrogenase (GAPDH), β2-microglobulin and Ywhaz (tyrosine 3-monooxygenase/tryptophan 5-monooxygenase activation protein, ζ) for presentation of relative mRNA levels. Data were analysed with Biogazelle qBasePlus version 2.3 (Biogazelle) and graphs are represented as a normalized expression scaled to average of all samples. Gene-specific primers used are listed in **Table 3.5.**

Table 3.5. qPCR primers. Table of qPCR primers used in experimental procedures disclosed by gene name and sequence 5´-3´.(Fw: Forward, Rv: Reverse).

Gene	Sequence (5´-3´)	
Atg12	**Fw:** AACAAAGAAATGGGCTGTGGAGCG	**Rv**: TTCCGAGGCCACCAGTTTAAGGAA
Atg2	**Fw:** CCACCTCTGCAAATCGGCA	**Rv:** CCAGTTGTCCTGATACCTCCA
Atg5	**Fw:** GACAAAGATGTGCTTCGAGATGTG	**Rv:** GTAGCTCAGATGCTCGCTCAG
Atg7	**Fw:** ATGCCAGGACACCCTGTGAACTTC	**Rv:** ACATCATTGCAGAAGTAGCAGCCA
Beclin-1	**Fw:** GGCCAATAAGATGGGTCTGA	**Rv:** CACTGCCTCCAGTGTCTTCA
CXCL10	**Fw:** CCAAGTGCTGCCGTCATTTTC	**Rv:** TCCCTATGGCCCTCATTCTCA
CXCL5	**Fw:** TGCGTTGTGTTTGCTTAACCG	**Rv:** CTTCCACCGTAGGGCACTG
CXCR1	**Fw:** TCTGGACTAATCCTGAGGGTG	**Rv:** GCCTGTTGGTTATTGGAACTCTC
GAPDH	**Fw:** AGCTTGTCATCAACGGGAAG	**Rv:** TTTGATGTTAGTGGGGTCTCG
HDAC1	**Fw:** CAGTCATGTCCAAAGTAAT	**Rv:** GTCCTTTGATGGTCAGATTG
HDAC10	**Fw:** ACAGCCACTCGACTGCTCT	**Rv:** GATGCCTCACAAGCTGACAAA
HDAC11	**Fw:** GTGTACTCACCACGTTACAACA	**Rv:** GCTCGTTGAGATAGCGCCTC
HDAC2	**Fw:** TGAAATTCCCAATGAGTTGC	**Rv:** GTTCTGGTTTGTCATGTTTG
HDAC3	**Fw:** GTGACATGTATGAAGTTGGAG	**Rv:** AAAAGGTGCTTGTAACTCTG
HDAC4	**Fw:** CTACTGGTATGGGAAGACAC	**Rv:** TTTCCTAAGAGGGAAGTCA
HDAC5	**Fw:** AAGACCTAGAAGAGGAGGAG	**Rv:** GCGAACAACTTTTTGTAACC
HDAC6	**Fw:** TCCACCGGCCAAGATTCTTC	**Rv:** CAGCACACTTCTTTCCACCAC
HDAC6b	**Fw:** TCGCTGTCTCATCCTACCTGCT	**Rv:** GTCAAAGTTGGCACCTTCACGG
HDAC6-Ex12	**Fw:** CTGGCTAAGGGAGTCAGTGC	**Rv:** TAGCACGGCTTCTTCCACTT
HDAC7	**Fw:** GAACTCTTGAGCCCTTGGACA	**Rv:** GGTGTGCTGCTACTACTGGG
HDAC8	**Fw:** ACTATTGCCGGAGATCCAATGT	**Rv:** CCTCCTAAAATCAGAGTTGCCAG
HDAC9	**Fw:** GCGGTCCAGGTTAAAACAGAA	**Rv:** GCCACCTCAAACACTCGCTT
IFIT3	**Fw:** GTGGACTGAGATTTCTGAACTGC	**Rv:** CAGAGATTCCCGGTTGACCT
IFN-β	**Fw:** TCAGAATGAGTGGTGGTTGC	**Rv:** GACCTTTCAAATGCAGTAGATTCA
IL12p40	**Fw:** GGAAGCACGGCAGCAGAAT	**Rv:** AACTTGAGGGAGAAGTAGGAATGG
IL-1β	**Fw:** GCAACTGTTCCTGAACTCAACT	**Rv:** ATCTTTTGGGGTCCGTCAACT
ISG15	**Fw:** GGTGTCCGTGACTAACTCCAT	**Rv:** TGGAAAGGGTAAGACCGTCCT
LAMP-1	**Fw:** AGCATACCGGTGTGTCAGTG	**Rv:** GTTGGGGAAGGTCCATCCTG
LAMP-2a	**Fw:** TGGCTAATGGCTCAGCTTTC	**Rv:** ATGGGCACAAGGAAGTTGTC
LC3A	**Fw:** TTGGTCAAGATCATCCGGC	**Rv:** GCTCACCATGCTGTGCTGG
LC3B	**Fw:** CCCACCAAGATCCCAGTGAT	**Rv:** CCAGGAACTTGGTCTTGTCCA
Mx1	**Fw:** GACCATAGGGGTCTTGACCAA	**Rv:** AGACTTGCTCTTTCTGAAAAGCC
p62	**Fw:** ATGTGGAACATGGAGGGAAGA	**Rv:** GGAGTTCACCTGTAGATGGGT
PanIFN-α	**Fw:** CCTGAGARAGAAGAAACACAGCC	**Rv:** GGCTCTCCAGAYTTCTGCTCT
Sirtuin-1	**Fw:** ATGACGCTGTGGCAGATTGTT	**Rv:** CCGCAAGGCGAGCATAGAT
Sirtuin-2	**Fw:** ATCGTGTTTTTCGGTGAGAACC	**Rv:** TTCCTTGTTAATGAGCAGCCG
Sirtuin-3	**Fw:** CTTCCGCTAAACTTCTCCCG	**Rv:** ACAGAGGGATATGGGCCTTCT
Sirtuin-4	**Fw:** TCTGACGATTTGGCTTGCCT	**Rv:** TTCAGAGTTGGAGCGGCATT
Sirtuin-5	**Fw:** CTCCGGGCCGATTCATTTCC	**Rv:** GCGTTCGCAAAACACTTCCG
Sirtuin-6	**Fw:** ATGTCGGTGAATTATGCAGCA	**Rv:** GCTGGAGGACTGCCACATTA
Sirtuin-7	**Fw:** AGCATCACCCGTTTGCATGA	**Rv:** GGCAGTACGCTCAGTCACAT
TLR-1	**Fw:** TGAGGGTCCTGATAATGTCCTAC	**Rv:** AGAGGTCCAAATGCTTGAGGC
TLR-2	**Fw:** GCAAACGCTGTTCTGCTCAG	**Rv:** AGGCGTCTCCCTCTATTGTATT
TLR-6	**Fw**: TGAGCCAAGACAGAAAACCCA	**Rv:** GGGACATGAGTAAGGTTCCTGTT
TNF-α	**Fw:** CCCTTCCTCCGATGGCTAC	**Rv:** CGCCTCCTTCTTGTTCTGG
Ywhaz	**Fw:** CGTTGTAGGAGCCCGTAGGTCAT	**Rv:** TCTGGTTGCGAAGCATTGGG
β2-M	**Fw:** TTCTGGTGCTTGTCTCACTGA	**Rv:** CAGTATGTTCGGCTTCCCATTC
β-actin	**Fw:** CAGAAGGAGATTACTGCTCTGGCT	**Rv:** TACTCCTGCTTGCTGATCCACATC

Primers HDAC6-Ex12 were designed to amplify the exon 12 of *Hdac6* gene and were included in experiments as a control to check *Hdac6*$^{-/-}$ mice (deletion of the fragment corresponding to exons 10-13). Amplification after cycle 30-35 was observed in *Hdac6*$^{-/-}$ DCs, indicating the absence of exon 12. HDAC6 and HDAC6b primer pairs were designed to amplify exons before 10-13 fragment, so they were used as positive controls of amplification in *Hdac6*$^{+/+}$ and *Hdac6*$^{-/-}$ GM-CSF DCs.

16. Soluble embryonic alkaline phosphatase (SEAP)-NF-κB detection

Transfected HEK-Blue hTLR2 cells (50.000 per well) with different HDAC6 constructions were placed in bottom p96 well plates resuspended in HEK-Blue Detection medium (Invivogen) without stimulus (negative control) and with TLR-2 agonists (HKLM stimulus, MOI=10). After 8-12 h of incubation, SEAP activity was measured by optical density at 620 nm with a microplate reader. To calculate the NF-κB induction, the signal obtained from each mutant condition without stimuli (background) was depleted of the signal of each condition of activation with Pam2GSK4, Pam3GSK4 or HKLM.

17. ELISAs and nitrite measurement

Cytokine and Nitric Oxide (NO) production was analysed in the supernatants of BMDC cultures at 6, 12 and 24 h after stimulation with *Lm*, heat-killed *Listeria monocytogenes* (HKLM), heat-killed *Salmonella* Typhimurium (HKST), Pam3CSK4, Flagellin, Imiquimod, polyinosinic-polycytidylic acid (Poly(I:C)) (InvivoGen, San Diego, CA), or LPS from *Escherichia coli* (Sigma-Aldrich). TNF-α and IL12p70 were analysed with OptEIA Enzyme-Linked Immunosorbent Assay (ELISA) kits (BD Biosciences, San Diego, CA), IL-1β and IL-6 with the mouse ELISA Ready-SET-Go! kit from eBioscience (Affymetrix, San Diego, CA) and Interferon-β was measured with Legend max mouse IFN-β ELISA kit (Biolegend). The detection was based on colorimetric quantification of absorbance at 450 nm, corrected with subtraction at 570 nm measured in a microplate reader (Bio-Rad Model 550). Nitric oxide (NO) was estimated from the nitrite concentration measured with a Griess reagent kit at 548 nm (Molecular Probes/Life Technologies, Thermo Fisher Scientific). Results were expressed as the means of duplicate wells.

18. Immunoblotting

Total cell extracts from GM-CSF DCs stimulated with *Lm*, HKLM or the indicated TLR ligands for the indicated times were prepared in lysis buffer (0.5% Triton X100, 25 mM Tris-HCl pH 7.5, 0.5 mM EGTA, 0.5 mM EDTA, 25 mM NaF, 0.5 sodium glycerol-phosphate, 2.5 mM pyrophosphate, 0.135 M sacarose) with a cocktail of protease and phosphatase inhibitors (Roche). Cell lysates were cleared of nuclei by centrifugation at 15,000 g for 15 min. Protein extracts were quantified using Bio-Rad Protein Assay Dye Reagent Concentrate (Bio-Rad) and sample buffer Laemmli were added to protein lysates.

Protein extracts were separated by 8-15% SDS-PAGE using acrylamide/bisacrylamide 29:1 reactive (Biorad) following the Laemmli method with Tris-glycine buffer. Proteins were transferred to a PVDF membrane (Biorad) or 0.45 µm pore-size nitrocellulose membranes (Biorad). Membranes were blocked with TBS-Tween20 5% BSA. Proteins were visualized with LAS-3000 using Luminata Forte and Luminata Crescendo Western horseradich peroxidase (HRP) substrate (Millipore) after membrane incubation with specific antibodies (**Table 3.6**) and peroxidase-conjugated secondary antibodies (using 5 µg ml^{-1} approximately) (**Table 3.7**). Band intensities were quantified using Image Gauge software (Fuji Photo Film, Co., Ltd) and results are expressed relative to loading controls. For quantification of western-blots, phosphorylated/total ratios were divided by loading control signal. Non-infection (NI) time was considered as 100%, and following times were relativized to it.

Table 3.6. Primary antibodies for WB. Table of antibodies used in WB experimental procedures disclosed by reference, brand, host and dilution (WB: Western blot).

Primary Antibodies	Reference	Brand	Host	Dilution
AKT	#9272	Cell Signaling	rabbit	WB (1:1000)
ERK1/2	#9102	Cell Signaling	mouse	WB (1:1000)
HDAC6	C0226	Assay bioTech	rabbit	WB (1:500)
iNOS	# 2982S	Cell Signaling	rabbit	WB (1:500)
LC3b	# 2775S	Cell Signaling	rabbit	WB (1:500)
MyD88	D80F5 #4283	Cell Signaling	rabbit	WB (1:500)
MyD88	sc-11356 (HFL-296)	Santa Cruz	rabbit	WB (1:500)
MyD88	sc-136970 (B-1)	Santa Cruz	mouse	WB (1:500)
MyD88	MA5-15762 (2E9C2)	TermoFisher Scientific	mouse	WB (1:500)
p62	P0067	Sigma-Aldrich	rabbit	WB (1:1000)
p70S6K	#2703	Cell Signaling	rabbit	WB (1:1000)
phAKT (Ser473)	#9271	Cell Signaling	rabbit	WB (1:1000)
phERK1/2 (Thr202/Thr204)	#9101	Cell Signaling	rabbit	WB (1:1000)
php70S6K	#9205	Cell Signaling	rabbit	WB (1:1000)
phS6 (Ser235/236)	#2211	Cell Signaling	rabbit	WB (1:1000)
S6	#2717	Cell Signaling	rabbit	WB (1:1000)
tubulin	T9026 (DH1A)	Sigma-Aldrich	mouse	WB (1:2000)
β-actin	A2228 (AC-74)	Sigma-Aldrich	mouse	WB (1:2000)

Table 3.7. Secondary antibodies for WB. Table of antibodies used in WB experimental procedures disclosed by reference, brand, host and dilution (WB: Western blot).

Secondary Antibodies	Reference	Brand	Host	Dilution
Goat anti-mouse-HRP	#31430	Thermofisher Scientific	goat	WB (1:5000)
Goat anti-rabbit-HRP	#31460	Thermofisher Scientific	goat	WB (1:5000)

Membrane strippings were performed using BlotFresh Western Blot Stripping reagent (SigmaGen Laboratories), followed by several Tris-buffered saline (TBS)-Tween 1% washes and TBS-Bovine serum albumin (BSA) 5% blockade previously to other primary antibody incubation.

19. Immunoprecipitation of MyD88 and HDAC6 proteins

19.1. From human monocyte-derived dendritic cells (moDCs)

Human moDCs (1×10^7 per condition) were lysed (10 mM Tris pH 7.4, 150 mM NaCl, 5% glycerol, 1mM EDTA, 1mM $MgCl_2$, 1mM $CaCl_2$, 1% CHAPS (Sigma) and protease and phosphatase inhibitors (Roche)) for 1 h at 4°C. Lysates were incubated for pre-clearing with pre-washed Protein G Dynabeads (Invitrogen; 50 µl per condition; 2 h, 4 °C). Pre-cleared lysates were incubated with 6 µg rabbit anti-MyD88 antibody (Cell Signaling) or 6 µg rabbit anti-HDAC6 antibody (Assay BioTech) per condition O/N at 4 °C. Similar µg of control isotype antibody for rabbit were used. Fifty microlitres of Dynabeads per condition were washed three times in wash buffer (10 mM Tris pH 7.4, 150 mM NaCl, 5% glycerol, 1mM EDTA, 1mM $MgCl_2$, 1mM $CaCl_2$, 0.1% CHAPS) and added to antibody-conjugated lysates for 2 h 4C. Antibody-conjugated Dynabeads were washed six times with wash buffer and transferred to clean tubes.

19.2. From HEK cell lines

HEK293T cells or HEK-Blue hTLR2 (1×10^7 per condition) were lysed (25 mM Tris pH 8, 150 mM NaCl, 0.5% NP-40 and protease and phosphatase inhibitors) and incubated for pre-clearing with pre-washed Protein G Dynabeads (Invitrogen; 50 µl per condition; 3 h, 4 °C). Fifty µg of Dynabeads per condition were washed three times in wash buffer (25 mM Tris pH 8, 150 mM NaCl, 0.05% NP-40) and re-suspended in 600 µl of wash buffer containing 1-2 µg mouse anti-HA antibody (Roche) per condition and incubated 3 h at 4 °C. Similar µg of control isotype antibody for mouse were used. Pre-cleared lysates were incubated with antibody-conjugated Dynabeads (O/N, 4 °C). Antibody-conjugated Dynabeads were washed six times with lysis buffer and transferred to clean tubes. Then, were washed twice with wash buffer. Protein loading buffer was added, samples were boiled at 95 °C for 5 min and processed for immunoblotting.

Antibodies used for IP approach are listed in **Table 3.8** indicating the reference, brand, host and concentration of use.

Table 3.8. Primary antibodies for IP. Table of antibodies used in IP experimental procedures disclosed by reference, brand, host and dilution (IP: Immunoprecipitation).

Primary Antibodies	Reference	Brand	Host	Dilution
Anti-HA	000000011583816001 (12CA5)	Roche (Sigma-Aldrich)	mouse	IP (5 µg/point)
Anti-HA	A190-108A	Bethyl	rabbit	IP (5 µg/point)
Control isotype of mouse	sc-2025	Santa Cruz	rat	IP (1-5 µg/point)
Control isotype of rabbit	sc-2027	Santa Cruz	rabbit	IP (5 µg/point)

20. Flow cytometry

Cells were stained in ice-cold PBS containing FBS (0.5%) and EDTA (5 mM) using appropriate antibody-fluorophore conjugates. Multiparameter analysis was performed on a FACSCANTO II flow cytometer (BD Biosciences) and analysed with FlowJo software (Tree Star). Prior to fixing, cells were resuspended in PBS/0.5% BSA/5 mM EDTA solution containing yellow fluorescent reactive dye to exclude dead cells (Life Technologies). For intracellular staining, cells were fixed and permeabilized using the CytoFix/Cytoperm kit (BD). Human cells were blocked with human gamma-globulin from human blood (Sigma), whereas mouse cells were blocked using Fc-Block (CD16/32) (Tombo biociencies). Complete primary and secondary antibody used for FC are listed in **Table 3.9** and **Table 3.10**.

Table 3.9. Primary antibodies for FC. Table of antibodies used in FC experimental procedures disclosed by reference, brand, host and dilution (FC: Flow cytometry).

Primary Antibodies	Reference	Brand	Host	Dilution
B220-PerCP-cyanine5.5	65-0452-U100 (RA 3-6B2)	Tombo biociences	rat	FC (1:200)
CD11b-FITC	553310 (M1/70)	BD Pharmingen	rat	FC (1:200)
CD11c-PE	557401 (HL3)	BD Pharmingen	hamster	FC (1:200)
CD11c-PE	555392 (B-ly6)	BD biociences	mouse	FC (1:200)
CD11c-PeCy7	558079 (HL3)	BD Pharmingen	hamster	FC (1:200)
CD11c-PeCy7	55079	BD Pharmingen	hamster	FC (1:200)
CD14-FITC	14F-100T (47-3D6)	Immunostep	mouse	FC (1:200)
CD16/32 Fc-block	(clone 2.4G)	BD Pharmingen	rat	FC (1:200)
CD19-VioletFluor450	75-0193-U100 (1D3)	Tombo biociences	rat	FC (1:200)
CD24-PE	12-0241-82 (30-F1)	ebiocience	rat	FC (1:200)
CD3e	T3b hybridoma	[158]	mouse	FC (5 µg/ml)
CD3-VioletFluor450	75-0032-U100 (17A2)	Tombo biociences	rat	FC (1:200)
CD40-APC	558695	BD Pharmingen	rat	FC (1:200)
CD86-biotinylated	553690 (GL1)	BD Pharmingen	rat	FC (1:200)
CD8-APC	558079 (HL3)	BD Pharmingen	rat	FC (1:200)
DC-SIGN (CD209)	sc-59157 (MR-1)	Santa Cruz	mouse	FC (1:200)
DX5 (CD49b)-V450	561638	BD biociences	rat	FC (1:200)
Gr-1-APC	553129 (RB6-8C5)	BD Pharmingen	rat	FC (1:200)
HLA-DR-PerCP	560652 (G46-6)	BD biociences	mouse	FC (1:200)
Lm	0400-0030	AbDSerotec	rabbit	FC (1:200)
Ly6C-PerCP-Cy5.5	560525	Becton Dickinson	rat	FC (1:200)
Ly6G-PE	551461 (1A8)	BD biociences	rat	FC (1:200)
MHC-II I-A/I-E-APC	17-5321-81 (145/1/4.15.2)	ebiocience	rat	FC (1:200)
MHC-II I-A/I-E-FITC	553623 (2G9)	BD Pharmingen	rat	FC (1:500)
p62	P0067	Sigma-Aldrich	rabbit	FC (1:200)

Table 3.10. Secondary antibodies for FC. Table of antibodies used in FC experimental procedures disclosed by reference, brand, host and dilution (FC: Flow cytometry).

Secondary Antibodies	Reference	Brand	Host	Dilution
Chicken anti-mouse 647	A-21463	Life technologies	chicken	FC (1:500)
Chicken anti-rabbit 647	A-21443	Life technologies	chicken	FC (1:500)
Streptavidin-APC	554067	BD Pharmingen	-	FC (1:300)
Streptavidin-BV421	563259	BD biociences	-	FC (1:300)

21. Fluorescence confocal microscopy

For immunofluorescence assays, cells were plated onto slides coated with poly-L-lysine (50 µg ml^{-1}) and incubated for 1 h at 37ºC. Infection experiments were carried out at the indicated times. Cells were then fixed, blocked and stained with the indicated primary antibodies (5 µg ml^{-1}) (**Table 3.11**) followed by Alexa488- or Rhodamine Red X-labelled secondary antibodies highly cross-adsorbed (Hx)(5 µg ml^{-1}) (**Table 3.11** and **Table 3.10**).

Table 3.11. Primary antibodies for IF. Table of antibodies used in IF experimental procedures disclosed by reference, brand, host and dilution (IF: Immunofluorescence).

Primary Antibodies	Reference	Brand	Host	Dilution
Acetylated cortactin	09-881	Millipore	rabbit	IF (1:100)
p62	P0067	Sigma-Aldrich	rabbit	IF (1:200)
K63 polyUb chain	05-1308 (clone Apu3)	Merk-Millipore	rabbit	IF (1:100)

Table 3.12. Secondary antibodies for IF. Table of antibodies used in IF experimental procedures disclosed by reference, brand, host and dilution (IF: Immunofluorescence).

Secondary Antibodies	Reference	Brand	Host	Dilution
Goat anti-rabbit A488 Hx	A-11008	Thermofisher Scientific	goat	IF (1:500)
Goat anti-rabbit Rhodamin Red-X Hx	111-295-144	Jackson	goat	IF (1:500)

Samples were examined under a Leica SP5 confocal microscope (Leica) fitted with a 63X objective. Images were acquired with sequential xyz acquisition mode scans with laser ranges of 418-473 nm for DAPI, 502-548 nm for Alexa-488, 584-644 nm for Rhodamine Red-X and 737-779 nm for Alexa-647. Z-stacks of 2-5 µm were obtained using a maximum z-step size of 0.3 µm.

22. Imaris quantification

Images were processed and assembled using Image J 1.51p (Fiji). Confocal 3D images assembled with Imaris 7.7.2 (Bitplane) using the ImarisCell module. Every cell and its corresponding intracellular bacteria were calculated in each image. Surfaces corresponding to bacteria were used to calculate the maximal fluorescence intensity of the channels to co-localize with bacteria. Two-channel co-localization was quantified in at least 10 images per genotype, corresponding to 10 biological samples. Each image contains from 60 to 80 cells.

23. In-gel protein digestion

Proteins were in-gel digested using a previously described protocol [27]. Briefly, the coimmunoprecipitate was heated at 95 °C for 5 min, after which the magnetic beads were removed using a magnet. The resulting solution was added sample buffer and loaded in 0.5-cm-wide wells of an SDS-PAGE gel. The run was stopped as soon as the front entered into the resolving gel. The protein band was visualized by Coomassie Blue staining, excised, and digested overnight at 37 °C with 60 ng/µl

sequencing-grade modified trypsin (Promega) at 10:1 protein:enzyme (w/w) ratio in 50 mM ammonium bicarbonate, pH 8.8, containing 10% acetonitrile. The resulting tryptic peptides were desalted onto C18 OMIX tips (Agilent), dried down and kept at -80 °C until further use.

24. Mass spectrometry

The resulting peptides were analyzed by liquid chromatography coupled to tandem mass spectrometry (LC-MS/MS) on an Easy nLC-1000 nano-HPLC apparatus (Thermo Scientific, San Jose, CA, USA) coupled to a hybrid quadrupole-orbitrap mass spectrometer (Q Exactive HF, Thermo Scientific). The dried peptides were taken up in 0.1% (v/v) formic acid and then loaded onto a PepMap100 C18 LC pre-column (75 µm I.D., 2 cm, Thermo Scientific) and eluted on line onto an analytical NanoViper PepMap 100 C18 LC column (75 µm I.D., 50 cm, Thermo Scientific) with a continuous gradient consisting of 8-31% B in 240 min (B = 80% ACN, 0.1% formic acid) at 200 nL/min. Peptides were ionized using a Picotip emitter nanospray needle (New Objective). Each MS run consisted of enhanced FT-resolution spectra (120,000 resolution) in the 400–1,200 m/z range followed by data-dependent MS/MS spectra of the 20 most intense parent ions acquired along the chromatographic run. The AGC target value in the Orbitrap for the survey scan was set to 1,000,000. Fragmentation in the linear ion trap was performed at 30% normalized collision energy with a target value of 10,000 ions. The full target was set to 30,000, with 1 microscan and 50 ms injection time, and the dynamic exclusion was set to 0.5 min.

25. Peptide identification

For peptide identification the MS/MS spectra were searched with the Sequest algorithm implemented in Proteome Discoverer 1.4 (Thermo Scientific). Database searching against human protein sequences from the UniProt database (March 2017, 158,382 entries) was performed with the following parameters: trypsin digestion with 4 maximum missed cleavage sites; precursor and fragment mass tolerances of 800 ppm and 0.02 Da, respectively; Cys carbamidomethylation as static modifications; and Met oxidation and Lys acetylation as dynamic modifications. The results were analyzed using the probability ratio method [149] and a false discovery rate (FDR) for peptide identification was calculated based on the search results against a decoy database using the refined method [168].

26. Statistical analysis

Data were analysed with GraphPad prism software (La Jolla, CA) for normality (Kolmogorov-Smirnov test for small samples). Normal data were analysed by Student t-test, non-normal data by Mann-Whitney test, and grouped data by 2-tailed One-way ANOVA with a Bonferroni post-test. Graphs show

the distribution of every sample and the mean of all samples ± the standard deviation of the mean (SEM).

For western blot quantification, the sample with the maximum signal was assigned a value of 100%, and signals in other samples were expressed as a percentage of this; significance was determined by a one-sample test.

Long-rank (Mantel-Cox) test and Cehan-Breslow-Wilcoxon test were used for the analysis of the Kaplan-Meier curve (survival curve).

Statistical significant differences were considered when $p \leq 0.05$, expressed as *, whereas ** was used for differences $p \leq 0.01$ and *** for differences $p \leq 0.001$. Non-significant differences were designed as ns ($p > 0.05$).

Results

4. RESULTS

4.1. Analysis of HDAC6 contribution to cellular mechanisms that eliminate intracellular bacteria by phagocytic cells

4.1.1. Effect of HDAC6 absence in the intracellular pathogen clearance of dendritic cells

To assess the possible role of HDAC6 in innate immune responses during bacterial pathogenesis, we performed a time-course infection with *Lm* in bone marrow (BM)-derived granulocyte and monocyte colony-stimulating factor (GM-CSF)-derived dendritic cells (DCs) from *Hdac6*$^{+/+}$ and *Hdac6*$^{-/-}$ mice. Increasing levels of HDAC6 expression were detected in the *Hdac6*$^{+/+}$ DCs as the infection progressed, reaching a peak at 4 hpi (**Figure 4.1**).

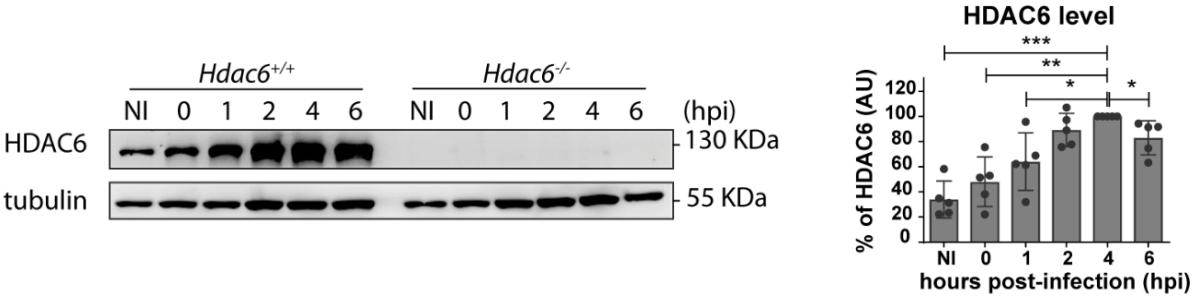

Figure 4.1. HDAC6 protein induction during Lm infection. *Left:* Western blot analysis of HDAC6 in a time-course of infection of GM-CSF DCs with *Lm.* Samples of non-infected (NI) cells and 0, 1, 2, 4 and 6 hpi cells are displayed. Tubulin was used as a loading control. *Right:* HDAC6 levels were quantified and are expressed relatively to its respective tubulin signal. Two-tailed t-test, ***p≤0.001, ** p≤0.01, *p≤0.05; n=5.

However, GM-CSF-derived DC differentiation was not noticeably affected in the absence of HDAC6, since there are the same levels of CD11c+MHC-II+, CD11c+MHC-II- and Gr-1+ populations between *Hdac6*$^{+/+}$ and *Hdac6*$^{-/-}$ DCs at day 11 of *in vitro* differentiation (**Figure 4.2**).

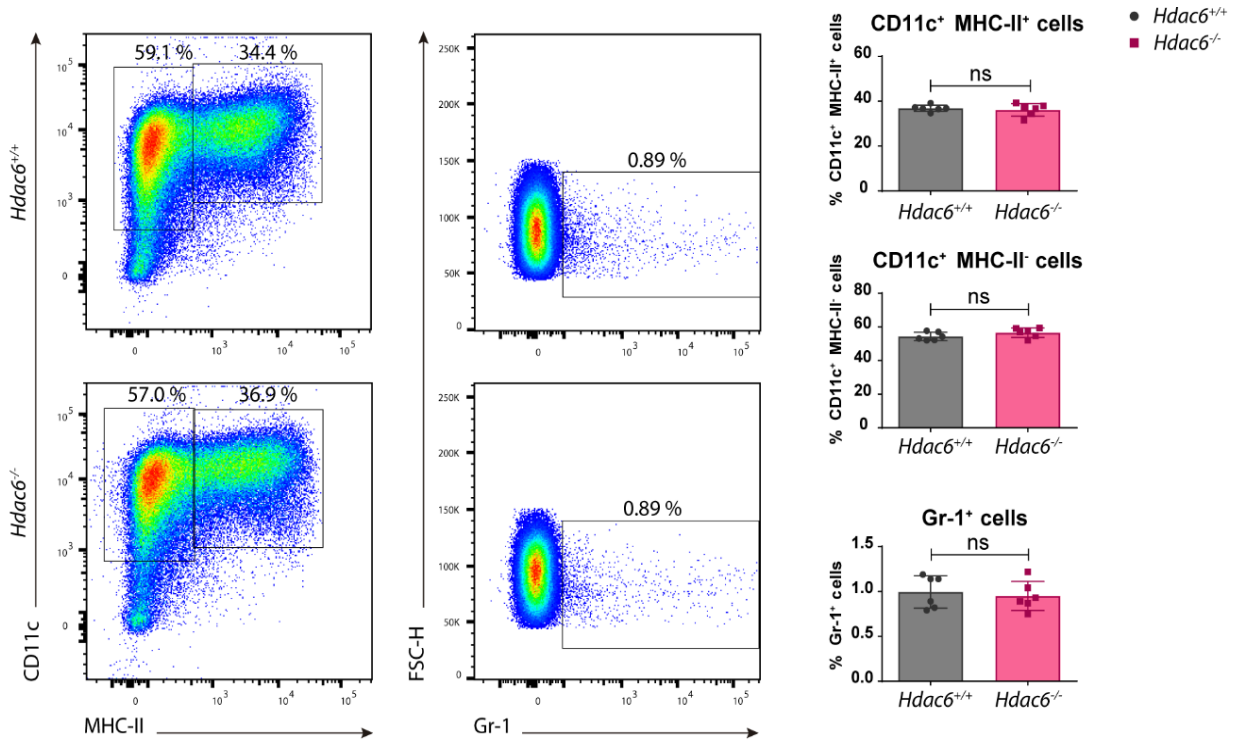

Figure 4.2. Differentiation of GM-CSF-derived DCs at day 11 of culture. *Left:* Dot-plots showing CD11c and MHC-II markers, with gating for $CD11c^+MHC\text{-}II^+$ and $CD11c^+MHC\text{-}II^-$ populations (percentages indicated). *Middle:* Dot-plots on differentiation day 11 showing FSC-H versus Gr-1, gating the $Gr\text{-}1^+$ population corresponding to neutrophil contamination in GM-CSF-derived DC cultures. *Right:* Charts show the percentages of $CD11c^+MHC\text{-}II^+$, $CD11c^+MHC\text{-}II^-$ and $Gr\text{-}1^+$ populations. ns>0.05 non-significant; n=6.

Next, *Hdac6*$^{+/+}$ and *Hdac6*$^{-/-}$ BMDCs were infected for different times with *Gram*-negative bacteria (*Salmonella* Typhimurium and *Escherichia coli DH5α*) and *Gram*-positive bacteria (*Listeria monocytogenes* and *Staphylococcus aureus*) at a multiplicity of infection (MOI) of 10, with colony-formed units (CFUs) corresponding to intracellular live bacteria (**Figure 4.3**). Bacterial entry was similar in *Hdac6*$^{+/+}$ and *Hdac6*$^{-/-}$ DCs at 0 h post-infection (hpi), while bacterial proliferation, measured at 6 hpi, was significantly higher in *Hdac6*$^{-/-}$ DCs for both types of intracellular pathogens, *Lm* and *S.* Typhimurium (**Figure 4.3. A**).

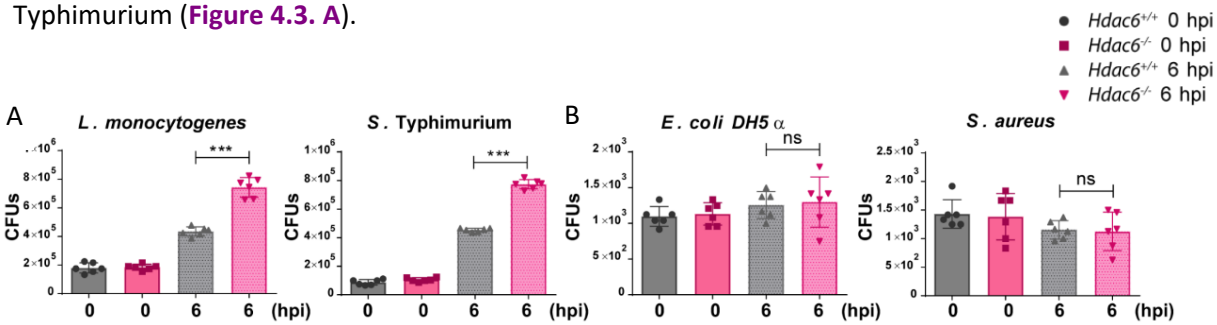

Figure 4.3. Intracellular bacteria entry and proliferation in GM-CSF-DCs infected with various types of bacteria. CFUs obtained at 0 and 6 hpi from DCs infected with **(A)** intracellular pathogens (*L. monocytogenes*, *S.* Typhimurium), and **(B)** extracellular pathogenes (*E. coli DHDα*, and *S. aureus*) at a MOI of 10. Data from 0 hpi are shown as bacteria entry control. Two-tailed t-test, ***p≤0.001, ns>0.05 non-significant; n=6.

This was not due to differences in cell viability after 6 hpi (**Figure 4.4. A**). However, cell viability of *Hdac6*$^{+/+}$ DCs is lower than *Hdac6*$^{-/-}$ ones at 24 hpi (**Figure 4.4. A**). No-significant differences were observed between *Hdac6*$^{+/+}$ and *Hdac6*$^{-/-}$ DCs after the addition of Heat Killed *Lm* (HKLM) at any time (**Figure 4.4. B**). These data indicate a phenotype in cell viability only with live bacteria at 24 hpi. In contrast, no significant difference was observed in the proliferation of the non-intracellular pathogens *S. aureus* and *E. coli*, indicating that HDAC6 is an important component of cellular mechanisms for the clearance of intracellular pathogens (**Figure 4.3. B**).

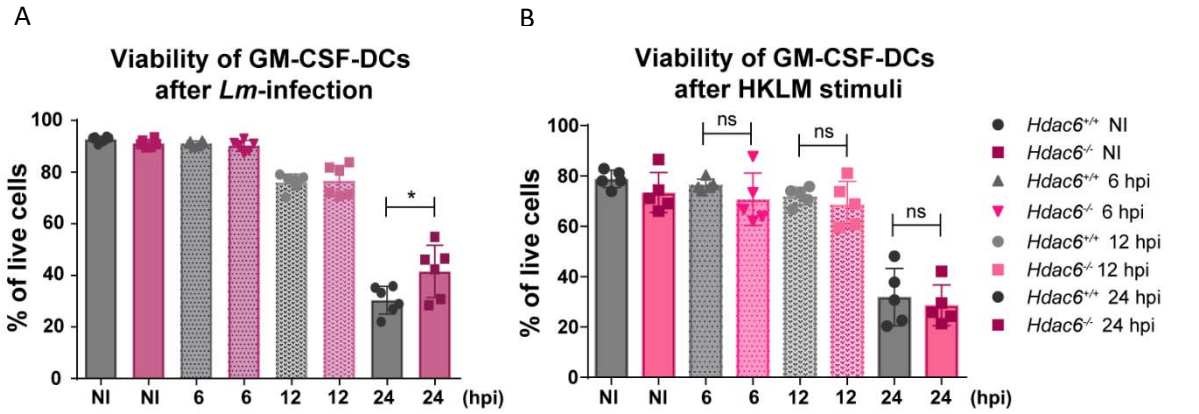

Figure 4.4. Viability of GM-CSF-DCs after Lm infection and HKLM stimuli at different times. Percentage viability of GM-CSF-DCs before and after **(A)** the infection with *Lm* MOI=10 or **(B)** HKLM stimuli MOI=50 at different times, NI: non-infected, 6, 12 and 24 h. Two-tailed t-test, **p≤0.01, ns>0.05 non- significant; n=6.

4.1.2. Measurement of *Lm* load in HDAC6-deficient myeloid cells

Time-course analysis showed that differences between *Lm* infection in *Hdac6*$^{+/+}$ and *Hdac6*$^{-/-}$ DCs CFUs peaked at 6 hpi and were sustained until 24 hpi (**Figure 4.5. A**). This effect was clearly observed at a MOI of 10, which did not affect cell viability (**Figure 4.5. B** and **Figure 4.4**).

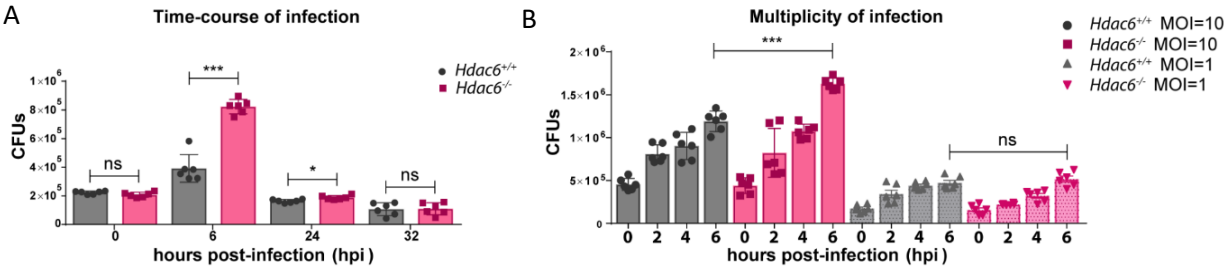

Figure 4.5. Time-course of Lm infection in GM-CSF-DCs and multiplicity of infection. (A) CFUs of *Lm*-infected GM-CSF DCs obtained at 0, 6, 24 and 32 hpi with a MOI=10. ***p≤0.001, *p≤0.05, ns>0.05 non-significant; n=6. **(B)** CFUs of *Lm*-infected DCs obtained at 0, 2, 4 and 6 hpi with a MOI=10 and 1. Two-tailed t-test, ***p≤0.001, *p≤0.05, ns>0.05 non-significant; n=6.

The lack of difference in bacterial load at 32 hpi between both genotypes is indicating that *Hdac6*$^{-/-}$ DCs do not succumb to the infection (**Figure 4.5**). This result suggests that other HDACs can be

compensating HDAC6 function during the ellimination of intracellular *Lm* at long times of infection. To address this question, qPCRs of every mouse deacetylase, HDACs (1-5 and 7-11) and sirtuins (1-7), were performed in *Lm* infected DCs at 6 and 24 hpi (**Figure 4.6**, **Figure 4.7**, **Figure 4.8** and **Figure 4.9**).

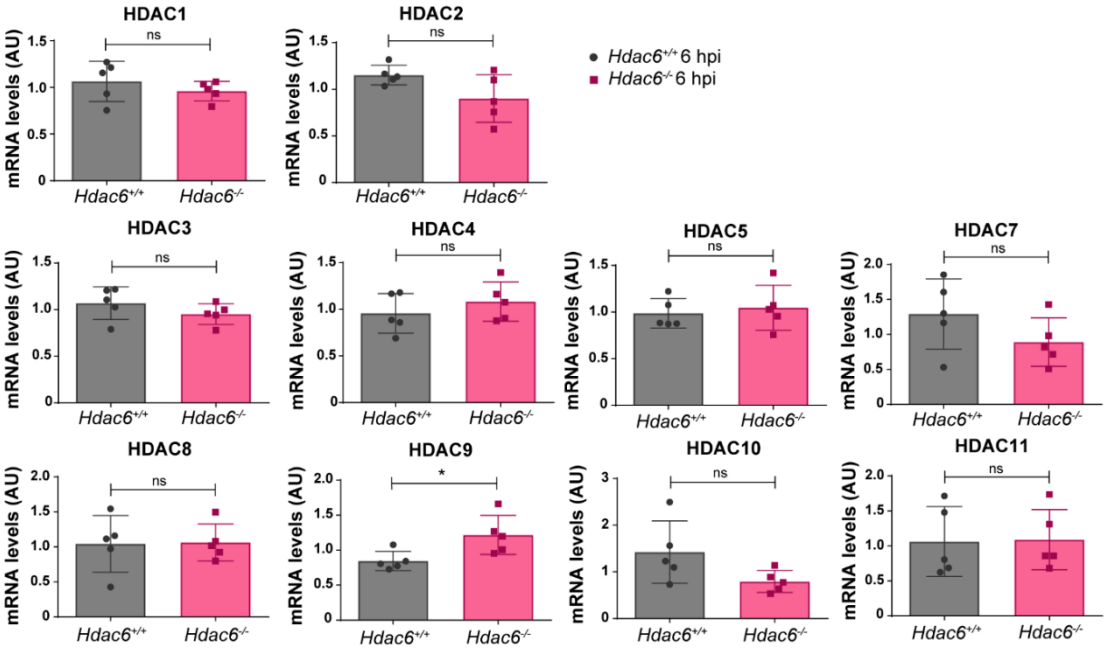

Figure 4.6. Expression of HDACs in DCs after *Lm* infection at 6 hpi. PCR analysis of HDACs (HDAC1, 2, 3, 4, 5, 7, 8, 9, 10 and 11) in *Hdac6*$^{+/+}$ and *Hdac6*$^{-/-}$ GM-CSF DCs infected with *Lm* at 6 hpi (AU: arbitrary units). Two-tailed t-test, * p≤0.05, ns>0.05 non-significant; n=5.

In this regard, higher expression levels of HDAC5 were detected in *Hdac6*$^{-/-}$ DCs at 24 hpi, whereas similar results were obtained for HDAC9 at 6 hpi (**Figure 4.6** and **Figure 4.7**).

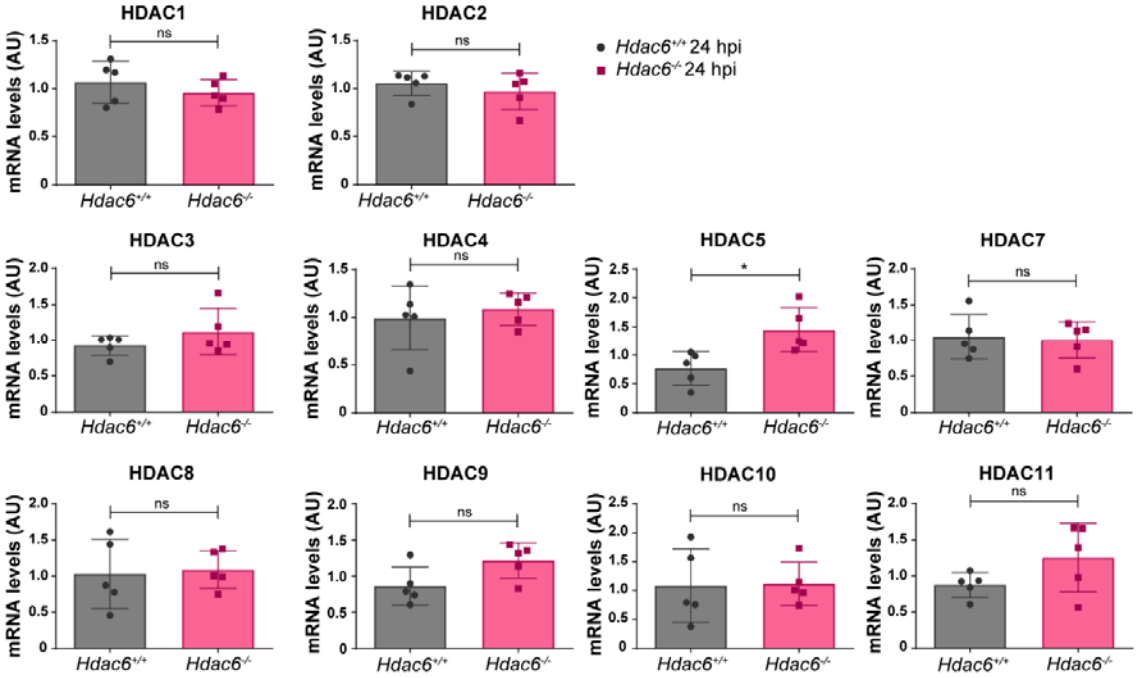

Figure 4.7. Expression of HDACs in DCs after *Lm* infection at 24 hpi. PCR analysis of HDACs (HDAC1, 2, 3, 4, 5, 7, 8, 9, 10 and 11) in *Hdac6*$^{+/+}$ and *Hdac6*$^{-/-}$ GM-CSF DCs infected with *Lm* at 24 hpi (AU: arbitrary units). Two-tailed t-test, * p≤0.05, ns>0.05 non-significant; n=5.

However, no significant differences were observed in sirtuins expresion between *Hdac6*$^{+/+}$ and *Hdac6*$^{-/-}$ DCs at any time (**Figure 4.8** and **Figure 4.9**).

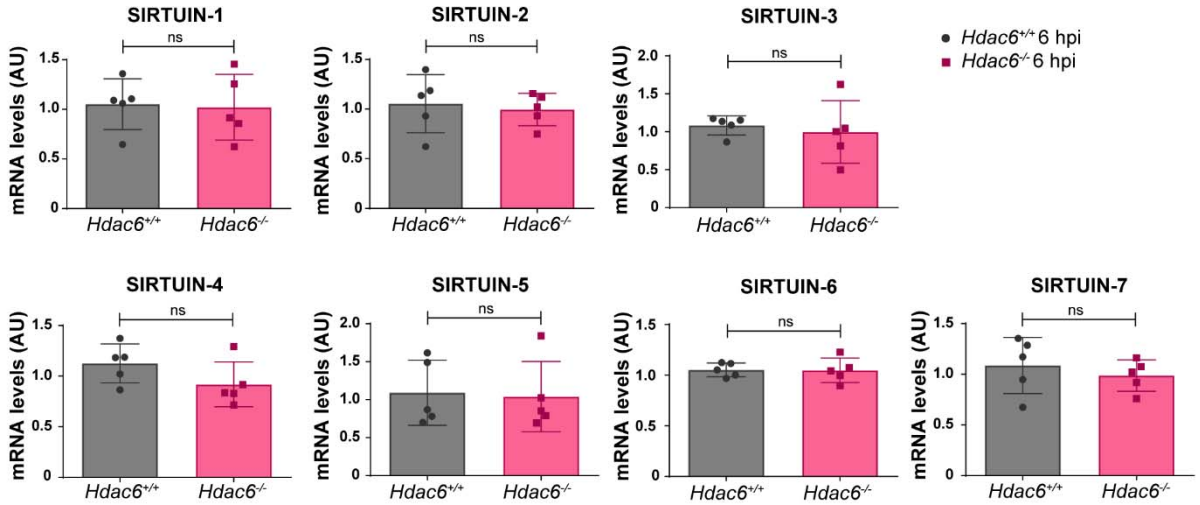

Figure 4.8. Expression of Sirtuins in DCs after *Lm* infection at 6 hpi. PCR analysis of Sirtuins (1, 2, 3, 4, 5, 6 and 7)in *Hdac6*$^{+/+}$ and *Hdac6*$^{-/-}$ GM-CSF DCs infected with *Lm* at 6 hpi (AU: arbitrary units). Two-tailed t-test, * p≤0.05, ns>0.05 non-significant; n=5.

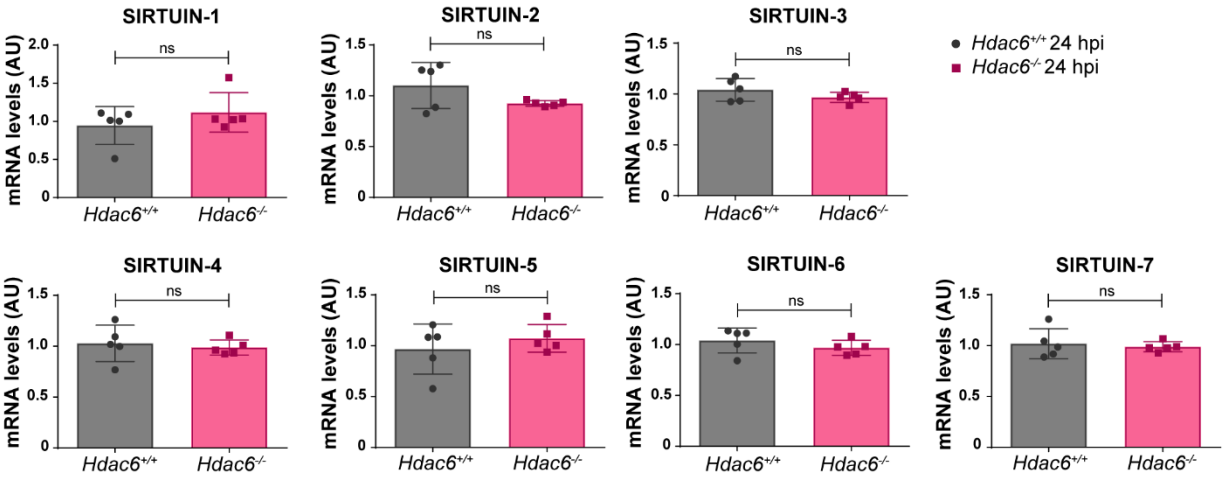

Figure 4.9. Expression of Sirtuins in DCs after *Lm* infection at 24 hpi. PCR analysis of Sirtuins (1, 2, 3, 4, 5, 6 and 7) in *Hdac6*$^{+/+}$ and *Hdac6*$^{-/-}$ GM-CSF DCs infected with *Lm* at 24 hpi (AU: arbitrary units). Two-tailed t-test, * p≤0.05, ns>0.05 non-significant; n=5.

A similar pattern was observed with macrophage colony-stimulating factor (M-CSF)-derived macrophages, demonstrating the lineage independence of the role of HDAC6 in bacterial clearance (**Figure 4.10**). Although the difference between *Hdac6*$^{+/+}$ and *Hdac6*$^{-/-}$ cells was observed in both macrophages and DCs, the clearance capacity of macrophages was ten-fold higher than that of DCs at 6 hpi (**Figure 4.10**).

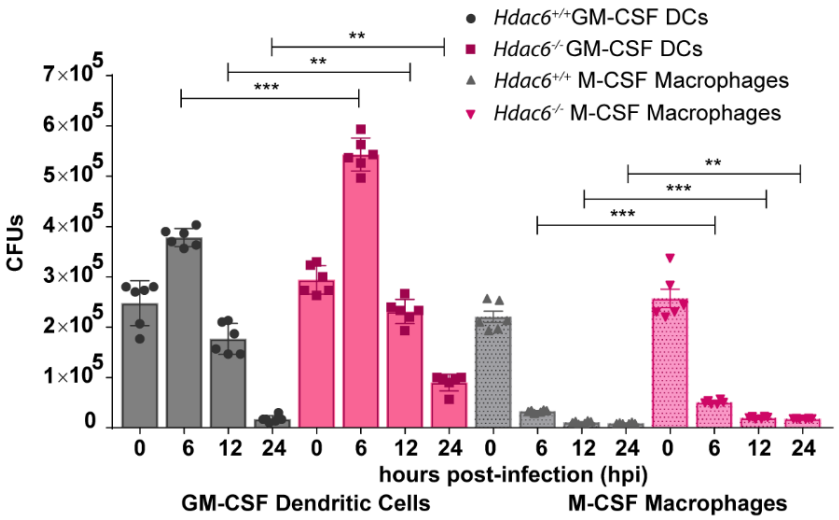

Figure 4.10. Comparison of intracellular bacteria in GM-CSF-derived DCs and M-CSF-derived macrophages over the time-course of *Lm*-infection. CFUs of DCs and macrophages are shown at 0, 6, 12 and 24 hpi. In both cases *Hdac6*$^{-/-}$ cells display higher intracellular bacterial load. Two-tailed t-test, ***p≤0.001, ** p≤0.01, ns>0.05 non-significant; n=6.

Bacterial load was also determined by flow cytometry using two strategies: a specific antibody against *Lm*, and RFP-expressing bacteria. Both approaches showed that *Hdac6*-deficient DCs contained more bacteria at 6 hpi (**Figure 4.11**).

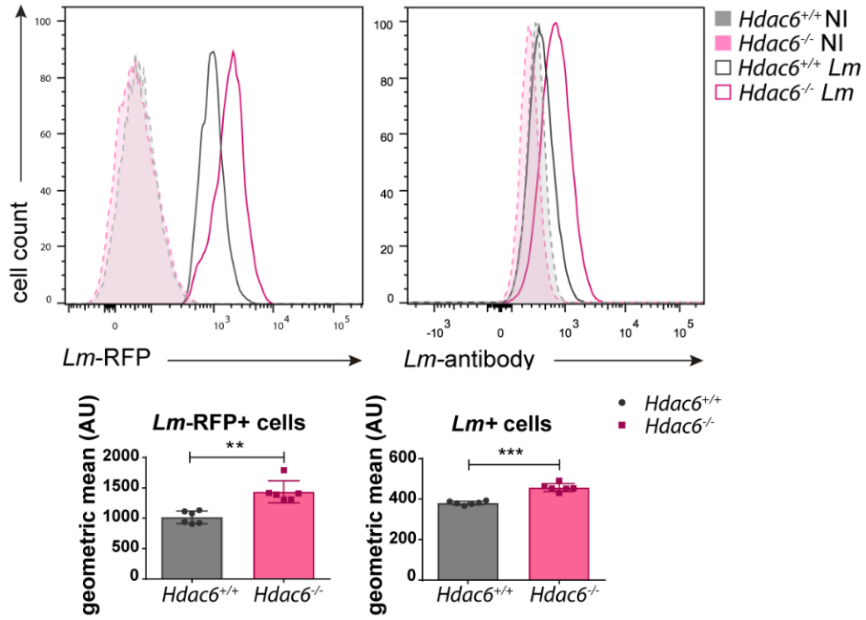

Figure 4.11. GM-CSF DCs were infected with *Lm*-RFP or *Lm* for 6 h and the bacterial signal was determined by flow cytometry. *Top panel:* The panel shows representative histograms of *Lm*-RFP and *Lm* antibody signals. *Bottom panel:* Graphs show geometric mean of the *Lm* signals. Each dot represents the number of samples and the mean with SEM is indicated in colour. Two-tailed t-test, ***p≤0.001, ** p≤0.01; n=6.

Higher numbers of bacteria in *Hdac6*$^{-/-}$ GM-CSF DCs were also detected by confocal fluorescence microscopy at 6 hpi (**Figure 4.12**). Some bacteria co-localized with filamentous actin, showing clear actin rockets (**Figure 4.12. A** and **B**). Image quantification confirmed that *Hdac6*$^{-/-}$ DCs contained more bacteria per cell and more total bacteria, remarking a higher percentage of cells hosting a large number of bacteria in *Hdac6*$^{-/-}$ cells (see distribution of bacteria per cell, 6-7) (**Figure 4.12. C** and **D**). ImarisCell Module view of images showed the number of bacteria per cell using actin transparency to easily visualize individual bacteria (**Figure 4.12. B**).

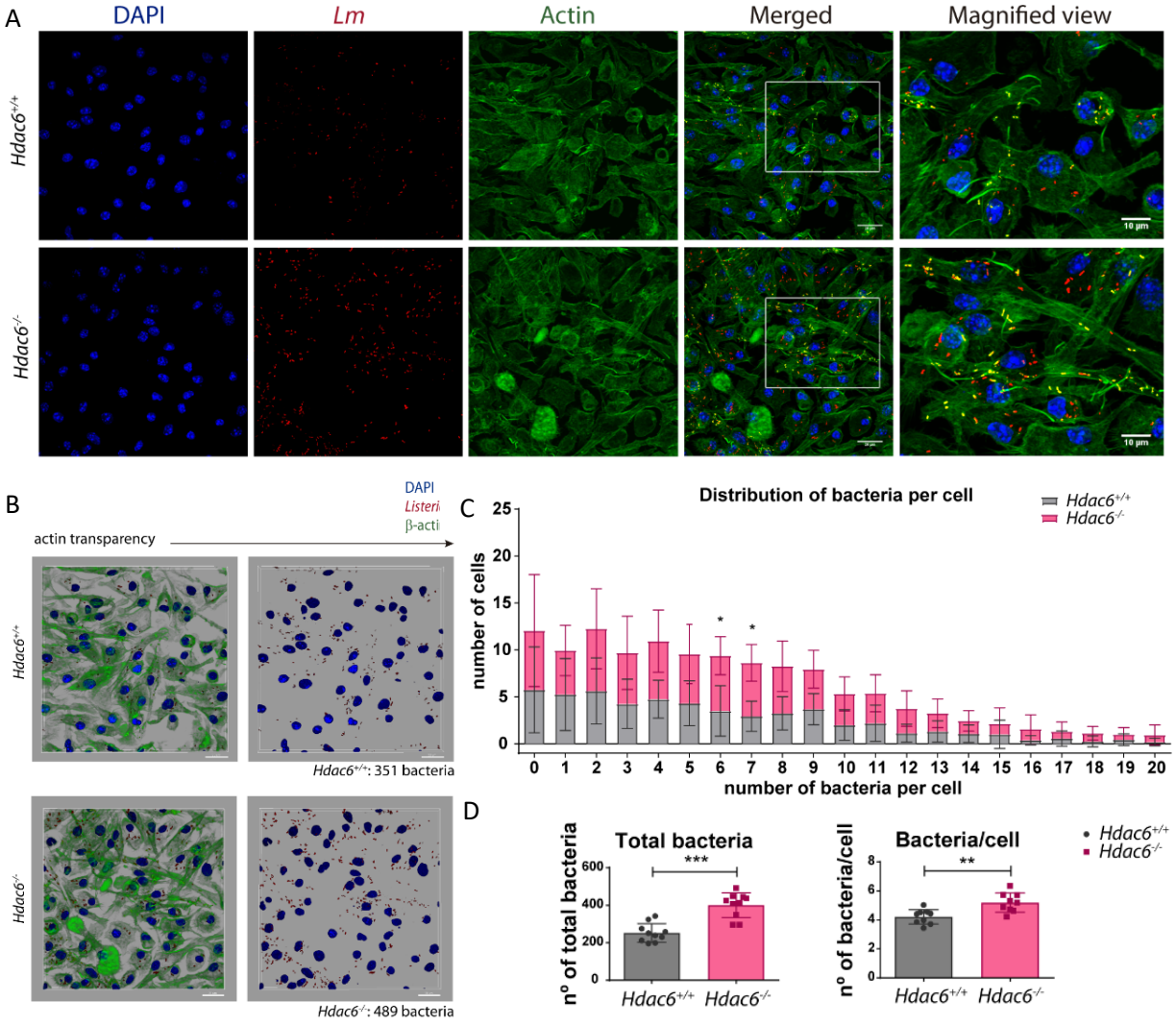

Figure 4.12. Confocal microscopy determination of bacterial load at 6 hpi. **(A)** Maximum intensity z-projections of confocal microscopy images of *Lm*-infected *Hdac6*$^{+/+}$ and *Hdac6*$^{-/-}$ GM-CSF DCs at 6 hpi. The panel shows DAPI (blue), *Lm* (red), β-actin (green), merged views of three channels, and magnified views of the boxed areas from the merged view. Yellow indicates *Lm* and β-actin co-localization. Scale bars 20 µm (main panels) and 10 µm magnified views). **(B)** Confocal microscopy determination of bacterial load of **Figure 4.12.A.** Maximum intensity z-projections of confocal microscopy images of *Lm*-infected *Hdac6*$^{+/+}$ and *Hdac6*$^{-/-}$ DCs at 6 hpi. ImarisCell Module view of the number of nucleus and bacteria per cell. Actin transparency is used to visualize bacteria (number indicated on the right). Images show DAPI (blue), *Lm* (red), β-actin (green). Scale bars 20 µm. **(C)** ImarisCell Module analysis of the number of cells and the number of bacteria per cell in all pictures (10 pictures per genotype). The graph shows the distribution of cells with a specific number of bacteria per cell. The number of cells with 6 and 7 bacteria differed significantly between the *Hdac6*$^{+/+}$ and *Hdac6*$^{-/-}$ genotypes. Two-way Anova, * p≤0.05; n=10 . **(D)** Graphs show statistical analysis of Imaris quantification of total bacteria and bacteria per cell in *Hdac6*$^{+/+}$ and *Hdac6*$^{-/-}$ DCs. Two-tailed t-test, ***p≤0.001, ** p≤0.01; n=10.

4.1.3. Determination of *in vivo* bacterial burden

To ascertain whether *Hdac6*$^{-/-}$ cells display higher bacterial burden than *Hdac6*$^{+/+}$ cells *in vivo*, *Hdac6*$^{+/+}$ and *Hdac6*$^{-/-}$ mice were intravenously injected with *Lm* and total CFUs per gram of liver and spleen were determined at 6 hpi. In agreement with the higher numbers of *Lm* observed in GM-CSF-DCs and M-CSF-Macrophages, we observed increased bacterial titres in spleen and liver cell suspensions (**Figure 4.13**).

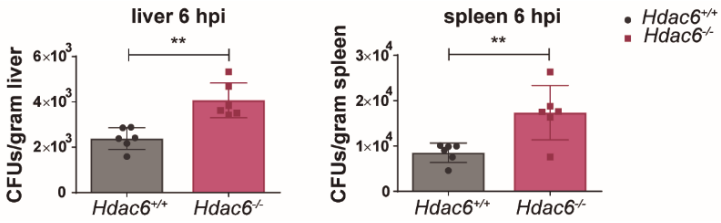

Figure 4.13. Deficient intracellular bacteria clearance in target organs of *Hdac6*$^{-/-}$ mice. Quantification of bacterial load in target organs (spleen and liver) at 6 hpi in *Hdac6*$^{+/+}$ and *Hdac6*$^{-/-}$ mice injected with a lethal dose of *Lm*. Bacterial load is expressed by CFUs per gram of liver (left graph) and per gram of spleen (right graph). Two-tailed t-test, **p≤0.01, n=6.

Next, to determine the specific cell populations underlying this phenotype, a multicolour gating strategy was used to identify the myeloid cell compartment, including monocytes, neutrophils, Tips DCs, total cDCs, CD8^{-} cCDs and CD8^{+} cDCs (**Figure 4.14**).

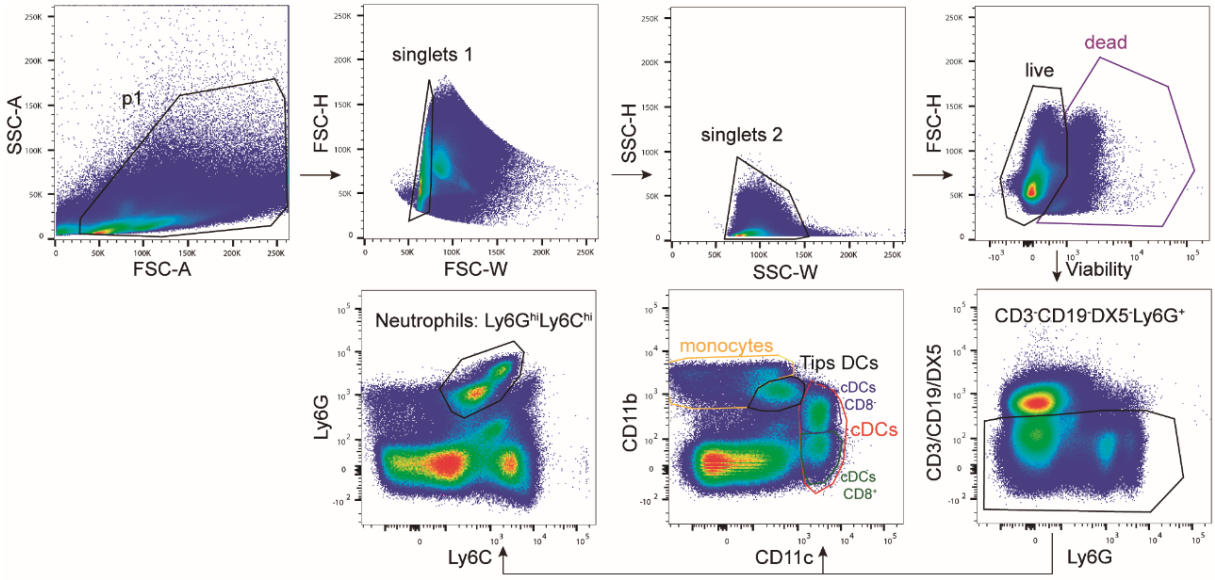

Figure 4.14. Gating strategy of myeloid populations of the spleen. Dot-plots showing the gating of myeloid populations of spleen. Dot-plots showing SSC-A versus FSC-A indicates p1, FSC-H versus FSC-W and SSC-H versus SSC-W were used to avoid doublets and FSC-H versus viability shows live and dead cells. Singlets and live cells were used to choose CD3^{-}CD19^{-}DX5^{-}Ly6G^{+} cell population. From this population, neutrophils were gated as Ly6G^{+}Ly6C^{+} cells, monocytes as CD11b^{+}CD11c^{lo}, Tips DCs as intermedium levels of CD11b and CD11c, conventional dendritic cells (cDCs) as CD11c^{hi}; inside this population CD8^{-} cDCs were distinguished as CD11c^{hi}CD11b^{+} and CD8^{-} cDCs as CD11c^{hi}CD11b^{lo}.

Non-significant differences were detected in the total number of myeloid splenic populations between *Hdac6*$^{+/+}$ and *Hdac6*$^{-/-}$genotypes at 6 hpi of *Lm*-infection (**Figure 4.15**).

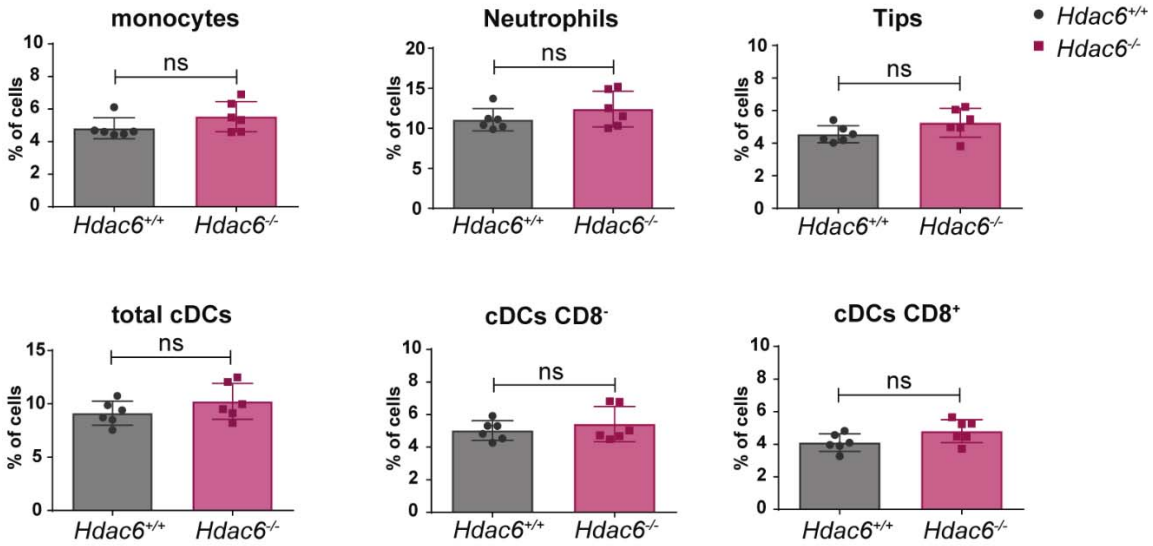

Figure 4.15. Comparison of myeloid populations of the spleen between *Hdac6*$^{+/+}$ and *Hdac6*$^{-/-}$ genotypes. The charts show percentage of cells of the different splenic populations (monocytes, neutrophils, Tips DCs, total cDCs, CD8$^-$ cDCs and CD8$^+$cDCs) gated in the live CD3$^-$CD19$^-$DX5$^-$ population of *Hdac6*$^{+/+}$ and *Hdac6*$^{-/-}$ mice injected with a lethal dose of *Lm* at 6 hpi. Two-tailed t-test, ns>0.05 non-significant; n=6.

However, higher numbers of *Lm* were observed in different myeloid cells at 6 hpi (**Figure 4.16**). These data highlight the impairment of intracellular *Lm* clearance in *Hdac6*$^{-/-}$ myeloid cells.

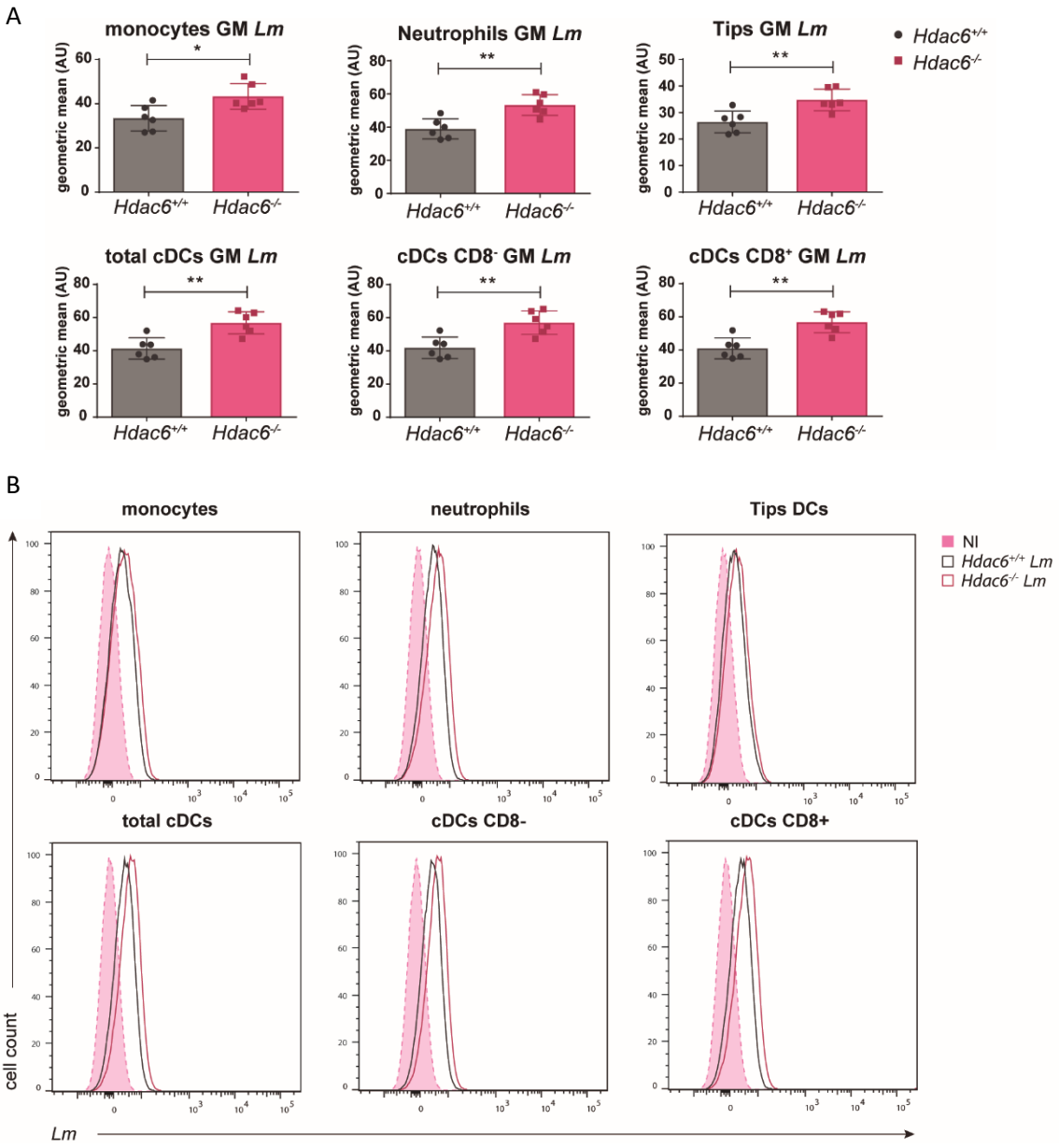

Figure 4.16. Deficient intracellular bacteria clearance in *Hdac6*$^{-/-}$ splenic myeloid populations. (A) The charts show geometric means (GM) of *Lm* of different splenic populations (monocytes, neutrophils, Tips DCs, total cDCs, cDCs CD8^{-} and cDCs CD8^{+}) gated in the live CD3^{-}CD19^{-}DX5^{-} population of *Hdac6*$^{+/+}$ and *Hdac6*$^{-/-}$ mice injected with a lethal dose of *Lm* at 6 hpi. Two-tailed t-test, **p≤0.01, * p≤0.05; n=6. **(B)** Representative histograms of different splenic populations (monocytes, neutrophils, Tips DCs, total cDCs, CD8^{-} cDCs and CD8^{+}cDCs) show *Lm* signal of *Hdac6*$^{+/+}$ and *Hdac6*$^{-/-}$ mice injected with a lethal dose of *Lm* at 6 hpi. A pool of *Hdac6*$^{+/+}$ and *Hdac6*$^{-/-}$ non-infected spleens was used as a control sample without infection (NI).

4.1.4. Evaluation of cellular clearance mechanisms of *Lm*

To test the involvement of autophagy in the mechanism by which HDAC6 regulates *Lm* infection, we treated GM-CSF-derived DCs with 3-methyladenine (3-MA), an inhibitor of autophagosome formation. Treatment with 3-MA increased bacterial load in *Hdac6*$^{+/+}$ DCs at 6 hpi, while having no effect on *Hdac6*$^{-/-}$ DCs (**Figure 4.17. B**), suggesting autophagy as the bacterial clearance mechanism impaired in *Hdac6*-deficient DCs. A similar result was observed upon treatment of DCs with bafilomycin A1, an inhibitor of vacuolar proton pump that indirectly inhibits phagosome-lysosome fusion, and with the lysosome acidification inhibitors chloroquine and NH_4Cl (**Figure 4.17. B** and **C**). In contrast, increasing autophagy flux with rapamycin did not restore the impaired autophagy in *Hdac6*$^{-/-}$ DCs (**Figure 4.17. D**). No significant effects were observed with control vehicles (**Figure 4.17. A**). To explore other possible mechanisms, we treated DCs with inhibitors of NADPH oxidase (DPI) and iNOS (1400W). These treatments did not alter the difference in CFU number at 6 hpi between treated and non-treated *Hdac6*$^{+/+}$ and *Hdac6*$^{-/-}$ DCs, indicating that the activity of either enzyme is not accounting for the existing phenotype (**Figure 4.17. E**).

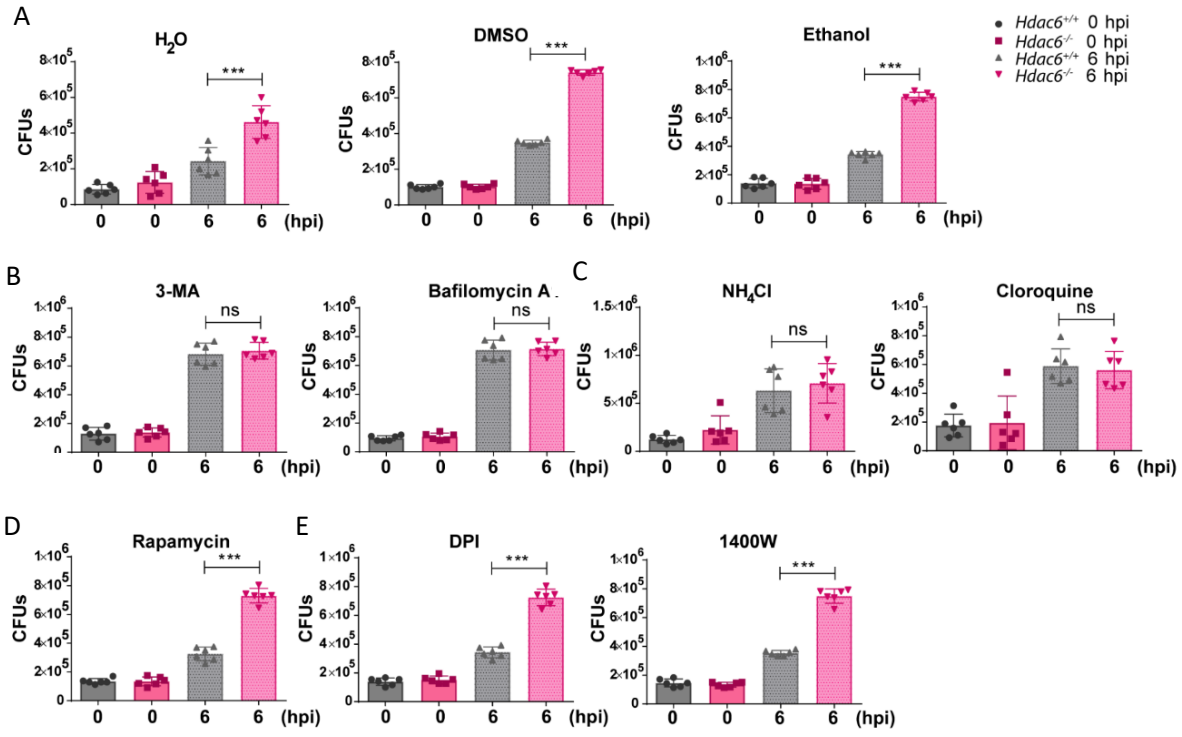

Figure 4.17. Intracellular bacteria after treatment with different inhibitors of principal clearance mechanisms of the cell. **(A)** Total CFUs at 0 and 6 hpi in *Lm*-infected GM-CSF DCs (MOI of 10) treated with different control vehicles (H_2O, DMSO and ethanol). Total CFUs in *Lm*-infected DCs treated with inhibitors. CFUs were detected at entry (0 hpi) and 6 hpi (bacterial proliferation) using: **(B)** the autophagy inhibitors (3-MA and bafilomycin A1, **(C)** the lysosome acidification inhibitors (NH_4Cl and cloroquine), and **(D)** the autophagy activator (rapamycin), **(E)** the NADPH oxidase inhibitor (DPI) and the iNOS inhibitor (1400W). Two-tailed t-test, ***p≤0.001, ns>0.05 non-significant; n=6. *Specification of control vehicles:* H_2O were the control vehicle used for NH_4Cl and cloroquine, DMSO for 3-MA, bafilomycin A1, DPI and 1400W and ethanol for rapamycin. Time 0 hpi is included as a bacterial entry control.

4.1.5. Consequence of the lack of HDAC6 in the autophagy of *Lm*

The defective autophagy phenotype of *Hdac6*$^{-/-}$ GM-CSF-derived DCs was not due to transcriptional alterations of autophagy or lysosome components, since *Lm*-infected *Hdac6*$^{+/+}$ and *Hdac6*$^{-/-}$ DCs showed no mRNA expression differences at 6 hpi in the autophagy components LC3 A and B, p62, ATG2, 5, 7 and 12, and Beclin-1 or in the lysosome components LAMP-1 and 2 (**Figure 4.18**).

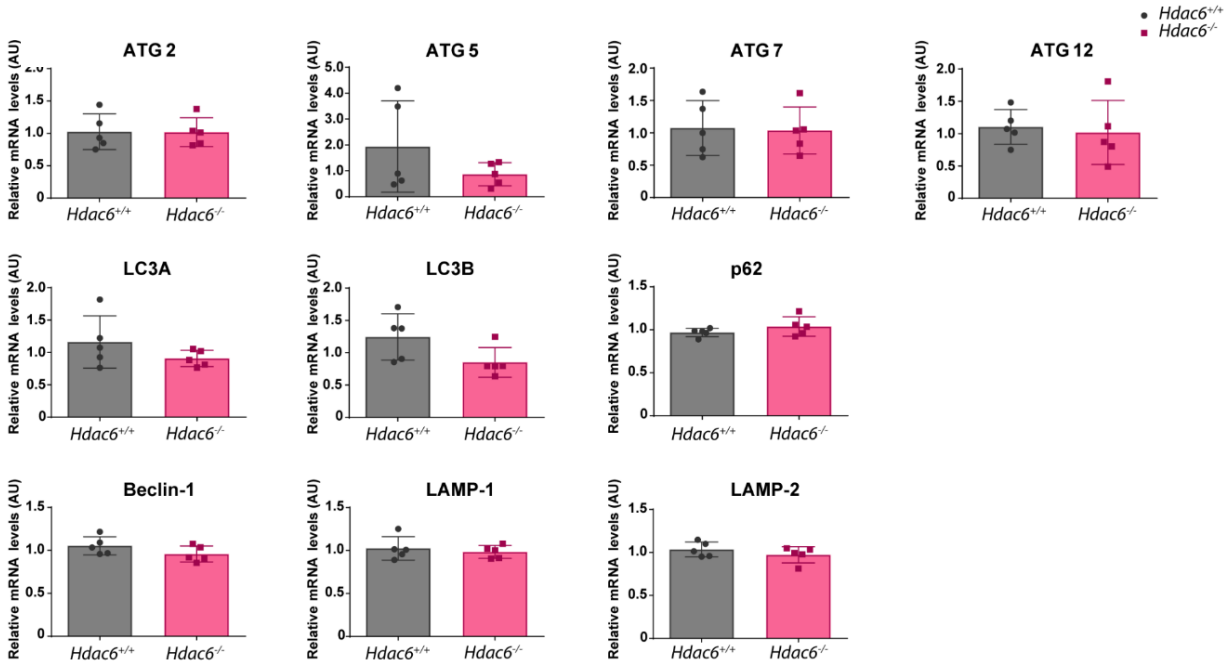

Figure 4.18. Expression of relevant autophagy and lysosome markers in Lm-infected GM-CSF-DCs at 6 hpi. PCR analysis of autophagy markers (ATG-2, 5, 7 and 12, LC3A and B, p62 and Beclin-1) and lysosome markers (LAMP-1 and 2) (AU: arbitrary units) after 6 hpi with *Lm*. Two-tailed t-test, ns>0.05 non-significant; n=5.

To determine whether these findings can be extended to other phagocytic cells, we carried out CFU assays with macrophages obtained from *Hdac6*$^{+/+}$ and *Hdac6*$^{-/-}$ mice four days after intraperitoneal thioglycollate injection. Higher bacterial load was observed only in *Hdac6*$^{-/-}$ macrophages at 6 hpi, and this difference was abrogated by treatment with bafilomycin A1 (**Figure 4.19**).

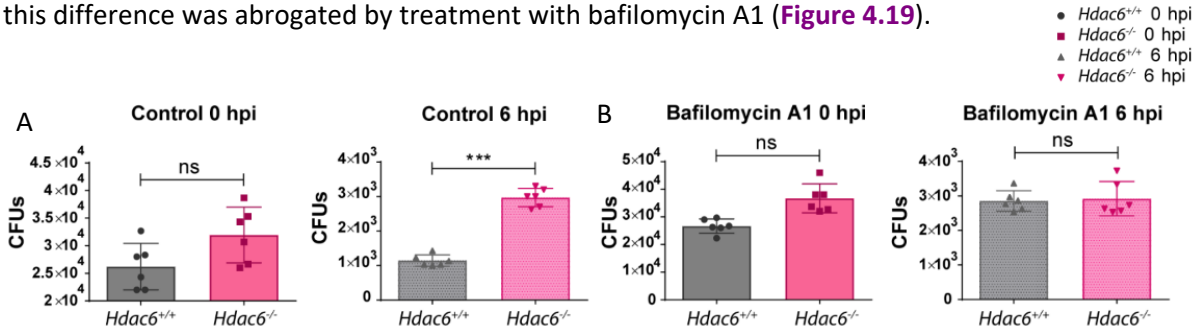

Figure 4.19. Intracellular bacteria in peritoneal macrophages. (A) Total CFUs at 0 and 6 hpi in *Lm*-infected thioglycollate-elicited macrophages. **(B)** Total CFUs at 0 and 6 hpi in *Lm*-infected TEMs treated with bafilomycin A1. Two-tailed t-test, ***p≤0.001, ns>0.05 non-significant; n=6.

These data indicate that the phenotype observed in DCs is also extendable to other *Hdac6*-deficient phagocytic cells such as peritoneal macrophages, indicating a widespread defect in intracellular killing ability due to lack of HDAC6. Moreover, the killing ability shown by peritoneal macrophages is similar to that of M-CSF-derived macrophages and higher than GM-CSF-derived DCs (**Figure 4.19** compared with **Figure 4.10**).

To gain further insight into the autophagy mechanism affected by HDAC6, we monitored the autophagosome markers p62 and LC3bI and II in *Lm*-infected GM-CSF DCs (**Figure 4.20**).

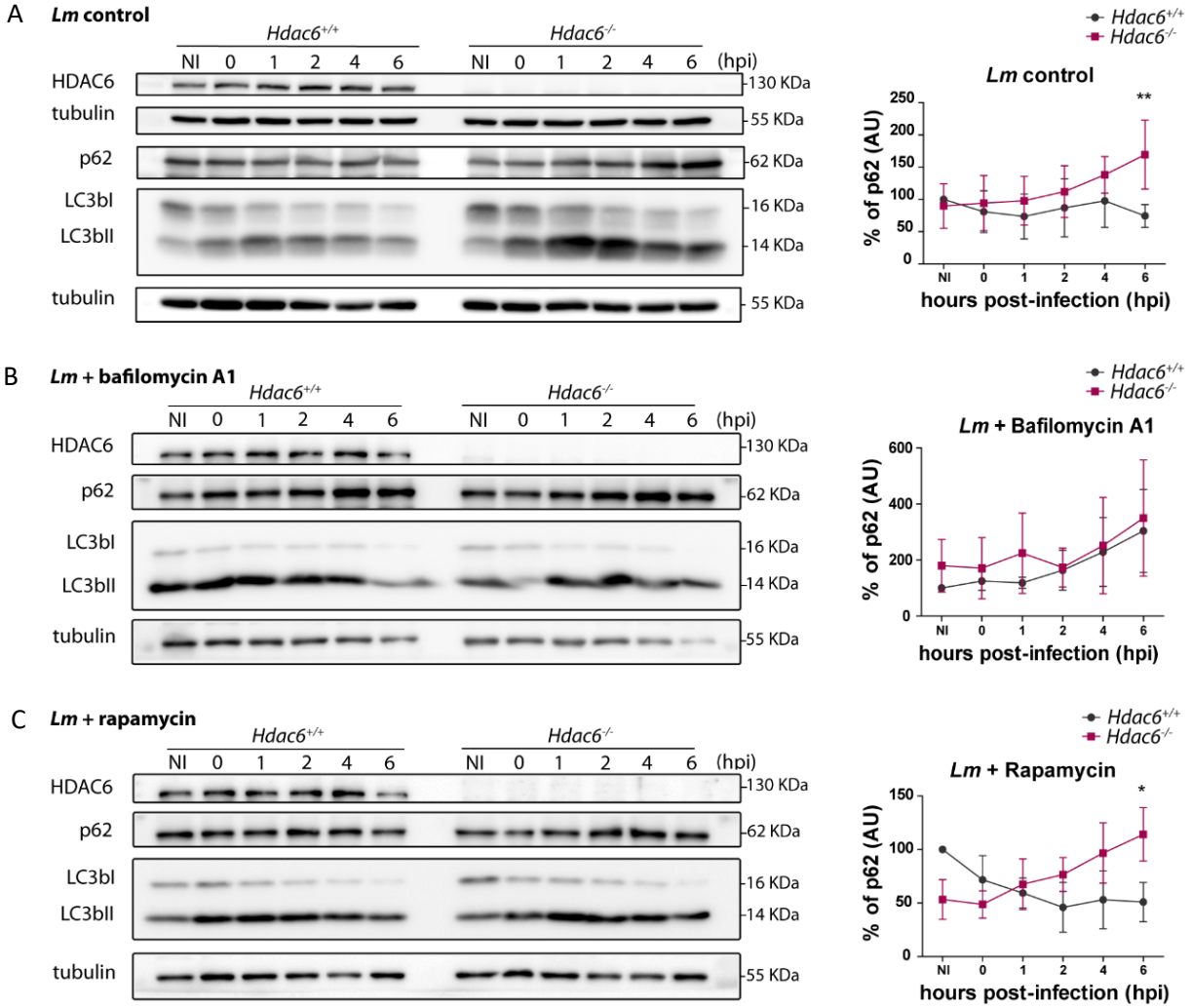

Figure 4.20. Western-blot levels of autophagy markers during infection with Lm in GM-CSF DCs treated with or without various autophagy inhibitors or an autophagy inducer. *Left panels:* Western-blot analysis of autophagy markers over the time-course of *Lm* infection in *Hdac6*$^{+/+}$ and *Hdac6*$^{-/-}$ DCs. *Left panels:* Levels of p62, LC3bI and II and HDAC6 were detected in **(A)** control cells and cells treated with **(B)** the inhibitor of phagosome maturation bafilomycin A1 and **(C)** the activator of autophagy rapamycin. Tubulin was used as a loading control. HDAC6 was used as a genotype check of *Hdac6*$^{+/+}$ and *Hdac6*$^{-/-}$ DCs and to monitor HDAC6 induction during infection. *Right panels:* Accompanying charts show quantification of the p62 percentage of control, bafilomycin A1 and rapamycin western blots in non-infected cells (NI) and 0, 1, 2, 4 and 6 hpi. NI time was considered the 100% point to refer other times as percentage from this sample. Two-tailed t-test, ** p≤0.01, * p≤0.05, ns>0.05 non-significant; n=5.

Hdac6$^{-/-}$ DCs showed a 2-fold higher accumulation of p62 than *Hdac6*$^{+/+}$ cells at 6 hpi and increased LC3bII level in *Hdac6*$^{+/+}$ cells from 1 to 6 hpi (**Figure 4.20. A**). However, differences in p62 and LC3b levels were not found at early times of *Lm* infection of *Hdac6*$^{+/+}$ and *Hdac6*$^{-/-}$ DCs, indicating that the induction of autophagy is not affected in the absence of HDAC6 (**Figure 4.20. A**).

The treatment with bafilomycin A1 enhances the accumulation of p62 during the infection up to the same level in both genotypes, abrogating the deficiency in autophagy observed in *Hdac6*$^{+/+}$ DCs (**Figure 4.20. B**). Although rapamycin also increased p62 accumulation at early times in *Hdac6*$^{+/+}$ and *Hdac6*$^{-/-}$ DCs, only *Hdac6*$^{+/+}$ cells are able to diminished p62 at 6 hpi (**Figure 4.20. C**). This treatment confirmed the results obtained in the CFUs functional assays with this inhibitor (**Figure 4.20. C** compared with **Figure 4.17. B**). The similarity of the autophagy defect detected in *Hdac6*$^{-/-}$ DCs in control condition to that in rapamycin-treated *Hdac6*$^{-/-}$ cells, suggests an impairment in phagocytic vesicle fusion with the lysosome.

To show all the information about autophagy drugs in a single Western blot, samples of non-infected *Hdac6*$^{+/+}$ and *Hdac6*$^{-/-}$ DCs and *Lm*-infected at 6 hpi, without inhibitors, and treated with an autophagy inhibitor (bafilomycin A1) and an activator of autophagy (rapamycin) were shown (**Figure 4.21**). In accordance with data of the previous figure, an increment in p62 level in control *Hdac6*$^{-/-}$ DCs can be observed at 6 hpi, similar p62 levels in bafilomycin A1-treated *Hdac6*$^{+/+}$ and *Hdac6*$^{-/-}$ DCs at 6 hpi, and more p62 signal in rapamycin-treated *Hdac6*$^{-/-}$ DCs (**Figure 4.21**).

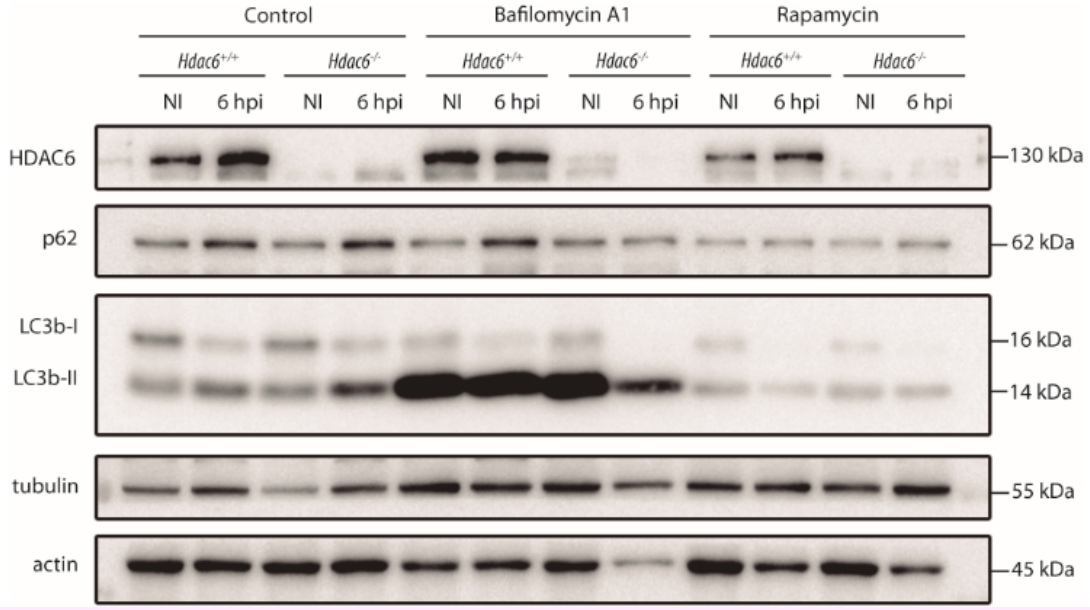

Figure 4.21. Western-blot levels of autophagy markers in untreated and treated with bafilomycin A1 and rapamycin DCs. Western-blot analysis of autophagy markers during *Lm* infection in *Hdac6*$^{+/+}$ and *Hdac6*$^{-/-}$ GM-CSF-derived DCs without treatment and treated with bafilomycin A1 and rapamycin. Levels of p62, LC3bI and II and HDAC6 were detected. Tubulin and actin were used as a loading controls. HDAC6 was as a genotype check of *Hdac6*$^{+/+}$ and *Hdac6*$^{-/-}$ DCs and to monitor HDAC6 induction during infection.

4.1.6. Effect of HDAC6 absence in the accumulation of autophagy marker p62

In order to further understand the defective autophagy of *Hdac6*$^{-/-}$ DCs, the accumulation of p62 was studied in more detail. Flow cytometry at 6 hpi revealed significantly higher p62 content in *Hdac6*$^{-/-}$ GM-CSF DCs, indicating accumulation of this phagosome marker due to defective fusion of this organelle with the lysosome (**Figure 4.22**). Bafilomycin A1 treatment completely abrogated this difference, suggesting that *Hdac6*$^{-/-}$ DCs displayed an impairment in the final step of autophagy (**Figure 4.22**). More signal of *Lm* is displayed in *Hdac6*$^{-/-}$ DCs (**Figure 4.22**). In this regard, bafilomycin A1 treatment increased the low *Lm* signal in *Hdac6*$^{+/+}$ DCs to the level observed in *Hdac6*$^{-/-}$ cells (**Figure 4.22**).

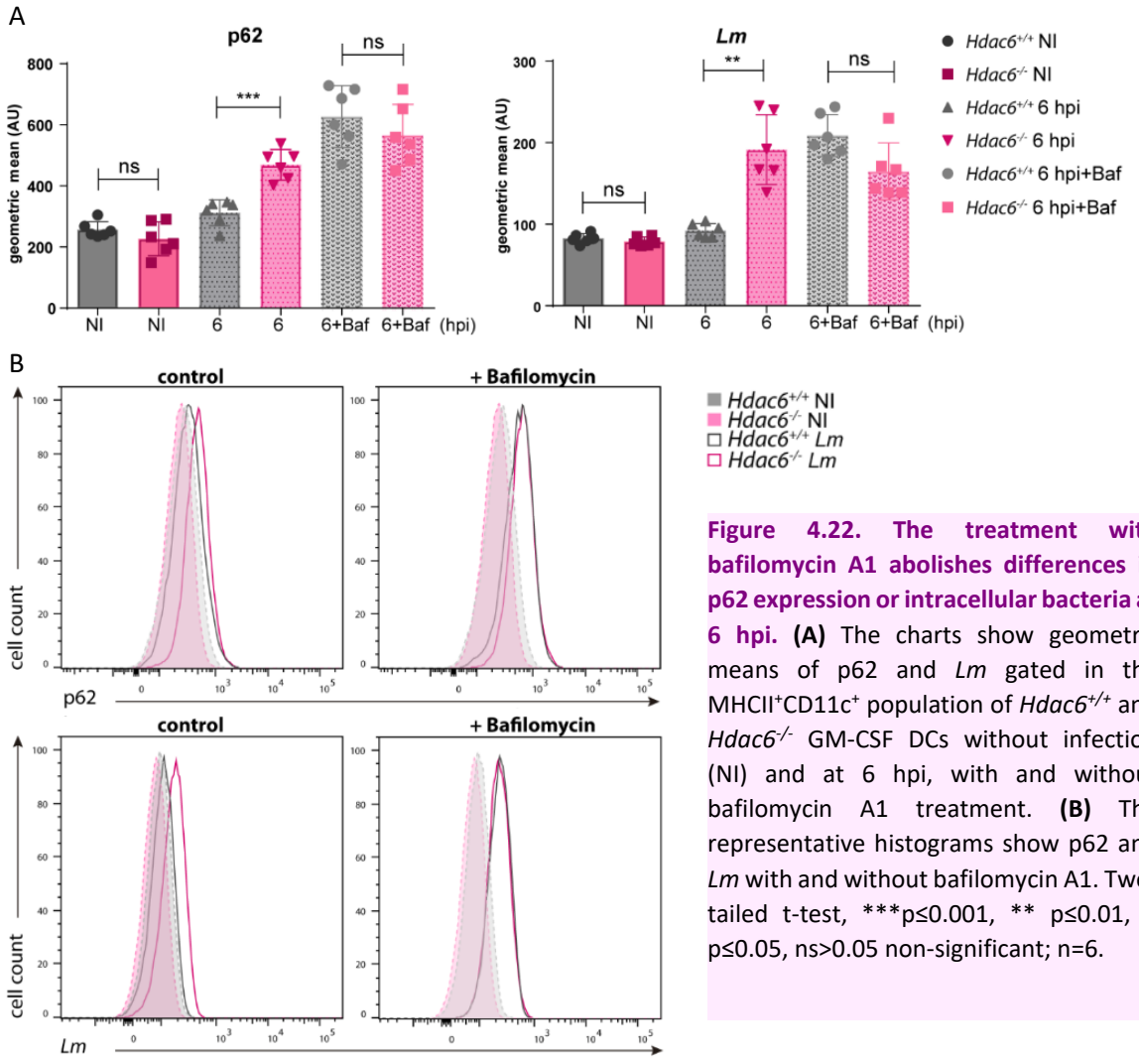

Figure 4.22. The treatment with bafilomycin A1 abolishes differences in p62 expression or intracellular bacteria at 6 hpi. (A) The charts show geometric means of p62 and *Lm* gated in the MHCII^{+}CD11c^{+} population of *Hdac6*$^{+/+}$ and *Hdac6*$^{-/-}$ GM-CSF DCs without infection (NI) and at 6 hpi, with and without bafilomycin A1 treatment. **(B)** The representative histograms show p62 and *Lm* with and without bafilomycin A1. Two-tailed t-test, ***p≤0.001, ** p≤0.01, * p≤0.05, ns>0.05 non-significant; n=6.

Confocal fluorescence analysis of *Lm*-infected DCs revealed increased levels of p62 in *Hdac6*$^{-/-}$ GM-CSF DCs (**Figure 4.23**). *Hdac6*$^{-/-}$ DCs also showed a higher percentage of p62-*Lm* co-localization than *Hdac6*$^{+/+}$ cells, indicating that *Hdac6*$^{-/-}$ cells have higher number of phagosome-contained bacteria (**Figure 4.23** in accordance with p62 accumulation observed in **Figure 4.20. A** and **Figure 4.22**).

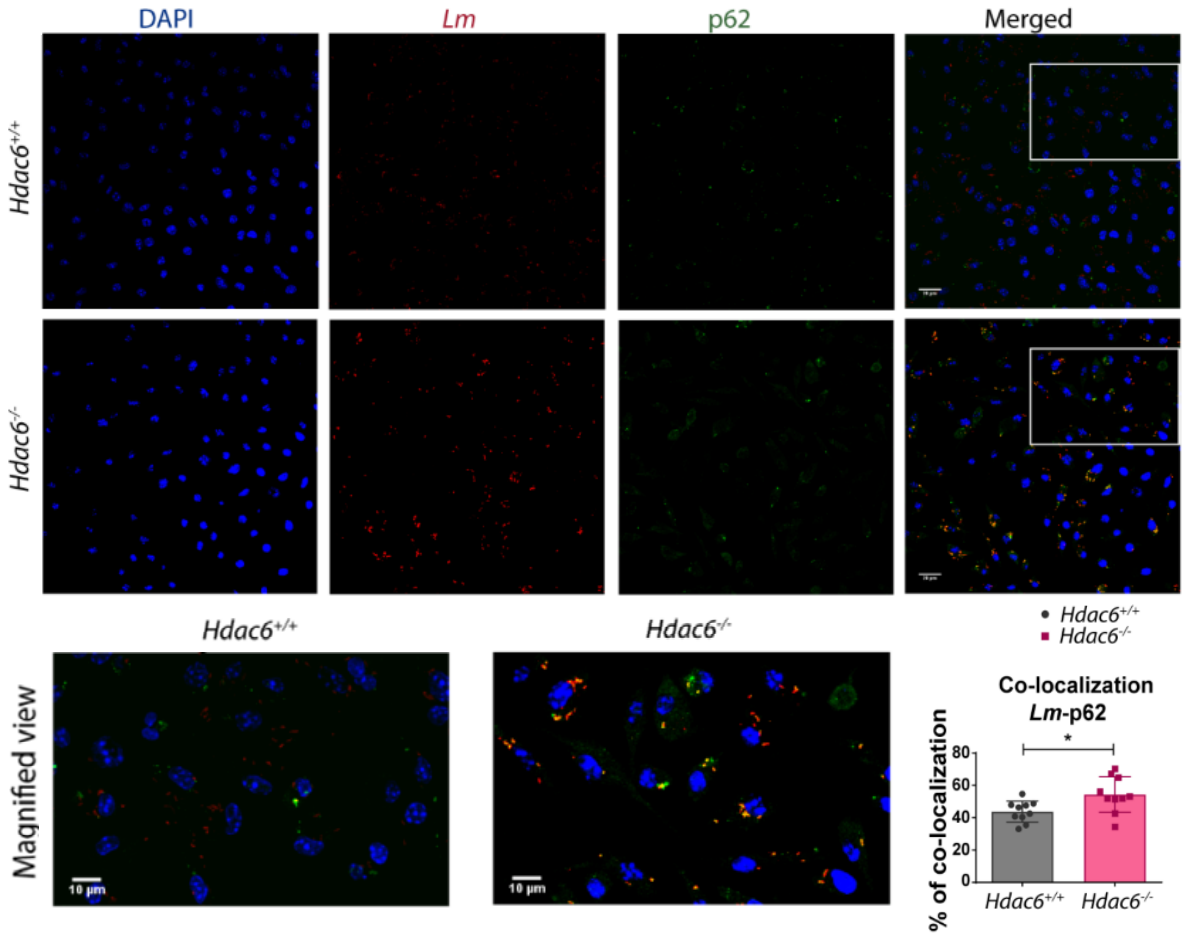

Figure 4.23. Confocal microscopy of the phagosome marker p62 co-localization with *Lm*. Confocal microscopy analysis of p62-*Lm* co-localization in *Lm*-infected *Hdac6*$^{+/+}$and *Hdac6*$^{-/-}$ DCs at 6 hpi. *Left panel:* Panels show DAPI (blue), *Lm* (red), p62 (green), and merged views of the three channels, with magnified views of the boxed areas. Yellow indicates p62-*Lm* co-localization. Scale bars 20 µm (main panels) and 10 µm (magnified views). *Right panel:* The chart shows ImarisCell Module analysis of the number of cells and the number of bacteria per cell in all pictures (10 pictures per genotype). Co-localization percentages were obtained by measuring the p62 channel on the bacterial surface using a threshold of 100. The statistical analysis of Imaris quantifications corresponds to the percentage of p62-*Lm* co-localization at 6 hpi. Two-tailed t-test, *p≤0.05; n=10.

Increase of the autophagosomal marker p62 and the consequent accumulation of post-translational modification K63-linked poly-ubiquitin chains have been reported during impaired phagosome-lysosome fusion. Confocal fluorescence microscopy images of K63-linked poly-ubiquitin chains with *Lm* at 6 hpi reveal a higher accumulation of K63 poly-Ub in *Hdac6*$^{-/-}$ DCs, consistent with a stronger co-localization of bacteria tagged with this post-translational modification (PTM) (**Figure 4.24**).

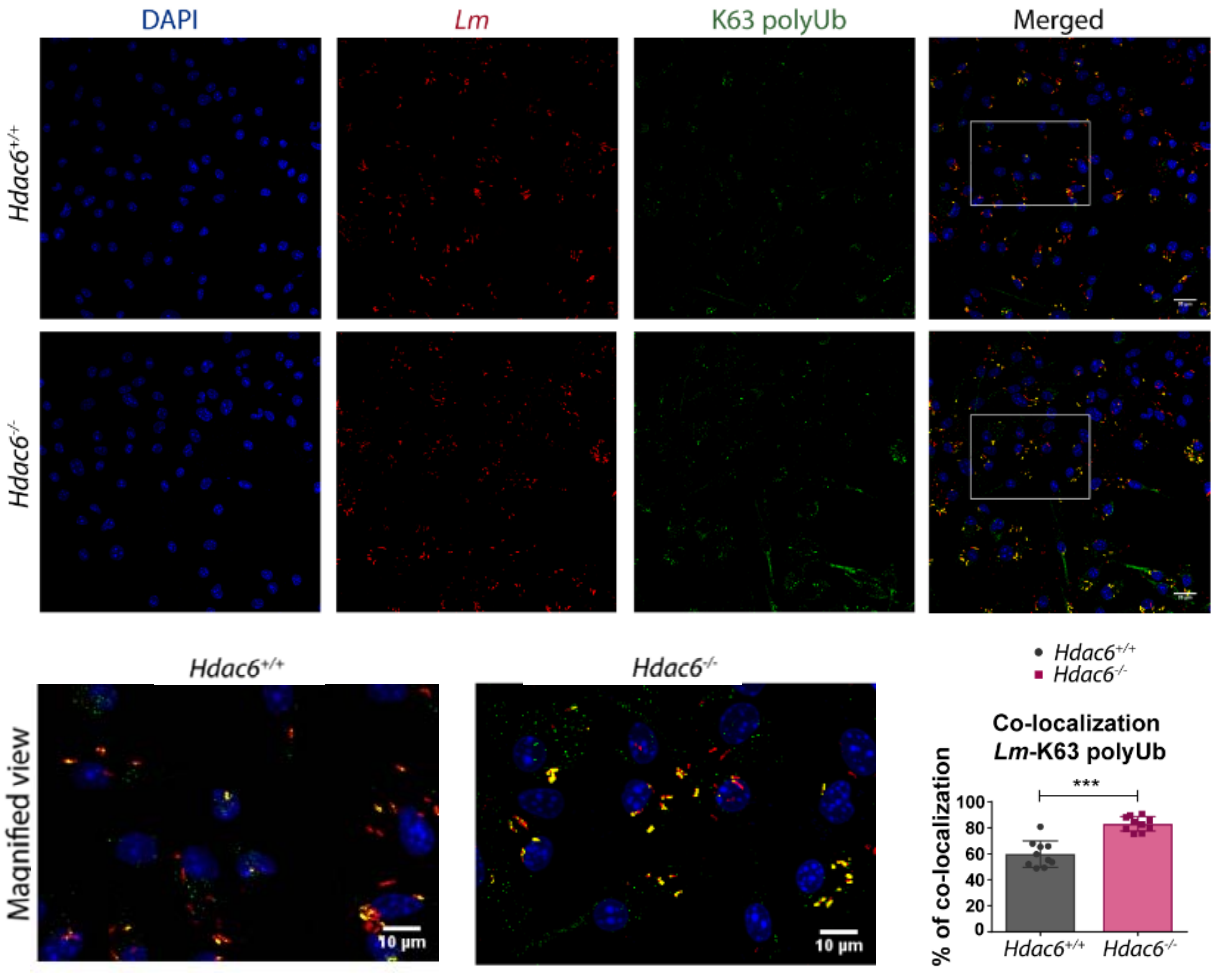

Figure 4.24. Confocal microscopy of K63 poly-ubiquitination co-localization with *Lm*. Maximum intensity z-projections of confocal microscopy images of K63 polyUb-*Lm* co-localization in *Lm*-infected *Hdac6*$^{+/+}$ and *Hdac6*$^{-/-}$ DCs at 6 hpi. *Left panel:* Panels show DAPI (blue), *Lm* (red), K63 polyUb (green), and merged views of the three channels, with magnified views of the boxed areas. Yellow indicates *Lm*-K63 polyUb co-localization. Scale bars 20 µm (main panels) and 10 µm (magnified views). *Right panel:* The chart shows ImarisCell Module analysis of the number of cells and the number of bacteria per cell in all pictures (10 pictures per genotype). Co-localization percentages were obtained by measuring the K63 polyUb channel on the bacterial surface using a threshold of 82. The statistical analysis of Imaris quantifications corresponds to the percentage of K63 polyUb-*Lm* co-localization at 6 hpi. Two-tailed t-test, *** p≤0.001; n=10.

Confocal fluorescence microscopy study of actin and *Lm* revealed more frequent co-localization in *Hdac6*$^{-/-}$ than in *Hdac6*$^{+/+}$ DCs, indicating that more bacteria are at the cytoplasm to form actin rockets in *Hdac6*-deficient cells (**Figure 4.25**).

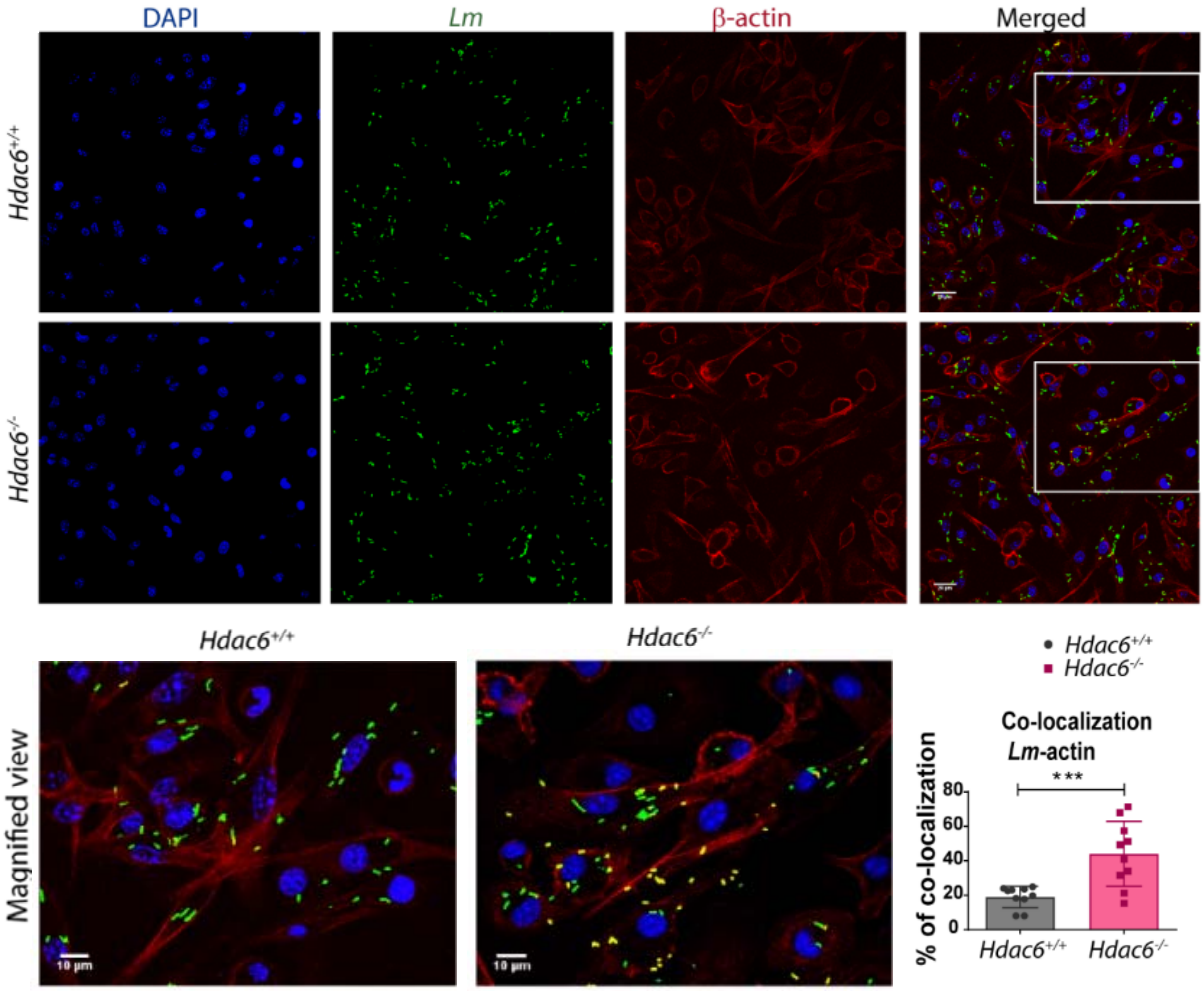

Figure 4.25. Confocal microscopy of β-actin co-localization with *Lm*. Confocal microscopy analysis of actin-*Lm* co-localization in *Lm*-infected *Hdac6*$^{+/+}$ and *Hdac6*$^{-/-}$ DCs at 6 hpi. *Left panel:* Panels show DAPI (blue), *Lm* (green), β-actin (red), and merged views of the three channels, with magnified views of the boxed areas. Yellow indicates *Lm*-β-actin co-localization. Scale bars 20 µm (main panels) and 10 µm (magnified views). *Right panel:* The chart shows ImarisCell Module analysis of the number of cells and the number of bacteria per cell in all pictures (10 pictures per genotype). Co-localization percentages were obtained by measuring the actin channel on the bacterial surface using a threshold of 40.6. The statistical analysis of Imaris quantifications corresponds to the percentage of actin-*Lm* co-localization at 6 hpi. Two-tailed t-test, *** p≤0.001; n=10.

4.1.7. Mechanism by which HDAC6 regulates autophagy of *Lm*

More signal of acetylated-cortactin is detected in *Hdac6*$^{-/-}$ DCs and also higher percentage of acetylated-cortactin-*Lm* co-localization (**Figure 4.26**).

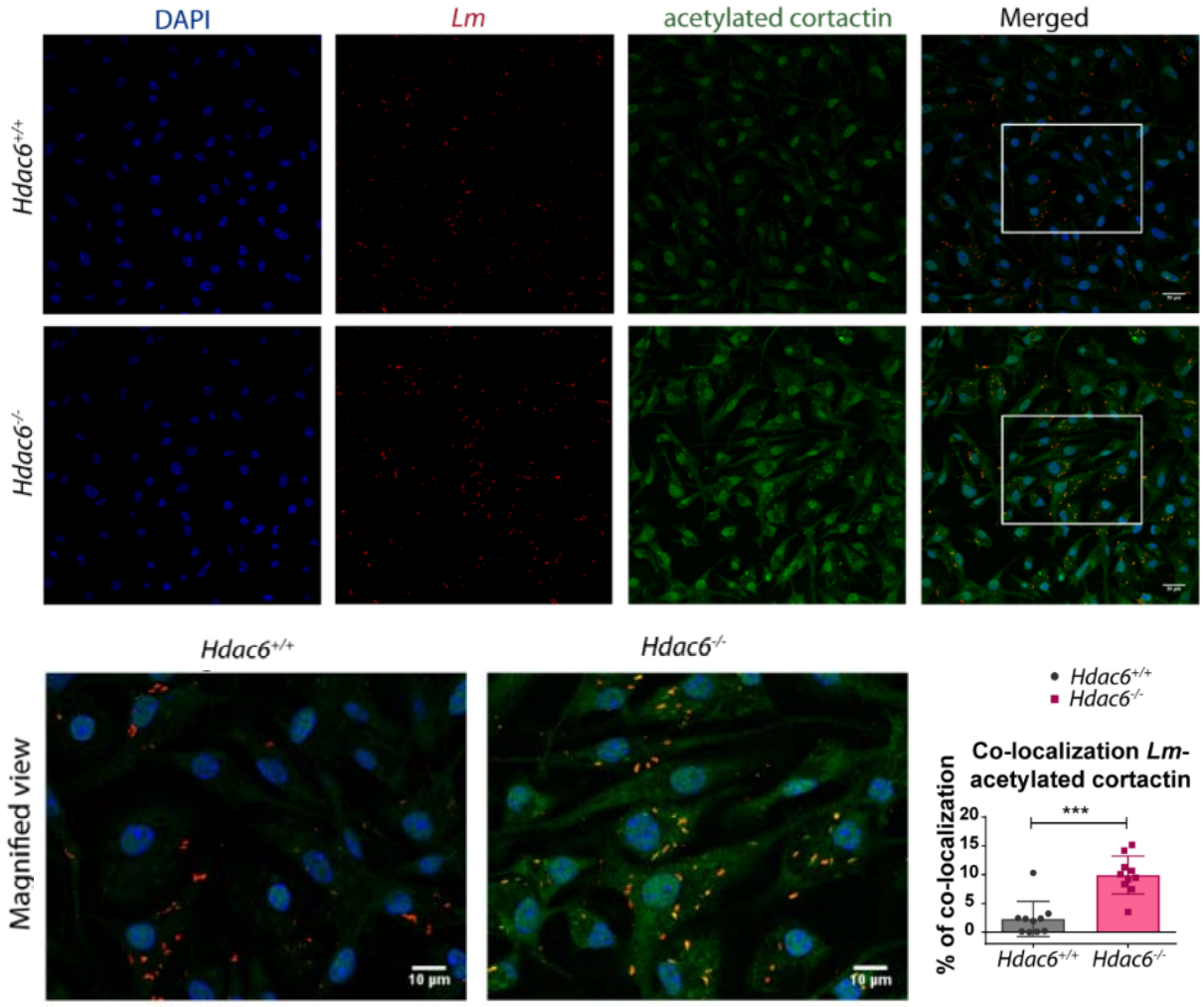

Figure 4.26. Confocal microscopy of acetylated cortactin co-localization with *Lm*. Confocal microscopy analysis of acetylated cortactin-*Lm* co-localization in *Lm*-infected *Hdac6*$^{+/+}$ and *Hdac6*$^{-/-}$ DCs at 6 hpi. *Left panel:* Panels show DAPI (blue), *Lm* (red), acetylated cortactin (green), and merged views of the three channels, with magnified views of the boxed areas. Yellow indicates *Lm*-acetylated cortactin co-localization. Scale bars 20 µm (main panels) and 10 µm (magnified views). *Right panel:* The chart shows ImarisCell Module analysis of the number of cells and the number of bacteria per cell in all pictures (10 pictures per genotype). Co-localization percentages were obtained by measuring the acetylated cortactin channel on the bacterial surface using a threshold of 184. The statistical analysis of Imaris quantifications corresponds to the percentage of acetylated cortactin-*Lm* co-localization at 6 hpi. Two-tailed t-test, *** p≤0.001; n=10.

These data could explain the accumulation of p62 and the delay in phagocytic vesicle fusion observed in *Hdac6*$^{-/-}$ DCs, necessary to degrade phagocytosed *Lm*.

4.2. Study of the role of HDAC6 in the activation of dendritic cell functions by bacterial infection and stimulation of TLRs

4.2.1. Determination of pro-inflammatory genes expression

The effect of HDAC6 on the response of DCs to *Lm* was evaluated by measuring pro-inflammatory cytokine gene induction. The relative mRNA levels of type I interferons (interferons α and β) were lower in *Hdac6*$^{-/-}$ DCs at 6 hpi (**Figure 4.27. A**).

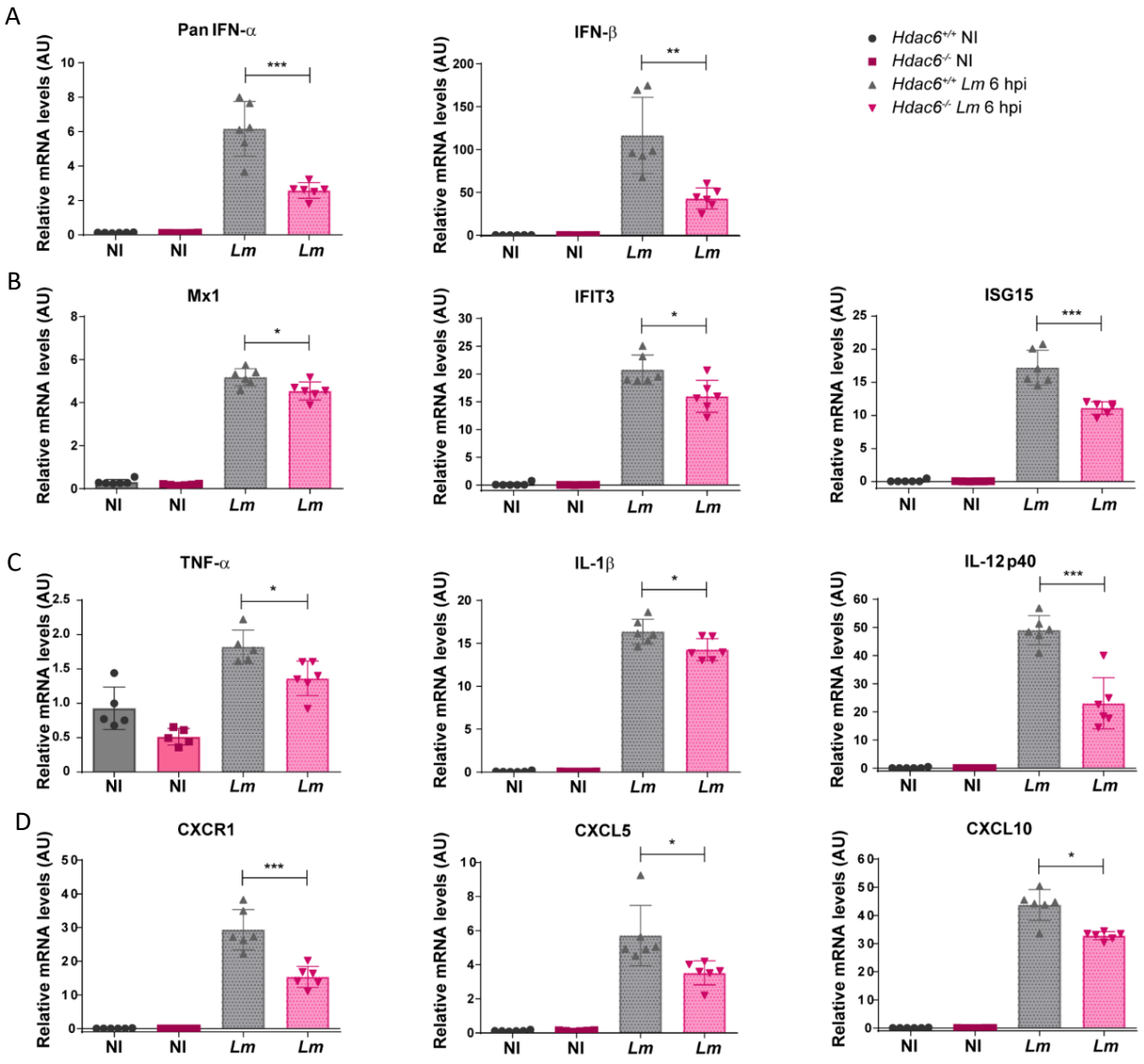

Figure 4.27. Expression of Type I interferons, interferon down-stream proteins, pro-inflammatory cytokines, chemokine receptor and chemokines in DCs after Lm infection at 6 hpi. PCR analysis of **(A)** Type-I interferons (PanIFN-α and IFN-β), **(B)** interferon downstream proteins (Mx1, IFIT3 and ISG15), **(C)** pro-inflammatory cytokines (TNF-α, IL-1β and IL-12p40), **(D)** chemokine receptor (CXCR1) and chemokines (CXCL5 and CXCL10) of *Hdac6*$^{+/+}$ and *Hdac6*$^{-/-}$ DCs non-infected (NI) and infected with *Lm* at 6 hpi (AU: arbitrary units). Two-tailed t-test, ***p≤0.001, ** p≤0.01, * p≤0.05; n=5-6.

Accordingly, expression of downstream interferon-response genes such as Mx1, IFN-induced protein with tetratricopeptide repeats 3 (IFIT3), and ISG15 was also lower in *Hdac6*$^{-/-}$ DCs (**Figure 4.27. B**). Lack of HDAC6 also decreased the relative mRNA levels of the pro-inflammatory cytokines TNFα, IL-1β and IL12p40, indicating impaired cytokine activation after infection (**Figure 4.27. C**). Similarly, *Hdac6*$^{-/-}$ DCs expressed lower levels than their *Hdac6*$^{+/+}$ counterparts of the chemokine receptor CXCR1 and chemokines CXCL5 and CXCL10 (**Figure 4.27. D**). These data demonstrate that *Hdac6*-deficient DCs have a weakened activation response to *Lm* infection at 6 hpi, which suggests a defect in bacterial clearance, consistent with the increased bacterial load in these cells.

4.2.2. Effect of HDAC6 in pro-inflammatory cytokine secretion after *Lm* infection

To confirm these data, we monitored pro-inflammatory cytokines and IFN-β in the supernatants of *Lm*-infected DCs. Early after infection, TNFα, IL-1β, IL-6, IL12p70 and IFN-β levels were lower in supernatants from *Hdac6*$^{-/-}$ cells than in those from *Hdac6*$^{+/+}$ cells, and this difference held at 12 and 24 hpi (**Figure 4.28**).

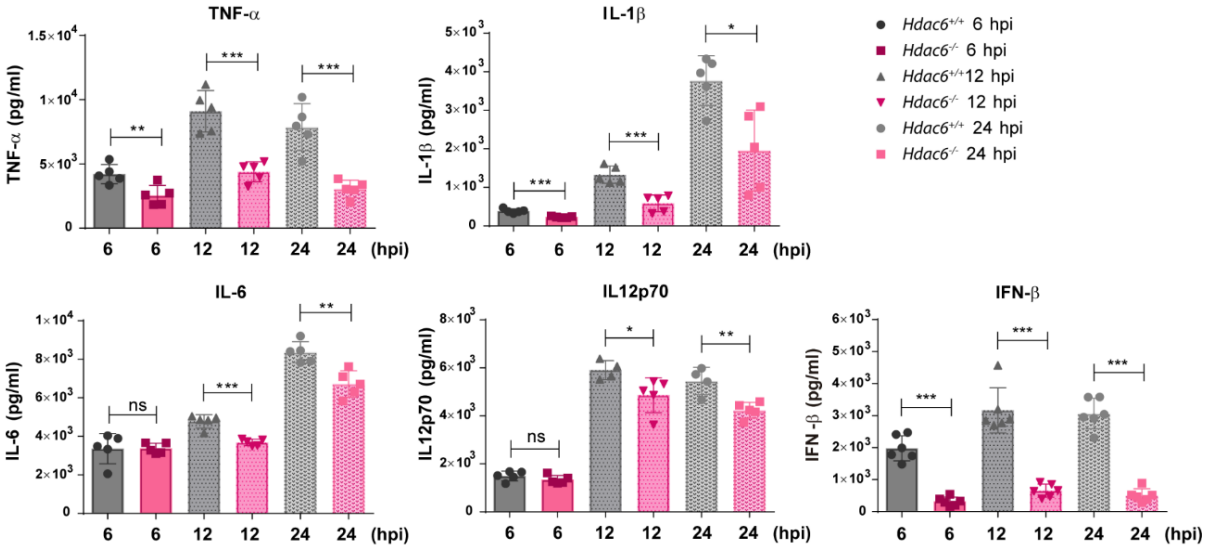

Figure 4.28. Pro-inflammatory cytokines secreted by *Lm*-infected DCs. ELISA analysis of the pro-inflammatory cytokines TNFα, IL1β, IL6 and IL12p70 (pg/ml) and IFN-β in supernatants of *Hdac6*$^{+/+}$ and *Hdac6*$^{-/-}$ DCs at 6, 12 and 24 hpi with *Lm*. Two-tailed t-test, ***p≤0.001, ** p≤0.01, * p≤0.05 ns>0.05 non-significant; n=5-6.

To exclude a defect in cytokine secretion, we compared cytokine levels in supernatants (S) with the levels in supernatants plus their corresponding cell pellets (S+P). Both analyses showed decreased cytokine levels in *Hdac6*$^{-/-}$ cells, indicating an impaired antibacterial response in *Hdac6*-deficient DCs (**Figure 4.29**).

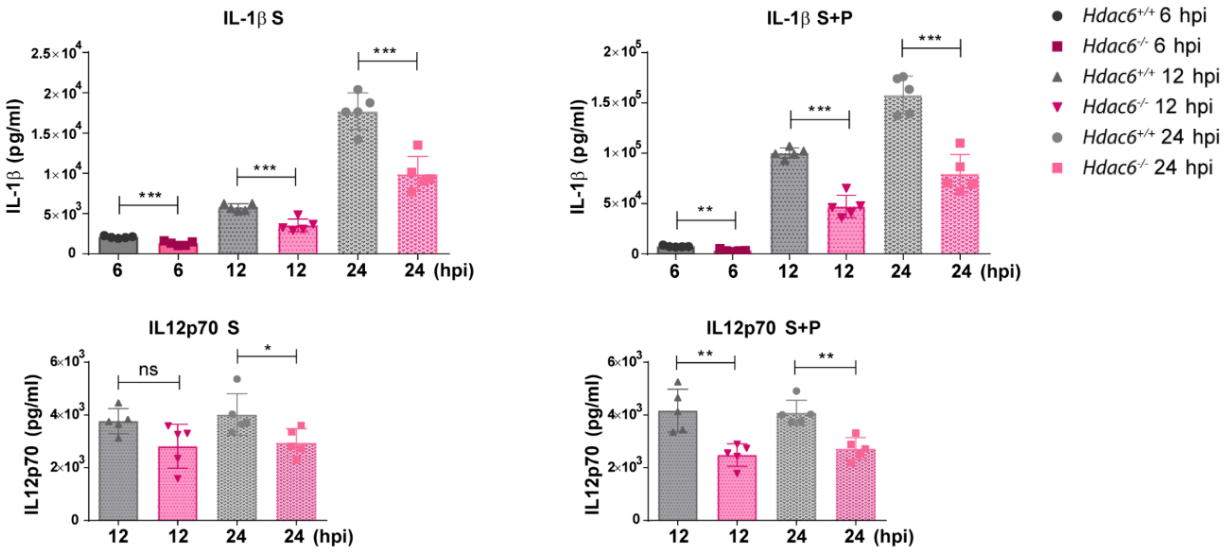

Figure 4.29. Comparison of secreted versus intracellular+secreted pro-inflammatory cytokines. ELISA detection of the pro-inflammatory cytokines IL-1β and IL12p70 (pg/ml) in supernatants (S) and in supernatants plus the corresponding cell pellets (S+P) of *Lm*-infected *Hdac6*$^{+/+}$ and *Hdac6*$^{-/-}$ DCs at 6, 12 and 24 hpi. Two-tailed t-test, ***p≤0.001, ** p≤0.01, * p≤0.05, ns>0.05 non-significant; n=5.

4.2.3. Influence of HDAC6 in the microbicidal activity of iNOS

Measurement of nitrite in supernatants of infected-DCs revealed higher nitric oxide production by *Hdac6*$^{+/+}$ DCs than in *Hdac6*$^{-/-}$ DCs at 24 hpi (**Figure 4.30. A**).

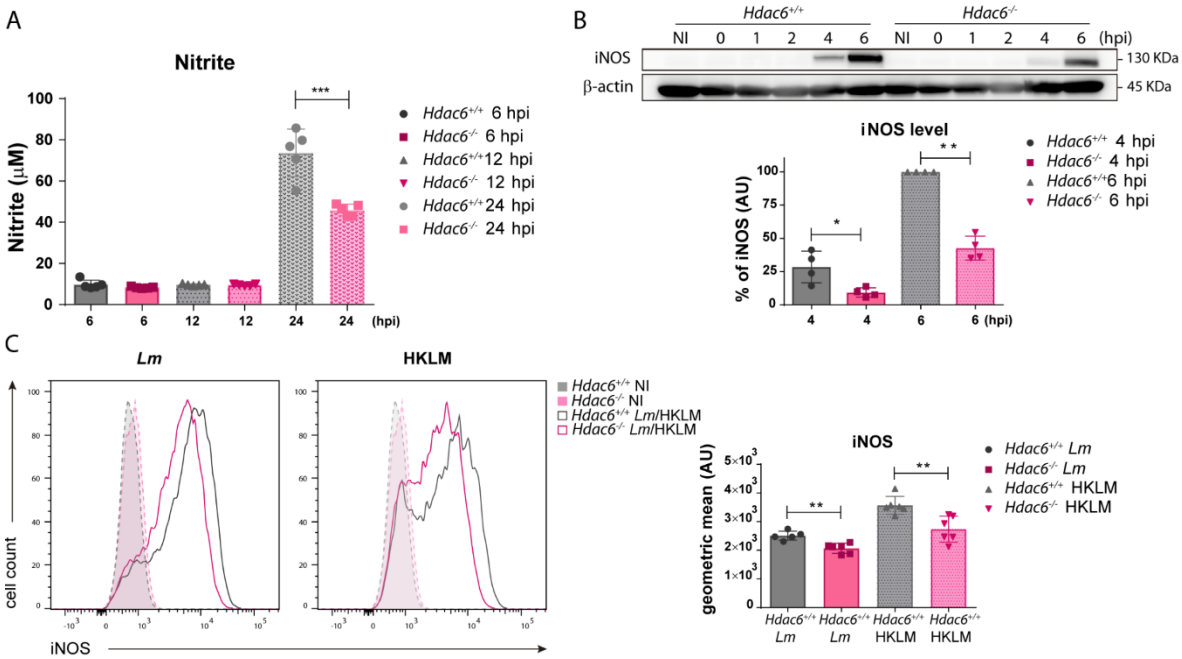

Figure 4.30. *Lm* activated iNOS activity in DCs. (A) Nitrite levels in supernatants of *Lm*-infected DCs at 6, 12 and 24 hpi. Two-tailed t-test, ***p≤0.001; n=5. **(B)** *Top panel:* Western-blot analysis of iNOS over the time-course of infection. β-actin was used as a loading control. *Lower panel:* The chart shows quantification of iNOS at 4 and 6 hpi. Two-tailed t-test, ** p≤0.01, * p≤0.05; n=4 **(C)** *Left:* The panel shows representative histograms of iNOS expressed by *Hdac6*$^{+/+}$ and *Hdac6*$^{-/-}$ DCs after exposure to live *Lm* or HKLM for 24 h (left). *Right:* The chart shows the geometric mean of iNOS expression. Non-infected (NI) DCs were used as a control of iNOS induction. Two-tailed t-test, **p≤0.01; n=6.

In agreement, western blot revealed lower levels of inducible nitric oxide synthase (iNOS) in *Hdac6*$^{-/-}$ DCs at 4 and 6 hpi (**Figure 4.30. B**), indicating a delay of the enzyme induction in *Hdac6*$^{-/-}$ DCs. Likewise, flow cytometry after exposure of DCs to live or heat-killed *Listeria monocytogenes* (HKLM) revealed higher expression of iNOS in *Hdac6*$^{+/+}$ DCs in both cases (**Figure 4.30. C**). These data support the involvement of HDAC6 in the activation of DC-mediated iNOS microbicidal responses to *Lm* infection and in the clearance of this intracellular pathogen.

4.2.4. Study of the expression of MHC co-stimulatory molecules on the membrane

Flow cytometry assay of *Lm* infected-GM-CSF-DCs at 24 hpi showed higher level of expression of membrane CD86 and CD40, both molecules routinely used as markers of co-stimulation of MHC (**Figure 4.31**).

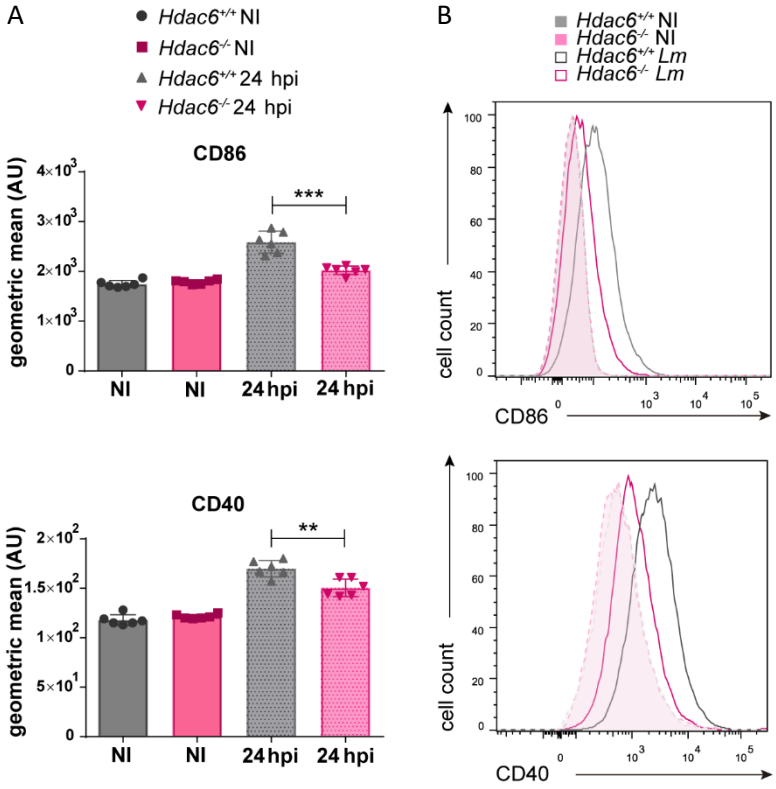

Figure 4.31. CD86 and CD40 membrane expression after *Lm* infection. **(A)** The charts show geometric means of CD86 and CD40 gated in live MHCII^{+}CD11c^{+} population of *Hdac6*$^{+/+}$ and *Hdac6*$^{-/-}$ DCs without infection (NI) and 24 h after exposure to *Lm*. Two-tailed t-test, ***p≤0.001, ** p≤0.01, ns>0.05 non-significant; n=6. **(B)** The representative histograms show CD86 and CD40. Non-infected NI DCs were used as a control of CD86 and CD40 induction.

The MHC-II+CD11c+ population of DCs were gated to check geometric means of CD86 and CD40, and non-significant differences in the percentage of this population were detected between *Hdac6*$^{+/+}$ and *Hdac6*$^{-/-}$ DCs (**Figure 4.32**). However, the MHC-II+CD11c+ population express higher levels of MHC-II and CD11c molecules on the cell surface in *Hdac6*$^{+/+}$ DCs (**Figure 4.32**). These results are in accordance with the observation of iNOS and pro-inflammatory cytokines, supporting the hypothesis of a stronger activation of *Hdac6*$^{+/+}$ DCs after *Lm* infection than *Hdac6*$^{-/-}$ ones.

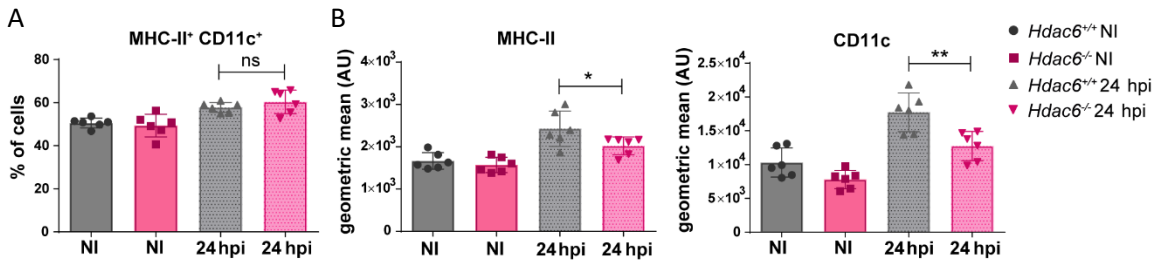

Figure 4.32. MHC-II and CD11c membrane expression after activation of DCs with *Lm* infection. (A)The chart displays the percentage of live cells of *Hdac6*$^{+/+}$ and *Hdac6*$^{-/-}$ DCs gated as MHC-II+CD11c+.Non-infected (NI) and 24 hpi *Lm*-infected conditions were tested. Two-tailed t-test, ns>0.05 non-significant; n=6. **(B)** The charts show geometric means of MHC-II and CD11c gated in live MHCII^{+}CD11c^{+} population of *Hdac6*$^{+/+}$ and *Hdac6*$^{-/-}$ DCs without infection (NI) and 24 h after infection with *Lm*. Two-tailed t-test, ** p≤0.01, * p≤0.05, ns>0.05 non-significant; n=6.

4.2.5. Function of HDAC6 in the activation of MAPK- and mTOR-signalling pathways

The diminished activation response against *Lm* in *Hdac6*$^{-/-}$ DCs is consistent with impaired TLR-related signalling. To investigate this question, we determined the phosphorylation levels of TLR downstream mediators by western blot. Compared with *Hdac6*$^{+/+}$ DCs, *Hdac6*$^{-/-}$ DCs showed weaker phosphorylation signals for ERK and AKT after *Lm* infection (**Figure 4.33. A** and **B**).

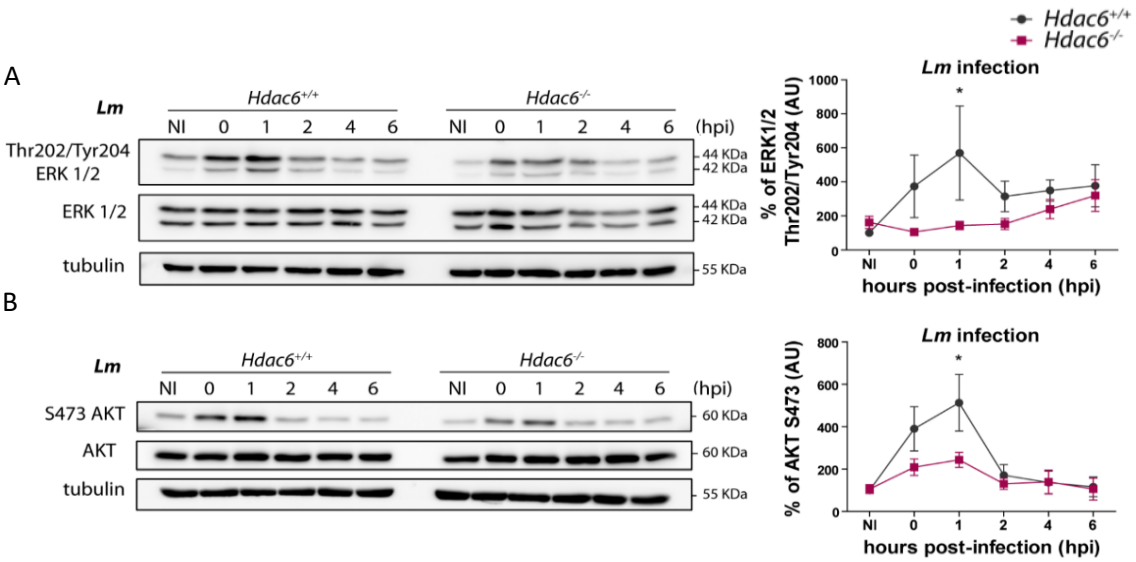

Figure 4.33. MAPK and AKT activation after *Lm* infection. Western-blot analysis of MAPK activation ERK1/2 and AKT over the time-course of *Lm* infection in *Hdac6*$^{+/+}$ and *Hdac6*$^{-/-}$ DCs. *Left:* Total and phosphorylated **(A)** ERK and **(B)** AKT were detected. Tubulin was used as a loading control. *Right:* Accompanying charts show quantification of **(A)** phERK/totalERK and **(B)** phAKT/totalAKT ratios relative to the loading control, ns non-significant; n=7 (right).

We next examined the effect of HDAC6 deficiency on TLR-signalling pathways using other TLR stimuli, including HKLM and LPS. AKT phosphorylation in *Hdac6*$^{-/-}$ DCs was decreased after LPS or HKLM treatment compared to *Hdac6*$^{+/+}$, confirming defective TLR activation (**Figure 4.34. A** and **B**).

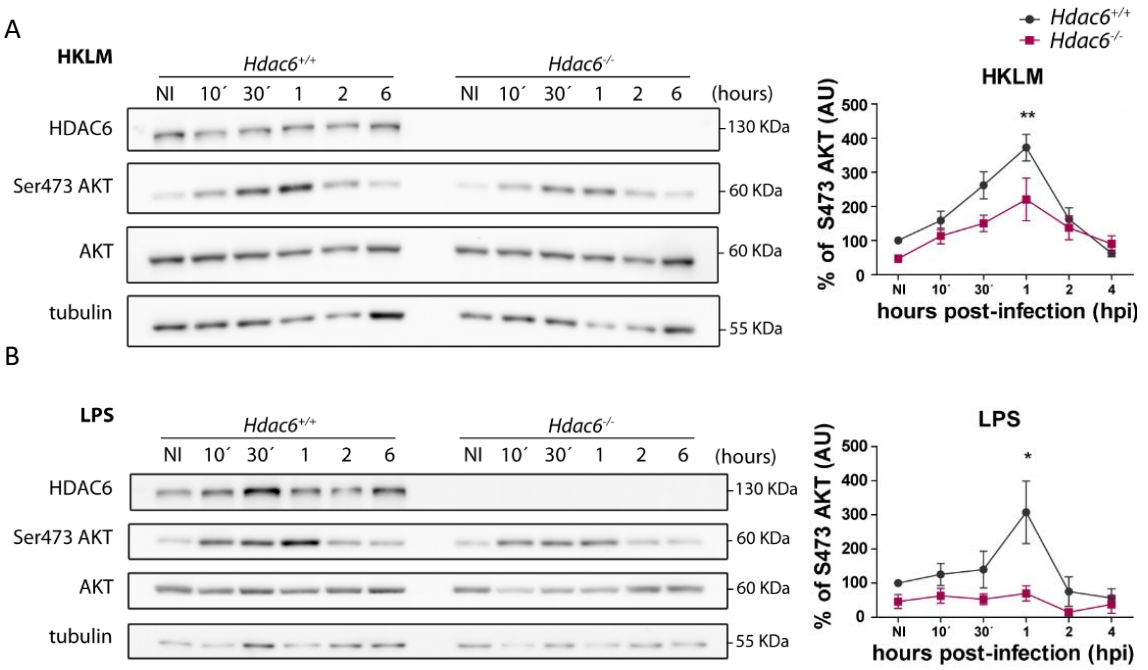

Figure 4.34. Induction of AKT phosphorylation in BMDCs after stimuli with HKLM and LPS. *Left:* Western-blot analysis in *Hdac6*$^{+/+}$ and *Hdac6*$^{-/-}$ DCs over the time-course of **(A)** HKLM or **(B)** LPS treatment. Total and phosphorylated AKT were detected for both treatments. *Right:* Accompanying charts on the right show quantification, indicating the percentage of phAKT/total AKT ratio. Two-tailed t-test, ** p≤0.01, * p≤0.05; n=4.

These effects are not related to a defect in *Lm*-induced transcriptional induction since mRNA levels of different *Lm*-related TLRs (TLR1, 2, and 6) were similar in *Hdac6*$^{+/+}$ and *Hdac6*$^{-/-}$ GM-CSF DCs (**Figure 4.35**).

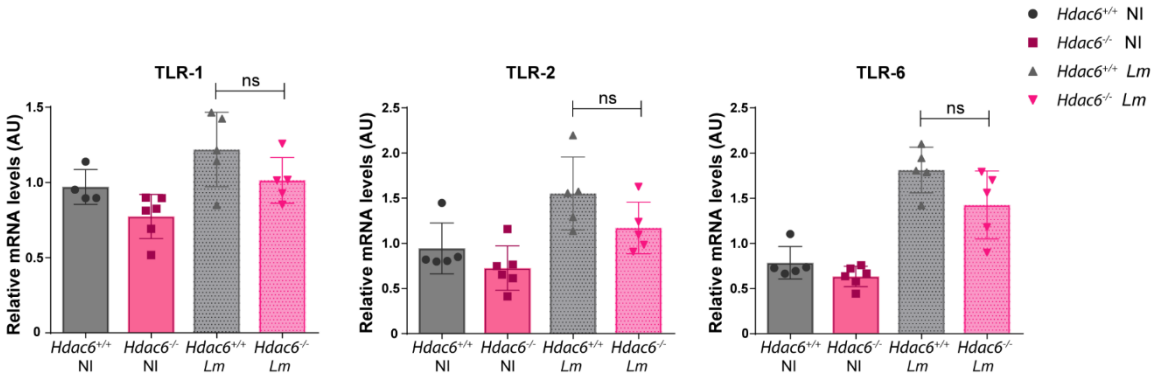

Figure 4.35. mRNA expression of TLRs involved in the detection of *Lm* PAMPs. RT-q-PCR analysis of TLR-1, 2 and 6 (AU: arbitrary units) in *Hdac6*$^{+/+}$ and *Hdac6*$^{-/-}$ DCs non-infected (NI) and after *Lm*-infection at 6 hpi. Two-tailed t-test, ns>0.05 non-significant; n=6.

Moreover, *Hdac6*$^{-/-}$ DCs showed weaker phosphorylation of mammalina target of rapamycin complex 1 (mTORC1) pathway proteins (mTORC1 downstream substrates p70S6K and S6), consistent with a less pronounced pro-inflammatory response after TLR-activation by pathogen-associated molecular patterns (PAMPs) (**Figure 4.36**).

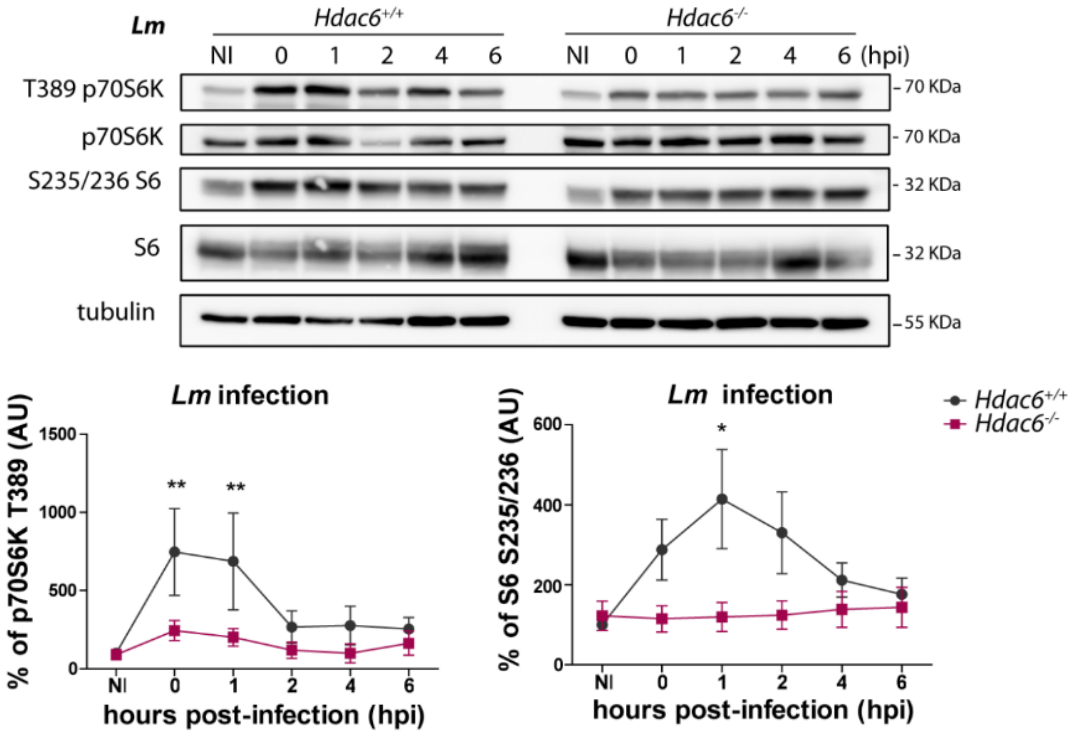

Figure 4.36. mTOR activation after *Lm* infection. *Top panel:* Western-blot analysis of mTORC1 pathway activation over the time-course of *Lm* infection in *Hdac6*$^{+/+}$ and *Hdac6*$^{-/-}$ DCs. Levels of phosphorylated and total p70S6K and S6 were detected. Tubulin was used as a loading control. *Lower panel:* Accompanying charts show quantification of php70S6K/total70S6K (n=5) and phS6/totalS6 (n=7) ratios relative to the loading control. Two-tailed t-test, ** p≤0.01, ns non-significant.

4.2.6. Pro-inflammatory cytokine secretion after stimulation with TLR agonists

To determine whether *Hdac6*$^{-/-}$ DCs showed a similar defective response to other TLR agonists, we first examined secretion of pro-inflammatory cytokines in response to agonists of TLR1-2 (Pam3GSK4), TLR-4 (LPS), TLR-7-9 (Imiquimod), and multiple TLRs (heat-killed *Salmonella* Typhimurium; HKST). *Hdac6*$^{-/-}$ DCs showed a defective cytokine response to these stimuli, determined from the release of TNFα, IL-6, IL-1β and IL12p70 (**Figure 4.37. A-D**).

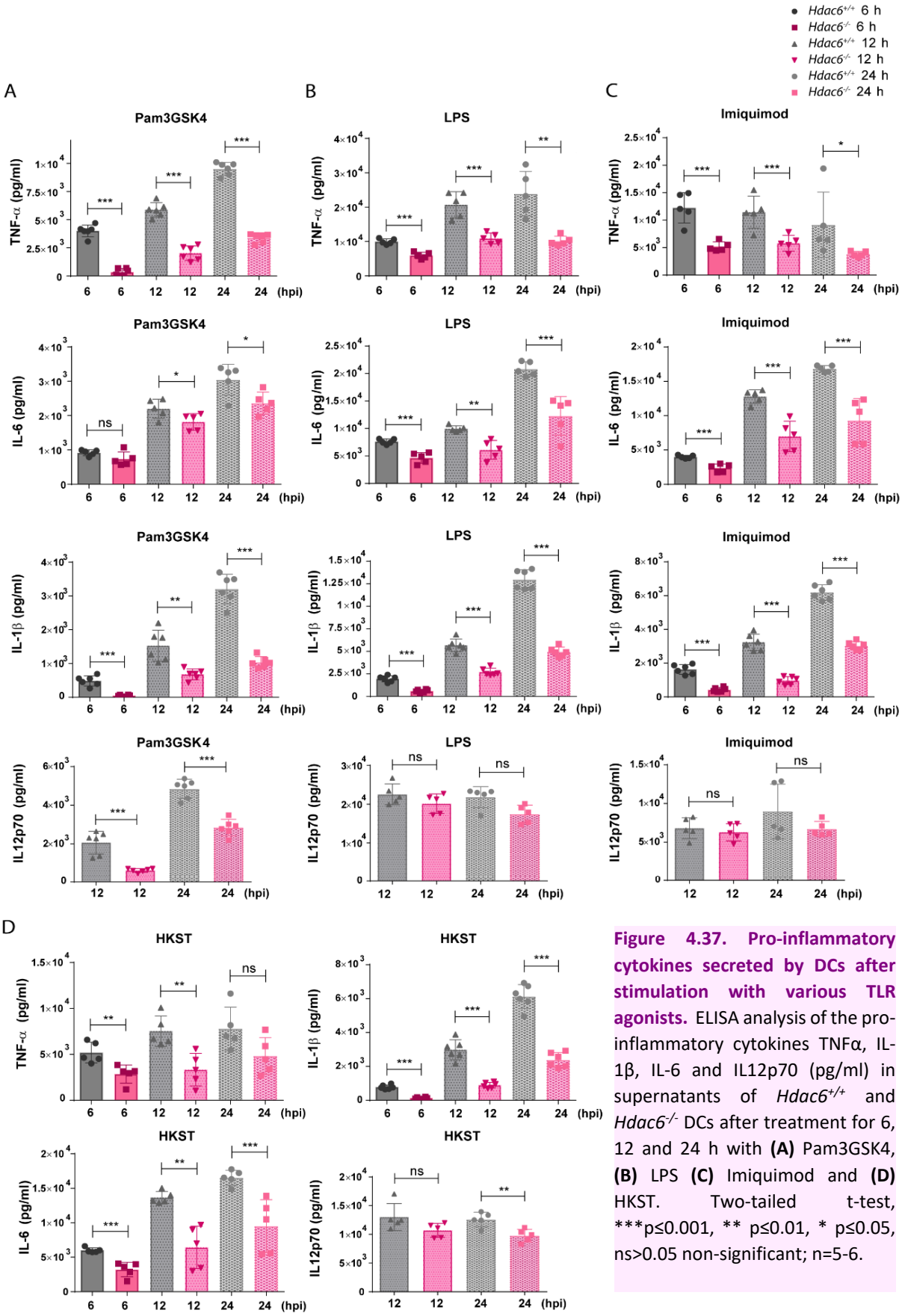

Figure 4.37. Pro-inflammatory cytokines secreted by DCs after stimulation with various TLR agonists. ELISA analysis of the pro-inflammatory cytokines TNFα, IL-1β, IL-6 and IL12p70 (pg/ml) in supernatants of *Hdac6*$^{+/+}$ and *Hdac6*$^{-/-}$ DCs after treatment for 6, 12 and 24 h with **(A)** Pam3GSK4, **(B)** LPS **(C)** Imiquimod and **(D)** HKST. Two-tailed t-test, ***p≤0.001, ** p≤0.01, * p≤0.05, ns>0.05 non-significant; n=5-6.

To assess the pro-inflammatory cytokine response to TLR3 and TLR5 ligands, we generated Fms-related tyrosine kinase 3 ligand-derived dendritic cells (FLT3L-derived DCs). Differentiation with the cytokine FLT3L yielded similar percentages of $CD24^+$ and $CD24^-$ subpopulations ($CD11c^+CD11b^+B220^-CD24^+$ and $CD11c^+CD11b^+B220^-CD24^-$, respectively) from *Hdac6*$^{+/+}$ and *Hdac6*$^{-/-}$ DCs, indicating that differentiation is unaffected by HDAC6 absence (**Figure 4.38**).

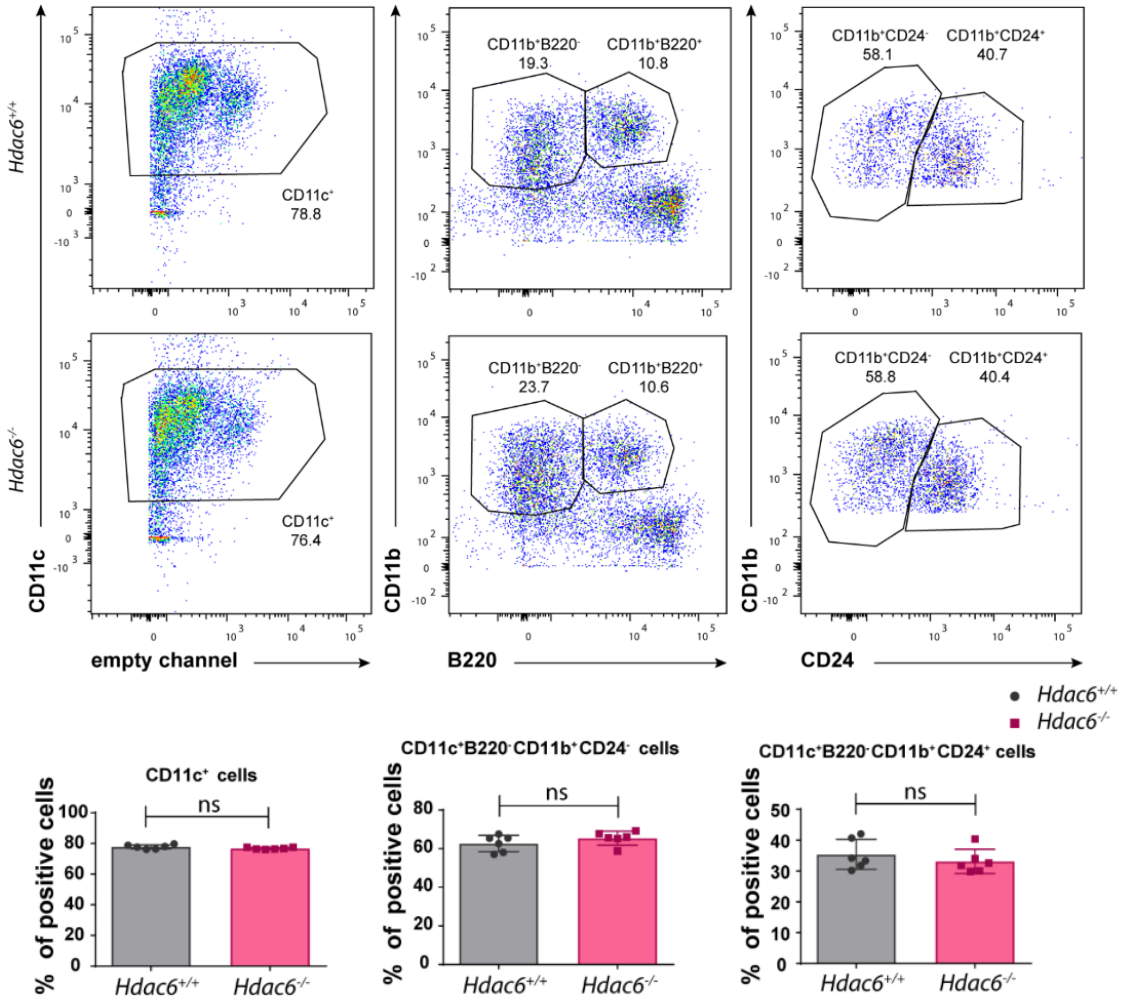

Figure 4.38. Characterization of FLT3L-derived DCs at day 11 of differentiation. *Left:* Dot-plots of FLT3L-derived DC cultures at day 11 of differentiation, showing gating for the CD11c+ population (percentages indicated). *Centre:* Dot-plots showing CD11b versus B220 to select two populations: $CD11c^+CD11b^+B220^+$ (plasmacytoid DCs, pDCs) and $CD11c^+CD11b^+B220^-$ (conventional DCs, cDCs) (percentages indicated). *Right:* Dot-plots showing CD11b versus CD24 to select the $CD11b^+CD24^+$ and $CD11b^+CD24^-$ populations (gated from cDCs) (percentages indicated). The charts on the right show the percentages of $CD11c^+$, $CD11c^+CD11b^+B220^-CD24^-$ and $CD11c^+CD11b^+B220^-CD24^+$ populations. Two-tailed t-test, ns>0.05 non-significant; n=6.

The TLR agonists Pam3GSK4 (TLR1-2), Poly(I:C) (TLR3), LPS (TLR4), flagellin (TLR5), Imiquimod (TLR-7-9), *Lm*, HKLM, and HKST (which activates several TLRs simultaneously) elicited similar cytokine secretion profiles in GM-CSF DCs and FLT3L-DCs (**Figure 4.39. A** and **Figure 4.39. B** compared to **Figure**

4.37. A-D). *Hdac6*$^{-/-}$ DCs of both origins showed an impaired cytokine response to each TLR agonist, indicating that HDAC6 likely regulates a common TLR signalling adaptor.

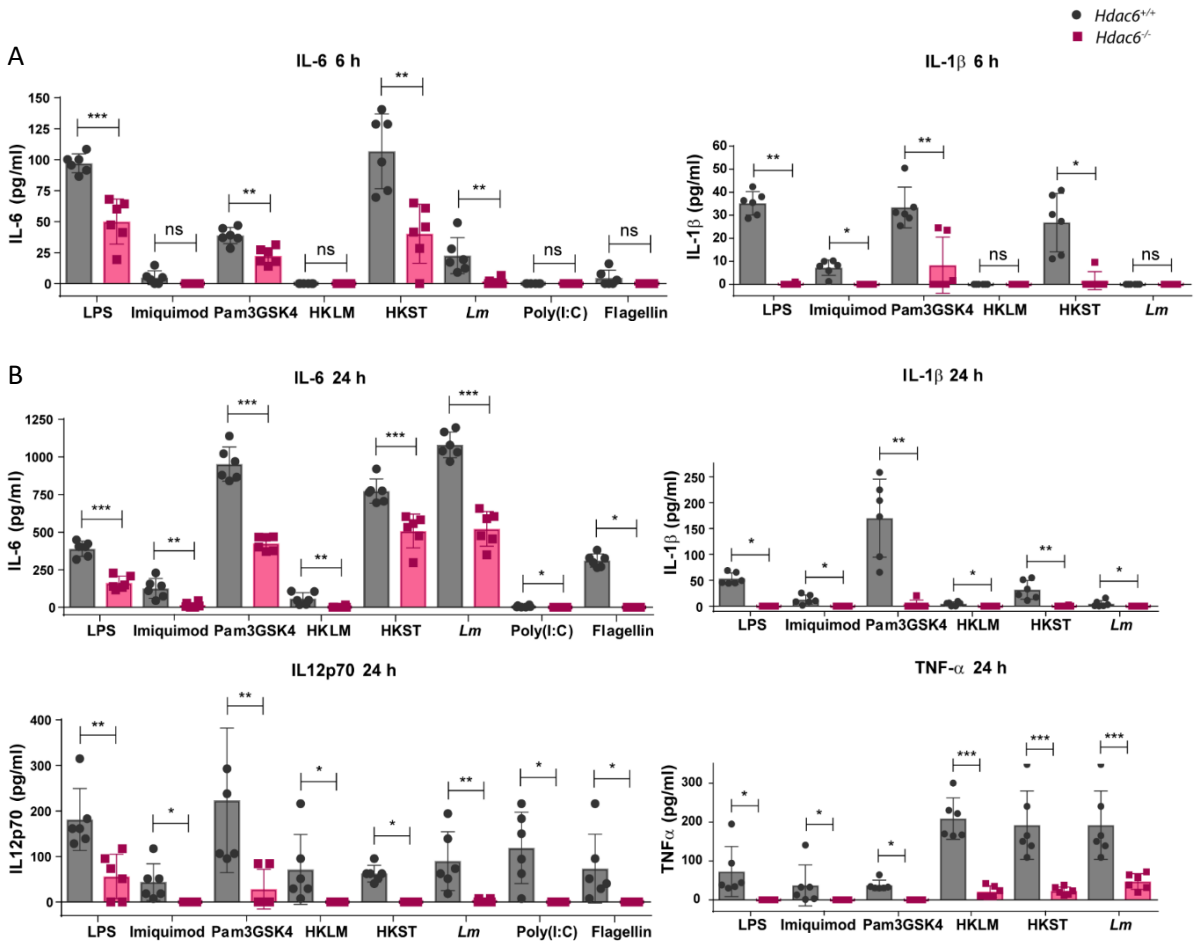

Figure 4.39. Pro-inflammatory cytokines IL-6, IL-1β, IL-12p70 and TNF-α secreted by FLT3L-derived DCs after the stimulation with various TLR agonist. ELISA detection of the pro-inflammatory cytokines IL-6, IL-1β, IL-12p70 and TNF-α (pg/ml) in supernatants of *Hdac6*$^{+/+}$ and *Hdac6*$^{-/-}$ FLT3L-derived DCs activated with LPS, Imiquimod, Pam3GSK4, HKLM, HKST, *Lm*, Poly(I:C) or flagellin for (**A)** 6 h and **(B)** 24 h. Two-tailed t-test, ***p≤0.001, ** p≤0.01, * p≤0.05; n=6.

4.2.7. Consequence of HDAC6 defect in the activation of TLR-signalling pathway

In this view, the TLR adaptor MyD88 participates in the transmission of signals by all TLRs except for TLR3. We decided to study MyD88 levels in a time-course infection with *Lm* by western blot, demonstrating that the quantity of this molecule was the same in *Hdac6*$^{+/+}$ and *Hdac6*$^{-/-}$ DCs and remained stable during infection (**Figure 4.40**).

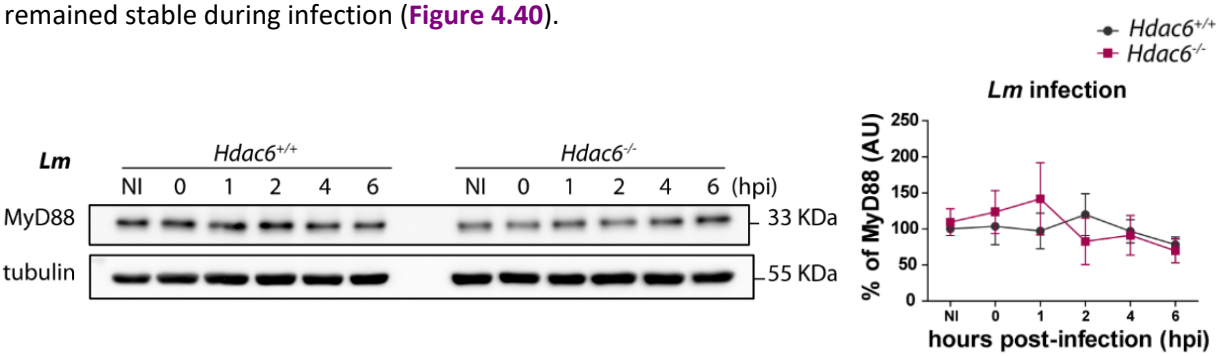

Figure 4.40. Levels of MyD88 adaptor protein during *Lm* infection. *Left:* Western-blot analysis of MyD88 protein level over the time-course of *Lm* infection in *Hdac6*$^{+/+}$ and *Hdac6*$^{-/-}$ DCs. Tubulin was used as a load control. NI correspond to non-infected cells and infected cells are displayed as 0, 1, 2, 4 and 6 hpi. *Right:* Accompanying charts show quantification of the percentage of MyD88. MyD88 levels were normalized with its corresponding tubulin and expressed as percentage in arbitrary units. NI sample is considered as 100% of signal and the rest of samples are relativized to it. Two-tailed t-test, ns non-significant; n=5.

Remarkably, MyD88-HDAC6 molecular association was observed by co-immunoprecipitations of endogenous proteins using human dendritic cells after Pam2GSK4, Pam3GSK4 and HKLM stimulation (**Figure 4.41**).

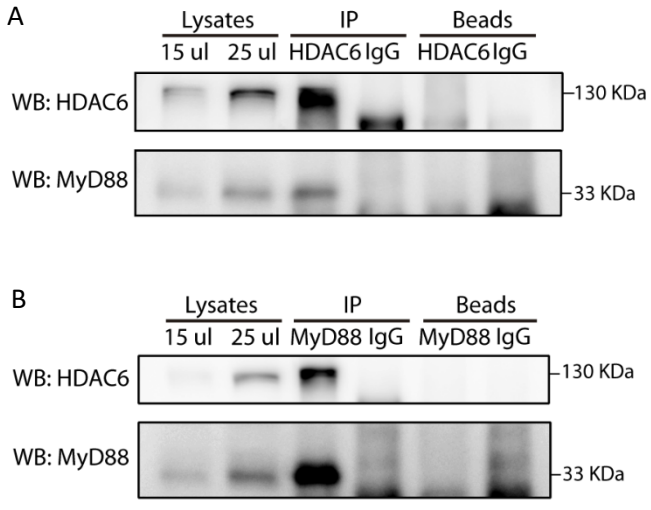

Figure 4.41. Molecular association of HDAC6 with the MyD88 adaptor protein. Immunoprecipitation of endogenous **(A)** HDAC6 and **(B)** MyD88 followed by western-blot for both proteins. Immunoprecipitations were carried out using human moDCs after 30 min of stimulation with Pam2GSK4, Pam3GSK4 and HKLM. Molecular weight of endogenous HDAC6 (130 KDa) and MyD88 (33 KDa) are indicated at the right of western-blot. Similar results were obtained in two independent experiments.

Likewise, the MyD88 immunoprecipitation in *MyD88*- and *HDAC6*-overexpressing HEK cells was also able to co-precipitate HDAC6 (**Figure 4.42**).

A

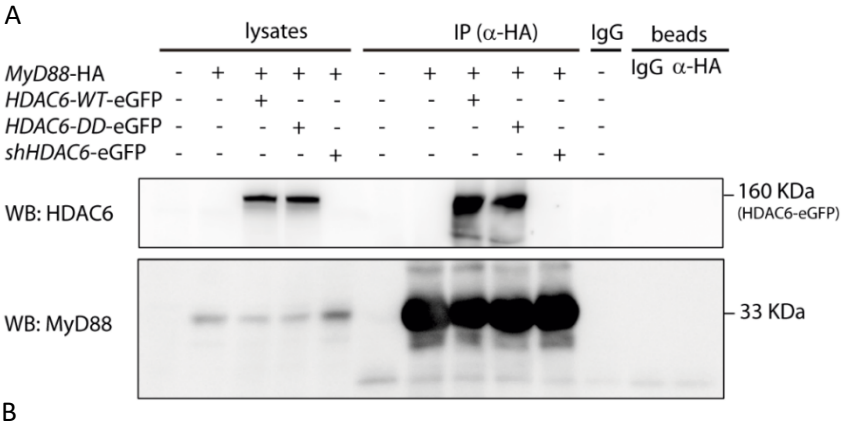

B

IP α-HA	*MyD88*-HA	*MyD88*-HA+ *HDAC6-WT*-eGFP	*MyD88*-HA+ *HDAC6-DD*-eGFP	*MyD88*-HA+ *shHDAC6*-eGFP	Beads + α-HA	Beads + α-IgG
MyD88 peptides	40 (*)	40	40 (*)	54 (*)	13	8
HDAC6 peptides	0	32	30	1	1	0

Figure 4.42. Molecular association of HDAC6 and MyD88 adaptor protein. **(A)** Immunoprecipitation of HA (MyD88) followed by western-blot for HDAC6 and MyD88. Immunoprecipitations were carried out using different *HDAC6-eGFP* plasmids co-transfected with *MyD88-HA* in HEK cell line. Over-expressed (HDAC6-eGFP, 160 kDa) is indicated at right of western-blot. Similar results were obtained in three independent experiments. **(B)** Immunoprecipitation of HA (MyD88) followed by mass spectrometry analysis. Immunoprecipitations were carried out using different *HDAC6-eGFP* plasmids co-transfected with *MyD88-HA* in HEK cell line. The number of unique MyD88 and HDAC6 peptides identified is indicated. **(*)** indicates the presence of acetylated MyD88 peptides. Similar results were obtained in three independent experiments.

These results were corroborated by mass spectrometry analysis of MyD88 immunoprecipitates; which in addition detected two acetylated peptides corresponding to MyD88 (**Figure 4.42. B** and **Figure 4.43**).

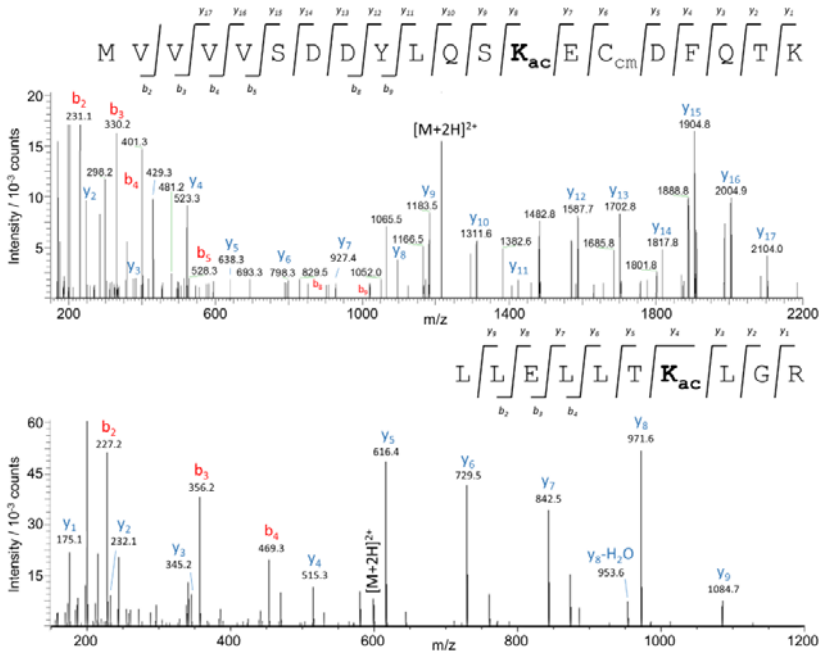

Figure 4.43. Acetylated lysines on MyD88 adaptor protein. MS^2 fragmentation spectra from the peptides showing at 1217.0699 (Top), and 599.3803 (Bottom). Ion adscription to carboxy- (*y* ions, blue) and amino-terminal (*b* ions, red) fragmentation series is indicated. K_{ac} denotes acetylated lysine and C_{cm} indicates carbamidomethylated cysteine. Fragment ion sequence coverage is schematically indicated. Similar results were obtained in three independent experiments.

The same approach was used to determine MyD88-HDAC6 molecular association after TLR-2 activation with HKLM using a constitutively expressed human TLR-2 HEK cell line, rendering the same result (**Figure 4.44**). This association is also maintained using a double-deacetylase domain mutant of HDAC6 (H216A:H611A), called *HDAC6-DD*, indicating that HDAC6-MyD88 interaction is independent of its catalytic activity (**Figure 4.42** and **Figure 4.44**). The knock-down of HDAC6 expression using a small hairpin plasmid (*sh-HDAC6*) blocked this interaction (**Figure 4.42** and **Figure 4.44**).

However, no acetylated peptides could be detected in the mass spectrometry analysis of the MyD88 immunoprecipitation from HKLM-stimulated TLR-2 HEK cell line (**Figure 4.44. B**).

A

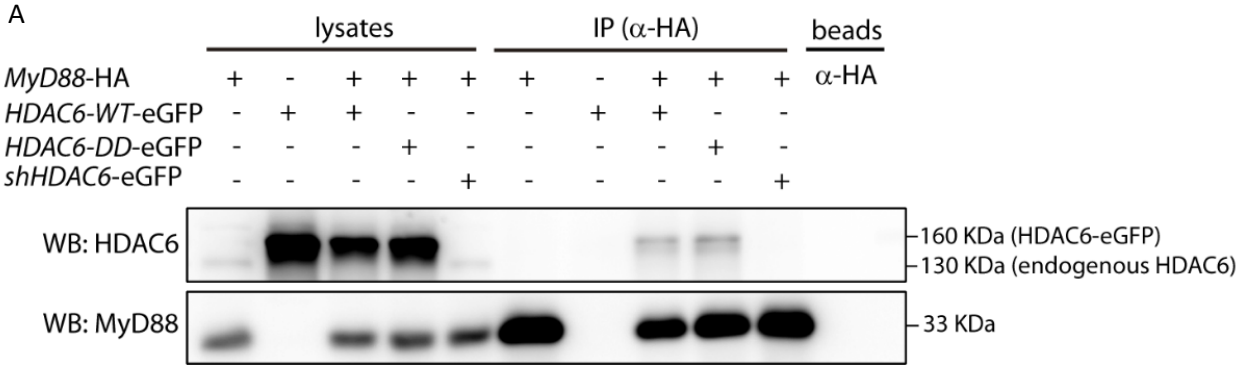

B

IP α-HA	*MyD88*-HA	*HDAC6-WT*-eGFP	*MyD88*-HA+ *HDAC6-WT*-eGFP	*MyD88*-HA+ *HDAC6-DD*-eGFP	*MyD88*-HA+ *shHDAC6*-eGFP	Beads + α-HA	Beads + α-IgG
MyD88 peptides	14	1	22	10	13	0	0
HDAC6 peptides	0	3	13	3	0	0	0

Figure 4.44. Molecular interaction of HDAC6 with the MyD88 adaptor protein. (A) Immunoprecipitation of HA (MyD88) followed by western-blot for HDAC6 and MyD88. Immunoprecipitations were carried out using different *HDAC6-eGFP* plasmids co-transfected with *MyD88-HA* in HEK-Blue hTLR2 cell line after 30 min of stimulation with HKLM. Over-expressed (HDAC6-eGFP, 160 KDa) and endogenous HDAC6 (130 KDa) are indicated at right of western-blot. Similar results were obtained in four independent experiments. **(B)** Immunoprecipitation of HA (MyD88) followed by mass spectrometry analysis. Immunoprecipitations were carried out using different *HDAC6-eGFP* plasmids co-transfected with *MyD88-HA* in HEK-Blue hTLR2 cell line after 30 min of stimulation with HKLM. The number of unique MyD88 and HDAC6 peptides is indicated. No acetylated peptides from MyD88 were detected in any sample. Similar results were obtained in four independent experiments.

Moreover, assessment of Nuclear factor-κB (NF-κB) induction in TLR-2-expressing HEK cells after HKLM, Pam2GSK4 and Pam3GSK4 stimulation shows lower activation only in *shHDAC6* transfected cells, without affecting the activity of *HDAC6-DD*-transfected cells (**Figure 4.45**).

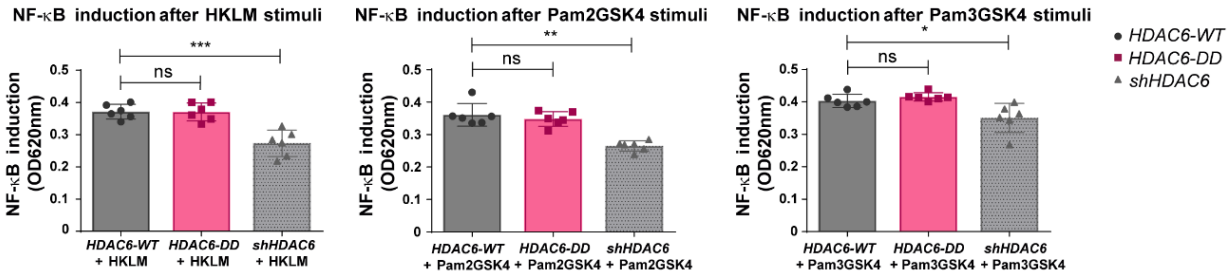

Figure 4.45. NF-κB induction after TLR-2 activation. Graph of NF-κB induction in transfected *HDAC6-WT*, *HDAC6-DD* and *shHDAC6* HEK-Blue hTLR2 cell line after activation with HKLM, Pam2GSK4 and Pam3GSK4 during 8 h. NF-κB induction was calculated by the ratio of the signal of stimulated cells with its corresponding transfected cells in basal condition (without stimuli). Two-tailed t-test, ***p≤0.001, ** p≤0.01, * p≤0.05, ns>0.05 non-significant; n=6.

Taking into account all these data, we concluded that HDAC6 associates with the TLR-adaptor molecule MyD88, and the absence of HDAC6 in DCs seems to diminish the TLR-response after a variety of stimuli, underlining the scaffold role of HDAC6 in determining the ability of MyD88 to mediate TLR signalling.

4.2.8. Evaluation of the HDAC6 role in the *in vivo* TLR-dependent inflammatory response

To ascertain the defective TLR-dependent inflammatory response *in vivo* due to the molecular MyD88-HDAC6 association, *Hdac6*$^{+/+}$ and *Hdac6*$^{-/-}$ mice were intravenously injected with a lethal dose of *Lm* (**Figure 4.46. A**) [150]. A protective effect against *Lm*-induced septic shock was observed from 3 to 10 days post-infection (dpi) (**Figure 4.46. A**). Accordingly, lower levels of the pro-inflammatory cytokine IL-6 were detected in the serum of *Hdac6*$^{-/-}$ mice at 72 hpi, highlighting a reduced systemic cytokine-driven inflammatory response after *Lm* infection in these mice (**Figure 4.46. B**).

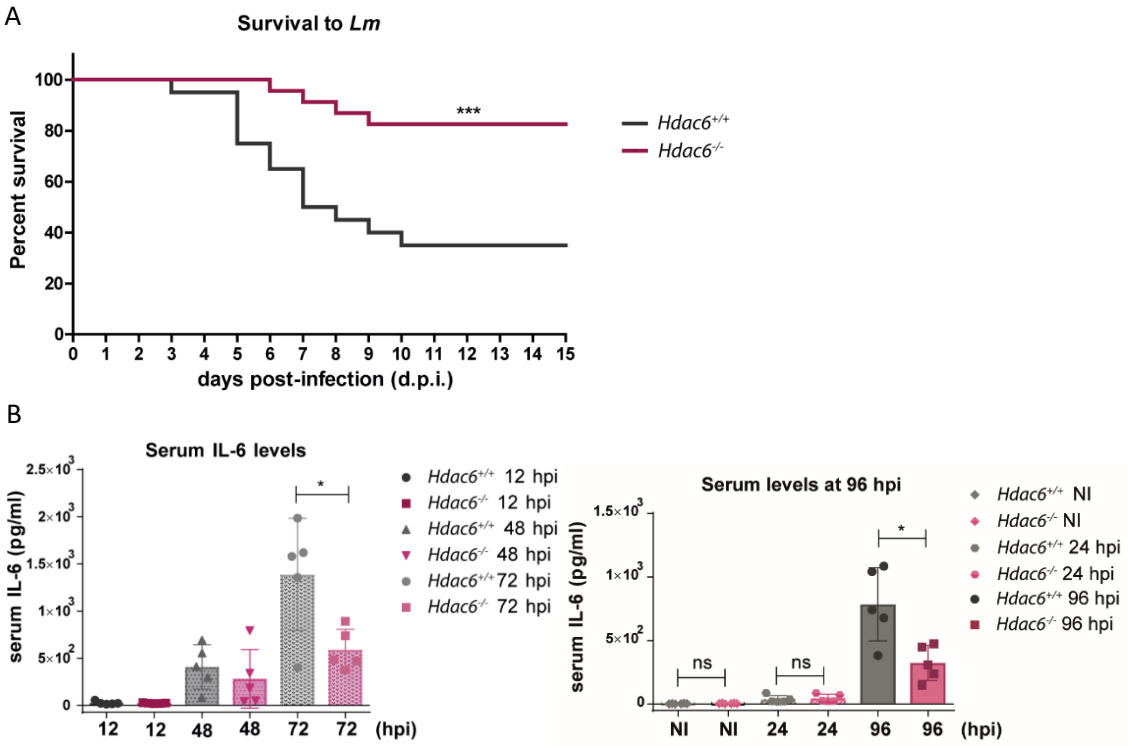

Figure 4.46. Inflammatory response of *Hdac6*$^{-/-}$ mice to *Lm*. **(A)** Survival curve to intravenous injection with a lethal dose of *Lm* in *Hdac6*$^{+/+}$ and *Hdac6*$^{-/-}$ is showed. This curve corresponds to two different experiments of survival to *Lm* with a n=24-21. Long-rank (Mantel-Cox) test and Cehan-Breslow-Wilcoxon test, ***p≤0.001. **(B)** Pro-inflammatory cytokine IL-6 was measured in sera of *Hdac6*$^{+/+}$ and *Hdac6*$^{-/-}$ mice intravenously injected with a lethal dose of *Lm* at 12, 24, 48, 72 and 96 hpi and NI (non-infected). Two-tailed t-test, *p≤0.05, n=5.

No significant differences in spleen and liver bacterial load were found between *Hdac6*$^{+/+}$and *Hdac6*$^{-/-}$ from 12 to 48 hpi (**Figure 4.47**). However, higher bacterial burden was distinguished in target organs of *Lm*-induced septic shock *Hdac6*$^{+/+}$ mice at 72 hpi (**Figure 4.47**). This observation is in accordance with the increased IL-6 level in *Hdac6*$^{+/+}$ mice sera at 72 hpi, suggesting an impairment of the anti-bacterial clearance response in these animals (**Figure 4.47** and compared with **Figure 4.46. B**).

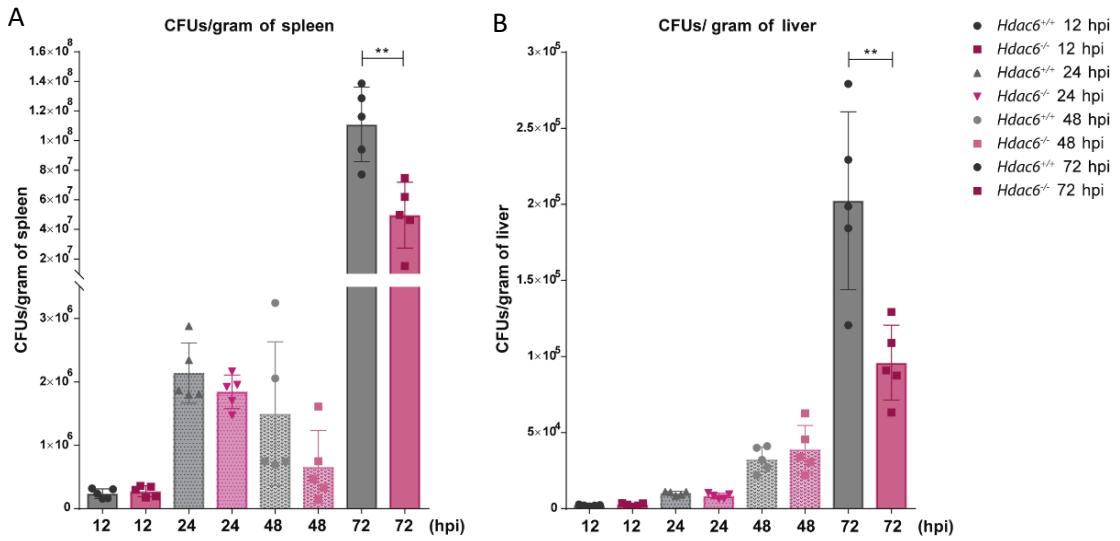

Figure 4.47. Bacterial burden in target organs of *Hdac6*$^{-/-}$ mice. Quantification of bacterial load in target organs, **(A)** spleen and **(B)** liver, at 12, 24, 48 and 72 hpi in *Hdac6*$^{+/+}$ and *Hdac6*$^{-/-}$ mice injected with a lethal dose of *Lm*. Bacterial load is expressed by CFUs per gram of spleen and per gram of liver. Two-tailed t-test, **p≤0.01, n=6.

Discussion

5. DISCUSSION

Here we present evidence suggesting a critical role for HDAC6 in the regulation of innate immune responses. Our results underscore a fundamental role of HDAC6 in almost every step of dendritic cell functions against the intracellular bacteria *Lm*, starting with the control of bacterial degradation by autophagy, cytokine production and regulation of the outcome of anti-bacterial host response. By regulating the fusion of autophagosomes with lysosomes, HDAC6 is able to degrade invading pathogens and reduce bacterial burden, which is critical to efficiently initiate the signalling pathways involved in anti-bacterial response. In addition, our results on the functional regulation of HDAC6 during TLR stimulation of pro-inflammatory cytokine production after *Lm* infection demonstrate the scaffold role of HDAC6 in the TLR-signalling pathway as a MyD88-interacting protein, providing a novel role of HDAC6 in the activation of innate immune responses against intracellular bacteria infection. Finally, we present evidence indicating a major role of HDAC6 in the context of pro-inflammatory cytokine production, which is associated with the exhacerbated inflammatory cytokine storm found during septic shock caused by *Gram*-positive bacteria. These results open a new field for the application of HDAC6 specific inhibitors in septic shock cases to avoid exacerbated inflammation.

5.1. Analysis of HDAC6 contribution to cellular mechanisms that eliminate intracellular bacteria by phagocytic cells

Recent studies have revealed the involvement of HDAC6 in the innate immune response against Influenza Virus A (IVA), Sendai virus (SeV), and vesicular stomatitis virus (VSV) [243,271,15,93]. Given the similarities between the innate responses to viruses and intracellular bacteria, this prompted us to investigate the role of HDAC6 in a model of *Listeria monocytogenes* infection. In this work, we demonstrate a dual role of HDAC6 in the innate response against *Lm*, not only due to its enzymatic activity but also dependent of its function as a scaffold protein (**Figure 5.1** and **Figure 5.3**).

5.1.1. Effect of HDAC6 absence in the intracellular pathogen clearance of dendritic cells

Our results describe an internalization up to 20 bacteria per DC as it has been previously described in phagocytic cells [195]. The significant median bacterial uptake by GM-CSF DCs was observed in cases of 6-7 bacteria per cell, although the distribution of the number of phagocyted bacteria per cell indicates that *Hdac6*$^{-/-}$ DCs display higher *Lm* titres than *Hdac6*$^{+/+}$ DCs independently of the number of bacteria per cell. Our data clearly demonstrate that *Hdac6*$^{-/-}$ DCs have an impaired immune response against *Lm* and *S.* Typhimurium infection *in vitro*. Moreover, higher *Lm* titres observed in *Hdac6*$^{-/-}$ DCs,

M-CSF-derived macrophages and peritoneal macrophages were corroborated during *in vivo Lm* infection at 6 hpi in various myeloid subsets of the spleen, including monocytes, neutrophils, cDCs, and TipDCs. The absence of this effect during DC *in vitro* infection by the non-intracellular bacteria *S. aureus* and *E. coli* DH5α indicates that *Hdac6*$^{-/-}$ DCs are specifically unable to efficiently clear intracellular pathogens.

5.1.2. Evaluation of cellular clearance mechanisms of *Lm*

Intracellular pathogens have developed specialized tools to evade cellular clearance mechanisms. For instance, *S.* Typhimurium uses a type-III secretion system to escape form *Salmonella*-containing vacuoles (SCVs), whereas *Lm* uses the pore-forming enzyem LLO and two phospholypases, PlcA and PlcB, to reach the host cell cytosol.

Additionaly, HDAC6 is involved in two of the most important cellular clearance systems, autophagy and ubiquitin-proteasome pathway (UPP) [127,186]. In the case of *Lm* and *S.* Typhimurium, the main molecular mechanism for degradation of vesicle-contained bacteria is fusion with lysosomes in a process called autophagy [205,197,24]. In agreement with this, our data show that impaired phagosome-lysosome fusion underlies the phenotype observed in *Hdac6*$^{-/-}$ DCs.

It has been previously reported that unsuccessful phago-lysosomal fusion depends on acetylated-cortactin in *Hdac6*-deficient cells [127]. This mechanism was first described in *Hdac6*-deficient mouse embryonic fibroblasts (MEFs) during quality-control autophagy [127]. Quality-control autophagy is a selective autophagy as well as the specific autophagy of *Lm* that we have observed in this work, which is commonly known as xenophagy. We demonstrate here that in *Hdac6*$^{-/-}$ DCs co-localize higher levels of acetylated-cortactin with intracellular *Lm.* The delay in vesicle fusion caused by the acetylation of cortactin, impairs the phagosome-lysosome fusion and provides more opportunities for phagosome-containing bacteria to escape to the cytosol, resulting in the higher bacterial load detected in *Hdac6*$^{-/-}$ DCs. Based on this experimental evidence, it is conceivable to postulate that the enzymatic activity of HDAC6 on its substrate cortactin controls autophagy of intracellular bacteria for their efficient clearance (**Figure 5.1 part 1** and **Figure 5.3 part 1**). Hence, *Hdac6*$^{-/-}$ DCs displays higher levels of acetylated cortactin and consequently more *Lm* burden.

5.1.3. Consequence of the lack of HDAC6 in the autophagy of *Lm*

Pharmacological autophagy inhibitors erased the observed differences between *Hdac6*$^{+/+}$ and *Hdac6*$^{-/-}$ DCs, remarking the impaired autophagy detected in *Hdac6*$^{-/-}$ DCs. Conversely, rapamycin did not overcome the *Hdac6*$^{-/-}$ autophagy defect. Rapamycin inhibits mTOR activity, causing an increment of the autophagic flux. Increased p62 levels were observed after rapamicyn treatment, although *Hdac6*$^{-}$

$^{/-}$ DCs accumulated higher p62 levels at 6 hpi compared to *Hdac6*$^{+/+}$ DCs, indicating a defect in the last step of the autophagy, the phagosome-lysosome fusion. Accordingly, similar results were obtained after the treatment with inhibitors of acidification of lysosomal enzymes, such as NH_4Cl and cloroquine, further sopporting this observation. However, other authors have reported opposite observations using pan-HDAC inhibitors (HDACi) or specific inhibitors of HDAC6 (HDAC6i) during infection of human macrophages with the *Gram*-negative intracellular pathogens *S.* Typhimurium and *E. coli* [5]. These inhibitors, when added at the time of infection, increase mitochondrial ROS production [5]. Overnight pre-treatment with HDACi before infection hampers bacterial clearance and reduces phagocytosis [5]. These data indicate that specific HDAC6 chemical inhibitors can have side-effects, including effects on other HDAC members, potentially interfering with the acetylation of other substrates upstream of cortactin that also have a role during bacterial infection. We have not observed any significant difference during bacterial entry between *Hdac6*$^{-/-}$ and *Hdac6*$^{-/-}$ DCs. Results obtained after overnight pre-treatment with HDAC6i in phagocytosis indicate additional acetylations on cytoskeleton proteins that do not occur in *Hdac6*$^{-/-}$ DCs. Hence, our genetic approach unequivocally assigns a specific role to HDAC6 in innate cells during bacterial infection.

5.1.4. Effect of HDAC6 absence in the accumulation of autophagy marker p62

Although we observed an impairment in phagosome-lysosome fusion, we cannot rule out an involvement of HDAC6 in the anti-microbial response through its BUZ domain, with a contribution from ubiquitin. The characterized interaction between p62 and HDAC6 through their ubiquitin-binding domains provides a clue about the possible role of ubiquitin in the activation of innate immunity through the recognition of ubiquitinated-molecules [262]. For example, the ubiquitin-binding regions of HDAC6 and p62 are both essential for MyD88 aggregation and the downstream activation of MyD88-dependent signal transduction [97]. Furthermore, ubiquitin-binding platforms formed by HDAC6 and p62 are able to interact with interferon stimulated gene 15 (ISG15) to eliminate ISGylated proteins tagged after interferon stimulation by autophagy [166]. These ubiquitin-binding platforms also bind protein aggregates tagged by lysine 63 (K63)-linked polyubiquitin (polyUb) chains and degrade them by autophagy. HDAC6 is able to bind to either mono- and poly-Ub proteins, but shows a preference for proteins modified with K63-linked polyUb chains, which share structural similarities with ISG15 [180,179]. *S.* Typhimurium is decorated with this kind of ubiquitin topology for recognition by host cells, and can be recovered with phagosome proteins to initiate autophagy [210]. Nevertheless, we were not able to detect K63 polyUb signal at early times of infection in our *Lm*-infected DC samples (data not shown). Consequently, our data demonstrate that autophagy induction does not differ between *Hdac6*$^{+/+}$ and *Hdac6*$^{-/-}$ DCs, indicating that this phenotype is due to p62 accumulation in

Hdac6$^{-/-}$ BMDCs as a consequence of impaired phagosome-lysosome fusion. Intact autophagy activation in *Hdac6*$^{-/-}$ DCs could be explained by compensatory p62 binding to ubiquitinated bacteria in the absence of HDAC6. However, higher K63 polyUb signal detected in in *Hdac6*$^{-/-}$ DCs at late time of infection (about 6 hpi) is clearly in accordance with the observation of higher p62 levels co-localizing with *Lm* in these DCs. Besides, it has been previously reported that an impaired autophagy results in the accumulation of the p62 autophagy adaptor and the subsequent increased amount of polyUb proteins. Together, these data indicates that HDAC6-deficient cells display an altered accumulation of p62 and K63 polyUb proteins due to the impared phago-lysosomal fusion.

5.2. Study of the role of HDAC6 in the activation of dendritic cell functions by bacterial infection and stimulation of TLRs

Our data also underscore another different function of HDAC6 in the innate immune response to intracellular bacteria and various TLR stimuli, independent of its enzymatic activity on cortactin (**Figure 5.1** and **Figure 5.3**). Upon infection, the activation of pro-inflammatory responses to alert immune system cells is an essential step for the elimination of intracellular pathogens.

5.2.1. Impaired inflammatory response

We provide evidence for a dampened inflammatory response in the absence of HDAC6, as shown by lower RNA levels of pro-inflammatory cytokines, chemokines, type-I interferons, and interferon-related proteins in *Hdac6*$^{-/-}$ DCs than in *Hdac6*$^{+/+}$ cells at 6 hpi, as well as the lower pro-inflammatory cytokine production of IL-1β, IL-6, IL-12p70 and TNF-α by *Lm* infected *Hdac6*$^{-/-}$ DCs from 6 to 24 hpi. This global diminished production of pro-inflammatory cytokines could reflect a defect in the TLR-signalling pathway.

Whole pathogens and their constituents contain Pathogen-asssociated molecular patterns (PAMPs) that activate TLRs, NLRs and other cytosolic receptors in host cells [108,162]. These receptors recognize general molecular patterns of microbes to rapidly activate the immune response. Upon *Lm* entry, heterodimers of TLR-2/6 and TLR-1/2 recognize respectively di-acyl- and tri-acyl-lipopeptides of *Lm*. Then, a receptor-signalling complex is triggered upon TLR activation where signalling proteins are modified by PTMs such as phosphorylation and ubiquitinaiton [234,198]. Both are reversible PTMs that allow transient protein-protein interactions occurring during signal transduction.

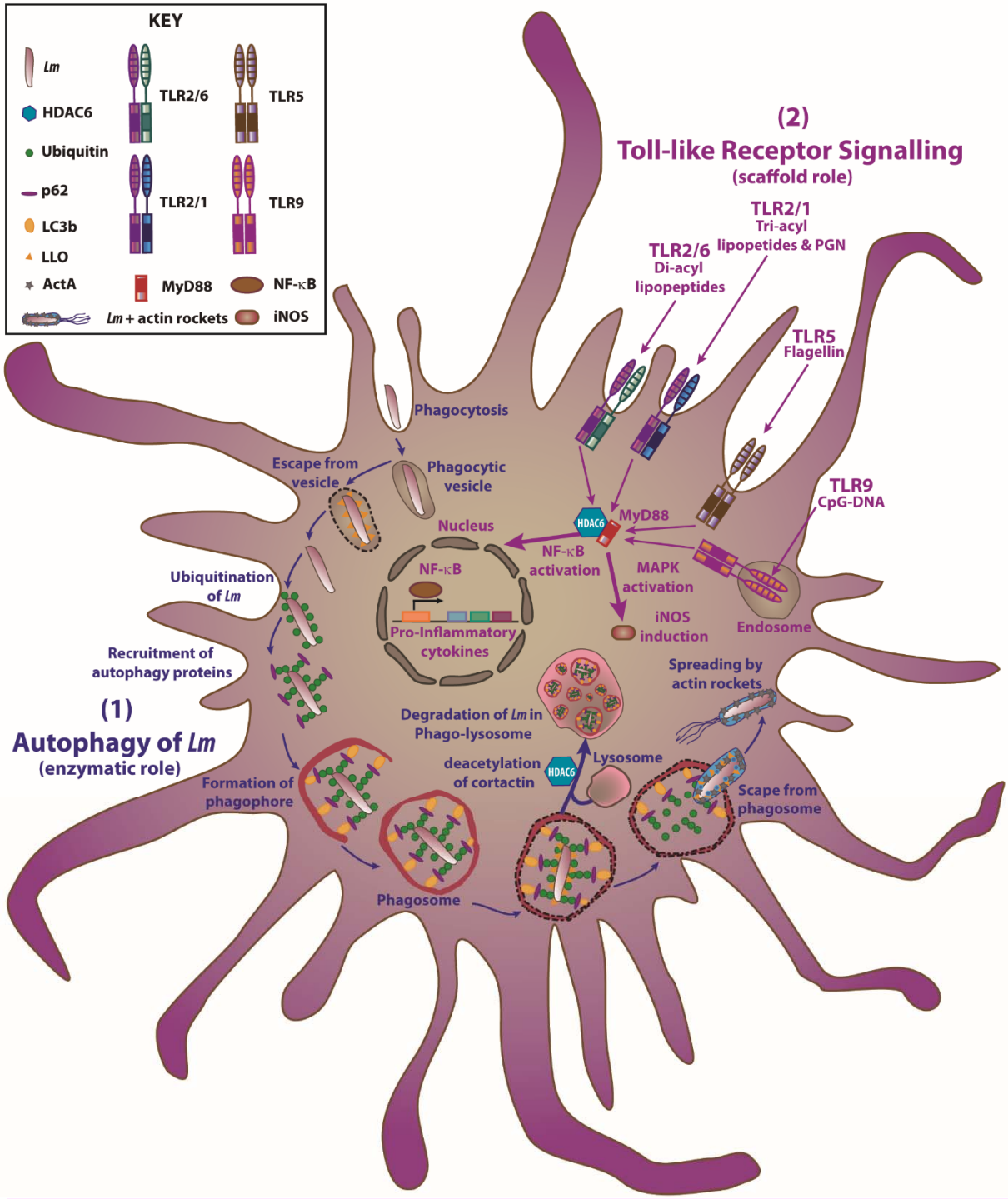

Figure 5.1. Dual role of HDAC6 during *Lm* infection in DCs. The figure shows two HDAC6 functions in *Lm*-infected DCs, the autophagy and the TLR signalling. **(1)** Autophagy: The deacetylation of cortactin by HDAC6 allows the correct phago-lysosomal fusion and the subsequent clearance of *Lm*. However, this bacterium is able to avoid autophagic degradation by the expression of LLO protein. Besides, *Lm* spread through the cytosol using ActA protein to polymerize cell host actin. **(2)** TLR-signalling pathway: Di- and tri-acyl lipopeptides and peptidoglycan (PGN) of *Lm* are recognized by TLR-2/6 and TLR-1/2, flagellin by TLR-5 and CpG DNA by TLR-9 upon *Lm* entry. HDAC6 interacts with the TLR-adaptor protein MyD88, enhancing down-stream TLR-signalling, (increasing NF-κB and MAPK activation). This stronger activation seems to be independent of HDAC6 enzymatic activity and causes higher pro-inflammatory cytokine production and more iNOS induction, necessary for the correct activation of anti-bacterial transcription program. Note that both processes occur during *Lm* infection and the pro-inflammatory cytokines and iNOS induction can impact on the autophagic process. The images in the figure are not scaled.

The TLR universal adaptor protein MyD88 is also activated, together with other adaptor protein called TIRAP (Toll/Interleukin-1 receptor domain containing adapter protein) or MAL (MyD88-adapter-like), followed by Interleukin-1 receptor-associated kinases (IRAK) 1, 2 and 4, TNF receptor-associated factor 6 (TRAF-6), finally transducing nuclear signals through Activator Protein 1 (AP-1) and NF-κB TFs leading to pro-inflammatory cytokine secretion [172]. In this regard, the E3-ubiquitin protein ligase TRAF-6 catalizes the formation of K63-linked polyUb chains and participates in the canonical NF-κB activation pathway, ubiquitinating Transforming growth factor-β (TGF-β) Activated Kinase 1 (TAK1): TAK-1 binding proteins 1, 2 and 3 (TAB1-3) and NF-κB essential modulator (NEMO):IκB kinase (IKK) complexes [48,105,139]. The canonical IKK complex is formed by two kinases, IKKα and IKKβ and their regulatory protein NEMO, which has an ubiquitin-binding domain (UBD) that recognizes K63-linked polyUb chains, an essential step for the activation of the NF-κB pathway [64,258]. In this case, K63-Ub chains function as molecular scaffolds for the recruitment of both IKK and TAK1 complexes, enhancing the TAK1-dependent activation of the IKKs [64,258]. Hence, ubiquitination of proteins belonging to the TLR signalling complex can fine tune innate immune responses to pathogens [142].

It has been also described that the expression of HDAC6 in the nucleus deacetylates p65 subunit of NF-κB, reducing its capacity to bind the Matrix metalloproteinase 2 (MMP2) promoter thereby causing the inhibition of tumour invasion [263]. Hence, deacetylation of NF-κB by HDAC6 adds more complexity to signalling regulation. Moreover, a suppressed activation of NF-κB and AP-1 pathways has been observed in HDAC6-silenced cells after HIV-1 Tat-stimulation [226]. In addition, *Lm*-derived lipoteichoic acids and LLO induce NF-κB signalling during infection, which seems to be MyD88-independent [87,109]. TAB2 and TAB3 are receptors which preferentially bind K63-linked polyUb chains through a highly conserved zinc finger domain (ZnF), very similar to the HDAC6 BUZ domain [105]. PolyUb-binding domains represent a new class of signaling structures that regulate protein kinase activity through a nonproteolytic mechanism. This issue may suggest a specific role of HDAC6 as an Ub-binding receptor in the NF-κB pathway, and this is in accordance with the lower phosphorylation observed in downstream MAPK signalling pathway in *Hdac6*$^{-/-}$ DCs. The **Figure 5.2** summarizes the tentative model of HDAC6 regulation of MyD88-dependent TLR-signalling pathway during *Lm* infection.

Moreover, during TLR-signalling MAPKs are also activated and the microbicidal activity of iNOS is induced [108]. For instance, HIV-1 Tat-induced activation in HDAC6-silenced cells shows a reduced induction of MAPKs, including ERK, c-Jun N-terminal kinase (JNK) and p38 signalling pathways [226]. In fact, *Hdac6*$^{-/-}$ DCs show diminished iNOS induction at 6 hpi associated with low nitrite production and iNOS expression at longer times of *Lm* infection (24 hpi). These results are in accordance with a lower phosphorylation of the MAPK pathway after *Lm* infection in *Hdac6*$^{-/-}$ DCs, controlling the activation of the AP-1 family of TFs, which is necessary to switch-on pro-inflammatory responses [108].

Additionally, the lower phosphorylation of mTORC1 pathway components in *Hdac6*$^{-/-}$ DCs is consistent with a lower pro-inflammatory response, as reported in trained macrophages and dendritic cells, in which a metabolic switch to glycolysis has been described [169]. These data may indicate that HDAC6 also appears to play a role in the activation of the mTOR pathway upon *Lm* infection to initiate the anti-bacterial transcriptional response to combat this pathogen.

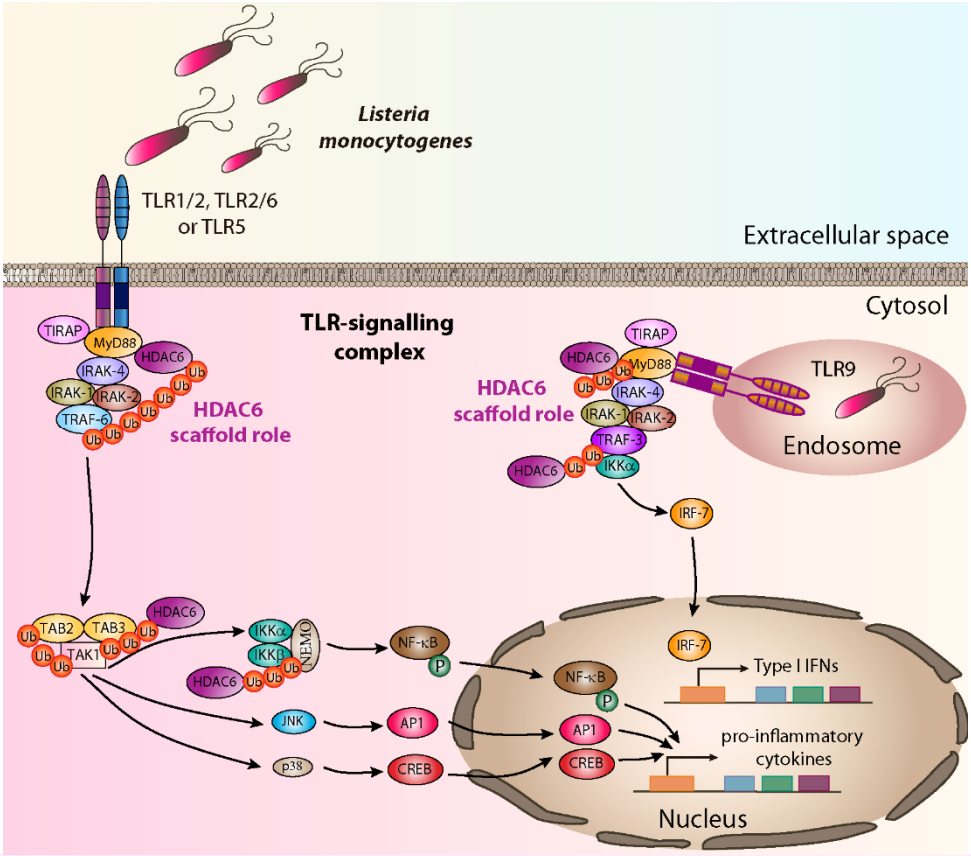

Figure 5.2. Proposed model of HDAC6 functions in Lm sensing. Activation of membrane TLR1/2, TLR2/6 or TLR5 or endosomal TLR-9 by *Gram*-positive bacteria as *Listeria monocytogenes* initiates the TLR-signalling complex. HDAC6 binds to MyD88 independently of its deacetylases domains, suggesting a scaffold role of HDAC6 in this signalling complex, likely mediated by K63-polyUb chain recognition through HDAC6 ubiquitin binding domain (BUZ domain). Other molecules of the TLR-signalling complex, like TAB2, TAB3 and IKK proteins, have been described to be modified with K63-polyUb chains by TRAF-6 and other E3-ubiquitin ligases. NF-κB promotes the transcription of pro-inflammatory genes, whereas IRF-7 activates the transcription of type I IFNs to enhance the cell microbicidal capacity against intracellular bacteria. The images in the figure are not scaled.

Lower IFN-β secretion was detected in *Lm*-infected *Hdac6*$^{-/-}$ DCs from 6 to 24 hpi. Upon vacuolar escape of *Lm*, the cytosolic surveillance pathway of host cell is activated [199]. Bacterial c-di-AMP and DNA mediate the activation of STING, whereas 5´pppRNAs are sensed by RIG-I, mediating the aggregation of mitochondrial and peroxisomal MAVS and the subsequent nuclear signalling of IRF-3 and 7 [1,77]. Aditionally, RIG-I deacetylation at K^{858} and K^{909} by HDAC6 is essental to engage MAVs for the activation of anti-viral response through IRF-3-IFN-β signalling [49,137]. The lack of RIG-I cytosolic response to *Lm* in *Hdac6*$^{-/-}$ DCs can partially explain the diminished pro-inflammatory production of IFN-β observed in this work.

Regarding the lower levels of RNA expression of some chemokines in *Hdac6*$^{-/-}$ DCs, a reduced expression of CXCL10 was also detected in HDAC6-silenced cells after HIV-1 Tat-activation [226]. However, further experiments are necessary to unveil the molecular mechanism by which HDAC6 could regulate this chemokine. In summary, our results reveal a defect in DC activation after *Lm* entry.

5.2.2. Pro-inflammatory cytokine secretion after stimulation with TLR agonists

The impaired anti-inflammatory response in *Hdac6*$^{-/-}$ DCs was also observed with other TLR-agonists such as LPS, Imiquimod, poly(I:C) and Pam3GSK4, highlighting HDAC6 as an important player in TLR signalling activation. This result remarks the possible involvement of HDAC6 in both MyD88-dependent and independent TLR-signalling pathways, because TLR-3 and non-cannonical TLR-4 pathway use TIR-domain containing adapter-inducing IFN-β (TRIF) adaptor instead of MyD88 [234].

Broad-spectrum HDAC inhibitors such as TSA exert immunosuppressive effects in TLR-2 and TLR-4 signalling pathways [208]. Genome-wide expression profiling arrays have revealed that 60% of genes transcriptionally increased by TLR-2 or TLR-4 stimulation are inhibited in TSA-treated cells, whereas 16 % of genes are potentiated [208]. However, these observations do not provide any demonstrative evidence for a specific role of HDAC6, since other HDACs may also be involved. At this point, our results with the genetic ablation of HDAC6 inequivocally endorse a specific role for this deacetylase in TLR-mediated cytokine secretion.

5.2.3. TLR-signalling pathway

Because GM-CSF-derived DCs express low levels of TLR-3 and TLR-5 in the membrane, we stimulated FLT3-L-derived DCs with poly(I:C) and flagellin to measure pro-inflammatory cytokines [55,260], noting maintained failure in the inflammatory response in *Hdac6*$^{-/-}$ cells. Moreover, we detected impaired responses to PAMPs activation in GM-CSF-derived and FLT3L-derived *Hdac6*$^{-/-}$ DCs. In addition, all TLRs except for TLR-3 signal through the adaptor MyD88, and the result obtained with the TLR-3 ligand poly(I:C) was similar to that showed for the rest of TLR stimuli, thereby indicating that the TLR3-response is also affected by absence of HDAC6. In this regard, these data are in agreement with a recent study showing that acetylated retinoic-acid-inducible gene-1 (RIG-1) makes *Hdac6*$^{-/-}$ cells less sensitive to the presence of RNA viruses, resulting in a higher viral titre [49]. While this mechanism could explain the difference between the response of *Hdac6*$^{+/+}$ and *Hdac6*$^{-/-}$ FLT3L-DCs to TLR-3 stimulation, the deficient activation by other TLRs in *Hdac6*$^{-/-}$ DCs also requires an explanation.

However, it has been observed that HDAC6 hampers the formation of MyD88-TRAF6 signalling complex, suppressing TLR-4 mediated activation in mouse macrophage cell line Raw 264.7 [97]. In this work, both p62 and HDAC6 are required for MyD88 aggregation and mediate the suppression of IL-6

and iNOS after TLR-ligand interaction [97]. However, these data are not in agreement with data obtained by other authors and our work [46,226,49,137].

5.2.4. HDAC6-MyD88 molecular association

Since the diminished pro-inflammatory reponse after TLR agonists in *Hdac6*$^{-/-}$ DCs can be explained by RIG-I acetylation, with the exception of poly(I:C), we decided to focus our mechanistic study in the general TLR-adaptor protein MyD88. In this respect, we demonstrate the molecular association of HDAC6 with MyD88 studing the endogenous proteins and an overexpression system. Conceivably, the depletion of HDAC6 and therefore the prevention of HDAC6-MyD88 binding, could inhibit TLR-2-signalling pathway activation, which is in accordance with a lower NF-κB induction measured in *Hdac6*$^{-/-}$ cells after stimulation with various TLR-2 agonists. A diminished NF-κB induction in *Hdac6*$^{-/-}$ cells could explain a reduced initiation of the pro-inflammatory response observed in *Hdac6*$^{-/-}$ DCs, needed to alert the innate and adaptive immune response to *Lm*. However, NF-κB activity of *HDAC6-DD*-transfected HEK cell line after different TLR-2 stimuli (HKLM, Pam2GSK4 and Pam3GSK4) did not display any significant change compared to *HDAC6-WT*-transfected cells, supporting that enzymatic activity of HDAC6 is not involved in this signalling pathway. Interestingly, we have assessed the acetylation of MyD88 by mass spectrometry, detecting acetylation of this molecule in two residues different to the one described previously [171]. The basal MyD88 IP detected "MVVVVSDDYLQS^{Ac}**K$_{231}$**ECDFQTK" sequence in *shHDAC6+MyD88*-HA and *HDAC6-DD+MyD88*-HA samples, and "LLELLT^{Ac}**K$_{95}$**LGR" sequence in *MyD88*-HA contruction. The acetylated peptides detected in basal condition correspond to the MyD88 sequences "MVVVVSDDYLQS^{Ac}**K$_{231}$**ECDFQTK" and "LLELLT^{Ac}**K$_{95}$**LGR", different from the residue described by New *et al*. "L^{Ac}**K$_{132}$**QQQEEAEKPL". In fact, the peptide described in New *et al* is surrounded by leucine residues, instead lysine or arginine, both produced by the trypsin digestion [171].

Our data suggest that the acetylation status of MyD88 does not appear to be regulated by HDAC6, as acetylation was detected not only in the *shHDAC6+MyD88*-HA sample, but also in the *HDAC6-DD+MyD88*-HA and *MyD88*-HA samples without any TLR stimuli. However, no changes in the acetylation marks on MyD88 were detected after HKLM incubation, highlighting the scaffold role of HDAC6 in the proper activation of TLR-signalling pathway (**Figure 5.1 part 2** and **Figure 5.3 part 2**). Therefore, we cannot assign the defect observed in TLR-signalling in *Hdac6*$^{-/-}$ DCs to this post-translational modification of MyD88, as it appears to be independent of the enzymatic activity of HDAC6.

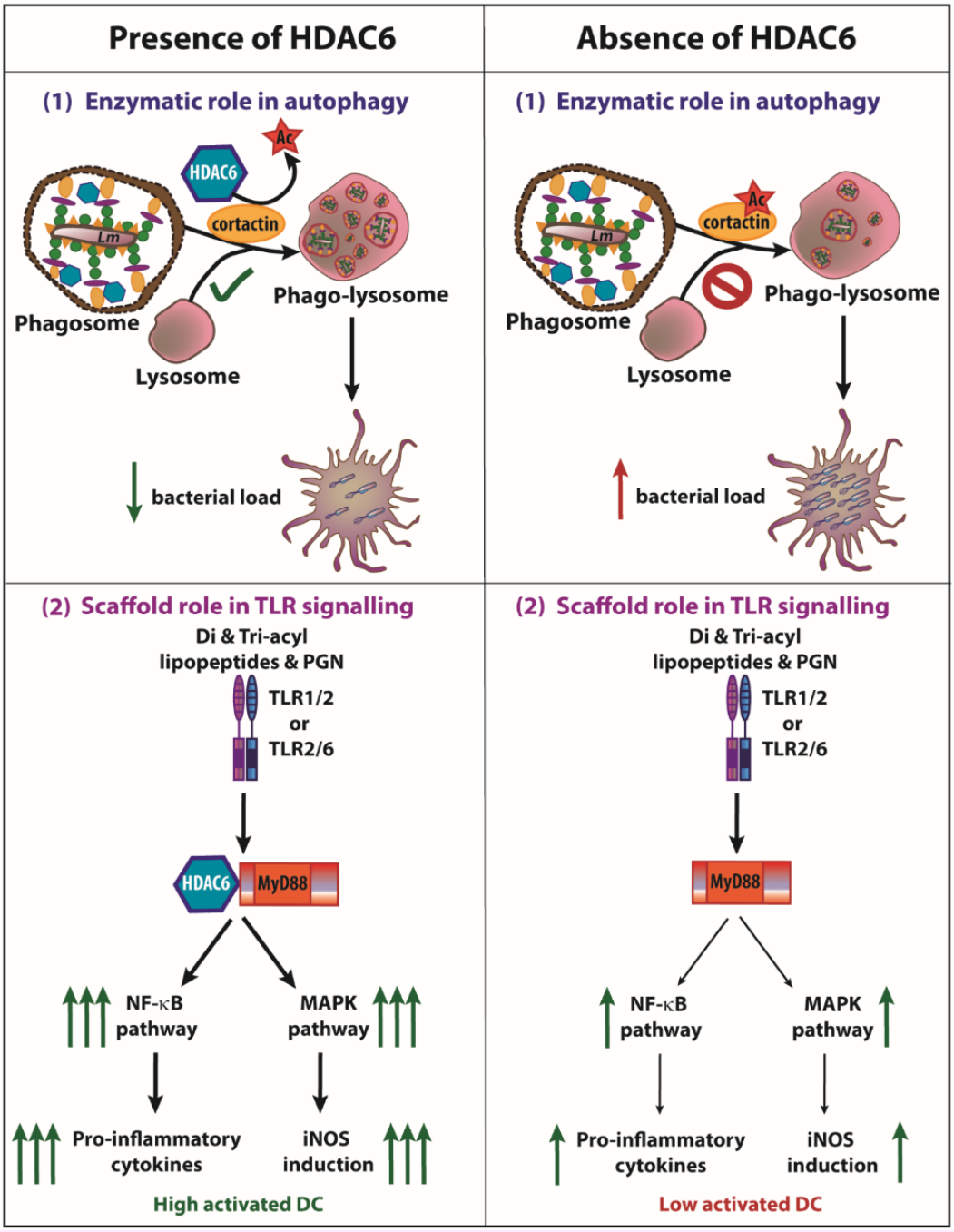

Figure 5.3. Graphical summary of HDAC6 role during DC response to *Lm* infection. The scheme shows the involvement of HDAC6 in two different functions of DC during *Lm* infection, the autophagy and the TLR signalling. **(1)** The fusion of phagosomes with lysosomes is dependent on cortactin and F-actin. The deacetylation of cortactin by HDAC6 allows the correct fusion, followed by an autophagic clearance of *Lm*. The absence of this enzyme delays the fusion of phagosome and lysosome, facilitating Lm to escape from phagosome leading to an increased bacterial load. **(2)** Di- and tri-acyl lipopeptides and peptidoglycan (PGN) of Lm are recognized by TLR1/2 or TLR2/6, activating the TLR pathway. HDAC6 is able to interact with the TLR-adaptor protein MyD88 which causes an enhanced down-stream signalling of the TLR pathway, increasing NF-κB and MAPK activation. This stronger activation (independent on HDAC6 enzymatic activity) results in higher pro-inflammatory cytokine production and iNOS induction, reinforcing the ability of the DC to combat against this intracellular pathogen. Although the absence of HDAC6 does not fully abolish DC activation, a lower induction of NF-κB and MAPK pathways promotes a lower activation of the anti-bacterial transcriptional program of the DCs. Note that both processes occur during *Lm* infection and the pro-inflammatory cytokines and iNOS induction can impact on the autophagic process. The images in the figure are not scaled.

It is conceivable that HDAC6 plays a scaffold role in the initial MyD88 complex in order to maintain the TLR-signalling the time necessary to achieve a proper TLR down-stream signalling. This scaffold role was previously described for HDAC6 in cell migration by Cabrero *et al* [36]. Comparison of induction of NF-κB with TLR-2 agonists in HEK-hTLR2 cells transfected with *HDAC6-WT*, *HDAC6-DD* and *sh-HDAC6* constructs demonstrate differences for silencing HDAC6 protein, but not for the double deacetylase mutant (DD), further supporting the scaffold role for HDAC6 in the maintenance of the TLR-signalling. However, we can not rule out that other PTMs regulate the function of MyD88 such as ubiquitination, because this molecule can be ubiquitinated at 95, 119, 231 and 262 K residues [131]. K48-linked polyubiquitinated-MyD88 seems to be degraded by Smad6-Smurf pathway after TLR-2 and TLR-4 stimulation [131]. Nevertheless, there are many types of ubiquitination and further studies are required to understand what kind of ubiquitin topology could be involved in MyD88-mediated TLR activation [114,233].

5.2.5. Evaluation of the HDAC6 role in the *in vivo* TLR-dependent inflammatory response

Unexpectedly, a protective effect against systemic infection to a lethal dose of *Lm* was observed in *Hdac6*$^{-/-}$ mice. The reduced level of the inflammatory cytokine IL-6 detected in *Hdac6*$^{-/-}$ mice are in accordance with its higher resistance to *Lm* infection. The defective systemic inflammatory response after *Lm* infection of *Hdac6*$^{-/-}$ mice may indicate an impaired TLR-response in the absence of HDAC6 and might therefore be attributed to the absence of the molecular association between MyD88 and HDAC6. In this regard, mice resistance to *Lm* infection can be mediated by sequential MyD88-independent and -dependent responses [217,66,239,218]. However, the role of TLR-2 during *Lm* infection does not appear to be clear enough [66,239]. On one hand, *Tlr-2*$^{-/-}$ mice display a deficit in circulating TNF-α and IL-12p40 production during intravenously injected *Lm* infection combined with a lower mice survival and increased bacterial burden in the liver [217,239]. Other authors have obtained similar resistance to intraperitoneal-injected *Lm* infection between *Tlr-2*$^{-/-}$ and *Tlr-2*$^{+/+}$ mice, indicating that different inoculation routes of bacteria may result in different immune outcomes [66].

Although handling and direct killing of *Lm* by activated macrophages can be mediated by TLR-2- and MyD88-independent mechanisms, the role of TLR-signalling has been found necessary for nitric oxide and cytokine production [217,239]. In fact, MyD88 not only works as TLR-adaptor protein, but also as adaptor of IL-1 and IL-18 receptors, both cytokine responses affected in *Lm*-infected *Myd88*$^{-/-}$ mice [66,239,6]. Although *Myd88*$^{-/-}$ mice are more suceptible to *Lm* infection, mice that lack caspase-1, which is responsible for the processing of immature forms of IL-1 and IL-18 into secreted forms, are only slightly more sensitive to infection than *wt* mice [66,241,217]. These data indicate that the protective immune response of MyD88 is mainly mediated through TLR-dependent signalling, rather

than IL-1 and IL-18 receptors. The recruitment of monocytes to *Lm*-infected spleens is mediated by MCP-1, which is MyD88-independent [218]. Hence, MyD88 deficiency does not impair monocyte recruitment, but prevents monocyte activation due to TNF-α and IL12p70 cytokine secretions are MyD88-dependent [218]. However, the protective $CD8^+$ T-cell response to *Lm* is maintained in *Myd88*$^{-/-}$ mice [252].

The apparently contradictory results obtained using *Tlr-2*$^{-/-}$ mice can be explained by different inoculation routes of *Lm*. On one hand, Torres *et al.* reported an increased susceptibility of these animals to intravenous injection of *Lm*, whereas Edelson *et al* did not observe any difference compared to *wt* mice using intraperitoneal injection [66,239]. Moreover, *Lm* is not only recognized by TLR-2, but also by other TLRs such as TLR-9. In the case of MyD88, it does not appear to be necessary to clear bacteria in *in vitro* infections of macrophages, but this adaptor is essential for cytokine and nitric oxide production, particularly during *in vivo* infections [66,239]. Hence, MyD88 is required for early *Lm* resistance and for proper activation of innate immune responses [66].

Innate immune responses against *Lm* are essential for host survival, because the lack of various innate immunity molecules increase the suceptibility to this pathogen [242]. The fundamental role of innate immunity to combact *Lm* is hihlighted in studies carried out with severe combined immunodeficient (SCID) and nude mice, which display a remarkable resitance to early time points of *Lm*-infection, but are unable to clear bacteria in the long term [14,173]. Further works have demonstrated that the IFN-γ produced by natural killer cells is responsible for macrophage activation at early times of infection [240,34,191,209,85]. Besides, mice lacking IFN-γ and TNF-α rapidly succumb to *Lm*-infection, remarking the importance of both cytokines in the control of the early infection [34,88,191,209]. However, mice that lack the receptor for type I IFNs (IFNAR1) or IRF-3 are more resistant to *Lm*-infection due to an increased apoptosis of T lymphocytes and the loss of TNF-α-producing cells [8,177,38]. Moreover, the lower suceptibility to *Lm* infection displayed by *Ifnar1*$^{-/-}$ mice was associated to a lack of cell-to-cell spreading of bacteria in *in vitro* infections of macrophages and *in vivo*, which is due to an alteration of actin-polymerization of ActA protein on the surface of *Lm* [8,230,182]. However, the existence of cellular factors that alter ActA localization of enclosing bacteria, or altered bacterial regulation mechanisms remains unknown. In this regard, HDAC6 could differently modulate host cell factors necessary for bacterial infection such as in the case of IFNARI absence.

Interestingly, here we detected decreased levels of the inflammatory cytokine IL-6 in *Hdac6*$^{-/-}$ mice serum at 72 and 96 hpi, indicating higher inflammation of *Hdac6*$^{+/+}$ animals in response to a lethal dose of *Lm.* Similar observations regarding lower inflammation in *Hdac6*$^{-/-}$ mice have been reported by other authors [46]. *Hdac6*$^{-/-}$ mice were more resistant to LPS injection, a model typically used to trigger a

septic shock [46]. Similarly, together the results reported in Chattopadhyay *et al.* and our *Lm* survival curves indicate that *Hdac6*$^{-/-}$ mice display a defect in inflammation that could protect *Hdac6*$^{-/-}$ mice from systemic pro-inflammatory cytokine response.

Although, the opposite results were expected based on the *in vitro* and *in vivo* data showing increased bacterial burden at early times in *Hdac6*$^{-/-}$ myeloid cells, a comparative of this short time with the *in vivo* response after various days of infection is hard to be interpret. Besides, HDAC6 overall effect on the inflammatory response to lethal dose of *Lm* should be taken into account when analyzing animal survival at long time points after a septic shock model. In this context, the defective response of inflammatory mediators in *Hdac6*$^{-/-}$ mice may be responsible for their higher survival. It has been described that MyD88 and TLR responses contribute to inflammation during infection [239]. *Tlr-2*$^{-/-}$ mice not only show a reduced production of TNF-α and IL-12, but also lower induction of iNOS, and the co-stimulatory molecules CD40 and CD86, necessary for the control of infection [239]. In this regard, *Lm*-infected *Hdac6*$^{-/-}$ GM-CSF DCs not only express lower CD86 and CD40 markers, but also a reduced nitrite production, fewer induction of iNOS and a reduced secretion of TNF-α and IL-12p70. However, bacterial burden can be controlled by other processes as well, e.g. macrophages directly kill *Lm* by autophagy, independently of TLR-2- and MyD88-mechanisms [66]. In this regard, the impared autophagy observed in *Hdac6*$^{-/-}$ GM-CSF DCs and peritoneal macrophages at 6 hpi is not maintained during the lethal dose of *Lm*-septic shock model. This issue could be explained by a compensatory activity of HDAC5 during the absence of HDAC6 as we have observed in GM-CSF DCs after 24 hpi of *Lm*-infection. Moreover, the *in vivo* quantification of bacterial burden in target organs from 12 to 48 hpi, did not display any significant results between *Hdac6*$^{+/+}$ and *Hdac6*$^{-/-}$mice, indicating that compensatory mechanisms are playing at these times or perhaps, the inflammatory cytokine storm is impairing the bacterial clearance at 72 hpi. Upon *Lm* infection, host cell Sirt-2 is shuttled to the nucleus to deacetylase histone 3, changing the chromatin packaging and the access of TFs. This step seems to be required for effective *Lm* infection because Sirt-2-deficient mice display decreased bacterial burden in target organs [67]. The molecular association between Sirt-2 and HDAC6 has been previously reported [164]. Although HDAC6 is able to bind to both phosphorylated and non-phosphorylated forms of Sirt-2, the ability of Sirt-2 to bind tubulin can only be mediated when it forms a complex with HDAC6 [164]. HDAC6-Sirt-2 interaction could mediate also a role in the nucleus by deacetylating histone 3, and the absence of HDAC6 may alter *Lm* adaptation in the host cell. This could explain why *Hdac6*$^{-/-}$ mice are protected from *Lm* infection as well as *Sirt-2*$^{-/-}$ mice.

The results obtained with *in vivo* long-term infection experiments may seem contradictory compared to *in vitro* assays and to short-term *in vivo* ones. Hence, further studies will be needed to uncover the consequences of HDAC6 deficiency in other mouse cell populations, in other kind of

bacterial inoculation, like intraperitoneal or oral infection models, or in other contexts of bacterial infection, such as *Gram*-negative bacteria.

Taking together, our data support a dual role for HDAC6 in the regulation of innate immunity against intracellular bacteria. An increased bacterial load in different *Hdac6*$^{-/-}$ myeloid cells can be explained by the autophagy mechanism, where a permanently acetylated cortactin may impair the phagosome-lysosome fusion, necessary for the clearance of this pathogen. Our experiments also show the importance of HDAC6 in DC activation, uncovering a novel mechanism of HDAC6 action mediated by the appropriate signalling via the TLR pathway, due to the association of HDAC6 with the TLR-adaptor protein MyD88. This molecular association seems to be required for a response to TLR stimuli to initiate the inflammatory response of an activated DC. Taken together, both HDAC6 functions described in this work, reinforce the importance of this molecule to combat the intracellular bacteria *Lm* by autophagy and to completely activate the inflammatory response after TLR activation. Overall, this work identifies for the first time part of the TLR regulatory machinery of the pro-inflammatory response after *Lm* infection. Moreover, the results obtained demonstate the importance of HDAC6 in the control of intracellular bacterial infection by innate immune system.

Conclusions

6. CONCLUSIONS

The findings presented herein support the following conclusions:

1. HDAC6 protein expression is increased during *Lm* infection in DCs.
2. *Hdac6*$^{-/-}$ myeloid cells display defective clearance of intracellular bacteria due to an impaired autophagy.
3. *Hdac6*$^{-/-}$ DCs display higher titres of *Lm* due to delayed fusion of autophagosome with lysosome, likely mediated by the acetylation state of cortactin.
4. *Hdac6*$^{-/-}$ DCs show impaired pro-inflammatory cytokine production in response to *Lm* infection and TLR agonist stimulation.
5. *Hdac6*$^{-/-}$ DCs exhibit weaker iNOS microbicidal activity after *Lm* infection and HKLM stimulation.
6. *Hdac6*$^{-/-}$ DCs show lower induction of MAPK and mTOR signalling pathways after *Lm* infection and TLR activation, indicating a defective anti-bacterial response.
7. There is a molecular association between HDAC6 and MyD88 responsible of a proper inflammatory response after TLR stimulation, which is independent of HDAC6 enzymatic activity.
8. The impaired TLR-signalling pathway observed in the absence of HDAC6 can explain the *Hdac6*$^{-/-}$ mice protection against septic shock model based in lethal dose-*Lm* infection.

Conclusiones

7. CONCLUSIONES

Los resultados presentados en esta tesis doctoral son respaldados con las siguientes conclusiones:

1. La expresión de la proteína HDAC6 se induce durante la infección de DCs con *Lm*.

2. Las células mieloides de ratones *Hdac6*$^{-/-}$ muestran un defecto en la eliminación de bacterias intracelulares debido a un defecto en la autofagia.

3. Las DCs de ratones *Hdac6*$^{-/-}$ contienen una mayor carga bacteriana debido a un retraso en la fusión del autophagosoma con el lisosoma, probablemente mediada por la acetilación de la cortactina.

4. En las DCs de ratones *Hdac6*$^{-/-}$ se detecta una producción de citoquinas pro-inflamatorias disminuida en respuesta a la infección por *Lm* y a la estimulación con ligandos de TLRs.

5. En las DCs de ratones *Hdac6*$^{-/-}$ se observa una menor inducción de la actividad microbicida de la enzima iNOS tras la infección con *Lm* y la estimulación con HKLM.

6. Las DCs de ratones *Hdac6*$^{-/-}$ tienen una menor inducción de las rutas de señalización de MAPK y mTOR por la infección de *Lm* y la activación de los TLR, lo que indica que la respuesta anti-bacteriana está afectada.

7. La asociación molecular existente ente HDAC6 y MyD88 es responsable de la correcta respuesta inflamatoria después de la estimulación de los TLRs, que parece ser independiente de la actividad enzimática de HDAC6.

8. La ruta de señalización de los TLRs afectada que se observa en la ausencia de la proteína HDAC6, podría explicar la protección de los ratones *Hdac6*$^{-/-}$ frente al modelo de shock séptico usando una dosis letal infectiva de *Lm*.

Bibliography

8. BIBLIOGRAPHY

1. Abdullah Z, Schlee M, Roth S, Mraheil MA, Barchet W, Bottcher J, Hain T, Geiger S, Hayakawa Y, Fritz JH, Civril F, Hopfner KP, Kurts C, Ruland J, Hartmann G, Chakraborty T, Knolle PA (2012) RIG-I detects infection with live Listeria by sensing secreted bacterial nucleic acids. EMBO J 31:4153-4164. doi:10.1038/emboj.2012.274

2. Ageta-Ishihara N, Miyata T, Ohshima C, Watanabe M, Sato Y, Hamamura Y, Higashiyama T, Mazitschek R, Bito H, Kinoshita M (2013) Septins promote dendrite and axon development by negatively regulating microtubule stability via HDAC6-mediated deacetylation. Nature communications 4:2532. doi:10.1038/ncomms3532

3. Aldana-Masangkay GI, Sakamoto KM (2011) The role of HDAC6 in cancer. J Biomed Biotechnol 2011:875824. doi:10.1155/2011/875824

4. Archer KA, Durack J, Portnoy DA (2014) STING-dependent type I IFN production inhibits cell-mediated immunity to Listeria monocytogenes. PLoS Pathog 10:e1003861. doi:10.1371/journal.ppat.1003861

5. Ariffin JK, das Gupta K, Kapetanovic R, Iyer A, Reid RC, Fairlie DP, Sweet MJ (2015) Histone deacetylase inhibitors promote mitochondrial reactive oxygen species production and bacterial clearance by human macrophages. Antimicrob Agents Chemother. doi:10.1128/AAC.01876-15

6. Arnold-Schrauf C, Dudek M, Dielmann A, Pace L, Swallow M, Kruse F, Kuhl AA, Holzmann B, Berod L, Sparwasser T (2014) Dendritic cells coordinate innate immunity via MyD88 signaling to control Listeria monocytogenes infection. Cell Rep 6:698-708. doi:10.1016/j.celrep.2014.01.023

7. Asthana J, Kapoor S, Mohan R, Panda D (2013) Inhibition of HDAC6 deacetylase activity increases its binding with microtubules and suppresses microtubule dynamic instability in MCF-7 cells. The Journal of biological chemistry 288:22516-22526. doi:10.1074/jbc.M113.489328

8. Auerbuch V, Brockstedt DG, Meyer-Morse N, O'Riordan M, Portnoy DA (2004) Mice lacking the type I interferon receptor are resistant to Listeria monocytogenes. J Exp Med 200:527-533. doi:10.1084/jem.20040976

9. Bae HJ, Jung KH, Eun JW, Shen Q, Kim HS, Park SJ, Shin WC, Yang HD, Park WS, Lee JY, Nam SW (2015) MicroRNA-221 governs tumor suppressor HDAC6 to potentiate malignant progression of liver cancer. J Hepatol 63:408-419. doi:10.1016/j.jhep.2015.03.019

10. Bahjat KS, Meyer-Morse N, Lemmens EE, Shugart JA, Dubensky TW, Brockstedt DG, Portnoy DA (2009) Suppression of cell-mediated immunity following recognition of phagosome-confined bacteria. PLoS Pathog 5:e1000568. doi:10.1371/journal.ppat.1000568

11. Bai J, Lei Y, An GL, He L (2015) Down-regulation of deacetylase HDAC6 inhibits the melanoma cell line A375.S2 growth through ROS-dependent mitochondrial pathway. PloS one 10:e0121247. doi:10.1371/journal.pone.0121247

12. Bakardjiev AI, Theriot JA, Portnoy DA (2006) Listeria monocytogenes traffics from maternal organs to the placenta and back. PLoS Pathog 2:e66. doi:10.1371/journal.ppat.0020066

13. Bali P, Pranpat M, Bradner J, Balasis M, Fiskus W, Guo F, Rocha K, Kumaraswamy S, Boyapalle S, Atadja P, Seto E, Bhalla K (2005) Inhibition of histone deacetylase 6 acetylates and disrupts the chaperone function of heat shock protein 90: a novel basis for antileukemia activity of histone deacetylase inhibitors. The Journal of biological chemistry 280:26729-26734. doi:10.1074/jbc.C500186200

14. Bancroft GJ, Schreiber RD, Unanue ER (1991) Natural immunity: a T-cell-independent pathway of macrophage activation, defined in the scid mouse. Immunol Rev 124:5-24

15. Banerjee I, Miyake Y, Nobs SP, Schneider C, Horvath P, Kopf M, Matthias P, Helenius A, Yamauchi Y (2014) Influenza A virus uses the aggresome processing machinery for host cell entry. Science 346:473-477. doi:10.1126/science.1257037

16. Banreti A, Sass M, Graba Y (2013) The emerging role of acetylation in the regulation of autophagy. Autophagy 9:819-829. doi:10.4161/auto.23908

17. Beauregard KE, Lee KD, Collier RJ, Swanson JA (1997) pH-dependent perforation of macrophage phagosomes by listeriolysin O from Listeria monocytogenes. J Exp Med 186:1159-1163

18. Beier UH, Wang L, Han R, Akimova T, Liu Y, Hancock WW (2012) Histone deacetylases 6 and 9 and sirtuin-1 control Foxp3+ regulatory T cell function through shared and isoform-specific mechanisms. Sci Signal 5:ra45. doi:10.1126/scisignal.2002873

19. Bershadsky AD, Ballestrem C, Carramusa L, Zilberman Y, Gilquin B, Khochbin S, Alexandrova AY, Verkhovsky AB, Shemesh T, Kozlov MM (2006) Assembly and mechanosensory function of focal adhesions: experiments and models. European journal of cell biology 85:165-173. doi:10.1016/j.ejcb.2005.11.001

20. Bertos NR, Gilquin B, Chan GK, Yen TJ, Khochbin S, Yang XJ (2004) Role of the tetradecapeptide repeat domain of human histone deacetylase 6 in cytoplasmic retention. The Journal of biological chemistry 279:48246-48254. doi:10.1074/jbc.M408583200

21. Bertos NR, Wang AH, Yang XJ (2001) Class II histone deacetylases: structure, function, and regulation. Biochemistry and cell biology = Biochimie et biologie cellulaire 79:243-252

22. Bierne H, Sabet C, Personnic N, Cossart P (2007) Internalins: a complex family of leucine-rich repeat-containing proteins in Listeria monocytogenes. Microbes Infect 9:1156-1166. doi:10.1016/j.micinf.2007.05.003

23. Birmingham CL, Canadien V, Kaniuk NA, Steinberg BE, Higgins DE, Brumell JH (2008) Listeriolysin O allows Listeria monocytogenes replication in macrophage vacuoles. Nature 451:350-354. doi:10.1038/nature06479

24. Birmingham CL, Smith AC, Bakowski MA, Yoshimori T, Brumell JH (2006) Autophagy controls Salmonella infection in response to damage to the Salmonella-containing vacuole. The Journal of biological chemistry 281:11374-11383. doi:10.1074/jbc.M509157200

25. Bleriot C, Dupuis T, Jouvion G, Eberl G, Disson O, Lecuit M (2015) Liver-resident macrophage necroptosis orchestrates type 1 microbicidal inflammation and type-2-mediated tissue repair during bacterial infection. Immunity 42:145-158. doi:10.1016/j.immuni.2014.12.020

26. Bonazzi M, Veiga E, Pizarro-Cerda J, Cossart P (2008) Successive post-translational modifications of E-cadherin are required for InlA-mediated internalization of Listeria monocytogenes. Cell Microbiol 10:2208-2222. doi:10.1111/j.1462-5822.2008.01200.x

27. Bonzon-Kulichenko E, Perez-Hernandez D, Nunez E, Martinez-Acedo P, Navarro P, Trevisan-Herraz M, Ramos Mdel C, Sierra S, Martinez-Martinez S, Ruiz-Meana M, Miro-Casas E, Garcia-Dorado D, Redondo JM, Burgos JS, Vazquez J (2011) A robust method for quantitative high-throughput analysis of proteomes by 18O labeling. Mol Cell Proteomics 10:M110 003335. doi:10.1074/mcp.M110.003335

28. Boujemaa-Paterski R, Gouin E, Hansen G, Samarin S, Le Clainche C, Didry D, Dehoux P, Cossart P, Kocks C, Carlier MF, Pantaloni D (2001) Listeria protein ActA mimics WASp family proteins: it activates filament barbed end branching by Arp2/3 complex. Biochemistry 40:11390-11404

29. Boyault C, Gilquin B, Zhang Y, Rybin V, Garman E, Meyer-Klaucke W, Matthias P, Muller CW, Khochbin S (2006) HDAC6-p97/VCP controlled polyubiquitin chain turnover. EMBO J 25:3357-3366. doi:10.1038/sj.emboj.7601210

30. Boyault C, Khochbin S (2008) [HDAC6 orchestrates cell defense responses against cytotoxic protein aggregates]. Med Sci (Paris) 24:15-17. doi:10.1051/medsci/200824115

31. Boyault C, Sadoul K, Pabion M, Khochbin S (2007) HDAC6, at the crossroads between cytoskeleton and cell signaling by acetylation and ubiquitination. Oncogene 26:5468-5476. doi:10.1038/sj.onc.1210614

32. Boyault C, Zhang Y, Fritah S, Caron C, Gilquin B, Kwon SH, Garrido C, Yao TP, Vourc'h C, Matthias P, Khochbin S (2007) HDAC6 controls major cell response pathways to cytotoxic accumulation of protein aggregates. Genes Dev 21:2172-2181. doi:10.1101/gad.436407

33. Braun L, Cossart P (2000) Interactions between Listeria monocytogenes and host mammalian cells. Microbes Infect 2:803-811

34. Buchmeier NA, Schreiber RD (1985) Requirement of endogenous interferon-gamma production for resolution of Listeria monocytogenes infection. Proc Natl Acad Sci U S A 82:7404-7408

35. Burrack LS, Harper JW, Higgins DE (2009) Perturbation of vacuolar maturation promotes listeriolysin O-independent vacuolar escape during Listeria monocytogenes infection of human cells. Cell Microbiol 11:1382-1398. doi:10.1111/j.1462-5822.2009.01338.x

36. Cabrero JR, Serrador JM, Barreiro O, Mittelbrunn M, Naranjo-Suarez S, Martin-Cofreces N, Vicente-Manzanares M, Mazitschek R, Bradner JE, Avila J, Valenzuela-Fernandez A, Sanchez-Madrid F (2006) Lymphocyte chemotaxis is regulated by histone deacetylase 6, independently of its deacetylase activity. Molecular biology of the cell 17:3435-3445. doi:10.1091/mbc.E06-01-0008

37. Cameron LA, Giardini PA, Soo FS, Theriot JA (2000) Secrets of actin-based motility revealed by a bacterial pathogen. Nat Rev Mol Cell Biol 1:110-119. doi:10.1038/35040061

38. Carrero JA, Calderon B, Unanue ER (2004) Type I interferon sensitizes lymphocytes to apoptosis and reduces resistance to Listeria infection. J Exp Med 200:535-540. doi:10.1084/jem.20040769

39. Cohen TJ, Guo JL, Hurtado DE, Kwong LK, Mills IP, Trojanowski JQ, Lee VM (2011) The acetylation of tau inhibits its function and promotes pathological tau aggregation. Nature communications 2:252. doi:10.1038/ncomms1255

40. Condotta SA, Richer MJ, Badovinac VP, Harty JT (2012) Probing CD8 T cell responses with Listeria monocytogenes infection. Adv Immunol 113:51-80. doi:10.1016/B978-0-12-394590-7.00005-1

41. Conlan JW (1996) Early pathogenesis of Listeria monocytogenes infection in the mouse spleen. J Med Microbiol 44:295-302. doi:10.1099/00222615-44-4-295

42. Cossart P (2001) Met, the HGF-SF receptor: another receptor for Listeria monocytogenes. Trends Microbiol 9:105-107

43. Cossart P, Helenius A (2014) Endocytosis of viruses and bacteria. Cold Spring Harb Perspect Biol 6. doi:10.1101/cshperspect.a016972

44. Czuczman MA, Fattouh R, van Rijn JM, Canadien V, Osborne S, Muise AM, Kuchroo VK, Higgins DE, Brumell JH (2014) Listeria monocytogenes exploits efferocytosis to promote cell-to-cell spread. Nature 509:230-234. doi:10.1038/nature13168

45. Chang YW, Tseng CF, Wang MY, Chang WC, Lee CC, Chen LT, Hung MC, Su JL (2015) Deacetylation of HSPA5 by HDAC6 leads to GP78-mediated HSPA5 ubiquitination at K447 and suppresses metastasis of breast cancer. Oncogene. doi:10.1038/onc.2015.214

46. Chattopadhyay S, Fensterl V, Zhang Y, Veleeparambil M, Wetzel JL, Sen GC (2013) Inhibition of viral pathogenesis and promotion of the septic shock response to bacterial infection by IRF-3 are regulated by the acetylation and phosphorylation of its coactivators. MBio 4. doi:10.1128/mBio.00636-12

47. Chen S, Owens GC, Makarenkova H, Edelman DB (2010) HDAC6 regulates mitochondrial transport in hippocampal neurons. PloS one 5:e10848. doi:10.1371/journal.pone.0010848

48. Chen ZJ (2012) Ubiquitination in signaling to and activation of IKK. Immunol Rev 246:95-106. doi:10.1111/j.1600-065X.2012.01108.x

49. Choi SJ, Lee HC, Kim JH, Park SY, Kim TH, Lee WK, Jang DJ, Yoon JE, Choi YI, Kim S, Ma J, Kim CJ, Yao TP, Jung JU, Lee JY, Lee JS (2016) HDAC6 regulates cellular viral RNA sensing by deacetylation of RIG-I. EMBO J. doi:10.15252/embj.201592586

50. de Noordhout CM, Devleesschauwer B, Angulo FJ, Verbeke G, Haagsma J, Kirk M, Havelaar A, Speybroeck N (2014) The global burden of listeriosis: a systematic review and meta-analysis. Lancet Infect Dis 14:1073-1082. doi:10.1016/S1473-3099(14)70870-9

51. de Ruijter AJ, van Gennip AH, Caron HN, Kemp S, van Kuilenburg AB (2003) Histone deacetylases (HDACs): characterization of the classical HDAC family. The Biochemical journal 370:737-749. doi:10.1042/BJ20021321

52. de Zoeten EF, Wang L, Butler K, Beier UH, Akimova T, Sai H, Bradner JE, Mazitschek R, Kozikowski AP, Matthias P, Hancock WW (2011) Histone deacetylase 6 and heat shock protein 90 control the functions of Foxp3(+) T-regulatory cells. Mol Cell Biol 31:2066-2078. doi:10.1128/MCB.05155-11

53. de Zoeten EF, Wang L, Sai H, Dillmann WH, Hancock WW (2010) Inhibition of HDAC9 increases T regulatory cell function and prevents colitis in mice. Gastroenterology 138:583-594. doi:10.1053/j.gastro.2009.10.037

54. Deakin NO, Turner CE (2014) Paxillin inhibits HDAC6 to regulate microtubule acetylation, Golgi structure, and polarized migration. J Cell Biol 206:395-413. doi:10.1083/jcb.201403039

55. Dearman RJ, Cumberbatch M, Maxwell G, Basketter DA, Kimber I (2009) Toll-like receptor ligand activation of murine bone marrow-derived dendritic cells. Immunology 126:475-484. doi:10.1111/j.1365-2567.2008.02922.x

56. Destaing O, Saltel F, Gilquin B, Chabadel A, Khochbin S, Ory S, Jurdic P (2005) A novel Rho-mDia2-HDAC6 pathway controls podosome patterning through microtubule acetylation in osteoclasts. Journal of cell science 118:2901-2911. doi:10.1242/jcs.02425

57. Ding G, Liu HD, Huang Q, Liang HX, Ding ZH, Liao ZJ, Huang G (2013) HDAC6 promotes hepatocellular carcinoma progression by inhibiting P53 transcriptional activity. FEBS Lett 587:880-886. doi:10.1016/j.febslet.2013.02.001

58. Ding WX, Yin XM (2008) Sorting, recognition and activation of the misfolded protein degradation pathways through macroautophagy and the proteasome. Autophagy 4:141-150

59. Dompierre JP, Godin JD, Charrin BC, Cordelieres FP, King SJ, Humbert S, Saudou F (2007) Histone deacetylase 6 inhibition compensates for the transport deficit in Huntington's disease by increasing tubulin acetylation. J Neurosci 27:3571-3583. doi:10.1523/JNEUROSCI.0037-07.2007

60. Dortet L, Mostowy S, Samba-Louaka A, Gouin E, Nahori MA, Wiemer EA, Dussurget O, Cossart P (2011) Recruitment of the major vault protein by InlK: a Listeria monocytogenes strategy to avoid autophagy. PLoS Pathog 7:e1002168. doi:10.1371/journal.ppat.1002168

61. Du Y, Seibenhener ML, Yan J, Jiang J, Wooten MC (2015) aPKC phosphorylation of HDAC6 results in increased deacetylation activity. PloS one 10:e0123191. doi:10.1371/journal.pone.0123191

62. Duarte JH, Di Meglio P, Hirota K, Ahlfors H, Stockinger B (2013) Differential influences of the aryl hydrocarbon receptor on Th17 mediated responses in vitro and in vivo. PloS one 8:e79819. doi:10.1371/journal.pone.0079819

63. Dussurget O, Bierne H, Cossart P (2014) The bacterial pathogen Listeria monocytogenes and the interferon family: type I, type II and type III interferons. Front Cell Infect Microbiol 4:50. doi:10.3389/fcimb.2014.00050

64. Ea CK, Deng L, Xia ZP, Pineda G, Chen ZJ (2006) Activation of IKK by TNFalpha requires site-specific ubiquitination of RIP1 and polyubiquitin binding by NEMO. Molecular cell 22:245-257. doi:10.1016/j.molcel.2006.03.026

65. Edelson BT, Bradstreet TR, Hildner K, Carrero JA, Frederick KE, Kc W, Belizaire R, Aoshi T, Schreiber RD, Miller MJ, Murphy TL, Unanue ER, Murphy KM (2011) CD8alpha(+) dendritic cells are an obligate cellular entry point for productive infection by Listeria monocytogenes. Immunity 35:236-248. doi:10.1016/j.immuni.2011.06.012

66. Edelson BT, Unanue ER (2002) MyD88-dependent but Toll-like receptor 2-independent innate immunity to Listeria: no role for either in macrophage listericidal activity. Journal of immunology 169:3869-3875

67. Eskandarian HA, Impens F, Nahori MA, Soubigou G, Coppee JY, Cossart P, Hamon MA (2013) A role for SIRT2-dependent histone H3K18 deacetylation in bacterial infection. Science 341:1238858. doi:10.1126/science.1238858

68. Faralla C, Rizzuto GA, Lowe DE, Kim B, Cooke C, Shiow LR, Bakardjiev AI (2016) InlP, a New Virulence Factor with Strong Placental Tropism. Infect Immun 84:3584-3596. doi:10.1128/IAI.00625-16

69. Gaillard JL, Berche P, Frehel C, Gouin E, Cossart P (1991) Entry of L. monocytogenes into cells is mediated by internalin, a repeat protein reminiscent of surface antigens from gram-positive cocci. Cell 65:1127-1141

70. Gao YS, Hubbert CC, Lu J, Lee YS, Lee JY, Yao TP (2007) Histone deacetylase 6 regulates growth factor-induced actin remodeling and endocytosis. Mol Cell Biol 27:8637-8647. doi:10.1128/MCB.00393-07

71. Gedde MM, Higgins DE, Tilney LG, Portnoy DA (2000) Role of listeriolysin O in cell-to-cell spread of Listeria monocytogenes. Infect Immun 68:999-1003

72. Gediya LK, Khandelwal A, Patel J, Belosay A, Sabnis G, Mehta J, Purushottamachar P, Njar VC (2008) Design, synthesis, and evaluation of novel mutual prodrugs (hybrid drugs) of all-trans-retinoic acid and histone deacetylase inhibitors with enhanced anticancer activities in breast and prostate cancer cells in vitro. Journal of medicinal chemistry 51:3895-3904. doi:10.1021/jm8001839

73. Glaser P, Frangeul L, Buchrieser C, Rusniok C, Amend A, Baquero F, Berche P, Bloecker H, Brandt P, Chakraborty T, Charbit A, Chetouani F, Couve E, de Daruvar A, Dehoux P, Domann E, Dominguez-Bernal G, Duchaud E, Durant L, Dussurget O, Entian KD, Fsihi H, Garcia-del Portillo F, Garrido P, Gautier L, Goebel W, Gomez-Lopez N, Hain T, Hauf J, Jackson D, Jones LM, Kaerst U, Kreft J, Kuhn

M, Kunst F, Kurapkat G, Madueno E, Maitournam A, Vicente JM, Ng E, Nedjari H, Nordsiek G, Novella S, de Pablos B, Perez-Diaz JC, Purcell R, Remmel B, Rose M, Schlueter T, Simoes N, Tierrez A, Vazquez-Boland JA, Voss H, Wehland J, Cossart P (2001) Comparative genomics of Listeria species. Science 294:849-852. doi:10.1126/science.1063447

74. Guedes-Dias P, de Proenca J, Soares TR, Leitao-Rocha A, Pinho BR, Duchen MR, Oliveira JM (2015) HDAC6 inhibition induces mitochondrial fusion, autophagic flux and reduces diffuse mutant huntingtin in striatal neurons. Biochim Biophys Acta 1852:2484-2493. doi:10.1016/j.bbadis.2015.08.012

75. Haberland M, Montgomery RL, Olson EN (2009) The many roles of histone deacetylases in development and physiology: implications for disease and therapy. Nature reviews Genetics 10:32-42. doi:10.1038/nrg2485

76. Haggarty SJ, Koeller KM, Wong JC, Grozinger CM, Schreiber SL (2003) Domain-selective small-molecule inhibitor of histone deacetylase 6 (HDAC6)-mediated tubulin deacetylation. Proc Natl Acad Sci U S A 100:4389-4394. doi:10.1073/pnas.0430973100

77. Hagmann CA, Herzner AM, Abdullah Z, Zillinger T, Jakobs C, Schuberth C, Coch C, Higgins PG, Wisplinghoff H, Barchet W, Hornung V, Hartmann G, Schlee M (2013) RIG-I detects triphosphorylated RNA of Listeria monocytogenes during infection in non-immune cells. PloS one 8:e62872. doi:10.1371/journal.pone.0062872

78. Hai Y, Christianson DW (2016) Histone deacetylase 6 structure and molecular basis of catalysis and inhibition. Nat Chem Biol 12:741-747. doi:10.1038/nchembio.2134

79. Hamilton SE, Badovinac VP, Khanolkar A, Harty JT (2006) Listeriolysin O-deficient Listeria monocytogenes as a vaccine delivery vehicle: antigen-specific CD8 T cell priming and protective immunity. Journal of immunology 177:4012-4020

80. Hamon M, Bierne H, Cossart P (2006) Listeria monocytogenes: a multifaceted model. Nat Rev Microbiol 4:423-434. doi:10.1038/nrmicro1413

81. Hamon MA, Batsche E, Regnault B, Tham TN, Seveau S, Muchardt C, Cossart P (2007) Histone modifications induced by a family of bacterial toxins. Proc Natl Acad Sci U S A 104:13467-13472. doi:10.1073/pnas.0702729104

82. Hamon MA, Cossart P (2011) K+ efflux is required for histone H3 dephosphorylation by Listeria monocytogenes listeriolysin O and other pore-forming toxins. Infect Immun 79:2839-2846. doi:10.1128/IAI.01243-10

83. Hamon MA, Ribet D, Stavru F, Cossart P (2012) Listeriolysin O: the Swiss army knife of Listeria. Trends Microbiol 20:360-368. doi:10.1016/j.tim.2012.04.006

84. Han Y, Jeong HM, Jin YH, Kim YJ, Jeong HG, Yeo CY, Lee KY (2009) Acetylation of histone deacetylase 6 by p300 attenuates its deacetylase activity. Biochemical and biophysical research communications 383:88-92. doi:10.1016/j.bbrc.2009.03.147

85. Harty JT, Bevan MJ (1995) Specific immunity to Listeria monocytogenes in the absence of IFN gamma. Immunity 3:109-117

86. Harty JT, Tvinnereim AR, White DW (2000) CD8+ T cell effector mechanisms in resistance to infection. Annu Rev Immunol 18:275-308. doi:10.1146/annurev.immunol.18.1.275

87. Hauf N, Goebel W, Fiedler F, Sokolovic Z, Kuhn M (1997) Listeria monocytogenes infection of P388D1 macrophages results in a biphasic NF-kappaB (RelA/p50) activation induced by lipoteichoic acid and bacterial phospholipases and mediated by IkappaBalpha and IkappaBbeta degradation. Proc Natl Acad Sci U S A 94:9394-9399

88. Havell EA (1989) Evidence that tumor necrosis factor has an important role in antibacterial resistance. Journal of immunology 143:2894-2899

89. Honda K, Takaoka A, Taniguchi T (2006) Type I interferon [corrected] gene induction by the interferon regulatory factor family of transcription factors. Immunity 25:349-360. doi:10.1016/j.immuni.2006.08.009

90. Huang S, Wang S, Bian C, Yang Z, Zhou H, Zeng Y, Li H, Han Q, Zhao RC (2012) Upregulation of miR-22 promotes osteogenic differentiation and inhibits adipogenic differentiation of human adipose tissue-derived mesenchymal stem cells by repressing HDAC6 protein expression. Stem Cells Dev 21:2531-2540. doi:10.1089/scd.2012.0014

91. Hubbert C, Guardiola A, Shao R, Kawaguchi Y, Ito A, Nixon A, Yoshida M, Wang XF, Yao TP (2002) HDAC6 is a microtubule-associated deacetylase. Nature 417:455-458. doi:10.1038/417455a

92. Huo L, Li D, Sun X, Shi X, Karna P, Yang W, Liu M, Qiao W, Aneja R, Zhou J (2011) Regulation of Tat acetylation and transactivation activity by the microtubule-associated deacetylase HDAC6. The Journal of biological chemistry 286:9280-9286. doi:10.1074/jbc.M110.208884

93. Husain M, Cheung CY (2014) Histone deacetylase 6 inhibits influenza A virus release by downregulating the trafficking of viral components to the plasma membrane via its substrate, acetylated microtubules. Journal of virology 88:11229-11239. doi:10.1128/JVI.00727-14

94. Husain M, Harrod KS (2009) Influenza A virus-induced caspase-3 cleaves the histone deacetylase 6 in infected epithelial cells. FEBS Lett 583:2517-2520. doi:10.1016/j.febslet.2009.07.005

95. Hwang I, Lee E, Jeon SA, Yu JW (2015) Histone deacetylase 6 negatively regulates NLRP3 inflammasome activation. Biochemical and biophysical research communications 467:973-978. doi:10.1016/j.bbrc.2015.10.033

96. Impens F, Radoshevich L, Cossart P, Ribet D (2014) Mapping of SUMO sites and analysis of SUMOylation changes induced by external stimuli. Proc Natl Acad Sci U S A 111:12432-12437. doi:10.1073/pnas.1413825111

97. Into T, Inomata M, Niida S, Murakami Y, Shibata K (2010) Regulation of MyD88 aggregation and the MyD88-dependent signaling pathway by sequestosome 1 and histone deacetylase 6. The Journal of biological chemistry 285:35759-35769. doi:10.1074/jbc.M110.126904

98. Iwata A, Riley BE, Johnston JA, Kopito RR (2005) HDAC6 and microtubules are required for autophagic degradation of aggregated huntingtin. The Journal of biological chemistry 280:40282-40292. doi:10.1074/jbc.M508786200

99. Jahreiss L, Menzies FM, Rubinsztein DC (2008) The itinerary of autophagosomes: from peripheral formation to kiss-and-run fusion with lysosomes. Traffic 9:574-587. doi:10.1111/j.1600-0854.2008.00701.x

100. Jones GS, Bussell KM, Myers-Morales T, Fieldhouse AM, Bou Ghanem EN, D'Orazio SE (2015) Intracellular Listeria monocytogenes comprises a minimal but vital fraction of the intestinal burden following foodborne infection. Infect Immun 83:3146-3156. doi:10.1128/IAI.00503-15

101. Jones GS, D'Orazio SE (2017) Monocytes Are the Predominant Cell Type Associated with Listeria monocytogenes in the Gut, but They Do Not Serve as an Intracellular Growth Niche. Journal of immunology 198:2796-2804. doi:10.4049/jimmunol.1602076

102. Jung S, Unutmaz D, Wong P, Sano G, De los Santos K, Sparwasser T, Wu S, Vuthoori S, Ko K, Zavala F, Pamer EG, Littman DR, Lang RA (2002) In vivo depletion of CD11c+ dendritic cells abrogates priming of CD8+ T cells by exogenous cell-associated antigens. Immunity 17:211-220

103. Kaluza D, Kroll J, Gesierich S, Yao TP, Boon RA, Hergenreider E, Tjwa M, Rossig L, Seto E, Augustin HG, Zeiher AM, Dimmeler S, Urbich C (2011) Class IIb HDAC6 regulates endothelial cell migration and angiogenesis by deacetylation of cortactin. EMBO J 30:4142-4156. doi:10.1038/emboj.2011.298

104. Kamemura K, Ogawa M, Ohkubo S, Ohtsuka Y, Shitara Y, Komiya T, Maeda S, Ito A, Yoshida M (2012) Depression of mitochondrial metabolism by downregulation of cytoplasmic deacetylase, HDAC6. FEBS Lett 586:1379-1383. doi:10.1016/j.febslet.2012.03.060

105. Kanayama A, Seth RB, Sun L, Ea CK, Hong M, Shaito A, Chiu YH, Deng L, Chen ZJ (2004) TAB2 and TAB3 activate the NF-kappaB pathway through binding to polyubiquitin chains. Molecular cell 15:535-548. doi:10.1016/j.molcel.2004.08.008

106. Kaser A, Lee AH, Franke A, Glickman JN, Zeissig S, Tilg H, Nieuwenhuis EE, Higgins DE, Schreiber S, Glimcher LH, Blumberg RS (2008) XBP1 links ER stress to intestinal inflammation and confers genetic risk for human inflammatory bowel disease. Cell 134:743-756. doi:10.1016/j.cell.2008.07.021

107. Kawaguchi Y, Kovacs JJ, McLaurin A, Vance JM, Ito A, Yao TP (2003) The deacetylase HDAC6 regulates aggresome formation and cell viability in response to misfolded protein stress. Cell 115:727-738

108. Kawasaki T, Kawai T (2014) Toll-like receptor signaling pathways. Front Immunol 5:461. doi:10.3389/fimmu.2014.00461

109. Kayal S, Lilienbaum A, Join-Lambert O, Li X, Israel A, Berche P (2002) Listeriolysin O secreted by Listeria monocytogenes induces NF-kappaB signalling by activating the IkappaB kinase complex. Mol Microbiol 44:1407-1419

110. Kekatpure VD, Dannenberg AJ, Subbaramaiah K (2009) HDAC6 modulates Hsp90 chaperone activity and regulates activation of aryl hydrocarbon receptor signaling. The Journal of biological chemistry 284:7436-7445. doi:10.1074/jbc.M808999200

111. Khelef N, Lecuit M, Bierne H, Cossart P (2006) Species specificity of the Listeria monocytogenes InlB protein. Cell Microbiol 8:457-470. doi:10.1111/j.1462-5822.2005.00634.x

112. Kimura S, Noda T, Yoshimori T (2008) Dynein-dependent movement of autophagosomes mediates efficient encounters with lysosomes. Cell Struct Funct 33:109-122

113. Kocks C, Hellio R, Gounon P, Ohayon H, Cossart P (1993) Polarized distribution of Listeria monocytogenes surface protein ActA at the site of directional actin assembly. Journal of cell science 105 (Pt 3):699-710

114. Komander D, Rape M (2012) The ubiquitin code. Annu Rev Biochem 81:203-229. doi:10.1146/annurev-biochem-060310-170328

115. Kopito RR (2003) The missing linker: an unexpected role for a histone deacetylase. Molecular cell 12:1349-1351

116. Kovacs JJ, Murphy PJ, Gaillard S, Zhao X, Wu JT, Nicchitta CV, Yoshida M, Toft DO, Pratt WB, Yao TP (2005) HDAC6 regulates Hsp90 acetylation and chaperone-dependent activation of glucocorticoid receptor. Molecular cell 18:601-607. doi:10.1016/j.molcel.2005.04.021

117. Kuhbacher A, Emmenlauer M, Ramo P, Kafai N, Dehio C, Cossart P, Pizarro-Cerda J (2015) Genome-Wide siRNA Screen Identifies Complementary Signaling Pathways Involved in Listeria Infection and Reveals Different Actin Nucleation Mechanisms during Listeria Cell Invasion and Actin Comet Tail Formation. MBio 6:e00598-00515. doi:10.1128/mBio.00598-15

118. Kuo MH, Allis CD (1998) Roles of histone acetyltransferases and deacetylases in gene regulation. BioEssays : news and reviews in molecular, cellular and developmental biology 20:615-626. doi:10.1002/(SICI)1521-1878(199808)20:8<615::AID-BIES4>3.0.CO;2-H

119. Lafarga V, Aymerich I, Tapia O, Mayor F, Jr., Penela P (2012) A novel GRK2/HDAC6 interaction modulates cell spreading and motility. EMBO J 31:856-869. doi:10.1038/emboj.2011.466

120. Lam GY, Cemma M, Muise AM, Higgins DE, Brumell JH (2013) Host and bacterial factors that regulate LC3 recruitment to Listeria monocytogenes during the early stages of macrophage infection. Autophagy 9:985-995. doi:10.4161/auto.24406

121. Lambrechts A, Gevaert K, Cossart P, Vandekerckhove J, Van Troys M (2008) Listeria comet tails: the actin-based motility machinery at work. Trends Cell Biol 18:220-227. doi:10.1016/j.tcb.2008.03.001

122. Lebreton A, Job V, Ragon M, Le Monnier A, Dessen A, Cossart P, Bierne H (2014) Structural basis for the inhibition of the chromatin repressor BAHD1 by the bacterial nucleomodulin LntA. MBio 5:e00775-00713. doi:10.1128/mBio.00775-13

123. Lebreton A, Lakisic G, Job V, Fritsch L, Tham TN, Camejo A, Mattei PJ, Regnault B, Nahori MA, Cabanes D, Gautreau A, Ait-Si-Ali S, Dessen A, Cossart P, Bierne H (2011) A bacterial protein targets the BAHD1 chromatin complex to stimulate type III interferon response. Science 331:1319-1321. doi:10.1126/science.1200120

124. Lecuit M, Dramsi S, Gottardi C, Fedor-Chaiken M, Gumbiner B, Cossart P (1999) A single amino acid in E-cadherin responsible for host specificity towards the human pathogen Listeria monocytogenes. EMBO J 18:3956-3963. doi:10.1093/emboj/18.14.3956

125. Lecuit M, Vandormael-Pournin S, Lefort J, Huerre M, Gounon P, Dupuy C, Babinet C, Cossart P (2001) A transgenic model for listeriosis: role of internalin in crossing the intestinal barrier. Science 292:1722-1725. doi:10.1126/science.1059852

126. Lee JY, Kapur M, Li M, Choi MC, Choi S, Kim HJ, Kim I, Lee E, Taylor JP, Yao TP (2014) MFN1 deacetylation activates adaptive mitochondrial fusion and protects metabolically challenged mitochondria. Journal of cell science 127:4954-4963. doi:10.1242/jcs.157321

127. Lee JY, Koga H, Kawaguchi Y, Tang W, Wong E, Gao YS, Pandey UB, Kaushik S, Tresse E, Lu J, Taylor JP, Cuervo AM, Yao TP (2010) HDAC6 controls autophagosome maturation essential for ubiquitin-selective quality-control autophagy. EMBO J 29:969-980. doi:10.1038/emboj.2009.405

128. Lee JY, Nagano Y, Taylor JP, Lim KL, Yao TP (2010) Disease-causing mutations in parkin impair mitochondrial ubiquitination, aggregation, and HDAC6-dependent mitophagy. J Cell Biol 189:671-679. doi:10.1083/jcb.201001039

129. Lee JY, Yao TP (2010) Quality control autophagy: a joint effort of ubiquitin, protein deacetylase and actin cytoskeleton. Autophagy 6:555-557. doi:10.4161/auto.6.4.11812

130. Lee SW, Yang J, Kim SY, Jeong HK, Lee J, Kim WJ, Lee EJ, Kim HS (2015) MicroRNA-26a induced by hypoxia targets HDAC6 in myogenic differentiation of embryonic stem cells. Nucleic Acids Res 43:2057-2073. doi:10.1093/nar/gkv088

131. Lee YS, Park JS, Kim JH, Jung SM, Lee JY, Kim SJ, Park SH (2011) Smad6-specific recruitment of Smurf E3 ligases mediates TGF-beta1-induced degradation of MyD88 in TLR4 signalling. Nature communications 2:460. doi:10.1038/ncomms1469

132. Lewis AJ, Dhakal BK, Liu T, Mulvey MA (2016) Histone Deacetylase 6 Regulates Bladder Architecture and Host Susceptibility to Uropathogenic Escherichia coli. Pathogens 5. doi:10.3390/pathogens5010020

133. Leyk J, Goldbaum O, Noack M, Richter-Landsberg C (2015) Inhibition of HDAC6 modifies tau inclusion body formation and impairs autophagic clearance. J Mol Neurosci 55:1031-1046. doi:10.1007/s12031-014-0460-y

134. Li Y, Shin D, Kwon SH (2013) Histone deacetylase 6 plays a role as a distinct regulator of diverse cellular processes. FEBS J 280:775-793. doi:10.1111/febs.12079

135. Li Y, Zhang X, Polakiewicz RD, Yao TP, Comb MJ (2008) HDAC6 is required for epidermal growth factor-induced beta-catenin nuclear localization. The Journal of biological chemistry 283:12686-12690. doi:10.1074/jbc.C700185200

136. Liu H, Wang M, Li M, Wang D, Rao Q, Wang Y, Xu Z, Wang J (2008) Expression and role of DJ-1 in leukemia. Biochemical and biophysical research communications 375:477-483. doi:10.1016/j.bbrc.2008.08.046

137. Liu HM, Jiang F, Loo YM, Hsu S, Hsiang TY, Marcotrigiano J, Gale M, Jr. (2016) Regulation of Retinoic Acid Inducible Gene-I (RIG-I) Activation by the Histone Deacetylase 6. EBioMedicine 9:195-206. doi:10.1016/j.ebiom.2016.06.015

138. Liu KP, Zhou D, Ouyang DY, Xu LH, Wang Y, Wang LX, Pan H, He XH (2013) LC3B-II deacetylation by histone deacetylase 6 is involved in serum-starvation-induced autophagic degradation. Biochemical and biophysical research communications 441:970-975. doi:10.1016/j.bbrc.2013.11.007

139. Liu S, Chen ZJ (2011) Expanding role of ubiquitination in NF-kappaB signaling. Cell Res 21:6-21. doi:10.1038/cr.2010.170

140. Liu W, Fan LX, Zhou X, Sweeney WE, Jr., Avner ED, Li X (2012) HDAC6 regulates epidermal growth factor receptor (EGFR) endocytic trafficking and degradation in renal epithelial cells. PloS one 7:e49418. doi:10.1371/journal.pone.0049418

141. Liu Y, Peng L, Seto E, Huang S, Qiu Y (2012) Modulation of histone deacetylase 6 (HDAC6) nuclear import and tubulin deacetylase activity through acetylation. The Journal of biological chemistry 287:29168-29174. doi:10.1074/jbc.M112.371120

142. Liu YC, Penninger J, Karin M (2005) Immunity by ubiquitylation: a reversible process of modification. Nature reviews Immunology 5:941-952. doi:10.1038/nri1731

143. Lwin T, Zhao X, Cheng F, Zhang X, Huang A, Shah B, Zhang Y, Moscinski LC, Choi YS, Kozikowski AP, Bradner JE, Dalton WS, Sotomayor E, Tao J (2013) A microenvironment-mediated c-Myc/miR-548m/HDAC6 amplification loop in non-Hodgkin B cell lymphomas. J Clin Invest 123:4612-4626. doi:10.1172/JCI64210

144. MacMicking JD, Nathan C, Hom G, Chartrain N, Fletcher DS, Trumbauer M, Stevens K, Xie QW, Sokol K, Hutchinson N, et al. (1995) Altered responses to bacterial infection and endotoxic shock in mice lacking inducible nitric oxide synthase. Cell 81:641-650

145. Mak AB, Nixon AM, Kittanakom S, Stewart JM, Chen GI, Curak J, Gingras AC, Mazitschek R, Neel BG, Stagljar I, Moffat J (2012) Regulation of CD133 by HDAC6 promotes beta-catenin signaling to suppress cancer cell differentiation. Cell Rep 2:951-963. doi:10.1016/j.celrep.2012.09.016

146. Malet JK, Cossart P, Ribet D (2017) Alteration of epithelial cell lysosomal integrity induced by bacterial cholesterol-dependent cytolysins. Cell Microbiol 19. doi:10.1111/cmi.12682

147. Mansini AP, Lorenzo Pisarello MJ, Thelen KM, Cruz-Reyes M, Peixoto E, Jin S, Howard BN, Trussoni CE, Gajdos GB, LaRusso NF, Perugorria MJ, Banales JM, Gradilone SA (2018) MiR-433 and miR-22

dysregulations induce HDAC6 overexpression and ciliary loss in cholangiocarcinoma. Hepatology. doi:10.1002/hep.29832

148. Marquis H, Doshi V, Portnoy DA (1995) The broad-range phospholipase C and a metalloprotease mediate listeriolysin O-independent escape of Listeria monocytogenes from a primary vacuole in human epithelial cells. Infect Immun 63:4531-4534

149. Martinez-Bartolome S, Navarro P, Martin-Maroto F, Lopez-Ferrer D, Ramos-Fernandez A, Villar M, Garcia-Ruiz JP, Vazquez J (2008) Properties of average score distributions of SEQUEST: the probability ratio method. Mol Cell Proteomics 7:1135-1145. doi:10.1074/mcp.M700239-MCP200

150. Martinez del Hoyo G, Ramirez-Huesca M, Levy S, Boucheix C, Rubinstein E, Minguito de la Escalera M, Gonzalez-Cintado L, Ardavin C, Veiga E, Yanez-Mo M, Sanchez-Madrid F (2015) CD81 controls immunity to Listeria infection through rac-dependent inhibition of proinflammatory mediator release and activation of cytotoxic T cells. Journal of immunology 194:6090-6101. doi:10.4049/jimmunol.1402957

151. Matsuyama A, Shimazu T, Sumida Y, Saito A, Yoshimatsu Y, Seigneurin-Berny D, Osada H, Komatsu Y, Nishino N, Khochbin S, Horinouchi S, Yoshida M (2002) In vivo destabilization of dynamic microtubules by HDAC6-mediated deacetylation. EMBO J 21:6820-6831

152. McFarland AP, Luo S, Ahmed-Qadri F, Zuck M, Thayer EF, Goo YA, Hybiske K, Tong L, Woodward JJ (2017) Sensing of Bacterial Cyclic Dinucleotides by the Oxidoreductase RECON Promotes NF-kappaB Activation and Shapes a Proinflammatory Antibacterial State. Immunity 46:433-445. doi:10.1016/j.immuni.2017.02.014

153. Medler TR, Craig JM, Fiorillo AA, Feeney YB, Harrell JC, Clevenger CV (2016) HDAC6 Deacetylates HMGN2 to Regulate Stat5a Activity and Breast Cancer Growth. Mol Cancer Res 14:994-1008. doi:10.1158/1541-7786.MCR-16-0109

154. Michel E, Reich KA, Favier R, Berche P, Cossart P (1990) Attenuated mutants of the intracellular bacterium Listeria monocytogenes obtained by single amino acid substitutions in listeriolysin O. Mol Microbiol 4:2167-2178

155. Min SW, Cho SH, Zhou Y, Schroeder S, Haroutunian V, Seeley WW, Huang EJ, Shen Y, Masliah E, Mukherjee C, Meyers D, Cole PA, Ott M, Gan L (2010) Acetylation of tau inhibits its degradation and contributes to tauopathy. Neuron 67:953-966. doi:10.1016/j.neuron.2010.08.044

156. Miyake Y, Keusch JJ, Wang L, Saito M, Hess D, Wang X, Melancon BJ, Helquist P, Gut H, Matthias P (2016) Structural insights into HDAC6 tubulin deacetylation and its selective inhibition. Nat Chem Biol 12:748-754. doi:10.1038/nchembio.2140

157. Monack DM, Theriot JA (2001) Actin-based motility is sufficient for bacterial membrane protrusion formation and host cell uptake. Cell Microbiol 3:633-647

158. Montoya MC, Sancho D, Bonello G, Collette Y, Langlet C, He HT, Aparicio P, Alcover A, Olive D, Sanchez-Madrid F (2002) Role of ICAM-3 in the initial interaction of T lymphocytes and APCs. Nat Immunol 3:159-168. doi:10.1038/ni753

159. Mortenson JB, Heppler LN, Banks CJ, Weerasekara VK, Whited MD, Piccolo SR, Johnson WE, Thompson JW, Andersen JL (2015) Histone deacetylase 6 (HDAC6) promotes the pro-survival activity of 14-3-3zeta via deacetylation of lysines within the 14-3-3zeta binding pocket. The Journal of biological chemistry 290:12487-12496. doi:10.1074/jbc.M114.607580

160. Mostowy S, Sancho-Shimizu V, Hamon MA, Simeone R, Brosch R, Johansen T, Cossart P (2011) p62 and NDP52 proteins target intracytosolic Shigella and Listeria to different autophagy pathways. The Journal of biological chemistry 286:26987-26995. doi:10.1074/jbc.M111.223610

161. Moura A, Criscuolo A, Pouseele H, Maury MM, Leclercq A, Tarr C, Bjorkman JT, Dallman T, Reimer A, Enouf V, Larsonneur E, Carleton H, Bracq-Dieye H, Katz LS, Jones L, Touchon M, Tourdjman M, Walker M, Stroika S, Cantinelli T, Chenal-Francisque V, Kucerova Z, Rocha EP, Nadon C, Grant K, Nielsen EM, Pot B, Gerner-Smidt P, Lecuit M, Brisse S (2016) Whole genome-based population biology and epidemiological surveillance of Listeria monocytogenes. Nat Microbiol 2:16185. doi:10.1038/nmicrobiol.2016.185

162. Moynagh PN (2005) TLR signalling and activation of IRFs: revisiting old friends from the NF-kappaB pathway. Trends Immunol 26:469-476. doi:10.1016/j.it.2005.06.009

163. Murray EGD, Webb, M. A. and Swann, M. B. R. A. (1926) Disease of rabbits characterised by a large mononuclear leucocytosis, caused by a hitherto underscribed bacillus *Bacterium monocytogenens* (n. sp.). J Pathol 29:407-439

164. Nahhas F, Dryden SC, Abrams J, Tainsky MA (2007) Mutations in SIRT2 deacetylase which regulate enzymatic activity but not its interaction with HDAC6 and tubulin. Mol Cell Biochem 303:221-230. doi:10.1007/s11010-007-9478-6

165. Nakashima H, Kaufmann JK, Wang PY, Nguyen T, Speranza MC, Kasai K, Okemoto K, Otsuki A, Nakano I, Fernandez S, Goins WF, Grandi P, Glorioso JC, Lawler S, Cripe TP, Chiocca EA (2015)

Histone deacetylase 6 inhibition enhances oncolytic viral replication in glioma. J Clin Invest 125:4269-4280. doi:10.1172/JCI80713

166. Nakashima H, Nguyen T, Goins WF, Chiocca EA (2015) Interferon-stimulated gene 15 (ISG15) and ISG15-linked proteins can associate with members of the selective autophagic process, histone deacetylase 6 (HDAC6) and SQSTM1/p62. The Journal of biological chemistry 290:1485-1495. doi:10.1074/jbc.M114.593871

167. Nakka KK, Chaudhary N, Joshi S, Bhat J, Singh K, Chatterjee S, Malhotra R, De A, Santra MK, Dilworth FJ, Chattopadhyay S (2015) Nuclear matrix-associated protein SMAR1 regulates alternative splicing via HDAC6-mediated deacetylation of Sam68. Proc Natl Acad Sci U S A 112:E3374-3383. doi:10.1073/pnas.1418603112

168. Navarro P, Vazquez J (2009) A refined method to calculate false discovery rates for peptide identification using decoy databases. J Proteome Res 8:1792-1796. doi:10.1021/pr800362h

169. Netea MG, Joosten LA, Latz E, Mills KH, Natoli G, Stunnenberg HG, O'Neill LA, Xavier RJ (2016) Trained immunity: A program of innate immune memory in health and disease. Science 352:aaf1098. doi:10.1126/science.aaf1098

170. Neuenhahn M, Kerksiek KM, Nauerth M, Suhre MH, Schiemann M, Gebhardt FE, Stemberger C, Panthel K, Schroder S, Chakraborty T, Jung S, Hochrein H, Russmann H, Brocker T, Busch DH (2006) CD8alpha+ dendritic cells are required for efficient entry of Listeria monocytogenes into the spleen. Immunity 25:619-630. doi:10.1016/j.immuni.2006.07.017

171. New M, Sheikh S, Bekheet M, Olzscha H, Thezenas ML, Care MA, Fotheringham S, Tooze RM, Kessler B, La Thangue NB (2016) TLR Adaptor Protein MYD88 Mediates Sensitivity to HDAC Inhibitors via a Cytokine-Dependent Mechanism. Cancer research 76:6975-6987. doi:10.1158/0008-5472.CAN-16-0504

172. Ni CY, Wu ZH, Florence WC, Parekh VV, Arrate MP, Pierce S, Schweitzer B, Van Kaer L, Joyce S, Miyamoto S, Ballard DW, Oltz EM (2008) Cutting edge: K63-linked polyubiquitination of NEMO modulates TLR signaling and inflammation in vivo. Journal of immunology 180:7107-7111

173. Nickol AD, Bonventre PF (1977) Anomalous high native resistance to athymic mice to bacterial pathogens. Infect Immun 18:636-645

174. Nikitas G, Deschamps C, Disson O, Niault T, Cossart P, Lecuit M (2011) Transcytosis of Listeria monocytogenes across the intestinal barrier upon specific targeting of goblet cell accessible E-cadherin. J Exp Med 208:2263-2277. doi:10.1084/jem.20110560

175. North RJ, Dunn PL, Conlan JW (1997) Murine listeriosis as a model of antimicrobial defense. Immunol Rev 158:27-36

176. Nunez-Andrade N, Iborra S, Trullo A, Moreno-Gonzalo O, Calvo E, Catalan E, Menasche G, Sancho D, Vazquez J, Yao TP, Martin-Cofreces NB, Sanchez-Madrid F (2016) HDAC6 regulates the dynamics of lytic granules in cytotoxic T lymphocytes. Journal of cell science 129:1305-1311. doi:10.1242/jcs.180885

177. O'Connell RM, Saha SK, Vaidya SA, Bruhn KW, Miranda GA, Zarnegar B, Perry AK, Nguyen BO, Lane TF, Taniguchi T, Miller JF, Cheng G (2004) Type I interferon production enhances susceptibility to Listeria monocytogenes infection. J Exp Med 200:437-445. doi:10.1084/jem.20040712

178. O'Riordan M, Portnoy DA (2002) The host cytosol: front-line or home front? Trends Microbiol 10:361-364

179. Olzmann JA, Chin LS (2008) Parkin-mediated K63-linked polyubiquitination: a signal for targeting misfolded proteins to the aggresome-autophagy pathway. Autophagy 4:85-87

180. Olzmann JA, Li L, Chudaev MV, Chen J, Perez FA, Palmiter RD, Chin LS (2007) Parkin-mediated K63-linked polyubiquitination targets misfolded DJ-1 to aggresomes via binding to HDAC6. J Cell Biol 178:1025-1038. doi:10.1083/jcb.200611128

181. Orsi RH, Wiedmann M (2016) Characteristics and distribution of Listeria spp., including Listeria species newly described since 2009. Appl Microbiol Biotechnol 100:5273-5287. doi:10.1007/s00253-016-7552-2

182. Osborne SE, Sit B, Shaker A, Currie E, Tan JM, van Rijn J, Higgins DE, Brumell JH (2017) Type I interferon promotes cell-to-cell spread of Listeria monocytogenes. Cell Microbiol 19. doi:10.1111/cmi.12660

183. Ouyang H, Ali YO, Ravichandran M, Dong A, Qiu W, MacKenzie F, Dhe-Paganon S, Arrowsmith CH, Zhai RG (2012) Protein aggregates are recruited to aggresome by histone deacetylase 6 via unanchored ubiquitin C termini. The Journal of biological chemistry 287:2317-2327. doi:10.1074/jbc.M111.273730

184. Palazzo A, Ackerman B, Gundersen GG (2003) Cell biology: Tubulin acetylation and cell motility. Nature 421:230. doi:10.1038/421230a

185. Pamer EG (2004) Immune responses to Listeria monocytogenes. Nature reviews Immunology 4:812-823. doi:10.1038/nri1461

186. Pandey UB, Nie Z, Batlevi Y, McCray BA, Ritson GP, Nedelsky NB, Schwartz SL, DiProspero NA, Knight MA, Schuldiner O, Padmanabhan R, Hild M, Berry DL, Garza D, Hubbert CC, Yao TP, Baehrecke EH, Taylor JP (2007) HDAC6 rescues neurodegeneration and provides an essential link between autophagy and the UPS. Nature 447:859-863. doi:10.1038/nature05853

187. Parmigiani RB, Xu WS, Venta-Perez G, Erdjument-Bromage H, Yaneva M, Tempst P, Marks PA (2008) HDAC6 is a specific deacetylase of peroxiredoxins and is involved in redox regulation. Proc Natl Acad Sci U S A 105:9633-9638. doi:10.1073/pnas.0803749105

188. Pentecost M, Kumaran J, Ghosh P, Amieva MR (2010) Listeria monocytogenes internalin B activates junctional endocytosis to accelerate intestinal invasion. PLoS Pathog 6:e1000900. doi:10.1371/journal.ppat.1000900

189. Perelman SS, Abrams ME, Eitson JL, Chen D, Jimenez A, Mettlen M, Schoggins JW, Alto NM (2016) Cell-Based Screen Identifies Human Interferon-Stimulated Regulators of Listeria monocytogenes Infection. PLoS Pathog 12:e1006102. doi:10.1371/journal.ppat.1006102

190. Perez M, Santa-Maria I, Gomez de Barreda E, Zhu X, Cuadros R, Cabrero JR, Sanchez-Madrid F, Dawson HN, Vitek MP, Perry G, Smith MA, Avila J (2009) Tau--an inhibitor of deacetylase HDAC6 function. J Neurochem 109:1756-1766. doi:10.1111/j.1471-4159.2009.06102.x

191. Pfeffer K, Matsuyama T, Kundig TM, Wakeham A, Kishihara K, Shahinian A, Wiegmann K, Ohashi PS, Kronke M, Mak TW (1993) Mice deficient for the 55 kd tumor necrosis factor receptor are resistant to endotoxic shock, yet succumb to L. monocytogenes infection. Cell 73:457-467

192. Pillich H, Loose M, Zimmer KP, Chakraborty T (2012) Activation of the unfolded protein response by Listeria monocytogenes. Cell Microbiol 14:949-964. doi:10.1111/j.1462-5822.2012.01769.x

193. Pizarro-Cerda J, Cossart P (2009) Listeria monocytogenes membrane trafficking and lifestyle: the exception or the rule? Annu Rev Cell Dev Biol 25:649-670. doi:10.1146/annurev.cellbio.042308.113331

194. Pizarro-Cerda J, Kuhbacher A, Cossart P (2012) Entry of Listeria monocytogenes in mammalian epithelial cells: an updated view. Cold Spring Harb Perspect Med 2. doi:10.1101/cshperspect.a010009

195. Portnoy DA, Auerbuch V, Glomski IJ (2002) The cell biology of Listeria monocytogenes infection: the intersection of bacterial pathogenesis and cell-mediated immunity. J Cell Biol 158:409-414. doi:10.1083/jcb.200205009

196. Pugacheva EN, Jablonski SA, Hartman TR, Henske EP, Golemis EA (2007) HEF1-dependent Aurora A activation induces disassembly of the primary cilium. Cell 129:1351-1363. doi:10.1016/j.cell.2007.04.035

197. Py BF, Lipinski MM, Yuan J (2007) Autophagy limits Listeria monocytogenes intracellular growth in the early phase of primary infection. Autophagy 3:117-125

198. Radoshevich L, Cossart P (2018) Listeria monocytogenes: towards a complete picture of its physiology and pathogenesis. Nat Rev Microbiol 16:32-46. doi:10.1038/nrmicro.2017.126

199. Radoshevich L, Dussurget O (2016) Cytosolic Innate Immune Sensing and Signaling upon Infection. Front Microbiol 7:313. doi:10.3389/fmicb.2016.00313

200. Radoshevich L, Impens F, Ribet D, Quereda JJ, Nam Tham T, Nahori MA, Bierne H, Dussurget O, Pizarro-Cerda J, Knobeloch KP, Cossart P (2015) ISG15 counteracts Listeria monocytogenes infection. Elife 4. doi:10.7554/eLife.06848

201. Rajabian T, Gavicherla B, Heisig M, Muller-Altrock S, Goebel W, Gray-Owen SD, Ireton K (2009) The bacterial virulence factor InlC perturbs apical cell junctions and promotes cell-to-cell spread of Listeria. Nat Cell Biol 11:1212-1218. doi:10.1038/ncb1964

202. Rao R, Fiskus W, Yang Y, Lee P, Joshi R, Fernandez P, Mandawat A, Atadja P, Bradner JE, Bhalla K (2008) HDAC6 inhibition enhances 17-AAG--mediated abrogation of hsp90 chaperone function in human leukemia cells. Blood 112:1886-1893. doi:10.1182/blood-2008-03-143644

203. Reed NA, Cai D, Blasius TL, Jih GT, Meyhofer E, Gaertig J, Verhey KJ (2006) Microtubule acetylation promotes kinesin-1 binding and transport. Curr Biol 16:2166-2172. doi:10.1016/j.cub.2006.09.014

204. Ribet D, Hamon M, Gouin E, Nahori MA, Impens F, Neyret-Kahn H, Gevaert K, Vandekerckhove J, Dejean A, Cossart P (2010) Listeria monocytogenes impairs SUMOylation for efficient infection. Nature 464:1192-1195. doi:10.1038/nature08963

205. Rich KA, Burkett C, Webster P (2003) Cytoplasmic bacteria can be targets for autophagy. Cell Microbiol 5:455-468

206. Richter-Landsberg C, Leyk J (2013) Inclusion body formation, macroautophagy, and the role of HDAC6 in neurodegeneration. Acta Neuropathol 126:793-807. doi:10.1007/s00401-013-1158-x

207. Riolo MT, Cooper ZA, Holloway MP, Cheng Y, Bianchi C, Yakirevich E, Ma L, Chin YE, Altura RA (2012) Histone deacetylase 6 (HDAC6) deacetylates survivin for its nuclear export in breast cancer. The Journal of biological chemistry 287:10885-10893. doi:10.1074/jbc.M111.308791

208. Roger T, Lugrin J, Le Roy D, Goy G, Mombelli M, Koessler T, Ding XC, Chanson AL, Reymond MK, Miconnet I, Schrenzel J, Francois P, Calandra T (2011) Histone deacetylase inhibitors impair innate immune responses to Toll-like receptor agonists and to infection. Blood 117:1205-1217. doi:10.1182/blood-2010-05-284711

209. Rothe J, Lesslauer W, Lotscher H, Lang Y, Koebel P, Kontgen F, Althage A, Zinkernagel R, Steinmetz M, Bluethmann H (1993) Mice lacking the tumour necrosis factor receptor 1 are resistant to TNF-mediated toxicity but highly susceptible to infection by Listeria monocytogenes. Nature 364:798-802. doi:10.1038/364798a0

210. Rytkonen A, Poh J, Garmendia J, Boyle C, Thompson A, Liu M, Freemont P, Hinton JC, Holden DW (2007) SseL, a Salmonella deubiquitinase required for macrophage killing and virulence. Proc Natl Acad Sci U S A 104:3502-3507. doi:10.1073/pnas.0610095104

211. Sabet C, Lecuit M, Cabanes D, Cossart P, Bierne H (2005) LPXTG protein InlJ, a newly identified internalin involved in Listeria monocytogenes virulence. Infect Immun 73:6912-6922. doi:10.1128/IAI.73.10.6912-6922.2005

212. Salemi LM, Almawi AW, Lefebvre KJ, Schild-Poulter C (2014) Aggresome formation is regulated by RanBPM through an interaction with HDAC6. Biol Open 3:418-430. doi:10.1242/bio.20147021

213. Scher MB, Vaquero A, Reinberg D (2007) SirT3 is a nuclear NAD+-dependent histone deacetylase that translocates to the mitochondria upon cellular stress. Genes Dev 21:920-928. doi:10.1101/gad.1527307

214. Schlech WF, 3rd, Lavigne PM, Bortolussi RA, Allen AC, Haldane EV, Wort AJ, Hightower AW, Johnson SE, King SH, Nicholls ES, Broome CV (1983) Epidemic listeriosis--evidence for transmission by food. N Engl J Med 308:203-206. doi:10.1056/NEJM198301273080407

215. Schofield AV, Gamell C, Bernard O (2013) Tubulin polymerization promoting protein 1 (TPPP1) increases beta-catenin expression through inhibition of HDAC6 activity in U2OS osteosarcoma cells. Biochemical and biophysical research communications 436:571-577. doi:10.1016/j.bbrc.2013.05.076

216. Seigneurin-Berny D, Verdel A, Curtet S, Lemercier C, Garin J, Rousseaux S, Khochbin S (2001) Identification of components of the murine histone deacetylase 6 complex: link between acetylation and ubiquitination signaling pathways. Mol Cell Biol 21:8035-8044. doi:10.1128/MCB.21.23.8035-8044.2001

217. Seki E, Tsutsui H, Tsuji NM, Hayashi N, Adachi K, Nakano H, Futatsugi-Yumikura S, Takeuchi O, Hoshino K, Akira S, Fujimoto J, Nakanishi K (2002) Critical roles of myeloid differentiation factor 88-dependent proinflammatory cytokine release in early phase clearance of Listeria monocytogenes in mice. Journal of immunology 169:3863-3868

218. Serbina NV, Kuziel W, Flavell R, Akira S, Rollins B, Pamer EG (2003) Sequential MyD88-independent and -dependent activation of innate immune responses to intracellular bacterial infection. Immunity 19:891-901

219. Serbina NV, Salazar-Mather TP, Biron CA, Kuziel WA, Pamer EG (2003) TNF/iNOS-producing dendritic cells mediate innate immune defense against bacterial infection. Immunity 19:59-70

220. Serrador JM, Cabrero JR, Sancho D, Mittelbrunn M, Urzainqui A, Sanchez-Madrid F (2004) HDAC6 deacetylase activity links the tubulin cytoskeleton with immune synapse organization. Immunity 20:417-428

221. Shen Y, Naujokas M, Park M, Ireton K (2000) InIB-dependent internalization of Listeria is mediated by the Met receptor tyrosine kinase. Cell 103:501-510

222. Shiloh MU, MacMicking JD, Nicholson S, Brause JE, Potter S, Marino M, Fang F, Dinauer M, Nathan C (1999) Phenotype of mice and macrophages deficient in both phagocyte oxidase and inducible nitric oxide synthase. Immunity 10:29-38

223. Shirakawa K, Chavez L, Hakre S, Calvanese V, Verdin E (2013) Reactivation of latent HIV by histone deacetylase inhibitors. Trends Microbiol 21:277-285. doi:10.1016/j.tim.2013.02.005

224. Simon D, Laloo B, Barillot M, Barnetche T, Blanchard C, Rooryck C, Marche M, Burgelin I, Coupry I, Chassaing N, Gilbert-Dussardier B, Lacombe D, Grosset C, Arveiler B (2010) A mutation in the 3'-UTR of the HDAC6 gene abolishing the post-transcriptional regulation mediated by hsa-miR-433 is linked to a new form of dominant X-linked chondrodysplasia. Hum Mol Genet 19:2015-2027. doi:10.1093/hmg/ddq083

225. Skoble J, Portnoy DA, Welch MD (2000) Three regions within ActA promote Arp2/3 complex-mediated actin nucleation and Listeria monocytogenes motility. J Cell Biol 150:527-538

226. Soo Youn G, Ju SM, Choi SY, Park J (2015) HDAC6 mediates HIV-1 tat-induced proinflammatory responses by regulating MAPK-NF-kappaB/AP-1 pathways in astrocytes. Glia. doi:10.1002/glia.22865

227. Stavru F, Bouillaud F, Sartori A, Ricquier D, Cossart P (2011) Listeria monocytogenes transiently alters mitochondrial dynamics during infection. Proc Natl Acad Sci U S A 108:3612-3617. doi:10.1073/pnas.1100126108

228. Stavru F, Cossart P (2011) Listeria infection modulates mitochondrial dynamics. Commun Integr Biol 4:364-366. doi:10.4161/cib.4.2.15506

229. Stavru F, Palmer AE, Wang C, Youle RJ, Cossart P (2013) Atypical mitochondrial fission upon bacterial infection. Proc Natl Acad Sci U S A 110:16003-16008. doi:10.1073/pnas.1315784110

230. Stockinger S, Reutterer B, Schaljo B, Schellack C, Brunner S, Materna T, Yamamoto M, Akira S, Taniguchi T, Murray PJ, Muller M, Decker T (2004) IFN regulatory factor 3-dependent induction of type I IFNs by intracellular bacteria is mediated by a TLR- and Nod2-independent mechanism. Journal of immunology 173:7416-7425

231. Stoner MW, Thapa D, Zhang M, Gibson GA, Calderon MJ, St Croix CM, Scott I (2016) alpha-Lipoic acid promotes alpha-tubulin hyperacetylation and blocks the turnover of mitochondria through mitophagy. The Biochemical journal 473:1821-1830. doi:10.1042/BCJ20160281

232. Subramanian C, Jarzembowski JA, Opipari AW, Jr., Castle VP, Kwok RP (2011) HDAC6 deacetylates Ku70 and regulates Ku70-Bax binding in neuroblastoma. Neoplasia 13:726-734

233. Swatek KN, Komander D (2016) Ubiquitin modifications. Cell Res 26:399-422. doi:10.1038/cr.2016.39

234. Takeda K, Akira S (2004) TLR signaling pathways. Semin Immunol 16:3-9

235. Tala, Sun X, Chen J, Zhang L, Liu N, Zhou J, Li D, Liu M (2014) Microtubule stabilization by Mdp3 is partially attributed to its modulation of HDAC6 in addition to its association with tubulin and microtubules. PloS one 9:e90932. doi:10.1371/journal.pone.0090932

236. Tam MA, Wick MJ (2004) Dendritic cells and immunity to Listeria: TipDCs are a new recruit. Trends Immunol 25:335-339. doi:10.1016/j.it.2004.05.004

237. Theisen E, Sauer JD (2016) Listeria monocytogenes and the Inflammasome: From Cytosolic Bacteriolysis to Tumor Immunotherapy. Curr Top Microbiol Immunol 397:133-160. doi:10.1007/978-3-319-41171-2_7

238. Tokesi N, Lehotzky A, Horvath I, Szabo B, Olah J, Lau P, Ovadi J (2010) TPPP/p25 promotes tubulin acetylation by inhibiting histone deacetylase 6. The Journal of biological chemistry 285:17896-17906. doi:10.1074/jbc.M109.096578

239. Torres D, Barrier M, Bihl F, Quesniaux VJ, Maillet I, Akira S, Ryffel B, Erard F (2004) Toll-like receptor 2 is required for optimal control of Listeria monocytogenes infection. Infect Immun 72:2131-2139

240. Tripp CS, Wolf SF, Unanue ER (1993) Interleukin 12 and tumor necrosis factor alpha are costimulators of interferon gamma production by natural killer cells in severe combined immunodeficiency mice with listeriosis, and interleukin 10 is a physiologic antagonist. Proc Natl Acad Sci U S A 90:3725-3729

241. Tsuji NM, Tsutsui H, Seki E, Kuida K, Okamura H, Nakanishi K, Flavell RA (2004) Roles of caspase-1 in Listeria infection in mice. Int Immunol 16:335-343

242. Unanue ER (1997) Studies in listeriosis show the strong symbiosis between the innate cellular system and the T-cell response. Immunol Rev 158:11-25

243. Valenzuela-Fernandez A, Alvarez S, Gordon-Alonso M, Barrero M, Ursa A, Cabrero JR, Fernandez G, Naranjo-Suarez S, Yanez-Mo M, Serrador JM, Munoz-Fernandez MA, Sanchez-Madrid F (2005) Histone deacetylase 6 regulates human immunodeficiency virus type 1 infection. Molecular biology of the cell 16:5445-5454. doi:10.1091/mbc.E05-04-0354

244. Valenzuela-Fernandez A, Cabrero JR, Serrador JM, Sanchez-Madrid F (2008) HDAC6: a key regulator of cytoskeleton, cell migration and cell-cell interactions. Trends Cell Biol 18:291-297. doi:10.1016/j.tcb.2008.04.003

245. Valera MS, de Armas-Rillo L, Barroso-Gonzalez J, Ziglio S, Batisse J, Dubois N, Marrero-Hernandez S, Borel S, Garcia-Exposito L, Biard-Piechaczyk M, Paillart JC, Valenzuela-Fernandez A (2015) The HDAC6/APOBEC3G complex regulates HIV-1 infectiveness by inducing Vif autophagic degradation. Retrovirology 12:53. doi:10.1186/s12977-015-0181-5

246. Vaquero A, Sternglanz R, Reinberg D (2007) NAD+-dependent deacetylation of H4 lysine 16 by class III HDACs. Oncogene 26:5505-5520. doi:10.1038/sj.onc.1210617

247. Vaudaux P, Waldvogel FA (1979) Gentamicin antibacterial activity in the presence of human polymorphonuclear leukocytes. Antimicrob Agents Chemother 16:743-749

248. Veiga E, Cossart P (2005) Listeria hijacks the clathrin-dependent endocytic machinery to invade mammalian cells. Nat Cell Biol 7:894-900. doi:10.1038/ncb1292

249. Wang D, Meng Q, Huo L, Yang M, Wang L, Chen X, Wang J, Li Z, Ye X, Liu N, Li Q, Dai Z, Ouyang H, Li N, Zhou J, Chen L, Liu L (2015) Overexpression of Hdac6 enhances resistance to virus infection in embryonic stem cells and in mice. Protein Cell 6:152-156. doi:10.1007/s13238-014-0120-6

250. Wang XC, Ma Y, Meng PS, Han JL, Yu HY, Bi LJ (2015) miR-433 inhibits oral squamous cell carcinoma (OSCC) cell growth and metastasis by targeting HDAC6. Oral Oncol 51:674-682. doi:10.1016/j.oraloncology.2015.04.010

251. Watabe M, Nakaki T (2011) Protein kinase CK2 regulates the formation and clearance of aggresomes in response to stress. Journal of cell science 124:1519-1532. doi:10.1242/jcs.081778

252. Way SS, Kollmann TR, Hajjar AM, Wilson CB (2003) Cutting edge: protective cell-mediated immunity to Listeria monocytogenes in the absence of myeloid differentiation factor 88. Journal of immunology 171:533-537

253. Wickstrom SA, Masoumi KC, Khochbin S, Fassler R, Massoumi R (2010) CYLD negatively regulates cell-cycle progression by inactivating HDAC6 and increasing the levels of acetylated tubulin. EMBO J 29:131-144. doi:10.1038/emboj.2009.317

254. Williams KA, Zhang M, Xiang S, Hu C, Wu JY, Zhang S, Ryan M, Cox AD, Der CJ, Fang B, Koomen J, Haura E, Bepler G, Nicosia SV, Matthias P, Wang C, Bai W, Zhang X (2013) Extracellular signal-regulated kinase (ERK) phosphorylates histone deacetylase 6 (HDAC6) at serine 1035 to stimulate cell migration. The Journal of biological chemistry 288:33156-33170. doi:10.1074/jbc.M113.472506

255. Witte CE, Archer KA, Rae CS, Sauer JD, Woodward JJ, Portnoy DA (2012) Innate immune pathways triggered by Listeria monocytogenes and their role in the induction of cell-mediated immunity. Adv Immunol 113:135-156. doi:10.1016/B978-0-12-394590-7.00002-6

256. Wojcik C, Yano M, DeMartino GN (2004) RNA interference of valosin-containing protein (VCP/p97) reveals multiple cellular roles linked to ubiquitin/proteasome-dependent proteolysis. Journal of cell science 117:281-292. doi:10.1242/jcs.00841

257. Woodward JJ, Iavarone AT, Portnoy DA (2010) c-di-AMP secreted by intracellular Listeria monocytogenes activates a host type I interferon response. Science 328:1703-1705. doi:10.1126/science.1189801

258. Wu CJ, Conze DB, Li T, Srinivasula SM, Ashwell JD (2006) Sensing of Lys 63-linked polyubiquitination by NEMO is a key event in NF-kappaB activation [corrected]. Nat Cell Biol 8:398-406. doi:10.1038/ncb1384

259. Xie R, Nguyen S, McKeehan WL, Liu L (2010) Acetylated microtubules are required for fusion of autophagosomes with lysosomes. BMC Cell Biol 11:89. doi:10.1186/1471-2121-11-89

260. Xu Y, Zhan Y, Lew AM, Naik SH, Kershaw MH (2007) Differential development of murine dendritic cells by GM-CSF versus Flt3 ligand has implications for inflammation and trafficking. Journal of immunology 179:7577-7584

261. Yan B, Xie S, Liu Z, Ran J, Li Y, Wang J, Yang Y, Zhou J, Li D, Liu M (2014) HDAC6 deacetylase activity is critical for lipopolysaccharide-induced activation of macrophages. PloS one 9:e110718. doi:10.1371/journal.pone.0110718

262. Yan J, Seibenhener ML, Calderilla-Barbosa L, Diaz-Meco MT, Moscat J, Jiang J, Wooten MW, Wooten MC (2013) SQSTM1/p62 interacts with HDAC6 and regulates deacetylase activity. PloS one 8:e76016. doi:10.1371/journal.pone.0076016

263. Yang CJ, Liu YP, Dai HY, Shiue YL, Tsai CJ, Huang MS, Yeh YT (2015) Nuclear HDAC6 inhibits invasion by suppressing NF-kappaB/MMP2 and is inversely correlated with metastasis of non-small cell lung cancer. Oncotarget 6:30263-30276. doi:10.18632/oncotarget.4749

264. Yang XJ, Seto E (2008) The Rpd3/Hda1 family of lysine deacetylases: from bacteria and yeast to mice and men. Nat Rev Mol Cell Biol 9:206-218. doi:10.1038/nrm2346

265. Yang Y, Ran J, Liu M, Li D, Li Y, Shi X, Meng D, Pan J, Ou G, Aneja R, Sun SC, Zhou J (2014) CYLD mediates ciliogenesis in multiple organs by deubiquitinating Cep70 and inactivating HDAC6. Cell Res 24:1342-1353. doi:10.1038/cr.2014.136

266. Yoshikawa Y, Ogawa M, Hain T, Yoshida M, Fukumatsu M, Kim M, Mimuro H, Nakagawa I, Yanagawa T, Ishii T, Kakizuka A, Sztul E, Chakraborty T, Sasakawa C (2009) Listeria monocytogenes ActA-mediated escape from autophagic recognition. Nat Cell Biol 11:1233-1240. doi:10.1038/ncb1967

267. Zhang L, Liu S, Liu N, Zhang Y, Liu M, Li D, Seto E, Yao TP, Shui W, Zhou J (2015) Proteomic identification and functional characterization of MYH9, Hsc70, and DNAJA1 as novel substrates of HDAC6 deacetylase activity. Protein Cell 6:42-54. doi:10.1007/s13238-014-0102-8

268. Zhang X, Yuan Z, Zhang Y, Yong S, Salas-Burgos A, Koomen J, Olashaw N, Parsons JT, Yang XJ, Dent SR, Yao TP, Lane WS, Seto E (2007) HDAC6 modulates cell motility by altering the acetylation level of cortactin. Molecular cell 27:197-213. doi:10.1016/j.molcel.2007.05.033

269. Zhang Y, Gilquin B, Khochbin S, Matthias P (2006) Two catalytic domains are required for protein deacetylation. The Journal of biological chemistry 281:2401-2404. doi:10.1074/jbc.C500241200

270. Zheng K, Jiang Y, He Z, Kitazato K, Wang Y (2017) Cellular defence or viral assist: the dilemma of HDAC6. J Gen Virol 98:322-337. doi:10.1099/jgv.0.000679

271. Zhu J, Coyne CB, Sarkar SN (2011) PKC alpha regulates Sendai virus-mediated interferon induction through HDAC6 and beta-catenin. EMBO J 30:4838-4849. doi:10.1038/emboj.2011.351

272. Zilberman Y, Ballestrem C, Carramusa L, Mazitschek R, Khochbin S, Bershadsky A (2009) Regulation of microtubule dynamics by inhibition of the tubulin deacetylase HDAC6. Journal of cell science 122:3531-3541. doi:10.1242/jcs.046813

273. Zou H, Wu Y, Navre M, Sang BC (2006) Characterization of the two catalytic domains in histone deacetylase 6. Biochemical and biophysical research communications 341:45-50. doi:10.1016/j.bbrc.2005.12.144

List of Figures

9. LIST OF FIGURES

Introduction

Materials and Methods

Results

Discussion

List of Tables

11. LIST OF TABLES

Introduction

Materials and Methods

Annexes

10.ANNEXES

10.1. Publications related to this thesis

1. **HDAC6 controls innate immune and autophagy responses to the intracellular bacteria *Listeria monocytogenes.*** Moreno-Gonzalo O, Ramírez-Huesca M, Blas-Rus N, Cibrián D, Saiz M.L, Jorge I, Camafeita E, Vázquez J, Sánchez-Madrid F. *PLOS Pathogens.* 2017. doi: 10.1371/journal.ppat.1006799. PMID:29281743.

2. **HDAC6 at crossroads of infection and innate immunity.** Moreno-Gonzalo O, Mayor F Jr, Sánchez-Madrid F. *Trends in Immunology*. 2018. *(submitted).*

10.2. Other Publications

1. **Tetraspanin CD9 limits mucosal healing in experimental colitis.** Saiz ML, Cibrián C, Ramírez-Huesca M, Torralba D, Moreno-Gonzalo O, Sánchez-Madrid F. *Frontiers in Immunology*. 2017. https://doi.org/10.3389/fimmu.2017.01854

2. **Post-Translational add-ons mark the path in exosomal protein sorting**. Moreno-Gonzalo O, Fernandez-Delgado I, Sánchez-Madrid F. *Cellular and Mollecular Life Science.* 2017. doi: 10.1007/s00018-017-2690-y. PMID:29080091.

3. **ISGylation controls exosome secretion by promoting lysosomal degradation of MVB proteins.** Villarroya-Beltri C, Baixauli F, Mittelbrunn M, Fernández-Delgado I, Torralba D, Moreno-Gonzalo O, Baldanta S, Enrich C, Guerra S, Sánchez-Madrid F. *Nature Communications* (2016) 7; 13588. doi: 10.1038/ncomms13588. PMID: 27882925.

4. **CD69 controls the uptake of L-tryptophan through LAT1-CD98 and AhR-dependent secretion of IL-22 in psoriasis.** Cibrian D, Saiz ML, de la Fuente H, Sánchez-Díaz R, Moreno-Gonzalo O, Jorge I, Ferrarini A, Vázquez J, Punzón C, Fresno M, Vicente-Manzanares M, Daudén E, Fernández-Salguero PM, Martín P, Sánchez-Madrid F. *Nature Immunology*. 2016 Aug;17(8):985-96. doi: 10.1038/ni.3504. Epub 2016 Jul 4. PMID: 27376471.

5. **HDAC6 regulates the dynamics of lytic granules in cytotoxic T lymphocytes.** Núñez-Andrade N, Iborra S, Trullo A, Moreno-Gonzalo O, Calvo E, Catalán E, Menasche G, Sancho D, Vázquez J, Yao TP, Martín-Cófreces NB, Sánchez-Madrid F. *Journal of Cell Science*. 2016 Apr 1;129(7):1305-11. doi: 10.1242/jcs.180885. Epub 2016 Feb 11. PMID: 26869226.

6. **Post-translational modifications of exosomal proteins.** Moreno-Gonzalo O, Villarroya-Beltri C, Sánchez-Madrid F. *Frontiers in Immunology*. 2014 Aug 11;5:383. doi: 10.3389/fimmu.2014.00383. eCollection 2014. Review. PMID: 25157254.

7. **The PDZ-adaptor protein syntenin-1 regulates HIV-1 entry.** Gordón-Alonso M, Rocha-Perugini V, Álvarez S, Moreno-Gonzalo O, Ursa A, López-Martín S, Izquierdo-Useros N, Martínez-Picado J, Muñoz-Fernández MÁ, Yáñez-Mó M, Sánchez-Madrid F. *Molecular Biology of the Cell*. 2012 Jun;23(12):2253-63. doi: 10.1091/mbc.E11-12-1003. Epub 2012 Apr 25. PMID: 22535526.

Selected Articles

12. SELECTED ARTICLES

PLOS | PATHOGENS

RESEARCH ARTICLE

HDAC6 controls innate immune and autophagy responses to TLR-mediated signalling by the intracellular bacteria *Listeria monocytogenes*

Olga Moreno-Gonzalo[1,2], Marta Ramírez-Huesca[1,2], Noelia Blas-Rus[1,2], Danay Cibrián[1,2,3], María Laura Saiz[1,2], Inmaculada Jorge[4], Emilio Camafeita[4], Jesús Vázquez[3,4], Francisco Sánchez-Madrid[1,2,3]*

1 Cell-cell Communication Laboratory, Vascular Pathophysiology Area, Centro Nacional Investigaciones Cardiovasculares (CNIC), Madrid, Spain, **2** Servicio de Inmunología, Hospital Universitario de la Princesa, Instituto Investigación Sanitaria Princesa (IIS-IP)-Universidad Autónoma de Madrid (UAM), Madrid, Spain, **3** CIBER CARDIOVASCULAR, Madrid, Spain, **4** Proteomics Unit, Vascular Pathophysiology Area, Centro Nacional Investigaciones Cardiovasculares (CNIC), Madrid, Spain

* fsmadrid@salud.madrid.org

Citation: Moreno-Gonzalo O, Ramírez-Huesca M, Blas-Rus N, Cibrián D, Saiz ML, Jorge I, et al. (2017) HDAC6 controls innate immune and autophagy responses to TLR-mediated signalling by the intracellular bacteria *Listeria monocytogenes*. PLoS Pathog 13(12): e1006799. https://doi.org/10.1371/journal.ppat.1006799

Editor: Igor Eric Brodsky, University of Pennsylvania, UNITED STATES

Received: May 29, 2017

Accepted: December 8, 2017

Published: December 27, 2017

Data Availability Statement: All relevant data are within the paper and its Supporting Information files.

Funding: The funders had no role in study design, data collection and analysis, decision to publish, or preparation of the manuscript. This study was supported by the following grants to FSM: SAF2014-55579-R from the Spanish Ministry of Economy and Competitiveness, INDISNET-S2011/BMD-2332 from the Comunidad de Madrid, CIBER

Abstract

Recent evidence on HDAC6 function underlines its role as a key protein in the innate immune response to viral infection. However, whether HDAC6 regulates innate immunity during bacterial infection remains unexplored. To assess the role of HDAC6 in the regulation of defence mechanisms against intracellular bacteria, we used the *Listeria monocytogenes* (*Lm*) infection model. Our data show that *Hdac6*$^{-/-}$ bone marrow-derived dendritic cells (BMDCs) have a higher bacterial load than *Hdac6*$^{+/+}$ cells, correlating with weaker induction of IFN-related genes, pro-inflammatory cytokines and nitrite production after bacterial infection. *Hdac6*$^{-/-}$ BMDCs have a weakened phosphorylation of MAPK signalling in response to *Lm* infection, suggesting altered Toll-like receptor signalling (TLR). Compared with *Hdac6*$^{+/+}$ counterparts, *Hdac6*$^{-/-}$ GM-CSF-derived and FLT3L-derived dendritic cells show weaker pro-inflammatory cytokine secretion in response to various TLR agonists. Moreover, HDAC6 associates with the TLR-adaptor molecule Myeloid differentiation primary response gene 88 (*MyD88*), and the absence of HDAC6 seems to diminish the NF-κB induction after TLR stimuli. *Hdac6*$^{-/-}$ mice display low serum levels of inflammatory cytokine IL-6 and correspondingly an increased survival to a systemic infection with *Lm*. The impaired bacterial clearance in the absence of HDAC6 appears to be caused by a defect in autophagy. Hence, *Hdac6*$^{-/-}$ BMDCs accumulate higher levels of the autophagy marker p62 and show defective phagosome-lysosome fusion. These data underline the important function of HDAC6 in dendritic cells not only in bacterial autophagy, but also in the proper activation of TLR signalling. These results thus demonstrate an important regulatory role for HDAC6 in the innate immune response to intracellular bacterial infection.

CARDIOVASCULAR and grant PIE13/00041 from the Instituto de Salud Carlos III (Fondo de Investigación Sanitaria del Instituto de Salud Carlos III with co-funding from the Fondo Europeo de Desarrollo Regional; FEDER), and ERC-2011-AdG 294340- GENTRIS and COST-Action BM1202 from the European Comission. The Centro Nacional de Investigaciones Cardiovasculares (CNIC) is supported by the Spanish Ministry of Economy and Competitiveness (MINECO) and the Pro-CNIC Foundation and is a Severo Ochoa Center of Excellence (MINECO award SEV-2015-0505). OMG was supported by the fellowship FPU programme (Spanish Ministry of Education). MLS was supported by the fellowship FPI programme (Spanish Ministry of Economy).

Competing interests: The authors have declared that no competing interests exist.

Author summary

Listeria monocytogenes (Lm) is a food-borne intracellular bacterium that causes listeriosis to 1.600 people each year, being responsible of approximately 260 deaths. This pathogen mostly affects immunocompromised individuals and pregnant women. It is particularly dangerous for the later due to its ability to pass across the placenta and the blood-brain barrier. *Lm* is extensively used as a *Gram* positive infection model in the laboratory to study innate and adaptive immune responses. HDAC6 is an important regulatory enzyme of the tubulin and actin cytoskeletons. Its inhibition or deficiency quells the immune response against different virus infections. Previous work has shown its involvement in the regulation of viral RNA-sensing activity and in interferon signalling. In this study, we report that HDAC6 is an essential component of the innate immune response to fight against intracellular bacterial infections. Genetic ablation of HDAC6 impairs activation of the pertinent Toll-like receptor pathway to induce the pro-inflammatory transcriptional program of the cell. Moreover, this enzyme controls cytoskeletal proteins that mediate the fusion of phagosome-contained bacteria with the lysosome during pathogen degradation.

Introduction

Histone deacetylase 6 (HDAC6) is a cytoplasmic deacetylase involved in the regulation of several biological processes, including migration, transport, angiogenesis, and tumour progression [1–5]. This enzyme is able to deacetylate α-tubulin and cortactin, regulating not only the microtubule cytoskeleton, but also actin [6, 7]. Both cytoskeletal interactions underline a crucial role of HDAC6 in many cellular functions such as phagosome-lysosome fusion, cargo transport through microtubules, and cell motility [8–10]. The role of HDAC6 has also been described in two of the main cellular degradation mechanisms: autophagy, through interaction with the autophagy marker p62; and the proteasome, mediated by deacetylation of HSP90 and its intersection with the ubiquitin-proteasome system (UPS) [11–15]. In addition, HDAC6 is involved in the transport of damaged mitochondria (mitophagy) and misfolded proteins (aggrephagy) to lysosomes and the proteasome for degradation [16–18]. The absence of HDAC6 impairs the deacetylation of mitofusin 1, preventing the mitochondrial fusion induced by glucose deprivation and causing excessive ROS production that provokes oxidative damage [19].

HDAC6 regulates the replication of human immunodeficiency virus (HIV) by deacetylating Tat and thus inhibiting viral transactivation [20, 21]. HDAC6 also participates in Sendai virus infection through the deacetylation of β-catenin, which acts as a co-activator of IRF3-mediated transcription [22]. During infection with Influenza Virus A (IVA), HDAC6 appears to play a dual role. IVA capsids mimic misfolded-protein aggregates to take advantage of the host cell aggresome pathway, thereby achieving disassembly and successful viral uncoating [23]. On the other hand, HDAC6-mediated microtubule deacetylation impairs the IVA cycle, preventing trafficking of viral components to the viral assembly site in the host plasma membrane and the spread of infection to surrounding cells [24]. The role of HDAC6 in the adaptive CD4 + T-cell response has been studied in several autoimmune and inflammatory situations such as colitis and cardiac allograft rejection; however, little is known about its role in innate immunity and bacterial diseases [25, 26].

Listeria monocytogenes (*Lm*) is a *Gram*-positive bacteria that causes severe infection in immunocompromised individuals and is able to cross the blood-brain barrier and the placenta [27]. *Lm* is widely used as a model of innate and adaptive immune responses to intracellular

bacterial infection [27–29]. From the first hours of infection, professional phagocytic cells trap bacteria in the blood and target organs, exerting a degree of control on bacterial growth [28]. After internalization by phagocytic cells, *Lm* is eliminated by fusion of the phagosome with lysosomes; however, some bacteria escape the phagosome into the cytoplasm through the action of listeriolysin O (LLO). In the cytoplasm, *Lm* replicates and is able to infect neighbouring cells [30–32]. Interestingly, phagosome-contained bacteria are also eliminated by the action of reactive oxygen species (ROS) and nitric oxide (NO), produced by NADPH oxidase 2 (NOX2) and inducible NO synthase (iNOS), respectively [33]. Moreover, *Lm* bacteria contain an ARP2/3-mimicking protein that enables their propulsion to neighbouring cells through the directional assembly of actin filaments (actin rockets) [34]. *Lm* can spread from cell to cell without exiting the intracellular compartment by a process called paracytophagy, which evades immune detection. However, the host cell is able to develop a specific $CD8^+$T cell response to cytosolic *Lm*, which is crucial for the control of infection [35–38].

Early control of *Listeria* burden largely depends on the innate immune response occurring in the spleen, which relies on two main cell populations of dendritic cells (DCs). On one hand, a subset of monocyte-derived DCs namely TNF/iNOS–producing DCs (Tip-DCs) has the ability to produce TNFα and NO [39]. The other splenic DC subset is $CD8\alpha^+$ conventional DCs (cDCs), and it is responsible for the final resolution of infection against *Listeria* through the antigen presentation of bacterial-derived antigens to specific CD8+T cells to induce cytotoxicity [40, 41]. The response of dendritic cells (DC) to live *Lm* is mediated by toll-like receptors (TLRs), nucleotide-binding oligomerization domain (NODs)-like receptors (NLRs), and other cytosolic receptors and involves two signalling pathways: TLR-dependent and independent signalling. TLR-dependent signalling, triggered by sensing of cell-surface and endo-phagosomal bacteria, mediating the activation of a MyD88-dependent response; and the cytosolic pathway, triggered by bacterial DNA after the escape of *Lm* into the cytosol, is responsible for the activation of sensor stimulator of interferon (IFN) genes (STING). STING activation leads to IFN regulatory factor (IRF)3–dependent production of IFN-β and activation of downstream signals that control the transcription of IFN target genes essential for antiviral and antibacterial responses [42, 43].

To determine the role of HDAC6 in the innate response to bacterial infection, we explored the impact of HDAC6 deficiency on the response of myeloid cells to *Lm*. Our results reveal that *Hdac6*$^{-/-}$ BMDCs are less efficient than *Hdac6*$^{+/+}$ at clearing *Lm*. This is due to defective maturation of phagosome-contained bacteria. Moreover, *Hdac6*$^{-/-}$ DCs display lower activation after *Lm* infection and TLR stimuli. These data support the view that HDAC6 positively regulates innate defence mechanisms against *Lm* and that its absence weakens the pro-inflammatory response.

Results

Deficient intracellular bacteria clearance in *Hdac6*$^{-/-}$ BMDCs

To assess the possible role of HDAC6 in innate immune responses during bacterial pathogenesis, we performed a time-course infection with *Lm* in granulocyte and monocyte colony-stimulating factor (GM-CSF)-derived BMDCs from *Hdac6*$^{+/+}$ and *Hdac6*$^{-/-}$ mice. Increasing levels of HDAC6 expression were detected in the *Hdac6*$^{+/+}$ DCs as the infection progressed (Fig 1A). However, BMDC differentiation was not noticeably affected in the absence of HDAC6 (S1 Fig part A). Next, *Hdac6*$^{+/+}$ and *Hdac6*$^{-/-}$ BMDCs were infected for different times with *Gram*-negative bacteria (*Salmonella* Typhimurium and *Escherichia coli DH5α*) and *Gram*-positive bacteria (*Listeria monocytogenes* and *Staphylococcus aureus*) at a multiplicity of infection (MOI) of 10, with colony-formed units (CFUs) corresponding to intracellular live bacteria. Bacterial

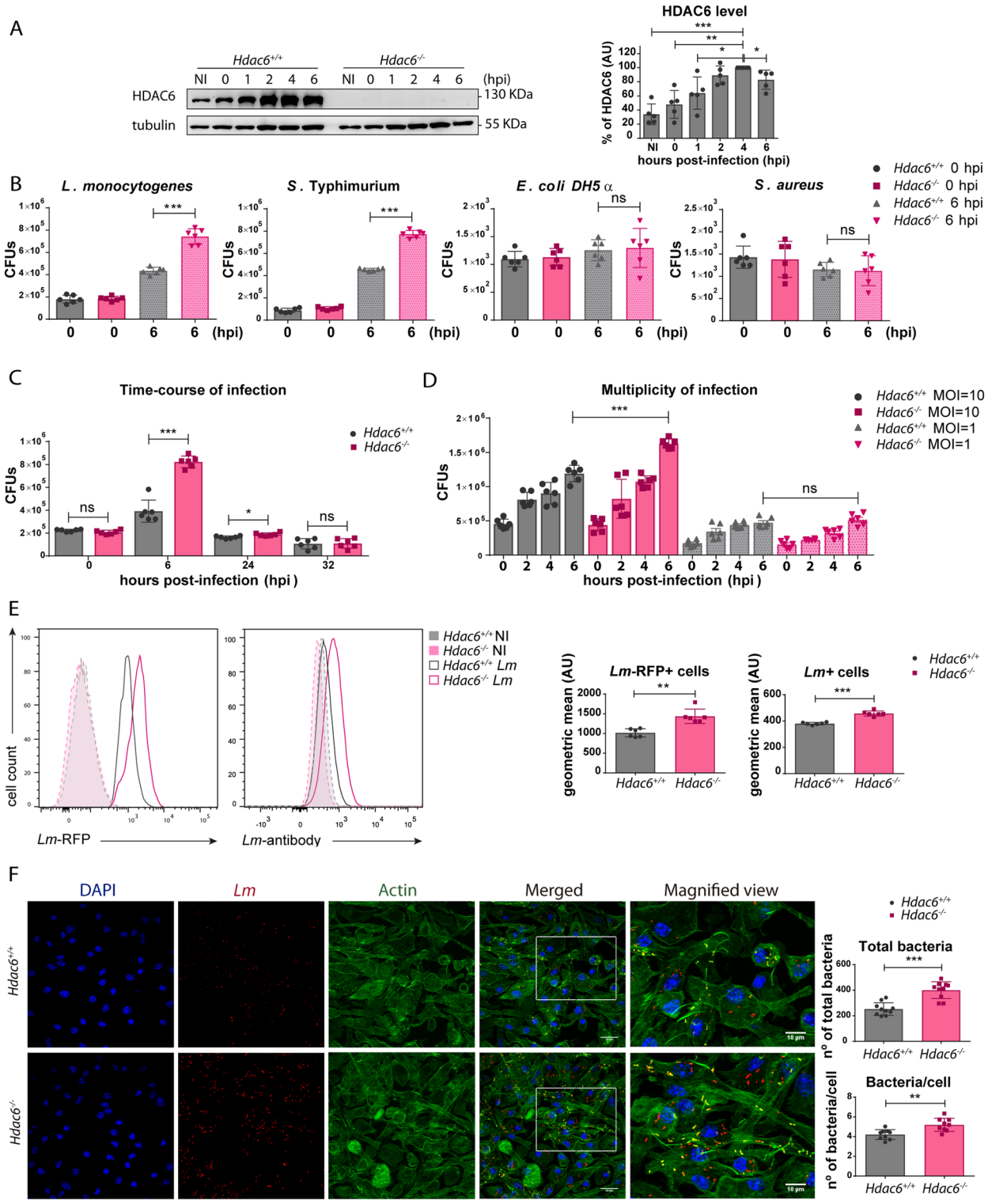

Fig 1. Deficient intracellular bacteria clearance in *Hdac6*$^{-/-}$ BMDCs. A) Western blot analysis of HDAC6 in a time-course of infection of BMDCs with *Lm*. Tubulin was used as a loading control. HDAC6 levels were quantified in five independent experiments. $^{***}p\leq0.001$, $^{**}p\leq0.01$ $^{*}p\leq0.05$. B) CFUs obtained at 0 and 6 hpi from BMDCs infected with *L. monocytogenes*, *S.* Typhimurium, *E. coli DHDα*, and *S. aureus* at a MOI of 10. Data from 0 hpi are shown as a bacteria entry control. $^{***}p\leq0.001$, ns>0.05 non-significant; n = 6. C) CFUs of *Lm*-infected BMDCs obtained at 0, 6, 24 and 32 hpi with a MOI = 10. $^{***}p\leq0.001$, $^{*}p\leq0.05$, ns>0.05 non-significant; n = 6. D) CFUs of *Lm*-infected BMDCs obtained at 0, 2, 4 and 6 hpi with a MOI = 10 and 1. $^{***}p\leq0.001$, $^{*}p\leq0.05$, ns>0.05 non-significant; n = 6. E) BMDCs were infected with *Lm* or *Lm*-RFP for 6 h and the bacterial signal

was determined by flow cytometry. The panel shows representative histograms and the geometric mean of the *Lm* signal. $^{***}p\leq0.001$, ** $p\leq0.01$; n = 6. F) Confocal microscopy determination of bacterial load at 6 hpi. *Left panel*: Maximum intensity z-projections of confocal microscopy images of *Lm*-infected *Hdac6*$^{+/+}$ and *Hdac6*$^{-/-}$ BMDCs at 6 hpi. The panel shows DAPI (blue), *Lm* (red), β-actin (green), merged views of three channels, and magnified views of the boxed areas from the merged view. Yellow indicates *Lm* and β-actin co-localization. Scale bars 20 μm (main panels) and 10 μm magnified views). *Right panel*: ImarisCell Module analysis of the number of cells and the number of bacteria per cell in all pictures (10 pictures per genotype). Statistical analysis of Imaris quantification of total bacteria and bacteria per cell in *Hdac6*$^{+/+}$ and *Hdac6*$^{-/-}$ BMDCs. $^{***}p\leq0.001$, ** $p\leq0.01$; n = 10.

https://doi.org/10.1371/journal.ppat.1006799.g001

entry was similar in *Hdac6*$^{+/+}$ and *Hdac6*$^{-/-}$ DCs at 0 h post-infection (hpi), while bacterial proliferation, measured at 6 hpi, was significantly higher in *Hdac6*$^{-/-}$ BMDCs for both types of intracellular pathogens, *Lm* and *S*. Typhimurium (Fig 1B). This was not due to differences in cell viability at 6 hpi (S1 Fig part B). In contrast, no significant difference was observed in the proliferation of the non-intracellular pathogens *S. aureus* and *E. coli*, indicating that HDAC6 is an important component of cellular mechanisms for the clearance of intracellular pathogens (Fig 1B).

Time-course analysis showed that differences between *Lm* infection in *Hdac6*$^{+/+}$ and *Hdac6*$^{-/-}$ BMDCs CFUs peaked at 6 hpi and were sustained until 24 hpi (Fig 1C). This effect was clearly observed at a MOI of 10, which did not affect cell viability (Fig 1D and S1 Fig part B). A similar pattern was observed with macrophage colony-stimulating factor (M-CSF)-derived macrophages, demonstrating the lineage independence of the role of HDAC6 in bacterial clearance (S1 Fig part C). Although the difference between *Hdac6*$^{+/+}$ and *Hdac6*$^{-/-}$ cells was observed in both macrophages and DCs, the clearance capacity of macrophages was ten-fold higher than that of DCs at 6 hpi (S1 Fig part C).

Bacterial load was also determined by flow cytometry using two strategies: a specific antibody against *Lm*, and RFP-expressing bacteria. Both approaches showed that *Hdac6*-deficient DCs contained more bacteria at 6 hpi (Fig 1E). Higher numbers of bacteria in *Hdac6*$^{-/-}$ BMDCs were also detected by confocal fluorescence microscopy at 6 hpi (Fig 1F). Some bacteria co-localized with filamentous actin, showing clear actin rockets (Fig 1F). Image quantification confirmed that *Hdac6*$^{-/-}$ BMDCs contained more bacteria per cell and more total bacteria, remarking a higher percentage of cells hosting a large number of bacteria in *Hdac6*$^{-/-}$ cells (see distribution of bacteria per cell, 6–7) (S1 Fig part D). ImarisCell Module view of Fig 1F images showed the number of bacteria per cell using actin transparency to easily visualize individual bacteria (S1 Fig part E).

To ascertain whether *Hdac6*$^{-/-}$ cells display higher bacterial burden than *Hdac6*$^{+/+}$ cells *in vivo*, *Hdac6*$^{+/+}$ and *Hdac6*$^{-/-}$ mice were intravenously injected with *Lm* and total CFUs per gram of liver and spleen were determined at 6 hpi. In agreement with the higher numbers of *Lm* observed in GM-CSF-DCs and M-CSF-Macrophages, we observed increased bacterial titres in spleen and liver cell suspensions (Fig 2A). Next, to determine the specific cell populations underlying this phenotype, a multicolour gating strategy was used to identify the myeloid cell compartment, including monocytes, neutrophils, Tips DCs, total cDCs, cCDs CD8^{-} and cDCs CD8^{+} (S2 Fig part A). Higher numbers of *Lm* were observed in different myeloid cells at 6 hpi (Fig 2B and S2 Fig part B). These data highlight the impairment of *Hdac6*$^{-/-}$ myeloid cells to clear intracellular *Lm*.

Impaired bacterial clearance in *Hdac6*$^{-/-}$ BMDCs is caused by a defect in autophagy

To test the involvement of autophagy in the mechanism by which HDAC6 regulates *Lm* infection, we treated DCs with 3-methyladenine (3-MA), an inhibitor of autophagosome formation. Treatment with 3-MA increased bacterial load in *Hdac6*$^{+/+}$ BMDCs at 6 hpi, while having no

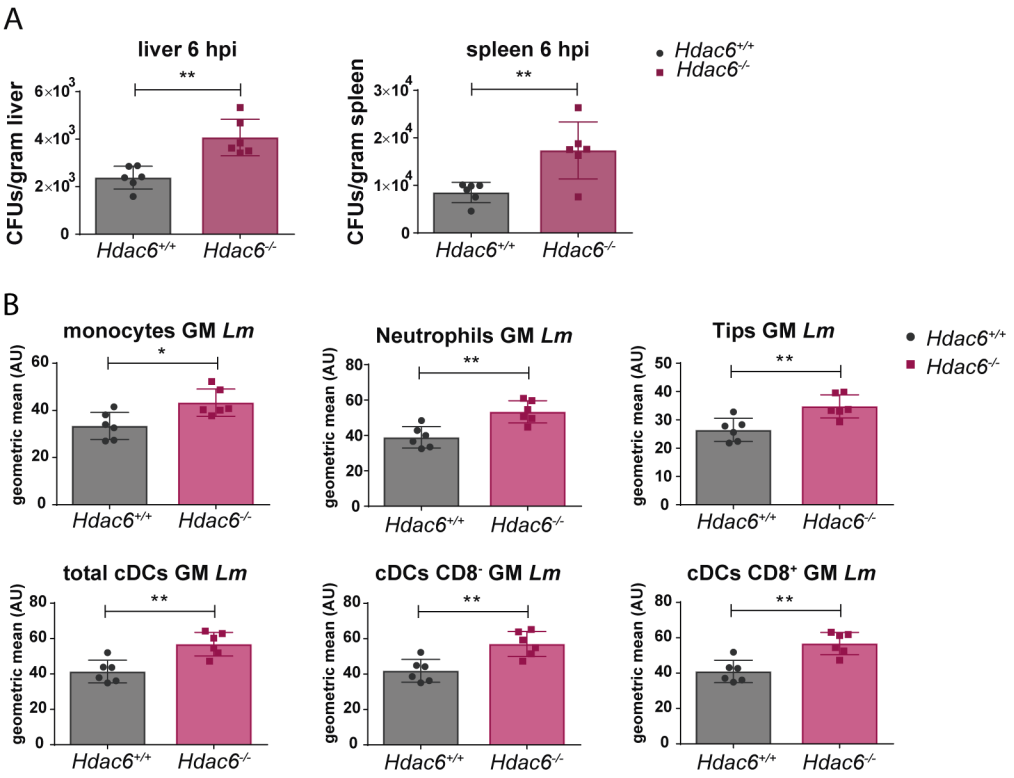

Fig 2. Deficient intracellular bacteria clearance in *Hdac6*$^{-/-}$ splenic myeloid populations. A) Quantification of bacterial load in target organs (spleen and liver) at 6 hpi in *Hdac6*$^{+/+}$ and *Hdac6*$^{-/-}$ mice injected with a lethal dose of *Lm*. Bacterial load is expressed by CFUs per gram of liver (left graph) and per gram of spleen (right graph). $^{**}p \leq 0.01$, n = 6. B) The charts show geometric means of *Lm* of different splenic populations (monocytes, neutrophils, Tips DCs, total cDCs, cDCs CD8$^-$ and cDCs CD8$^+$) gated in the live CD3$^-$CD19$^-$DX5$^-$ population of *Hdac6*$^{+/+}$ and *Hdac6*$^{-/-}$ mice injected with a lethal dose of *Lm* at 6 hpi. $^{**}p \leq 0.01$; n = 6.

https://doi.org/10.1371/journal.ppat.1006799.g002

effect on *Hdac6*$^{-/-}$ BMDCs (Fig 3A), suggesting autophagy as the bacterial clearance mechanism impaired in *Hdac6*-deficient DCs. A similar result was observed upon treatment of BMDCs with bafilomycin A1, an inhibitor of vascular proton pump that indirectly inhibits phagosome-lysosome fusion, and with the lysosome acidification inhibitors chloroquine and NH_4Cl (Fig 3A). In contrast, increasing autophagy flux with rapamycin did not restore the impaired autophagy in *Hdac6*$^{-/-}$ BMDCs (Fig 3B). No significant effects were observed with control vehicles (S3 Fig part A). To explore other possible mechanisms, we treated BMDCs with inhibitors of NADPH oxidase (DPI) and iNOS (1400W). These treatments did not alter the difference in CFU number at 6 hpi between treated and non-treated *Hdac6*$^{+/+}$ and *Hdac6*$^{-/-}$ BMDCs, indicating that the activity of either enzyme is not accounting for the existing phenotype (Fig 3B).

The defective autophagy phenotype of *Hdac6*$^{-/-}$ BMDCs was not due to transcriptional alterations to autophagy or lysosome components, since *Lm*-infected *Hdac6*$^{+/+}$ and *Hdac6*$^{-/-}$ BMDCs showed no mRNA expression differences at 6 hpi in the autophagy components LC3A and B, p62, ATG2, 5, 7 and 12, and Beclin-1 or in the lysosome components LAMP-1 and 2 (S3 Fig part B).

To determine whether these findings can be extended to other phagocytic cells, we carried out CFU assays with macrophages obtained from *Hdac6*$^{+/+}$ and *Hdac6*$^{-/-}$ mice four days after intraperitoneal thioglycollate injection. Higher bacterial load was observed only in *Hdac6*$^{-/-}$

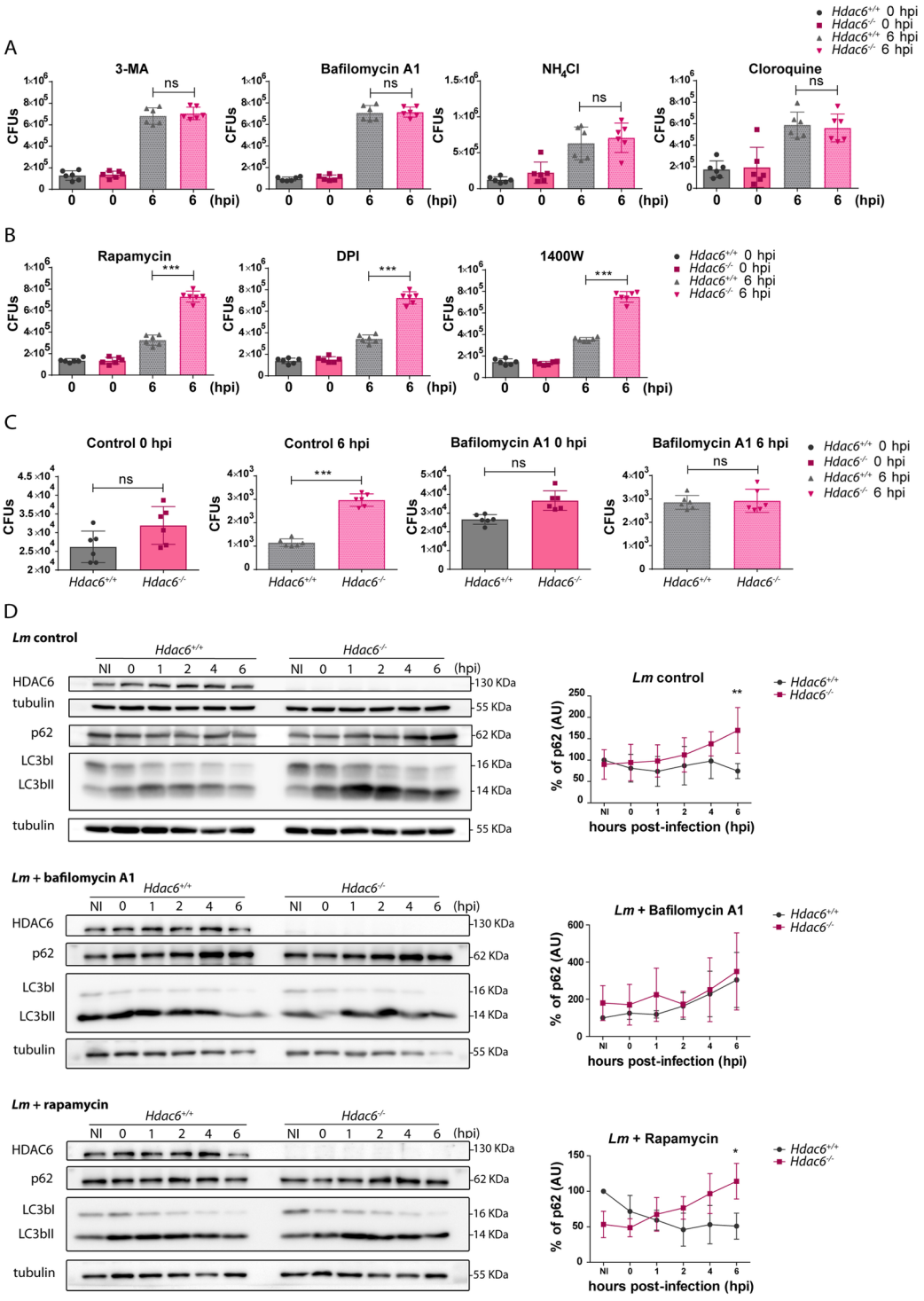

Fig 3. Impaired bacterial clearance in *Hdac6*$^{-/-}$ BMDCs is caused by a defect in autophagy. A) Total CFUs in *Lm*-infected BMDCs treated with inhibitors. CFUs were detected at entry (0 hpi) and 6 hpi (bacterial proliferation) using the autophagy inhibitors (3-MA and bafilomycin A1 and the lysosome acidification inhibitors (NH4Cl and cloroquine), ns>0.05 non-significant; n = 6. B) Total CFUs at 0 and 6 hpi in *Lm*-infected BMDCs treated with the autophagy activator (rapamycin), the NADPH oxidase inhibitor (DPI) and the iNOS inhibitor (1400W). $^{***}p\leq0.001$; n = 6. C) Total CFUs at 0 and 6 hpi in *Lm*-infected thioglycollate-elicited macrophages treated with or without bafilomycin A1. $^{***}p\leq0.001$, ns>0.05 non-significant; n = 6. D) Western-blot analysis of autophagy markers over the time-course of *Lm* infection in *Hdac6*$^{+/+}$ and *Hdac6*$^{-/-}$ BMDCs. *Left panels*: Levels were detected of p62, LC3bI and II and HDAC6 in control cells and cells treated

with bafilomycin A1 and rapamycin. Tubulin was used as a loading control. HDAC6 was as a genotype check of *Hdac6*$^{+/+}$ and *Hdac6*$^{-/-}$ BMDCs and to monitor HDAC6 induction during infection. *Right panels*: Accompanying charts show quantification of the p62 percentage of control, bafilomycin A1 and rapamycin western blots. ** $p \leq 0.01$, * $p \leq 0.05$, ns>0.05 non-significant; n = 5.

https://doi.org/10.1371/journal.ppat.1006799.g003

macrophages at 6 hpi, and this difference was abrogated by treatment with bafilomycin A1 (Fig 3C). These data indicate that the phenotype observed in BMDCs is also extendable in other *Hdac6*-deficient phagocytic cells such as peritoneal macrophages, indicating a widespread defect in intracellular killing ability due to lack of HDAC6. Moreover, the killing ability shown by peritoneal macrophages is similar to that of M-CSF-derived macrophages and higher than GM-CSF-derived DCs (Fig 3C compared with S1 Fig part C).

To gain further insight into the autophagy mechanism affected by HDAC6, we monitored the autophagosome markers p62 and LC3bI and II in *Lm*-infected BMDCs. *Hdac6*$^{-/-}$ BMDCs showed a 2-fold higher accumulation of p62 than *Hdac6*$^{+/+}$ cells at 6 hpi and increased LC3bII level in *Hdac6*$^{+/+}$ cells from 1 to 6 hpi (Fig 3D). However, differences in p62 and LC3b levels were not noticed at early times of *Lm* infection of *Hdac6*$^{+/+}$ and *Hdac6*$^{-/-}$ BMDCs, indicating that the induction of autophagy is not affected in the absence of HDAC6 (Fig 3D). The treatment with bafilomycin A1 enhances the accumulation of p62 during the infection at the same level in both genotypes, abrogating the deficiency in autophagy observed in *Hdac6*$^{+/+}$ BMDCs (Fig 3D). Although rapamycin also increased p62 accumulation at early times in *Hdac6*$^{+/+}$ and *Hdac6*$^{-/-}$ BMDCs, only *Hdac6*$^{+/+}$ cells are able to diminished p62 at 6 hpi (Fig 3D). This treatment confirmed the results obtained in the CFUs functional assays with this inhibitor (Fig 3D compared with Fig 3B). The similarity of the autophagy defect detected in *Hdac6*$^{-/-}$ BMDCs in control condition to that in rapamycin-treated *Hdac6*$^{-/-}$ cells, suggests an impairment in phagocytic vesicle fusion with the lysosome.

Hdac6$^{-/-}$ BMDCs accumulate p62

In order to further understand the defective autophagy of *Hdac6*$^{-/-}$ BMDCs, the accumulation of p62 was studied in more detail. Flow cytometry at 6 hpi revealed significantly higher p62 content in *Hdac6*$^{-/-}$ BMDCs, indicating accumulation of this phagosome marker due to defective fusion of this organelle with the lysosome (Fig 4A). Bafilomycin A1 treatment completely abrogated this difference, suggesting that *Hdac6*$^{-/-}$ BMDCs displayed an impairment in the final step of autophagy (Fig 4A). More signal of *Lm* is displayed in *Hdac6*$^{-/-}$ DCs (Fig 4A). In this regard, bafilomycin A1 treatment increased the low *Lm* signal in *Hdac6*$^{+/+}$ DCs to the level observed in *Hdac6*$^{-/-}$ cells (Fig 4A).

Confocal fluorescent analysis of *Lm*-infected DCs revealed increased levels of p62 in *Hdac6*$^{-/-}$ BMDCs (Fig 4B). *Hdac6*$^{-/-}$ BMDCs also showed a higher percentage of p62-*Lm* co-localization than *Hdac6*$^{+/+}$ cells, indicating that *Hdac6*$^{-/-}$ cells have more number of phagosome-contained bacteria (Fig 4B in accordance with p62 accumulation observed in Figs 3D and 4A). Confocal fluorescent microscopy study of actin and *Lm* revealed more frequent co-localization in *Hdac6*$^{-/-}$ than in *Hdac6*$^{+/+}$ BMDCs, indicating that more bacteria are at the cytoplasm to form actin rockets in *Hdac6*-deficient cells (Fig 4C). Moreover, more signal of acetylated-cortactin is detected in *Hdac6*$^{-/-}$ BMDCs and also higher percentage of acetylated-cortactin-*Lm* co-localization (Fig 4D). These data could explain the accumulation of p62 and the delay in phagocytic vesicle fusion observed in *Hdac6*$^{-/-}$ BMDCs, necessary to degrade phagocytosed *Lm*.

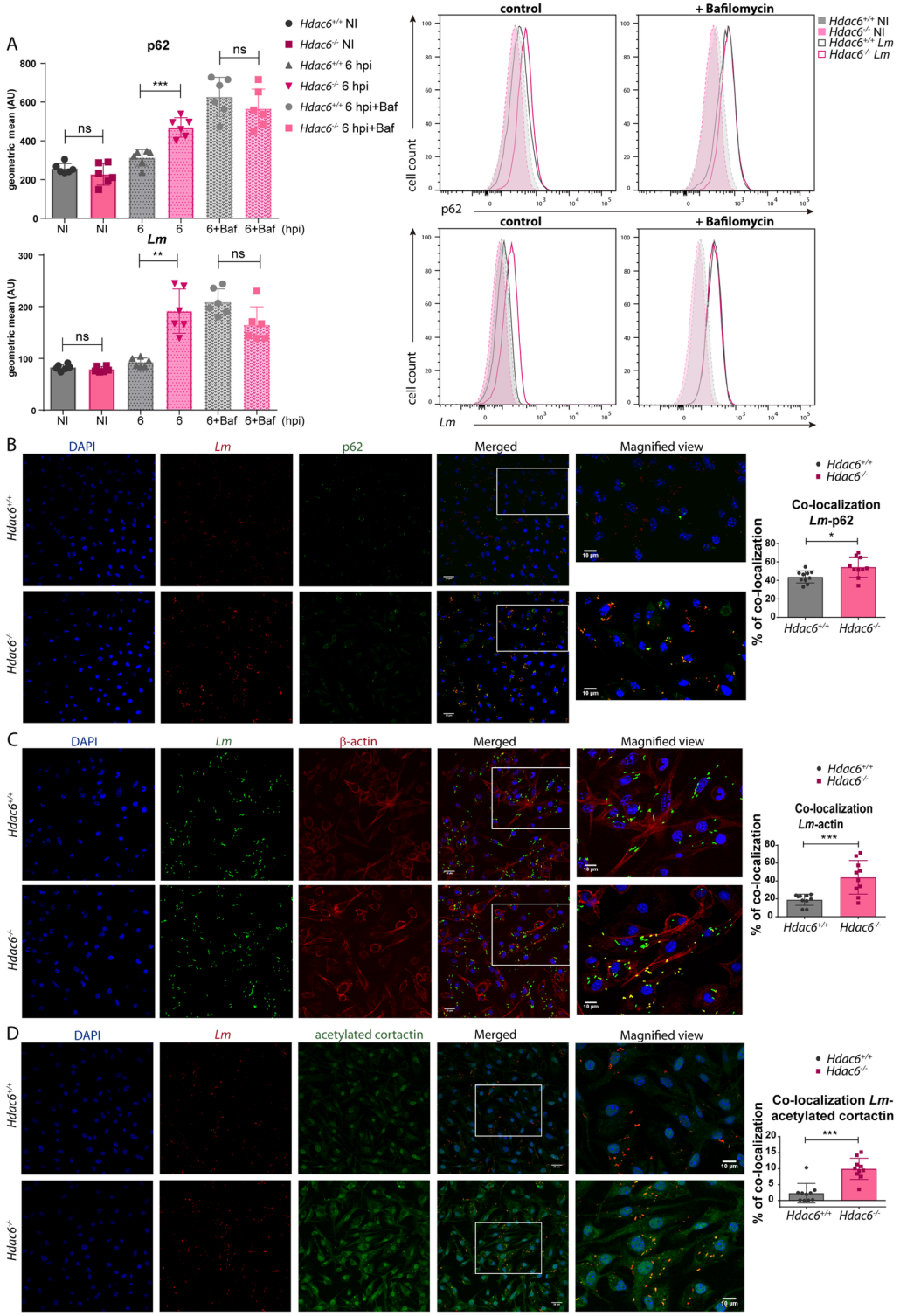

Fig 4. *Hdac6*$^{-/-}$ BMDCs accumulate higher levels of p62. A) *Left panels*: The charts show geometric means of p62 *and* *Lm* gated in the MHCII^{+}CD11c^{+} population of *Hdac6*$^{+/+}$ and *Hdac6*$^{-/-}$ BMDCs without infection (NI) and at 6 hpi, with and without bafilomycin A1 treatment. The representative histograms on the right show p62 and *Lm* with and without bafilomycin A1. $^{***}p \leq 0.001$, $^{**}p \leq 0.01$, ns>0.05 non-significant; n = 6. B) Confocal microscopy analysis of p62-*Lm* co-localization in *Lm*-infected *Hdac6*$^{+/+}$ and *Hdac6*$^{-/-}$ BMDCs at 6 hpi. Panels show DAPI (blue), *Lm* (red), p62 (green), and merged views of the three channels, with magnified views of the boxed areas. Yellow indicates p62-*Lm* co-localization.

Scale bars 20 μm (main panels) and 10 μm (magnified views). *Right panel*: The chart shows ImarisCell Module analysis of the number of cells and the number of bacteria per cell in all pictures (10 pictures per genotype). Co-localization percentages were obtained by measuring the p62 channel on the bacterial surface using a threshold of 100. The statistical analysis of Imaris quantifications corresponds to the percentage of p62-*Lm* co-localization at 6 hpi. $^{*}p \leq 0.05$; n = 10. C) Confocal microscopy analysis of actin-*Lm* co-localization in *Lm*-infected *Hdac6*$^{+/+}$ and *Hdac6*$^{-/-}$ BMDCs at 6 hpi. Panels show DAPI (blue), *Lm* (green), β-actin (red), and merged views of the three channels, with magnified views of the boxed areas. Yellow indicates β-actin-*Lm* co-localization. Scale bars 20 μm (main panels) and 10 μm (magnified views). *Right panel*: The chart shows ImarisCell Module analysis of the number of cells and the number of bacteria per cell in all pictures (10 pictures per genotype). Co-localization percentages were obtained by measuring the actin channel on the bacterial surface using a threshold of 40.6. The statistical analysis of Imaris quantifications corresponds to the percentage of actin-*Lm* co-localization at 6 hpi. *** $p \leq 0.001$; n = 10. D) Confocal microscopy analysis of acetylated cortactin-*Lm* co-localization in *Lm*-infected *Hdac6*$^{+/+}$ and *Hdac6*$^{-/-}$ BMDCs at 6 hpi. Panels show DAPI (blue), *Lm* (red), acetylated cortactin (green), and merged views of the three channels, with magnified views of the boxed areas. Yellow indicates acetylated cortactin-*Lm* co-localization. Scale bars 20 μm (main panels) and 10 μm (magnified views). *Right panel*: The chart shows ImarisCell Module analysis of the number of cells and the number of bacteria per cell in all pictures (10 pictures per genotype). Co-localization percentages were obtained by measuring the acetylated cortactin channel on the bacterial surface using a threshold of 184. The statistical analysis of Imaris quantifications corresponds to the percentage of acetylated cortactin-*Lm* co-localization at 6 hpi. *** $p \leq 0.001$; n = 10.

https://doi.org/10.1371/journal.ppat.1006799.g004

Defective pro-inflammatory cytokine response to *Lm* in *Hdac6*$^{-/-}$ BMDCs

The effect of HDAC6 on the response of BMDCs to *Lm* was evaluated by measuring pro-inflammatory cytokine gene induction. The relative mRNA levels of type I interferons (interferons α and β) were lower in *Hdac6*$^{-/-}$ BMDCs at 6 hpi (Fig 5A). Accordingly, expression of downstream interferon-response genes such as Mx1, IFIT3, and ISG15 was also lower in *Hdac6*$^{-/-}$ BMDCs (Fig 5A). Lack of HDAC6 also decreased the relative mRNA levels of the pro-inflammatory cytokines TNFα, IL-1β and IL12p40, indicating impaired cytokine activation after infection (Fig 5A). Similarly, *Hdac6*$^{-/-}$ DCs expressed lower levels than their *Hdac6*$^{+/+}$ counterparts of the chemokine receptor CXCR1 and chemokines CXCL5 and CXCL10 (Fig 5A). These data demonstrate that *Hdac6*-deficient DCs have a weakened activation response to *Lm* infection at 6 hpi, which suggests a defect in bacterial clearance, consistent with the increased bacterial load in these cells. To confirm these data, we monitored pro-inflammatory cytokines and IFN-β in the supernatants of *Lm*-infected DCs. Early after infection, TNFα, IL-1β, IL-6, IL12p70 and IFN-β levels were lower in supernatants from *Hdac6*$^{-/-}$ cells than in those from *Hdac6*$^{+/+}$ cells, and this difference held at 12 and 24 hpi (Fig 5B). To exclude a defect in cytokine secretion, we compared cytokine levels in supernatants (S) with the levels in supernatants plus their corresponding cell pellets (S+P). Both analyses showed decreased cytokine levels in *Hdac6*$^{-/-}$ cells, indicating an impaired antibacterial response in *Hdac6*-deficient DCs (S4 Fig).

Measurement of nitrite in supernatants of infected-BMDCs revealed higher nitric oxide production by *Hdac6*$^{+/+}$ DCs than in *Hdac6*$^{-/-}$ DCs at 24 hpi (Fig 6A). In agreement, western blot revealed lower levels of inducible nitric oxide synthase (iNOS) in *Hdac6*$^{-/-}$ BMDCs at 4 and 6 hpi (Fig 6B), indicating a delay of the enzyme induction in *Hdac6*$^{-/-}$ BMDCs. Likewise, flow cytometry after exposure of DCs to live or heat-killed *L. monocytogenes* (HKLM) revealed higher expression of iNOS in *Hdac6*$^{+/+}$ BMDCs in both cases (Fig 6C). These data support the involvement of HDAC6 in the activation of DC-mediated iNOS microbicidal responses to *Lm* infection and in the clearance of this intracellular pathogen.

Hdac6$^{-/-}$ BMDCs show defective activation of Toll-like receptor signalling pathway

The diminished activation response against *Lm* in *Hdac6*$^{-/-}$ BMDCs is consistent with impaired TLR-related signalling. To investigate this question, we determined the phosphorylation levels

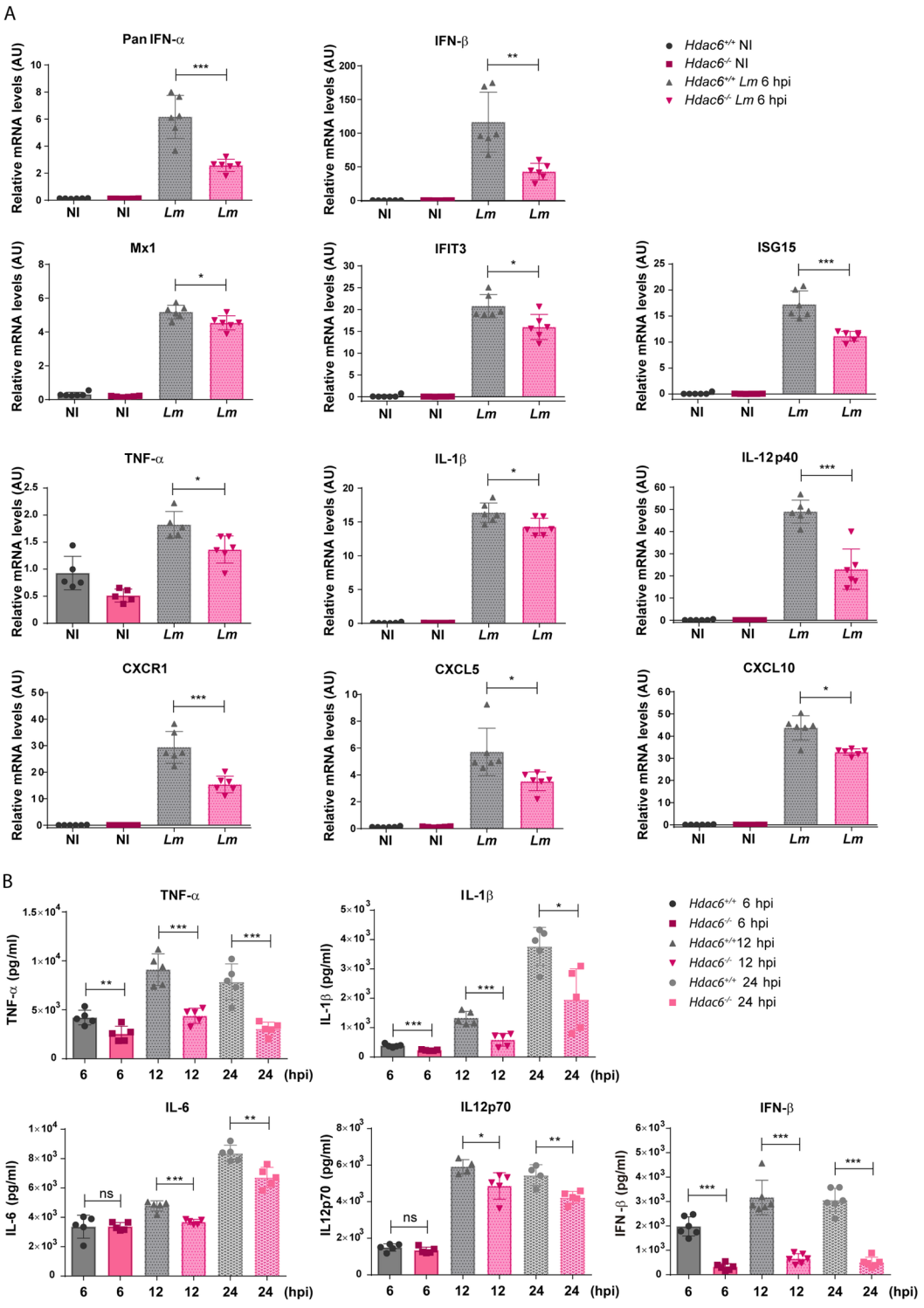

Fig 5. Defective pro-inflammatory cytokine response to *Lm* in *Hdac6*$^{-/-}$ BMDCs. A) PCR analysis of type-I interferons (PanIFN-α and IFN-β), interferon downstream proteins (Mx1, IFIT3 and ISG15), pro-inflammatory cytokines (TNF-α, IL-1β and IL-12p40) chemokine receptor (CXCR1) and chemokines (CXCL5 and CXCL10) of *Hdac6*$^{+/+}$ and *Hdac6*$^{-/-}$ BMDCs non-infected (NI) and infected with *Lm* at 6 hpi (arbitrary units). $^{***}p\leq0.001$, ** $p\leq0.01$, * $p\leq0.05$; n = 5–6. B) ELISA analysis of the pro-inflammatory cytokines TNFα, IL1β, IL6 and IL12p70 (pg/ml) and IFN-β in supernatants of *Hdac6*$^{+/+}$ and *Hdac6*$^{-/-}$ BMDCs at 6, 12 and 24 hpi with *Lm*. $^{***}p\leq0.001$, ** $p\leq0.01$, * $p\leq0.05$ ns>0.05 non-significant; n = 5–6.

https://doi.org/10.1371/journal.ppat.1006799.g005

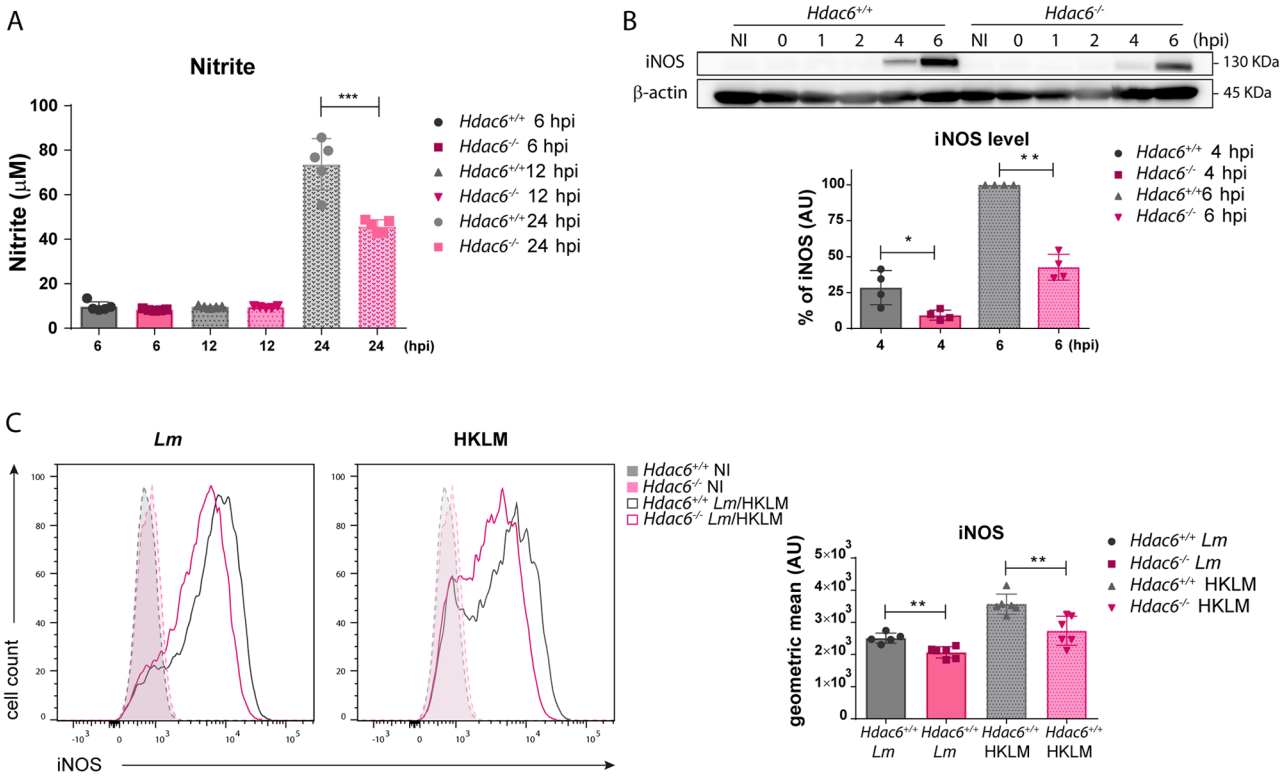

Fig 6. Defective iNOS response to *Lm* in *Hdac6*$^{-/-}$ BMDCs. A) *Lm*-activated iNOS activity. Nitrite levels in supernatants of *Lm*-infected BMDCs at 6, 12 and 24 hpi. ***p≤0.001; n = 5. B) Western-blot analysis of iNOS induction over the time-course of *Lm* infection. β-actin was used as a loading control (top panel). The chart shows quantification of iNOS at 4 and 6 hpi. ** p≤0.01, * p≤0.05; n = 4 (lower panel). C) The panel shows representative histograms of iNOS expressed by *Hdac6*$^{+/+}$ and *Hdac6*$^{-/-}$ BMDCs after exposure to live *Lm* or HKLM for 24 h (left). The right chart shows the geometric mean of iNOS expression. Non-infected (NI) BMDCs were used as a control of iNOS induction. **p≤0.01; n = 6.

https://doi.org/10.1371/journal.ppat.1006799.g006

of TLR downstream mediators by western blot. Compared with *Hdac6*$^{+/+}$ BMDCs, *Hdac6*$^{-/-}$ BMDCs showed weaker phosphorylation signals for ERK and AKT after *Lm* infection (Fig 7A). We next examined the effect of HDAC6 deficiency on TLR-signalling pathways using other TLR stimuli, including HKLM and LPS. AKT phosphorylation in *Hdac6*$^{-/-}$ BMDCs was decreased after LPS or HKLM treatment compared to *Hdac6*$^{+/+}$, confirming defective TLR activation (S5 Fig part A). These effects are not related to a defect in *Lm*-induced transcriptional induction since mRNA levels of different *Lm*-related TLRs (TLR1, 2, and 6) were similar in *Hdac6*$^{+/+}$ and *Hdac6*$^{-/-}$ BMDCs (S5 Fig part B). Moreover, *Hdac6*$^{-/-}$ BMDCs showed weaker phosphorylation of mTORC1 pathway proteins (mTORC1 downstream substrates p70S6K and S6), consistent with a less pronounced pro-inflammatory response after TLR-activation by pathogen-associated molecular patterns (PAMPs) (Fig 7B).

To determine if *Hdac6*$^{-/-}$ BMDCs showed a similarly defective response to other TLR agonists, we first examined secretion of pro-inflammatory cytokines in response to agonists of TLR1-2 (Pam3GSK4), TLR-4 (LPS), TLR-7-9 (Imiquimod), and multiple TLRs (heat-killed *Salmonella* Typhimurium; HKST). *Hdac6*$^{-/-}$ BMDCs showed a defective cytokine response to these stimuli, determined from the release of TNFα, IL-6, IL-1β and IL12p70 (Fig 8A–8D).

To assess the pro-inflammatory cytokine response to TLR3 and TLR5 ligands, we generated Fms-related tyrosine kinase 3 ligand dendritic cells (FLT3L-DCs). Differentiation with the cytokine FLT3L yielded similar percentages of CD24^{+} and CD24^{-} subpopulations (CD11c^{+}CD11b^{+}B220^{-}CD24^{+} and CD11c^{+}CD11b^{+}B220^{-}CD24^{-}, respectively) from *Hdac6*$^{+/+}$

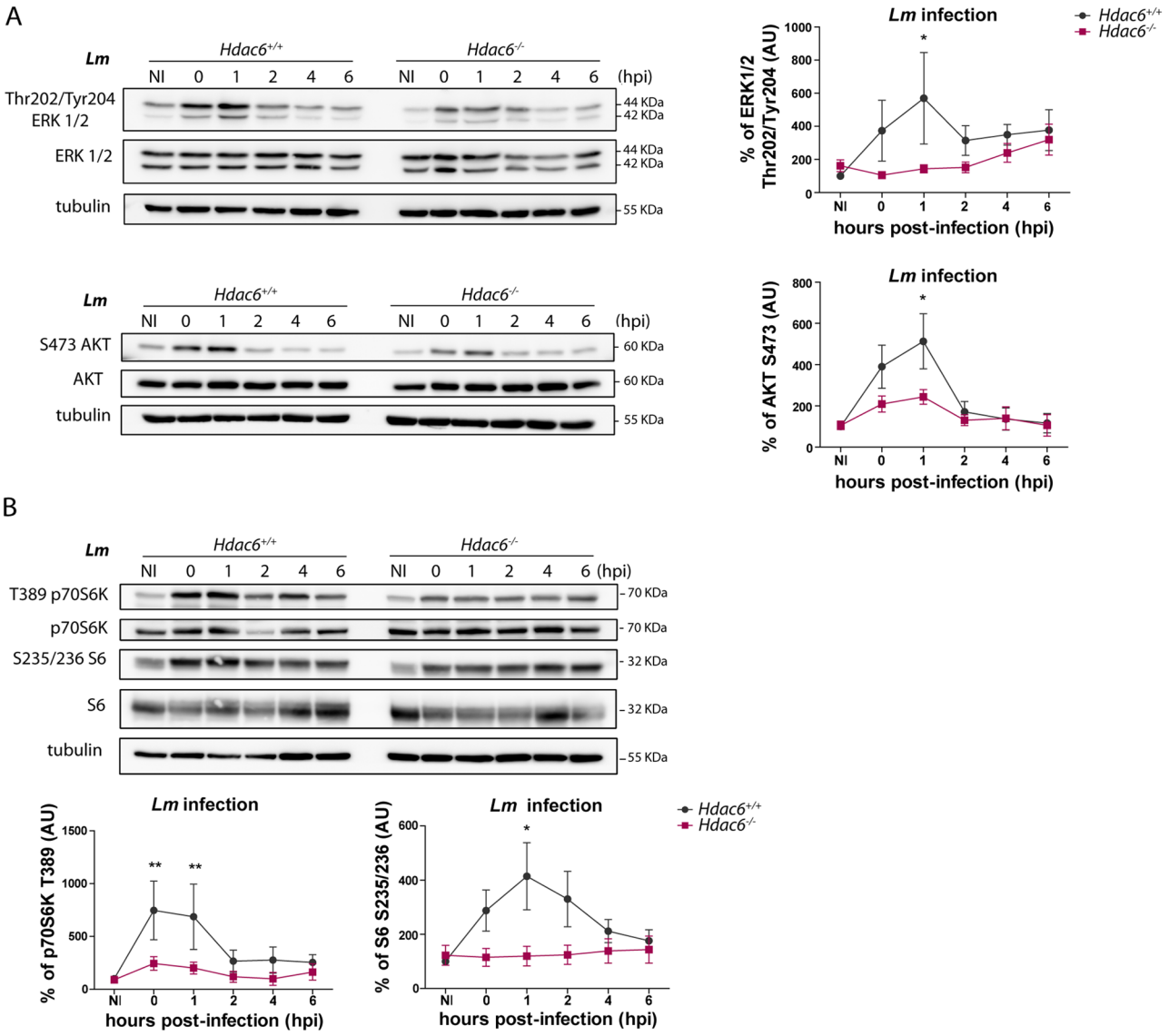

Fig 7. *Hdac6*$^{-/-}$ BMDCs show defective activation of the Toll-like receptor signalling pathway. A) Western-blot analysis of MAPK activation over the time-course of *Lm* infection in *Hdac6*$^{+/+}$ and *Hdac6*$^{-/-}$ BMDCs. Total and phosphorylated ERK and AKT were detected. Tubulin was used as a loading control (left). Accompanying charts show quantification of phERK/totalERK and phAKT/totalAKT ratios relative to the loading control, ns non-significant; n = 7 (right). B) Western-blot analysis of mTORC1 pathway activation over the time-course of *Lm* infection in *Hdac6*$^{+/+}$ and *Hdac6*$^{-/-}$ BMDCs. Levels of phosphorylated and total p70S6K and S6 were detected. Tubulin was used as a loading control (top panel). Accompanying charts show quantification of php70S6K/total70S6K (n = 5) and phS6/totalS6 (n = 7) ratios relative to the loading control. ** $p \leq 0.01$, ns non-significant; (lower panel).

https://doi.org/10.1371/journal.ppat.1006799.g007

and *Hdac6*$^{-/-}$ DCs, indicating that differentiation is unaffected by HDAC6 absence (S6 Fig part A). The TLR agonists Pam3GSK4 (TLR1-2), Poly(I:C) (TLR3), LPS (TLR4), flagellin (TLR5), Imiquimod (TLR-7-9), *Lm*, HKLM, and HKST (which activates several TLRs simultaneously) elicited similar cytokine secretion profiles in GM-CSF DCs and FLT3L-DCs (Fig 9A and S6 Fig part B compared to Fig 8A–8D). *Hdac6*$^{-/-}$ DCs of both derivations showed an impaired cytokine response to each TLR agonist, indicating that HDAC6 likely regulates a common TLR signalling adaptor.

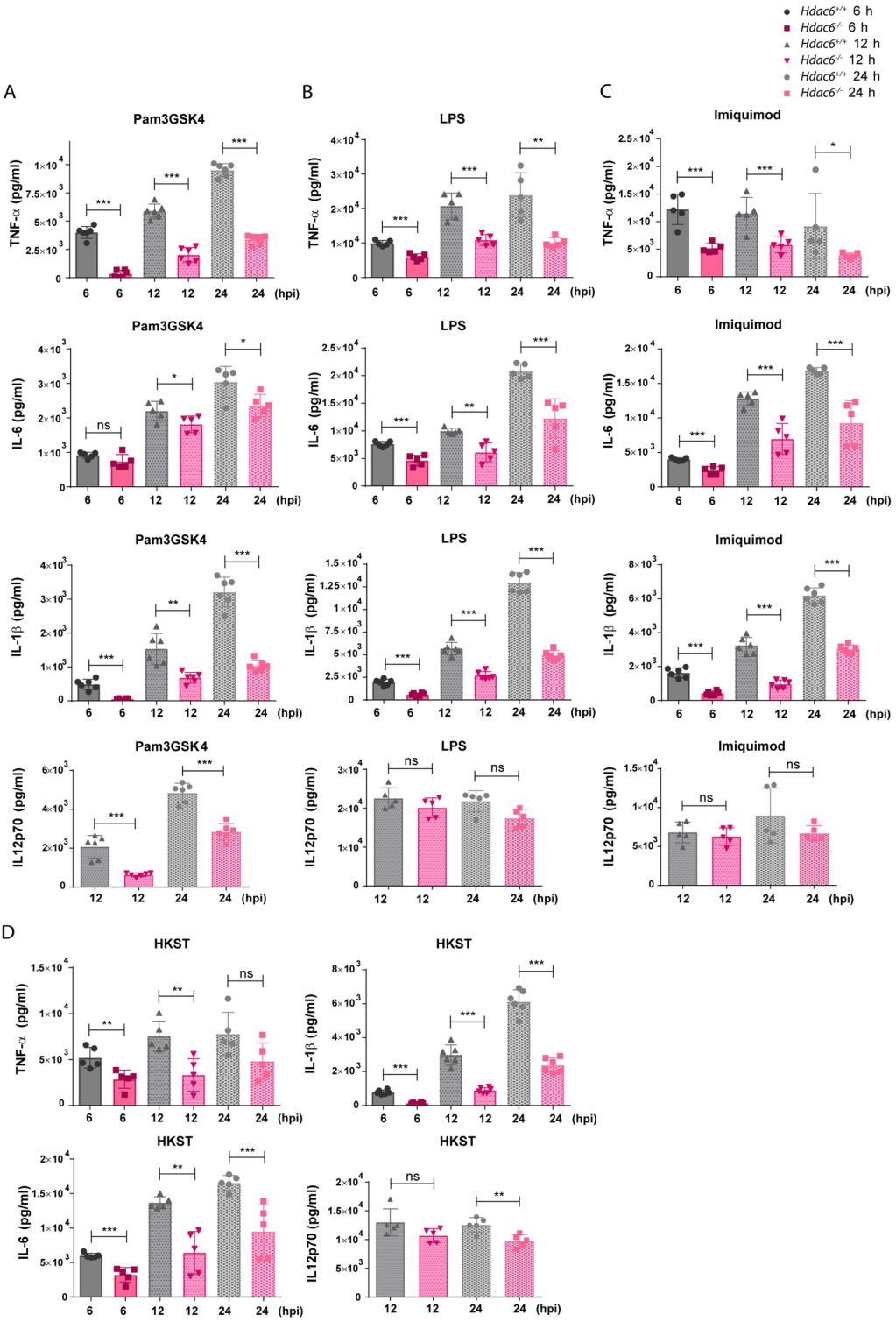

Fig 8. *Hdac6*$^{-/-}$ BMDCs show defective inflammatory cytokine response to Toll-like receptor stimuli. A) ELISA analysis of the pro-inflammatory cytokines TNFα, IL-1β, IL-6 and IL12p70 (pg/ml) in supernatants of *Hdac6*$^{+/+}$ and *Hdac6*$^{-/-}$ BMDCs after treatment for 6, 12 and 24 h with Pam3GSK4. $^{***}p \leq 0.001$, ** $p \leq 0.01$, * $p \leq 0.05$, ns>0.05 non-significant; n = 5–6. B) ELISA analysis of the pro-inflammatory cytokines TNFα, IL-1β, IL-6 and IL12p70 (pg/ml) in supernatants of *Hdac6*$^{+/+}$ and *Hdac6*$^{-/-}$ BMDCs after treatment for 6, 12 and 24 h with LPS. $^{***}p \leq 0.001$, ** $p \leq 0.01$, ns>0.05 non-significant; n = 5–6. C) ELISA analysis of the pro-inflammatory cytokines TNFα, IL-1β, IL-6 and IL12p70

(pg/ml) in supernatants of *Hdac6*$^{+/+}$ and *Hdac6*$^{-/-}$ BMDCs after treatment for 6, 12 and 24 h with Imiquimod. $^{***}p \leq 0.001$, * $p \leq 0.05$, ns>0.05 non-significant; n = 5–6. D) ELISA analysis of the pro-inflammatory cytokines TNFα, IL-1β, IL-6 and IL12p70 (pg/ml) in supernatants of *Hdac6*$^{+/+}$ and *Hdac6*$^{-/-}$ BMDCs after treatment for 6, 12 and 24 h with HKST. $^{***}p \leq 0.001$, ** $p \leq 0.01$, ns>0.05 non-significant; n = 5–6.

https://doi.org/10.1371/journal.ppat.1006799.g008

In this view, the TLR adaptor MyD88 participates in the transmission of signals by all TLRs except for TLR3. We decided to study MyD88 levels in a time-course infection with *Lm* by western blot, demonstrating that the quantity of this molecule was the same between *Hdac6*$^{+/+}$ and *Hdac6*$^{-/-}$ DCs and remaining stable during infection (S6 Fig part C). Remarkably, MyD88-HDAC6 molecular association was observed by co-immunoprecipitations of endogenous proteins using human dendritic cells after Pam2GSK4, Pam3GSK4 and HKLM stimulation (Fig 9B). Likewise, the MyD88 immunoprecipitation in *MyD88*- and *HDAC6*-overexpressed HEK cell line was also able to co-precipitate HDAC6 (S6 Fig part D). These results were corroborated by mass spectrometry analysis of MyD88 immunoprecipitates; which in addition detected two acetylated peptides corresponding to MyD88 (S6 Fig parts E and F). The same approach was used to determine MyD88-HDAC6 molecular association after TLR-2 activation with HKLM using a constitutively expressed human TLR-2 HEK cell line, rendering the same result (Fig 9C). This association is also maintained using a double-deacetylase domain mutant of HDAC6 (H216A:H611A), called HDAC6-DD, indicating that HDAC6-MyD88 interaction is independent of its catalytic activity (Fig 9C and S6 Fig part D). The knock-down of HDAC6 expression using a small harping plasmid (sh-HDAC6) blocked this interaction (Fig 9C and S6 Fig part D). However, no acetylated peptides could be detected in the mass spectrometry analysis of the MyD88 immunoprecipitation from HKLM-stimulated TLR-2 HEK cell line (Fig 9D). Moreover, assessment of NF-κB induction in TLR-2-expressing HEK cell line after HKLM, Pam2GSK4 and Pam3GSK4 stimulation shows lower activation only in shHDAC6 transfected cells, without affecting the activity of HDAC6-DD-transfected ones (Fig 9E).

Taking into account all these data, HDAC6 associates with the TLR-adaptor molecule MyD88, and the absence of HDAC6 in DCs seems to diminish the TLR-response after a variety of stimuli, underlining the scaffold role of HDAC6 in determining the ability of MyD88 to mediate TLR signalling.

To ascertain the defective TLR-dependent inflammatory response *in vivo* due to the molecular association of MyD88-HDAC6, *Hdac6*$^{+/+}$ and *Hdac6*$^{-/-}$ mice were intravenously injected with a lethal dose of *Lm* (Fig 9F) [44]. A protective effect against *Lm*-induced septic shock was observed from 3 to 10 days post-infection (dpi) (Fig 9F). Accordingly, lower levels of the pro-inflammatory cytokine IL-6 were detected in the serum of *Hdac6*$^{-/-}$ mice at 72 hpi, highlighting a reduced systemic cytokine-driven inflammatory response after *Lm* infection in these mice (Fig 9G).

Discussion

Recent studies have revealed the involvement of HDAC6 in the innate immune response against Influenza Virus A (IVA), Sendai virus (SeV), and vesicular stomatitis virus (VSV) [21–24]. Given the similarities between the innate responses to viruses and intracellular bacteria, this prompted us to investigate the role of HDAC6 in a model of *Lm* infection. In this work, we demonstrated a dual role of HDAC6 in the innate response against *Lm*, not only due to its enzymatic activity but also dependent of its function as a scaffold (Fig 10). Our data clearly demonstrate that *Hdac6*$^{-/-}$ BMDCs have an impaired immune response against *Lm* and *S.* Typhimurium infection *in vitro*. Moreover, higher *Lm* titres observed in *Hdac6*$^{-/-}$ dendritic cells, M-CSF-derived macrophages and peritoneal macrophages were corroborated during *in*

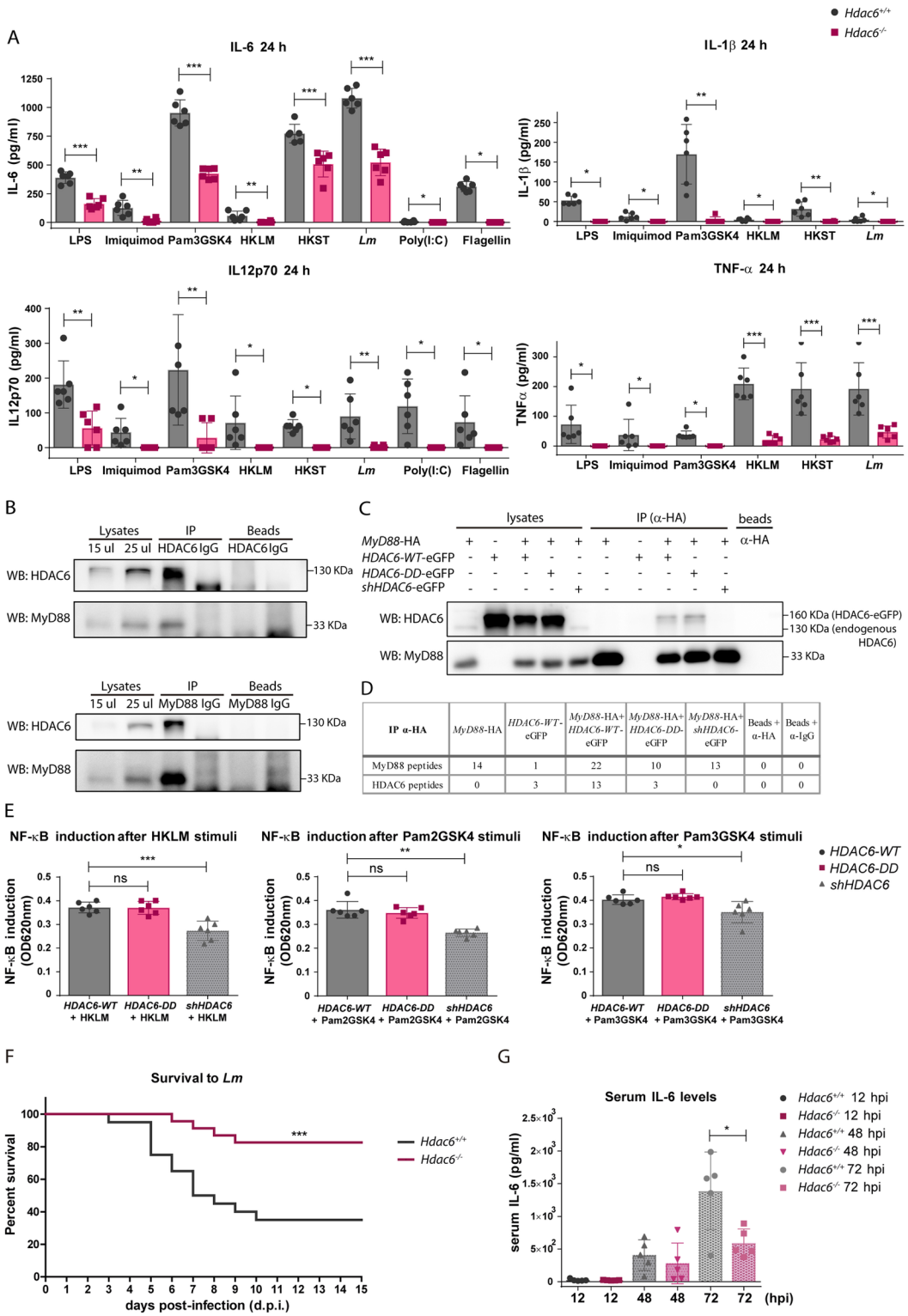

Fig 9. Association of HDAC6 with TLR-adaptor MyD88 and its contribution to the inflammatory response to *Lm*. A) ELISA analysis of the pro-inflammatory cytokines TNFα, IL-1β, IL-6 and IL12p70 (pg/ml) in supernatants of *Hdac6*$^{+/+}$ and *Hdac6*$^{-/-}$ FLT3L-DCs activated with LPS, Imiquimod, Pam3GSK4, HKLM, HKST, *Lm*, Poly(I:C) and flagellin for 24 h. $^{***}p \leq 0.001$, ** $p \leq 0.01$, * $p \leq 0.05$; n = 6. B) Immunoprecipitation of endogenous HDAC6 and MyD88 followed by western-blot for both proteins. Immunoprecipitations were carried out using human moDCs after 30 min of stimulation with

Pam2GSK4, Pam3GSK4 and HKLM. Endogenous HDAC6 (130 KDa) and MyD88 (33 KDa) are indicated at right of western-blot. Similar results were obtained in two independent experiments. C) Immunoprecipitation of HA (MyD88) followed by western-blot for HDAC6 and MyD88. Immunoprecipitations were carried out using different HDAC6-eGFP plasmids co-transfected with MyD88-HA in HEK-Blue hTLR2 cell line after 30 min of stimulation with HKLM. Over-expressed (HDAC6-eGFP, 160 KDa) and endogenous HDAC6 (130 KDa) are indicated at right of western-blot. Similar results were obtained in four independent experiments. D) Immunoprecipitation of HA (MyD88) followed by mass spectrometry analysis. Immunoprecipitations were carried out using different HDAC6-eGFP plasmids co-transfected with MyD88-HA in HEK-Blue hTLR2 cell line after 30 min of stimulation with HKLM. The number of unique MyD88 and HDAC6 peptides is indicated. No acetylated peptides from MyD88 were detected in any sample. Similar results were obtained in four independent experiments. E) Graph of NF-κB induction in transfected *HDAC6-WT*, *HDAC6-DD* and *shHDAC6* HEK-Blue hTLR2 cell line after activation with HKLM, Pam2GSK4 and Pam3GSK4 during 8 h. NF-κB induction was calculated by the ratio of the signal of stimulated cells with its corresponding transfected cells in basal condition (without stimuli), $^{***}p\leq0.001$, ** $p\leq0.01$, * $p\leq0.05$, ns>0.05 non-significant; n = 6. F) Survival curve to intravenous injection with a lethal dose of *Lm* in $Hdac6^{+/+}$ and $Hdac6^{-/-}$ is showed. This curve corresponds to two different experiment of survival to *Lm* with a n = 24–21. $^{***}p\leq0.001$. G) Pro-inflammatory cytokine IL-6 was measured in sera of $Hdac6^{+/+}$ and $Hdac6^{-/-}$ mice intravenously injected with a lethal dose of *Lm* at 12, 48 and 72 hpi. $^{*}p\leq0.05$, n = 5.

https://doi.org/10.1371/journal.ppat.1006799.g009

vivo Lm infection at 6 hpi in various myeloid subsets of the spleen. The absence of this effect during BMDC *in vitro* infection by the non-intracellular bacteria *S. aureus* and *E. coli* DH5α indicates that $Hdac6^{-/-}$ BMDCs are specifically unable to efficiently clear intracellular pathogens. HDAC6 is involved in two of the most important cellular clearance systems, autophagy and ubiquitin-proteasome system (UPS) [9, 13]. In the case of *Lm* and *S.* Typhimurium, the main molecular mechanism for degradation of vesicle-contained bacteria is fusion with lysosomes in a process called autophagy [45–47]. In agreement with this, our data show that impaired phagosome-lysosome fusion underlies the phenotype observed in $Hdac6^{-/-}$ BMDCs. Unsuccessful fusion depends on acetylated-cortactin in *Hdac6*-deficient cells [9]. A similar mechanism has been described in *Hdac6*-deficient MEFs during quality-control autophagy [9]. We demonstrated that in $Hdac6^{-/-}$ BMDCs co-localized higher levels of acetylated-cortactin with intracellular *Lm*. The delay in vesicle fusion caused by the acetylation of cortactin, impairs the phagosome-lysosome fusion and provides more opportunities for phagosome-containing bacteria to escape to the cytosol, resulting in the higher bacterial load detected in $Hdac6^{-/-}$ BMDCs. Based on this experimental evidence, it is conceivable to postulate that the enzymatic activity of HDAC6 on its substrate cortactin controls autophagy of intracellular bacteria for their efficient clearance (Fig 10).

Pharmacological autophagy inhibitors erased the observed differences between $Hdac6^{+/+}$ and $Hdac6^{-/-}$ BMDCs. Conversely, rapamycin did not overcome the $Hdac6^{-/-}$ autophagy defect, indicating a defect in phagosome-lysosome fusion. However, other authors have reported opposite observations using pan-HDAC inhibitors or specific inhibitors of HDAC6 during infection of human macrophages with the *Gram*-negative intracellular pathogens *S.* Typhimurium and *E. coli* [48]. These inhibitors, when added at the time of infection, increase mitochondrial ROS production [48]. However, overnight pre-treatment before infection hampered bacterial clearance and reduced phagocytosis [48]. These data indicate that specific HDAC6 chemical inhibitors can have side-effects, including effects on other HDAC members, potentially interfering with the acetylation of other substrates upstream of cortactin that also have a role during bacterial infection. Our genetic approach unequivocally assigns a specific role to HDAC6 in innate cells during bacterial infection.

Although we observed an impairment in phagosome-lysosome fusion, we cannot rule out an involvement of HDAC6 in the anti-microbial response through its BUZ domain, with a contribution from ubiquitin. The characterized interaction between p62 and HDAC6 through their ubiquitin-binding domains provides a clue about the possible role of ubiquitin in the activation of innate immunity through the recognition of ubiquitinated-molecules [15]. For example, the ubiquitin-binding regions of HDAC6 and p62 are both essential for MyD88

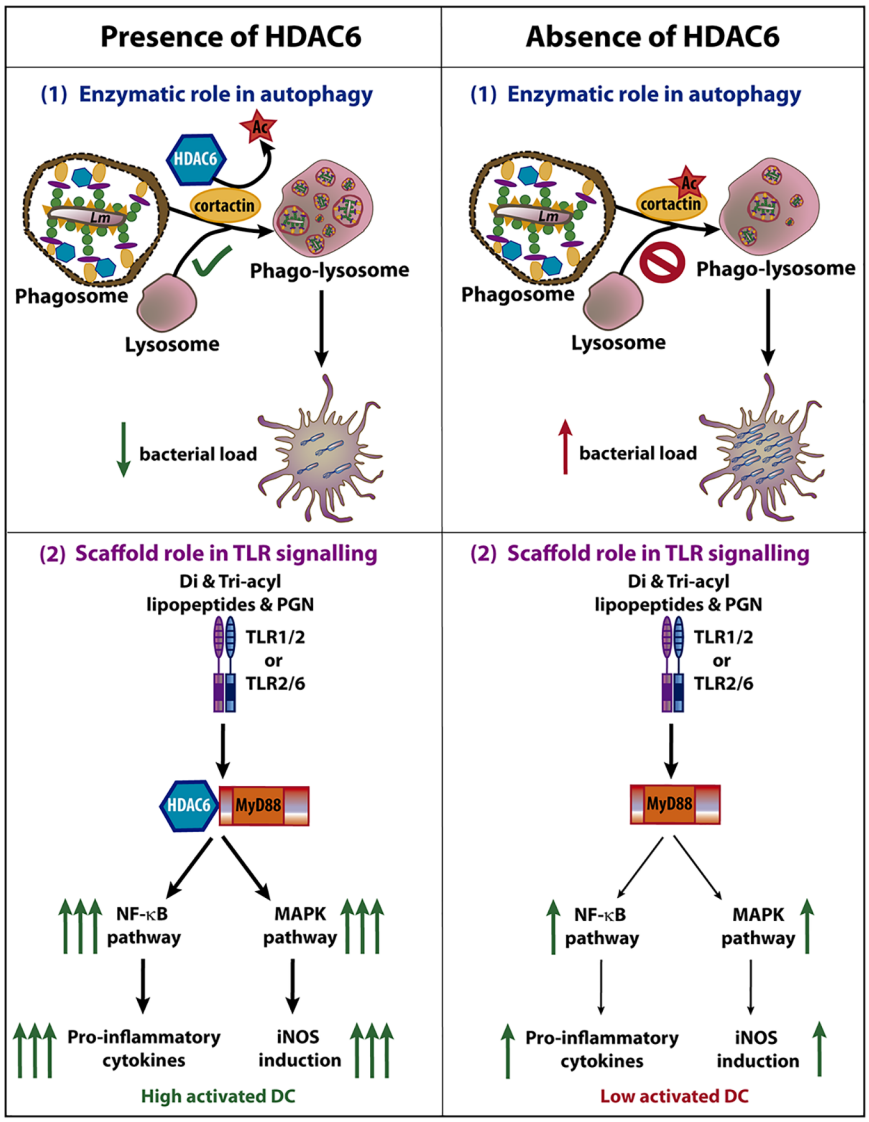

Fig 10. Dual role of HDAC6 during *Lm* infection in dendritic cells. The scheme shows the involvement of HDAC6 in two different functions of dendritic cell during *Lm* infection, the autophagy and the TLR signalling. **(1)** The fusion of phagosome with lysosome is dependent on cortactin and F-actin. The deacetylation of cortactin by HDAC6 allows the correct fusion, followed by an autophagic clearance of *Lm*. The absence of this enzyme delays the fusion of phagosome and lysosome, facilitating *Lm* to escape from phagosome leading to an increased bacterial load. **(2)** Di- and tri-acyl lipopeptides and peptidoglycan (PGN) of *Lm* are recognized by TLR1/2 or TLR2/6, activating the TLR pathway. HDAC6 is able to interact with the TLR-adaptor protein MyD88 which caused an enhanced down-stream signalling of TLR pathway, increasing NF-κB and MAPK activation. This stronger activation (independent on HDAC6 enzymatic activity) results in higher pro-inflammatory cytokine production and iNOS induction, reinforcing the ability of the DC to combat against this intracellular pathogen. Although the absence of HDAC6 does not fully abolish the activation of the DC, a lower induction of NF-κB and MAPK pathways promotes a lower activation of the anti-bacterial transcriptional program of the DCs. Note that both processes occur during *Lm* infection and the pro-inflammatory cytokines and iNOS induction can impact on the autophagic process. The images in the figure are not scaled.

https://doi.org/10.1371/journal.ppat.1006799.g010

aggregation and the downstream activation of MyD88-dependent signal transduction [49]. Furthermore, ubiquitin-binding platforms formed by HDAC6 and p62 are able to interact with interferon stimulated gene 15 (ISG15) to eliminate ISGylated proteins tagged after interferon stimulation by autophagy [50]. HDAC6 is able to bind to either mono- and poly-

ubiquitinated proteins, but shows a preference for proteins modified with k63-linked ubiquitin chains, which share structural similarities with ISG15 [51]. *S*. Typhimurium is decorated with this kind of ubiquitin chain for recognition by host cells, and can be recovered with phagosome proteins to initiate autophagy [52, 53]. Nevertheless, our data demonstrate that autophagy induction does not differ between *Hdac6*$^{+/+}$ and *Hdac6*$^{-/-}$ BMDCs, indicating that this phenotype is due to p62 accumulation in *Hdac6*$^{-/-}$ BMDCs as a consequence of impaired phagosome-lysosome fusion. Intact autophagy activation in *Hdac6*$^{-/-}$ BMDCs could be explained by compensatory p62 binding to ubiquitinated bacteria in the absence of HDAC6.

Our data also underscore other different function of HDAC6, independent of its enzymatic activity, in innate immune response to intracellular bacteria and various TLR stimuli (Fig 10). Hence, we provide evidence for a dampened inflammatory response in the absence of HDAC6, as shown by lower RNA levels of pro-inflammatory cytokines, chemokines, type-I interferons, and interferon-related proteins in *Hdac6*$^{-/-}$ BMDCs than in *Hdac6*$^{+/+}$ cells at 6 hpi, as well as the lower pro-inflammatory cytokine production and IFN-β secretion by infected *Hdac6*$^{-/-}$ BMDCs from 6 to 24 hpi. Moreover, *Hdac6*$^{-/-}$ BMDCs showed diminished iNOS induction at 6 hpi associated with low nitrite production and iNOS expression at longer times of *Lm* infection (24 hpi). These results agree with a lower phosphorylation of the MAPK pathway after *Lm* infection in *Hdac6*$^{-/-}$ dendritic cells, controlling the activation of AP-1 family transcription factors, which is necessary to switch inflammatory responses on [54]. In addition, the lower phosphorylation of mTORC1 pathway components in *Hdac6*$^{-/-}$ DCs is consistent with a lower pro-inflammatory response, as reported in trained macrophages and dendritic cells, in which a metabolic switch to glycolysis has been described [55]. These data may indicate that HDAC6 also appears to play a role in the activation of mTOR pathway after *Lm* infection to initiate the antibacterial transcriptional response to combat this pathogen. In summary, our results reveal a defect in DC activation after *Lm* entry.

Remarkably, this impaired anti-inflammatory response in *Hdac6*$^{-/-}$ BMDCs was also observed with other TLR-agonists such as LPS, Imiquimod, poly(I:C) and Pam3GSK4, highlighting HDAC6 as an important player in TLR signalling activation. Broad-spectrum HDAC inhibitors such as TSA exert immunosuppressive effects [56]. Genome-wide expression profiling arrays have revealed that 60% of genes transcriptionally increased by TLR2 or TLR4 stimulation are inhibited in TSA-treated cells, whereas 16% of genes are potentiated [56]. However, these observations do not provide any demonstrative evidence for a specific role of HDAC6, since other HDACs may also be involved.

Because GM-CSF-derived DCs express low levels of TLR3 and 5 in the membrane, we stimulated FLT3-L-derived DCs with poly(I:C) and flagellin to measure pro-inflammatory cytokines [57, 58], noting maintained failure in the inflammatory response in *Hdac6*$^{-/-}$ cells. Moreover, we detected impaired responses to PAMPs activation in GM-CSF-derived and FLT3L-derived *Hdac6*$^{-/-}$ DCs. In addition, all TLRs except for TLR3 signal through the adaptor MyD88, and the result obtained with the TLR3 ligand poly(I:C) was similar to that showed for the rest of TLR stimuli, thereby indicating that the TLR3-response is also affected by absence of HDAC6. In this regard, these data are in agreement with a recent study showing that acetylated retinoic-acid-inducible gene-1 (RIG-1) makes *Hdac6*$^{-/-}$ cells less sensitive to the presence of RNA viruses, resulting in a higher viral titre [59]. While this mechanism could explain the difference between the response of *Hdac6*$^{+/+}$ and *Hdac6*$^{-/-}$ FLT3L-DCs to TLR3 stimulation, the deficient activation by other TLRs in *Hdac6*$^{-/-}$ DCs also requires an explanation. In this respect, we demonstrate the molecular association of HDAC6 with MyD88 with endogenous proteins and in an overexpression system. Conceivably, the depletion of HDAC6 and therefore prevention of HDAC6-MyD88 binding, could inhibit TLR-2-signalling pathway activation, which is in accordance with a lower NF-κB induction measured in *Hdac6*$^{-/-}$ cells after various

TLR-2 agonist stimulation. A diminished NF-κB induction in *Hdac6*$^{-/-}$ cells could explain a reduced initiation of the pro-inflammatory response observed in *Hdac6*$^{-/-}$ dendritic cells, needed to alert the innate and adaptive immune response to *Lm*. However, NF-κB activity of HDAC6-DD-transfected HEK cell line after TLR-2 stimuli did not display any significant change compared to HDAC6-WT-transfected ones, supporting that enzymatic activity of HDAC6 is not involved in this signalling pathway. Two acetylated peptides corresponding to MyD88 have been found in basal condition in HEK transfected with HDAC6-DD and shHDAC6 constructions, which are different from the residue previously described in MyD88 [60]. However, no changes in the acetylation marks on MyD88 were detected after HKLM incubation, highlighting the scaffold role of HDAC6 in the proper activation of TLR-signalling pathway (Fig 10). Unexpectedly, a protective effect against systemic infection to a lethal dose of *Lm* were observed in *Hdac6*$^{-/-}$ mice. The reduced level of the inflammatory cytokine IL-6 detected in *Hdac6*$^{-/-}$ mice are in accordance with its higher resistance to *Lm* infection. The defective systemic inflammatory response after *Lm* infection of *Hdac6*$^{-/-}$ mice may indicate an impaired TLR-response in the absence of HDAC6 and might therefore be attributed to the absence of the molecular association of MyD88 and HDAC6. In this regard, mice resistance to *Lm* infection can be mediated by sequential MyD88-independent and -dependent responses [61–64]. However, the role of TLR-2 during *Lm* infection does not appear to be clear enough [62, 63]. On one hand, *Tlr-2*$^{-/-}$ mice display a deficit in circulating TNF-α and IL-12p40 production during intravenously injected *Lm* infection combined with a lower mice survival and increased bacterial burden in the liver [61, 63]. Other authors have obtained similar resistance to intraperitoneal-injected *Lm* infection between *Tlr-2*$^{-/-}$ and *Tlr-2*$^{+/+}$ mice, indicating that different inoculation routes of bacteria may render different immune outcomes [62]. Although handling and direct killing of *Lm* by activated macrophages can be mediated by TLR-2- and MyD88-independent mechanisms, the role of TLR-signalling has been observed necessary for nitric oxide and cytokine production [61, 63]. In fact, MyD88 not only works as TLR-adaptor protein, but also as adaptor of IL-1 and IL-18 receptors, both cytokine responses affected in *Lm*-MyD88$^{-/-}$ mice [62, 63, 65].

Overall, our data support a dual role for HDAC6 in the regulation of innate immunity against intracellular bacteria. An increased bacterial load in different *Hdac6*$^{-/-}$ myeloid cells can be explained by the autophagy mechanism, where a permanently acetylated cortactin may impair the phagosome-lysosome fusion, necessary for the clearance of this pathogen. Our experiments also show the importance of HDAC6 in DC activation, uncovering a novel mechanism of HDAC6 action mediated by the appropriate signalling via the TLR pathway, due to the association of HDAC6 with the TLR-adaptor protein MyD88. This molecular association seems to be required for a response to TLR stimuli to initiate the inflammatory response of an activated dendritic cell. Taken together, both HDAC6 functions described in this manuscript, reinforce the importance of this molecule to combat intracellular bacteria as *Lm* by autophagy and to completely activate the inflammatory response after TLR activation.

Materials and methods

Ethical statement

Mice were housed under specific pathogen-free conditions at the Centro Nacional de Investigaciones Cardiovasculares Carlos III (CNIC), and experiments were approved by the CNIC Ethical Committee for Animal Welfare and by the Spanish Ministry of Agriculture, Food, and the Environment. Animal care and animal procedures license were reviewed and approved by the local Ethics Committee for Basic research at the CNIC Ethical Committee for Animal Welfare and the Órgano Encargado del Bienestar Animal (OEBA) del Gabinete Veterinario de la

Universidad Autónoma de Madrid (UAM). This committee approved the document with an associated identification number PROEX 158/15 (CNIC 04/15).

Buffy coats of healthy donors were received from the Blood Transfusion Center of Comunidad de Madrid, and all donors signed their consent for the use of samples for research purposes. All the procedures using primary human cells were approved by the Ethics Committee of the Hospital Universitario de la Princesa.

Mice

HDAC6$^{-/-}$ mice were generated through targeting of exons from 10 to 13 by inserting a neomycin (Neo) and zeocin (Zeo) cassette, resulting in the disruption of the first catalytic domain of HDAC6 [66]. These mice were intercrossed on a C57BL/6 background to generate sex and age matched wild-type (*wt*) and knockout.

Bacteria strains

We used the *Listeria monocytogenes EGD* (BUG 600) strain, provided by Dr. Esteban Veiga (Centro Nacional de Biotecnología, CNB, Madrid). *Staphylococcus aureus* 132 and *Escherichia coli* K12, strain DH5α, were purchased from Invitrogen. BUG600 and *S. aureus* bacteria were grown in BHI broth. RFP-expressing *Listeria monocytogenes* (RFP-*Lm*) was provided by Dr Carlos Ardavín´s laboratory (Centro Nacional de Biotecnología, CNB, Madrid). *Salmonella enterica* serovar Thyphimurium strain SL1344 was provided by Dr. J. Garaude (Centro Nacional de Investigaciones Cardiovasculares, CNIC, Madrid). SL1344 and DH5α bacteria were grown in LB broth supplemented with 50 μg/ml streptomycin (Sigma). For phagocytosis experiments, *Lm* and *S. aureus* were grown overnight in Brain Herat Infusion (BHI) broth and *E. coli* and *S.* Thyphimurium in Luria-Bertani (LB) broth with shaking, diluted 1/50, and grown until log-phase (optical density 0.8–1.2 at 600 nm) without shaking. Bacteria were washed with phosphate-buffered saline (PBS) to remove LB salts before addition to cells.

Cell culture

The HEK293T cell line (ATCC) was cultured in DMEM medium (Sigma) containing 10% FBS (Invitrogen), 2 mM L-glutamine, 100 mg/ml penicillin and 100 mg/ml streptomycin. HEK Blue hTLR2 cell line (Invivogen), the HEK293 cell line expressing human TLR2, CD14 and NF-κB-SEAP (secreted embryonic alkaline phosphatase) reporter gene was cultured in DMEM medium (Sigma) containing 10% FBS (Invitrogen), 2 mM L-glutamine, 100 μg/ml Normocin (Invivogen) and 1X HEK-Blue Selection (Invitrogen).

Generation of bone marrow-derived dendritic cells (GM-CSF) and macrophages (M-CSF)

Mouse primary dendritic cells (BMDCs) and macrophages (BMDMs) were obtained from bone marrow cell suspensions after culture on non-treated 150-mm Petri dishes in complete RPMI 1640 supplemented with 10% FBS, 2 mM L-glutamine, 100 mg/ml penicillin, 100 mg/ml streptomycin, 50 mM 2-ME, and 20 ng/ml granulocyte-macrophage colony-stimulating factor (GM-CSF, PeproTech, London, U.K.) for BMDCs and macrophage colony-stimulating factor (30% mycoplasma-free L929 cell supernatant, NCBI Biosample accession number SAMN00155972) for BMDMs. BMDCs were collected at day 9 and BMDCs were characterized as $CD11c^{+}MHC\text{-}II^{+}Gr\text{-}1^{-}$ cells by flow cytometry. BMDMs were collected at day 6 and BMDMs were characterized as $CD11b^{+}F4/80^{+}$ or $CD11b^{+}CD64^{+}$ cells.

Generation of bone marrow-derived dendritic cells (FLT3L)

Bone marrow cell suspensions were culture on treated 6 well plates in complete RPMI 1640 supplemented with 10% FBS, 2 mM L-glutamine, 100 mg/ml penicillin, 100 mg/ml streptomycin, 50 mM 2-ME, and 150 ng/ml (FLT3L, PeproTech, London, U.K.). After 9–11 days of differentiation cells were collected to be characterized by flow cytometry as $CD11c^{+}B220^{-}CD11b^{+}CD24^{-}$ (60% of the culture) and $CD11c^{+}B220^{-}CD11b^{+}CD24^{+}$(40%).

Obtainment of thioglycollate-elicited macrophages (TEMs)

Mice received peritoneal injections with 1ml 4% TG. The peritoneal exudate was collected after 4 days and cultured in complete RPMI 1640 supplemented with 10% FBS, 2 mM L-glutamine, 100 mg/ml penicillin, 100 mg/ml streptomycin, and 50 mM 2-ME. To enrich the culture for macrophages, non-adherent cells were eliminated after a few hours by washing five times with warm PBS and gentle swirling.

Obtainment of human monocyte-derived dendritic cells (moDCs)

Peripheral blood mononuclear cells (PBMCs) from Buffy coats of healthy donors were isolated using Biocoll separating solution (Millipore) by centrifugation at 700 g 30 min at RT. Monocytes were purified from peripheral blood mononuclear cells (PBMCs) by an adherence step at 37˚C in incomplete RPMI 1640 medium during 1 h. Non-adherent cells were removed and adherent monocytes were washed three times with warm 1xPBS to remove residual PBMCs. Monocytes were cultured in complete RPMI 1640 supplemented with 10% FBS, 2 mM L-glutamine, 100 mg/ml penicillin, 100 mg/ml streptomycin, 500 U/ml IL-4 (R&D) and 500 U/ml GM-CSF (Immunotools) for 6 days. Fresh medium and cytokines were added every 48 hours to differentiate monocytes to immature human dendritic cells. Cells were characterized by flow cytometry as $HLA\text{-}DR^{+}CD3^{-}DC\text{-}SIGN^{+}CD14^{-}CD11c^{+}$. Activation of dendritic cells was induced with Pam2GSK4, Pam3GSK4 and HKLM for 30 min (Invivogen).

In vitro Lm-infection of BMDCs, BMDMs and TEMs

Cells were incubated with *Lm* and assessed for survival to gentamicin exposure [67]. Cells were infected with *Lm* at a multiplicity of infection (MOI) of 10 for 30 min at 37˚C. To determine the number of bacteria entering the cells, extracellular bacteria were killed by treatment with 100 μg/ml gentamicin (Sigma-Aldrich, St. Louis, MO) for an additional 30 min at 37˚C. Then, infected cells were washed with PBS three times and lysed with 0.05% Triton X-100 (Sigma-Aldrich, St. Louis, MO) in distilled water. Serial dilutions were seeded on brain-heart infusion (BHI) agar plates and CFUs were counted after 36 hours.

In vivo Lm systemic infections

$Hdac6^{+/+}$ and $Hdac6^{-/-}$ were intravenously injected with *Listeria monocytogenes* EGD (125.000 CFUs/mouse) using a 29-gauge needle. For survival experiments mice were monitored twice a day in order to detect casualties during 15 days of infection.

Determination of CFUs in target organs

After 12, 24, 48 and 72 hpi, mice were perfused with 1X PBS to clean blood form organs and spleens and livers were weight. To determine bacterial load, spleens and livers were digested with 0.1 mg/ml type IV collagenase and 0.5 mg/ml DNAse I (Roche, Mannheim, Germany) for 30 min at 37˚C. After digestion, organs were homogenized in 70 μm filters and red blood cells were lysed with ammonium chloride potassium lysis buffer (ACK, Sigma). Splenic cell

suspensions were resuspended in PBS and cells were counted. Serial dilutions were grown on BHI agar plates. CFUs were counted after 36 hours of incubation at 37˚C. CFUs were calculated by cell number and by gram per organ.

Antibodies and reagents

Antibodies were used in western blotting, flow cytometry and immunofluorescence; detailed information is available in S1 Table. Poly-L-lysine (PLL) was purchased from Sigma. Phalloidin-Alexa488 and 647 were from BD Biosciences. Zenon Alexa Fluor 488 rabbit IgG labelling kit, DAPI and Prolong Gold anti-fade mounting medium were from Thermofisher Scientific. Anti-human CD3 antibody (T3b hybridoma) was generated in Dr. F. Sánchez-Madrid laboratory (Hospital Universitario de la Princesa, HUP, Madrid) [68]. Rapamycin, bafilomycin A1, 3-MA, cloroquine, NH_4Cl, 1400W and DPI were from Sigma-Aldrich.

Gene overexpression and silencing

HEK293 cells were co-transfected with plasmids encoding human MyD88 fused to the HA-tag (Addgene plasmid #12287) together with plasmids encoding *HDAC6-WT* or double deacetylase domain mutant DD (mutated human HDAC6-H216A/H611A) fused to the eGFP tag (*HDAC6-WT* and *HDAC6-DD* have been previously described [26]. When indicated, cells were co-transfected with the appropriate small harping RNA plasmid pLVX-IRES-ZsGreen1, where *shHDAC6*-2049 (TRCN0000004842) was cloned between BamH1 and EcoR1 sites. Cells were transfected using Lipofectamine 2000 (Invitrogen). Experiments were performed after 24 h after transfection.

RNA extraction and real-time quantitative PCR

RNA from mouse BMDCs was isolated with the QIAGEN RNeasy Kit (Qiagen). Residual DNA contamination was removed with the Turbo DNA-free Kit (Ambion). Total RNA (1–2 μg) was reverse transcribed to cDNA with a Reverse Trancription Kit (Applied Biosystems). Quantitative PCR was then performed in an AB7900-384 thermocycler (Applied Biosystem) using SYBR Green master mix (Applied Biosystems, Warrington, UK) as the reporter. Expression levels of target genes were normalized to the expression of housekeeping genes β-actin, GAPDH, β2-microglobulin and Yhwaz (tyrosine 3-monooxygenase/tryptophan 5-monooxygenase activation protein, ζ) for presentation of relative mRNA levels. Data were analysed with Biogazelle qBasePlus version 2.3 (Biogazelle) and graphs are represented as a normalized expression scaled to average of all samples. Gene-specific primers used are listed in S2 Table.

Soluble embryonic alkaline phosphatase (SEAP)-NF-κB detection

50.000 transfected HEK-Blue hTLR2 cells with different HDAC6 constructions were place in bottom p96 well plates resuspended in HEK-Blue Detection medium (Invivogen) without stimulus (negative control) and with TLR-2 agonists (HKLM stimulus, MOI = 10). After 8–12 h of incubation, SEAP activity was measured by optical density at 620 nm with a microplate reader. To calculate the NF-κB induction, the signal obtained from each mutant condition without stimuli (background) was depleted of the signal of each condition of activation with Pam2GSK4, Pam3GSK4 or HKLM.

ELISAs and nitrite measurement

Cytokine and NO production was analysed in the supernatants of BMDC cultures at 6, 12 and 24 h after stimulation with *Lm*, heat-killed *Listeria monocytogenes* (HKLM), heat-killed

Salmonella Typhimurium (HKST), Pam3CSK4, Flagellin, Imiquimod, polyinosinic-polycytidylic acid (Poly(I:C)) (InvivoGen, San Diego, CA), or LPS from *Escherichia coli* (Sigma-Aldrich). TNF-α and IL12p70 were analysed with OptEIA ELISA kits (BD Biosciences, San Diego, CA), IL-1β and IL-6 with the mouse ELISA Ready-SET-Go! kit from eBioscience (Affymetrix, San Diego, CA) and Interferon-β was measured with Legend max mouse IFN-β ELISA kit (Biolegend). The detection was based on colorimetric quantification of absorbance at 450 nm, corrected with subtraction at 570 nm measured in a microplate reader (Bio-Rad Model 550). NO was estimated from the nitrite concentration measured with a Griess reagent kit at 548 nm (Molecular Probes/Life Technologies, Thermo Fisher Scientific). Results were expressed as the means of duplicate wells.

Immunoblotting

Total cell extracts from BMDCs stimulated with *Lm*, HKLM or the indicated TLR ligands for the indicated times were prepared in lysis buffer (0.5% Triton X100, 25 mM Tris-HCl pH 7.5, 0.5 mM EGTA, 0.5 mM EDTA, 25 mM NaF, 0.5 sodium glycerol-phosphate, 2.5 mM pyrophosphate, 0.135 M sacarose) with a cocktail of protease and phosphatase inhibitors (Roche). Cell lysates were cleared of nuclei by centrifugation at 15,000 g for 15 min. Protein extracts were separated by 8–15% SDS-PAGE and transferred to a PVDF membrane (Biorad). Proteins were visualized with LAS-3000 after membrane incubation with specific antibodies (see S1 Table) and peroxidase-conjugated secondary antibodies (5 μg ml^{-1}). Band intensities were quantified using Image Gauge software (Fuji Photo Film, Co., Ltd) and results are expressed relative to loading controls. For quantification of western-blots, phosphorylated/total ratios were divided by loading control signal. Non-infection (NI) time was considered as 100%, and following times were relativized to it.

Immunoprecipitation of MyD88 and HDAC6 proteins

Human moDCs (1×10^7 per condition) were lysed (10 mM Tris pH 7.4, 150 mM NaCl, 5% glycerol, 1mM EDTA, 1mM $MgCl_2$, 1mM $CaCl_2$, 1% CHAPS (Sigma) and protease and phosphatase inhibitors (Roche)) for 1 h at 4˚C. Lysates were incubated for pre-clearing with pre-washed Protein G Dynabeads (Invitrogen; 50 μl per condition; 2 h, 4˚C). Pre-cleared lysates were incubated with 6 μg rabbit anti-MyD88 antibody (Cell Signaling) or 6 μg rabbit anti-HDAC6 antibody (Assay bioTech) per condition O/N at 4˚C. Similar μg of control isotype antibody for rabbit were used. Fifty microlitres of Dynabeads per condition were washed three times in wash buffer (10 mM Tris pH 7.4, 150 mM NaCl, 5% glycerol, 1mM EDTA, 1mM $MgCl_2$, 1mM $CaCl_2$, 0.1% CHAPS) and added to antibody-conjugated lysates for 2 h 4C. Antibody-conjugated Dynabeads were washed six times with wash buffer and transferred to clean tubes.

HEK293T cells or HEK-Blue hTLR2 (1×10^7 per condition) were lysed (25 mM Tris pH 8, 150 mM NaCl, 0.5% NP-40 and protease and phosphatase inhibitors) and incubated for pre-clearing with pre-washed Protein G Dynabeads (Invitrogen; 50 μl per condition; 3 h, 4˚C). Fifty microlitres of Dynabeads per condition were washed three times in wash buffer (25 mM Tris pH 8, 150 mM NaCl, 0.05% NP-40) and re-suspended in 600 μl of wash buffer containing 1–2 μg mouse anti-HA antibody (Roche) per condition and incubated 3 h at 4˚C. Similar μg of control isotype antibody for mouse were used. Pre-cleared lysates were incubated with antibody-conjugated Dynabeads (O/N, 4˚C). Antibody-conjugated Dynabeads were washed six times with lysis buffer and transferred to clean tubes. Then, were washed twice with wash buffer. Protein loading buffer was added, samples were boiled at 95˚C for 5 min and processed for immunoblotting.

Flow cytometry

Cells were stained in ice-cold PBS containing FBS (0.5%) and EDTA (5 mM) using appropriate antibody-fluorophore conjugates. Multiparameter analysis was performed on a FACSCANTO II flow cytometer (BD Biosciences) and analysed with FlowJo software (Tree Star). Prior to fixing, cells were resuspended in PBS/0.5% BSA/5 mM EDTA solution containing yellow fluorescent reactive dye to exclude dead cells (Life Technologies). For intracellular staining, cells were fixed and permeabilized using the CytoFix/Cytoperm kit (BD).

Fluorescence confocal microscopy

For immunofluorescence assays, cells were plated onto slides coated with poly-L-lysine (50 μg ml^{-1}) and incubated for 1 h at 37˚C. Infection experiment were carried out at the indicated times. Cells were then fixed, blocked and stained with the indicated primary antibodies (5 μg ml^{-1}) followed by alexa488- or Rhodamine Red X-labelled secondary antibodies (5 μg ml^{-1}). Samples were examined under a Leica SP5 confocal microscope (Leica) fitted with a 63X objective. Images were acquired with sequential xyz acquisition mode scans with laser ranges of 418–473 nm for DAPI, 502–548 nm for Alexa-488, 584–644 nm for Rhodamine X and 737–779 nm for Alexa-647. Z-stacks of 2–5 μm were obtained using a maximum z-step size of 0.3 μm.

Imaris quantification

Images were processed and assembled using Image J 1.51p (Fiji). Confocal 3D images assembled with Imaris 7.7.2 (Bitplane) using the ImarisCell module. Every cell and its corresponding intracellular bacteria were calculated in each image. Surfaces corresponding to bacteria were used to calculate the maximal fluorescence intensity of the channels to co-localize with bacteria. Two-channel co-localization was quantified in at least 10 images per genotype, corresponding to 10 biological samples.

In-gel protein digestion

Proteins were in-gel digested using a previously described protocol [69]. Briefly, the coimmunoprecipitate was heated at 95˚C for 5 min, after which the magnetic beads were removed using a magnet. The resulting solution was added sample buffer and loaded in 0.5-cm-wide wells of an SDS-PAGE gel. The run was stopped as soon as the front entered into the resolving gel. The protein band was visualized by Coomassie Blue staining, excised, and digested overnight at 37˚C with 60 ng/μl sequencing-grade modified trypsin (Promega) at 10:1 protein: enzyme (w/w) ratio in 50 mM ammonium bicarbonate, pH 8.8, containing 10% acetonitrile. The resulting tryptic peptides were desalted onto C18 OMIX tips (Agilent), dried down and kept at -80˚C until further use.

Mass spectrometry

The resulting peptides were analyzed by liquid chromatography coupled to tandem mass spectrometry (LC-MS/MS) on an Easy nLC-1000 nano-HPLC apparatus (Thermo Scientific, San Jose, CA, USA) coupled to a hybrid quadrupole-orbitrap mass spectrometer (Q Exactive HF, Thermo Scientific). The dried peptides were taken up in 0.1% (v/v) formic acid and then loaded onto a PepMap100 C18 LC pre-column (75 μm I.D., 2 cm, Thermo Scientific) and eluted on line onto an analytical NanoViper PepMap 100 C18 LC column (75 μm I.D., 50 cm, Thermo Scientific) with a continuous gradient consisting of 8–31% B in 240 min (B = 80% ACN, 0.1% formic acid) at 200 nL/min. Peptides were ionized using a Picotip emitter

nanospray needle (New Objective). Each MS run consisted of enhanced FT-resolution spectra (120,000 resolution) in the 400–1,200 m/z range followed by data-dependent MS/MS spectra of the 20 most intense parent ions acquired along the chromatographic run. The AGC target value in the Orbitrap for the survey scan was set to 1,000,000. Fragmentation in the linear ion trap was performed at 30% normalized collision energy with a target value of 10,000 ions. The full target was set to 30,000, with 1 microscan and 50 ms injection time, and the dynamic exclusion was set to 0.5 min.

Peptide identification

For peptide identification the MS/MS spectra were searched with the Sequest algorithm implemented in Proteome Discoverer 1.4 (Thermo Scientific). Database searching against human protein sequences from the UniProt database (March 2017, 158,382 entries) was performed with the following parameters: trypsin digestion with 4 maximum missed cleavage sites; precursor and fragment mass tolerances of 800 ppm and 0.02 Da, respectively; Cys carbamidomethylation as static modifications; and Met oxidation and Lys acetylation as dynamic modifications. The results were analyzed using the probability ratio method [70] and a false discovery rate (FDR) for peptide identification was calculated based on the search results against a decoy database using the refined method [71].

Statistical analysis

Data were analysed with GraphPad prism software (La Jolla, CA) for normality (Kolmogorov-Smirnov test for small samples). Normal data were analysed by Student t-test, non-normal data by Mann-Whitney test, and grouped data by 2-tailed One-way ANOVA with a Bonferroni post-test. For western blot quantification, the sample with the maximum signal was assigned a value of 100%, and signals in other samples were expressed as a percentage of this; significance was determined by a one-sample test. Long-rank (Mantel-Cox) test and Cehan-Breslow-Wilcoxon test were used for the analysis of the Kaplan-Meier curve (survival curve).

Supporting information

S1 Fig. Differentiation of GM-CSF-derived DCs, their viability at 6 hpi, comparison of CFUs of GM-CSF- and M-CSF-derived cells and fluorescent confocal microscopy of *Lm*. A) Left: Dot-plots showing CD11c and MHC-II markers, with gating for $CD11c^{+}MHC\text{-}II^{+}$ and $CD11c^{+}MHC\text{-}II^{-}$ populations (percentages indicated). Right: Dot-plots on differentiation day 11 showing FSC-H versus Gr-1, gating the $Gr\text{-}1^{+}$ population corresponding to neutrophil contamination in GM-CSF-derived DC cultures. Charts show the percentages of $CD11c^{+}MHC\text{-}II^{+}$, $CD11c^{+}MHC\text{-}II^{-}$ and $Gr\text{-}1^{+}$ populations. ns>0.05 non-significant; n = 6. B) Percentage viability of BMDCs before infections and at 6 hpi with *Lm*, ns>0.05 non-significant; n = 6. C) Comparison of CFUs in GM-CSF-derived DCs and M-CSF-derived macrophages over the time-course of *Lm* infection. $^{***}p\leq0.001$, $^{**}p\leq0.01$, ns>0.05 non-significant; n = 6. D) ImarisCell Module analysis of the number of cells and the number of bacteria per cell in all pictures (10 pictures per genotype). The graph shows the distribution of cells with a specific number of bacteria per cell. The number of cells with 6 and 7 bacteria differed significantly between the $Hdac6^{+/+}$ and $Hdac6^{-/-}$ genotypes. $^{*}p\leq0.05$, n = 10. E) Confocal microscopy determination of bacterial load of the Fig 1F. Maximum intensity z-projections of confocal microscopy images of *Lm*-infected $Hdac6^{+/+}$ and $Hdac6^{-/-}$ BMDCs at 6 hpi. ImarisCell Module view of the number of nucleus and bacteria per cell. Actin transparency is used to visualize bacteria (number indicated on the right). Images show DAPI (blue),

Lm (red), β-actin (green). Scale bars 20 μm.
(TIF)

S2 Fig. Gating strategy of myeloid populations of the spleen. A) Dot-plots showing the gating of myeloid populations of spleen. Dot-plots showing SSC-A versus FSC-A indicates p1, FSC-H versus FSC-W and SSC-H versus SSC-W were used to avoid doublets and FSC-H versus viability shows live and dead cells. Singlets and live cells were used to choose $CD3^-CD19^-DX5^-Ly6G^+$ cell population. From this population, neutrophils were gated as Ly6G +Ly6C+ cells, monocytes as $CD11b^+CD11c^{lo}$, Tips DCs as intermedium levels of CD11b and CD11c, conventional dendritic cells (cDCs) as $CD11c^{hi}$; inside this population cDCs $CD8^-$ were distinguish as $CD11c^{hi}CD11b^+$ and cDCs $CD8^-$ as $CD11c^{hi}CD11b^{lo}$. B) Representative histograms of different splenic populations (monocytes, neutrophils, Tips DCs, total cDCs, cDCs $CD8^-$ and cDCs $CD8^+$) show *Lm* signal of $Hdac6^{+/+}$ and $Hdac6^{-/-}$ mice injected with a lethal dose of *Lm* at 6 hpi. A pool of $Hdac6^{+/+}$ and $Hdac6^{-/-}$ spleens non-infected was used as a control sample without infection (NI). $^{**}p\leq0.01$, $^{*}p\leq0.05$; n = 6.
(TIF)

S3 Fig. Control vehicles and autophagy markers. A) Total CFUs at 0 and 6 hpi in *Lm*-infected BMDCs (MOI of 10) treated with different control vehicles (H_2O, DMSO and ethanol). H_2O were the control vehicle used for NH_4Cl and cloroquine, DMSO for 3-MA, bafilomycin A1, DPI and 1400W and ethanol for rapamycin. Time 0 is included as a bacterial entry control. $^{***}p\leq0.001$, ns>0.05 non-significant; n = 6. B) PCR analysis of autophagy markers (ATG-2, 5, 7 and 12, LC3A and B, p62 and Beclin-1) and lysosome markers (LAMP-1 and 2) (arbitrary units) after 6 hpi with *Lm*, ns>0.05 non-significant; n = 5.
(TIF)

S4 Fig. Pro-inflammatory cytokine secretion. ELISA detection of the pro-inflammatory cytokines IL-1β and IL12p70 (pg/ml) in supernatants (S) and in supernatants plus the corresponding cell pellets (S+P) of *Lm*-infected $Hdac6^{+/+}$ and $Hdac6^{-/-}$ BMDCs at 6, 12 and 24 hpi. $^{***}p\leq0.001$, $^{**}p\leq0.01$, $^{*}p\leq0.05$, ns>0.05 non-significant; n = 5.
(TIF)

S5 Fig. TLR expression and TLR-signalling pathway activation by LPS and HKLM. A) Western-blot analysis in $Hdac6^{+/+}$ and $Hdac6^{-/-}$ BMDCs over the time-course of LPS or HKLM treatment. Total and phosphorylated AKT were detected for both treatments. Accompanying charts on the right show quantification, indicating the percentage of phAKT/total AKT ratio. $^{**}p\leq0.01$, $^{*}p\leq0.05$; n = 4. B) PCR analysis of TLR-1, 2 and 6 (arbitrary units) in $Hdac6^{+/+}$ and $Hdac6^{-/-}$ BMDCs non-infected (NI) and after *Lm*-infection at 6 hpi. ns>0.05 non-significant; n = 6.
(TIF)

S6 Fig. Differentiation of FLT3-L DCs, their pro-inflammatory cytokine secretion at 6 hpi and association of HDAC6 with TLR-adaptor MyD88. A) Left: Dot-plots of FLT3-L DC cultures at day 11 of differentiation, showing gating for the CD11c+ population (percentages indicated). Centre: Dot-plots showing CD11b versus B220 to select two populations: $CD11c^+CD11b^+B220^+$ (plasmacytoid DCs, pDCs) and $CD11c^+CD11b^+B220^-$ (conventional DCs, cDCs) (percentages indicated). Right: Dot-plots showing CD11b versus CD24 to select the $CD11b^+CD24^+$ and $CD11b^+CD24^-$ populations (gated from cDCs) (percentages indicated). The charts on the right show the percentages of $CD11c^+$, $CD11c^+CD11b^+B220^-CD24^-$ and $CD11c^+CD11b^+B220^-CD24^+$ populations, ns>0.05 non-significant; n = 6. B) ELISA detection of the pro-inflammatory cytokines IL-1β and IL-6 (pg/ml) in supernatants of

Hdac6$^{+/+}$ and *Hdac6*$^{-/-}$ FLT3L-DCs activated with LPS, Imiquimod, Pam3GSK4, HKLM, HKST, *Lm*, Poly(I:C) or flagellin for 6 h. $^{***}p \leq 0.001$, ** $p \leq 0.01$, * $p \leq 0.05$; n = 6. C) MyD88 adaptor protein in *Hdac6*$^{+/+}$ and *Hdac6*$^{-/-}$ BMDCs. Western-blot analysis of MyD88 over the time-course of *Lm* infection in *Hdac6*$^{+/+}$ and *Hdac6*$^{-/-}$ BMDCs (left). Accompanying charts on the right show quantification of the percentage of MyD88; ns non-significant; n = 5. D) Immunoprecipitation of HA (MyD88) followed by western-blot for HDAC6 and MyD88. Immunoprecipitations were carried out using different HDAC6-eGFP plasmids co-transfected with MyD88-HA in HEK cell line. Over-expressed (HDAC6-eGFP, 160 kDa) is indicated at right of western-blot. E) Immunoprecipitation of HA (MyD88) followed by mass spectrometry analysis. Immunoprecipitations were carried out using different HDAC6-eGFP plasmids co-transfected with MyD88-HA in HEK cell line. The number of unique MyD88 and HDAC6 peptides identified is indicated. (*) indicates the presence of acetylated MyD88 peptides. Similar results were obtained in three independent experiments. F) MS^2 fragmentation spectra from the peptides showing at 1217.0699 (Top), and 599.3803 (Bottom). Ion adscription to carboxy- (*y* ions, blue) and amino-terminal (*b* ions, red) fragmentation series is indicated. K_{ac} denotes acetylated lysine and C_{cm} indicates carbamidomethylated cysteine. Fragment ion sequence coverage is schematically indicated. Similar results were obtained in three independent experiments.
(TIF)

S1 Table. Antibody table. Table of antibodies used in experimental procedures disclosed by reference, brand, host, application and dilution.
(PDF)

S2 Table. qPCR primers. Table of qPCR primers used in experimental procedures disclosed by gene name and sequence 5′-3′.
(PDF)

Acknowledgments

We thank Dr S. Bartlett for assistance with English editing and M.V. Manzanares for critical reading of the manuscript. Some experiments were performed in the CNIC Proteomics Units.

Author Contributions

Conceptualization: Olga Moreno-Gonzalo, Danay Cibrián, María Laura Saiz, Francisco Sánchez-Madrid.

Data curation: Inmaculada Jorge, Emilio Camafeita, Jesús Vázquez.

Formal analysis: Olga Moreno-Gonzalo, María Laura Saiz, Inmaculada Jorge, Emilio Camafeita.

Funding acquisition: Francisco Sánchez-Madrid.

Investigation: Olga Moreno-Gonzalo, Marta Ramírez-Huesca, Noelia Blas-Rus, Danay Cibrián, María Laura Saiz, Francisco Sánchez-Madrid.

Methodology: Olga Moreno-Gonzalo, Marta Ramírez-Huesca, Noelia Blas-Rus, Danay Cibrián, María Laura Saiz, Inmaculada Jorge, Emilio Camafeita, Jesús Vázquez.

Project administration: Francisco Sánchez-Madrid.

Supervision: Francisco Sánchez-Madrid.

Validation: Olga Moreno-Gonzalo, Marta Ramírez-Huesca, Noelia Blas-Rus.

Writing – original draft: Olga Moreno-Gonzalo, Emilio Camafeita, Francisco Sánchez-Madrid.

Writing – review & editing: Olga Moreno-Gonzalo, Francisco Sánchez-Madrid.

References

1. Valenzuela-Fernandez A, Cabrero JR, Serrador JM, Sanchez-Madrid F. HDAC6: a key regulator of cytoskeleton, cell migration and cell-cell interactions. Trends Cell Biol. 2008; 18(6):291–7. https://doi.org/10.1016/j.tcb.2008.04.003 PMID: 18472263.
2. Kaluza D, Kroll J, Gesierich S, Yao TP, Boon RA, Hergenreider E, et al. Class IIb HDAC6 regulates endothelial cell migration and angiogenesis by deacetylation of cortactin. EMBO J. 2011; 30(20):4142–56. https://doi.org/10.1038/emboj.2011.298 PMID: 21847094.
3. Birdsey GM, Dryden NH, Shah AV, Hannah R, Hall MD, Haskard DO, et al. The transcription factor Erg regulates expression of histone deacetylase 6 and multiple pathways involved in endothelial cell migration and angiogenesis. Blood. 2012; 119(3):894–903. https://doi.org/10.1182/blood-2011-04-350025 PMID: 22117042.
4. Schulz R, Marchenko ND, Holembowski L, Fingerle-Rowson G, Pesic M, Zender L, et al. Inhibiting the HSP90 chaperone destabilizes macrophage migration inhibitory factor and thereby inhibits breast tumor progression. J Exp Med. 2012; 209(2):275–89. https://doi.org/10.1084/jem.20111117 PMID: 22271573.
5. Cabrero JR, Serrador JM, Barreiro O, Mittelbrunn M, Naranjo-Suarez S, Martin-Cofreces N, et al. Lymphocyte chemotaxis is regulated by histone deacetylase 6, independently of its deacetylase activity. Molecular biology of the cell. 2006; 17(8):3435–45. https://doi.org/10.1091/mbc.E06-01-0008 PMID: 16738306.
6. Zhang X, Yuan Z, Zhang Y, Yong S, Salas-Burgos A, Koomen J, et al. HDAC6 modulates cell motility by altering the acetylation level of cortactin. Molecular cell. 2007; 27(2):197–213. https://doi.org/10.1016/j.molcel.2007.05.033 PMID: 17643370.
7. Hubbert C, Guardiola A, Shao R, Kawaguchi Y, Ito A, Nixon A, et al. HDAC6 is a microtubule-associated deacetylase. Nature. 2002; 417(6887):455–8. https://doi.org/10.1038/417455a PMID: 12024216.
8. Matsuyama A, Shimazu T, Sumida Y, Saito A, Yoshimatsu Y, Seigneurin-Berny D, et al. In vivo destabilization of dynamic microtubules by HDAC6-mediated deacetylation. EMBO J. 2002; 21(24):6820–31. https://doi.org/10.1093/emboj/cdf682 PMID: 12486003.
9. Lee JY, Koga H, Kawaguchi Y, Tang W, Wong E, Gao YS, et al. HDAC6 controls autophagosome maturation essential for ubiquitin-selective quality-control autophagy. EMBO J. 2010; 29(5):969–80. https://doi.org/10.1038/emboj.2009.405 PMID: 20075865.
10. Lafarga V, Aymerich I, Tapia O, Mayor F Jr., Penela P. A novel GRK2/HDAC6 interaction modulates cell spreading and motility. EMBO J. 2012; 31(4):856–69. https://doi.org/10.1038/emboj.2011.466 PMID: 22193721.
11. Iwata A, Riley BE, Johnston JA, Kopito RR. HDAC6 and microtubules are required for autophagic degradation of aggregated huntingtin. The Journal of biological chemistry. 2005; 280(48):40282–92. https://doi.org/10.1074/jbc.M508786200 PMID: 16192271.
12. Pandey UB, Batlevi Y, Baehrecke EH, Taylor JP. HDAC6 at the intersection of autophagy, the ubiquitin-proteasome system and neurodegeneration. Autophagy. 2007; 3(6):643–5. PMID: 17912024.
13. Pandey UB, Nie Z, Batlevi Y, McCray BA, Ritson GP, Nedelsky NB, et al. HDAC6 rescues neurodegeneration and provides an essential link between autophagy and the UPS. Nature. 2007; 447(7146):859–63. https://doi.org/10.1038/nature05853 PMID: 17568747.
14. Boyault C, Gilquin B, Zhang Y, Rybin V, Garman E, Meyer-Klaucke W, et al. HDAC6-p97/VCP controlled polyubiquitin chain turnover. EMBO J. 2006; 25(14):3357–66. https://doi.org/10.1038/sj.emboj.7601210 PMID: 16810319.
15. Yan J, Seibenhener ML, Calderilla-Barbosa L, Diaz-Meco MT, Moscat J, Jiang J, et al. SQSTM1/p62 interacts with HDAC6 and regulates deacetylase activity. PloS one. 2013; 8(9):e76016. https://doi.org/10.1371/journal.pone.0076016 PMID: 24086678.
16. Ding WX, Yin XM. Sorting, recognition and activation of the misfolded protein degradation pathways through macroautophagy and the proteasome. Autophagy. 2008; 4(2):141–50. PMID: 17986870.
17. Lee JY, Nagano Y, Taylor JP, Lim KL, Yao TP. Disease-causing mutations in parkin impair mitochondrial ubiquitination, aggregation, and HDAC6-dependent mitophagy. J Cell Biol. 2010; 189(4):671–9. https://doi.org/10.1083/jcb.201001039 PMID: 20457763.

18. Kawaguchi Y, Kovacs JJ, McLaurin A, Vance JM, Ito A, Yao TP. The deacetylase HDAC6 regulates aggresome formation and cell viability in response to misfolded protein stress. Cell. 2003; 115(6):727–38. PMID: 14675537.

19. Lee JY, Kapur M, Li M, Choi MC, Choi S, Kim HJ, et al. MFN1 deacetylation activates adaptive mitochondrial fusion and protects metabolically challenged mitochondria. Journal of cell science. 2014; 127 (Pt 22):4954–63. https://doi.org/10.1242/jcs.157321 PMID: 25271058.

20. Huo L, Li D, Sun X, Shi X, Karna P, Yang W, et al. Regulation of Tat acetylation and transactivation activity by the microtubule-associated deacetylase HDAC6. The Journal of biological chemistry. 2011; 286(11):9280–6. https://doi.org/10.1074/jbc.M110.208884 PMID: 21220424.

21. Valenzuela-Fernandez A, Alvarez S, Gordon-Alonso M, Barrero M, Ursa A, Cabrero JR, et al. Histone deacetylase 6 regulates human immunodeficiency virus type 1 infection. Molecular biology of the cell. 2005; 16(11):5445–54. https://doi.org/10.1091/mbc.E05-04-0354 PMID: 16148047.

22. Zhu J, Coyne CB, Sarkar SN. PKC alpha regulates Sendai virus-mediated interferon induction through HDAC6 and beta-catenin. EMBO J. 2011; 30(23):4838–49. https://doi.org/10.1038/emboj.2011.351 PMID: 21952047.

23. Banerjee I, Miyake Y, Nobs SP, Schneider C, Horvath P, Kopf M, et al. Influenza A virus uses the aggresome processing machinery for host cell entry. Science. 2014; 346(6208):473–7. https://doi.org/10.1126/science.1257037 PMID: 25342804.

24. Husain M, Cheung CY. Histone deacetylase 6 inhibits influenza A virus release by downregulating the trafficking of viral components to the plasma membrane via its substrate, acetylated microtubules. Journal of virology. 2014; 88(19):11229–39. https://doi.org/10.1128/JVI.00727-14 PMID: 25031336.

25. de Zoeten EF, Wang L, Butler K, Beier UH, Akimova T, Sai H, et al. Histone deacetylase 6 and heat shock protein 90 control the functions of Foxp3(+) T-regulatory cells. Mol Cell Biol. 2011; 31(10):2066–78. https://doi.org/10.1128/MCB.05155-11 PMID: 21444725.

26. Serrador JM, Cabrero JR, Sancho D, Mittelbrunn M, Urzainqui A, Sanchez-Madrid F. HDAC6 deacetylase activity links the tubulin cytoskeleton with immune synapse organization. Immunity. 2004; 20 (4):417–28. PMID: 15084271.

27. Pamer EG. Immune responses to Listeria monocytogenes. Nature reviews Immunology. 2004; 4 (10):812–23. https://doi.org/10.1038/nri1461 PMID: 15459672.

28. Tam MA, Wick MJ. Dendritic cells and immunity to Listeria: TipDCs are a new recruit. Trends Immunol. 2004; 25(7):335–9. https://doi.org/10.1016/j.it.2004.05.004 PMID: 15207498.

29. Hamon M, Bierne H, Cossart P. Listeria monocytogenes: a multifaceted model. Nat Rev Microbiol. 2006; 4(6):423–34. https://doi.org/10.1038/nrmicro1413 PMID: 16710323.

30. Pizarro-Cerda J, Cossart P. Listeria monocytogenes membrane trafficking and lifestyle: the exception or the rule? Annu Rev Cell Dev Biol. 2009; 25:649–70. https://doi.org/10.1146/annurev.cellbio.042308.113331 PMID: 19575658.

31. Burrack LS, Harper JW, Higgins DE. Perturbation of vacuolar maturation promotes listeriolysin O-independent vacuolar escape during Listeria monocytogenes infection of human cells. Cell Microbiol. 2009; 11(9):1382–98. https://doi.org/10.1111/j.1462-5822.2009.01338.x PMID: 19500109.

32. Birmingham CL, Canadien V, Kaniuk NA, Steinberg BE, Higgins DE, Brumell JH. Listeriolysin O allows Listeria monocytogenes replication in macrophage vacuoles. Nature. 2008; 451(7176):350–4. https://doi.org/10.1038/nature06479 PMID: 18202661.

33. MacMicking JD, Nathan C, Hom G, Chartrain N, Fletcher DS, Trumbauer M, et al. Altered responses to bacterial infection and endotoxic shock in mice lacking inducible nitric oxide synthase. Cell. 1995; 81 (4):641–50. PMID: 7538909.

34. Kocks C, Hellio R, Gounon P, Ohayon H, Cossart P. Polarized distribution of Listeria monocytogenes surface protein ActA at the site of directional actin assembly. Journal of cell science. 1993; 105 (Pt 3):699–710. PMID: 8408297.

35. Michel E, Reich KA, Favier R, Berche P, Cossart P. Attenuated mutants of the intracellular bacterium Listeria monocytogenes obtained by single amino acid substitutions in listeriolysin O. Mol Microbiol. 1990; 4(12):2167–78. PMID: 1965218.

36. Hamilton SE, Badovinac VP, Khanolkar A, Harty JT. Listeriolysin O-deficient Listeria monocytogenes as a vaccine delivery vehicle: antigen-specific CD8 T cell priming and protective immunity. Journal of immunology. 2006; 177(6):4012–20. PMID: 16951364.

37. Bahjat KS, Meyer-Morse N, Lemmens EE, Shugart JA, Dubensky TW, Brockstedt DG, et al. Suppression of cell-mediated immunity following recognition of phagosome-confined bacteria. PLoS Pathog. 2009; 5(9):e1000568. https://doi.org/10.1371/journal.ppat.1000568 PMID: 19730694.

38. Condotta SA, Richer MJ, Badovinac VP, Harty JT. Probing CD8 T cell responses with Listeria monocytogenes infection. Adv Immunol. 2012; 113:51–80. https://doi.org/10.1016/B978-0-12-394590-7.00005-1 PMID: 22244579.

39. Serbina NV, Salazar-Mather TP, Biron CA, Kuziel WA, Pamer EG. TNF/iNOS-producing dendritic cells mediate innate immune defense against bacterial infection. Immunity. 2003; 19(1):59–70. PMID: 12871639.

40. Edelson BT, Bradstreet TR, Hildner K, Carrero JA, Frederick KE, Kc W, et al. CD8alpha(+) dendritic cells are an obligate cellular entry point for productive infection by Listeria monocytogenes. Immunity. 2011; 35(2):236–48. https://doi.org/10.1016/j.immuni.2011.06.012 PMID: 21867927.

41. Jung S, Unutmaz D, Wong P, Sano G, De los Santos K, Sparwasser T, et al. In vivo depletion of CD11c + dendritic cells abrogates priming of CD8+ T cells by exogenous cell-associated antigens. Immunity. 2002; 17(2):211–20. PMID: 12196292.

42. Witte CE, Archer KA, Rae CS, Sauer JD, Woodward JJ, Portnoy DA. Innate immune pathways triggered by Listeria monocytogenes and their role in the induction of cell-mediated immunity. Adv Immunol. 2012; 113:135–56. https://doi.org/10.1016/B978-0-12-394590-7.00002-6 PMID: 22244582.

43. Honda K, Takaoka A, Taniguchi T. Type I interferon [corrected] gene induction by the interferon regulatory factor family of transcription factors. Immunity. 2006; 25(3):349–60. https://doi.org/10.1016/j.immuni.2006.08.009 PMID: 16979567.

44. Martinez del Hoyo G, Ramirez-Huesca M, Levy S, Boucheix C, Rubinstein E, Minguito de la Escalera M, et al. CD81 controls immunity to Listeria infection through rac-dependent inhibition of proinflammatory mediator release and activation of cytotoxic T cells. Journal of immunology. 2015; 194(12):6090–101. https://doi.org/10.4049/jimmunol.1402957 PMID: 25972472.

45. Rich KA, Burkett C, Webster P. Cytoplasmic bacteria can be targets for autophagy. Cell Microbiol. 2003; 5(7):455–68. PMID: 12814436.

46. Py BF, Lipinski MM, Yuan J. Autophagy limits Listeria monocytogenes intracellular growth in the early phase of primary infection. Autophagy. 2007; 3(2):117–25. PMID: 17204850.

47. Birmingham CL, Smith AC, Bakowski MA, Yoshimori T, Brumell JH. Autophagy controls Salmonella infection in response to damage to the Salmonella-containing vacuole. The Journal of biological chemistry. 2006; 281(16):11374–83. https://doi.org/10.1074/jbc.M509157200 PMID: 16495224.

48. Ariffin JK, das Gupta K, Kapetanovic R, Iyer A, Reid RC, Fairlie DP, et al. Histone deacetylase inhibitors promote mitochondrial reactive oxygen species production and bacterial clearance by human macrophages. Antimicrob Agents Chemother. 2015. https://doi.org/10.1128/AAC.01876-15 PMID: 26711769.

49. Into T, Inomata M, Niida S, Murakami Y, Shibata K. Regulation of MyD88 aggregation and the MyD88-dependent signaling pathway by sequestosome 1 and histone deacetylase 6. The Journal of biological chemistry. 2010; 285(46):35759–69. https://doi.org/10.1074/jbc.M110.126904 PMID: 20837465.

50. Nakashima H, Nguyen T, Goins WF, Chiocca EA. Interferon-stimulated gene 15 (ISG15) and ISG15-linked proteins can associate with members of the selective autophagic process, histone deacetylase 6 (HDAC6) and SQSTM1/p62. The Journal of biological chemistry. 2015; 290(3):1485–95. https://doi.org/10.1074/jbc.M114.593871 PMID: 25429107.

51. Olzmann JA, Li L, Chudaev MV, Chen J, Perez FA, Palmiter RD, et al. Parkin-mediated K63-linked polyubiquitination targets misfolded DJ-1 to aggresomes via binding to HDAC6. J Cell Biol. 2007; 178 (6):1025–38. https://doi.org/10.1083/jcb.200611128 PMID: 17846173.

52. Rytkonen A, Poh J, Garmendia J, Boyle C, Thompson A, Liu M, et al. SseL, a Salmonella deubiquitinase required for macrophage killing and virulence. Proc Natl Acad Sci U S A. 2007; 104(9):3502–7. https://doi.org/10.1073/pnas.0610095104 PMID: 17360673.

53. Olzmann JA, Chin LS. Parkin-mediated K63-linked polyubiquitination: a signal for targeting misfolded proteins to the aggresome-autophagy pathway. Autophagy. 2008; 4(1):85–7. PMID: 17957134.

54. Kawasaki T, Kawai T. Toll-like receptor signaling pathways. Front Immunol. 2014; 5:461. https://doi.org/10.3389/fimmu.2014.00461 PMID: 25309543.

55. Netea MG, Joosten LA, Latz E, Mills KH, Natoli G, Stunnenberg HG, et al. Trained immunity: A program of innate immune memory in health and disease. Science. 2016; 352(6284):aaf1098. https://doi.org/10.1126/science.aaf1098 PMID: 27102489.

56. Roger T, Lugrin J, Le Roy D, Goy G, Mombelli M, Koessler T, et al. Histone deacetylase inhibitors impair innate immune responses to Toll-like receptor agonists and to infection. Blood. 2011; 117(4):1205–17. https://doi.org/10.1182/blood-2010-05-284711 PMID: 20956800.

57. Dearman RJ, Cumberbatch M, Maxwell G, Basketter DA, Kimber I. Toll-like receptor ligand activation of murine bone marrow-derived dendritic cells. Immunology. 2009; 126(4):475–84. https://doi.org/10.1111/j.1365-2567.2008.02922.x PMID: 18778283.

58. Xu Y, Zhan Y, Lew AM, Naik SH, Kershaw MH. Differential development of murine dendritic cells by GM-CSF versus Flt3 ligand has implications for inflammation and trafficking. Journal of immunology. 2007; 179(11):7577–84. PMID: 18025203.

59. Choi SJ, Lee HC, Kim JH, Park SY, Kim TH, Lee WK, et al. HDAC6 regulates cellular viral RNA sensing by deacetylation of RIG-I. EMBO J. 2016. 15; 35(4):429–42. https://doi.org/10.15252/embj.201592586 PMID: 26746851.

60. New M, Sheikh S, Bekheet M, Olzscha H, Thezenas ML, Care MA, et al. TLR Adaptor Protein MYD88 Mediates Sensitivity to HDAC Inhibitors via a Cytokine-Dependent Mechanism. Cancer research. 2016; 76(23):6975–87. https://doi.org/10.1158/0008-5472.CAN-16-0504 PMID: 27733371.

61. Seki E, Tsutsui H, Tsuji NM, Hayashi N, Adachi K, Nakano H, et al. Critical roles of myeloid differentiation factor 88-dependent proinflammatory cytokine release in early phase clearance of Listeria monocytogenes in mice. Journal of immunology. 2002; 169(7):3863–8. PMID: 12244183.

62. Edelson BT, Unanue ER. MyD88-dependent but Toll-like receptor 2-independent innate immunity to Listeria: no role for either in macrophage listericidal activity. Journal of immunology. 2002; 169 (7):3869–75. PMID: 12244184.

63. Torres D, Barrier M, Bihl F, Quesniaux VJ, Maillet I, Akira S, et al. Toll-like receptor 2 is required for optimal control of Listeria monocytogenes infection. Infect Immun. 2004; 72(4):2131–9. https://doi.org/10.1128/IAI.72.4.2131-2139.2004 PMID: 15039335.

64. Serbina NV, Kuziel W, Flavell R, Akira S, Rollins B, Pamer EG. Sequential MyD88-independent and -dependent activation of innate immune responses to intracellular bacterial infection. Immunity. 2003; 19(6):891–901. PMID: 14670305.

65. Arnold-Schrauf C, Dudek M, Dielmann A, Pace L, Swallow M, Kruse F, et al. Dendritic cells coordinate innate immunity via MyD88 signaling to control Listeria monocytogenes infection. Cell Rep. 2014; 6 (4):698–708. https://doi.org/10.1016/j.celrep.2014.01.023 PMID: 24529704.

66. Gao YS, Hubbert CC, Lu J, Lee YS, Lee JY, Yao TP. Histone deacetylase 6 regulates growth factor-induced actin remodeling and endocytosis. Mol Cell Biol. 2007; 27(24):8637–47. https://doi.org/10.1128/MCB.00393-07 PMID: 17938201.

67. Vaudaux P, Waldvogel FA. Gentamicin antibacterial activity in the presence of human polymorphonuclear leukocytes. Antimicrob Agents Chemother. 1979; 16(6):743–9. PMID: 533256.

68. Montoya MC, Sancho D, Bonello G, Collette Y, Langlet C, He HT, et al. Role of ICAM-3 in the initial interaction of T lymphocytes and APCs. Nat Immunol. 2002; 3(2):159–68. https://doi.org/10.1038/ni753 PMID: 11812993.

69. Bonzon-Kulichenko E, Perez-Hernandez D, Nunez E, Martinez-Acedo P, Navarro P, Trevisan-Herraz M, et al. A robust method for quantitative high-throughput analysis of proteomes by 18O labeling. Mol Cell Proteomics. 2011; 10(1):M110 003335. https://doi.org/10.1074/mcp.M110.003335 PMID: 20807836.

70. Martinez-Bartolome S, Navarro P, Martin-Maroto F, Lopez-Ferrer D, Ramos-Fernandez A, Villar M, et al. Properties of average score distributions of SEQUEST: the probability ratio method. Mol Cell Proteomics. 2008; 7(6):1135–45. https://doi.org/10.1074/mcp.M700239-MCP200 PMID: 18303013.

71. Navarro P, Vazquez J. A refined method to calculate false discovery rates for peptide identification using decoy databases. J Proteome Res. 2009; 8(4):1792–6. https://doi.org/10.1021/pr800362h PMID: 19714873.

Supplemental Figure 1

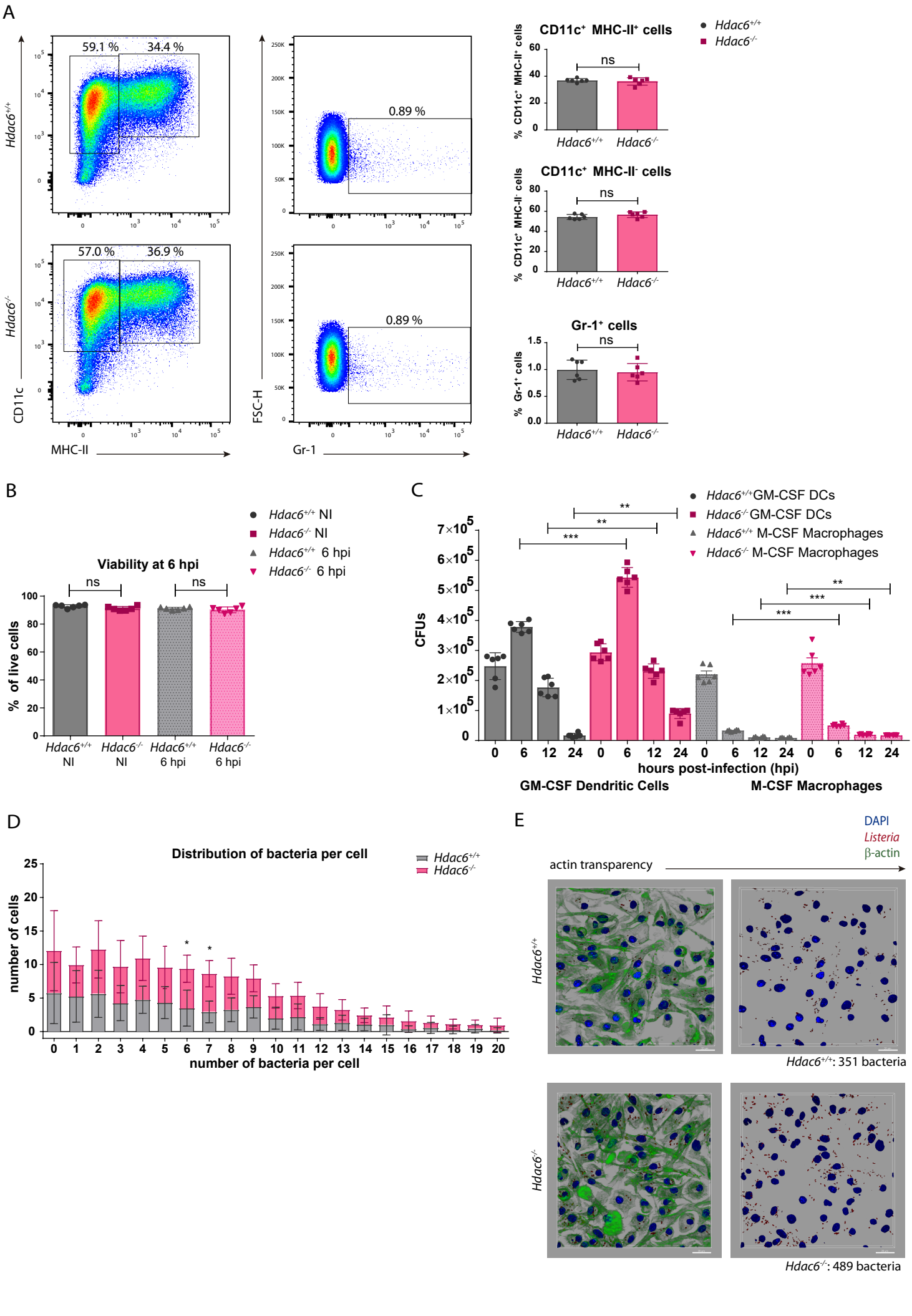

Supplemental Figure 2

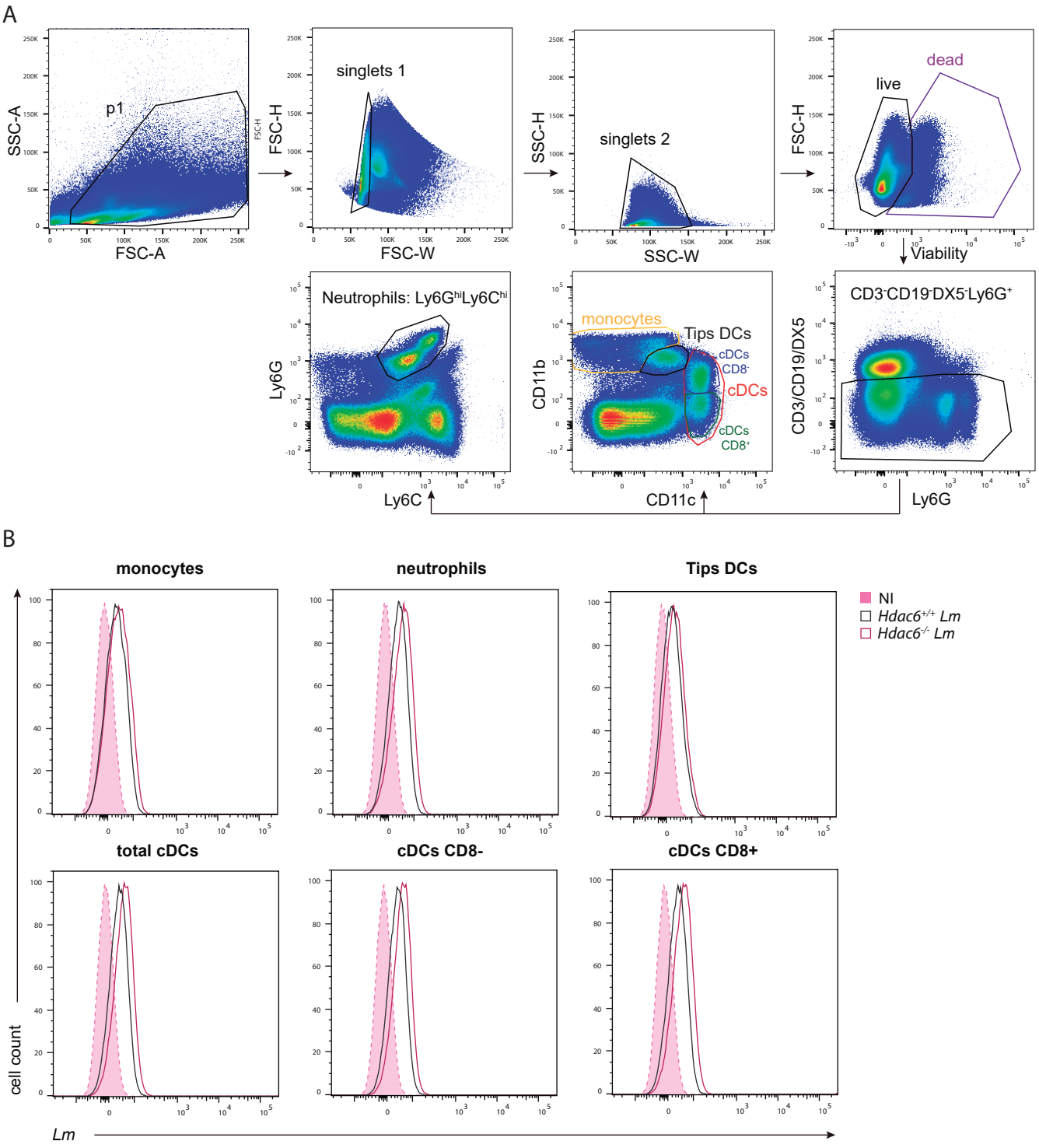

Supplemental Figure 3

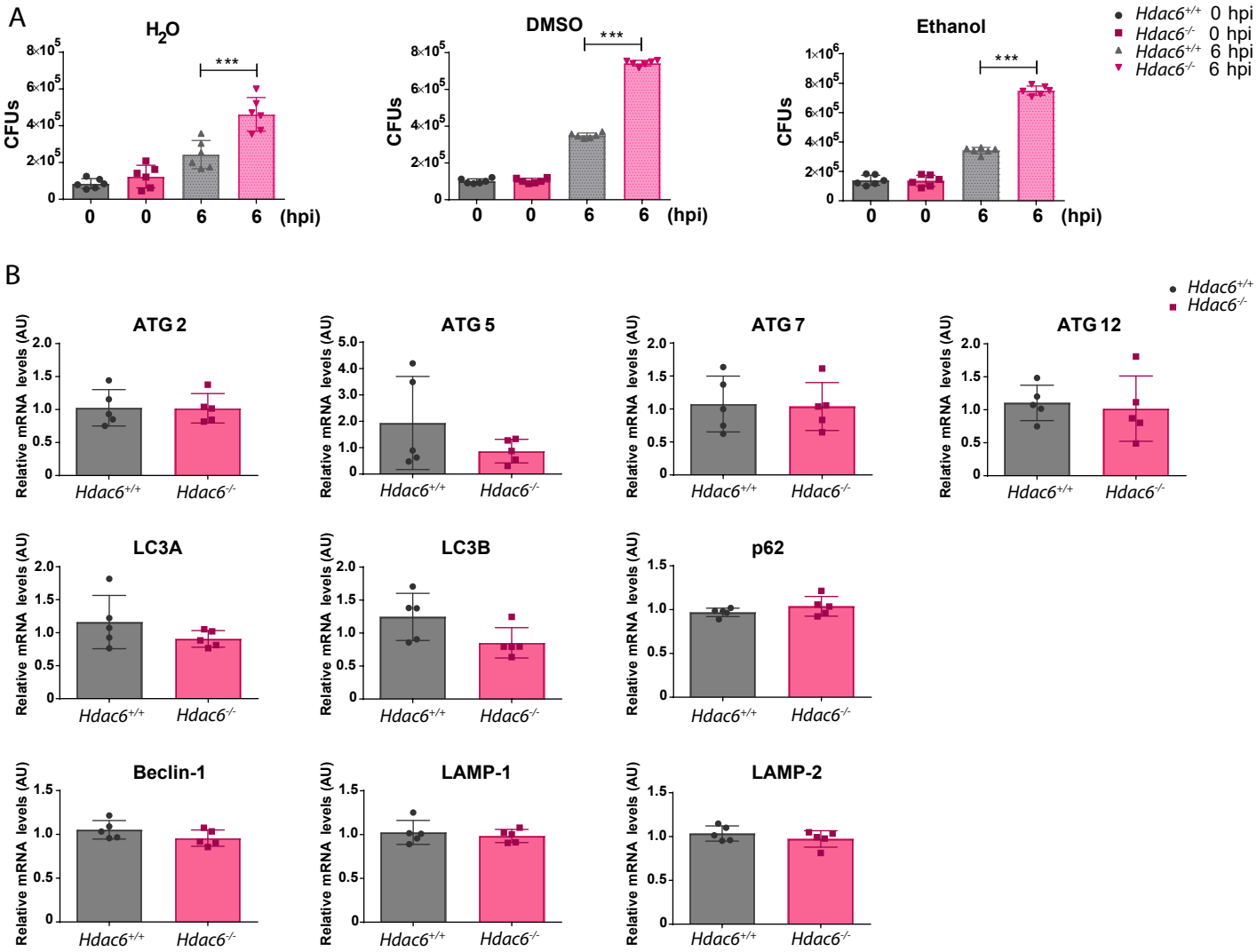

Supplemental Figure 4

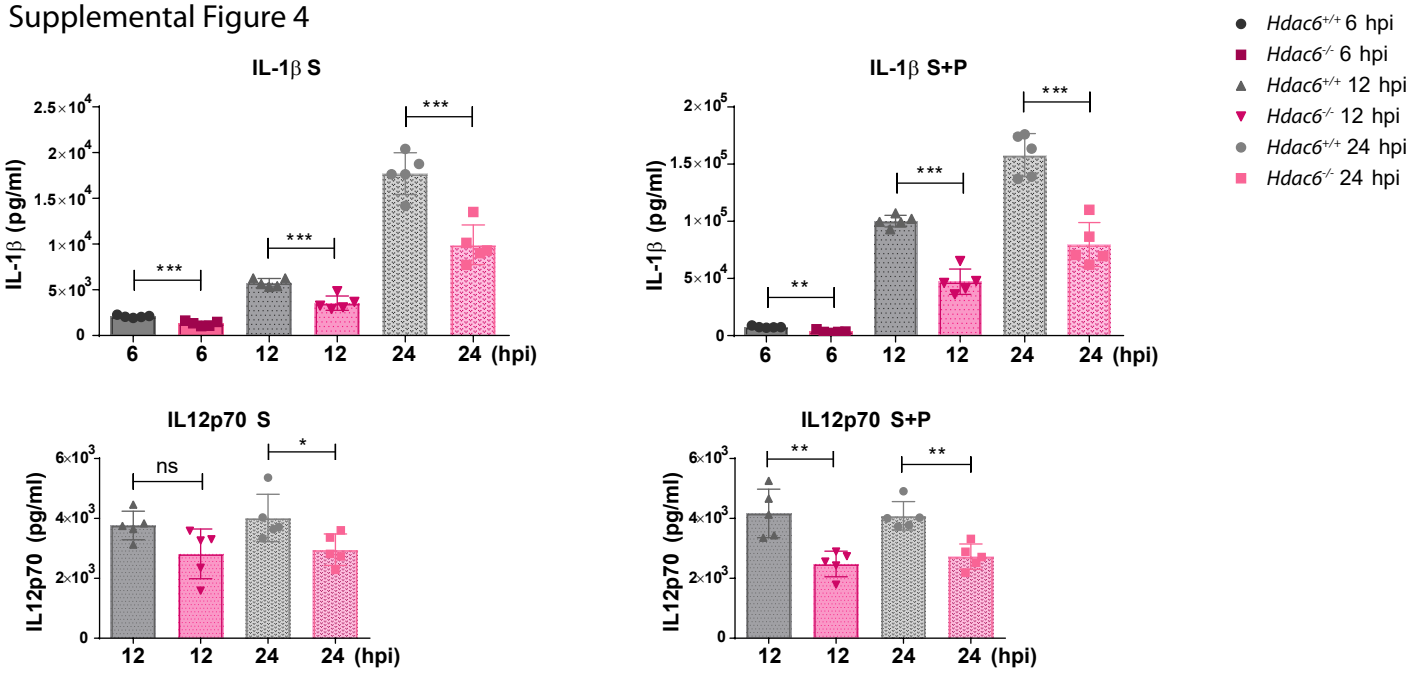

Supplemental Figure 5

A

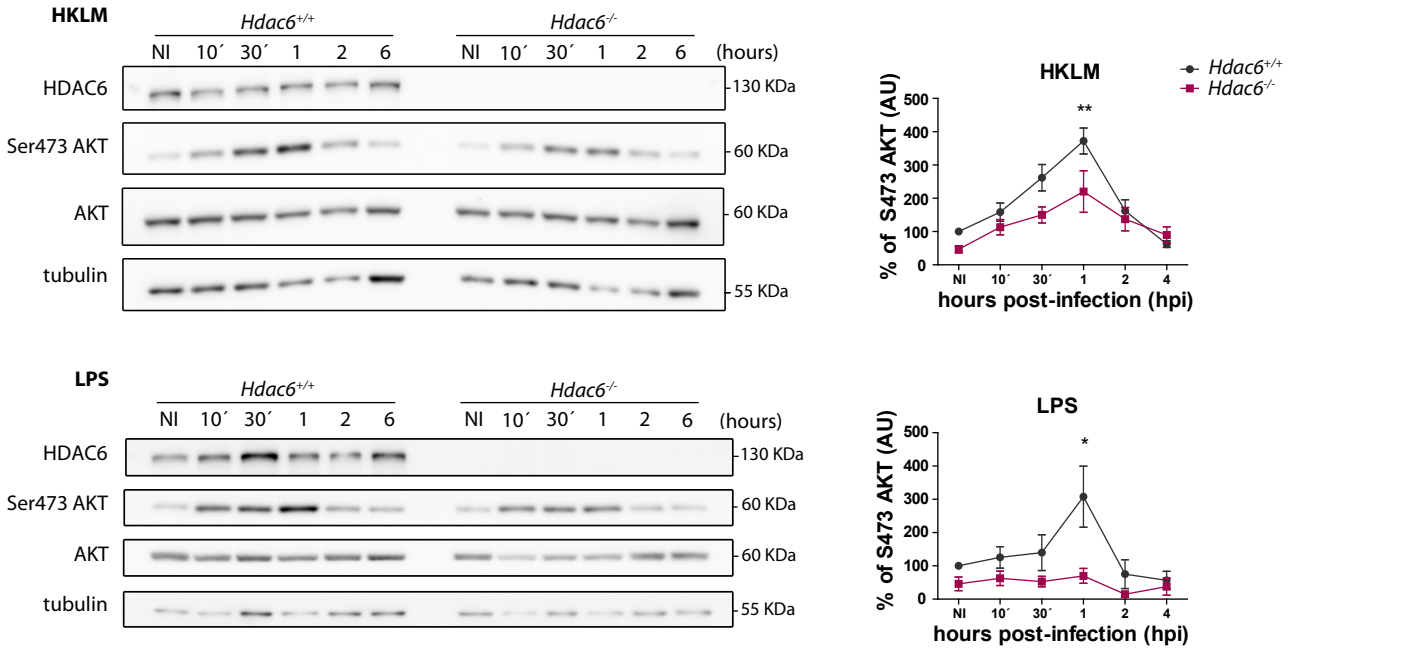

B

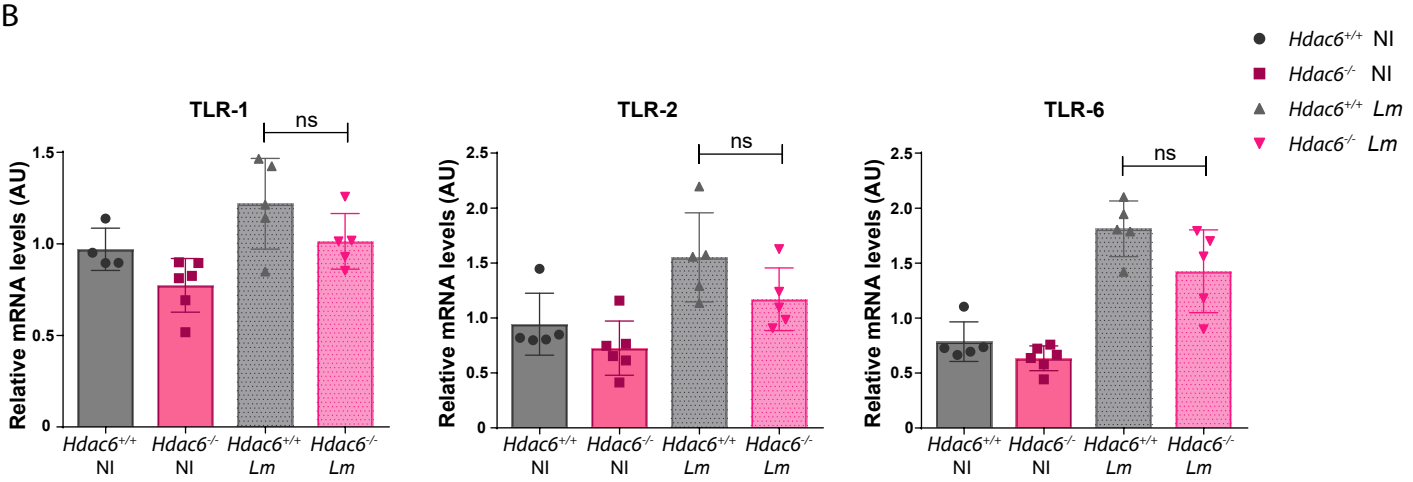

Supplemental Figure 6

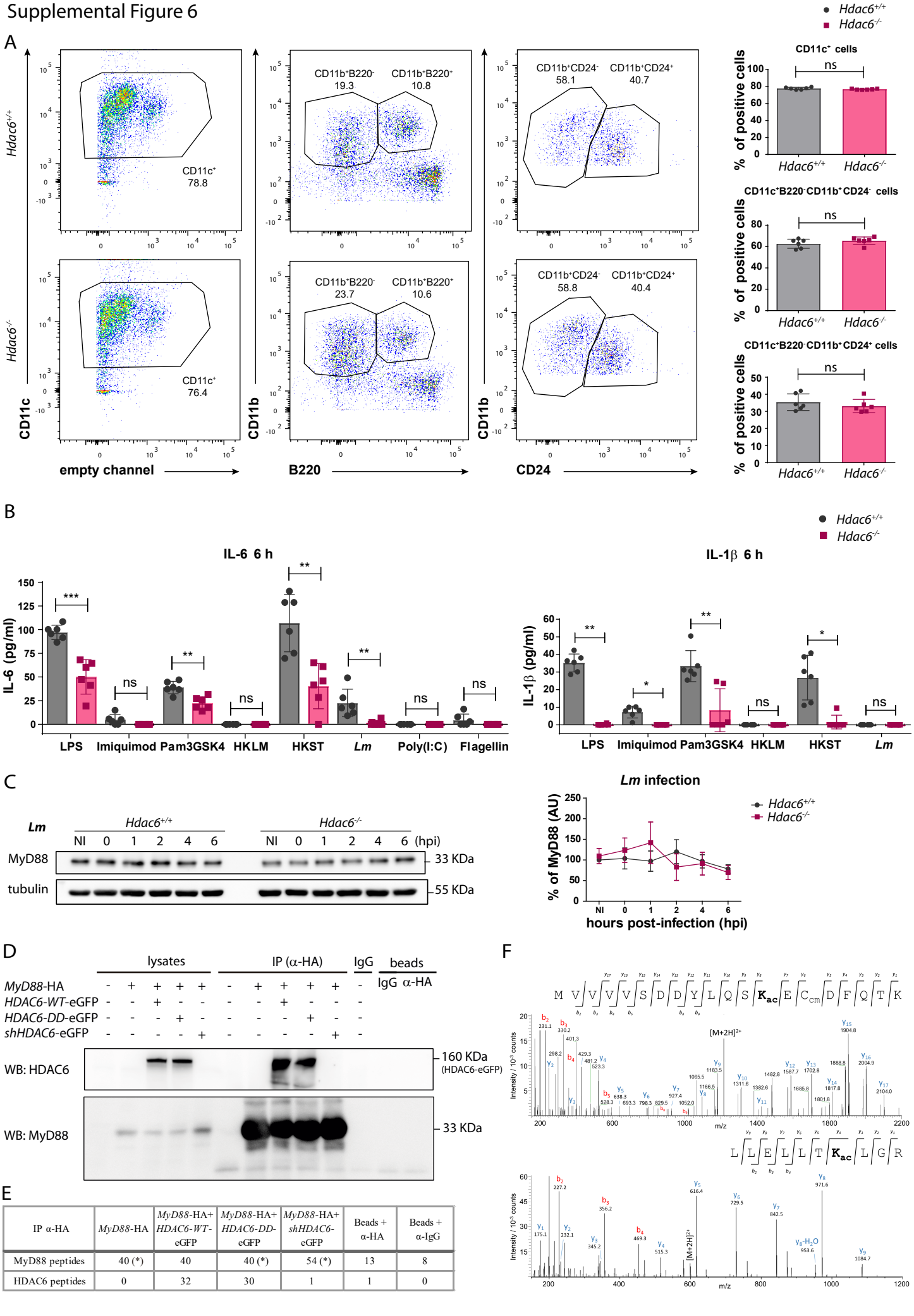

E

IP α-HA	*MyD88*-HA	*MyD88*-HA+ *HDAC6-WT*-eGFP	*MyD88*-HA+ *HDAC6-DD*-eGFP	*MyD88*-HA+ *shHDAC6*-eGFP	Beads + α-HA	Beads + α-IgG
MyD88 peptides	40 (*)	40	40 (*)	54 (*)	13	8
HDAC6 peptides	0	32	30	1	1	0

Published in final edited form as:
J Cell Sci. 2016 April 1; 129(7): 1305–1311. doi:10.1242/jcs.180885.

HDAC6 regulates the dynamics of lytic granules in cytotoxic T lymphocytes

Norman Núñez-Andrade[1,2], **Salvador Iborra**[3], **Antonio Trullo**[4,5], **Olga Moreno-Gonzalo**[1,2], **Enrique Calvo**[6], **Elena Catalán**[7], **Gaël Menasche**[8], **David Sancho**[3], **Jesús Vázquez**[6], **Tso-Pang Yao**[9], **Noa Beatriz Martín-Cófreces**[#1,2], and **Francisco Sánchez-Madrid**[#1,2]

[1]Servicio de Inmunología, Hospital Universitario de la Princesa, UAM, IIS-IP. Madrid, 28006 Spain

[2]Laboratory of Intercellular communication, Fundación CNIC, Madrid, 28029 Spain

[3]Immunobiology of inflammation, Fundación CNIC, Madrid, 28029 Spain

[4]Microscopy and Dynamic Imaging Unit, Fundación CNIC, Madrid, 28029 Spain

[5]Spettroscopia biomedica in fluorescenza dinamica, Center of Experimental Imaging, Ospedale San Raffaele, Milan, 20132, Italy

[6]Proteomic Unit. Fundación CNIC, Madrid, 28029 Spain

[7]Dept. Biochemistry and Molecular and Cell Biology, Universidad de Zaragoza, 500009, Spain

[8]Laboratory of Normal and Pathological Homeostasis of the Immune System, INSERM Unité Mixte de Recherche 1163, Paris France

[9]Departments of Pharmacology and Cancer Biology Duke University, Medical Center, Durham, North Carolina 27710, U.S.

[#] These authors contributed equally to this work.

Abstract

HDAC6 is a tubulin deacetylase involved in many cellular functions related to cytoskeleton dynamics including cell migration and autophagy. In addition, HDAC6 affects antigen-dependent $CD4^+$ T cell activation. In this study, we show that HDAC6 contributes to the cytotoxic function of $CD8^+$ T cells. Immunization studies revealed defective cytotoxic activity *in vivo* in the absence of HDAC6. Adoptive transfer of wild-type or *Hdac6*$^{-/-}$ $CD8^+$ T cells to *Rag1*$^{-/-}$ mice demonstrated specific impairment in $CD8^+$ T cell responses against vaccinia infection. Mechanistically, HDAC6-deficient cytotoxic T lymphocytes (CTLs) showed defective *in vitro* cytolytic activity related to altered dynamics of lytic granules, inhibited kinesin 1 – dynactin mediated terminal transport of lytic granules to the immune synapse and deficient exocytosis, but not to target cell recognition, T cell receptor (TCR) activation or interferon (IFNγ) production. Our results establish

Contact information: Francisco Sánchez-Madrid, Laboratorio de Comunicación Intercelular, Servicio de Inmunología, Hospital de La Princesa, Diego de León 62. 28006, Madrid. Spain, fsmadrid@salud.madrid.org, Phone: +34915202307, FAX: +34915202374.

Author contribution. NNA, NBMC and FSM designed experiments, made the figures and wrote the manuscript; NNA, SI, NBMC, OMG, JV, DS, GM and TSY and EC collected and/or analyzed data; AT developed the Quant Application.

Conflict of interest. Authors declare that they have no conflict of interest.

Europe PMC Funders Author Manuscripts

HDAC6 as an effector of the immune cytotoxic response that acts by affecting the dynamics, transport and secretion of lytic granules by CTLs.

Introduction

Cytotoxic T Lymphocytes (CTLs) are a specialized population of $CD8^+$ T cells that provides defense against virus-infected cells and tumors. Naïve $CD8^+$ T cells differentiate into CTLs upon antigen recognition, a process involving the synthesis and storage of cytotoxic mediators into lysosomal-derived lytic granules (LG) (Williams and Bevan, 2007). CTLs eliminate target cells by different mechanisms, including secretion of pro-inflammatory cytokines, e.g. tumor necrosis factor (TNF)α or interferon (IFN)γ (de Saint Basile et al., 2010), FAS-L (FAS ligand) ligation to its receptor as well as granule-mediated apoptosis upon cell-cell contact and immune synapse (IS) formation (Ritter et al., 2013). LG fuse with the plasma membrane and release granzymes, cathepsins and perforins (Prf) (Lopez et al., 2013; Pardo et al., 2009). The IS acts as a focal point for exocytosis of LG. LG polarization towards the target cell depends on T cell receptor (TCR) engagement, driven by the relocation of the centrosome to IS. The LG degranulate at a secretory domain adjacent to the TCR-enriched region within the IS (de Saint Basile et al., 2010; Ritter et al., 2013).

Histone deacetylase 6 (HDAC6) is an ubiquitous, cytosolic protein from the class II HDACs family with X-linked inheritance, that binds to and deacetylates α-tubulin at lys40 (Hubbert et al., 2002; Valenzuela-Fernandez et al., 2008). HDAC6 also modulates other substrates, e.g. cortactin or hsp90. HDAC6 controls cell migration (Zhang et al., 2007), T-regulatory functions (de Zoeten et al., 2011) and $CD4^+$ T cell activation (Serrador et al., 2004). Consistent with this, HDACs inhibitors impair some immune functions (Mosley et al., 2006; Tsuji et al., 2015). However, the precise contribution *in vivo* (by using *Hdac6*$^{-/-}$ mice) has not been assessed, and the mechanisms involved remain unsolved. HDAC6 also functions as a scaffold protein in T cell migration (Cabrero et al., 2006) and the transport of misfolded proteins (Kawaguchi et al., 2003). In this report, we describe the impaired killing capacity of *Hdac6*$^{-/-}$ CTLs. The molecular mechanism underlying this defect involves a scaffold role that positions HDAC6 as a protein that oversees the proper movement of LG, their transport to the IS and secretion towards the target cell.

Results and Discussion

HDAC6 deficiency reduces the cytolytic capacity of $CD8^+$ T lymphocytes

We examined the ability of cytotoxic T cells from *Hdac6*$^{-/-}$ mice to kill target cells *in vitro*. $CD8^+$ T cells from wild-type (WT) and *Hdac6*$^{-/-}$ mice expressing the transgenic ovalbumin (OVA)-specific TCR (OT-I) were activated *in vitro* and cultured to generate CTLs. Cell cytotoxicity was subsequently analyzed by survival of dye-labeled EL4 target cells pulsed or not with $OVA_{257\text{-}264}$ peptide (SIINFEKL). *Hdac6*$^{-/-}$ CTLs showed decreased killing activity (Fig. 1A), consistent with reduced expression of CD107a (also known as Lamp1) in *Hdac6*$^{-/-}$ CTLs upon degranulation (Fig. 1B). Likewise, CTLs from OT-I mice treated treated with tubastatin A, a potent HDAC6 inhibitor, displayed a reduced killing ability (Suppl. Fig. 1A). We also detected decreased Prf1 secretion from activated (i.e. induced by anti-CD3 and anti-

CD28 monoclonal antibodies) *Hdac6*$^{-/-}$ CTLs (Fig. 1C, left). Next, we assessed the secretion promoted by phorbol-12-myristate-13-acetate (PMA), to bypass TCR stimulation. Both cathepsins D and Prf1 decreased in supernatants from activated *Hdac6*$^{-/-}$ CTLs (Fig. 1C, right). Taken together, our data demonstrate that *Hdac6*$^{-/-}$ CTLs show reduced cytotoxic activity, and suggest that HDAC6 controls exocytosis.

We next tested IFN-γ production; the frequency of CTLs producing IFNγ and its secretion was unaffected in activated *Hdac6*$^{-/-}$ CTLs (Fig. 1D-E), in contrast to what has been described when cells are treated with ACY-1215, a recently described inhibitor that is ten-fold more selective for HDAC6 than for HDAC1, HDAC2 and HDAC3 and that shows slight activity against HDAC8 (Tsuji et al., 2015). Likewise, treatment of CTLs from OT-I mice with tubastatin A had no significant effect (Suppl. Fig. 1B). Importantly, T-cell signaling induced by anti-CD3/anti-CD28 mAbs in *Hdac6*$^{-/-}$ was comparable to control, as determined by assessing PLCγ1 and erk1/2 (Erk1/2; also known as MAPK3 and MAPK1, respectively)phosphorylation (Fig. 1F). Likewise, the increase in intracellular calcium remained unchanged upon activation (Fig. 1G). As expected, tubulin acetylation at Lys40 was increased in *Hdac6*$^{-/-}$ CTLs (Fig. 1F). These results suggest that the killing defect observed does not result from a general impairment of CTLs function.

Defective *in vivo* and *ex vivo* killing in HDAC6 knockout mice

The effector activity of *Hdac6*$^{-/-}$ CD8^{+} T cells was tested *in vivo* following mouse immunization using SIINFEKL-pulsed dendritic cells. The *in vivo* killing activity against the injected target cells (pulsed or not with SIINFEKL) was analyzed upon recovery by peritoneal lavage. Notably, *Hdac6*$^{-/-}$ mice showed reduced specific killing of target cells (Fig. 2A, left panel). However, the proportion of SIINFEKL-specific CD8^{+} T cells from the endogenous repertoire was not affected in *Hdac6*$^{-/-}$ mice (Fig. 2A, right panel), suggesting that the cytotoxic function rather than the number of antigen-specific CTLs could underlie the defect. Next, we examined whether the decreased cytotoxic function of the CTLs resulted in an impaired ability to prevent morbidity and/or mortality during a viral infection. To restrict HDAC6 deficiency to CD8^{+} T cells, we adoptively transferred *Rag1*$^{-/-}$ mice with WT or *Hdac6*$^{-/-}$ naïve CD8^{+} T cells and subsequently challenged with a fully replicative vaccinia virus (VACV) WR strain. This infection model mimics the immunological and clinical features of smallpox vaccination in humans (Mota et al., 2011). CD8^{+} T cell proliferation was comparable, or even increased (division 4) in *Hdac6*$^{-/-}$ (Fig. 2B). *Rag1*$^{-/-}$ mice passively transferred with *Hdac6*$^{-/-}$ CD8^{+} T cells showed increased morbidity at 9 and 11 days post-infection (p.i.) (Fig. 2C). Virus titration from the lesion tissue demonstrated that *Hdac6*$^{-/-}$ immune cells exerted a less-efficient virus clearance (Fig. 2D). Consistent with our findings on the lack of effect in endogenous antigen-specific CD8^{+} T cell numbers, CTL expansion tracked at 13 d.p.i. was not affected in *Hdac6*$^{-/-}$ (Fig. 2E, left). The proportion of activated CD8^{+} T cells (CD44^{high}) at early (5 d.p.i) and late stages (13-30 d.p.i.) of the disease were similar for WT and *Hdac6*$^{-/-}$ mice (tested in peripheral blood and spleen, respectively; Fig. 2E, right). These *in vivo* results emphasize the role of HDAC6 in the CD8^{+} T cell-dependent protection against VACV infection without affecting effector CD8^{+} CTLs differentiation.

HDAC6 drives the terminal transport of LG to the target cell

CTL killing is limited to target cells (and not neighbor cells) by the confinement of secretion to the immune synapse established between the CTL and the target cell (de Saint Basile et al., 2010). Interestingly, the intracellular colocalization between cathepsinD and lamp1 (CD107a) was affected in *Hdac6*$^{-/-}$ CTLs conjugated with target cells, pointing to the mislocalization of lytic mediators in these cells (Fig. 3A; images and middle graphs). The decreased secretion of lytic proteins from *Hdac6*$^{-/-}$ CTLs suggests that HDAC6 regulates exocytosis of LG (Fig. 1C). Indeed, the translocation of the centrosome to the contact area with the target cell was even more pronounced in *Hdac6*$^{-/-}$ CTLs than in WT cells (Fig. 3A, right graph), in accordance with the effect described with the HDAC inhibitor Trichostatin A on the centrosomal polarization in CD4^{+} T cells (Serrador et al., 2004). This suggests that the defective exocytosis might rely on the movement of LG themselves.

We thus monitored the dynamics of LG at the subcortical immune synapse cytoskeleton and their release by Total Internal Reflection Fluorescence microscopy (TIRFm). CTLs were loaded with a pH-dependent, lysosomal tracker which allows the visualization of the LG and settled on to a stimulating surface to form an IS-like structure (Fig. 3B). These experiments revealed significant changes in the distribution of the LG and their dynamics, with a marked decrease in the number of LG detected at the immune synapse-like structure in *Hdac6*$^{-/-}$, suggesting alterations to the active transport of the granules from the centrosomal region to the plasma membrane. Indeed, the mean fluorescence intensity detected for *Hdac6*$^{-/-}$ granules was lower, which suggests a higher pH and therefore a different degree of maturation, although the LG displayed similar sizes in WT and *Hdac6*$^{-/-}$ cells (Fig. 3C). The most remarkable difference pertained to the *x*-*y* distribution of the LG, which was wider (diffusion surface) in the *Hdac6*$^{-/-}$ CTLs, with a higher diffusion coefficient, although maintaining similar duration times and path lengths (Fig. 3D). These data suggest that the LG from *Hdac6*$^{-/-}$ CTLs are not properly targeted and/or that they dock inefficiently at the immune synapse.

Tubulin motors control the delivery of LG to the plasma membrane. Whereas dynein controls LG targeting to the centrosome (Burkhardt et al., 1993; Mentlik et al., 2010), the kinesin-1/Slp3/Rab27a (Slp3 is also known as SYTL3) complex directs terminal transport to the plasma membrane for exocytosis (Kurowska et al., 2012). Dynactin might also be part of this complex, linking the cargo to kinesin-1 motor (Haghnia et al., 2007; Hendricks et al., 2010). We then hypothesized that HDAC6 regulates the movement and delivery of the LG at the IS through kinesin-1. Using a biochemical approach, we observed that HDAC6 formed a complex with kinesin-1 light chain (KLC1) upon triggering with anti-CD3 and anti-CD28 monoclonal antibodies (Fig. 3E). Moreover, interaction of the kinesin-activator complex dynactin subunits p150-glued (also known as DCTN1) and p50-dynamitin (also known as DCTN2) was impaired in *Hdac6*$^{-/-}$ (Fig. 3F).

In summary, our data support a specific role for HDAC6 in the intracellular localization of lytic mediators and, particularly, in their exocytosis. Therefore, the catalytic and scaffold activities of HDAC6 might act at multiple levels in the control of cytotoxic-related pathways, making HDAC6 a potential candidate that could be targeted to modulate CTLs in specific diseases.

Materials and Methods

Mice

Hdac6$^{-/-}$ mice were generated through targeting of exons 10 to 13 (Gao et al., 2007). They were intercrossed in a C57BL/6 background to generate wild-type and knockout littermates. Mice presenting transgenic inserts for mouse *Tcra*-Variable 2 and *Tcrb*-Variable 5 genes, which TCR recognizes ovalbumin$_{257-264}$ peptide in the context of H2Kb MHC-I (OT-I), were crossed to female *Hdac6*$^{+/-}$ mice to generate WT and KO littermates; males were used for *in vivo* experimentation since *Hdac6* is a X-linked gene. *Rag1*$^{-/-}$ mice were used for adoptive transfer experiments. These studies were approved by the local Ethics Committee for Basic Research at the CNIC and the Comunidad Autónoma de Madrid.

Cell culture

Cytotoxic cells were produced by culturing cells upon stimulation with SIINFEKL peptide (0.5 μM, 24h) or concanavalin A (2.5 μg/ml, 36 h) and cultured in presence of IL-2 (50-100 IU/ml) for at least 7 days. All other cells were cultured and treated as described previously (Cascio et al., 2015; Martin-Cofreces et al., 2006; Sancho et al., 2008).

Immunoprecipitation, CTL signaling and immunoblotting

Experimentation was performed as described (Martin-Cofreces et al., 2012; Martin-Cofreces et al., 2008; Martin-Cofreces et al., 2006).); KLC1 antibody was from Merck Millipore (5 μg/ml for Immunoprecipitation and 1 μg/ml for Western blot; Darmstadt, Germany; KLC), anti-HDAC6 from Assay Biotech (0.1 μg/ml for Western blot; Sunnyvale, California, US) and anti-p50 (0.25 μg/ml for Western blot) and -p150 (1 μg/ml for Immunoprecipitation and 0.25 μg/ml) for Western blot from BD Pharmingen (Franklin Lakes, New Jersey,US).

Measurement of intracellular variations in Calcium ions by flow cytometry

The method used for intracellular calcium influx is described (June and Moore, 2004). In particular, 5x10^6 purified CD8$^+$ CTLs generated *in vitro* were loaded with 2 μg.ml^{-1} INDO-1 AM (Invitrogen Corporation) and stimulated with anti-CD3 and anti-CD28 monoclonal antibodies (BD Biosciences; Franklin Lakes, New Jersey, US) plus goat anti-Armenian-hamster IgG antibodies (Jackson Immunoresearch Laboratories; West Grove, PA, US. 6, 3 and 6 μg/ml, respectively).

In vitro degranulation assay

CD107a expression was monitored with anti-CD107a-Alexa647 antibody (BD Biosciences) in monensin-pretreated CD8$^+$ OTI cells (5 mM) stimulated with SIINFEKL-pulsed EL4 (1 μM; 3 h, 37 ºC). Cells were stained with anti-CD8-PE and anti-CD44-FITC, analyzed by FACS and data were processed with FlowJo 7.6.5 (TreeStar Inc; Ashland, Oregon; US).

Confocal and Total Internal Reflection Fluorescence Microscopy analysis

Cell conjugates between CTLs and EL4 cells were allowed to form (15 min) and processed as described (Cascio et al., 2015; Martin-Cofreces et al., 2006) under a Leica SP5 confocal microscope (Leica Microsystems; Manheim, Germany) mounted on an inverted DMI6000

microscope fitted with a HCX PL APO 63x/1.40-0.6 oil objective. Images were processed using Imaris software (Bitplane; Zurich, Switzerland), Image J software (http://rsbweb.nih.gov/ij/) and assembled with Photoshop 6 software. 3D distance from the centrosomal centre of mass to the target cell-edge was measured by generating image masks from fluorescence with Imaris Software. TIRFm imaging was performed with a Leica AM-TIRF-MC-M system mounted on a Leica DMI-6000B microscope coupled to an Andor-DU8285_VP-4094 camera (Andor; Belfast, UK) fitted with a HCX-PL-APO 100.0x1.46 OIL objective as described (Baixauli et al., 2011; Martin-Cofreces et al., 2012). The laser penetrance used was 90 nm (561 nm laser). The LG mechanical properties were determined with a user-customized routine developed in Python. The software can be freely downloaded from: https://dl.dropboxusercontent.com/u/4050954/VesiclesAnalyser.zip. For more information, see the tutorial included.

Vaccinia virus (VACV) infection and virus titration

Tails were scarified with VACV ($2x10^6$ PFU/mouse) by gently scratching (x25) with a 28 1/2 G needle. For virus titration, tails were mechanical disaggregated (1ml of PBS), subjected to freeze-thaw cycles and sonication. Serial dilutions of the homogenates were added to monolayers of CV-1 cells seeded in 24 well plates. Cells were stained with Cristal violet 24 h later. We observed a detection limit of 5 PFU/tail, the number of plaques was multiplied by the reciprocal of sample dilution and converted to p.f.u./g of tissue.

In vitro and *in vivo* cytotoxicity assay

For *in vitro* experiments, EL4 target cells were incubated with 1 μM Cell Violet pulsed with 1 μM SIINFEKL or with 0.1 μM Cell Violet and no SIINFEKL, washed extensively, mixed (1:1), pooled with different dilutions of effectors, plated in a 96-well U-bottom plate for 5 h (37ºC) by triplicate and analyzed by FACS. Dead cells were excluded on the basis of propidium iodide staining. The mean percentage of survival in antigen-loaded targets was calculated relative to antigen-negative internal controls in each sample. Specific lysis was calculated using the following equation: percentage specific lysis = 100 * (1 - (percentage of cells staining for Cell Violet 1μM/percentage of cells staining for Cell Violet 0,1μM). All data were normalized to the basal specific lysis in absence of effector cells. For *in vivo* assays, WT and *Hdac6*$^{-/-}$ mice were immunized by i.p. injection of bone marrow dendritic cells pulsed with 1 μM of SIINFEKL and LPS (1 $\mu g ml^{-1}$) for 1 h. After 7 days, CD45.1 splenocytes were prepared as targets as described above and injected i.p. into recipients. Cells were recovered 24 h later by peritoneal lavage and *in vivo* killing measured (Hermans et al., 2004; Iborra et al., 2012; Sancho et al., 2008; Schulz et al., 2005).

Statistical analysis

Data were analyzed with GraphPad Prism software (La Jolla, California, US) for normality (D'Agostino-Pearson or the Kolmogorov-Smirnov test for small sAMples). Student's *t*-tests or Mann-Whitney tests were used for normal or non-normal data, respectively and two-tailed ANOVA for grouped data (Bonferroni post-test).

Europe PMC Funders Author Manuscripts

Supplementary Material

Refer to Web version on PubMed Central for supplementary material.

Acknowledgements

We thank Manuel Gomez and Miguel Vicente for critical reading of the manuscript. Experimentation was performed at Cellomics and Microscopy Units (CNIC) and Flow Cytometry Core Unit (CNIO).

Funding. This work was supported by the Ministerio de Economía y Competitividad (MINECO) [grant number SAF2014-55579-R], CAM [grant numbers INDISNET01592006, BIOMID-PIE13/041 and RD12/0042/0056]; from Universidad Carlos III de Madrid; and FEDER and ERC-2011-AdG 294340-GENTRIS. CNIC is supported by the MINECO and Pro-CNIC Foundation.

References

Baixauli F, Martin-Cofreces NB, Morlino G, Carrasco YR, Calabia-Linares C, Veiga E, Serrador JM, Sanchez-Madrid F. The mitochondrial fission factor dynamin-related protein 1 modulates T-cell receptor signalling at the immune synapse. The EMBO journal. 2011; 30:1238–50. [PubMed: 21326213]

Burkhardt JK, McIlvain JM Jr, Sheetz MP, Argon Y. Lytic granules from cytotoxic T cells exhibit kinesin-dependent motility on microtubules in vitro. Journal of cell science. 1993; 104(Pt 1):151–62. [PubMed: 8449993]

Cabrero JR, Serrador JM, Barreiro O, Mittelbrunn M, Naranjo-Suarez S, Martin-Cofreces N, Vicente-Manzanares M, Mazitschek R, Bradner JE, Avila J, et al. Lymphocyte chemotaxis is regulated by histone deacetylase 6, independently of its deacetylase activity. Molecular biology of the cell. 2006; 17:3435–45. [PubMed: 16738306]

Cascio G, Martin-Cofreces NB, Rodriguez-Frade JM, Lopez-Cotarelo P, Criado G, Pablos JL, Rodriguez-Fernandez JL, Sanchez-Madrid F, Mellado M. CXCL12 Regulates through JAK1 and JAK2 Formation of Productive Immunological Synapses. Journal of immunology. 2015; 194:5509–19.

de Saint Basile G, Menasche G, Fischer A. Molecular mechanisms of biogenesis and exocytosis of cytotoxic granules. Nature reviews Immunology. 2010; 10:568–79.

de Zoeten EF, Wang L, Butler K, Beier UH, Akimova T, Sai H, Bradner JE, Mazitschek R, Kozikowski AP, Matthias P, et al. Histone deacetylase 6 and heat shock protein 90 control the functions of Foxp3(+) T-regulatory cells. Molecular and cellular biology. 2011; 31:2066–78. [PubMed: 21444725]

Gao YS, Hubbert CC, Lu J, Lee YS, Lee JY, Yao TP. Histone deacetylase 6 regulates growth factor-induced actin remodeling and endocytosis. Molecular and cellular biology. 2007; 27:8637–47. [PubMed: 17938201]

Haghnia M, Cavalli V, Shah SB, Schimmelpfeng K, Brusch R, Yang G, Herrera C, Pilling A, Goldstein LS. Dynactin is required for coordinated bidirectional motility, but not for dynein membrane attachment. Molecular biology of the cell. 2007; 18:2081–9. [PubMed: 17360970]

Hendricks AG, Perlson E, Ross JL, Schroeder HW 3rd, Tokito M, Holzbaur EL. Motor coordination via a tug-of-war mechanism drives bidirectional vesicle transport. Current biology: CB. 2010; 20:697–702. [PubMed: 20399099]

Hermans IF, Silk JD, Yang J, Palmowski MJ, Gileadi U, McCarthy C, Salio M, Ronchese F, Cerundolo V. The VITAL assay: a versatile fluorometric technique for assessing CTL- and NKT-mediated cytotoxicity against multiple targets in vitro and in vivo. J Immunol Methods. 2004; 285:25–40. [PubMed: 14871532]

Hubbert C, Guardiola A, Shao R, Kawaguchi Y, Ito A, Nixon A, Yoshida M, Wang XF, Yao TP. HDAC6 is a microtubule-associated deacetylase. Nature. 2002; 417:455–8. [PubMed: 12024216]

Iborra S, Izquierdo HM, Martinez-Lopez M, Blanco-Menendez N, Reis e Sousa C, Sancho D. The DC receptor DNGR-1 mediates cross-priming of CTLs during vaccinia virus infection in mice. The Journal of clinical investigation. 2012; 122:1628–43. [PubMed: 22505455]

Europe PMC Funders Author Manuscripts

June CH, Moore JS. Measurement of intracellular ions by flow cytometry. Curr Protoc Immunol. 2004; Chapter 5 Unit 5 5.

Kawaguchi Y, Kovacs JJ, McLaurin A, Vance JM, Ito A, Yao TP. The deacetylase HDAC6 regulates aggresome formation and cell viability in response to misfolded protein stress. Cell. 2003; 115:727–38. [PubMed: 14675537]

Kurowska M, Goudin N, Nehme NT, Court M, Garin J, Fischer A, de Saint Basile G, Menasche G. Terminal transport of lytic granules to the immune synapse is mediated by the kinesin-1/Slp3/Rab27a complex. Blood. 2012; 119:3879–89. [PubMed: 22308290]

Lopez JA, Jenkins MR, Rudd-Schmidt JA, Brennan AJ, Danne JC, Mannering SI, Trapani JA, Voskoboinik I. Rapid and unidirectional perforin pore delivery at the cytotoxic immune synapse. Journal of immunology. 2013; 191:2328–34.

Martin-Cofreces NB, Baixauli F, Lopez MJ, Gil D, Monjas A, Alarcon B, Sanchez-Madrid F. End-binding protein 1 controls signal propagation from the T cell receptor. The EMBO journal. 2012; 31:4140–52. [PubMed: 22922463]

Martin-Cofreces NB, Robles-Valero J, Cabrero JR, Mittelbrunn M, Gordon-Alonso M, Sung CH, Alarcon B, Vazquez J, Sanchez-Madrid F. MTOC translocation modulates IS formation and controls sustained T cell signaling. The Journal of cell biology. 2008; 182:951–62. [PubMed: 18779373]

Martin-Cofreces NB, Sancho D, Fernandez E, Vicente-Manzanares M, Gordon-Alonso M, Montoya MC, Michel F, Acuto O, Alarcon B, Sanchez-Madrid F. Role of Fyn in the rearrangement of tubulin cytoskeleton induced through TCR. Journal of immunology. 2006; 176:4201–7.

Mentlik AN, Sanborn KB, Holzbaur EL, Orange JS. Rapid lytic granule convergence to the MTOC in natural killer cells is dependent on dynein but not cytolytic commitment. Molecular biology of the cell. 2010; 21:2241–56. [PubMed: 20444980]

Mosley AJ, Meekings KN, McCarthy C, Shepherd D, Cerundolo V, Mazitschek R, Tanaka Y, Taylor GP, Bangham CR. Histone deacetylase inhibitors increase virus gene expression but decrease CD8+ cell antiviral function in HTLV-1 infection. Blood. 2006; 108:3801–7. [PubMed: 16912225]

Mota BE, Gallardo-Romero N, Trindade G, Keckler MS, Karem K, Carroll D, Campos MA, Vieira LQ, da Fonseca FG, Ferreira PC, et al. Adverse events post smallpox-vaccination: insights from tail scarification infection in mice with Vaccinia virus. PloS one. 2011; 6:e18924. [PubMed: 21526210]

Pardo J, Aguilo JI, Anel A, Martin P, Joeckel L, Borner C, Wallich R, Mullbacher A, Froelich CJ, Simon MM. The biology of cytotoxic cell granule exocytosis pathway: granzymes have evolved to induce cell death and inflammation. Microbes and infection / Institut Pasteur. 2009; 11:452–9. [PubMed: 19249384]

Ritter AT, Angus KL, Griffiths GM. The role of the cytoskeleton at the immunological synapse. Immunological reviews. 2013; 256:107–17. [PubMed: 24117816]

Sancho D, Mourao-Sa D, Joffre OP, Schulz O, Rogers NC, Pennington DJ, Carlyle JR, Reis e Sousa C. Tumor therapy in mice via antigen targeting to a novel, DC-restricted C-type lectin. J Clin Invest. 2008; 118:2098–110. [PubMed: 18497879]

Schulz O, Diebold SS, Chen M, Naslund TI, Nolte MA, Alexopoulou L, Azuma YT, Flavell RA, Liljestrom P, Reis e Sousa C. Toll-like receptor 3 promotes cross-priming to virus-infected cells. Nature. 2005; 433:887–92. [PubMed: 15711573]

Serrador JM, Cabrero JR, Sancho D, Mittelbrunn M, Urzainqui A, Sanchez-Madrid F. HDAC6 deacetylase activity links the tubulin cytoskeleton with immune synapse organization. Immunity. 2004; 20:417–28. [PubMed: 15084271]

Tsuji G, Okiyama N, Villarroel VA, Katz SI. Histone deacetylase 6 inhibition impairs effector CD8 T-cell functions during skin inflammation. The Journal of allergy and clinical immunology. 2015; 135:1228–39. [PubMed: 25458911]

Valenzuela-Fernandez A, Cabrero JR, Serrador JM, Sanchez-Madrid F. HDAC6: a key regulator of cytoskeleton, cell migration and cell-cell interactions. Trends in cell biology. 2008; 18:291–7. [PubMed: 18472263]

Williams MA, Bevan MJ. Effector and memory CTL differentiation. Annual review of immunology. 2007; 25:171–92.

Zhang X, Yuan Z, Zhang Y, Yong S, Salas-Burgos A, Koomen J, Olashaw N, Parsons JT, Yang XJ, Dent SR, et al. HDAC6 modulates cell motility by altering the acetylation level of cortactin. Molecular cell. 2007; 27:197–213. [PubMed: 17643370]

Europe PMC Funders Author Manuscripts

Europe PMC Funders Author Manuscripts

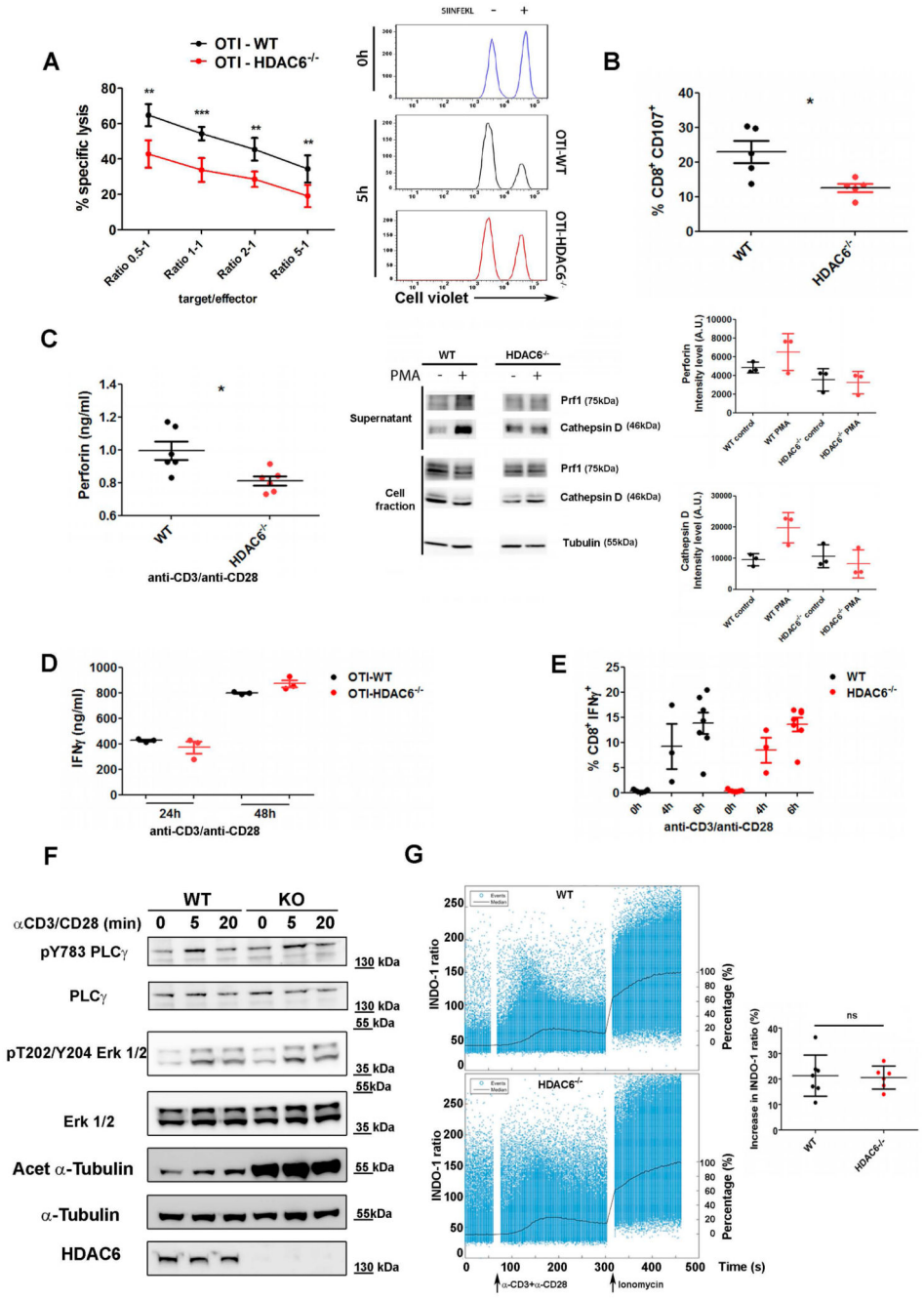

Figure 1. HDAC6 modulates the efficiency of target cell killing and degranulation of lytic mediators.

(A) Graph showing *in vitro* cytotoxic assay for specific lysis of SIINFEKL-pulsed EL4 target cells by OT-I-WT or -*Hdac6*$^{-/-}$ CTLs. Mean ± SEM of specific lysis for 5 h are shown at the indicated target to effector ratios. All killing assay where performed by triplicate. *, P < 0.05; **, P < 0.01; ***, P < 0.001. Unpaired T-test (n=5 mice for each genotype). Histograms, representative FACS profile. (B) Degranulation is shown as the percentage of CD107a^{+} cells detected by FACS in activated vs non-stimulated WT and *Hdac6*$^{-/-}$ CD8^{+} CTLs. Results are mean±s.e.m. n=5 for each genotype. (C) Exocytosis of lytic mediators

upon T cell activation. Left, Perforin content in culture cell supernatants was determined by ELISA. CTLs were stimulated with anti-CD3 and anti-CD28 monoclonal antibodies and 'goat' anti-Armenian-hamster 'IgG' anyibodies (5 h). Graphs show mean±s.e.m. (n=6 mice for each genotype). *P<0.05 (unpaired t-test). Middle panel, representative Western blot showing exocytosis. PMA stimulation (1 h). Normalization was performed against cell fractions. Right graphs, Mean +/-SEM (3 independent experiments). (D) Graph, IFNγ secretion supernatants from anti-CD3/anti-CD28 mAbs activated WT and *Hdac6*$^{-/-}$ CTLs by ELISA. Results are mean±s.e.m. n=3 for each genotype. Mann-Whitney test. (E) Percentage of IFNγ^{+} cells in WT and *Hdac6*$^{-/-}$ CTLs activated with anti-CD3 and anti-CD28 monoclonal antibodies. Results are mean±s.e.m. n=6 (0 and 6 h) and n= 3 (4 h) for each genotype. Mann-Whitney test. (F) Effector CD8^{+} CTLs isolated from WT and *Hdac6*$^{-/-}$ mice were activated (anti-CD3/anti-CD28 mAbs), lysed and blotted against PLCγ1 (pY783) and erk1/2 (pT202/Y204) phosphorylation and tubulin acetylation. (G) Calcium flux. WT and *Hdac6*$^{-/-}$ purified CTLs pre-loaded with the INDO-1 AM probe were analyzed for free and bound Ca^{2+} by flow cytometry. Left graphs, time course ratiometric variation (left Y axis). Black line, Median function normalized to basal (0%) and total activation by ionomycin treatment (100%; right Y axis). Stimuli are indicated. A representative experiment is shown. Right graph, Mean of the increase in the ratio +/-SD (WT, n=7; *Hdac6*$^{-/-}$ n=6. Mann Whitney test).

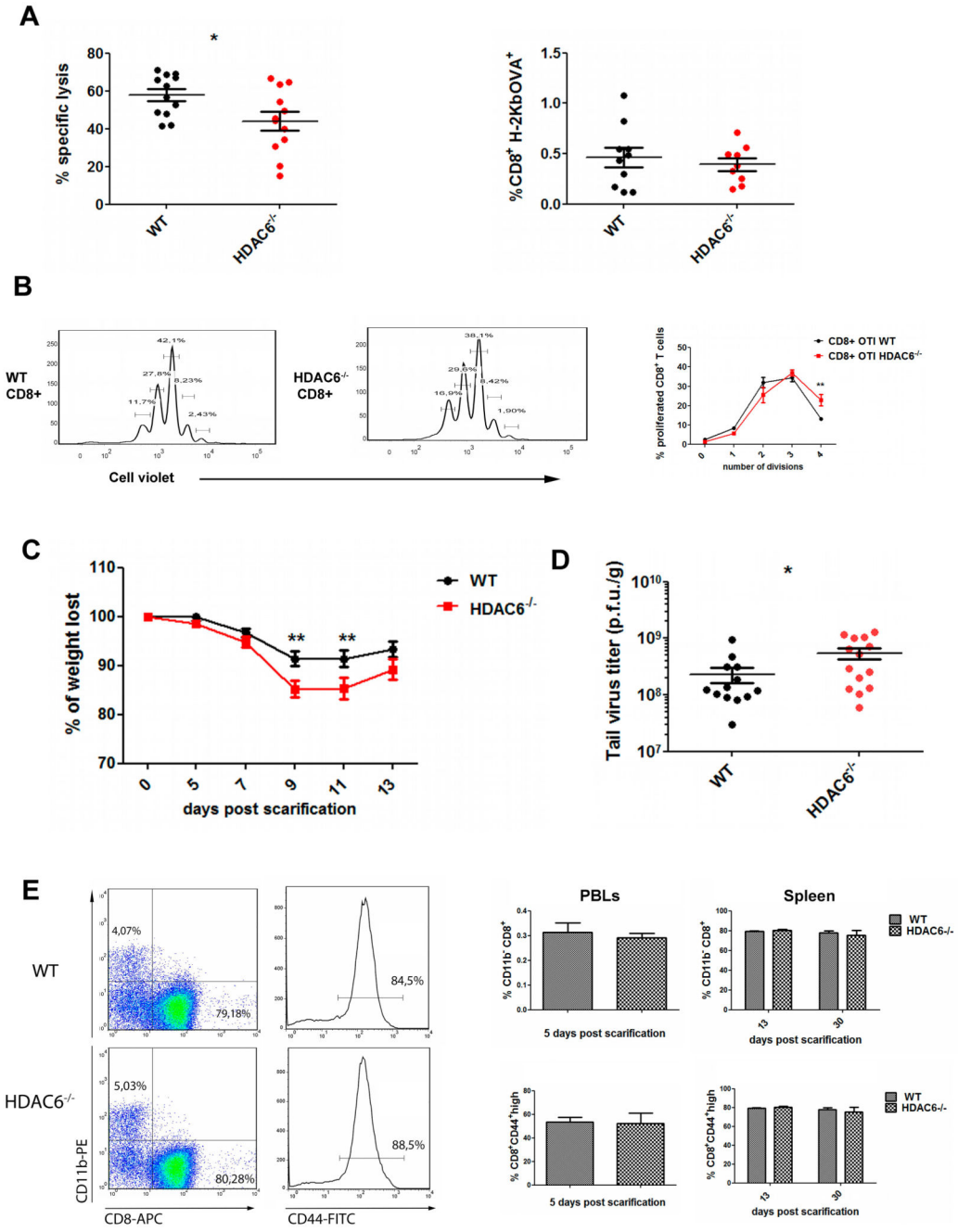

Figure 2. In vivo function of CTLs is impaired in HDAC6 knockout mice.

(A) WT and *Hdac6*$^{-/-}$ were immunized against SIINFEKL peptide. 7 days after immunization, cell violet-labelled, SIINFEKL-pulsed or not target cells (1 μM) were injected i.p., recovered through intraperitoneal lavage (24 h) and cell survival assessed by FACs (left panel). Data represent mean±s.e.m. (n= 12 for each genotype from three independent experiments). *P<0.05, Mann-Whitney test. Relative percentage of $CD8^+$ $H\text{-}2Kb^+$ was determined to control avidity towards SIINFEKL (right panel, results are mean ±s.e.m. (WT, n= 10; *Hdac6*$^{-/-}$, n= 9 from three independent experiments. Mann-Whitney's

test). (B) Proliferation of $CD8^+$ cells in VACV-OVA infected WT and *Hdac6*$^{-/-}$ mice. Results are means±s.e.m. (n= 5 for each genotype). **P<0.01 (Mann-Whitney test). (C) *Rag1*$^{-/-}$ mice inoculated i.v. with $0.8x10^6$ $CD8^+$ naïve cells and infected with VACV-WR by tail scarification were weighted every 2 days. Results are means±s.e.m. (n=10 for each genotype). **P<0.01 (Mann-Whitney test). (D) Titration of viral particles from scarified tails (13 d.p.i). The colonies of CV-1 cells infected *in vitro* with different dilutions of tail extracts were counted, and normalized to the tail tissue weight. Results are means±s.e.m. (WT, n= 13; *Hdac6*$^{-/-}$ n= 14). *P<0.05 (Mann-Whitney test). (E) Percentage of $CD8^+$ expansion and CD44 expression by FACs analysis in peripheral blood (5 d.p.i) and in spleen populations (13 and 30 d.p.i.). CD11b was used as negative control. Results are means ±s.e.m. (n= 5) (Mann-Whitney test).

Europe PMC Funders Author Manuscripts

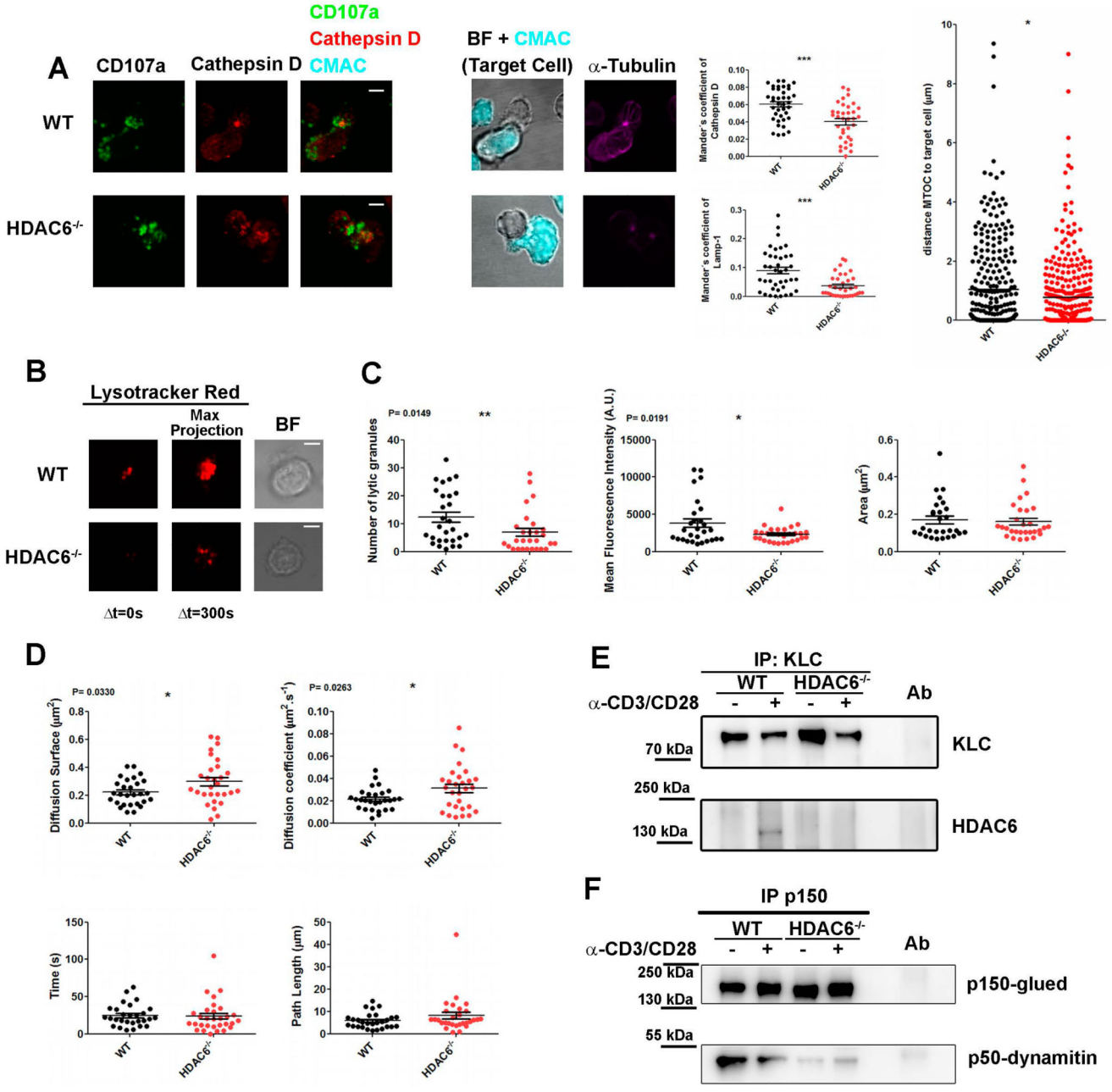

Figure 3. HDAC6 drives the terminal transport of LG to the target cell.

(A) Confocal microscopy images of WT and *Hdac6*$^{-/-}$ OT-I-derived CTLs conjugated with CMAC-loaded, OVA pre-pulsed target cell EL4 (500 nM SIINFEKL, Cyan) for 15 min. Green, CD107a. Red, CathepsinD. Magenta, α-tubulin. Bright-field (BF) images correspond to a unique plane and fluorescence images, to maximal projections from Z-stacks. Middle graphs, Mander's coefficient for co-localization of Lamp1 and CathepsinD. Results are mean±???? (WT, n=39; Hdac6−/−, n=35). ***P<0.001 (Mann–Whitney test). Right graph, quantification of MTOC translocation. Results are mean±s.e.m. (n>270, from 3 independent experiments); *P<0.05 (unpaired *t*-test). (B) Representative TIRFm images of Lysotracker

Red-loaded WT and *Hdac6*$^{-/-}$ CTLs in glass-bottom chambers coated with anti-CD3 and anti-CD28 monoclonal antibodies. Video recording was initiated upon cell adhesion (37ºC and 5% CO_2). Images were acquired for 5 min every 0.5 s. (C-D) Quantification for LG parameters at the IS-like was performed for each cell Results are means±s.e.m. (n=28 for each genotype, 3 independent experiments). *P<0.05; **P<0.01. Mann-Whitney test. (E-F) Western blots showing immunoprecipitates from resting or activated WT and *Hdac6*$^{-/-}$ CTLs (15 min) from a representative experiment out of three. Antibodies anti-KLC1 (E) or anti-p150 glued (p150) were used (F). Samples were blotted against indicated antibodies. Ab, pre-immune control antibody. Scale bars: 4 μm.

The PDZ-adaptor protein syntenin-1 regulates HIV-1 entry

Mónica Gordón-Alonso[a], Vera Rocha-Perugini[b], Susana Álvarez[c], Olga Moreno-Gonzalo[a], Ángeles Ursa[a], Soraya López-Martín[d], Nuria Izquierdo-Useros[e], Javier Martínez-Picado[e], Maria Ángeles Muñoz-Fernández[c], María Yáñez-Mó[d], and Francisco Sánchez-Madrid[a,b]

[a]Servicio de Inmunología, Instituto de Investigación Sanitaria de la Princesa, Hospital Universitario de la Princesa, 28006 Madrid, Spain; [b]Centro Nacional de Investigaciones Cardiovasculares, 28029 Madrid, Spain; [c]Servicio de Inmunobiología Molecular del Hospital Universitario Gregorio Marañon, 28007 Madrid, Spain; [d]Instituto de Investigación Sanitaria de la Princesa, Hospital Santa Cristina, 28007 Madrid, Spain; [e]Institut de Recerca de la SIDA IrsiCaixa, University Hospital Germans Trias i Pujol, Universitat Autónoma de Barcelona, 08916 Badalona, Spain

ABSTRACT **Syntenin-1 is a cytosolic adaptor protein involved in several cellular processes requiring polarization. Human immunodeficiency virus type 1 (HIV-1) attachment to target CD4$^+$ T-cells induces polarization of the viral receptor and coreceptor, CD4/CXCR4, and cellular structures toward the virus contact area, and triggers local actin polymerization and phosphatidylinositol 4,5-bisphosphate (PIP_2) production, which are needed for successful HIV infection. We show that syntenin-1 is recruited to the plasma membrane during HIV-1 attachment and associates with CD4, the main HIV-1 receptor. Syntenin-1 overexpression inhibits HIV-1 production and HIV-mediated cell fusion, while syntenin depletion specifically increases HIV-1 entry. Down-regulation of syntenin-1 expression reduces F-actin polymerization in response to HIV-1. Moreover, HIV-induced PIP_2 accumulation is increased in syntenin-1–depleted cells. Once the virus has entered the target cell, syntenin-1 polarization toward the viral nucleocapsid is lost, suggesting a spatiotemporal regulatory role of syntenin-1 in actin remodeling, PIP_2 production, and the dynamics of HIV-1 entry.**

Monitoring Editor
Mark H. Ginsberg
University of California, San Diego

Received: Dec 12, 2011
Revised: Mar 21, 2012
Accepted: Apr 19, 2012

INTRODUCTION

The adaptor protein syntenin-1 was originally described in relation to its association with the syndecan receptor and its recycling (Grootjans *et al.*, 1997; Zimmermann *et al.*, 2005). It was also termed melanoma differentiation-associated gene-9 (mda-9) for its up-regulated expression in several types of tumors, which correlates with high invasiveness (Sarkar *et al.*, 2004, 2008). Structurally, syntenin-1 contains a regulatory N-terminal region and two tandem postsynaptic density protein, *Drosophila* disk large, and zonula occludens-1 (PDZ) domains. The N-terminal region is composed of two Tyr-based domains: one ITIM and one ITAM domain, the ITIM domain being important for CXCR4-mediated T-cell migration (Sala-Valdes *et al.*, 2012). PDZ domains are involved in the formation of macromolecular complexes that often link transmembrane proteins to the actin cytoskeleton, mediating their clustering and polarized subcellular distribution (Fanning and Anderson, 1999; Brone and Eggermont, 2005; Hirbec *et al.*, 2005; Ludford-Menting *et al.*, 2005). PDZ domains interact with short amino acid sequences at the C-terminal end of plasma membrane proteins. Three consensus sequences bind PDZ domains: class I ([S/T]-X-Φ), class II (Φ-X-Φ), and class III ([D/E]-X-Φ), where X is any amino acid and Φ is a hydrophobic residue (Chimura *et al.*, 2011). Through its PDZ domains, syntenin-1 binds to transmembrane proteins, such as CD6 (Gimferrer *et al.*, 2005) and the tetraspanin CD63 (Latysheva *et al.*, 2006); signaling proteins, such as the tyrosine kinase Src (Boukerche *et al.*, 2008);

This article was published online ahead of print in MBoC in Press (http://www.molbiolcell.org/cgi/doi/10.1091/mbc.E11-12-1003) on April 25, 2012.

Address correspondence to: Francisco Sánchez-Madrid (fsanchez.hlpr@salud.madrid.org).

Abbreviations used: APC, antigen presenting cell; BSA, bovine serum albumin; CD4, cluster of differentation-4; CMTMR, 5-(and-6)(((4chloromethyl)benzoyl)amino) tetramethylrhodamine; CNBr, cyanogen bromide; CXCR4, C-X-C chemokine receptor type-4; ELISA, enzyme-linked immunosorbent assay; ENV, viral envelope glycoprotein complex gp120/gp41; FBS, fetal bovine serum; FITC, fluorescein isothiocyanate; GFP, green fluorescent protein; GST, glutathione *S*-transferase; HA, hemagglutinin; HIV-1, human immunodeficiency virus type 1; ITAM, immunoreceptor tyrosine-based activating motif; ITIM, immunoreceptor tyrosine-based inhibitory motif; mda-9, melanoma differentiation-associated gene-9; PDZ, postsynaptic density protein, *Drosophila* disk large, and zonula occludens-1; PI4P5K-Ia, phosphatidylinositol-4-phosphate-5 kinase type I-alpha; PIP_2, phosphatidylinositol 4,5-bisphosphate; PLC-delta-PH-GFP, pleckstrin homology domain of phospholipase C-delta tagged to GFP protein; siRNA, small interfering RNA; TBS, Tris-buffered saline; VLP, virus-like particle; VSV, vesicular stomatitis virus.

and the actin-linker protein merlin (Jannatipour *et al.*, 2001). Recruitment of syntenin-1 to the plasma membrane is also regulated through its PDZ-mediated interaction with the lipid second messenger phosphatidylinositol 4,5-bisphosphate (PIP_2; Zimmermann, 2006).

Syntenin-1 has a cytosolic distribution, being enriched in vesicles and F-actin structures (Zimmermann *et al.*, 2001). It is implicated in several actin-polarized processes, such as cell migration, immune synapse formation, intracellular trafficking, cell-surface targeting, axonal outgrowth, and synaptic transmission (Gimferrer *et al.*, 2005; Hirbec *et al.*, 2005; Zimmermann *et al.*, 2005; Beekman and Coffer, 2008; Sarkar *et al.*, 2008). We recently reported the involvement of syntenin-1 in CXCR4-mediated T-chemotaxis and T-APC antigen presentation, in which it regulates Rac-triggered actin polymerization (Sala-Valdes *et al.*, 2012).

CD4/CXCR4-derived signaling and Rac-induced actin remodeling are also important for human immunodeficiency virus type 1 (HIV-1) infection (Pontow *et al.*, 2004; Carter *et al.*, 2009). Soon after HIV-1 contact with $CD4^+$ T-cells, the viral envelope glycoprotein complex gp120/gp41 (Env) engages with CD4 and CXCR4, inducing several signaling pathways that trigger receptor clustering (Jimenez-Baranda *et al.*, 2007; Barrero-Villar *et al.*, 2009) in a structure called "cap" (Dianzani *et al.*, 1995; Nguyen *et al.*, 2005), local actin polymerization (Iyengar *et al.*, 1998; Jolly *et al.*, 2004), T-cell activation (Popik *et al.*, 1998; Hiscott *et al.*, 2001), and HIV-1 replication (Popik and Pitha, 2000; Mettling *et al.*, 2008). These rearrangements enhance viral entry (Wu and Yoder, 2009; Juno and Fowke, 2010) by supplying an optimal density of CD4/CXCR4 complexes through actin-mediated surface reorganization (Iyengar *et al.*, 1998; Doms, 2000; Jolly *et al.*, 2004). Thus the actin-binding proteins moesin and filamin-A accumulate at the F-actin–enriched capping areas and influence CD4/CXCR4 clustering (Jimenez-Baranda *et al.*, 2007; Barrero-Villar *et al.*, 2009). Moreover, we previously showed that HIV-1 gp120, through its interaction with CD4, induces local production of PIP_2 by activating PI4P5K-Iα (Barrero-Villar *et al.*, 2008).

After viral attachment to the plasma membrane, the local F-actin accumulation can constitute a physical barrier for entry of the viral nucleocapsid (Vasiliver-Shamis *et al.*, 2009). In this regard, CXCR4-gp120 interaction was recently shown to activate cofilin, which promotes actin clearance, facilitating nucleocapsid entry into the cytoplasm (Yoder *et al.*, 2008).

In this study, we assessed the possible role of syntenin-1 as a mediator of CD4/CXCR4 clustering and actin remodeling during HIV-1 infection. Our data indicate that syntenin-1 associates with CD4 and negatively regulates HIV-1 infection by affecting the dynamic reorganization of actin cytoskeleton and PIP_2 production triggered upon HIV-1 contact, specifically at the viral entry step.

RESULTS

Syntenin-1 is recruited to the plasma membrane by HIV-1 Env

PDZ proteins commonly determine the polarization of cellular events (Fanning and Anderson, 1999; Brone and Eggermont, 2005; Ludford-Menting *et al.*, 2005). Because HIV-1 contact with target cells triggers the polarization of cellular components (Dianzani *et al.*, 1995; Nguyen *et al.*, 2005), we investigated whether the PDZ protein syntenin-1 was recruited upon HIV-1 contact with target $CD4^+$ T-cells (CEM-T4). In the absence of HIV-1 virus, syntenin-1 displayed a diffuse cytosolic pattern with low clustering at the plasma membrane (Figure 1A). In contrast, after incubation of T-cells with free HIV-1 particles, syntenin-1 was clearly recruited toward the CD4/CXCR4 capping area (Figure 1, A and E). To confirm the specificity of syntenin-1 recruitment, we assessed CD45 distribution and observed that it did not accumulate at virus-induced capping areas (Figure 1, B and E). In addition, to assess that syntenin-1 recruitment was Env-mediated, target CEM-T4 cells were incubated with a Jurkat clone expressing the T-tropic HIV-1 envelope HxB (Env^+ HxBc2 cells). Syntenin-1 was found at the Env-driven cell contacts, together with CD4 (Figure 1, C and E). We also cocultured target CEM-T4 cells with T-cells directly infected with HIV–green fluorescent protein (GFP) virus (MT4-HIV-GFP). In these cocultures, syntenin-1 accumulated at cell–cell contacts, areas in which viral synapses are established (Figure 1, D and E), but not at unspecific Env-independent cell–cell contacts (Figure1E, right-hand white bar; exemplified in Supplemental Figure S1). Quantification confirmed significant accumulation of syntenin-1 at contacts with HIV-1 viral particles and infected cells, in comparison with CD45 (Figure 1E).

Syntenin-1 associates with the cytoplasmic tail of CD4

PDZ domains usually bind to specific consensus sequences at the C-terminal ends of transmembrane proteins (Chimura *et al.*, 2011). To determine whether syntenin-1 forms part of the CD4/CXCR4 complex at the capping areas, we first searched the CD4 and CXCR4 cytoplasmic domain sequences for potential PDZ-binding motifs. A class I PDZ-binding consensus sequence (Ser-Pro-Ile) was detected at the C-terminal end of CD4, suggesting potential direct interaction with syntenin-1 via its PDZ domains. To test this, we immobilized glutathione *S*-transferase (GST)-fused hemagglutinin (HA)- or Myc-tagged syntenin-1 on Sepharose beads, and incubated them with human primary lymphoblast lysates. GST-syntenin-HA and GST-syntenin-Myc, but not GST alone, precipitated CD4 (Figure 2A). Confirming this interaction, anti-CD4 antibody immunoprecipitated endogenous syntenin-1 from CEM T-cell lysates; syntenin-1 was detected with anti–syntenin-1 antibody as a double band of around 32 kDa (Figure 2B). To demonstrate the occurrence of CD4–syntenin-1 association in the context of HIV-1 infection, we performed reverse immunoprecipitation assays with Jurkat T-cells previously incubated with free viral particles. Immunoprecipitation of syntenin-1, followed by immunodetection of CD4, detected constitutive CD4–syntenin-1 interaction that was maintained during HIV-1 contact (Figure 2C). Together, these data suggest that syntenin-1 interacts with CD4 before and during HIV-1 infection.

Syntenin-1 overexpression inhibits HIV-1–induced cell fusion and viral production

To assess the specific role of syntenin-1 during HIV-1 infection, target T-cells were transfected with GFP-tagged, wild-type syntenin-1 (syntenin-GFP) or a mutated protein, syntenin-Y1-GFP (Synt-Y1-GFP), which carries a Y4>F point mutation in the ITIM motif of the regulatory N-terminal region. Phosphorylation of endogenous syntenin-1 at this tyrosine residue has been shown to be essential for CXCR4-induced chemotaxis (Sala-Valdes *et al.*, 2012). Syntenin-GFP and Synt-Y1-GFP showed a similar distribution to endogenous syntenin-1, being enriched at Env-driven cell–cell contacts (Figure 3A) and HIV-induced capping areas (Figure 3B and data not shown). Target J77 cells overexpressing these GFP-tagged proteins were infected with free HIV-1 particles, and viral production was measured 3 d later by p24 enzyme-linked immunosorbent assay (ELISA). Cells overexpressing syntenin-GFP produced lower viral titers than control cells (transfected with GFP alone). In contrast, overexpression of the mutated syntenin-1 had no effect on HIV-1 production (Figure 3C).

To investigate the potential effect of syntenin-1 plasma membrane recruitment on HIV-1–induced cell fusion, we measured Env-mediated cell fusion by flow cytometry. Env^+ HxBc2 cells

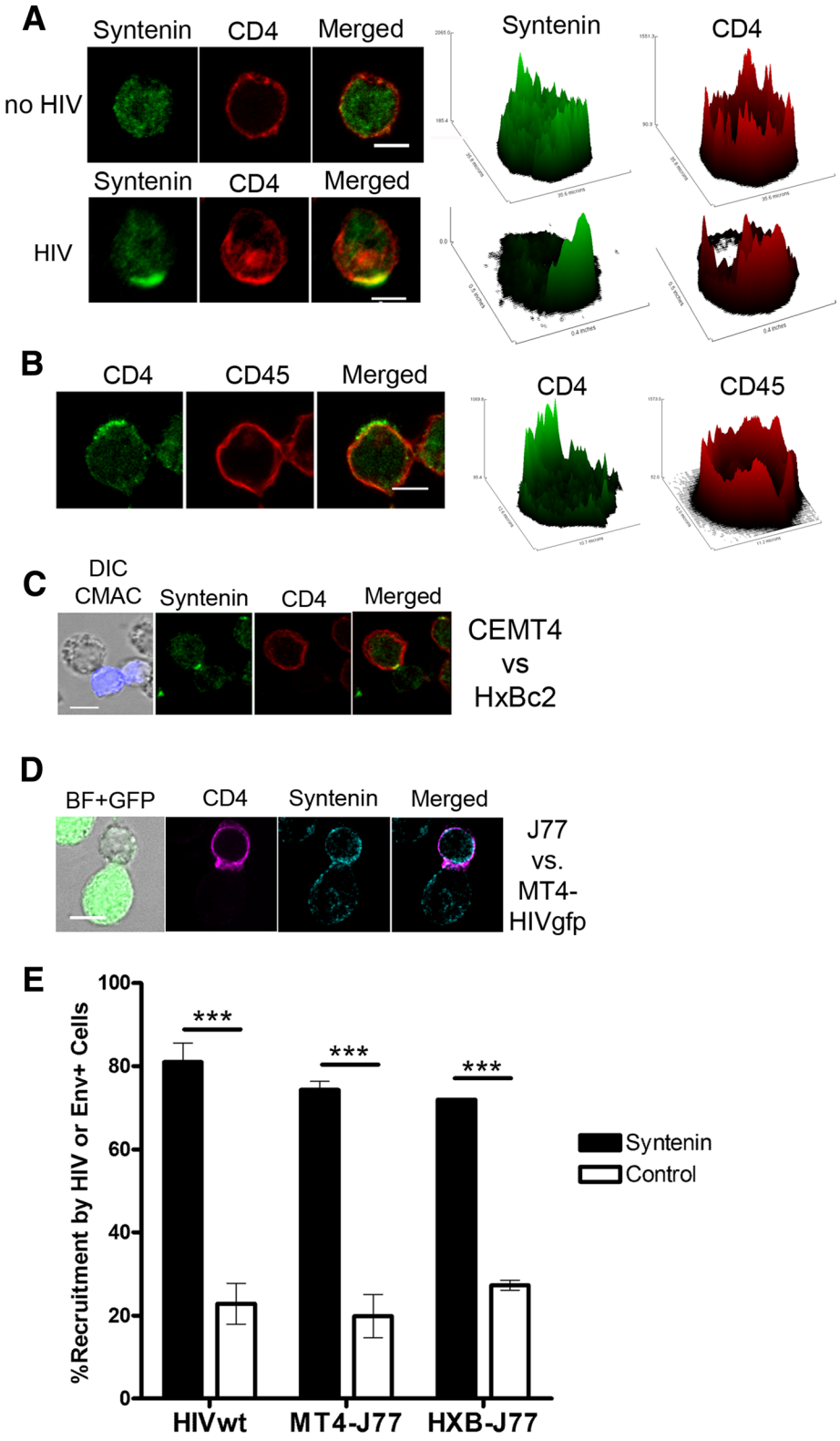

FIGURE 1: Syntenin-1 is recruited by HIV-1 envelope glycoproteins. (A) CEM-T4 cells incubated with or without HIV-1 particles for 30 min were fixed and immunostained for syntenin-1 and CD4 (HP2/6). Summative projections of confocal stack images are shown. Scale bars: 5 µm. Surface plots show fluorescence distribution and intensity for corresponding images. (B) CEM-T4 cells incubated with HIV-1 particles for 30 min were fixed and immunostained for CD4 (CD4v4-FITC) and CD45 (D3/9). Summative projections of confocal stack images are shown. Scale bar: 5 µm. Surface plots show fluorescence distribution and intensity for corresponding images.
(C) Immunofluorescence microscopy images of target CEMT4 cells incubated for 2 h with Env$^+$ HxBc2 cells (CMAC stained, blue) and stained for syntenin-1 and CD4 (HP2/6). Scale bars: 5 µm. (D) Target J77 cells were incubated for 2 h with HIV-1–infected T-cells (MT4-HIV-GFP) and immunostained for syntenin-1 and CD4 (HP2/6). Projections of confocal stack images are shown. Scale bar: 5 µm. (E) Quantification of syntenin-1 accumulation at HIV-1-induced capping areas (HIV-wt), contacts between target cells and HIV-infected cells (MT4-J77), or contacts between target cells and Env$^+$ cells (HxB-J77). The control (white bars) for HIV wild-type and MT4-J77 represent the recruitment of CD45. The control (white bar) for HxB-J77 corresponds to the recruitment of syntenin at Env-independent cell–cell contacts (between two target J77 cells). The chart represents the mean ± SD of three independent experiments; more than 100 conjugates were counted in each condition.

were labeled with red intracellular tracker (CMTMR; 5-(and-6)(((4chloromethyl)benzoyl)-amino) tetramethylrhodamine) and cocultured with target T-cells transfected with each GFP-tagged syntenin-1 construct. Env-driven cell fusion leads to syncytia formation, detected as double-fluorescence positive events of higher size and complexity. As a control of specificity, syncytia formation was blocked with the HIV-1 fusion inhibitor T-20 (Figure 3D). Quantification of these events showed that overexpression of wild-type syntenin-1 reduced Env-mediated cell fusion, whereas the Y4>F mutant had no significant effect (Figure 3D). These data suggest that syntenin-1 negatively regulates HIV-1–mediated membrane fusion through a mechanism requiring phosphorylation of tyrosine 4 in the ITIM motif. To assess whether the Y4>F point mutant was able to interact with CD4, cells were transfected with syntenin-GFP or Synt-Y1-GFP, immunoprecipitated with an anti-GFP, and blotted for CD4. As shown in Figure 3E, Synt-Y1-GFP also associated with CD4.

Knockdown of syntenin-1 expression increases HIV-1 cell fusion and viral entry

To further study syntenin-1 function during HIV-1 infection, we knocked down endogenous syntenin-1 expression using small interfering RNA (siRNA). Control cells were transfected with an siRNA sequence that does not hybridize with any eukaryotic mRNA. Syntenin-1 down-regulation was assessed for each experiment (Figure 4A and data not shown). Membrane expression levels of CD4 and CXCR4 were also routinely assessed to confirm that they were not affected by syntenin depletion (Figure 4B). To assess Env-driven cell fusion, silenced T-cells loaded with green cell tracker were cocultured with

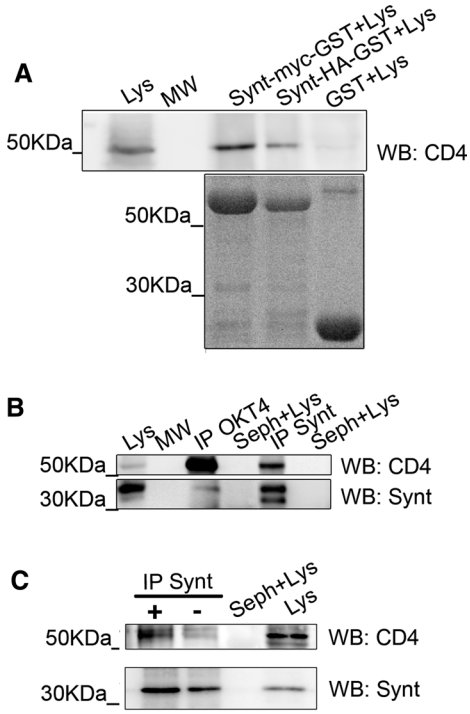

FIGURE 2: Syntenin-1 interacts with CD4 during HIV infection of T-cells. (A) T-lymphoblast cell lysates (Lys) were pulled down with GST, GST-syntenin-Myc, or GST-syntenin-HA, and blotted with anti-CD4 mAb MEM241. (B) CEM T-cell lysates were immunoprecipitated with anti-CD4 mAb OKT4 (IP-OKT4) and anti-syntenin pAb (IP-Synt), and then blotted for syntenin-1 (pAb) and CD4 (mAb MEM241). Total lysates (Lys) and Sepharose beads incubated with lysates (Seph+Lys) are shown. (C) Jurkat J77 T-cells incubated with or without HIV-1 particles were lysed, immunoprecipitated with anti–syntenin-1 pAb, and blotted with anti-CD4 mAb MEM241.

Env$^+$ HxBc2 cells labeled with red cell tracker. Syntenin-1–depleted cells exhibited enhanced cell fusion with Env$^+$ cells compared with control cells (Figure 4C). Furthermore, syntenin-1–depleted cells produced higher viral titers than control cells upon infection with free HIV-1 virions (Figure 4D). Importantly, this effect could be rescued by syntenin-GFP overexpression in silenced T-cells (Figure 4E). Taken together, these results confirm the inhibitory role of syntenin-1 in HIV-1 infection.

Syntenin-1 restricts HIV-1 entry

Syntenin-1 recruitment at the plasma membrane suggested its involvement during HIV-1 attachment or entry steps. To distinguish between these possibilities, we incubated syntenin-1–depleted cells with HIV-1 particles for 2 h at 4°C, a temperature that does not allow Env-induced membrane fusion, thus arresting the virus at the attachment step, or at 37°C, a permissive temperature for membrane fusion and consequently for viral entry. For both conditions a low infection rate was used to avoid superinfection and cooperative virion entry. The amount of p24 in the lysates was measured by ELISA (Figure 5A) and Western blot (data not shown); HIV-1 attachment was estimated from the p24 level at 4°C, and HIV entry was estimated from the difference between the levels at 37 and 4°C. Syntenin-1 silencing enhanced virus entry without affecting viral attachment (4°C), suggesting that syntenin-1 specifically impairs HIV entry (Figure 5A). To confirm these observations, we infected target cells with a one-cycle luciferase virus displaying a T-tropic envelope (X4-Luc), or the vesicular stomatitis virus (VSV) envelope (VSV-Luc) as a control. Higher luciferase levels were found in X4-Luc–infected syntenin-1–silenced cells, confirming that syntenin-1 knockdown specifically increases viral entry (Figure 5B). VSV infection was similar in silenced and control cells, demonstrating that the effect observed is HIV-1 Env-dependent (Figure S2). These results indicate that syntenin-1 negatively regulates HIV-1 entry without affecting viral attachment.

To study the behavior of syntenin-1 during viral attachment and entry in more detail, we incubated Gag-GFP fluorescent virus-like particles (VLPs) with T-cells at 4°C or 37°C. At 4°C, VLPs attached preferentially to one pole of the target cell (Figure S3; see Supplemental Movie S1 for three-dimensional reconstruction), which suggests that the capping area behaves as the main site for viral entry, as has been proposed (Doms, 2000; Nguyen *et al.*, 2005). At 37°C, VLPs could be observed inside target cells, usually accumulated at one pole of the cytoplasm (Figure S3; see Movie S2 for three-dimensional reconstruction).

We next examined the localization of endogenous syntenin-1 by confocal immunostaining of T-cells exposed to VLPs. To avoid false positives due to fortuitous superposition, we only analyzed planes in which VLPs were detected (usually one to two planes distanced by 0.25 μm). Syntenin-1 was enriched at VLP attachment sites in cells kept at 4°C (Figure 5, C and F), whereas barely any syntenin-1 localized at the internalized VLPs in cells incubated at 37°C (Figure 5, D and F). However, syntenin-1 did accumulate near VLPs positioned at cell–cell contacts at 37°C (Figure 5, E and F). Quantification of syntenin-1 accumulation at VLPs at each temperature and location confirmed that association of syntenin-1 with VLPs occurs only on the plasma membrane, and not once the particles are already internalized (Figure 5F).

Thus syntenin-1 is recruited to the plasma membrane by HIV-1 Env during the attachment and entry steps but affects only the effectiveness of viral entry, and it is released from the viral complex once the nucleocapsid has entered the cytoplasm.

Syntenin-1 regulates actin polymerization and PIP_2 accumulation upon HIV-1 contact

Syntenin-1 was recently found to regulate F-actin polymerization via Rac GTPase in T-cells during CXCR4-induced chemotaxis and superantigen presentation (Sala-Valdes *et al.*, 2012). This syntenin-1–mediated activation of Rac depends on phosphorylation of tyrosine 4 (Sala-Valdes *et al.*, 2012). Moreover, Rac-mediated actin reorganization is known to be essential for HIV-1 entry (Iyengar *et al.*, 1998; Pontow *et al.*, 2004; Harmon *et al.*, 2010). To analyze the relation between syntenin-1 and F-actin during HIV-1 infection, we incubated target cells with VLPs, stained them for syntenin-1 and F-actin, and analyzed them with confocal microscopy. Syntenin-1 clusters at the plasma membrane corresponded with the VLP contact area and partially overlapped with F-actin accumulation (Figure 6A; see Figure S4 for F-actin staining in noninfected target cells). Given that HIV-1 attachment to CD4 and CXCR4 triggers local actin polymerization (Jolly *et al.*, 2004), we analyzed this process in syntenin-1–depleted cells. A similar percentage of VLPs colocalized with F-actin in control and syntenin-1–depleted cells (Figure 6A). However, when actin polymerization after HIV-1 contact was monitored at different time points, control cells showed a marked increase in F-actin content 30 min after HIV-1 contact, whereas F-actin polymerization was markedly lower in syntenin-1–depleted cells (Figure 6B). These data indicate that syntenin-1 is required for HIV-1–triggered F-actin polymerization at early stages, when most virus particles are observed at the plasma membrane. Moreover, F-actin accumulation at cell–cell contacts between target and infected MT4 cells was reduced in cells knocked down for syntenin in comparison with control cells (Figure 6C).

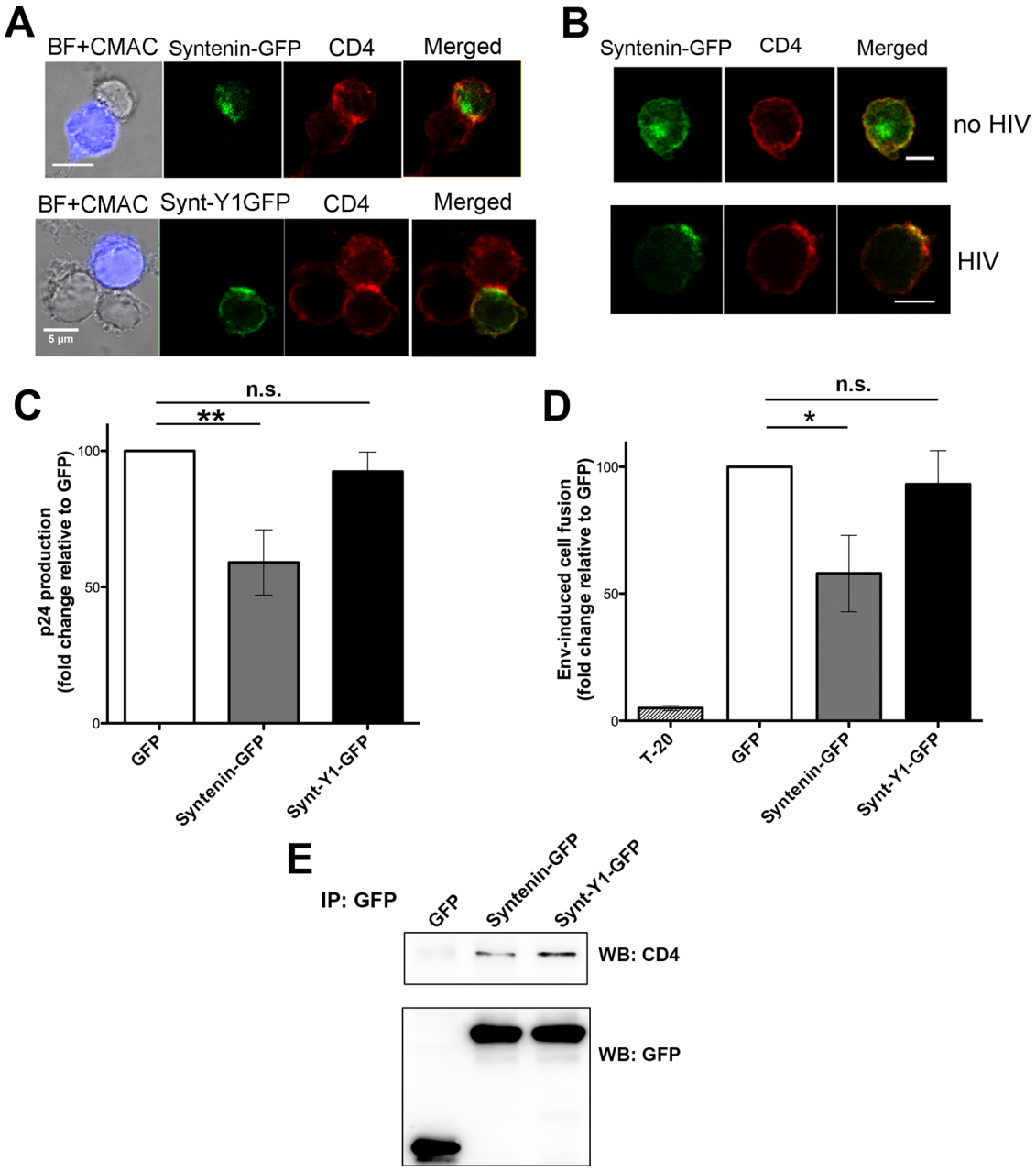

FIGURE 3: Overexpression of wild-type syntenin-1, but not a phosphorylation-defective mutant, in target T-cells impairs HIV-1 infection. (A) CEM-T4 cells overexpressing syntenin-GFP or Synt-Y1-GFP (containing the Y4>F point mutation) were incubated with Env+ HxBc2 cells (tracked with CMAC, blue) for 2 h, fixed, and stained for CD4 (HP2/6 mAb). Summative projections of confocal stack images are shown. Scale bars: 5 µm. (B) CEM-T4 cells overexpressing wild-type syntenin-1 (syntenin-GFP) were incubated for 30 min with or without HIV-1 particles, fixed, and stained for CD4 (HP2/6 mAb). Projections of confocal stack images are shown. Scale bars: 5 µm. (C) HIV-1 infection is inhibited by syntenin-GFP but not by Synt-Y1-GFP. Infection was measured as viral production, quantified as p24 viral protein content in supernatants (ELISA). Data are the fold induction relative to control cells transfected with GFP alone (mean ± SD of four experiments performed in triplicate; $p = 0.0058$). (D) Cell fusion triggered by HIV-1 envelope is reduced in cells overexpressing syntenin-GFP. As a control, syncytia formation was blocked by incubation with the fusion inhibitor T20 (10 nM). Data are the fold induction relative to GFP-transfected cells (mean ± SD of four experiments performed in duplicate; $p = 0.031$). (E) Cells were transfected with GFP, syntenin-GFP, or Synt-Y1-GFP; immunoprecipitated with pAb anti-GFP; and blotted for CD4 (MEM241) and GFP (mAb).

Interaction of the HIV-1 envelope with CD4 triggers PIP_2 production (Barrero-Villar *et al.*, 2008), and this lipid has been found to regulate not only syntenin-1 recruitment to the plasma membrane (Zimmermann *et al.*, 2005) but also many other actin-related proteins (Saarikangas *et al.*, 2010). We therefore assessed whether syntenin-1–dependent actin polymerization upon HIV-1 contact was related to local production of PIP_2. Control or syntenin-1–depleted cells were incubated with MT4-HIV-GFP cells for 2 h and then fixed and stained for PIP_2 with anti-PIP_2 mAb. Syntenin-1–depleted T-cells showed increased accumulation of PIP_2 at contacts with HIV-1–infected T-cells (Figure 6D). To confirm that this effect was related to HIV-1 Env-dependent contacts, we quantified PIP_2 accumulation in target cells

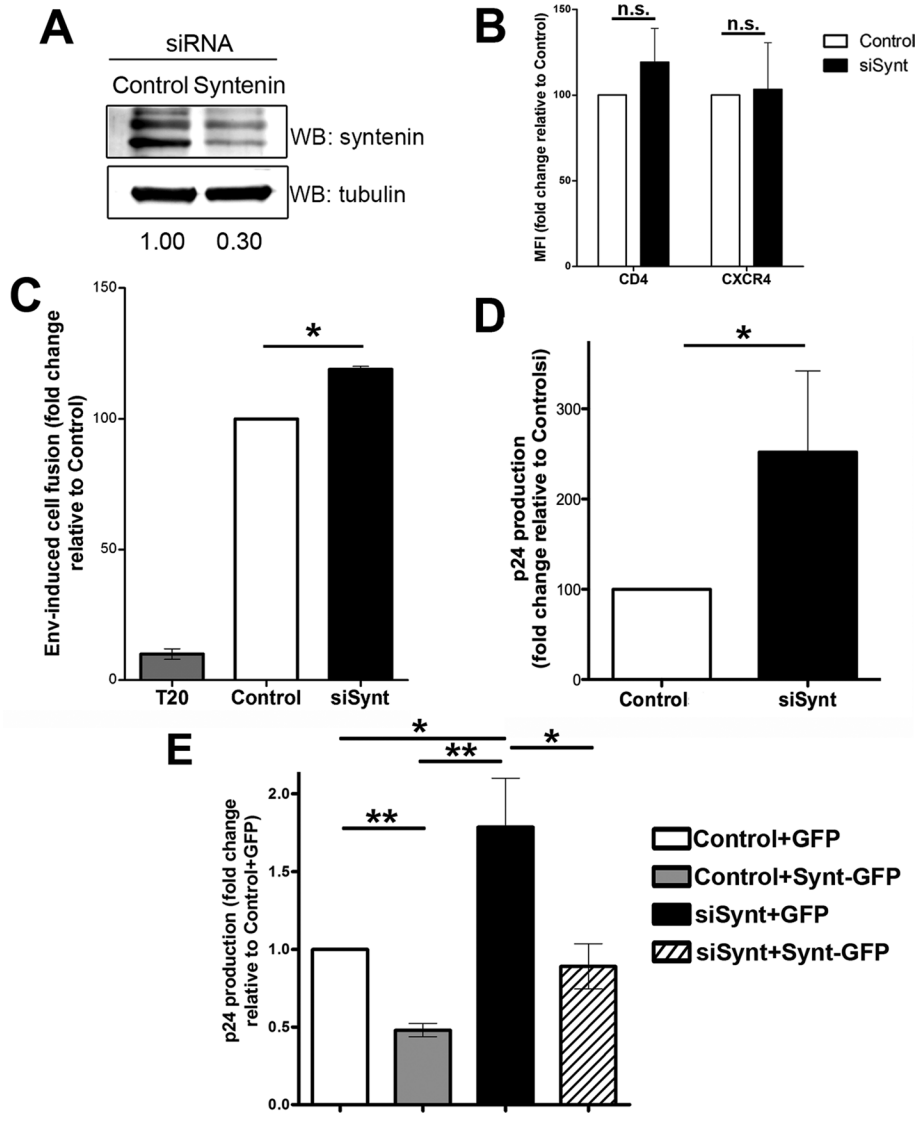

FIGURE 4: Knockdown of syntenin-1 expression increases HIV-1 entry and syncytia formation. (A) Representative Western blot showing silencing of endogenous syntenin-1 expression using oligonucleotide J-008270-08 in T-cells 48 h after siRNA transfection. Numbers below the blot show band intensity ratios between cells transfected with control siRNA and syntenin-1 siRNA, expressed relative to tubulin. (B) Bar chart showing surface expression levels (mean fluorescence intensity) of CD4 and CXCR4 in control and syntenin-depleted cells measured by flow cytometry. (C) Syntenin-1 silencing in target T-cells favors syncytia formation induced by Env$^+$ HxBc2 cells. Syncytia formation was quantified by flow cytometry detection of double-positive fluorescent cells and is presented as the fold induction relative to cells transfected with control siRNA (mean ± SD of four independent experiments performed in duplicate; $p = 0.017$). As a control, syncytia formation was blocked by incubation with the fusion inhibitor T20 (10 nM). (D) Effect of syntenin-1 silencing on HIV-1 infection. Infection was measured as viral production (p24 viral protein content in supernatants [ELISA]) and depicted as the mean fold induction relative to cells transfected with control siRNA (mean ± SD of four experiments performed in triplicate; $p = 0.025$). (E) Syntenin-1-GFP overexpression on cells knocked down for the endogenous syntenin-1 rescues the level of HIV-1 infection. Infection was measured as p24 viral protein content in supernatants (ELISA) and quantified as the mean fold induction relative to cells transfected with control siRNA + GFP (mean ± SD of two experiments performed in triplicate).

cocultured with Env$^+$ HxBc2 cells (heterotypic, Env-driven contacts) or cultured alone (homotypic, Env-independent contacts between target cells; Figure 6E and see Figure S5 for an example image). Syntenin-1 knockdown specifically increased PIP_2 accumulation at Env-driven contacts, while having no effect on Env-independent contacts (Figure 6E).

To assess whether syntenin-1 depletion increases PIP_2 accumulation in virus–cell contacts, we transfected control and syntenin-1–depleted cells with PLCδ-PH-GFP (pleckstrin homology domain of PLC-delta tagged to GFP), a biosensor that binds to PIP_2-enriched membranes (Varnai and Balla, 1998), and incubated them with Cherry-fluorescent VLPs expressing HxB (T-tropic) envelope. Patches of PLCδ-PH-GFP were frequently observed on the target cell surface at sites of VLP attachment (a representative image is shown in Figure 6F). The frequency of these events was higher in syntenin-1–depleted cells (Figure 6F). Taken together, these data indicate that syntenin-1 depletion increases PIP_2 accumulation at Env-driven contacts both of cell–cell and of virus–cell interactions, correlating with lower F-actin polymerization and higher viral entry.

DISCUSSION

In this study we show that syntenin-1 is recruited toward HIV-1 Env-driven virus–cell and cell–cell contacts, associates with CD4, limits HIV-1–induced cell fusion and viral entry, and modulates Env-triggered F-actin remodeling and PIP_2 production.

HIV-1 binding to CD4/CXCR4 complexes at the T-cell surface activates several signaling pathways and triggers local actin polymerization (Iyengar *et al.*, 1998; Jolly *et al.*, 2004), which is essential for receptor clustering at the plasma membrane (Iyengar *et al.*, 1998; Jolly *et al.*, 2004, 2007; Pontow *et al.*, 2004). The actin-binding proteins filamin-A and ERMs are known to favor CD4/CXCR4 clustering during HIV-1 attachment (Jimenez-Baranda *et al.*, 2007; Barrero-Villar *et al.*, 2009). Filamin-A is needed for a transient cofilin inactivation through a RhoA-ROCK–dependent mechanism that stabilizes F-actin during HIV-1 attachment (Jimenez-Baranda *et al.*, 2007). ERMs are activated by phosphorylation upon HIV-1 contact and are essential for F-actin polarization and CD4/CXCR4 clustering (Barrero-Villar *et al.*, 2009). In contrast with these actin-binding proteins, syntenin-1 does not affect HIV-1 attachment and therefore does not seem to be involved in HIV-1–induced CD4/CXCR4 clustering.

Instead, syntenin-1 binding to CD4 might block Lck activation or other CD4-derived pathways, thus hampering HIV-1 entry. However, since syntenin-1 depletion reduces actin polymerization soon after HIV-1 contact, the most plausible explanation for its inhibitory effect is that it induces an actin accumulation at the viral attachment site that hinders viral nucleocapsid entry at the cell surface. Localized actin clearance during HIV-1 entry has been proposed as a mechanism for overcoming this physical restriction (Yoder *et al.*, 2008; Liu *et al.*, 2009; Vasiliver-Shamis *et al.*, 2009), and

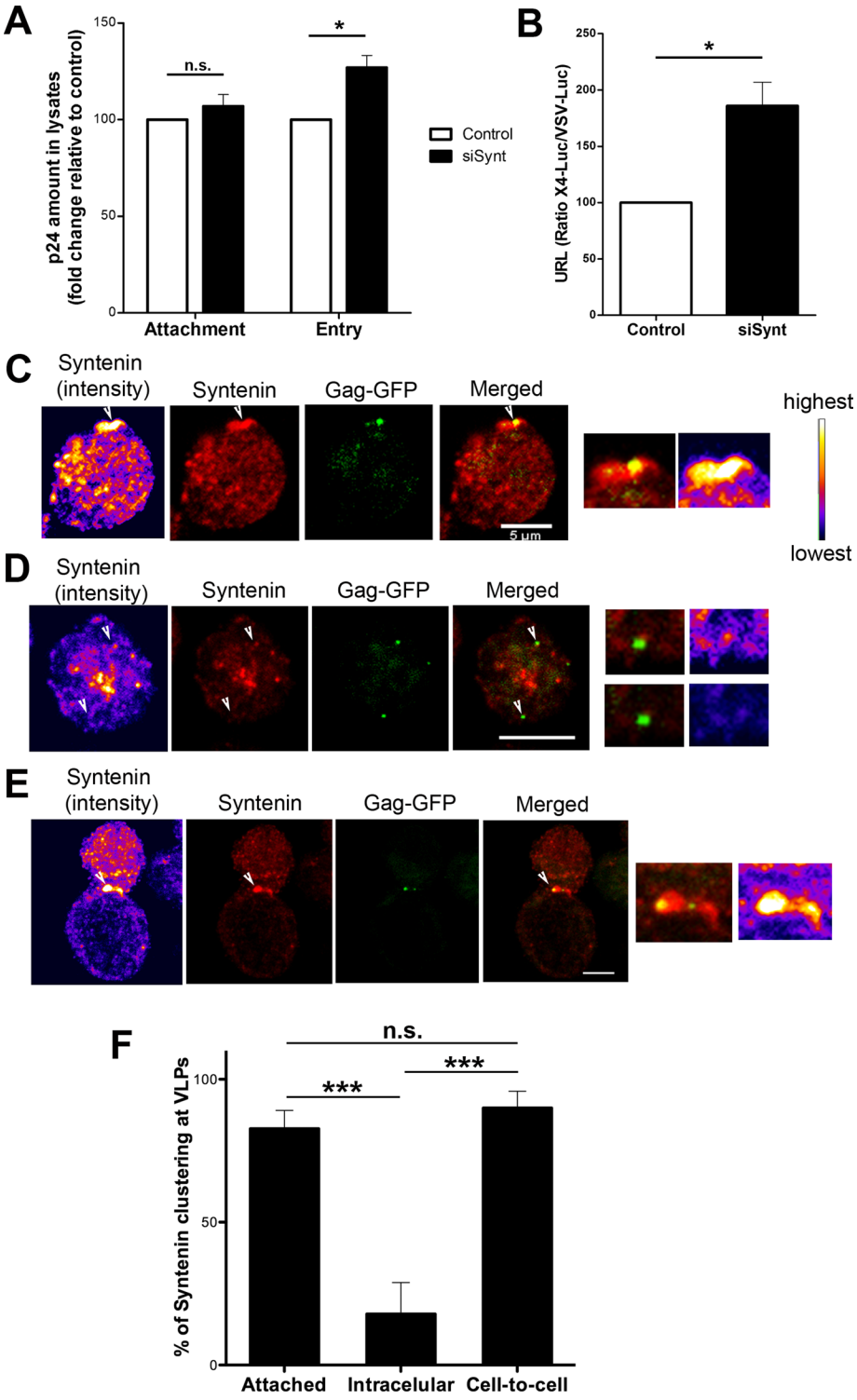

FIGURE 5: Syntenin-1 specifically inhibits viral entry and coclusters with fluorescent VLPs at the plasma membrane. (A) Effect of syntenin-1 silencing on HIV-1 attachment (4°C) and entry (37–4°C) into target T-cells. Data present the fold induction relative to control cells (mean ± SD of three experiments performed in triplicate; $p = 0.016$). (B) HIV-1 entry in syntenin-silenced cells measured by infection with one-cycle viral particles carrying a luciferase reporter gene. Data present the fold induction of luciferase-HIV-1-envelope virus relative to control cells and normalized to values obtained with luciferase-VSV-envelope virus (mean ± SD from four independent experiments performed in triplicate; $p = 0.038$). (C) Confocal images showing the recruitment of endogenous syntenin-1 toward attached VLPs (Gag-GFP) at 4°C. Images are projections of the planes in which each individual VLP is observed. Scale bar: 5 µm. Syntenin-1 staining is shown in pseudocolor intensity-coding format next to the confocal image. The small panels are zoomed views of VLP contacts from pseudocolor syntenin-1 and merged immunostaining images (×3). Note that the maximum intensity of syntenin-1 staining (white on the pseudocolor scale images) overlaps the VLP attachment site. (D) Confocal images showing endogenous syntenin-1 distribution in target T-cells with internalized VLPs (37°C). Two VLPs are shown: one with low syntenin-1 clustering and another with no clustering. Scale bar: 5 µm. Small panels as in (C). (E) Confocal images showing endogenous syntenin-1 distribution in target T-cells forming cell–cell contacts with cells infected with VLPs. Contacts are productive sites for viral transfer and also recruit syntenin-1. Scale bar: 5 µm. Small panels as in (C). (F) Quantification of the number of VLPs that cluster syntenin-1 at the surface of target T-cells (4°C, attached particles), in the cytoplasm (37°C, intracellular particles) or at cell–cell contacts (37°C). Results are from at least three independent experiments and more than 100 VLPs were quantified for each condition.

cofilin activation and its actin-severing function have been linked to enhanced HIV entry (Yoder *et al.*, 2008). Thus a reduced F-actin structure after HIV-1 attachment renders cells more susceptible to subsequent HIV-1 nucleocapsid entry, as occurs in syntenin-depleted cells.

Higher HIV-1–mediated cell fusion and viral entry in syntenin-1–depleted target T-cells also correlates with increased PIP_2 production at Env-mediated cell–cell contacts. PIP_2 is an important second messenger that targets proteins to the plasma membrane and regulates many actin-related proteins, such as ERMs, filamin, cofilin, and α-actinin (Saarikangas *et al.*, 2010). Generation of PIP_2 triggers local actin cytoskeleton changes by activating ERMs (Nakamura *et al.*, 1999), recruiting cofilin (van Rheenen *et al.*, 2009), and inhibiting α-actinin bundling activity (Corgan *et al.*, 2004). Overall, these pathways might favor HIV-1 membrane fusion by facilitating receptor clustering and subsequent actin clearance (Liu *et al.*, 2009). Remarkably, although PIP2-associated cofilin is inactive in tumor cells, cofilin activation in leukocytes is mainly regulated by dephosphorylation (van Rheenen *et al.*, 2009), which is in fact induced upon HIV-1 contact through CXCR4-derived signaling (Yoder *et al.*, 2008). Thus PIP2 might switch the association of membrane receptors and their cytosolic partners (Zimmermann *et al.*, 2005; Saarikangas *et al.*, 2010), modulating the links between transmembrane proteins and the subcortical actin cytoskeleton, and subsequently altering the association of proteins belonging to the same signaling pathway. In this

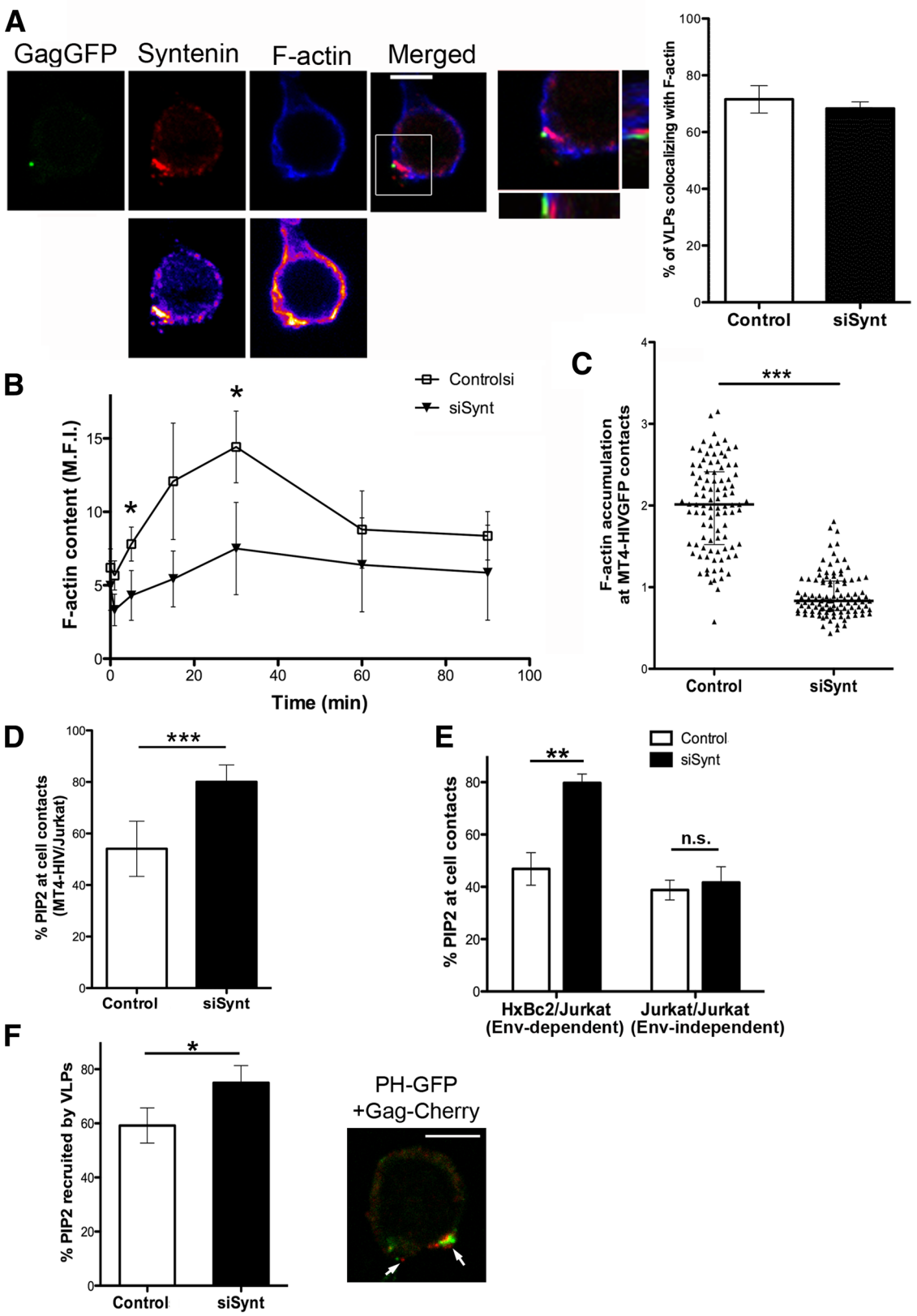

FIGURE 6: Actin polymerization is reduced in syntenin-1–depleted T-cells. (A) J77 T-cells were incubated with fluorescent VLPs (Gag-GFP) for 30 min, fixed, and stained for syntenin-1 and F-actin. The panels show projections of selected confocal planes in which a VLP was observed, with corresponding pseudocolor images below. Scale bar: 5 μm. The zoomed image shows the particle site (boxed region in merged image) together with orthogonal sections. Quantification of VLPs that colocalized with F-actin in cells silenced or not for syntenin-1 is shown at the right. No significant difference was observed. (B) Time profile of F-actin content upon contact with HIV-1 particles, measured by flow cytometry in control or syntenin-depleted cells. Data are means ± SD of four independent experiments. (C) F-actin accumulation at

regard, in a preliminary attempt to assess syntenin-1 partners, we have observed its association with ERMs and PI4P5K-I (Gordon-Alonso *et al.*, unpublished data). One possibility is that syntenin-1 may be able to prevent ERMs from fulfilling their role of in facilitating HIV-1 entry but without affecting CD4/CXCR4 clustering. A second option is that syntenin-1 is limiting PI4P5K-I PIP2 production, and therefore, inhibiting HIV-1 entry (Barrero-Villar *et al.*, 2008). The complexity of syntenin-1 relationships deserves further investigation. Alternatively, depletion of syntenin-1 might simply allow a higher pool of free PIP2 to accumulate at the plasma membrane after HIV-1 attachment, where it could mediate the recruitment of proteins, such as, ERMs, that facilitate HIV entry (Barrero-Villar *et al.*, 2008, 2009).

The fact that syntenin-1 clustering around the virus-like particle vanishes after viral entry is consistent with participation of syntenin-1 at the plasma membrane during HIV-1 entry, probably as a consequence of its association with CD4 or its recruitment through PIP_2. We therefore propose a dynamic model in which syntenin-1 is first recruited to the viral attachment site through CD4 and/or PIP_2. At this location, syntenin-1 would trigger F-actin polymerization via Rac GTPase, as has also been suggested for other processes mediated by this GTPase (Sala-Valdes *et al.*, 2012). This is consistent with the fact that Rac is the Rho GTPase specifically activated during HIV-1 entry (Pontow *et al.*, 2004; Harmon *et al.*, 2010). Because syntenin-1 regulates Rac-triggered F-actin polymerization through the adaptor protein M-Rip during T chemotaxis (Sala-Valdes *et al.*, 2012), it is conceivable that this or a similar signaling axis could be involved during HIV-1 entry. Indeed, syntenin-1 Tyr-4 is essential for Rac-mediated T-cell chemotaxis and superantigen presentation (Sala-Valdes *et al.*, 2012) and seems also to be crucial for syntenin-mediated inhibition of HIV infection. Subsequently, F-actin must be locally depolymerized to facilitate the nucleocapsid entry (Yoder *et al.*, 2008; Vasiliver-Shamis *et al.*, 2009), which is favored (F-actin depolymerization) in the absence of syntenin-1. In this context, PIP_2 induction by HIV-1 might be the signal that shuts down local F-actin polymerization while activating F-actin clearance.

In summary, our results have unveiled a critical regulatory role for syntenin-1 in controlling HIV-1 entry into target T-cells through altering actin polymerization, most likely in a PIP_2-regulated manner.

MATERIALS AND METHODS

Cell lines and reagents

The Jurkat-derived human T-cell line J77 $V\beta8^+$ J77cl20 was grown in RPMI 1640 medium supplemented with 10% fetal bovine serum (FBS; Cambrex Bioscience, Charles City, IA). The CEM-T4 human T-lymphoblast–like cell line (courtesy of Paul Clapman), and the HxBc2 Jurkat-derived T-cell line (courtesy of Joseph Sodrowski) were obtained from the National Institutes of Health (NIH) AIDS Research and Reference Reagent Program and were cultured according to NIH instructions. The chronically infected MT4-NL4.3-GFP cell line (MT4-HIV-GFP) was generated by Nuria Izquierdo-Useros at the laboratory of Martinez-Picado (IrsiCaixa, Barcelona, Spain).

The biotinylated monoclonal anti-CXCR4 antibody was from BD PharMingen. Mouse monoclonal anti–α-tubulin was from Sigma-Aldrich (Saint Louis, MO). Anti-CD4 monoclonal antibodies used were HP2/6 (Gordon-Alonso *et al.*, 2006), OKT4 (eBioscience), RPA-T4 (eBioscience, San Diego, CA), CD4v4-FITC (BD PharMingen, Franklin Lakes, NJ), and MEM 241 (Abcam, Cambridge, UK). Rabbit polyclonal anti–syntenin-1 was from Synaptic Systems (Göttingen, Germany). The anti-CD45 mAb was clone D3/9, previously described (Gordon-Alonso *et al.*, 2006). Anti-PIP_2 mAb was from Santa Cruz Biotechnology (clone 2C11; Santa Cruz, CA). Anti-GFP antibodies (pAb for IP and mAb for WB) were from Living colors (Clontech, Mountain View, CA). HRP-conjugated secondary antibodies were from Pierce (Rockford, IL).

The intracellular fluorescent trackers CMAC, Calcein-AM, and CM-TMR and all fluorochrome-conjugated secondary antibodies and phalloidins were from Molecular Probes (Camarillo, CA). The HIV-1-specific fusion inhibitor T20 (Enfuvirtide) was from Roche Diagnostics.

Cell transfection, DNA and siRNA

J77 cells (2×10^7) were electroporated in cold Optimem (Life Technologies-BRL, Camarillo, CA) with DNA (20 mg) or with siRNA (1.25 mM) using a Bio-Rad GenePulser II electroporator (240 V; 950°F). Fluorescent protein expression and siRNA knockdown were tested respectively by flow cytometry (24 h) and Western blot analysis (48 h).

The syntenin-1 GFP fusion proteins Psrα-HAGFP-syntenin-1 and syntenin-1-Y1-GFP have been described previously (Sala-Valdes *et al.*, 2012). PIP_2-enriched plasma membranes were monitored during Env-mediated membrane fusion or VLP attachment by transfecting cells with the biosensor PLCδ-PH-GFP (Varnai and Balla, 1998). GST-syntenin-1-HA and GST-syntenin-1-Myc were kindly donated by F. Lozano (Hospital Clinic, Barcelona, Spain).

Negative control siRNA was from Eurogentec (Serain, Belgium) and the specific siRNAs against syntenin-1 were from Thermo Scientific Dharmacon (oligonucleotides J-008270-08 and J-008270-06).

Preparation and production of HIV-1 and virus attachment and entry assay

Preparation of HIV-1 NL4.3 and measurement of viral replication were as previously described (Valenzuela-Fernandez *et al.*, 2005). Gag-GFP and Gag-Cherry fluorescent VLPs were produced as previously described (Izquierdo-Useros *et al.*, 2009) by cotransfecting 293T cells with the HIV Gag-eGFP/Cherry plasmids and the envelope plasmid pHXB2.

contacts between infected MT4-HIV-GFP cells and silenced or control target cells was quantified using the synapse-measure plug-in of Image J. The medians and interquartile ranges are shown. More than 100 conjugates were counted for each condition in two independent experiments ($p = 4.08 \times 10^{-31}$). (D) MT4-HIV-GFP infected T-cells were incubated with control or syntenin-depleted target T-cells for 2 h, fixed, and stained for PIP_2 with anti-PIP_2 mAb. Quantified PIP_2 labeling at Env-mediated cell contacts is presented as the percentage of PIP_2 accumulated at cell contacts. More than 100 conjugates were counted for each condition ($p = 1.1 \times 10^{-5}$). (E) Env+ HxBc2 T-cells were incubated with control or syntenin-depleted target T-cells for 2 h and then fixed, and the conjugates were stained for PIP_2 with anti-PIP_2 mAb. Quantified PIP_2 labeling at cell contacts is presented as the percentage of PIP_2 accumulated at heterotypic Env-driven cell–cell contacts and at homotypic Env-independent contacts (between two target T-cells). More than 100 conjugates were counted for each condition ($p = 2.1 \times 10^{-4}$). (F) Control or syntenin-depleted cells expressing PLCδ-PH-GFP were incubated with fluorescent VLPs (Gag-Cherry) for 30 min, fixed, and analyzed by confocal microscopy. The bar chart shows quantification of PIP_2 enrichment at VLP contacts, presented as the percentage of PIP_2 recruited to VLP–cell contacts. More than 100 VLP contacts were counted for each condition ($p = 0.038$). The right panel shows a sample confocal image in which several VLPs are attached to one pole of the target T-cell (arrows). Scale bar: 5 μm.

For p24 production, T-cells were infected with 100 ng of HIV-1 NL4.3 per million cells for 2 h at 37°C (which is equivalent to 1–2 multiplicity of infection or viral particles per cell), and then extensively washed with medium to remove nonattached viral particles. Infected T-cells were kept in culture for 3 d, at which time supernatants were harvested and p24 concentration measured by ELISA (Innotest HIV-1 antigen mAb; Innogenetic, Ghent, Belgium).

For HIV attachment and entry measurements, T-cells were infected with 20 ng of HIV-1 NL4.3 per million cells for 2 h at 4°C (attachment) or 37°C (attachment + entry), and then extensively washed to remove viral input and lysed with RIPA buffer (50 mM Tris HCl, pH 8, 150 mM NaCl, 1% NP-40, 0.5% sodium deoxycholate, 0.1% SDS). p24 was measured by ELISA (Innotest HIV-1antigen mAb; Innogenetic).

Luciferase virus assay

Replication-deficient luciferase-HIV-1 particles were kindly provided by Suryaram Gummuluru (Boston University, Boston, MA). Replication-deficient viral particles were produced by cotransfecting 293T cells with the luciferase-expressing reporter virus, HIV/Δnef/Δenv/luc$^+$, which contains the luciferase gene inserted into the *nef* open reading frame and does not express *env* glycoprotein (Yamashita and Emerman, 2004), and a CXCR4-tropic (Lai) *env* glycoprotein or non–T-tropic VSV glycoprotein. Virus stocks were generated by PolyFect transient cotransfection of HEK293T cells (Gummuluru *et al.*, 2002). Two days after transfection, cell-free virus-containing supernatants were clarified of cell debris and concentrated by centrifugation (16,000 × *g*, 1 h at 4°C) and stored at –80°C until required. HIV-1 virus preparations were titrated by p24-ELISA. T-cells were infected with 200 ng of luciferase-based virus with X4-tropic HIV-1 envelope or VSV envelope per million cells for 2 h. Cells were washed extensively and luciferase activity was measured at 48 h after infection with a luciferase assay kit (Promega Corporation, Madison, WI) on a 1450 Microbeta Luminescence Counter (Walax, Trilux).

Env-induced cell fusion assay

A dual-fluorescence cell-fusion assay was performed as described previously (Gordon-Alonso *et al.*, 2006). Briefly, CMTMR-loaded Env$^+$ Jurkat-Hxbc2 cells were mixed with calcein-AM–loaded parental or transfected CEM-T4 cells. Fluorescence events were detected 14 h later by flow cytometry. Fusion was quantified as the ratio of double-positive events to single-positive target cells.

Immunoprecipitation

T lymphoblasts and CEM T-cells were lysed in 1% NP-40, 1 mM $MgCl_2$, 1 mM $CaCl_2$ in Tris-buffered saline (TBS) supplemented with protease and phosphatase inhibitor cocktails. J77 T-cells (4×10^7) were lysed in 1% NP-40 in TBS supplemented with a protease inhibitor cocktail. Lysates were centrifuged at 11,000 rpm for 10 min at 4°C, and cell lysate supernatants were incubated for 2 h at 4°C with cyanogen bromide (CNBr) beads (Amersham, Uppsala, Sweden) blocked with bovine serum albumin (BSA). Supernatants were then incubated with the indicated antibody covalently coupled to CNBr beads for 2 h at 4°C. Pellets were washed with lysis buffer, resuspended in reducing Laemmli buffer, and processed for Western blotting with the indicated antibodies.

Immunofluorescence and confocal microscopy

T-cells incubated with viral particles, Env$^+$ cells (HxBc2), or HIV-1 infected cells (MT4-HIV-GFP) were seeded on 50 μg/ml poly-L-lysine for 30 min and fixed with 3% paraformaldehyde. For staining of intracellular proteins (endogenous syntenin-1, F-actin, and PIP_2), samples were permeabilized for 5 min with 0.5% Triton X-100 in TBS, stained and mounted in Prolong (Invitrogen, Camarillo, CA). Images were obtained with a photomicroscope (DMR; Leica, Germany) fitted with an HCX PL APO 63×/1.32-210.6 oil-immersion objective (Leica; Germany) and coupled to a COHU 4912–5010 charge-coupled camera.

Confocal images were obtained with a Leica TCS-SP5 confocal scanning laser microscope fitted with either an HCX PL APO lambda blue 63×/1.4 or an HCX PL APO lambda blue 100×/1.4 oil-immersion objective and analyzed with Image J. For clustering quantification, staining intensities were transformed with the pseudocolor-intensity look-up-table (LUT). Yellow-white patches at VLP locations were considered positive for clustering. For analyzing F-actin accumulation at cell–cell contacts, Image J software was used as previously described (Calabia-Linares *et al.*, 2011).

Western blotting

J77 T-cells were lysed in 1% NP-40 in TBS supplemented with a cocktail of protease inhibitors and phosphatase inhibitors. Lysates were centrifuged at 11,000 rpm for 10 min at 4°C, and supernatants were mixed with reducing Laemmli buffer and boiled for 5 min. Lysates were separated by SDS–PAGE and immunoblotted with specific antibodies. Protein bands were analyzed using the LAS-1000 CCD system and Image Gauge 3.4 software (Fuji Photo Film, Tokyo, Japan).

Flow cytometry

Cells were incubated with TBS 5% BSA for 30 min at 4°C and then with primary monoclonal antibody (30 min at 4°C). After being washed, cells were incubated with a fluorescein isothiocyanate (FITC)-conjugated secondary antibody and analyzed in a FACScalibur flow cytometer (Becton Dickinson, Franklin Lakes, NJ). Data were analyzed with Cell-Quest Pro (Becton Dickinson).

F-actin quantification

Cells were stimulated with HIV NL4.3 free virions (100 ng/million cells), fixed with 4% formaldehyde at different time points, permeabilized with TBS 0.5% Triton X-100 (5 min), and stained with Phalloidin-Alexa647 (Molecular Probes, Camarillo, CA). Mean fluorescence intensity of F-actin staining was analyzed on a FACScalibur cytometer (BD Biosciences, Franklin Lakes, NJ).

Statistical analysis

Statistical significance was calculated using Student's *t* test or the parametric one-way analysis of variance with Bonferroni's post hoc multiple-comparison test. Significant differences are labeled (*, $p < 0.05$; **, $p < 0.01$; ***, $p < 0.001$).

ACKNOWLEDGMENTS

The authors thank José Román Cabrero for helpful biochemical advice, Manuel Perez-Martinez for confocal assistance, and Miguel Vicente-Manzanares for critical reading of the manuscript. Simon Barlett (CNIC) provided English editing. This work was supported by SAF2008-02635, SAF2011-25834 (from Ministerio de Economía y Competitividad), INSINET-0159/2006 (from the Comunidad de Madrid), and FIPSE 36658/07 (from the Spanish Society against AIDS), all to F.S.-M. M.G.-A. was funded by RECAVA and V.R.-P. by the CNIC.

REFERENCES

Barrero-Villar M, Barroso-Gonzalez J, Cabrero JR, Gordon-Alonso M, Alvarez-Losada S, Munoz-Fernandez MA, Sanchez-Madrid F, Valenzuela-Fernandez A (2008). PI4P5-kinase Iα is required for efficient HIV-1 entry and infection of T cells. J Immunol 181, 6882–6888.

Barrero-Villar M, Cabrero JR, Gordon-Alonso M, Barroso-Gonzalez J, Alvarez-Losada S, Munoz-Fernandez MA, Sanchez-Madrid F, Valenzuela-Fernandez A (2009). Moesin is required for HIV-1-induced CD4-CXCR4 interaction, F-actin redistribution, membrane fusion and viral infection in lymphocytes. J Cell Sci 122, 103–113.

Beekman JM, Coffer PJ (2008). The ins and outs of syntenin, a multifunctional intracellular adaptor protein. J Cell Sci 121, 1349–1355.

Boukerche H, Su ZZ, Prevot C, Sarkar D, Fisher PB (2008). mda-9/syntenin promotes metastasis in human melanoma cells by activating c-Src. Proc Natl Acad Sci USA 105, 15914–15919.

Brone B, Eggermont J (2005). PDZ proteins retain and regulate membrane transporters in polarized epithelial cell membranes. Am J Physiol Cell Physiol 288, C20–C29.

Calabia-Linares C *et al.* (2011). Endosomal clathrin drives actin accumulation at the immunological synapse. J Cell Sci 124, 820–830.

Carter GC, Bernstone L, Baskaran D, James W (2009). HIV-1 infects macrophages by exploiting an endocytic route dependent on dynamin, Rac1 and Pak1. Virology 409, 234–250.

Chimura T, Launey T, Ito M (2011). Evolutionarily conserved bias of amino-acid usage refines the definition of PDZ-binding motif. BMC Genomics 12, 300.

Corgan AM, Singleton C, Santoso CB, Greenwood JA (2004). Phosphoinositides differentially regulate α-actinin flexibility and function. Biochem J 378, 1067–1072.

Dianzani U, Bragardo M, Buonfiglio D, Redoglia V, Funaro A, Portoles P, Rojo J, Malavasi F, Pileri A (1995). Modulation of CD4 lateral interaction with lymphocyte surface molecules induced by HIV-1 gp120. Eur J Immunol 25, 1306–1311.

Doms RW (2000). Beyond receptor expression: the influence of receptor conformation, density, and affinity in HIV-1 infection. Virology 276, 229–237.

Fanning AS, Anderson JM (1999). PDZ domains: fundamental building blocks in the organization of protein complexes at the plasma membrane. J Clin Invest 103, 767–772.

Gimferrer I *et al.* (2005). The lymphocyte receptor CD6 interacts with syntenin-1, a scaffolding protein containing PDZ domains. J Immunol 175, 1406–1414.

Gordon-Alonso M, Yanez-Mo M, Barreiro O, Alvarez S, Munoz-Fernandez MA, Valenzuela-Fernandez A, Sanchez-Madrid F (2006). Tetraspanins CD9 and CD81 modulate HIV-1-induced membrane fusion. J Immunol 177, 5129–5137.

Grootjans JJ, Zimmermann P, Reekmans G, Smets A, Degeest G, Durr J, David G (1997). Syntenin, a PDZ protein that binds syndecan cytoplasmic domains. Proc Natl Acad Sci USA 94, 13683–13688.

Gummuluru S, KewalRamani VN, Emerman M (2002). Dendritic cell-mediated viral transfer to T cells is required for human immunodeficiency virus type 1 persistence in the face of rapid cell turnover. J Virol 76, 10692–10701.

Harmon B, Campbell N, Ratner L (2010). Role of Abl kinase and the Wave2 signaling complex in HIV-1 entry at a post-hemifusion step. PLoS Pathog 6, e1000956.

Hirbec H, Martin S, Henley JM (2005). Syntenin is involved in the developmental regulation of neuronal membrane architecture. Mol Cell Neurosci 28, 737–746.

Hiscott J, Kwon H, Genin P (2001). Hostile takeovers: viral appropriation of the NF-κB pathway. J Clin Invest 107, 143–151.

Iyengar S, Hildreth JE, Schwartz DH (1998). Actin-dependent receptor colocalization required for human immunodeficiency virus entry into host cells. J Virol 72, 5251–5255.

Izquierdo-Useros N *et al.* (2009). Capture and transfer of HIV-1 particles by mature dendritic cells converges with the exosome-dissemination pathway. Blood 113, 2732–2741.

Jannatipour M, Dion P, Khan S, Jindal H, Fan X, Laganiere J, Chishti AH, Rouleau GA (2001). Schwannomin isoform-1 interacts with syntenin via PDZ domains. J Biol Chem 276, 33093–33100.

Jimenez-Baranda S *et al.* (2007). Filamin-A regulates actin-dependent clustering of HIV receptors. Nat Cell Biol 9, 838–846.

Jolly C, Kashefi K, Hollinshead M, Sattentau QJ (2004). HIV-1 cell to cell transfer across an Env-induced, actin-dependent synapse. J Exp Med 199, 283–293.

Jolly C, Mitar I, Sattentau QJ (2007). Requirement for an intact T-cell actin and tubulin cytoskeleton for efficient assembly and spread of human immunodeficiency virus type 1. J Virol 81, 5547–5560.

Juno JA, Fowke KR (2010). Clarifying the role of G protein signaling in HIV infection: new approaches to an old question. AIDS Rev 12, 164–176.

Latysheva N, Muratov G, Rajesh S, Padgett M, Hotchin NA, Overduin M, Berditchevski F (2006). Syntenin-1 is a new component of tetraspanin-enriched microdomains: mechanisms and consequences of the interaction of syntenin-1 with CD63. Mol Cell Biol 26, 7707–7718.

Liu Y, Belkina NV, Shaw S (2009). HIV infection of T cells: actin-in and actin-out. Sci Signal 2, pe23.

Ludford-Menting MJ *et al.* (2005). A network of PDZ-containing proteins regulates T cell polarity and morphology during migration and immunological synapse formation. Immunity 22, 737–748.

Mettling C, Desmetz C, Fiser AL, Reant B, Corbeau P, Lin YL (2008). Gαi protein-dependent extracellular signal-regulated kinase-1/2 activation is required for HIV-1 reverse transcription. AIDS 22, 1569–1576.

Nakamura F, Huang L, Pestonjamasp K, Luna EJ, Furthmayr H (1999). Regulation of F-actin binding to platelet moesin in vitro by both phosphorylation of threonine 558 and polyphosphatidylinositides. Mol Biol Cell 10, 2669–2685.

Nguyen DH, Giri B, Collins G, Taub DD (2005). Dynamic reorganization of chemokine receptors, cholesterol, lipid rafts, and adhesion molecules to sites of CD4 engagement. Exp Cell Res 304, 559–569.

Pontow SE, Heyden NV, Wei S, Ratner L (2004). Actin cytoskeletal reorganizations and coreceptor-mediated activation of rac during human immunodeficiency virus-induced cell fusion. J Virol 78, 7138–7147.

Popik W, Hesselgesser JE, Pitha PM (1998). Binding of human immunodeficiency virus type 1 to CD4 and CXCR4 receptors differentially regulates expression of inflammatory genes and activates the MEK/ERK signaling pathway. J Virol 72, 6406–6413.

Popik W, Pitha PM (2000). Inhibition of CD3/CD28-mediated activation of the MEK/ERK signaling pathway represses replication of X4 but not R5 human immunodeficiency virus type 1 in peripheral blood CD4(+) T lymphocytes. J Virol 74, 2558–2566.

Saarikangas J, Zhao H, Lappalainen P (2010). Regulation of the actin cytoskeleton-plasma membrane interplay by phosphoinositides. Physiol Rev 90, 259–289.

Sala-Valdes M, Gordon-Alonso M, Tejera E, Ibanez A, Cabrero JR, Ursa A, Mittelbrunn M, Lozano F, Sanchez-Madrid F, Yanez-Mo M (2012). Association of syntenin-1 with M-RIP polarizes Rac-1 activation during chemotaxis and immune interactions. J Cell Sci 125, 1235–1246.

Sarkar D, Boukerche H, Su ZZ, Fisher PB (2004). mda-9/syntenin: recent insights into a novel cell signaling and metastasis-associated gene. Pharmacol Ther 104, 101–115.

Sarkar D, Boukerche H, Su ZZ, Fisher PB (2008). mda-9/syntenin: more than just a simple adapter protein when it comes to cancer metastasis. Cancer Res 68, 3087–3093.

Valenzuela-Fernandez A *et al.* (2005). Histone deacetylase 6 regulates human immunodeficiency virus type 1 infection. Mol Biol Cell 16, 5445–5454.

van Rheenen J, Condeelis J, Glogauer M (2009). A common cofilin activity cycle in invasive tumor cells and inflammatory cells. J Cell Sci 122, 305–311.

Varnai P, Balla T (1998). Visualization of phosphoinositides that bind pleckstrin homology domains: calcium- and agonist-induced dynamic changes and relationship to myo-[3H]inositol-labeled phosphoinositide pools. J Cell Biol 143, 501–510.

Vasiliver-Shamis G, Cho MW, Hioe CE, Dustin ML (2009). Human immunodeficiency virus type 1 envelope gp120-induced partial T-cell receptor signaling creates an F-actin-depleted zone in the virological synapse. J Virol 83, 11341–11355.

Wu Y, Yoder A (2009). Chemokine coreceptor signaling in HIV-1 infection and pathogenesis. PLoS Pathog 5, e1000520.

Yamashita M, Emerman M (2004). Capsid is a dominant determinant of retrovirus infectivity in nondividing cells. J Virol 78, 5670–5678.

Yoder A *et al.* (2008). HIV envelope-CXCR4 signaling activates cofilin to overcome cortical actin restriction in resting CD4 T cells. Cell 134, 782–792.

Zimmermann P (2006). The prevalence and significance of PDZ domain-phosphoinositide interactions. Biochim Biophys Acta 1761, 947–956.

Zimmermann P, Tomatis D, Rosas M, Grootjans J, Leenaerts I, Degeest G, Reekmans G, Coomans C, David G (2001). Characterization of syntenin, a syndecan-binding PDZ protein, as a component of cell adhesion sites and microfilaments. Mol Biol Cell 12, 339–350.

Zimmermann P, Zhang Z, Degeest G, Mortier E, Leenaerts I, Coomans C, Schulz J, N'Kuli F, Courtoy PJ, David G (2005). Syndecan recycling [corrected] is controlled by syntenin-PIP_2 interaction and Arf6. Dev Cell 9, 377–388.

nature COMMUNICATIONS

ARTICLE

Received 24 Nov 2015 | Accepted 18 Oct 2016 | Published 24 Nov 2016

DOI: 10.1038/ncomms13588 OPEN

ISGylation controls exosome secretion by promoting lysosomal degradation of MVB proteins

Carolina Villarroya-Beltri[1,2], Francesc Baixauli[1,2], María Mittelbrunn[1], Irene Fernández-Delgado[1,2], Daniel Torralba[1,2], Olga Moreno-Gonzalo[1,2], Sara Baldanta[3], Carlos Enrich[4], Susana Guerra[3,*] & Francisco Sánchez-Madrid[1,2,*]

Exosomes are vesicles secreted to the extracellular environment through fusion with the plasma membrane of specific endosomes called multivesicular bodies (MVB) and mediate cell-to-cell communication in many biological processes. Posttranslational modifications are involved in the sorting of specific proteins into exosomes. Here we identify ISGylation as a ubiquitin-like modification that controls exosome release. ISGylation induction decreases MVB numbers and impairs exosome secretion. Using ISG15-knockout mice and mice expressing the enzymatically inactive form of the de-ISGylase USP18, we demonstrate *in vitro* and *in vivo* that ISG15 conjugation regulates exosome secretion. ISG15 conjugation triggers MVB co-localization with lysosomes and promotes the aggregation and degradation of MVB proteins. Accordingly, inhibition of lysosomal function or autophagy restores exosome secretion. Specifically, ISGylation of the MVB protein TSG101 induces its aggregation and degradation, being sufficient to impair exosome secretion. These results identify ISGylation as a novel ubiquitin-like modifier in the control of exosome production.

[1] Centro Nacional de Investigaciones Cardiovasculares (CNIC), 28029 Madrid, Spain. [2] Immunology Service, Hospital de la Princesa, Instituto Investigación Sanitaria Princesa, Universidad Autónoma de Madrid, 28006 Madrid, Spain. [3] Department of Preventive Medicine, Public Health and Microbiology, Universidad Autónoma de Madrid, 28029 Madrid, Spain. [4] Departament de Biomedicina, Unitat de Biologia Cel·lular, Centre de Recerca Biomèdica CELLEX, Institut d'Investigacions Biomèdiques August Pi i Sunyer (IDIBAPS), Facultat de Medicina, Universitat de Barcelona, 08036 Barcelona, Spain. * These authors contributed equally to this work. Correspondence and requests for materials should be addressed to F.S.-M. (email: fsmadrid@salud.madrid.org).

Exosomes are vesicles secreted to the extracellular environment by most cell types. They are key mediators of cell-to-cell communication in many different contexts, including the immune response[1,2] and tumour progression[3,4]. Exosomes originate in endosomal compartments called multivesicular bodies (MVBs), which are late endosomes containing multiple intraluminal vesicles (ILVs) formed by the invagination of the endosomal membrane. When MVBs fuse with the plasma membrane, ILVs are released as exosomes[5]. Alternatively, MVBs can fuse with the lysosomal compartment, resulting in degradation of their content.

Exosome composition is not a mere copy of cytosolic content; rather, specific proteins and nucleic acids are selectively sorted into exosomes. The amount and content of exosomes can moreover change in response to different stimuli[6,7]. Such changes in exosome composition determine the final outcome of exosome-mediated communication[8,9].

The mechanisms that control exosome composition and content are still not well understood[10]. Posttranslational modifications such as ubiquitination may play an important role in the sorting of proteins into exosomes[11–13]. The endosomal sorting complex required for transport (ESCRT) recognizes ubiquitinated proteins and sorts them into ILVs[14]. The ESCRT complex is essential for the sorting of proteins such as epidermal growth factor receptor into MVBs that are degraded through fusion with lysosomes[15], but is also involved in the regulation of exosome composition and secretion[16,17]. Another ubiquitin-like protein (UBL) that can modify exosomal proteins is SUMO, whose conjugation to hnRNPA2B1 is essential for the sorting of microRNAs into exosomes[18], and enhances the secretion of α-synuclein into extracellular vesicles (EVs) in an ESCRT-dependent manner[19].

ISG15 is an interferon (IFN)-α/β-induced UBL[20], which exerts its functions in two distinct states: as a free molecule (intracellular and extracellular)[21] or conjugated to target proteins (ISGylation)[22,23]. Analogous to ubiquitin, ISG15 conjugation is mediated by the consecutive action of an E1-activating enzyme (Ube1L), an E2-conjugating enzyme (UbCH8) and E3 ligases (mHERC6/hHERC5)[24–26], and counteracted by the specific isopeptidase USP18 (ref. 27). ISGylation was shown to occur in a co-translational process favouring modification of viral proteins in infected cells, which, in turn, interferes with virus assembly or function[28–30]. Furthermore, cellular proteins involved in antiviral defense or export of viral particles have been shown to be ISGylated, supporting the antiviral function of ISG15 (ref. 28). Studies in mice have demonstrated a role for ISG15 in antiviral immunity. Hence, mice lacking ISG15 exhibit a higher susceptibility to several pathogens including virus[31] and bacteria[32], and this is reverted in USP18-mutant mice, in which high levels of ISG15 conjugation are observed[33]. However, human ISG15 seems to have critical immune functions but not in antiviral immunity; unlike mice, ISG15 deficiency increased viral resistance in humans[34]. Specifically, free extracellular human ISG15 is important in IFN-γ-dependent anti-mycobacterial immunity[21], whereas free intracellular ISG15 is involved in USP18-mediated downregulation of IFN-α/β signalling[35].

ISG15 expression blocks the process of virus-budding by different mechanisms such as the blockage of ESCRT machinery in HIV-infected cells[36], or in the case of Ebola and other enveloped virus infections, inhibiting the Nedd4 E3 ubiquitin ligase[37]. Interestingly, exosomes and viruses share many features, and some viruses have been shown to exploit exosome and microvesicle secretion pathways[38,39]. In addition, exosomes are enriched in ISGylation targets, such as TSG101 (ref. 40) and heat-shock proteins[41].

Here we show that IFN-I inhibits exosome secretion by inducing protein ISGylation. We demonstrate that the ISGylation of the MVB protein TSG101 induces its aggregation and degradation, and this is sufficient for impairing exosome secretion. Moreover, the ISGylation-induced defect in exosome secretion is rescued on inhibition of lysosomal function or autophagy.

Results

ISGylation inhibits exosome secretion. To analyse the role of ISGylation on exosome production, we first treated Jurkat T cells with IFN-I, to induce ISG15 expression and conjugation (Supplementary Fig. 1A), and purified the secreted EVs from their culture supernatants by a serial ultracentrifugation protocol. IFN-I treatment inhibited the secretion of the classical exosome markers CD63, TSG101 and CD81 in the purified EVs (Fig. 1a). A concomitant decrease in the exosomal markers on IFN-I treatment was also observed after an additional purification step by ultracentrifugation in a sucrose gradient (Supplementary Fig. 1B). Interestingly, the few EVs secreted by IFN-treated cells were recovered in different fractions than the EVs from non-treated cells, suggesting that they might be of different nature. To further investigate the function of ISGylation in controlling EVs secretion, we next overexpressed ISG15 and the machinery responsible for ISGylation (E1, E2 and E3) in HEK293 cells, which mimics the activation of the ISG15 pathway (Supplementary Fig. 1A)[24,28] without activating other pathways induced by IFN-I treatment. ISGylation induction inhibited the secretion of EVs containing CD63, TSG101 and CD81 (Fig. 1b). To dissect whether the inhibition in exosomal markers secretion was due to ISG15 overexpression itself or to increased ISG15 conjugation to proteins, we overexpressed the ISGylation machinery together with an ISG15 mutated at the carboxy-terminal (ISG15MUT), thus disabling protein conjugation. Cells overexpressing ISG15MUT showed higher levels of exosomal markers in comparison with ISG15WT (Fig. 1c), demonstrating that ISG15 conjugation to proteins, but not free ISG15, is required for the inhibition of exosomal markers secretion. Nanoparticle tracking analysis (NTA) showed a decrease in the number of particles secreted on ISG15WT overexpression in comparison with ISG15MUT-expressing cells (Supplementary Fig. 1C), indicating that ISGylation is not causing a mere decrease in the sorting of exosomal markers in EVs, but an actual decrease in exosome secretion. However, NTA did not reveal any significant decrease in the secretion of nanoparticles on IFN-I treatment (Supplementary Fig. 1D).

To study the role of ISG15 in exosome secretion in a more physiological context, we analysed the secretion of exosomes by primary cells from wild-type (*WT*), ISG15 knockout (*ISG15KO*)[42] and *USP18C61A* mice, which have the ISG15 de-conjugating enzyme USP18 enzymatically inactive and thus show higher levels of protein ISGylation[33]. Consistent with the inhibition of exosome secretion induced by ISGylation, IFN-I treatment decreased exosome secretion in primary bone marrow-derived macrophages (BMDMs) from *WT* mice but not in ISG15-deficient macrophages (Fig. 1d). Furthermore, BMDMs from *USP18C61A* mice secrete less exosomes than either *WT* or *ISG15KO* mice on ISGylation induction by IFN-I, supporting the role of ISG15 protein conjugation in the regulation of exosome secretion. Similar results were also obtained with primary T lymphoblasts (Supplementary Fig. 1E). To assess the role of ISGylation *in vivo,* poly (I:C) was injected intraperitoneally into *WT*, *ISG15KO* and *USP18C61A* mice, to induce ISG15 expression[43], and exosomes from blood serum analysed. Interestingly, there were less exosomes in serum from poly (I:C)-injected *WT* than *ISG15KO* mice, and even less exosomes in

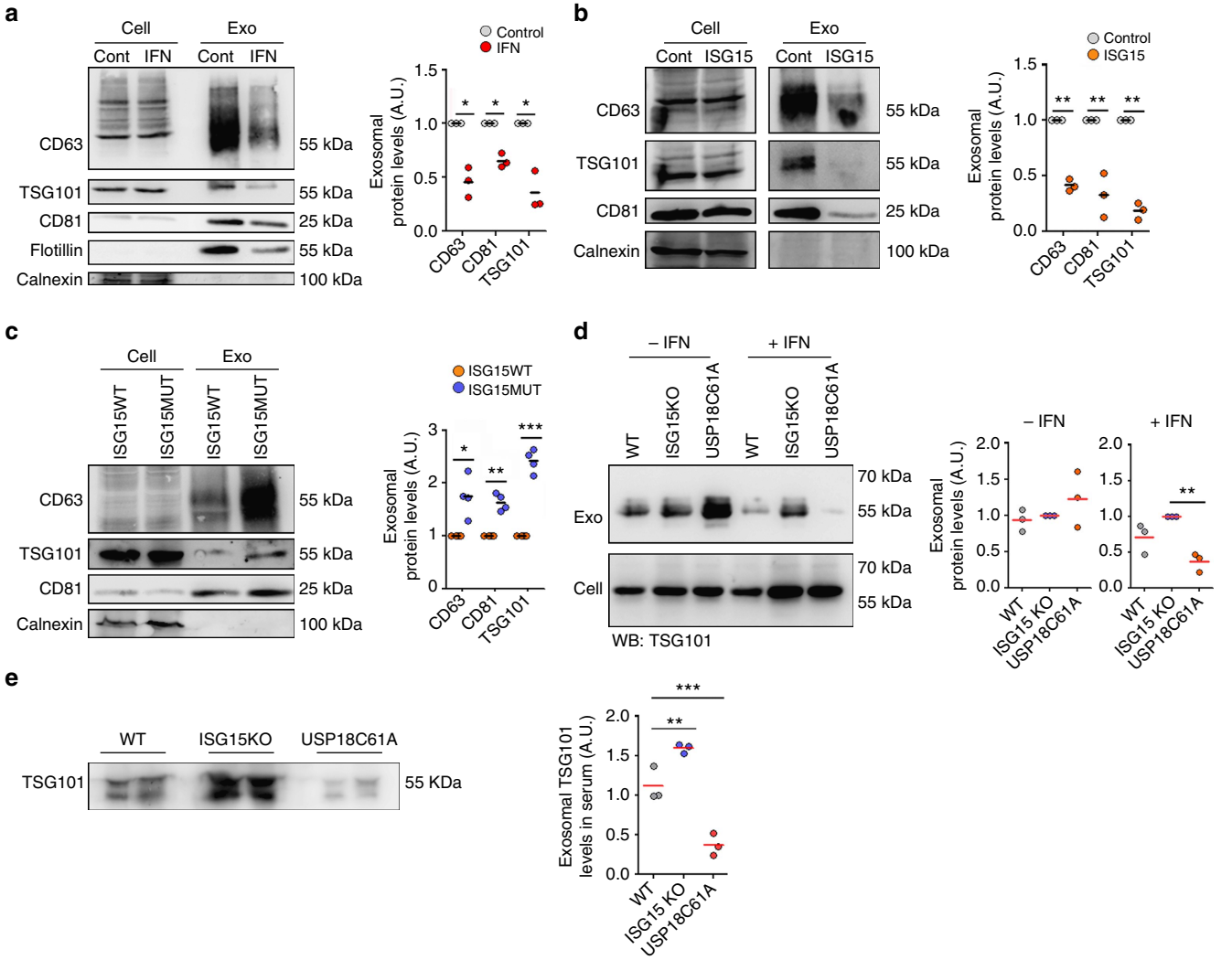

Figure 1 | ISGylation inhibits exosome secretion. (**a**) Western blot analysis of EVs purified by serial ultracentrifugation from cell culture supernatants from equal numbers of Jurkat T cells untreated (Cont) or treated with 1,000 U ml^{-1} IFN-I for 16 h. Cells and EVs (Exo) were blotted for the exosomal markers CD63, TSG101, Flotillin and CD81, and for the endoplasmic reticulum marker Calnexin. Right graph: quantification of exosomal protein levels in the EVs obtained from IFN-I-treated and untreated cells in three independent experiments. (**b**) Western blot analysis of the EVs obtained from equal numbers of untransfected HEK293 cells (Cont) or co-transfected with ISG15 and the ISGylation machinery; E1, E2, E3 ligases (ISG15). Cells and EVs (Exo) were blotted for CD63, TSG101, CD81 and Calnexin. Right graph: quantification of exosomal protein levels in the EVs obtained from untransfected HEK293 cells or co-transfected with ISG15 and the ISGylation machinery in three independent experiments. (**c**) Western blot analysis of the EVs obtained from equal numbers of HEK293 cells co-transfected with plasmids encoding the ISGylation machinery and the functional (ISG15WT) or mutated ISG15 (ISG15MUT). Cells and EVs (Exo) were blotted for CD63, CD81 and Calnexin. Right graph: quantification of exosomal protein levels in four independent experiments. (**d**) Western blot analysis of the EVs obtained from equal numbers of *WT*, *ISG15KO* and *USP18C61A* BMDMs treated 16 h with IFN-I or left untreated. Cells and EVs were blotted for TSG101 and quantification of exosomal protein levels of IFN-I-treated and -untreated cells is shown for three independent experiments. (**e**) Western blot analysis of the EVs obtained in blood serum from poly(I:C)-injected *WT*, *ISG15KO* and *USP18C61A* mice. EVs were isolated from 250 µl of serum and blotted for TSG101. Right graphs: quantification of exosomal TSG101 protein levels of three mice per genotype; *t*-test **P*-value < 0.05, ***P*-value < 0.001 and ****P*-value < 0.0001.

serum from injected *USP18C61A* mice (Fig. 1e), demonstrating the role of ISGylation in the inhibition of exosome secretion *in vivo*. Overall, our gain- and loss-of-function experiments strongly support the role of ISGylation in the regulation of exosome secretion *in vitro* and *in vivo*.

ISGylation decreases MVB numbers. To investigate the mechanisms by which ISGylation controls exosome secretion, MVBs were studied. Hepatocyte growth factor-regulated tyrosine kinase substrate (HRS) is involved in MVB formation and exosome secretion[17,44], and it has been previously used as a marker of MVBs, being present in intermediates between early and late MVBs positive for TSG101 and LBPA[44,45]. ISGylation induction resulted in a more perinuclear and clustered localization of HRS, as shown by the increase in the size of HRS$^+$ structures (Fig. 2a), and decreased the number of HRS$^+$ spots per cell (Supplementary Fig. 2A). Similar results were obtained with the MVB marker CD63 (Fig. 2a and Supplementary Fig. 2A), whereas the early endosome (EE) marker EEA1 did not show any apparent alteration (Supplementary Fig. 2B). Electron microscopy analyses revealed significant reduced MVBs numbers and density on ISGylation induction (Fig. 2b). In accordance, IFN-I treatment reduced HRS$^+$ spots in WT macrophages but not in *ISG15KO*

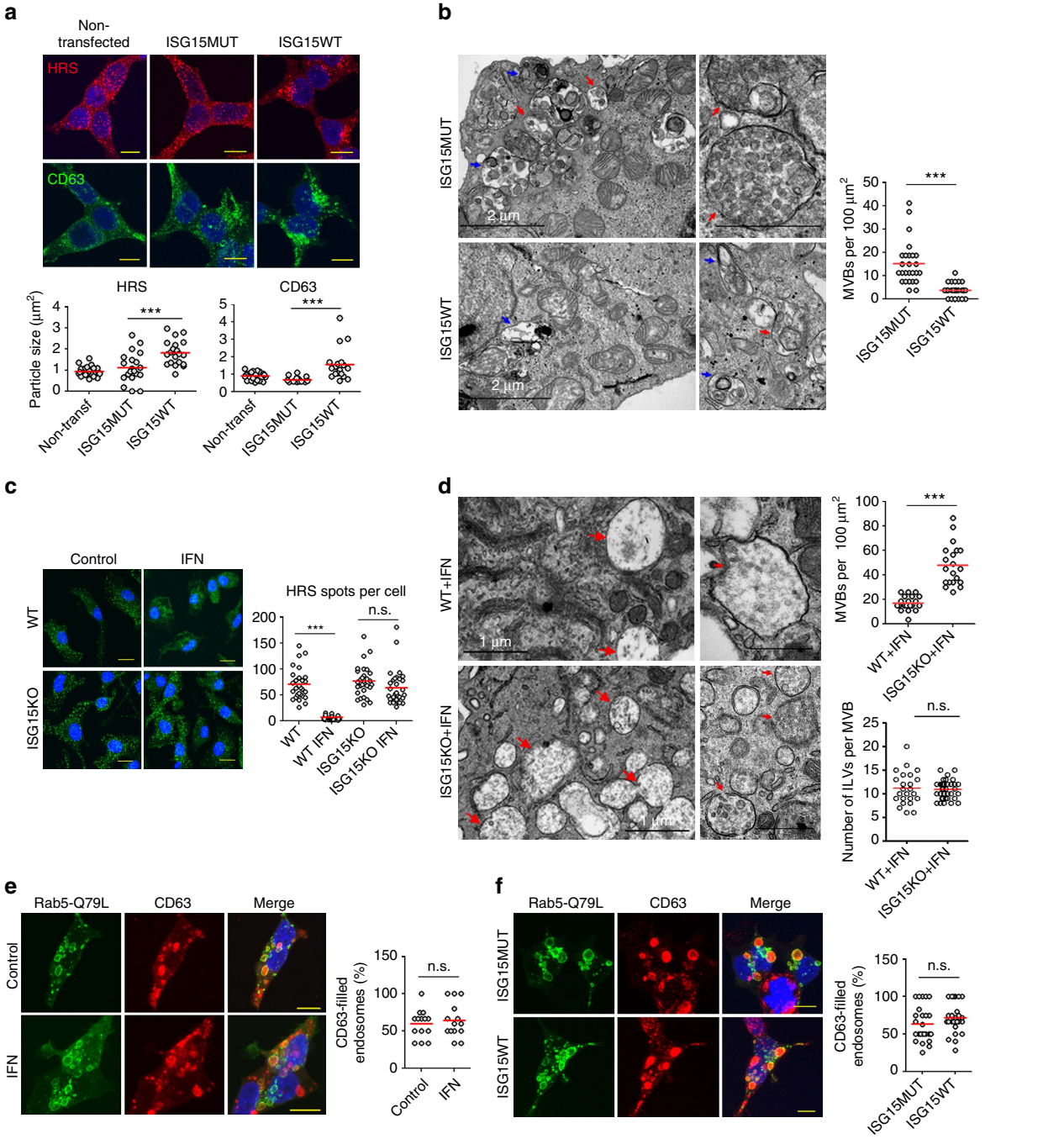

Figure 2 | ISGylation decreases MVB numbers. (**a**) Confocal microscopy analysis of the endosome markers HRS (red) and CD63 (green) in non-transfected HEK293 cells or HEK293 cells co-transfected with plasmids encoding the ISGylation machinery and the functional (ISG15WT) or mutated ISG15 (ISG15MUT). Scale bar, 10 μm. Right graph: quantification of HRS^+ and $CD63^+$ average particle size per cell ($n=20$). Each dot represents the average particle size from individual cells and mean is indicated in red lines. (**b**) Electron microscopy images showing representative fields with MVBs (red arrows) and lysosomes/autophagosomes (blue arrows) in HEK293 transfected as in **a**. Right graph: quantification of MVB numbers in more than 25 fields per condition. Each dot represents the number of MVBs per section and mean is indicated in red lines. Scale bar (insets), 500 nm. (**c**) Confocal microscopy analysis of HRS in *WT* or *ISG15KO* BMDMs left untreated or treated with 1,000 U ml^{-1} IFN for 16 h. Scale bar, 10 μm. Right graph: quantification of the number of HRS^+ particles per cell. Each dot represents the number of HRS^+ particles from individual cells and mean is indicated in red lines ($n=28$). (**d**) Electron microscopy images showing MVBs (red arrows) in *WT* or *ISG15KO* BMDMs treated with 1,000 U ml^{-1} IFN for 16 h. Upper graph, quantification of MVB numbers in 20 fields per condition. Each dot represents the number of MVBs per section and mean is indicated in red lines. Lower graph, quantification of ILV numbers per MVB. Each dot represents the number of ILVs per MVB and mean is indicated in red lines ($n\geq 24$). Scale bar (insets), 500 nm. (**e**) Confocal microscopy analysis of CD63 (red) in Rab5-Q79L-GFP^+ endosomes (green). HEK293 cells were transfected with Rab5-Q79L-GFP and treated 16 h with 1,000 U ml^{-1} IFN or left untreated. (**f**) Confocal microscopy analysis of CD63 (red) in Rab5-Q79L-GFP^+ endosomes (green). HEK293 cells were co-transfected with Rab5-Q79L-GFP mutant, the ISGylation machinery and ISG15WT or ISG15MUT. Images from **e**,**f**: Scale bar, 10 μm. Right graphs: each dot represents the percentage of CD63-filled endosomes per individual cell and mean is indicated in red lines; *t*-test; NS: *P*-value > 0.05 and ***P*-value < 0.0001.

macrophages (Fig. 2c), and MVBs were more abundant in *ISG15KO* macrophages than in their WT counterparts on IFN-I treatment (Fig. 2d), overall suggesting a role for ISG15 in regulating MVB numbers.

To ascertain whether ISGylation decreases MVB numbers by affecting MVB formation, we transfected HEK293 cells with the constitutively active Rab5-Q79L-GFP mutant, which forms large endosomes with a mixed morphology between EE and MVBs, which facilitates the study of the first steps in MVB biogenesis[46,47]. ISGylation induction by either IFN-I or ISG15 overexpression did not affect the sorting of the exosomal protein CD63 into Rab5-Q79L-GFP endosomes (Fig. 2e,f). Furthermore, quantitative electron microscopy analyses did not show any significant differences in the number of ILVs per MVB on ISGylation induction (Supplementary Fig. 2C,D). To rule out any possible side effect derived from the uneven distribution of small ILVs within enlarged MVBs[48], ILV numbers were also quantified in the absence of Rab5-Q79L-GFP overexpression. Accordingly, macrophages from *WT* and *ISG15KO* mice also showed similar levels of ILVs per MVB on ISGylation induction by IFN (Fig. 2d). Altogether, these data support that ISGylation does not impair the formation of ILVs, suggesting that it is mainly affecting later stages on the MVB pathway.

ISGylation induces protein aggregation and degradation. We then sought to understand how ISGylation regulates MVB numbers and exosome secretion. For this, we used ISG15 fusion proteins as models of protein ISGylation, as previously described for other posttranslational modifications such as ubiquitin or other UBLs[49–51]. Although fusion proteins are not exactly the same than endogenous ISGylation in lysines, in our ISG15 fusion proteins the C-terminal glycine of ISG15 is fused to the NH_2 group of the target protein in the N-terminal amino acid through a peptidic bond, which is chemically analogue to the isopeptidic bond formed between the endogenous ISG15 and the NH_2 group of a target protein lysine.

Confocal analysis showed partial co-localization of ISG15-GFP fusion protein with the MVB marker HRS and with the aggresome marker p62 (ref. 52 and Fig. 3a,b), whereas no co-localization was detected with the EE marker EEA1 (Supplementary Fig. 3A). Notably, ISGylation increased the co-localization of HRS with the lysosome marker LAMP1 (Fig. 3c), although neither LAMP1 content nor localization were affected (Supplementary Fig. 3B).

Despite its co-localization with MVB markers, green fluorescent protein (GFP) was not found in exosomes when fused to ISG15 (Fig. 3d) but rather promoted its accumulation in detergent-insoluble cell fractions (Fig. 3e), indicating that ISGylation promotes protein aggregation. Western blot analysis of cycloheximide-treated cells showed that when fused to ISG15, GFP is degraded faster than GFP alone or when fused to the ubiquitin-like modifier SUMO2, and that this degradation is delayed by the lysosome inhibitor Bafilomycin A1 but not by the proteasome inhibitor MG132 (Fig. 3f and Supplementary Fig. 3C–E), thus indicating that ISGylation of proteins promotes their degradation through the lysosome.

Inhibition of MVB–lysosome fusion rescues exosome secretion. To assess whether ISGylation inhibits exosome secretion by inducing MVB lysosomal degradation, we studied whether inhibition of MVB fusion with lysosomes could recover exosome secretion. Bafilomycin A1 is a proton pump inhibitor that increases the pH of lysosomes and inhibits trafficking between MVB and lysosomes[53,54]. Bafilomycin A1 treatment recovered exosome secretion in HEK293 cells in which ISGylation was induced by ISG15 overexpression (Fig. 4a), whereas it did not increase exosome secretion in control cells (Supplementary Fig. 4A), suggesting that ISGylation inhibits exosome secretion by re-routing MVB to lysosomes but is not impairing MVB biogenesis. This is also supported by the detection of ISGylated proteins in exosomes on secretion recovery (Supplementary Fig. 4B). Exosome secretion was also recovered despite ISGylation induction by IFN-I in Jurkat T cells when treated with Bafilomycin A1 (Supplementary Fig. 4C).

To avoid unspecific effects derived from the use of the inhibitor, we also studied exosome recovery on Rab7T22N dominant-negative mutant expression, which inhibits both endosome–lysosome and autophagosome–lysosome fusion[55–58]. Rab7T22N expression rescued exosome secretion in HEK293 cells despite ISGylation induction by ISG15 overexpression (Fig. 4b), whereas it did not increase exosome secretion in control cells (Supplementary Fig. 4D), supporting that the ISGylation-induced inhibition of exosome secretion is mediated by MVB fusion and degradation by the lysosome.

Fusion of MVBs with autophagosomes on induction of autophagy by rapamycin has been reported[56]. Interestingly, the secretion of exosomes on ISGylation induction was also recovered on silencing of the autophagy mediator ATG5 (Fig. 4c), indicating that autophagy probably contributes to the decreased exosome release induced by ISGylation. Accordingly, IFN-I treatment promoted the localization of the autophagy mediator LC3 in more acidic compartments, presumably lysosomes, supported by the loss of GFP fluorescent signal in mRFP-GFP-LC3 tandem reporter (Fig. 4d). Notably, ISGylation induction by IFN-I treatment or ISG15 overexpression did not induce general autophagy, as evidenced by unaltered levels of p62 and other autophagy markers (Supplementary Fig. 4E,F), indicating that ISGylation promotes selective autophagy and degradation of MVB without inducing a global autophagy response.

ISG15 impairs exosome secretion by modifying TSG101. To elucidate the molecular mechanism by which ISGylation regulates exosome secretion, we focused on TSG101, a component of the ESCRT machinery involved in exosome biogenesis that has been shown to be ISGylated and to regulate the secretion of virus[40]. To confirm TSG101 ISGylation, we overexpressed the ISGylation machinery together with *WT* or mutated ISG15 fused to the V5 tag and performed V5 immunoprecipitation. Western blot analysis of TSG101 in V5-ISG15 but not in control or V5-ISG15MUT immunoprecipitates confirmed endogenous TSG101 ISGylation (Fig. 5a). Moreover, ISGylation induction by ISG15 overexpression induced endogenous TSG101 aggregation and accumulation in insoluble fractions (Fig. 5b). To address whether ISGylation of TSG101 is sufficient to inhibit exosome secretion, we generated a TSG101-GFP plasmid that mimics TSG101 ISGylation (referred as ISG15-TSG101-GG), in which ISG15 terminal glycine is conjugated to TSG101 N-terminal through a peptide bound that can be cleaved by the USP18 de-ISGylase (Supplementary Fig. 5A). Consequently, both ISGylated and de-ISGylated TSG101-GFP are detected in cells transfected with this plasmid (Fig. 5c). Interestingly, ISGylated TSG101-GFP accumulated in insoluble fractions and was degraded faster than de-ISGylated TSG101-GFP (Fig. 5d,e), consistent with ISGylation promoting TSG101 protein aggregation and degradation. The expression of the ISG15-TSG101-GG plasmid rescued exosome secretion in cells targeted for endogenous TSG101 (Fig. 5f and Supplementary Fig. 5B), probably due to the presence of a functional de-ISGylated form of TSG101. To circumvent this, we

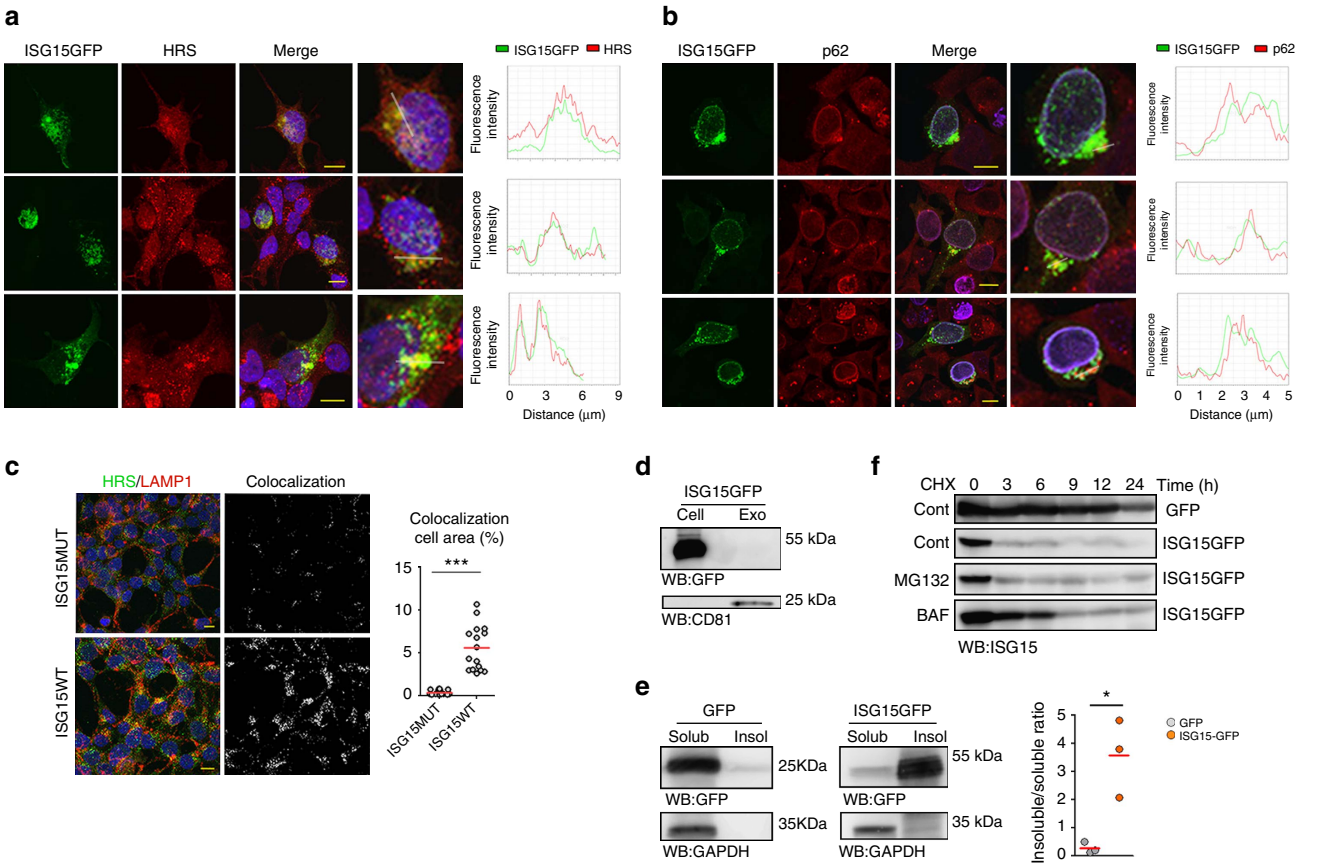

Figure 3 | ISG15 conjugation induces protein aggregation and degradation by lysosomes. (**a**) Confocal co-localization analysis of ISG15-GFP (green) and the MVB marker HRS (red). Right graphs: fluorescence intensity profiles of ISG15-GFP (green) and HRS (red) in the regions delineated by a white line. Nuclei were stained with DAPI. Scale bar, 10 μm. (**b**) Confocal co-localization analysis of ISG15-GFP (green) and p62 (red). Right graphs represent fluorescence intensity profiles of ISG15-GFP (green) and p62 (red) of the regions delineated by a white line. Nuclei were stained with DAPI. Scale bar, 10 μm. (**c**) Confocal microscopy analysis of HRS (green) and LAMP1 (red) co-localization in HEK293 cells co-transfected with ISGylation machinery and functional (ISG15WT) or mutated ISG15 (ISG15MUT). Nuclei were stained with DAPI. Scale bar, 10 μm. Co-localization area per cell was quantified by ImageJ ($n=16$). Each dot represents the percentage of co-localization area per cell surface and mean is indicated in red lines. (**d**) Western blot analysis of exogenous ISG15 in HEK293 cells transfected with ISG15-GFP. Cells and EVs (EXO) were blotted for GFP and CD81. (**e**) Western blot analysis of ISG15-GFP and GFP in 0.5% NP-40 soluble and insoluble cell fractions in HEK293 transfected with GFP or ISG15-GFP. Right graph: quantification of GFP and ISG15-GFP in the insoluble fraction respect to the soluble fraction in three independent experiments. (**f**) Western blot analysis of GFP and ISG15-GFP degradation kinetics in HEK293 cells transfected with GFP or ISG15-GFP and treated with cycloheximide to inhibit protein synthesis during the indicated times. Where specified, the medium was supplemented with the lysosome inhibitor Bafilomycin A1 (BAF) or the proteasome inhibitor MG132. A representative blot from two independent experiments is shown. Data from **c**,**e**: *t*-test $^{*}P$-value <0.05 and $^{***}P$-value <0.0001.

generated a non-de-ISGylable TSG101 mutant by changing ISG15 terminal glycines into alanines (ISG15-TSG101-AA), thus preventing TSG101 de-ISGylation (Fig. 5c). In cells devoid of endogenous TSG101, overexpression of the non-de-ISGylable TSG101 mutant did not restore the secretion of exosomes (Fig. 5g and Supplementary Fig. 5C), supporting that ISG15 conjugation to the ESCRT component TSG101 is sufficient to inhibit the secretion of exosomes.

Discussion

Cells secrete a variety of EVs including shedding vesicles, coming from the direct evagination of the plasma membrane, and exosomes, coming from endosomal compartments called MVBs. The membrane of MVB invaginates to form ILVs, which are secreted to the extracellular environment on MVB fusion with the plasma membrane[5]. MVBs can also fuse with the lysosomal compartment for the degradation of their content. There is evidence that different types of MVB co-exist in cells[59], although the differences in their composition and the mechanisms that control their biogenesis and final fusion with the lysosome or plasma membrane are not well understood[10]. In addition, on specific stimuli such as starvation or rapamycin treatment, MVBs can be re-routed to promote their fusion with the lysosomal compartment and thus avoid their fusion with the plasma membrane and the concomitant secretion of exosomes[56] demonstrating that the final fate of MVBs is not immutable but can change under specific conditions[60].

The role of the ESCRT complex in the sorting of ubiquitinated proteins into ILVs for their degradation in the lysosome is well known[61] and some of the ESCRT complex components are also involved in the secretion of exosomes and other EVs[12,17], although their precise role in the biogenesis of the different types of EVs is not known. Other ubiquitin-like modifiers have been shown to control the composition of EVs, for example, SUMOylation of hnRNPA2B1 promotes the sorting of specific microRNAs into exosomes[18], and also controls the sorting of α-synuclein into EVs[19]. Here we identify the ubiquitin-like modifier ISG15 as a novel regulator of the exosome pathway. We show that ISGylation induction by ISG15 machinery

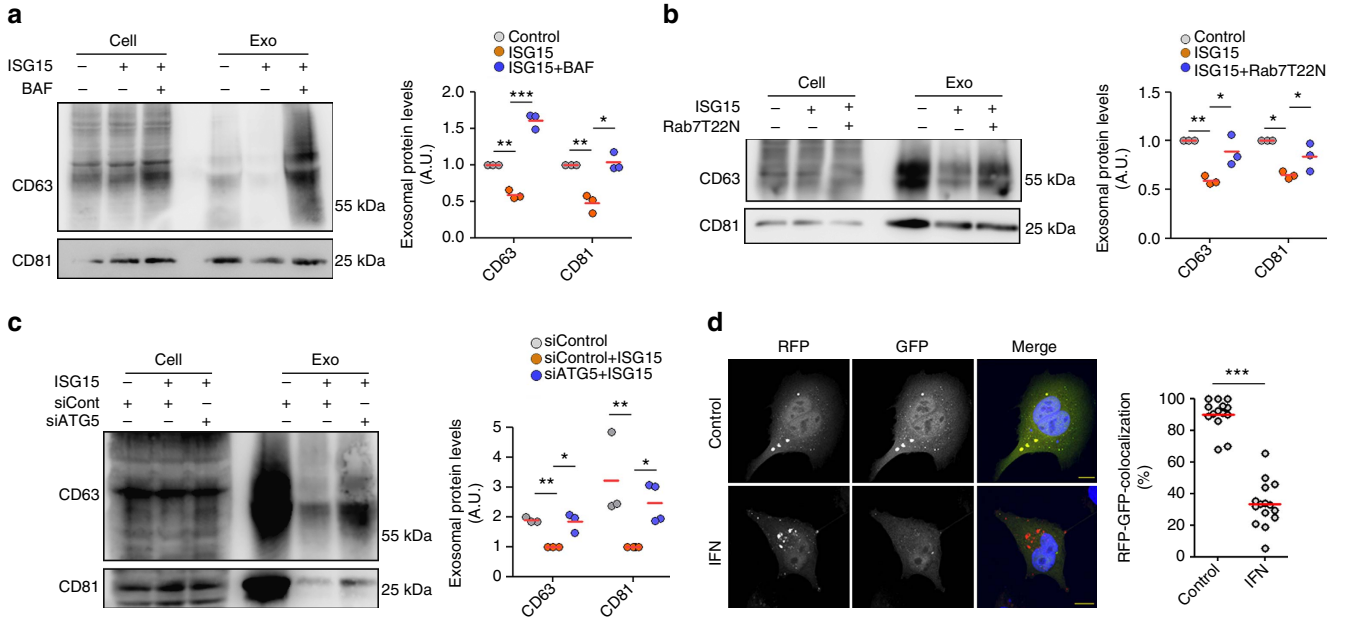

Figure 4 | Inhibition of lysosome function upon ISGylation induction rescues exosome secretion. (**a**) Western blot analysis of exosome secretion in untransfected HEK293 cells and HEK293 cells co-transfected with plasmids encoding the ISGylation machinery and ISG15, and treated with Bafilomycin A1 (BAF), when indicated. Cells and EVs (Exo) were blotted for CD63 and CD81. Right graph: quantification of exosomal protein levels in three independent experiments. (**b**) Western blot analysis of exosome secretion in HEK293 cells transfected with GFP or co-transfected with plasmids encoding ISG15 and the ISGylation machinery, and when indicated, with the Rab7T22N dominant-negative mutant. Cells and EVs were blotted for CD63 and CD81. Right graph: quantification of exosomal protein levels in three independent experiments. (**c**) Western blot analysis of exosome secretion in HEK293 cells transfected with control small interfering RNAs (siRNAs) or siRNAs targeting ATG5. After 48 h, cells were re-transfected with siRNAs together with plasmids encoding ISG15 and ISGylation machinery. Cells and EVs (Exo) were blotted for CD63 and CD81. Right: quantification of exosomal protein levels in three or four independent experiments. (**d**) Confocal analysis of LC3 localization into acidic compartments in HEK293 cells transfected with LC3-RFP-GFP tandem plasmid and treated 16 h with IFN-I where indicated. Nuclei were stained with DAPI. Scale bar, 10 μm. Images were processed by ImageJ and the number of RFP^+ and RFP^+GFP^+ dots quantified. Each dot represents the percentage of RFP^+GFP^+ dots per individual cell and mean is indicated in red lines; *t*-test; ***P-value < 0.001. Data **a**,**b**,**c**: analysis of variance; *P-value < 0.05, **P-value < 0.001 and ***P-value < 0.0001.

overexpression or IFN-I decreases the secretion of exosomal markers. Importantly, experiments with the non-conjugable ISG15MUT and with primary cells from mice with defective function of the specific ISG15 de-ISGylase USP18 demonstrated that this effect is mediated by ISG15 conjugation to proteins and not by free ISG15. ISGylation induction by ISG15 overexpression induces a decrease in microparticle secretion, indicating that ISGylation is not merely decreasing the sorting of certain exosomal markers into ILVs but is actually decreasing exosome secretion. However, ISGylation induction by IFN-I does not induce a significant decrease in the number of secreted microparticles. This could be due to the induction of the secretion of other types of EVs by IFN-I and this is in agreement with previous reports showing that IFN-I can promote the secretion of EVs loaded with antiviral components that are transferred to other cells[62]. In fact, on ultracentrifugation in sucrose gradients, the few EVs secreted by IFN-treated cells are recovered in different fractions than the EVs from non-treated cells, suggesting that they might have a different nature. Alternatively, the absence of effect of IFN on global particle secretion may indicate that only the EVs derived from MVBs are affected.

We also show that ISGylation decreases the numbers of MVBs, but does not prevent the formation of ILVs. The secretion of exosomes is recovered when the fusion of MVB with lysosomes or autophagosomes is inhibited, indicating that the observed inhibition of exosome secretion is mainly mediated by the induction of MVB degradation by the lysosome. In accordance, we show that ISGylation promotes the aggregation and degradation of proteins by the lysosome, and this is in agreement with previous reports in which ISG15-linked proteins associated with the proteins p62 and HDAC-6 involved in the autophagic process[52]. We have observed that ISGylation decreases the number of HRS^+ structures without preventing the formation of ILVs, possibly reflecting an accelerated degradation of endosomes. In addition, ISGylation increases the co-localization of the lysosome marker LAMP-1 with HRS, which is usually absent from LAMP-1-positive structures[44]. Whether ISGylation of MVB proteins induces the rapid fusion of MVB with lysosomes in an earlier stage of maturation, or whether it directly impairs HRS dissociation from endosomal membranes is not known.

A number of ISG15 target proteins are typically present in exosomes and MVBs[41], including several components of the ESCRT complex such as TSG101, CHMP2A, CHMP4B and CHMP6 (refs 40,63,64). It is therefore conceivable that ISG15 is recruited to MVB by conjugating endosomal proteins. There, it may promote protein aggregation and enhance MVB degradation by the autophagosome–lysosome compartment, thus preventing their fusion with the plasma membrane and the secretion of exosomes (Fig. 6). We have validated the ISGylation of TSG101, which has been previously shown to control the secretion of viral particles[40], and we show that TSG101 ISGylation is sufficient to impair exosome secretion. However, we cannot rule out the possibility that other endosomal proteins are being ISGylated and also contribute to the inhibition of exosome secretion induced by ISG15. TSG101 depletion has been previously shown to inhibit MVB formation[65] or to modify the size of MVBs and/or the number of ILVs[48]. However, there are significant differences

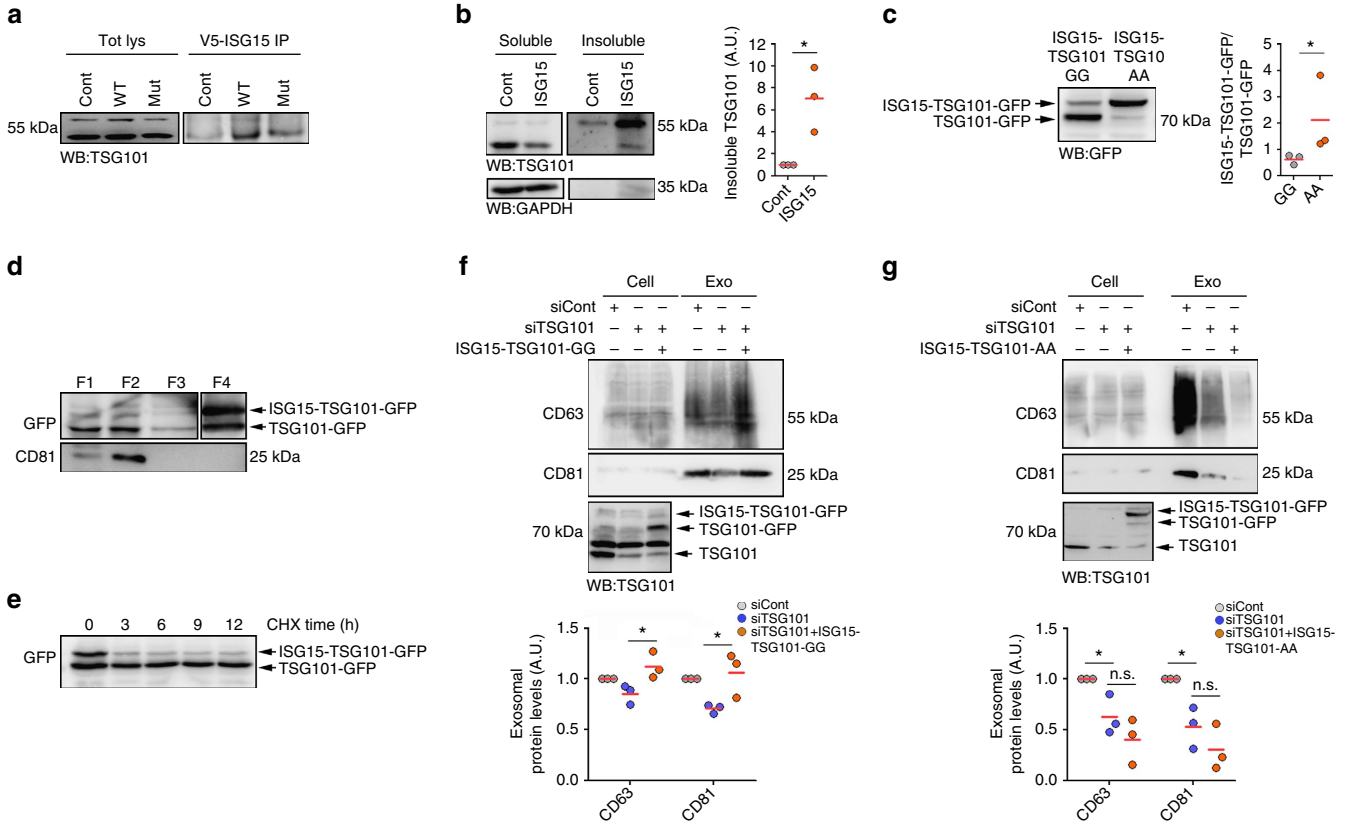

Figure 5 | ISG15 impairs exosome secretion by modifying TSG101. (**a**) Western blot analysis of TSG101 immunoprecipitation in HEK293 cells non-transfected or HEK293 cells co-transfected with plasmids encoding the ISGylation machinery and functional (ISG15WT) or mutated ISG15 (ISG15MUT). Total lysates and V5 immunoprecipitates were blotted for TSG101. (**b**) Western blot analysis of 0.5% NP-40 soluble and insoluble fractions from non-transfected HEK293 cells (Cont) or cells transfected with ISG15 and ISGylation machinery (ISG15). Soluble and insoluble fractions were blotted for TSG101 and GAPDH. Right graph: quantification of TSG101 protein levels in insoluble fractions in three independent experiments. (**c**) Western blot analysis of TSG101-GFP ISGylation in HEK293 cells transfected with ISG15-TSG101-GFP-GG or with the non-de-ISGylable mutant ISG15-TSG101-GFP-AA. Cell lysates were blotted for GFP. Right graph: quantification of ISG15-TSG101-GFP/TSG101-GFP ratio in three independent experiments. (**d**) Western blot analysis of ISG15-TSG101-GFP and TSG101-GFP subcellular distribution in HEK293 cells transfected with ISG15-TSG101-GFP-GG. Fractions corresponding to cytosol (F1), membranes (F2), nucleus (F3) and insoluble aggregates (F4) were extracted and blotted for GFP and CD81. A lower exposition of the same blot is shown for F4. (**e**) Western blot analysis of ISG15-TSG101-GFP and TSG101-GFP degradation kinetics in HEK293 cells transfected with ISG15-TSG101-GFP-GG and treated with cycloheximide during the indicated times. Cell lysates are blotted for GFP. (**f**) Western blot analysis of HEK293 cells transfected with control small interfering RNAs (siRNAs) or siRNAs targeting TSG101. When indicated, cells were co-transfected with ISG15-TSG101-GFP-GG. Cells and EVs (EXO) were blotted for CD63 and CD81. Lower gel shows cell lysates blotted for TSG101 to check TSG101 silencing and exogenous overexpression. Lower graph: quantification of exosomal protein levels in three independent experiments. (**g**) Western blot analysis of HEK293 cells transfected with control siRNAs or siRNAs targeting TSG101. When indicated, cells were co-transfected with the non-de-ISGylable mutant ISG15-TSG101-GFP-AA. Cells and EVs (EXO) were blotted for CD63 and CD81. Lower gel shows cell lysates blotted for TSG101 to check TSG101 silencing and exogenous overexpression. Lower graph: quantification of exosomal protein levels in three independent experiments. Data **b**,**c**: *t*-test; NS: *P*-value > 0.05 and **P*-value < 0.05. Data **f**,**g**: analysis of variance; NS: *P*-value > 0.05 and **P*-value < 0.05.

between depletion and ISGylation of TSG101. ISG15 may be directed to endosomes in a later stage of their maturation and here modify MVB proteins such as TSG101, and promote their aggregation and subsequent degradation by the lysosome without impairing ILV biogenesis. However, we could not completely rule out any effect of ISGylation on MVB biogenesis.

ISGylation has been previously shown to exert an antiviral activity by blocking the exit of viral particles[36,40,64,66]. The ISGylation of multiple MVB proteins and the consequent inhibition of exosome secretion induced by IFN-I would prevent the spreading of viruses that exploit the MVB pathway for their way out the cell. In addition, exosomes play important roles in cell-to-cell communication during the immune response, tumour progression, neuron survival and many other contexts[1,3,4,67]. Therefore, ISGylation induction by different stimuli such as viral infection, IFN, ischaemia[68] or ageing[69] can be an important mechanism to regulate exosome-mediated communication in many different situations.

Methods

Cell culture. The human Jurkat-derived T-cell line J77cl20 (TCR Vαl. 2 Vβ8) was cultured in RPMI (Sigma) containing 10% fetal bovine serum (FBS; Invitrogen). The HEK293T cell line was cultured in DMEM medium (Sigma) containing 10% FBS (Invitrogen).

Mouse primary macrophages (BMDMs) were obtained from the bone marrow of C57BL/6 *WT*, ISG15 knockout[42] and *USP18C61A* mice[33] (kindly provided by K. Knobeloch, Freiburg University, Germany). Cells were cultured RPMI-1640 supplemented with macrophage colony-stimulating factor (30% mycoplasma-free L929 cell supernatant, NCBI Biosample accession number SAMN00155972) for 6 days, to induce cell differentiation.

Mouse primary T lymphocytes were obtained from cell suspensions prepared from spleens and peripheral lymph nodes of C57BL/6 *WT*, *ISG15KO USP18C61A* mice. Cells were cultured for 36–48 h in RPMI with 2 μg ml^{-1} concanavalin A (Sigma) and subsequently 50 U ml^{-1} human recombinant IL-2 (Glaxo) was added

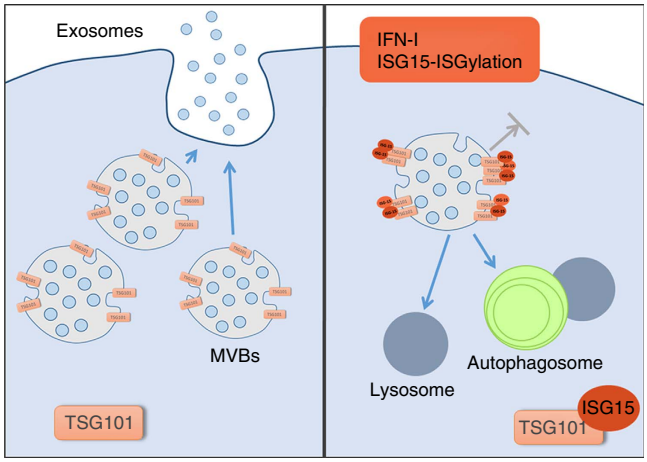

Figure 6 | Proposed model for the role of ISGylation in the regulation of exosome secretion. IFN-I induces ISG15 expression and conjugation to MVB proteins such as TSG101. ISGylation of MVB proteins promotes MVB fusion with lysosomes and degradation, thus inhibiting exosome secretion.

to the medium every 2 days for at least 4–6 days, to obtain differentiated T lymphoblasts.

Exosome purification. Cells were cultured in medium supplemented with 10% exosome-depleted FBS (bovine exosomes were removed by overnight centrifugation at 100,000 *g*). Supernatant fractions were collected from 16 to 20 h cell culture supernatants and exosomes were obtained by serial centrifugation as follows. Cells were pelleted (320 × *g* for 10 min) and the supernatant was centrifuged at 2,000 *g* for 15 min, to discard debris and dead cells. The supernatant was collected and ultracentrifuged at 10,000 *g* for 30 min at 4 °C (Beckman Coulter Optima L-100 XP, Beckman Coulter) and exosomes were pelleted by ultracentrifugation at 100,000 *g* for 70 min at 4 °C. The exosome pellet was washed in PBS and collected by ultracentrifugation at 100,000 *g* for 70 min (Beckman Coulter Optima L-100 XP, Beckman Coulter).

Nanoparticle tracking analysis. Exosome numbers and size distribution were determined by measuring the rate of Brownian motion using a NanoSight LM10 system, which is equipped with fast video capture and particle-tracking software (NanoSight, Amesbury, UK). Samples were diluted before analysis to between 2×10^8 and 20×10^8 particles per ml, and the relative concentration was calculated according to the dilution factor. Data analysis was performed with *NTA 2.1* software (Nanosight). Samples were analysed using manual shutter and gain adjustments, which resulted in shutter speeds of 15 or 30 ms, with camera gains between 280 and 560. The detection threshold was kept above 2; blur: auto; minimum expected particle size: 50 nm.

ISGylation induction by overexpression. HEK293 cells were co-transfected with plasmids encoding human E1, E2 and E3 ligases (kindly provided by A. García-Sastre, Mount Sinai Hospital, NYC) together with plasmids encoding WT or C-terminal mutated human ISG15 fused to the V5 tag. When indicated, cells were co-transfected with the appropriate small interfering RNAs or with the EGFP-Rab7A T22N plasmid (gift from Qing Zhong, Addgene plasmid 28048). Cells were transfected using Lipofectamine 2000 (Invitrogen). Twenty-four hours after transfection, cells were cultured in exosome-depleted medium for 20 h and exosomes were isolated from supernatants as described above. When indicated, cells were incubated overnight in exosome-depleted medium containing 20 nM Bafilomycin A1 (Merck).

Exosome extraction from blood serum. WT, *ISG15KO* and *USP18C61A* mice were treated with 5 μg g^{-1} body weight poly (I:C) (InvivoGen) intraperitoneally. Blood samples were extracted from the heart 24 h after poly (I:C) injection and allowed to clot 3 h at room temperature. Blood samples were kept 2 h at 4 °C and serum was obtained by centrifugation at 400 *g*, 10 min at 4 °C. Cell debris were removed by centrifugation at 3,000 *g*, 15 min at 4 °C and serum samples were stored at − 20 °C. Exosomes were extracted from serum as previously described[70]; briefly, 125 μl of Exoquick reagent were added to 250 μl of serum and incubated overnight at 4 °C. Samples were centrifuged at 1,500 *g*, 30 min and exosome pellets resuspended in RIPA buffer.

Gene silencing. HEK293 cells were transfected using Lipofectamine 2000 (Invitrogen) with the following small interfering RNAs: control (scrambled), ATG5 and TSG101 (SIGMA). Twenty-four hours after transfection, cells were cultured in exosome-depleted medium for 20 h and exosomes were isolated from supernatants as described above.

Western blotting. Cells or exosomes were lysed in RIPA buffer (50 mM Tris-HCl pH 8, 150 mM NaCl, 1% Triton X-100, 0.1% sodium deoxycholate and 0.1% SDS) containing a protease inhibitor cocktail (Complete, Roche). Proteins were separated on 10% acrylamide/bisacrylamide gels and transferred to a nitrocellulose membrane. Membranes were incubated with primary antibodies (1:1,000) and peroxidase-conjugated secondary antibodies (1:5,000), and proteins were visualized with LAS-3000. The following antibodies were used: rabbit anti-human ISG15 (Proteintech, 15981-1-AP), mouse anti-human CD63 (Calbiochem, OP171), mouse 5A6 anti-human CD81 (Santa Cruz, sc-23962), mouse anti-human TSG101 (Abcam, GTX70255), mouse anti-GFP (Living colors, 632381), rabbit anti-p62 (Sigma, P0067), mouse DM1A anti-tubulin (Sigma, F2168), rabbit anti-Calnexin (Abcam, ab10286), goat anti-mouse peroxidase (Thermo Scientific), goat anti-rabbit peroxidase (Thermo Scientific) and donkey anti-goat peroxidase (Thermo Scientific). Full immunoblots are provided in Supplementary Fig. 6.

Fluorescence confocal microscopy. For immunofluorescence assays, cells were plated onto slides coated with fibronectin (20 μg ml^{-1}), incubated for 16 h min, fixed with 2% paraformaldehyde and stained with the indicated primary antibodies (1:100) followed by secondary antibodies (1:500). When indicated, cells were previously transfected with GFP-Rab5CA (Q79L) plasmid (gift from Sergio Grinstein, Addgene plasmid 35140) or LC3-GFP-RFP tandem construct (gift from Tamotsu Yoshimori, Addgene plasmid 21074). Samples were examined with a Leica SP5 confocal microscope (Leica) fitted with a × 63 objective and images were processed and assembled using Leica software. The following antibodies were used: anti-CD63 (clone Tea 3/18, generated in the laboratory), anti-HRS (Abcam, ab72053), anti-EE1A (Santa Cruz, sc-6415), anti-LAMP1-647 (BioLegend, 328612), anti-p62 (Sigma, P0067), goat anti-mouse-488 and goat anti-rabbit-RX (Life Technologies). Images were processed and quantified using LAS-AF and ImageJ.

Cloning. ISG15-GFP plasmids were generated by excision of ISG15 from the pCAGG plasmid with XhoI and EcoICRI restriction enzymes, followed by insertion between the XhoI and AfeI sites of pAcGFP-N1. ISG15 stop codons were mutated using the QuickChange Site-Directed Mutagenesis kit (Agilent). ISG15-TSG101-GFP was obtained by inserting TSG101 into ISG15-GFP plasmid with XhoI and BamHI restriction enzymes. Non-de-ISGylable mutant ISG15-TSG101-GFP-AA was obtained by mutated terminal glycines into alanines using the QuickChange Site-Directed Mutagenesis kit (Agilent). Ubiquitin-GFP expressing plasmid was obtained from Addgene (gift from Nico Dantuma, Addgene plasmid 11928).

Protein aggregation. HEK293 cells were transfected with GFP or ISG15-GFP plasmids using Lipofectamine 2000 (Invitrogen) and 48 h later lysed in lysis buffer (10 mM Tris-HCl pH 8, 100 mM NaCl, 1 mM EDTA, 0.5% NP40 and 50 mM iodoacetamide) supplemented with protease inhibitor cocktail (Complete, Roche). Cells were centrifuged for 5 min a 13,000 *g*, and the supernatant (S1) and pellet (P1) were saved. P1 was resuspended in lysis buffer containing 2% SDS, sonicated and centrifuged at 16,000 *g* for 10 min. The pellet (P2) was resuspended in lysis buffer containing 2% SDS and sonicated. S1 and P2 were loaded on a poly-acrylamide gel and blotted for GFP. Subcellular fractionation was performed with ProteoExctarct Subcellular Proteome Extraction kit (Calbiochem).

Protein degradation. HEK293 cells were cultured in six-well-plates and transfected with GFP or ISG15-GFP using Lipofectamine 2000 (Invitrogen). Cells were treated with 40 μg ml^{-1} cycloheximide (Sigma) to inhibit protein synthesis and were lysed at the indicated time points. When indicated, the medium contained 20 nM Bafilomycin A1 (Merk) or 40 μM MG132 (Sigma).

Immunoprecipitation. 1×10^7 HEK293 cells per condition were lysed (25 mM Tris pH 8, 150 mM NaCl, 2 mM $MgCl_2$, 0.5% NP-40 and protease inhibitors) and incubated for pre-clearing with pre-washed Protein G Dynabeads (Invitrogen; 50 μl per condition; 1 h, 4 °C). Fifty microlitres of Dynabeads per condition were washed twice in 0.01% Tween PBS and resuspended in 200 μl of 0.01% Tween PBS containing 5 μg mouse anti-V5 antibody (Life Technologies) per condition and incubated 1 h at 4 °C. Pre-cleared lysates were incubated with antibody-conjugated Dynabeads (1.5 h, 4 °C). Antibody-conjugated Dynabeads were washed six times with lysis buffer and transferred to clean tubes. Protein loading buffer was added, samples were boiled at 95 °C for 5 min and processed for immunoblotting.

Electron microscopy and MVB quantification. Cells cultured on dishes were washed in PBS and fixed for 1 h in 2.5% glutaraldehyde in 0.1 M phosphate buffer at room temperature. Then, cells were slowly and gently scrapped and pelleted in eppendorf tubes. Pellets were washed in phosphate buffer and incubated with 1%

OsO_4 for 90 min at 4 °C. Then, samples were dehydrated, embedded in Spurr and sectioned using Leica ultramicrotome (Leica Microsystems). Ultrathin sections (50–70 nm) were stained with 2% uranyl acetate for 10 min and with a lead-staining solution for 5 min and observed using a transmission electron microscope, JEOL JEM-1010 fitted with a Gatan Orius SC1000 (model 832) digital camera.

For the calibration of images, quantification and analysis ImageJ was used. MVBs were identified and counted by morphology, having only discrete ILVs. Lysosomes contain multilamellar profiles. At least 20 MVBs were analysed per experiment from separate cells. Data were analysed from duplicate or triplicate separate experiments and two to four grids were used for each condition. The minimum number of cells scored for each condition was 20. Box scatter plots were generated using Prism GraphPad software and statistical tests were performed in Microsoft Excel. Data are means ± s.d. and ***P-value < 0.0001.

Data availability. The data that support the conclusions of this study are available from the corresponding author upon request.

References

1. Andreola, G. *et al.* Induction of lymphocyte apoptosis by tumor cell secretion of FasL-bearing microvesicles. *J. Exp. Med.* **195,** 1303–1316 (2002).
2. Thery, C. *et al.* Indirect activation of naive $CD4^+$ T cells by dendritic cell-derived exosomes. *Nat. Immunol.* **3,** 1156–1162 (2002).
3. Chalmin, F. *et al.* Membrane-associated Hsp72 from tumor-derived exosomes mediates STAT3-dependent immunosuppressive function of mouse and human myeloid-derived suppressor cells. *J. Clin. Invest.* **120,** 457–471 (2010).
4. Peinado, H. *et al.* Melanoma exosomes educate bone marrow progenitor cells toward a pro-metastatic phenotype through MET. *Nat. Med.* **18,** 883–891 (2012).
5. Kowal, J., Tkach, M. & Thery, C. Biogenesis and secretion of exosomes. *Curr. Opin. Cell Biol.* **29,** 116–125 (2014).
6. Blanchard, N. *et al.* TCR activation of human T cells induces the production of exosomes bearing the TCR/CD3/zeta complex. *J. Immunol.* **168,** 3235–3241 (2002).
7. van der Vlist, E. J. *et al.* CD4(+) T cell activation promotes the differential release of distinct populations of nanosized vesicles. *J. Extracell. Vesicles* **1,** 18364 (2012).
8. Hergenreider, E. *et al.* Atheroprotective communication between endothelial cells and smooth muscle cells through miRNAs. *Nat. Cell Biol.* **14,** 249–256 (2012).
9. Kucharzewska, P. *et al.* Exosomes reflect the hypoxic status of glioma cells and mediate hypoxia-dependent activation of vascular cells during tumor development. *Proc. Natl Acad. Sci. USA* **110,** 7312–7317 (2013).
10. Villarroya-Beltri, C., Baixauli, F., Gutierrez-Vazquez, C., Sanchez-Madrid, F. & Mittelbrunn, M. Sorting it out: regulation of exosome loading. *Semin. Cancer Biol.* **28,** 3–13 (2014).
11. Moreno-Gonzalo, O., Villarroya-Beltri, C. & Sanchez-Madrid, F. Post-translational modifications of exosomal proteins. *Front. Immunol.* **5,** 383 (2014).
12. Nabhan, J. F., Hu, R., Oh, R. S., Cohen, S. N. & Lu, Q. Formation and release of arrestin domain-containing protein 1-mediated microvesicles (ARMMs) at plasma membrane by recruitment of TSG101 protein. *Proc. Natl Acad. Sci. USA* **109,** 4146–4151 (2012).
13. Putz, U. *et al.* Nedd4 family-interacting protein 1 (Ndfip1) is required for the exosomal secretion of Nedd4 family proteins. *J. Biol. Chem.* **283,** 32621–32627 (2008).
14. Henne, W. M., Buchkovich, N. J. & Emr, S. D. The ESCRT pathway. *Dev. Cell* **21,** 77–91 (2011).
15. Levkowitz, G. *et al.* Ubiquitin ligase activity and tyrosine phosphorylation underlie suppression of growth factor signaling by c-Cbl/Sli-1. *Mol. Cell* **4,** 1029–1040 (1999).
16. Baietti, M. F. *et al.* Syndecan-syntenin-ALIX regulates the biogenesis of exosomes. *Nat. Cell Biol.* **14,** 677–685 (2012).
17. Colombo, M. *et al.* Analysis of ESCRT functions in exosome biogenesis, composition and secretion highlights the heterogeneity of extracellular vesicles. *J. Cell Sci.* **126,** 5553–5565 (2013).
18. Villarroya-Beltri, C. *et al.* Sumoylated hnRNPA2B1 controls the sorting of miRNAs into exosomes through binding to specific motifs. *Nat. Commun.* **4,** 2980 (2013).
19. Kunadt, M. *et al.* Extracellular vesicle sorting of alpha-Synuclein is regulated by sumoylation. *Acta Neuropathol.* **129,** 695–713 (2015).
20. Farrell, P. J., Broeze, R. J. & Lengyel, P. Accumulation of an mRNA and protein in interferon-treated Ehrlich ascites tumour cells. *Nature* **279,** 523–525 (1979).
21. Bogunovic, D. *et al.* Mycobacterial disease and impaired IFN-gamma immunity in humans with inherited ISG15 deficiency. *Science* **337,** 1684–1688 (2012).
22. Giannakopoulos, N. V. *et al.* ISG15 Arg151 and the ISG15-conjugating enzyme UbE1L are important for innate immune control of Sindbis virus. *J. Virol.* **83,** 1602–1610 (2009).
23. Lai, C. *et al.* Mice lacking the ISG15 E1 enzyme UbE1L demonstrate increased susceptibility to both mouse-adapted and non-mouse-adapted influenza B virus infection. *J. Virol.* **83,** 1147–1151 (2009).
24. Dastur, A., Beaudenon, S., Kelley, M., Krug, R. M. & Huibregtse, J. M. Herc5, an interferon-induced HECT E3 enzyme, is required for conjugation of ISG15 in human cells. *J. Biol. Chem.* **281,** 4334–4338 (2006).
25. Kim, K. I., Giannakopoulos, N. V., Virgin, H. W. & Zhang, D. E. Interferon-inducible ubiquitin E2, Ubc8, is a conjugating enzyme for protein ISGylation. *Mol. Cell Biol.* **24,** 9592–9600 (2004).
26. Yuan, W. & Krug, R. M. Influenza B virus NS1 protein inhibits conjugation of the interferon (IFN)-induced ubiquitin-like ISG15 protein. *EMBO J.* **20,** 362–371 (2001).
27. Ketscher, L. & Knobeloch, K. P. ISG15 uncut: dissecting enzymatic and non-enzymatic functions of USP18 *in vivo*. *Cytokine* **76,** 569–571 (2015).
28. Durfee, L. A., Lyon, N., Seo, K. & Huibregtse, J. M. The ISG15 conjugation system broadly targets newly synthesized proteins: implications for the antiviral function of ISG15. *Mol. Cell* **38,** 722–732 (2010).
29. Rahnefeld, A. *et al.* Ubiquitin-like protein ISG15 (interferon-stimulated gene of 15 kDa) in host defense against heart failure in a mouse model of virus-induced cardiomyopathy. *Circulation* **130,** 1589–1600 (2014).
30. Zhao, C., Hsiang, T. Y., Kuo, R. L. & Krug, R. M. ISG15 conjugation system targets the viral NS1 protein in influenza A virus-infected cells. *Proc. Natl Acad. Sci. USA* **107,** 2253–2258 (2010).
31. Lenschow, D. J. Antiviral Properties of ISG15. *Viruses* **2,** 2154–2168 (2010).
32. Radoshevich, L. *et al.* ISG15 counteracts *Listeria monocytogenes* infection. *eLife* **4,** e06848 (2015).
33. Ketscher, L. *et al.* Selective inactivation of USP18 isopeptidase activity *in vivo* enhances ISG15 conjugation and viral resistance. *Proc. Natl Acad. Sci. USA* **112,** 1577–1582 (2015).
34. Speer, S. D. *et al.* ISG15 deficiency and increased viral resistance in humans but not mice. *Nat. Commun.* **7,** 11496 (2016).
35. Zhang, X. *et al.* Human intracellular ISG15 prevents interferon-alpha/beta over-amplification and auto-inflammation. *Nature* **517,** 89–93 (2015).
36. Okumura, A., Lu, G., Pitha-Rowe, I. & Pitha, P. M. Innate antiviral response targets HIV-1 release by the induction of ubiquitin-like protein ISG15. *Proc. Natl Acad. Sci. USA* **103,** 1440–1445 (2006).
37. Malakhova, O. A. & Zhang, D. E. ISG15 inhibits Nedd4 ubiquitin E3 activity and enhances the innate antiviral response. *J. Biol. Chem.* **283,** 8783–8787 (2008).
38. Booth, A. M. *et al.* Exosomes and HIV Gag bud from endosome-like domains of the T cell plasma membrane. *J. Cell Biol.* **172,** 923–935 (2006).
39. Izquierdo-Useros, N. *et al.* Capture and transfer of HIV-1 particles by mature dendritic cells converges with the exosome-dissemination pathway. *Blood* **113,** 2732–2741 (2009).
40. Sanyal, S. *et al.* Type I interferon imposes a TSG101/ISG15 checkpoint at the Golgi for glycoprotein trafficking during influenza virus infection. *Cell Host Microbe* **14,** 510–521 (2013).
41. Giannakopoulos, N. V. *et al.* Proteomic identification of proteins conjugated to ISG15 in mouse and human cells. *Biochem. Biophys. Res. Commun.* **336,** 496–506 (2005).
42. Osiak, A., Utermohlen, O., Niendorf, S., Horak, I. & Knobeloch, K. P. ISG15, an interferon-stimulated ubiquitin-like protein, is not essential for STAT1 signaling and responses against vesicular stomatitis and lymphocytic choriomeningitis virus. *Mol. Cell Biol.* **25,** 6338–6345 (2005).
43. Doyle, S. *et al.* IRF3 mediates a TLR3/TLR4-specific antiviral gene program. *Immunity* **17,** 251–263 (2002).
44. Bache, K. G., Brech, A., Mehlum, A. & Stenmark, H. Hrs regulates multivesicular body formation via ESCRT recruitment to endosomes. *J. Cell Biol.* **162,** 435–442 (2003).
45. Gibbings, D. J., Ciaudo, C., Erhardt, M. & Voinnet, O. Multivesicular bodies associate with components of miRNA effector complexes and modulate miRNA activity. *Nat. Cell Biol.* **11,** 1143–1149 (2009).
46. Stenmark, H. *et al.* Inhibition of rab5 GTPase activity stimulates membrane fusion in endocytosis. *EMBO J.* **13,** 1287–1296 (1994).
47. Wegner, C. S. *et al.* Ultrastructural characterization of giant endosomes induced by GTPase-deficient Rab5. *Histochem. Cell Biol.* **133,** 41–55 (2010).
48. Edgar, J. R., Eden, E. R. & Futter, C. E. Hrs- and CD63-dependent competing mechanisms make different sized endosomal intraluminal vesicles. *Traffic* **15,** 197–211 (2014).
49. Carter, S. & Vousden, K. H. p53-Ubl fusions as models of ubiquitination, sumoylation and neddylation of p53. *Cell Cycle* **7,** 2519–2528 (2008).
50. Haglund, K. *et al.* Multiple monoubiquitination of RTKs is sufficient for their endocytosis and degradation. *Nat. Cell Biol.* **5,** 461–466 (2003).

51. Li, M. *et al.* Mono- versus polyubiquitination: differential control of p53 fate by Mdm2. *Science* **302,** 1972–1975 (2003).
52. Nakashima, H., Nguyen, T., Goins, W. F. & Chiocca, E. A. Interferon-stimulated Gene 15 (ISG15) and ISG15-linked proteins can associate with members of the selective autophagic process, histone deacetylase 6 (HDAC6) and SQSTM1/p62. *J. Biol. Chem.* **290,** 1485–1495 (2015).
53. van Deurs, B., Holm, P. K. & Sandvig, K. Inhibition of the vacuolar H(+)-ATPase with bafilomycin reduces delivery of internalized molecules from mature multivesicular endosomes to lysosomes in HEp-2 cells. *Eur. J. Cell Biol.* **69,** 343–350 (1996).
54. van Weert, A. W., Dunn, K. W., Geuze, H. J., Maxfield, F. R. & Stoorvogel, W. Transport from late endosomes to lysosomes, but not sorting of integral membrane proteins in endosomes, depends on the vacuolar proton pump. *J. Cell Biol.* **130,** 821–834 (1995).
55. Bucci, C., Thomsen, P., Nicoziani, P., McCarthy, J. & van Deurs, B. Rab7: a key to lysosome biogenesis. *Mol. Biol. Cell* **11,** 467–480 (2000).
56. Fader, C. M., Sanchez, D., Furlan, M. & Colombo, M. I. Induction of autophagy promotes fusion of multivesicular bodies with autophagic vacuoles in k562 cells. *Traffic* **9,** 230–250 (2008).
57. Gutierrez, M. G., Munafo, D. B., Beron, W. & Colombo, M. I. Rab7 is required for the normal progression of the autophagic pathway in mammalian cells. *J. Cell Sci.* **117,** 2687–2697 (2004).
58. Jager, S. *et al.* Role for Rab7 in maturation of late autophagic vacuoles. *J. Cell Sci.* **117,** 4837–4848 (2004).
59. Trajkovic, K. *et al.* Ceramide triggers budding of exosome vesicles into multivesicular endosomes. *Science* **319,** 1244–1247 (2008).
60. Baixauli, F., Lopez-Otin, C. & Mittelbrunn, M. Exosomes and autophagy: coordinated mechanisms for the maintenance of cellular fitness. *Front. Immunol.* **5,** 403 (2014).
61. Raiborg, C. & Stenmark, H. The ESCRT machinery in endosomal sorting of ubiquitylated membrane proteins. *Nature* **458,** 445–452 (2009).
62. Li, J. *et al.* Exosomes mediate the cell-to-cell transmission of IFN-alpha-induced antiviral activity. *Nat. Immunol.* **14,** 793–803 (2013).
63. Kuang, Z., Seo, E. J. & Leis, J. Mechanism of inhibition of retrovirus release from cells by interferon-induced gene ISG15. *J. Virol.* **85,** 7153–7161 (2011).
64. Pincetic, A., Kuang, Z., Seo, E. J. & Leis, J. The interferon-induced gene ISG15 blocks retrovirus release from cells late in the budding process. *J. Virol.* **84,** 4725–4736 (2010).
65. Razi, M. & Futter, C. E. Distinct roles for Tsg101 and Hrs in multivesicular body formation and inward vesiculation. *Mol. Biol. Cell* **17,** 3469–3483 (2006).
66. Okumura, A., Pitha, P. M. & Harty, R. N. ISG15 inhibits Ebola VP40 VLP budding in an L-domain-dependent manner by blocking Nedd4 ligase activity. *Proc. Natl Acad. Sci. USA* **105,** 3974–3979 (2008).
67. Fruhbeis, C. *et al.* Neurotransmitter-triggered transfer of exosomes mediates oligodendrocyte-neuron communication. *PLoS Biol.* **11,** e1001604 (2013).
68. Nakka, V. P. *et al.* Increased cerebral protein ISGylation after focal ischemia is neuroprotective. *J. Cereb. Blood Flow Metab.* **31,** 2375–2384 (2011).
69. Lou, Z. *et al.* Telomere length regulates ISG15 expression in human cells. *Aging (Albany NY)* **1,** 608–621 (2009).
70. Andreu, Z. *et al.* Comparative analysis of EV isolation procedures for miRNAs detection in serum samples. *J. Extracell Vesicles* **5,** 31655 (2016).

Acknowledgements

We thank Dr K. Knobeloch, Dr A. García-Sastre and Dr M.A. Alonso for providing reagents, and Dr S. Bartlett for assistance with English editing. C.E. is thankful to electron microscopy facility (campus Casanova), CCiT-University of Barcelona. This study was supported by grants SAF2014-55579-R from the Spanish Ministry of Economy and Competitiveness, INDISNET-S2011/BMD-2332 from the Comunidad de Madrid, Cardiovascular Network RD12-0042-0056 and PIE13/00041 from Instituto de Salud Carlos III (Fondo de Investigación Sanitaria del Instituto de Salud Carlos III and co-funding by Fondo Europeo de Desarrollo Regional FEDER), ERC-2011-AdG 294340-GENTRIS and COST-Action BM1202 to F.S.-M.; grant SAF2014-54623-R, FIS grant PI11/00127 (Fondo de Investigación Sanitaria del Instituto de Salud Carlos III and Ministry of Health of Spain, State secretary of R+D and FEDER/FSE) and Bayer Group Grants4Grants (ID 2013-08-0982) to S.G.; and grant BFU2015-66785-P from the Spanish Ministry of Economy and Competitiveness to C.E.; Centro Nacional de Investigaciones Cardiovasculares (CNIC) is supported by the Spanish Ministry of Economy and Competitiveness (MINECO) and the Pro-CNIC Foundation, and is a Severo Ochoa Center of Excellence (MINECO award SEV-2015-0505). C.V.-B. was supported by FPU programme (Spanish Ministry of Education). M.M. is supported by MS14/00219 from Instituto de Salud Carlos III.

Author contributions

C.V.-B., F.B., I.F.-D., D.T., O.M.-G., S.B. and C.E. performed experimental work. C.V.-B., F.B., M.M., S.G. and F.S.-M. designed research. C.V.-B., F.B. and F.S.-M. analysed data and wrote the manuscript.

Additional information

Supplementary Information accompanies this paper at http://www.nature.com/naturecommunications

Competing financial interests: The authors declare no competing financial interests.

Reprints and permission information is available online at http://npg.nature.com/reprintsandpermissions/

How to cite this article: Villarroya-Beltri, C. *et al.* ISGylation controls exosome secretion by promoting lysosomal degradation of MVB proteins. *Nat. Commun.* **7,** 13588 doi: 10.1038/ncomms13588 (2016).

Publisher's note: Springer Nature remains neutral with regard to jurisdictional claims in published maps and institutional affiliations.

Cell. Mol. Life Sci. (2018) 75:1–19
https://doi.org/10.1007/s00018-017-2690-y

Cellular and Molecular Life Sciences

VISIONS AND REFLECTIONS

Post-translational add-ons mark the path in exosomal protein sorting

Olga Moreno-Gonzalo[1,2] · Irene Fernandez-Delgado[1,2] · Francisco Sanchez-Madrid[1,2,3]

Received: 24 July 2017 / Revised: 11 October 2017 / Accepted: 23 October 2017 / Published online: 27 October 2017

Abstract Extracellular vesicles (EVs) are released by cells to the extracellular environment to mediate inter-cellular communication. Proteins, lipids, nucleic acids and metabolites shuttled in these vesicles modulate specific functions in recipient cells. The enrichment of selected sets of proteins in EVs compared with global cellular levels suggests the existence of specific sorting mechanisms to specify EV loading. Diverse post-translational modifications (PTMs) of proteins participate in the loading of specific elements into EVs. In this review, we offer a perspective on PTMs found in EVs and discuss the specific role of some PTMs, specifically Ubiquitin and Ubiquitin-like modifiers, in exosomal sorting of protein components. The understanding of these mechanisms will provide new strategies for biomedical applications. Examples include the presence of defined PTM marks on EVs as novel biomarkers for the diagnosis and prognosis of certain diseases, or the specific import of immunogenic components into EVs for vaccine generation.

Keywords Extracellular vesicles · Exosome · Post-translational modifications · Exosomal sorting · Ubiquitin

Olga Moreno-Gonzalo and Irene Fernandez-Delgado contributed equally to this work.

✉ Francisco Sanchez-Madrid
fsmadrid@salud.madrid.org

[1] Vascular Pathophysiology Research Area, Centro Nacional de Investigaciones Cardiovasculares Carlos III (CNIC), Madrid, Spain

[2] Servicio de Inmunología, Instituto Investigación Sanitaria Princesa, Universidad Autónoma de Madrid (UAM), Madrid, Spain

[3] CIBERCV, Madrid, Spain

Introduction

Extracellular vesicles

Extracellular vesicles (EVs) are 50–300 nm-sized nanovesicles secreted to the extracellular milieu by a vast variety of cell types to promote inter-cellular communication on cells that capture them. Such vesicle exchange is involved in many physio-pathological situations such as tumour progression, metastasis, immunomodulation and the spreading of infections [1]. EVs have a heterogeneous nature, thus they are classified according to their origin into three groups: exosomes, shedding vesicles and apoptotic bodies [2]. Exosomes are of endosomal origin. Cells release them by fusing multivesicular bodies (MVBs)-containing intraluminal vesicles (ILVs) with the plasma membrane. Shedding vesicles form directly at the plasma membrane. Finally, apoptotic bodies are vesicles that result from apoptosis and contain cellular waste [3, 4]. EVs are membrane-covered vesicles that contain proteins, nucleic acids (DNA, mRNA and miRNAs), lipids and metabolites [5]. Proteins that are enriched in exosomes include tetraspanins (CD9, CD63, CD81), cytoskeleton components (Syntenin, Drebrin, ERMs), Endosomal Sorting Complexes Required for Transport (ESCRT complex) (TSG101, ALIX), Heat-Shock proteins (HSP70 and 90), Annexins, Rab proteins, among others [6]. Exosome membranes are also different from the membrane of their producer cells, mainly enriched in ceramide, sphingolipids, glycerophospholipids and cholesterol [7, 8].

Almost every cell, prokaryotic and eukaryotic, can secrete EVs. These particles appear in many fluids, including urine, amniotic fluid, blood, bile, semen, cerebrospinal fluid, breast milk, ascites and cell cultures (reviewed in [2]). Moreover, EVs contain specific external and internal markers, which vary depending on their origin. For

instance, CD24 is a marker for urine and amniotic fluid exosomes [9]. In addition, a single cell type can simultaneously secrete different populations of exosomes [10, 11]. For example, polarized cells can deliver different populations of exosomes through the apical and basolateral poles [12].

Regarding cargo sorting, EVs receive cargoes through both ESCRT-dependent and independent mechanisms [13, 14]. The existence of heterogeneous MVBs populations becomes apparent when different components of endosomal trafficking or the ESCRT pathway are silenced or overexpressed, and when exosomal secretion is disturbed and not all exosomal markers are affected to the same extent [10, 15]. This enables distinguishing between global markers, e.g. TSG101, ALIX or HSP70; and cell-specific markers, e.g. class II Major Histocompatibility Complex (MHC-II) [3]. EV cargo also evolves with global changes to the whole cells. For example, oxidative stress modulates MVB biogenesis, endocytosis and consequently EVs composition [12].

Post-translational modifications

Post-translational modifications (PTMs) include a collection of add-ons that provide variability to a defined set of proteins that all cells use to enable most biological processes, adapting the functionality of those proteins by varying their interactive capability, resistance to degradation, etc. In this sense, PTMs exponentially increase the level of the proteome complexity [16]. These add-ons are molecules of diverse nature that attach to specific amino acids. Multiple amino acids can receive varied PTMs. The types of added molecule include chemical groups, carbohydrates, lipids, aminoacids, proteins and nucleotides. This process is controlled by specialized enzymes responsible for the addition or removal of each modification [17]. PTMs and their regulation constitute a cellular communication code to respond in a fast, versatile and accurate mode. The fulcrum of this review is that PTMs can direct exosome loading. Exosomes do not mirror the protein composition of their parental cells, and some proteins appear enriched in exosomes by selective mechanisms of protein cargo sorting controlled by specific PTMs [18]. The main PTMs are summarized in Table 1. These include addition of chemical groups (phosphorylation, acetylation, methylation, oxidation, hydroxylation, S-nitrosylation, sulfation or sulfonation, and others), carbohydrates [N-glycosylation, O-glycosylation, glycosylphosphatidylinositol (GPI)-anchoring], lipids (myristoylation, palmitoylation, prenylation) and nucleotides (ADP-rybosylation, PARylation). To make this large problem tractable, we focus in Ubiquitin and Ubiquitin-like modifiers (UBLs) as major controllers of EV protein loading.

Ubiquitination and Ubiquitin-like modifiers (UBLs)

This group of PTMs represents one of the most important regulatory systems of protein location, stability and function. The C-terminal (C-t) Gly of ubiquitin and most UBLs attaches covalently mainly to the ε-amino group of a Lys (K) residue of the substrate protein, forming an isopeptide bond. The conjugation of ubiquitin and UBLs requires the consecutive action of three specific enzymes: Ubl-activating enzymes (E1s), Ubl-conjugating enzymes (E2s) and Ubl-protein ligases (E3s). Specific proteases reverse this process, removing ubiquitin from target proteins [19, 20]. Ubiquitin is a highly conserved, small protein of 8.5 kDa involved in diverse functions, such as protein degradation, endocytic trafficking, signal transduction and DNA repair, among others. Mono-ubiquitination is the modification of a specific Lys in a target protein. The same protein can bear multiple mono-ubiquitinated residues simultaneously. Besides, the ubiquitin protein itself contains seven Lys (K6, 11, 27, 29, 33, 48 and 63) in its sequence. These Lys can bind to other molecules of ubiquitin, generating seven types of polymeric ubiquitin chains, constituting the so called "ubiquitin code". Moreover, M1 chains are polymeric chains formed by ubiquitin N-terminal (N-t) Met. All these chains vary in length, ranging from two to more than ten residues. They can be homotypic if the same residue is modified during elongation as in M1, K11, 48 or 63-linked chains, or heterotypic if the same chain displays different linkages [21, 22]. Moreover, a single ubiquitin can be modified with multiple chains or UBLs (NEDD8, SUMO, ISG15), generating branched chains or mixed chains, respectively. Finally, ubiquitin can be acetylated or phosphorylated [21–25]. K48-linked ubiquitin was the first described poly-ubiquitin chain related to degradation [21, 26]. On the other hand, K63-linked chains relate to many biological processes, and K63-modified proteins play important roles in diverse cellular signalling pathways, e.g. Toll-like receptor (TLR) cascade and endosomal transport [21, 27–30]. However, the specific functions of other mixed, branched or heterogeneous chains remain almost unknown [28] (Table 1). The consensus is that proteins modified with K29 and K48-linked chains are proteasome-bound for degradation. Nevertheless, M1, K6, K11, K27 and K63 chains and mono-ubiquitination regulate different cellular processes such as DNA repair, translation, inflammation and endocytic trafficking [21, 27–33] (Table 1).

UBLs share many features with ubiquitin, including their sequence and three-dimensional structure, which is a compact β-grasp fold. The main members of this group are SUMO1, SUMO2-3, SUMO4, ISG15, NEDD8, ATG12, FAT10, MNSFβ, UFM1, URM and UBL5 (reviewed in [34–38]). Neural precursor cells-Expressed Developmentally Down-regulated protein 8 (NEDD8) is the closest UBL to ubiquitin. NEDD8 mainly modifies proteins from the Cullin

Table 1 Post-translational modifications of proteins

Group	Subgroup	Molecule (donor)	Protein residues	Average mass (Da)	Structure	Adding Enzyme // Cleaving Enzyme	Ref
Chemical group	Phosphorylation	Phosphate (γ-phosphate ATP)	Ser/Thr Tyr His Asp, Arg*,Lys*	94.973		Kinases (phosphotransferases)// *Phosphatases*	[155]
	Acetylation	Acetate (Acetyl coenzyme A)	Lys(1,2) N-t(1,2)	43.045		Acetyl-trasferases (ATs)// *Desacetylases (DACs)*	[156,157]
	N- Methylation	Methyl group (S-adenosylmethionine, SAM)	Arg Lys	15.035		Methyltransferases // *Demethylases*	[158-160]
	Oxidation	*Reactive Oxygen species (ROS)*					[161]
	Oxidation	Anion superoxide	Cys Met	16.000		- // *Superoxide dismutases*	[161]
	Hydroxylation	Hydroxyl group	Pro Asn Lys	17.007		Iron-containing monooxygenases // *Pro-hydroxylase and oxygenases*	[162]
		Reactive Nitrogen species (RNS)					[161]
	Tyr-Nitration	Nitro group (NO_2) (Peroxynitrites)	Tyr	46.006		- // *Denitrase*	[163]
	S-Nitrosylation	Nitric oxide (NO)	Cys(1,2) Met	30.006		Nytrosylases // *Denitrosylases, S-Nitroglutathione reductase (GSNOR)*	[164]
	Other oxidative compound: hydrogen peroxide (peroxidation) and nitrate.						[161]
	Sulfation	Sulphate (Phosphoadenosyl-phosphosulfate)	Tyr	96.064		Tyrosylprotein sulfotransferases // *Sulfatase*	[165]
	Amidation	Amide	C-t[A]	16.023		Peptidylglysine α-amid monooxygenase (PAM)	[166]
	Formylation	Formate	Met Lys	28.010		Methionyl-tRNAMet transformylase	[167,168]
	Succinylation	Succinate (Succinyl-coenzyme A)	Lys	116.073		- // *Sirtuin 5*	[169]
	Malonylation	Malonate (Manolyl-coenzyme A)	Lys	102.047		- // *Sirtuin 5*	[170]
Carbohydrates	N-Glycosylation	Monosaccharides (dolilchol pyrophosphate or lipid-linked oligosaccharide, LLO)	Asn (NxT/S)	≥ 2372.1		Olygosaccaryl transferases (OST), glucosyl transferases // *glucosidases I and II, mannosidases*	[171-174]
	O-Glycosylation	Monosaccharides (GlcNAc, GalNAc, fucose, glucose, mannose,...)	Ser Thr Trp# Tyr*	~ 200	 GlcNAc	*O*-(monosaccharide)-transferase // *Hydrolases*	[171,172, 174,175]
	Others: C-mannossylation and glypiation						
	GPI	Glycosyl phosphatidyl-inositol	C-t(1)	~ 1900		GPI transamidase // *Phosphoinositol-specific phospholipase C*	[176-178]
Lipids	S-Palmitoylation	Palmitic acid (palmitoyl coenzyme A)	Cys Ser Thr	256.424		Palmitoyl acyl transferases (PATs) // *Thioesterases*	[179-181]
	N-Myristoylation	Myristic acid (myristoyl coenzyme A)	N-t Gly	228.371		N-myristoyltransferase (NMT)	[179-181]
	S-Prenylation						
	Farnesylation	Farnesyl (Farnesylpyrophosphate)	Cys[B] (CaaX box)	222.366	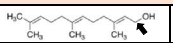	Proteinfarnesyl transferase (FT)	[181,182]
	Geranylgeranylation	Geranylgeranyl (Geranylgeranyl-pyroP)		290.483	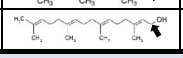	Proteingeranyl-geranyl transferases (GGT I and II)	[181,182]
Proteins	Aminoacids						
	Polyglutamylation	Glutamate (up to 20)	Internal Glu	> 147.13		Tubulin-tyrosine ligase-like (TTLL) protein family // Deglutamylase	[183]
	Polyglycylation	Glycine (up to 34)	Glu	> 75.067		Glycylase // Deglycylase	[184,185]
	Other: Citrullination (conversion of Arg to citrulline by PAD enzyme)						[186,187]
	Ubiquitination						
	MonoUb	Ubiquitin	Lys N-t Thr#, Cys#, Ser#	8565	 PDB: 1UBQ	E1 activating enzyme, E2 conjugating enzyme, E3 ligase E4// *Deubiquitinases*	[21,22,147]
	M1/K63	PolyUB Chain: C-t bond with N-t Met, Lys63		> 8565			[88,147]
	K6/K29/K33	PolyUB Chain: C-t bond with Lys6/Lys29/ Lys33		> 8565			
	K11/K27/K48	PolyUB Chain: C-t bond with Lys11/Lys27/ Lys48		> 8565			
	Ubiquitin-like proteins (UBLs)						[34-38]
	SUMOylation	SUMO1	Lys	11557	 PDB: 1WM3 (SUMO-2)	E1 (SAE), E2 (Ubc9), E3 // *DeSUMOylases (SENP)*	[188]
		SUMO 2-3		10871			
	ISGylation	ISG15		17888	 PDB: 1Z2M	E1 (UbE1L), E2 (UbCH8), E3 // *DeISGylase (USP18)*	[189]
	Neddylation	NEDD8		9072	 PDB: 1NDD	E1 (NAE), E2 (UbCH12), E3 // *Isopeptidase*	[40,41]
	Others UBLs: ATG12, FAT10, MNSFβ, UFM1, URM, UBL5, SUMO4						[34-38]
	Modification of Ub: Phospho-Ub and Acetyl-Ub			Polyubiquitin chains:	Branched chains PolyUb mixed chains (modified by SUMO, NEDD8, ISG15)		[21-25]
Nucleotides	ADP-ribosylation						
	Mono	ADP-ribose (NAD^+)	Tyr Asn Lys Arg Cys	559.316	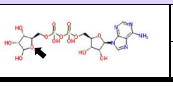	ADP-rybosyltransferases (ARTs) // *ADP-ribosylhydrolases*	[190,191]
	Poly (PARylation)		Glu Asp			Poly(ADP-ribose)polymerases (PARPs) // *Poly (ADP-ribose) glycohydrolase (PARG)*	[191]

* Found in prokaryotes
\# Rare
➡ Nucleophile or electrophile site
A Almost followed by a proline
B Cys - 5 aminoacids from the C-terminus
(1) Reversible
(2) Irreversible

Structures obtained from ChemSpider Search and share chemistry (Royal Society of Chemistry) and Protein Data Bank (PDB)

RING Ligases (CRLs) superfamily. RING E3 Ligases transfer ubiquitin directly from E2 enzymes to the substrate protein forming a complex scaffolding by Cullin. CRLs play an important role in protein ubiquitination for proteasomal degradation under the control of NEDD8 [39, 40]. NEDD8 also forms chains through one of its six Lys [41]. Small ubiquitin-related modifier (SUMO) is an UBL involved in nuclear transport and organization, DNA repair, transcription, chromatin remodelling and ribosome biogenesis. It is an essential modification to maintain cell homeostasis in stress responses and has become relevant in many diseases [42]. Interferon-stimulated gene 15 (ISG15) is induced by type I interferons (IFN-I), exposure to bacterial lipopolysaccharide (LPS), viral double-stranded RNA (dsRNA), ischemia and aging [43]. It is an essential part of the innate immune response to fight against bacterial and virus infections [44]. Besides, ISG15 is also overrepresented in various types of tumours [45]. Interestingly, ISG15 can also function as a free unconjugated form with an immunomodulatory role [46].

Exploring the sorting of modified proteins into EVs

Sorting mechanisms to MVBs

Exosomes originate in the endocytic pathway, whereas shedding vesicles form from direct budding of plasma membrane. Therefore, the mechanisms involved in protein secretion are different [18]. Here, we will discuss how PTMs could be involved in the sorting of proteins into EVs.

ESCRT-dependent and independent sorting mechanisms into ILVs

Presently, mechanisms of protein incorporation into the ILVs of MVBs for exosomal secretion or lysosomal degradation remain unclear. One key part of the machinery that controls the incorporation of ubiquitinated proteins into ILVs is the ESCRT complex [47, 48]. This complex includes four sub-complexes that sequentially recognize protein cargos and include them into ILVs. ESCRT-0 comprises HRS and STAM1/2 subunits, which are proteins with several distinct ubiquitin-binding domains (UBDs) that form a cargo-recognition module. HRS recognizes ubiquitinated proteins through a FYVE domain necessary to interact with phosphatidyl inositol 3-phosphate (PI3-P) molecules of endosomal membranes. HRS also displays PSAP domains that connect with the ESCRT-I subunit TSG101, which also binds ubiquitinated proteins. Moreover, the PSAP domains of small integral membrane protein of the lysosome/late endosome (SIMPLE) also bind TSG101. SIMPLE has a PPxY motif that interacts with NEDD4 to be ubiquitinated, and di-Leu and YKRL motives, which are signatures of endocytic functions [14, 49]. Mutations in these motifs impair the secretion of SIMPLE to exosomes, altering MVBs biogenesis [49]. Moreover, *Hrs* conditional knock-out (KO) in dendritic cells (DC) significantly reduces exosome release, pointing to an important role for ESCRT components in exosome secretion [50].

Deubiquitination is mandatory prior to packaging cargo into ILVs. To remove ubiquitin, ESCRT-III recruits deubiquitinating enzymes. ESCRT-III subunits CHMP2 A, B, CHMP3, CHMP4 A, B, C and CHMP6 bind to lipid membranes through their positively charged N-t domains, allowing high order oligomerization that results in structures over 600 kDa. Yeast ESCRT-III Snf7 (CHMP4 in humans), is not only implicated in neck-shaped oligomeric assembly for vesicle budding, but also in its scission. In this regard, the necessary energy to dissociate budding vesicles from membrane is provided by the ATPase activity of the Vacuolar protein 4 (VPS4) Complex (SKD1, CHMP5, LIP5) (reviewed in [47, 48]).

Ubiquitination of cargo proteins is necessary for recognition by ESCRT-0 components, whereas deubiquitination is a crucial step for sorting them into ILVs. However, whether ubiquitination is mandatory for driving proteins into exosomes is currently controversial. The sorting of some proteins seems independent of ubiquitination, e.g. MHCII loading into DC exosomes after T cell activation, which is associated to tetraspanin-enriched microdomains (TEMs) formed by CD9 [13, 51]. Furthermore, CD81 is important for the sorting of its associated proteins into exosomes [42]. Other studies support that the ubiquitination drives MHCII-containing MVBs to degradation upon fusion with the lysosomal system [52] (Fig. 1).

In addition, ESCRT components can be ubiquitinated themselves, for example HRS. HRS mono-ubiquitination prevents binding of ubiquitinated cargo, regulating the flow of specific proteins into MVBs [47]. The E3 ubiquitin ligase implicated in ubiquitin turnover can thus control the destiny of MVBs. For example, the activity of Mahogunin on TSG101 disrupts MVB lysosomal trafficking, whereas another E3 ubiquitin ligase called Tal abrogates MVB biogenesis [53, 54]. Associated molecule with the SH3 domain of STAM (AMSH) ubiquitin isopeptidase and ubiquitin isopeptidase Y (UBPY) removes mono-ubiquitin from HRS to recycle ESCRT components, preventing their degradation. Moreover, AMSH deubiquitinates cargoes modified with K63-linked chains, whereas UBPY recognizes both K63 and K48-linked chains. The action of these enzymes indicated a deubiquitination step that is required to sort cargoes into ILVs, and hence, into exosomes [55, 56].

However, mono and poly-ubiquitinated proteins can be found in exosomes, but not associated to the exosomal

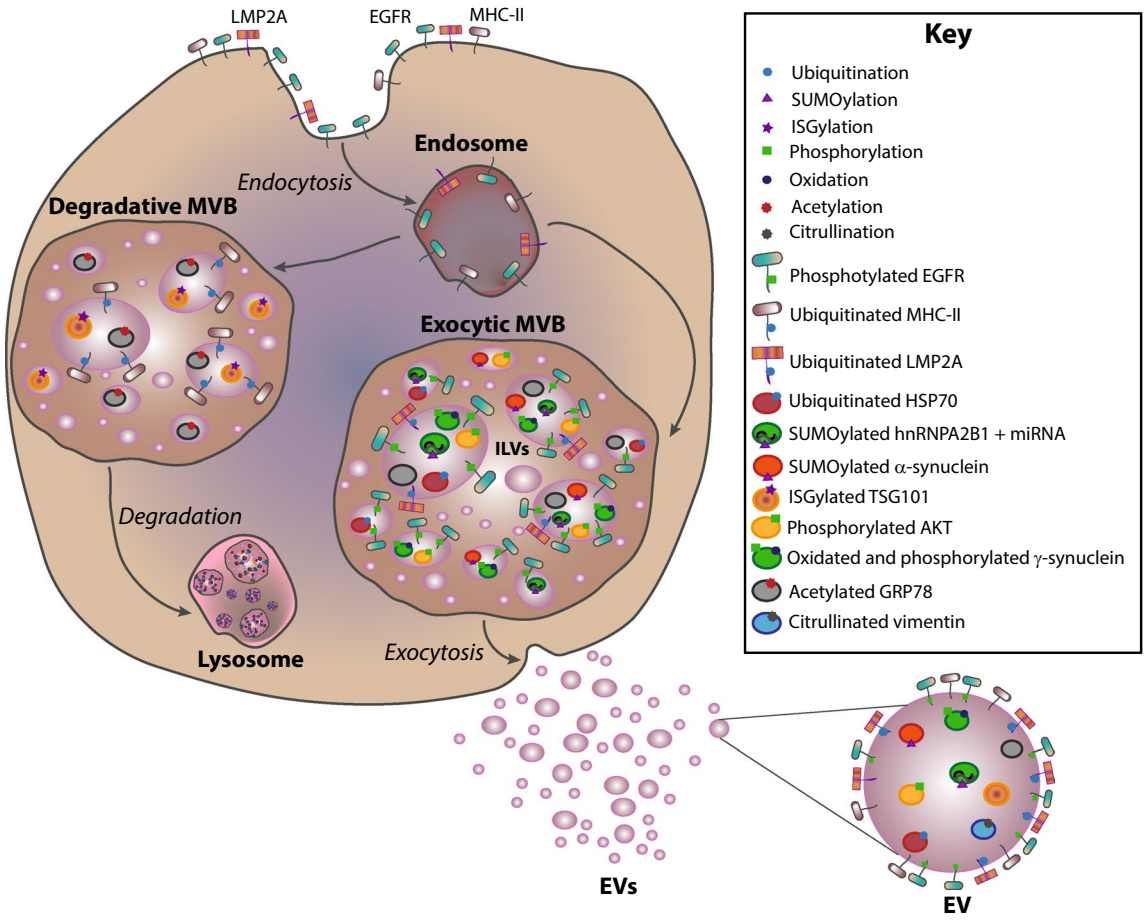

Fig. 1 Schematic representation of some PTMs found in EVs. Endocytosis of plasma membrane receptors (MHC-II, LMP2A and EGFR) transfer them into the endocytic pathway. Depending on the added PTMs, these receptors can have different fates. Ubiquitinated-MHC-II is preferentially directed to degradative MVBs for degradation in lysosomes, whereas, Ub-LMP2A and ph-EGFR are usually incorporated into ILVs of exocytic MVBs, which are fused with plasma membrane to be secreted as EVs [52, 77, 116]. In the case of acetylated-GRP78 and ISGylated-TSG101, these PTMs act as cellular retention tags, promoting their degradation in lysosomes [128, 129]. However, Ub-HSP70, SUMOylated-hnRNPA2B1, SUMOylated-α-synuclein, ph-AKT, oxidized and phosphorylated γ-synuclein and citrullinated vimentin are loaded into ILVs and driven to EVs [80, 104, 106, 108, 118, 154]. Besides, unmodified TSG101 and GRP78 proteins can also be present in EVs [128, 129]. Figure key is shown at the right side. The images in the figures are not scaled

membrane [57]. Cargo deubiquitination before its packaging into ILVs seems essential, but how some ubiquitinated proteins end up in exosomes remains controversial. These contradictory results suggest that ubiquitinated proteins can evade deubiquitination; or finish up in exosomes through ESCRT-independent mechanisms. Such mechanisms do exist. In these, sorting depends on tetraspanins, sphingolipids and ceramide [58–60]. For example, LYPX(n)L motifs in the protein ALIX are implicated in its interaction with CD63 tetraspanin, and together with transmembrane proteins syndecans and syntenin induce budding and membrane abscission of ILVs [61]. In fact, an extensive study of ESCRT components downregulation revealed that of 23 ESCRT proteins studied, not all of them interfered with exosome secretion in the same way [11]. When HRS, TSG101, VPS22 and VPS24 are simultaneously silenced, MVBs are still produced and only the formation of Epidermal Growth Factor $(EGF)^+$-MVBs is affected, highlighting a possible mechanism of substrate selectivity [62]. Proteolipid $(PLP)^+$-exosomes localize together with flotillin and GPI in endosomal compartments, but not with HRS. These vesicles were enriched in cholesterol and ceramide, and their secretion depended on ceramide production by the activity of sphingomyelinase 2 (nSMase2) [63]. The enzyme sphingomyelin synthase SMS2 regulates the secretion of amyloid-β (Aβ)-$peptide^+$-exosomes. In addition, the transfer of $CD63^+$-exosomes from T cells to APCs during immune synapse is ceramide-dependent [59, 60]. This is likely related to the fact that ceramide creates spontaneous curvature of endosomal membranes, triggering ILVs budding. Besides, other lipids metabolites such as sphingosine-1-phosphate (S1P), diacylglycerol (DAG), cholesterol, phosphatidyl choline, or

lysobisphosphatidic acid (LBPA) are involved in the MVB biogenesis and exosome secretion, although how protein cargoes are selectively transported into this kind of vesicles remains unknown [64–71].

Ubiquitinated proteins in EVs

Ubiquitin was first observed in human urine exosomes showing a wide range of molecular weight complexes by Western blot, which suggested the presence of ubiquitinated proteins in exosomes [72]. Specific antibodies for ubiquitin and poly-ubiquitin chains allowed to identify mono-, oligo- and poly-ubiquitinated proteins in exosomes [57]. Various studies and proteomic analysis identified specific ubiquitinated proteins (reviewed in [73]) (Table 2 and Fig. 1). For example, myeloid-derived suppressor cells (MDSC) secrete exosomes enriched in ubiquitinated proteins, including endosomal trafficking proteins and histones [74]. Moreover, high molecular weight complexes of non-classical human leukocyte antigen-G (HLA-G) are ubiquitinated, but not glycosylated, in exosomes obtained from ascitic and pleural exudates of patients [75]. Shedding vesicles also contain modified proteins such as arrestin domain-containing protein 1 (ARRDC1), which is ubiquitinated by the E3 ubiquitin ligase WW domain-containing protein 2 (WWP2). An arrestin domain in ARRDC1 anchors it to the plasma membrane, enabling its interaction with the PSAP domain of TSG101 to generate direct membrane budding [76]. In the case of ubiquitinated Epstein–Bar virus latent membrane protein 2A (LMP2A), exosome sorting depends on cholesterol, whereas the phosphorylated form was not detected in exosomes [77] (Table 2 and Fig. 1).

Phosphatase and tensin homolog deleted on chromosome 10 (PTEN) is ubiquitinated on Lys13 by the association and regulation of Nedd4 family-interacting protein 1 (Ndfip1), an adaptor protein of the Nedd4 family E3 ubiquitin ligases, appearing in this form in exosomes, although modified-Ndfip1 does not. However, its presence is necessary for the import of Nedd4, Nedd4-2 and ITCH to exosomes [14, 78]. Alanine replacement on di-Leu (LL) and YKRL motifs of SIMPLE reduces it secretion into exosomes, as well as a mutation on its PTAP motif, which controls SIMPLE binding to TSG101 for incorporation into ILVs. However, point mutations of the two PPxY motifs of SIMPLE, a binding domain for Nedd4 type E3 ubiquitin ligases, such as Nedd4 and ITCH, increase exosomal incorporation; hence SIMPLE ubiquitination does not direct its own sorting [49]. In other cases, such as Fas Ligand (FasL), ubiquitination of the proline-rich domain (PRD)-flanking Lys and phosphorylation of multiple tyrosines promote its internalization in MVBs and its secretion into EVs [79]. The COP9 signalosome (CSN)-associated protein CSN5 mediates ubiquitin isopeptidase activity. Deletion of its JAB1/MPN/Mov34 metalloenzyme (JAMM) domain increases the sorting of ubiquitinated HSP70 and HIV Gag proteins into exosomes; whereas a mutation of its associated deubiquitin activity domain promotes the enrichment of non-modified proteins in EVs [80]. These results highlight that CSN5 participates in ubiquitin-dependent and independent protein vectorization into exosomes [80] (Table 2). MARCH1, an E3 ubiquitin ligase for MHCII and CD86, is incorporated into exosomes dependent on its C-t tyrosin-based motifs [81]. This endosome sorting motif is also important for sorting of transferrin receptor into exosomes due to its interaction with ALIX [82]. Nevertheless, whether MARCH1 is ubiquitinated or not in exosomes remains unclear, although this region is important for MARCH1 auto-ubiquitination [83].

Human urine exosomes contain approximately 15% of ubiquitinated proteins. Of these, 21% are transmembrane proteins, underscoring that deubiquitination is not mandatory for the incorporation of protein cargo into MVBs and exosomes [84]. Although, ubiquitination-specific motifs remain unidentified, this PTM has preference for basic

Table 2 Post-translational modified proteins found in EVs

Target protein	PTM	Residue	References
CryAB	Phosphorylation	Ser-59/Ser-45	[112]
Tau	Phosphorylation	Hyperphosphorylated Tau	[110]
	Phosphorylation	Thr-181/Ser-396	[117]
	Phosphorylation	-	[113]
EGFR	Phosphorylation	Tyr-1068	[116]
IRS-1	Phosphorylation	Ser-312 and Pan-Tyr	[111]
PDK1*	Phosphorylation	Ser-241	[108]
AKT*	Phosphorylation	Thr-308	[108]
SRC*	Phosphorylation	Tyr-416	[108]
ELK1 *	Phosphorylation	Ser-383	[108]
ERK 1/2*	Phosphorylation	Thr-202/Tyr-204	[108]
AMPKα1 *	Phosphorylation	Ser-485	[108]
Acetyl-CoA carboxylase*	Phosphorylation	Ser-79	[108]
NCC	Phosphorylation	Thr-46, Thr-50 and Thr-55	[114]
Aquaporin 2*	Phosphorylation	Ser-256	[101]
GPRC5C*	Phosphorylation	Thr-435/Ser-395/Tyr-426	[101]
CHMP2B*	Phosphorylation	Ser-199	[101]
Fas Ligand	Phosphorylation	Tyr-7/Tyr-9/Tyr-13	[79]
	Ubiquitination	Mono-	[79]
Annexin A2	Phosphorylation	Tyr-23	[109]
γ-synuclein	Phosphorylation	-	[118]
	Oxidation	Met-38/Tyr-39	[118]
TyA*	Myristoylation	MGCINSKRKD N-t tag	[124]
CD55	GPI-anchor	-	[125]
Vimentin*	Citrullination	-	[154]
LGALS3BP$	Glycosylation	-	[120]
Histone H1.2*	Ubiquitination	-	[74]
HLA-G complex	Ubiquitination	-	[75]
ARRDC1	Ubiquitination	-	[76]
LMP2A	Ubiquitination	-	[77]
PTEN	Ubiquitination	Lys-13	[78]
HSP70	Ubiquitination	-	[80]
SIMPLE	Ubiquitination	-	[49]
Aquaporin-1*	Ubiquitination	Mono- and Poly-	[84]
Annexin A1*	Ubiquitination	Poly-	[84]
Plastin-3 isoform 1*	Ubiquitination	Multimono- at Lys-11 and Lys-18	[84]
HspX#	Ubiquitination	-	[136]
GroES#	Ubiquitination	-	[136]
GFP	Ubiquitination	Ubiquitin C-t tag	[137]
ATG85B- ESAT6	Ubiquitination	Ubiquitin C-t tag	[137]
nHer2	Ubiquitination	Ubiquitin C-t tag	[137]
GFP	SUMOylation	SUMO-1/SUMO-2 C-t tag	[106]
hnRNPA2B1	SUMOylation	-	[104]
α-synuclein	SUMOylation	-	[106]

* More proteins identified in a high-throughput screening approach, proteomics [74,84,101,108,120].
# Mycobacterial proteins detected in exosomes from human and mouse cell lines.
$ More glycosylated proteins identified by lectin blotting, NP-HPLC analysis and mass spectrometry [120].

amino acids and positively charged residues upstream of the ubiquitination site, hydrophobic residues adjacent to it and additional Lys 6 amino acids upstream [84]. Besides, poly-ubiquitin chains appear following this order of enrichment: K63 > K48 > K11 > K6 > K29 > K33 > K27. This shows that K63, K48 and K11-linked chains are the most representative poly-ubiquitin topologies in exosomes [84]. Furthermore, platelet exosomes contain poly-ubiquitin chains and in higher numbers compared to platelets microparticles [85] (Table 2).

Deciphering the ubiquitin code in EVs

The ubiquitin code comprises the combination of mono-, poly- and branched-ubiquitin chains and even other PTMs, which allow a wide range of possibilities for the regulation of proteins. K48-linked chains require at least four ubiquitin units to attach to the target protein to enable recognition by the 26S proteasome [86, 87]. In particular, the proteasome subunit S5a/Rpn10 contains an ubiquitin-interacting motif (UIM) in the hydrophobic patch of its C-t region, which enables recognition of this specific poly-ubiquitin chain. Inside the proteasome, ubiquitin molecules are removed from target proteins for recycling, whereas the rest of the proteins are cleaved into small peptides (3–25 amino acids of length). There is some evidence suggesting that other chains, e.g. M1, K6, K11, K27 and K29 could be involved in proteasomal degradation of target proteins [21, 30, 33, 86]. Moreover, a new conjugation factor, named E4, participates in the generation of efficient poly-ubiquitinated-linked chains under stress conditions to direct modified proteins to the proteasome, demonstrating the existence of an E4-dependent multi-ubiquitination pathway for degradation [88] (Fig. 2). K63-linked chains do not end up in the proteasome as they bind specifically to the ESCRT-0 complex, specifically to UIMs found in HRS and STAM1 components [27, 89]. These interactions condense proteins modified with K63-linked poly-ubiquitin chains into endosomes, promoting their import into ILVs of MVBs and possibly, their subsequent delivery into exosomes [90]. In fact, K63-linked chain is the most representative ubiquitin topology found in EVs [84] (Fig. 2).

How ubiquitin-binding proteins detect unequivocally a specific conformation of poly-ubiquitin chains may explain the selective targeting of a given protein within the cell. For example, M1 and K63-linked chains display a fairly linear or open space conformation, whereas K6, K11, and K48-linked chains create closed structures [21, 33, 91, 92] (Table 1). Open-conformation chains only limitation is that imposed by isopeptide bonds that connect them [21, 33]. However, closed conformation chains have multiple steric hindrances, which alters ubiquitin space structure by exposing and concealing different parts of ubiquitin residues, creating diverse topologies intrinsic to a specific type of linkage [21, 91]. In the cell, specific proteins bind to a unique type of ubiquitin linkage topology [91]. Because distances between ubiquitin units within a chain are different in K63 or K48-linked chains, UBDs of cellular machinery display small spaces between UIMs to specifically recognize K48-chains, whereas larger spacers are used for K63 binding [91, 92]. The use of a variety of UBDs structures not only allows discriminating between open and close conformations, it also enables distinguishing among different open structures such as K63- and M1-linked chains [91, 92]. All these possibilities of ubiquitin topologies and UBDs compose a fine and selective language among ubiquitinated-target proteins and ubiquitin-interacting proteins.

In a similar way, depending on the different distances between UIMs inside UBDs, certain E3-ubiquitin ligases elongate specific types of K-linked chains associated to target proteins. Besides, the wide variety of E3-ubiquitin ligases described in eukaryotic cells and their tissue restrictions amplify the code of ubiquitin chains. For example, the Cbl family of E3-ubiquitin ligases are highly expressed in hematopoietic cells and are involved in the downregulation of many signalling pathways controlling T and B cell receptors and integrins [93, 94]. However, MARCH1 is represented in antigen presenting cells (APCs), modifying class II MHC molecules, downregulating their expression in the plasma membrane, whereas MARCH-IV regulates class I MHC molecules using a similar mechanism [95, 96]. In this regard, a possible explanation regarding how K48-linked poly-ubiquitin chains evade proteasomal degradation and travel into exosome involves the collaboration of certain ubiquitin-binding proteins located in endosomal pathway (Fig. 2).

Branched poly-ubiquitin chains display the particular signalling properties of their K48 or K63 components, although they are recognized by multiple linkage-specific enzymes [97]. This underscores the predominance of certain chain topologies within a mixed-linkage poly-ubiquitin chain. The sorting of ubiquitin chains other than K63-linked requires mechanisms different from those dependent on ESCRT components. The incorporation of SUMO-2/3 following ubiquitination creates heterologous SUMO-2/3-Ubiquitin chains responsible for enhancing the degradation of IκBα by the proteasome after the activation of the Tumour Necrosis α (TNFα) signalling pathway [23]. In stress situations, NEDD8 can also modify ubiquitin Lys48 [25]. A recent study described how ISGylation of ubiquitin Lys29 negatively controls the turnover of ubiquitinated proteins [24].

Interestingly, ubiquitin can be phosphorylated on Ser65 by PTEN induced putative kinase 1 (PINK1), enhancing its interaction with the mitochondrial E3 ubiquitin ligase parkin [98]. This phosphorylation-dependent mechanism increases the enzymatic activity of parkin, decreasing the

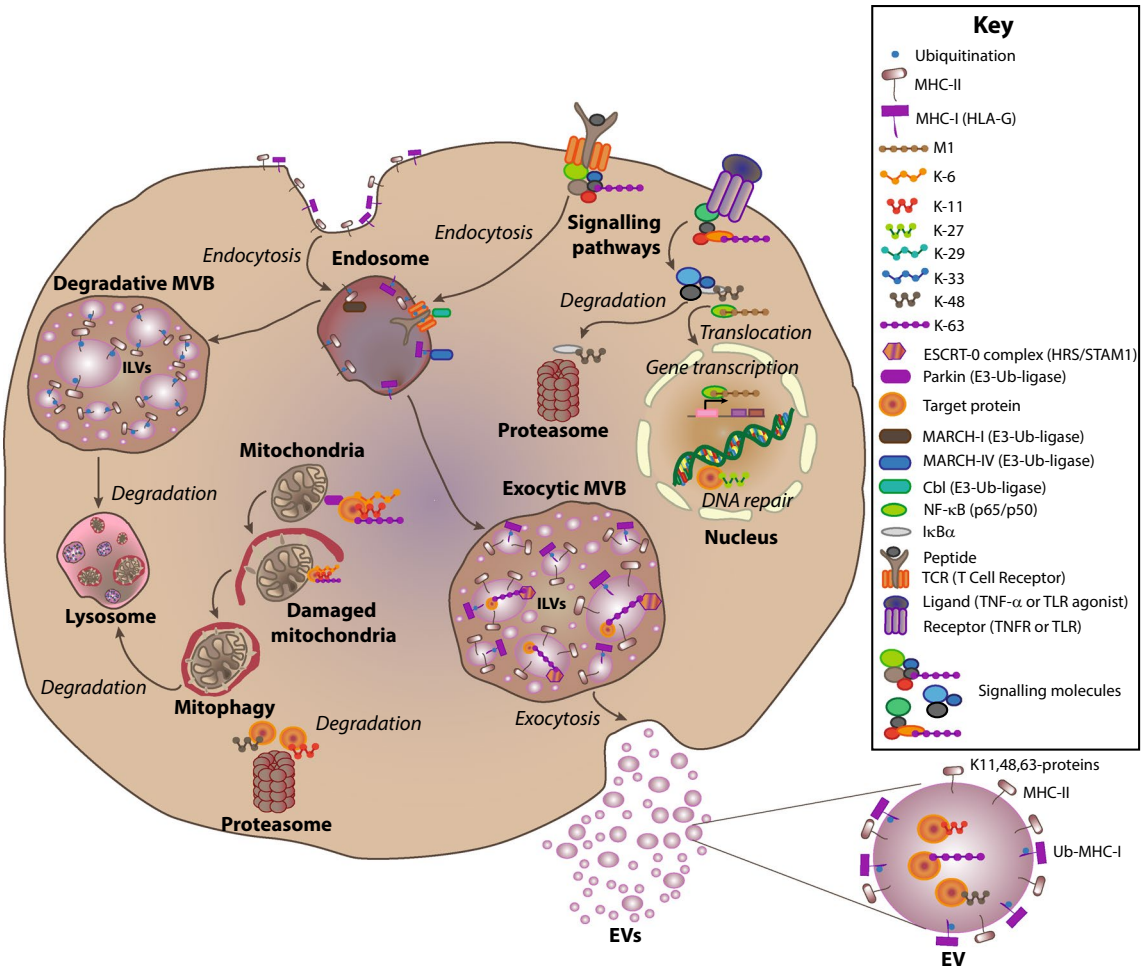

Fig. 2 The ubiquitin code in cellular functions. MHC-I and II and TCR are preferentially retained in endosomes by the action of specific E3-Ub-ligases MARCH-IV, I and Cbl, respectively. Whereas Ub-MHC-II is mainly degraded by lysosomes, Ub-MHC-I (HLA-G) can be sorted into EVs. Signalling proteins downstream of TCR, TNFR or TLR can be modified by K63-linked chains to mediate signal transduction or by K48-linked ones, such as IκBα to be degraded in the proteasome. M1-linked chain is added to NF-κB to allow its nuclear translocation to start gene transcription. K27-linked chains are related with DNA repair processes, while K6, K11 and K63 chains can modify mitochondrial proteins to initiate mitophagy of damaged mitochondria by the E3-Ub-ligase Parkin. Proteins with K11 and K48-chains are principally transported to the proteasome to be degraded. Most of the proteins modified with K63-linked chains interact with ESCRT-0 and are vectorised in ILVs of exocytic MVBs to be delivered into EVs. Although Ub-MHC-II is mainly degraded, unmodified MHC-II and Ub-MHC-I (HLA-G) are usually incorporated in exosome membrane. Besides, K11, K48 and K63-linked chains can be found in EVs. Figure key is shown at the right side. The images in the figures are not scaled

mitochondrial membrane potential [98]. Moreover, ubiquitin becomes acetylated in Lys6 and Lys48 without affecting substrate mono-ubiquitination of histone H2B [99]. However, both acetylations inhibit K11, K48 and K63-linked poly-ubiquitin chain elongation, providing a novel regulatory step of control of mono- and poly-ubiquitination [99].

Because many PTMs can modify proteins in the same residue, competition and crosstalk between different PTMs depending on different cell factors can change protein function and localization [100]. In summary, deciphering the sophisticated ubiquitin code is necessary to unveil specific functions of every chain topology in the selective import of proteins into exosomes.

Other PTMs in EVs

Proteomic studies have contributed extensively to define the protein composition of EVs [72, 84, 101–103]. Heterogeneous nuclear ribonucleoprotein A2/B1 (hnRNPA2B1) is present in exosomes in its sumoylated form, and that is necessary for the sorting of EXOmotif-containing microRNAs into exosomes [104]. On the other hand, a study suggested that SUMO-1 could modulate the toxicity of α-synuclein in neurodegenerative disorders such as Parkinson's disease (PD) [105]. Besides, EVs can contribute to disseminate neurotoxic proteins, which favours the development of PD pathogenesis. Hence,

sumoylated α-synuclein is incorporated into exosomes by a mechanism dependent on the ESCRT complex and phospholipids [106] (Table 2 and Fig. 1).

Nevertheless, ubiquitin and UBLs are not the only PTMs detected in EVs [73, 107]. For example, many phosphorylated proteins appear in exosomes, including the calcium-dependent phospholipid-binding protein Annexin A2, which is enriched in cholesterol-rich lipid raft micro-domains of exosome membranes [101, 108, 109]. The localization of this protein depends on the phosphorylation of Tyr23, which prevents its endosomal degradation and allows its incorporation into exosomal membranes [109]. Other phosphorylated proteins found in exosomes include Tau, type 1 insulin receptor substrate (IRS-1), Crystalline alphaB (CryAB), Epidermal Growth Factor Receptor (EGFR), Na^+-Cl^- co-transporter (NCC), Aquaporin 2, FasL and proteins implicated in cellular processes such as apoptosis, survival and metabolism [79, 101, 108, 110–117] (Table 2 and Fig. 1).

γ-Synuclein acquires features of prion-like proteins by oxidation, which triggers the aggregation of other proteins, e.g. α-synuclein [118]. The most frequent oxidized residues of γ-synuclein are Met38 and Tyr39. Oxidized γ-synuclein is released into exosomes and incorporated in neighbouring cells, amplifying the toxic protein-aggregation cascade that finally causes a degenerative synucleinopathy [118]. Besides, other oxidized proteins appear in EVs as described in other studies (reviewed in [107]) (Table 2 and Fig. 1). Moreover, several studies have revealed the presence of glycosylated proteins in EVs (reviewed in [73, 107]). Notably, EVs contain mainly mannose or sialic acid enriched-glycans and N-linked glycoproteins. In particular, exosomes contain large amounts of the sialoglycoprotein galectin-3-binding protein (LGALS3BP) [119–122] (Table 2).

Additionally, plasma membrane anchors induce vesicle budding directly from the plasma membrane of highly oligomeric proteins, such as the HIV Gag protein and the yeast cytoplasmic protein Tya [123, 124]. An evaluation of different membrane anchors for Tya demonstrated that myristoylation was the most effective enhancer of the formation of shedding vesicles, whereas other types such as, phosphatidylinositol-(4,5)-bisphosphate and phosphatidylinositol-(3,4,5)-trisphosphate-binding domains, prenylation/palmitoylation tag or the type-1 plasma membrane protein CD43 did not cause this effect [124]. This illustrates the role of protein anchors for the induction of shedding vesicles, which is similar to retrovirus budding [124] (Table 2). Besides, CD55 or decay-accelerating factor (DAF) anchored to a GPI molecules is selectively secreted to EVs [125].

The role of UBL and other PTMs in the sorting of proteins to EVs

The function of PTMs such as oxidation, phosphorylation, glycosylation and citrullination in the incorporation of proteins into EVs, has been recently reviewed in [107]. Briefly, these PTMs can regulate EVs release and uptake, acting as a disposal mechanism for cellular harmful components or as a repair mechanism in physio-pathological conditions [107]. Similar to ubiquitin, the UBL SUMO also plays an important role in protein sorting to EVs. For example, SUMOylation is necessary for α-synuclein sorting into exosomes in an ESCRT-dependent manner [106] (Table 2). A recent study showed that other UBL called autophagy-related protein 12 (ATG12) and its E3 ligase ATG3 interact with ALIX, regulating diverse functions carried out by ALIX, for example, viral budding and MVBs biogenesis [126]. This observation suggests that ATG12 could also participate in exosome biogenesis. Besides, isoprenylation and palmitoylation may also participate in protein delivery into exosomes, as in the case of the CINCCKVL palmitoylation and isoprenylation motif, which is present in human Ras Homolog Family Member B (RhoB), determines its incorporation into ILVs in a cholesterol-dependent way and consequently in exosomes [127]. Furthermore, the expression of reporter proteins containing this palmitoylation/isoprenylation motif is enough to define a late-endosomal fate for these proteins [127].

On the contrary, ISG15, which is recognized as an immune alarm signal by cells, has an opposite role in protein sorting to exosomes. A recent study showed that ISGylation tags proteins for degradation, thereby avoiding exosome secretion and spreading [43, 128] (Fig. 1). Besides, acetylation can abrogate the sorting of proteins into exosomes. High glucose-regulated protein 78 (GRP78) is expressed and secreted into exosomes by colon cancer cells to prepare the tumor microenvironment [129]. Its secretion in exosomes is impaired by chemical inhibitors of histone deacetylases (HDACs) and silencing of HDAC6 protein, which causes the dissociation of GRP78 from HDAC6 and promotes GRP78 aggregation and interaction with VPS34 complex [129]. The use of an acetylation mimetic mutant of GRP78 (K633Q) also impairs exosome sorting and blocks tumour cell growth in vivo [129] (Fig. 1).

On the other side, the role of the other PTMs, gathered in Table 1, remains largely unexplored. This could suggest that a role for these PTMs is unlikely, or that they can work as a cellular retaining signal for some proteins, directing them to other cellular processes such as the autophagy-lysosome degradation pathway.

Targeting post-translationally modified proteins into EVs for biomedical applications

Deciphering the role of PTMs for protein sorting into exosomes could be useful for medical purposes, such as association of certain modified proteins with concrete physio-pathological situations, highlighting PTMs of exosomal proteins as biomarkers for prognosis, diagnosis and treatment of diseases.

PTM marks in EVs as biomarkers for diagnosis and prognosis

EVs have potential as non-invasive biomarkers for several pathological conditions, particularly due to their accessibility from biological fluids, facilitating the detection of certain pathologies [130–133]. A specific PTM of a protein in EVs in particular diseases could constitute a potential biomarker (Fig. 3). For example, the secretion of modified Tau protein aggravates development and progression of neurodegenerative processes. The majority of modified (phospho-Thr-181) Tau detected in human cerebrospinal fluid samples is secreted via exosomes, constituting a well-characterized

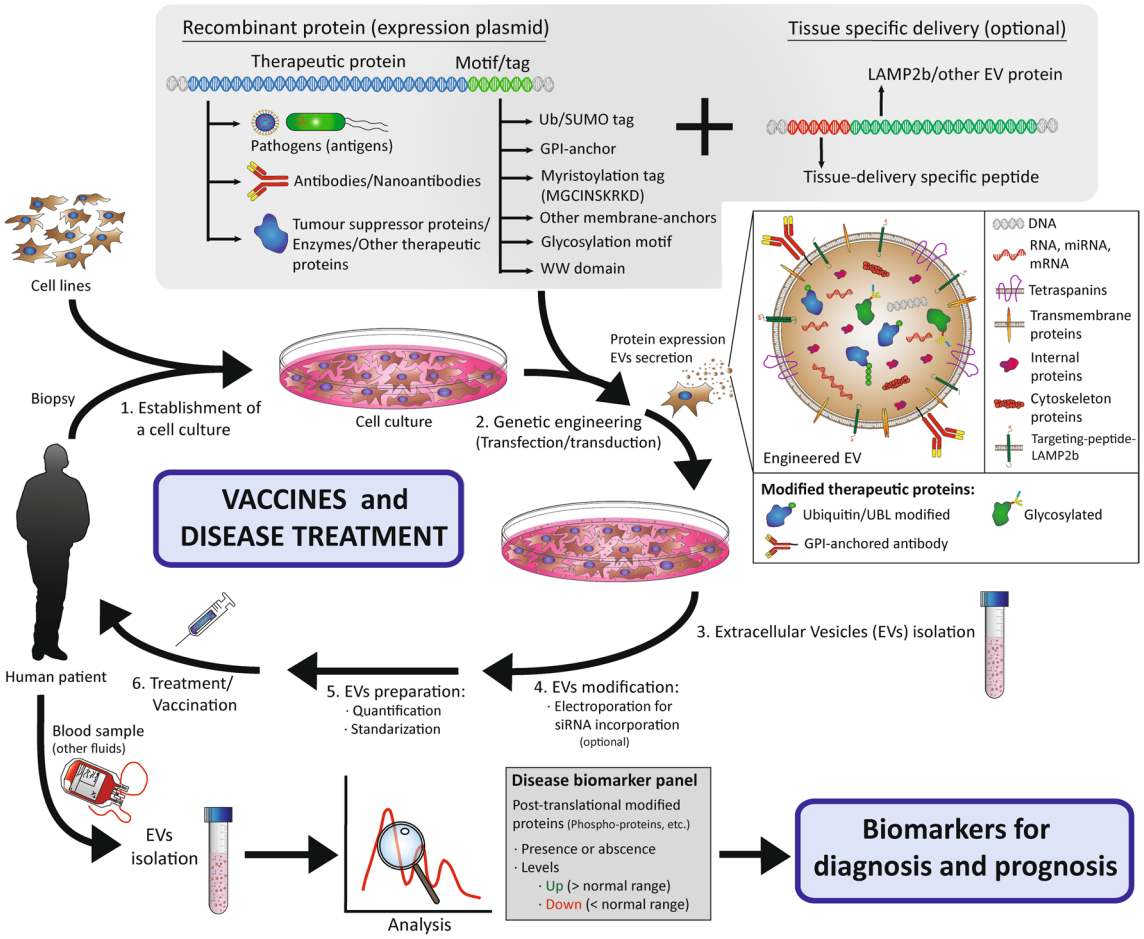

Fig. 3 Targeting post-translationally modified proteins into EVs for biomedical applications. The process for exosome engineering to use as a vaccine or treatment comprises various steps: (1) EVs can be isolated from different cell cultures, either cell lines or cells obtained from human biopsies. (2) These cells can be transfected or transduced with specific constructs coding for engineered therapeutic proteins, that will be targeted to EVs by the addition of a specific PTM motif or tag. Therapeutic proteins include: pathogen antigens for the generation of vaccines; antibodies or nanoantibodies for activation or blocking of signalling pathways, or any kind of protein with a therapeutic potential. Besides, the expression of LAMP2b fused to a tissue-delivery targeting-peptide defines a specific fate for these EVs once in the blood stream. (3) The EVs can be isolated by diverse procedures. (4) Additionally, an extra step can be performed to incorporate inside EVs therapeutic small interference RNAs by electroporation. (5, 6) Finally, EVs preparations, once standardized and quantified, could be administered intravenously for disease treatment or vaccination. On the other hand, EVs obtained from blood samples (or other fluids) can be analysed to identify certain condition biomarkers (post-translational modified protein) for disease prognosis and diagnosis. The images in the figures are not scaled

biomarker for Alzheimer's disease (AD) [115]. In fact, ph-Tau in combination with Aβ activate diverse signalling pathways, increasing the production of hyperphosphorylated Tau oligomers, which are then secreted by exosomes within the brain, accelerating neurodegeneration [110]. Moreover, some AD-related proteins such as ph-Tau, Aβ1-42, neurogranin (NRGN) and the repressor element 1-silencing transcription factor (REST) contained in neuronal-derived exosomes appear in plasma [117]. The transference of these proteins contained in exosomes isolated from AD patients' plasma into the central nervous system of a normal mouse causes Tau aggregation and induces AD-like neuropathology [117]. Other studies carried out with Tau-transgenic mice (rTg4510) revealed a high grade of pathology and higher accumulation of Tau in their exosomes compared to control ones [113].

On the other hand, several phosphorylations of IRS-1 in different residues associate to insulin resistance syndrome in diabetes mellitus as well as to degenerative diseases such as AD and fronto-temporal dementia [111]. Exosomes released by retinal pigment epithelial (RPE) cells into vitreous humour contain a vast subset of phosphorylated proteins in age-related macular degeneration (AMD) patients [108]. Oxidative stressed RPE cells modify the phosphorylation profile of exosomal proteins compared to control cells, thus their detection could represent a source of biomarkers for diagnosis and prognosis of eye-degenerative diseases [108].

Besides, detection of modified exosomal proteins bears potential as a biomarker of treatment progression. For instance, cetuximab works as a therapeutic antibody to block EGFR activation in tumour cells [116]. EVs coming from cetuximab-treated cells represent well their originating cells, containing lower level of phosphorylated EGFR after treatment [116]. Monitoring total and phosphorylated forms of EGFR present in EVs from patient blood could reflect the efficacy of anti-tumour therapy [116].

Moreover, detection of some exosomal biomarkers can reveal the existence of side effects during treatment. For example, a fraction of kidney transplant patients treated with tacrolimus as part of the immunosuppressive therapy developed hypertension 6 months after surgery [114]. Urinary exosomes of hypertensive patients are enriched in the phosphorylated form of thiazide-sensitive NCC compared to non-hypertensive patients [114]. Hence, the measurement of total and phosphorylated NCC in urinary exosomes can be used as a biomarker of hypertension [114].

Vaccines

EVs also represent a promising tool for other therapeutic applications, such as generation of vaccines. EVs and many viruses share common mechanisms for protein sorting and particle release [134]. The study of EVs physiology can help us to understand virus infections, but also to generate virus-like particles suitable for vaccination exploiting the exosome pathway by sorting virus proteins into exosomes. For instance, exosomes isolated from infected cells can prime mice and protect them from a following lethal infection [135]. In the case of macrophages infected with the intracellular bacteria *Mycobacterium tuberculosis*, more than 40 mycobacterial components appear in exosomes [136] (Table 2). In addition, the administration of soluble mycobacterial proteins in human epithelial and mouse macrophage cell lines promotes sorting of similar bacterial proteins into exosomes [136]. Ubiquitination of mycobacterial proteins such as HspX and GroES acts as a signal for their incorporation into ILVs and secretion as EVs [136]. Moreover, vaccination using these exosomes in mice protects them against subsequent aerosolized infection with the whole infective bacteria [136]. This is just an example of how vaccination with a PTM-protein is a new strategy to initiate a protective immune response against a specific pathogen. An option for heterologous protein sorting into exosomes, which can be used as a vaccine, consists of protein overexpression with the addition of an ubiquitin tag, avoiding strategies based on inactivated or non-replicative pathogens [128, 137] (Fig. 3). This approach enables the exosomal delivery of proteins not usually found in exosomes, e.g. GFP. For instance, the use of exosomes produced by a stable cell line and containing recombinant fusion proteins from *M. tuberculosis* evoked T cell immune responses [137]. However, although exosome-based vaccines could trigger antigen-specific immune responses, they also contain other proteins that could trigger side- or off-target effects. In addition to ubiquitin, GFP SUMOylation drives it into exosomes, suggesting that SUMO could work as a specific sorting tool for antigen incorporation into exosomes for vaccination schemes [106] (Fig. 3).

Disease treatment

EVs are a promising tool to design new strategies for disease treatment. The size of these small particles make them suitable to carry proteins, lipids, RNA, DNA or small chemical drugs, protecting them from external factors in the blood stream [138, 139]. They can be easily isolated in high amounts from diverse culture cells types. Furthermore, the target specificity of EVs prevents some secondary effects observed in traditional therapies [138]. One of the most potent advantages of exosomes is their capability of crossing the brain blood barrier (BBB), which opens a wide variety of possibilities for diagnosis and treatment of neurodegenerative diseases [140]. In fact, exosomes carrying a specific siRNA and a brain-delivery peptide signal could even silence the expression of the targeted gene [141]. Generating exosomes targeted to a certain type of tissue can be

accomplished by the expression of specific tissue-delivery peptide fused to the N-t of lysosome-associated membrane glycoprotein 2 (LAMP2), a transmembrane protein which causes their incorporation into EVs [141]. Engineered targeting peptides-LAMP2 sometimes undergo degradation even when localized to exosomes, reducing their potential as therapeutic tools. A recent study has discovered that the incorporation of glycosylating motifs enhances their delivery and protects them from damage [142].

The use of engineered EVs based on biologically active proteins could be used to treat some diseases. The addition of a WW tag (a domain-containing PPxY motif) to a certain protein determines its incorporation into exosomes [139]. The L-domains of Ndfip1 recognize this particular mark, targeting this protein to exosomes [14]. In the same way, we propose the use of known PTMs motifs, such as the myristoylation sequence MGCINSKRKD, in the N-t of the protein of interest to drive it specifically into exosomes, as other authors have described for Tya [124]. Moreover, addition of a C-t ubiquitin or SUMO tag could deliver proteins into exosomes, including targeting-peptides-LAMP2 with glycosylated motifs for specific tissue delivery [106, 137, 142]. Besides, protein glycosylation has improved the efficacy of therapeutic proteins [143]. Thus, addition of glycosylating motifs to the protein of interest could also mediate its incorporation to exosomes, although protein glycosylation is still technically complex for industrial production [73, 107] (Fig. 3).

PTM-dependent sorting approaches could contribute to halting tumour progression and development. PTEN, a tumour suppressor phosphatase, is ubiquitinated in exosomes and is active in recipient cells, promoting the dephosphorylation of AKT [78]. Hence, the uptake of exosomes containing the C-t domain of PTEN by cancer cells reduces proliferation, migration and metastasis, postulating such a strategy as an anti-tumour treatment [144]. On the other hand, GPI modification of blocking-nanoantibodies that recognize receptors present in tumour cells, favours their attachment to exosomes. Exosome-attached EGFR-nanoantibodies approach can confer a specific selectivity to EVs against tumour cells, decreasing their EGFR-proliferative signalling pathways [145]. Hence, GPI anchors can be used to target particular proteins to EVs for biomedical applications [146] (Fig. 3). To sum up, all these strategies remark the potential application of EVs-containing post-translational modified proteins for selective delivery of therapeutic components into specific tissues.

Concluding remarks

Although the mechanisms that define the sorting of proteins into EVs are not fully understood, PTMs are likely to play an important role. Many post-translationally modified proteins have been detected in EVs [73, 107], whereas others that have not been identified in EVs could have a role in protein delivery, participating in the incorporation of other proteins, or being removed before secretion. Ubiquitination or SUMOylation of some proteins have a clear role in their incorporation into exosomes, whereas others such as ISGylation or acetylation oppose such mechanisms, driving the modified protein to degradation [106, 128, 137]. Moreover, exosome secretion can be mediated by diverse mechanisms, such as the ESCRT complex, lipids and tetraspanins, increasing the complexity and diversity of ILV-protein sorting and exosome release [18]. In this regard, EVs populations are heterogeneous as each vesicle contains a specific repertoire of proteins potentially different from its neighbours [10, 11]. In addition, there are other factors that increase the complexity of this system, for example the fact that almost every cell can secrete EVs containing common and cell-type-specific markers. Then, the final destination of each population of EVs can be different, working as an autocrine or paracrine signal or even travelling throughout the blood stream to other tissues.

Regarding ubiquitination, its own structure and functional complexity increases the number of factors to be taken into consideration. Compartimentalization and specificity of the different E3 ligases participate in protein localization [93, 94]. In addition, competition or crosstalk with other PTMs such as SUMOylation or Neddylation alters the fate of the modified protein [100]. Also, the complexity of the ubiquitin code includes homotypic, heterotypic, mixed or branched chains that distribute protein populations among many cellular processes such as proteasome degradation or endocytic trafficking, forming a ubiquitin-based protein ZIP code that has yet to be revealed [20–25, 33, 147]. Finally, the study of ubiquitinated proteins or even UBLs is difficult technically. Proteomics approaches to find ubiquitinated proteins in whole proteome typically used trypsin digestion of the sample. Nowadays, the discovery of new UBLs highlights that the sole use of this enzyme may mask the appearance of additional variations due to the same di-Gly residue shared by all these kind of modifications [148]. Hence, this information can only be used to localize specific sites on proteins susceptible to be modified by these kind of PTMs [148]. Nevertheless, some approaches tried to discern among these PTMs by terminal mutation and protein overexpression [149]. Besides, these proteomic approaches could also help to discover or define any possible consensus sequence for protein delivery into EVs, either protein mono-ubiquitination and selective chain formation or other PTMs [102, 150, 151].

In addition, EVs represent a novel non-invasive and selective therapeutic tool to be developed for prognosis, diagnosis or treatment of diverse diseases, with very promising

preliminary results [138, 139, 152, 153]. PTMs confer specific properties to proteins, playing a relevant role in EVs protein sorting. Hence, the use of PTMs represents a useful tool for the generation of therapeutically engineered EVs.

Acknowledgements The authors thank Dr. Miguel Vicente-Manzanares and Dr. Manuel Gómez-Gutiérrez for assistance with English editing. This work was supported by Grants to Francisco Sánchez-Madrid, SAF2014-55579-R; INDISNET-S2011/BMD-2332; PIE13/00041; H2020 European Research Council (ERC-2011-AdG 294340-GENTRIS); and was co-funded by Fondo Europeo de Desarrollo Regional (FEDER). Irene Fernández-Delgado and Olga Moreno-Gonzalo are supported by Formación de Profesorado Universitario (FPU) program from the Spanish Ministry of Education, Culture and Sports. The CNIC is supported by the Spanish Ministry of Economy, Industry and Competitiveness (MINECO) and by the Pro CNIC Foundation.

References

1. Yanez-Mo M, Siljander PR, Andreu Z, Zavec AB, Borras FE, Buzas EI, Buzas K, Casal E, Cappello F, Carvalho J, Colas E, Cordeiro-da Silva A, Fais S, Falcon-Perez JM, Ghobrial IM, Giebel B, Gimona M, Graner M, Gursel I, Gursel M, Heegaard NH, Hendrix A, Kierulf P, Kokubun K, Kosanovic M, Kralj-Iglic V, Kramer-Albers EM, Laitinen S, Lasser C, Lener T, Ligeti E, Line A, Lipps G, Llorente A, Lotvall J, Mancek-Keber M, Marcilla A, Mittelbrunn M, Nazarenko I, Nolte-'t Hoen EN, Nyman TA, O'Driscoll L, Olivan M, Oliveira C, Pallinger E, Del Portillo HA, Reventos J, Rigau M, Rohde E, Sammar M, Sanchez-Madrid F, Santarem N, Schallmoser K, Ostenfeld MS, Stoorvogel W, Stukelj R, Van der Grein SG, Vasconcelos MH, Wauben MH, De Wever O (2015) Biological properties of extracellular vesicles and their physiological functions. J Extracell Vesicles 4:27066. https://doi.org/10.3402/jev.v4.27066
2. Raposo G, Stoorvogel W (2013) Extracellular vesicles: exosomes, microvesicles, and friends. J Cell Biol 200(4):373–383. https://doi.org/10.1083/jcb.201211138
3. Colombo M, Raposo G, Thery C (2014) Biogenesis, secretion, and intercellular interactions of exosomes and other extracellular vesicles. Annu Rev Cell Dev Biol 30:255–289. https://doi.org/10.1146/annurev-cellbio-101512-122326
4. Kowal J, Tkach M, Thery C (2014) Biogenesis and secretion of exosomes. Curr Opin Cell Biol 29:116–125. https://doi.org/10.1016/j.ceb.2014.05.004
5. Vallabhaneni KC, Penfornis P, Dhule S, Guillonneau F, Adams KV, Mo YY, Xu R, Liu Y, Watabe K, Vemuri MC, Pochampally R (2015) Extracellular vesicles from bone marrow mesenchymal stem/stromal cells transport tumor regulatory microRNA, proteins, and metabolites. Oncotarget 6(7):4953–4967. https://doi.org/10.18632/oncotarget.3211
6. Thery C, Zitvogel L, Amigorena S (2002) Exosomes: composition, biogenesis and function. Nat Rev Immunol 2(8):569–579. https://doi.org/10.1038/nri855
7. Llorente A, Skotland T, Sylvanne T, Kauhanen D, Rog T, Orlowski A, Vattulainen I, Ekroos K, Sandvig K (2013) Molecular lipidomics of exosomes released by PC-3 prostate cancer cells. Biochim Biophys Acta 1831(7):1302–1309
8. Skotland T, Sandvig K, Llorente A (2017) Lipids in exosomes: current knowledge and the way forward. Prog Lipid Res 66:30–41. https://doi.org/10.1016/j.plipres.2017.03.001
9. Keller S, Rupp C, Stoeck A, Runz S, Fogel M, Lugert S, Hager HD, Abdel-Bakky MS, Gutwein P, Altevogt P (2007) CD24 is a marker of exosomes secreted into urine and amniotic fluid. Kidney Int 72(9):1095–1102. https://doi.org/10.1038/sj.ki.5002486
10. Bobrie A, Colombo M, Krumeich S, Raposo G, Thery C (2012) Diverse subpopulations of vesicles secreted by different intracellular mechanisms are present in exosome preparations obtained by differential ultracentrifugation. J Extracell Vesicles. https://doi.org/10.3402/jev.v1i0.18397
11. Colombo M, Moita C, van Niel G, Kowal J, Vigneron J, Benaroch P, Manel N, Moita LF, Thery C, Raposo G (2013) Analysis of ESCRT functions in exosome biogenesis, composition and secretion highlights the heterogeneity of extracellular vesicles. J Cell Sci 126(Pt 24):5553–5565. https://doi.org/10.1242/jcs.128868
12. Sreekumar PG, Kannan R, Kitamura M, Spee C, Barron E, Ryan SJ, Hinton DR (2010) AlphaB crystallin is apically secreted within exosomes by polarized human retinal pigment epithelium and provides neuroprotection to adjacent cells. PLoS One 5(10):e12578. https://doi.org/10.1371/journal.pone.0012578
13. Buschow SI, Nolte-'t Hoen EN, van Niel G, Pols MS, ten Broeke T, Lauwen M, Ossendorp F, Melief CJ, Raposo G, Wubbolts R, Wauben MH, Stoorvogel W (2009) MHC II in dendritic cells is targeted to lysosomes or T cell-induced exosomes via distinct multivesicular body pathways. Traffic 10(10):1528–1542. https://doi.org/10.1111/j.1600-0854.2009.00963.x
14. Putz U, Howitt J, Lackovic J, Foot N, Kumar S, Silke J, Tan SS (2008) Nedd4 family-interacting protein 1 (Ndfip1) is required for the exosomal secretion of Nedd4 family proteins. J Biol Chem 283(47):32621–32627. https://doi.org/10.1074/jbc.M804120200
15. van der Vlist EJ, Arkesteijn GJ, van de Lest CH, Stoorvogel W, Nolte-'t Hoen EN, Wauben MH (2012) CD4(+) T cell activation promotes the differential release of distinct populations of nanosized vesicles. J Extracell Vesicles. https://doi.org/10.3402/jev.v1i0.18364
16. Khoury GA, Baliban RC, Floudas CA (2011) Proteome-wide post-translational modification statistics: frequency analysis and curation of the swiss-prot database. Sci Rep. https://doi.org/10.1038/srep00090
17. Knorre DG, Kudryashova NV, Godovikova TS (2009) Chemical and functional aspects of posttranslational modification of proteins. Acta Nat 1(3):29–51
18. Villarroya-Beltri C, Baixauli F, Gutierrez-Vazquez C, Sanchez-Madrid F, Mittelbrunn M (2014) Sorting it out: regulation of exosome loading. Semin Cancer Biol 28:3–13. https://doi.org/10.1016/j.semcancer.2014.04.009
19. Dye BT, Schulman BA (2007) Structural mechanisms underlying posttranslational modification by ubiquitin-like proteins. Annu Rev Biophys Biomol Struct 36:131–150. https://doi.org/10.1146/annurev.biophys.36.040306.132820
20. Pickart CM, Eddins MJ (2004) Ubiquitin: structures, functions, mechanisms. Biochim Biophys Acta 1695(1–3):55–72. https://doi.org/10.1016/j.bbamcr.2004.09.019
21. Komander D, Rape M (2012) The ubiquitin code. Annu Rev Biochem 81:203–229. https://doi.org/10.1146/annurev-biochem-060310-170328
22. Swatek KN, Komander D (2016) Ubiquitin modifications. Cell Res 26(4):399–422. https://doi.org/10.1038/cr.2016.39
23. Aillet F, Lopitz-Otsoa F, Egana I, Hjerpe R, Fraser P, Hay RT, Rodriguez MS, Lang V (2012) Heterologous SUMO-2/3-ubiquitin chains optimize IkappaBalpha degradation and NF-kappaB activity. PLoS One 7(12):e51672. https://doi.org/10.1371/journal.pone.0051672
24. Fan JB, Arimoto K, Motamedchaboki K, Yan M, Wolf DA, Zhang DE (2015) Identification and characterization of a novel ISG15-ubiquitin mixed chain and its role in regulating protein homeostasis. Sci Rep 5:12704. https://doi.org/10.1038/srep12704

25. Hjerpe R, Thomas Y, Kurz T (2012) NEDD8 overexpression results in neddylation of ubiquitin substrates by the ubiquitin pathway. J Mol Biol 421(1):27–29. https://doi.org/10.1016/j.jmb.2012.05.013
26. Johnson ES, Ma PC, Ota IM, Varshavsky A (1995) A proteolytic pathway that recognizes ubiquitin as a degradation signal. J Biol Chem 270(29):17442–17456
27. Bache KG, Raiborg C, Mehlum A, Stenmark H (2003) STAM and Hrs are subunits of a multivalent ubiquitin-binding complex on early endosomes. J Biol Chem 278(14):12513–12521. https://doi.org/10.1074/jbc.M210843200
28. Ikeda F, Dikic I (2008) Atypical ubiquitin chains: new molecular signals. 'Protein Modifications: beyond the Usual Suspects' review series. EMBO Rep 9(6):536–542. https://doi.org/10.1038/embor.2008.93
29. Mukhopadhyay D, Riezman H (2007) Proteasome-independent functions of ubiquitin in endocytosis and signaling. Science 315(5809):201–205. https://doi.org/10.1126/science.1127085
30. Schnell JD, Hicke L (2003) Non-traditional functions of ubiquitin and ubiquitin-binding proteins. J Biol Chem 278(38):35857–35860. https://doi.org/10.1074/jbc.R300018200
31. Hammond-Martel I, Yu H, el Affar B (2012) Roles of ubiquitin signaling in transcription regulation. Cell Signal 24(2):410–421. https://doi.org/10.1016/j.cellsig.2011.10.009
32. Hofmann K (2009) Ubiquitin-binding domains and their role in the DNA damage response. DNA Repair (Amst) 8(4):544–556. https://doi.org/10.1016/j.dnarep.2009.01.003
33. Michel MA, Elliott PR, Swatek KN, Simicek M, Pruneda JN, Wagstaff JL, Freund SM, Komander D (2015) Assembly and specific recognition of k29- and k33-linked polyubiquitin. Mol Cell 58(1):95–109. https://doi.org/10.1016/j.molcel.2015.01.042
34. Hochstrasser M (2009) Origin and function of ubiquitin-like proteins. Nature 458(7237):422–429. https://doi.org/10.1038/nature07958
35. Kerscher O, Felberbaum R, Hochstrasser M (2006) Modification of proteins by ubiquitin and ubiquitin-like proteins. Annu Rev Cell Dev Biol 22:159–180. https://doi.org/10.1146/annurev.cellbio.22.010605.093503
36. Taherbhoy AM, Schulman BA, Kaiser SE (2012) Ubiquitin-like modifiers. Essays Biochem 52:51–63. https://doi.org/10.1042/bse0520051
37. van der Veen AG, Ploegh HL (2012) Ubiquitin-like proteins. Annu Rev Biochem 81:323–357. https://doi.org/10.1146/annurev-biochem-093010-153308
38. Vierstra RD (2012) The expanding universe of ubiquitin and ubiquitin-like modifiers. Plant Physiol 160(1):2–14. https://doi.org/10.1104/pp.112.200667
39. Enchev RI, Schulman BA, Peter M (2015) Protein neddylation: beyond cullin-RING ligases. Nat Rev Mol Cell Biol 16(1):30–44. https://doi.org/10.1038/nrm3919
40. Kamitani T, Kito K, Nguyen HP, Yeh ET (1997) Characterization of NEDD8, a developmentally down-regulated ubiquitin-like protein. J Biol Chem 272(45):28557–28562
41. Jones J, Wu K, Yang Y, Guerrero C, Nillegoda N, Pan ZQ, Huang L (2008) A targeted proteomic analysis of the ubiquitin-like modifier nedd8 and associated proteins. J Proteome Res 7(3):1274–1287. https://doi.org/10.1021/pr700749v
42. Flotho A, Melchior F (2013) Sumoylation: a regulatory protein modification in health and disease. Annu Rev Biochem 82:357–385. https://doi.org/10.1146/annurev-biochem-061909-093311
43. Villarroya-Beltri C, Guerra S, Sanchez-Madrid F (2017) ISGylation—a key to lock the cell gates for preventing the spread of threats. J Cell Sci. https://doi.org/10.1242/jcs.205468
44. Morales DJ, Lenschow DJ (2013) The antiviral activities of ISG15. J Mol Biol 425(24):4995–5008. https://doi.org/10.1016/j.jmb.2013.09.041
45. Desai SD (2015) ISG15: a double edged sword in cancer. Oncoimmunology 4(12):e1052935. https://doi.org/10.1080/2162402X.2015.1052935
46. Campbell JA, Lenschow DJ (2013) Emerging roles for immunomodulatory functions of free ISG15. J Interferon Cytokine Res 33(12):728–738. https://doi.org/10.1089/jir.2013.0064
47. Henne WM, Buchkovich NJ, Emr SD (2011) The ESCRT pathway. Dev Cell 21(1):77–91. https://doi.org/10.1016/j.devcel.2011.05.015
48. Raiborg C, Stenmark H (2009) The ESCRT machinery in endosomal sorting of ubiquitylated membrane proteins. Nature 458(7237):445–452. https://doi.org/10.1038/nature07961
49. Zhu H, Guariglia S, Yu RY, Li W, Brancho D, Peinado H, Lyden D, Salzer J, Bennett C, Chow CW (2013) Mutation of SIMPLE in Charcot-Marie-Tooth 1C alters production of exosomes. Mol Biol Cell 24(11):1619–1637. https://doi.org/10.1091/mbc.E12-07-0544 **(S1611–S1613)**
50. Tamai K, Tanaka N, Nakano T, Kakazu E, Kondo Y, Inoue J, Shiina M, Fukushima K, Hoshino T, Sano K, Ueno Y, Shimosegawa T, Sugamura K (2010) Exosome secretion of dendritic cells is regulated by Hrs, an ESCRT-0 protein. Biochem Biophys Res Commun 399(3):384–390. https://doi.org/10.1016/j.bbrc.2010.07.083
51. Perez-Hernandez D, Gutierrez-Vazquez C, Jorge I, Lopez-Martin S, Ursa A, Sanchez-Madrid F, Vazquez J, Yanez-Mo M (2013) The intracellular interactome of tetraspanin-enriched microdomains reveals their function as sorting machineries toward exosomes. J Biol Chem 288(17):11649–11661. https://doi.org/10.1074/jbc.M112.445304
52. Gauvreau ME, Cote MH, Bourgeois-Daigneault MC, Rivard LD, Xiu F, Brunet A, Shaw A, Steimle V, Thibodeau J (2009) Sorting of MHC class II molecules into exosomes through a ubiquitin-independent pathway. Traffic 10(10):1518–1527. https://doi.org/10.1111/j.1600-0854.2009.00948.x
53. Kim BY, Olzmann JA, Barsh GS, Chin LS, Li L (2007) Spongiform neurodegeneration-associated E3 ligase Mahogunin ubiquitylates TSG101 and regulates endosomal trafficking. Mol Biol Cell 18(4):1129–1142. https://doi.org/10.1091/mbc.E06-09-0787
54. McDonald B, Martin-Serrano J (2008) Regulation of Tsg101 expression by the steadiness box: a role of Tsg101-associated ligase. Mol Biol Cell 19(2):754–763. https://doi.org/10.1091/mbc.E07-09-0957
55. McCullough J, Row PE, Lorenzo O, Doherty M, Beynon R, Clague MJ, Urbe S (2006) Activation of the endosome-associated ubiquitin isopeptidase AMSH by STAM, a component of the multivesicular body-sorting machinery. Curr Biol 16(2):160–165. https://doi.org/10.1016/j.cub.2005.11.073
56. Row PE, Prior IA, McCullough J, Clague MJ, Urbe S (2006) The ubiquitin isopeptidase UBPY regulates endosomal ubiquitin dynamics and is essential for receptor down-regulation. J Biol Chem 281(18):12618–12624. https://doi.org/10.1074/jbc.M512615200
57. Buschow SI, Liefhebber JM, Wubbolts R, Stoorvogel W (2005) Exosomes contain ubiquitinated proteins. Blood Cells Mol Dis 35(3):398–403. https://doi.org/10.1016/j.bcmd.2005.08.005
58. Mazurov D, Barbashova L, Filatov A (2013) Tetraspanin protein CD9 interacts with metalloprotease CD10 and enhances its release via exosomes. FEBS J 280(5):1200–1213. https://doi.org/10.1111/febs.12110
59. Mittelbrunn M, Gutierrez-Vazquez C, Villarroya-Beltri C, Gonzalez S, Sanchez-Cabo F, Gonzalez MA, Bernad A, Sanchez-Madrid F (2011) Unidirectional transfer of microRNA-loaded exosomes from T cells to antigen-presenting cells. Nat Commun 2:282. https://doi.org/10.1038/ncomms1285
60. Yuyama K, Sun H, Mitsutake S, Igarashi Y (2012) Sphingolipid-modulated exosome secretion promotes clearance of

amyloid-beta by microglia. J Biol Chem 287(14):10977–10989. https://doi.org/10.1074/jbc.M111.324616
61. Baietti MF, Zhang Z, Mortier E, Melchior A, Degeest G, Geeraerts A, Ivarsson Y, Depoortere F, Coomans C, Vermeiren E, Zimmermann P, David G (2012) Syndecan-syntenin-ALIX regulates the biogenesis of exosomes. Nat Cell Biol 14(7):677–685. https://doi.org/10.1038/ncb2502
62. Stuffers S, Sem Wegner C, Stenmark H, Brech A (2009) Multivesicular endosome biogenesis in the absence of ESCRTs. Traffic 10(7):925–937. https://doi.org/10.1111/j.1600-0854.2009.00920.x
63. Trajkovic K, Hsu C, Chiantia S, Rajendran L, Wenzel D, Wieland F, Schwille P, Brugger B, Simons M (2008) Ceramide triggers budding of exosome vesicles into multivesicular endosomes. Science 319(5867):1244–1247. https://doi.org/10.1126/science.1153124
64. Alonso R, Rodriguez MC, Pindado J, Merino E, Merida I, Izquierdo M (2005) Diacylglycerol kinase alpha regulates the secretion of lethal exosomes bearing Fas ligand during activation-induced cell death of T lymphocytes. J Biol Chem 280(31):28439–28450. https://doi.org/10.1074/jbc.M501112200
65. Aung T, Chapuy B, Vogel D, Wenzel D, Oppermann M, Lahmann M, Weinhage T, Menck K, Hupfeld T, Koch R, Trumper L, Wulf GG (2011) Exosomal evasion of humoral immunotherapy in aggressive B-cell lymphoma modulated by ATP-binding cassette transporter A3. Proc Natl Acad Sci USA 108(37):15336–15341. https://doi.org/10.1073/pnas.1102855108
66. Bollag WB, Xie D, Zheng X, Zhong X (2007) A potential role for the phospholipase D2-aquaporin-3 signaling module in early keratinocyte differentiation: production of a phosphatidylglycerol signaling lipid. J Investig Dermatol 127(12):2823–2831. https://doi.org/10.1038/sj.jid.5700921
67. Kajimoto T, Okada T, Miya S, Zhang L, Nakamura S (2013) Ongoing activation of sphingosine 1-phosphate receptors mediates maturation of exosomal multivesicular endosomes. Nat Commun 4:2712. https://doi.org/10.1038/ncomms3712
68. Kobayashi T, Stang E, Fang KS, de Moerloose P, Parton RG, Gruenberg J (1998) A lipid associated with the antiphospholipid syndrome regulates endosome structure and function. Nature 392(6672):193–197. https://doi.org/10.1038/32440
69. Laulagnier K, Grand D, Dujardin A, Hamdi S, Vincent-Schneider H, Lankar D, Salles JP, Bonnerot C, Perret B, Record M (2004) PLD2 is enriched on exosomes and its activity is correlated to the release of exosomes. FEBS Lett 572(1–3):11–14. https://doi.org/10.1016/j.febslet.2004.06.082
70. Matsuo H, Chevallier J, Mayran N, Le Blanc I, Ferguson C, Faure J, Blanc NS, Matile S, Dubochet J, Sadoul R, Parton RG, Vilbois F, Gruenberg J (2004) Role of LBPA and Alix in multivesicular liposome formation and endosome organization. Science 303(5657):531–534. https://doi.org/10.1126/science.1092425
71. Strauss K, Goebel C, Runz H, Mobius W, Weiss S, Feussner I, Simons M, Schneider A (2010) Exosome secretion ameliorates lysosomal storage of cholesterol in Niemann-Pick type C disease. J Biol Chem 285(34):26279–26288. https://doi.org/10.1074/jbc.M110.134775
72. Pisitkun T, Shen RF, Knepper MA (2004) Identification and proteomic profiling of exosomes in human urine. Proc Natl Acad Sci USA 101(36):13368–13373. https://doi.org/10.1073/pnas.0403453101
73. Moreno-Gonzalo O, Villarroya-Beltri C, Sanchez-Madrid F (2014) Post-translational modifications of exosomal proteins. Front Immunol 5:383. https://doi.org/10.3389/fimmu.2014.00383
74. Burke MC, Oei MS, Edwards NJ, Ostrand-Rosenberg S, Fenselau C (2014) Ubiquitinated proteins in exosomes secreted by myeloid-derived suppressor cells. J Proteome Res 13(12):5965–5972. https://doi.org/10.1021/pr500854x
75. Alegre E, Rebmann V, Lemaoult J, Rodriguez C, Horn PA, Diaz-Lagares A, Echeveste JI, Gonzalez A (2013) In vivo identification of an HLA-G complex as ubiquitinated protein circulating in exosomes. Eur J Immunol 43(7):1933–1939. https://doi.org/10.1002/eji.201343318
76. Nabhan JF, Hu R, Oh RS, Cohen SN, Lu Q (2012) Formation and release of arrestin domain-containing protein 1-mediated microvesicles (ARMMs) at plasma membrane by recruitment of TSG101 protein. Proc Natl Acad Sci USA 109(11):4146–4151. https://doi.org/10.1073/pnas.1200448109
77. Ikeda M, Longnecker R (2007) Cholesterol is critical for Epstein-Barr virus latent membrane protein 2A trafficking and protein stability. Virology 360(2):461–468. https://doi.org/10.1016/j.virol.2006.10.046
78. Putz U, Howitt J, Doan A, Goh CP, Low LH, Silke J, Tan SS (2012) The tumor suppressor PTEN is exported in exosomes and has phosphatase activity in recipient cells. Sci Signal 5(243):ra70. https://doi.org/10.1126/scisignal.2003084
79. Zuccato E, Blott EJ, Holt O, Sigismund S, Shaw M, Bossi G, Griffiths GM (2007) Sorting of Fas ligand to secretory lysosomes is regulated by mono-ubiquitylation and phosphorylation. J Cell Sci 120(Pt 1):191–199. https://doi.org/10.1242/jcs.03315
80. Liu Y, Shah SV, Xiang X, Wang J, Deng ZB, Liu C, Zhang L, Wu J, Edmonds T, Jambor C, Kappes JC, Zhang HG (2009) COP9-associated CSN5 regulates exosomal protein deubiquitination and sorting. Am J Pathol 174(4):1415–1425. https://doi.org/10.2353/ajpath.2009.080861
81. Bourgeois-Daigneault MC, Thibodeau J (2013) Identification of a novel motif that affects the conformation and activity of the MARCH1 E3 ubiquitin ligase. J Cell Sci 126(Pt 4):989–998. https://doi.org/10.1242/jcs.117804
82. Geminard C, De Gassart A, Blanc L, Vidal M (2004) Degradation of AP2 during reticulocyte maturation enhances binding of hsc70 and Alix to a common site on TFR for sorting into exosomes. Traffic 5(3):181–193. https://doi.org/10.1111/j.1600-0854.2004.0167.x
83. Bourgeois-Daigneault MC, Thibodeau J (2012) Autoregulation of MARCH1 expression by dimerization and autoubiquitination. J Immunol 188(10):4959–4970. https://doi.org/10.4049/jimmunol.1102708
84. Huebner AR, Cheng L, Somparn P, Knepper MA, Fenton RA, Pisitkun T (2016) Deubiquitylation of protein cargo is not an essential step in exosome formation. Mol Cell Proteom 15(5):1556–1571. https://doi.org/10.1074/mcp.M115.054965
85. Srikanthan S, Li W, Silverstein RL, McIntyre TM (2014) Exosome poly-ubiquitin inhibits platelet activation, downregulates CD36 and inhibits pro-atherothombotic cellular functions. J Thromb Haemost 12(11):1906–1917. https://doi.org/10.1111/jth.12712
86. Kravtsova-Ivantsiv Y, Ciechanover A (2012) Non-canonical ubiquitin-based signals for proteasomal degradation. J Cell Sci 125(Pt 3):539–548. https://doi.org/10.1242/jcs.093567
87. Lecker SH, Goldberg AL, Mitch WE (2006) Protein degradation by the ubiquitin-proteasome pathway in normal and disease states. J Am Soc Nephrol 17(7):1807–1819. https://doi.org/10.1681/ASN.2006010083
88. Koegl M, Hoppe T, Schlenker S, Ulrich HD, Mayer TU, Jentsch S (1999) A novel ubiquitination factor, E4, is involved in multiubiquitin chain assembly. Cell 96(5):635–644
89. Nathan JA, Kim HT, Ting L, Gygi SP, Goldberg AL (2013) Why do cellular proteins linked to K63-polyubiquitin chains not associate with proteasomes? EMBO J 32(4):552–565. https://doi.org/10.1038/emboj.2012.354
90. Erpapazoglou Z, Dhaoui M, Pantazopoulou M, Giordano F, Mari M, Leon S, Raposo G, Reggiori F, Haguenauer-Tsapis R (2012) A dual role for K63-linked ubiquitin chains in multivesicular

body biogenesis and cargo sorting. Mol Biol Cell 23(11):2170–2183. https://doi.org/10.1091/mbc.E11-10-0891
91. Hicke L, Schubert HL, Hill CP (2005) Ubiquitin-binding domains. Nat Rev Mol Cell Biol 6(8):610–621. https://doi.org/10.1038/nrm1701
92. Husnjak K, Dikic I (2012) Ubiquitin-binding proteins: decoders of ubiquitin-mediated cellular functions. Annu Rev Biochem 81:291–322. https://doi.org/10.1146/annurev-biochem-051810-094654
93. Huang F, Gu H (2008) Negative regulation of lymphocyte development and function by the Cbl family of proteins. Immunol Rev 224:229–238. https://doi.org/10.1111/j.1600-065X.2008.00655.x
94. Thien CB, Langdon WY (1998) c-Cbl: a regulator of T cell receptor-mediated signalling. Immunol Cell Biol 76(5):473–482. https://doi.org/10.1046/j.1440-1711.1998.00768.x
95. Bartee E, Mansouri M, Hovey Nerenberg BT, Gouveia K, Fruh K (2004) Downregulation of major histocompatibility complex class I by human ubiquitin ligases related to viral immune evasion proteins. J Virol 78(3):1109–1120
96. Jabbour M, Campbell EM, Fares H, Lybarger L (2009) Discrete domains of MARCH1 mediate its localization, functional interactions, and posttranscriptional control of expression. J Immunol 183(10):6500–6512. https://doi.org/10.4049/jimmunol.0901521
97. Nakasone MA, Livnat-Levanon N, Glickman MH, Cohen RE, Fushman D (2013) Mixed-linkage ubiquitin chains send mixed messages. Structure 21(5):727–740. https://doi.org/10.1016/j.str.2013.02.019
98. Koyano F, Okatsu K, Kosako H, Tamura Y, Go E, Kimura M, Kimura Y, Tsuchiya H, Yoshihara H, Hirokawa T, Endo T, Fon EA, Trempe JF, Saeki Y, Tanaka K, Matsuda N (2014) Ubiquitin is phosphorylated by PINK1 to activate parkin. Nature 510(7503):162–166. https://doi.org/10.1038/nature13392
99. Ohtake F, Saeki Y, Sakamoto K, Ohtake K, Nishikawa H, Tsuchiya H, Ohta T, Tanaka K, Kanno J (2015) Ubiquitin acetylation inhibits polyubiquitin chain elongation. EMBO Rep 16(2):192–201. https://doi.org/10.15252/embr.201439152
100. Venne AS, Kollipara L, Zahedi RP (2014) The next level of complexity: crosstalk of posttranslational modifications. Proteomics 14(4–5):513–524. https://doi.org/10.1002/pmic.201300344
101. Gonzales PA, Pisitkun T, Hoffert JD, Tchapyjnikov D, Star RA, Kleta R, Wang NS, Knepper MA (2009) Large-scale proteomics and phosphoproteomics of urinary exosomes. J Am Soc Nephrol 20(2):363–379. https://doi.org/10.1681/ASN.2008040406
102. Schey KL, Luther JM, Rose KL (2015) Proteomics characterization of exosome cargo. Methods 87:75–82. https://doi.org/10.1016/j.ymeth.2015.03.018
103. Marimpietri D, Petretto A, Raffaghello L, Pezzolo A, Gagliani C, Tacchetti C, Mauri P, Melioli G, Pistoia V (2013) Proteome profiling of neuroblastoma-derived exosomes reveal the expression of proteins potentially involved in tumor progression. PLoS One 8(9):e75054. https://doi.org/10.1371/journal.pone.0075054
104. Villarroya-Beltri C, Gutierrez-Vazquez C, Sanchez-Cabo F, Perez-Hernandez D, Vazquez J, Martin-Cofreces N, Martinez-Herrera DJ, Pascual-Montano A, Mittelbrunn M, Sanchez-Madrid F (2013) Sumoylated hnRNPA2B1 controls the sorting of miRNAs into exosomes through binding to specific motifs. Nat Commun 4:2980. https://doi.org/10.1038/ncomms3980
105. Vijayakumaran S, Wong MB, Antony H, Pountney DL (2015) Direct and/or indirect roles for SUMO in modulating alpha-synuclein toxicity. Biomolecules 5(3):1697–1716. https://doi.org/10.3390/biom5031697
106. Kunadt M, Eckermann K, Stuendl A, Gong J, Russo B, Strauss K, Rai S, Kugler S, Falomir Lockhart L, Schwalbe M, Krumova P, Oliveira LM, Bahr M, Mobius W, Levin J, Giese A, Kruse N, Mollenhauer B, Geiss-Friedlander R, Ludolph AC, Freischmidt A, Feiler MS, Danzer KM, Zweckstetter M, Jovin TM, Simons M, Weishaupt JH, Schneider A (2015) Extracellular vesicle sorting of alpha-synuclein is regulated by sumoylation. Acta Neuropathol 129(5):695–713. https://doi.org/10.1007/s00401-015-1408-1
107. Szabo-Taylor K, Ryan B, Osteikoetxea X, Szabo TG, Sodar B, Holub M, Nemeth A, Paloczi K, Pallinger E, Winyard P, Buzas EI (2015) Oxidative and other posttranslational modifications in extracellular vesicle biology. Semin Cell Dev Biol 40:8–16. https://doi.org/10.1016/j.semcdb.2015.02.012
108. Biasutto L, Chiechi A, Couch R, Liotta LA, Espina V (2013) Retinal pigment epithelium (RPE) exosomes contain signaling phosphoproteins affected by oxidative stress. Exp Cell Res 319(13):2113–2123. https://doi.org/10.1016/j.yexcr.2013.05.005
109. Valapala M, Vishwanatha JK (2011) Lipid raft endocytosis and exosomal transport facilitate extracellular trafficking of annexin A2. J Biol Chem 286(35):30911–30925. https://doi.org/10.1074/jbc.M111.271155
110. Chiarini A, Armato U, Gardenal E, Gui L, Dal Pra I (2017) Amyloid beta-exposed human astrocytes overproduce phospho-tau and overrelease it within exosomes, effects suppressed by calcilytic NPS 2143-further implications for Alzheimer's therapy. Front Neurosci 11:217. https://doi.org/10.3389/fnins.2017.00217
111. Kapogiannis D, Boxer A, Schwartz JB, Abner EL, Biragyn A, Masharani U, Frassetto L, Petersen RC, Miller BL, Goetzl EJ (2015) Dysfunctionally phosphorylated type 1 insulin receptor substrate in neural-derived blood exosomes of preclinical Alzheimer's disease. FASEB J 29(2):589–596. https://doi.org/10.1096/fj.14-262048
112. Kore RA, Abraham EC (2016) Phosphorylation negatively regulates exosome mediated secretion of cryAB in glioma cells. Biochim Biophys Acta 1863(2):368–377. https://doi.org/10.1016/j.bbamcr.2015.11.027
113. Polanco JC, Scicluna BJ, Hill AF, Gotz J (2016) Extracellular vesicles isolated from the brains of rTg4510 mice seed tau protein aggregation in a threshold-dependent manner. J Biol Chem 291(24):12445–12466. https://doi.org/10.1074/jbc.M115.709485
114. Rojas-Vega L, Jimenez-Vega AR, Bazua-Valenti S, Arroyo-Garza I, Jimenez JV, Gomez-Ocadiz R, Carrillo-Perez DL, Moreno E, Morales-Buenrostro LE, Alberu J, Gamba G (2015) Increased phosphorylation of the renal Na^+-Cl^- cotransporter in male kidney transplant recipient patients with hypertension: a prospective cohort. Am J Physiol Renal Physiol 309(10):F836–F842. https://doi.org/10.1152/ajprenal.00326.2015
115. Saman S, Kim W, Raya M, Visnick Y, Miro S, Saman S, Jackson B, McKee AC, Alvarez VE, Lee NC, Hall GF (2012) Exosome-associated tau is secreted in tauopathy models and is selectively phosphorylated in cerebrospinal fluid in early Alzheimer disease. J Biol Chem 287(6):3842–3849. https://doi.org/10.1074/jbc.M111.277061
116. van Dommelen SM, van der Meel R, van Solinge WW, Coimbra M, Vader P, Schiffelers RM (2016) Cetuximab treatment alters the content of extracellular vesicles released from tumor cells. Nanomedicine (Lond) 11(8):881–890. https://doi.org/10.2217/nnm-2015-0009
117. Winston CN, Goetzl EJ, Akers JC, Carter BS, Rockenstein EM, Galasko D, Masliah E, Rissman RA (2016) Prediction of conversion from mild cognitive impairment to dementia with neuronally derived blood exosome protein profile. Alzheimers Dement (Amst) 3:63–72. https://doi.org/10.1016/j.dadm.2016.04.001
118. Surgucheva I, Sharov VS, Surguchov A (2012) Gamma-synuclein: seeding of alpha-synuclein aggregation and transmission between cells. Biochemistry 51(23):4743–4754. https://doi.org/10.1021/bi300478w
119. Batista BS, Eng WS, Pilobello KT, Hendricks-Munoz KD, Mahal LK (2011) Identification of a conserved glycan

signature for microvesicles. J Proteome Res 10(10):4624–4633. https://doi.org/10.1021/pr200434y
120. Escrevente C, Grammel N, Kandzia S, Zeiser J, Tranfield EM, Conradt HS, Costa J (2013) Sialoglycoproteins and N-glycans from secreted exosomes of ovarian carcinoma cells. PLoS One 8(10):e78631. https://doi.org/10.1371/journal.pone.0078631
121. Krishnamoorthy L, Bess JW Jr, Preston AB, Nagashima K, Mahal LK (2009) HIV-1 and microvesicles from T cells share a common glycome, arguing for a common origin. Nat Chem Biol 5(4):244–250. https://doi.org/10.1038/nchembio.151
122. Palmisano G, Jensen SS, Le Bihan MC, Laine J, McGuire JN, Pociot F, Larsen MR (2012) Characterization of membrane-shed microvesicles from cytokine-stimulated beta-cells using proteomics strategies. Mol Cell Proteom 11(8):230–243. https://doi.org/10.1074/mcp.M111.012732
123. Fang Y, Wu N, Gan X, Yan W, Morrell JC, Gould SJ (2007) Higher-order oligomerization targets plasma membrane proteins and HIV gag to exosomes. PLoS Biol 5(6):e158. https://doi.org/10.1371/journal.pbio.0050158
124. Shen B, Wu N, Yang JM, Gould SJ (2011) Protein targeting to exosomes/microvesicles by plasma membrane anchors. J Biol Chem 286(16):14383–14395. https://doi.org/10.1074/jbc.M110.208660
125. Rabesandratana H, Toutant JP, Reggio H, Vidal M (1998) Decay-accelerating factor (CD55) and membrane inhibitor of reactive lysis (CD59) are released within exosomes during in vitro maturation of reticulocytes. Blood 91(7):2573–2580
126. Murrow L, Malhotra R, Debnath J (2015) ATG12-ATG3 interacts with Alix to promote basal autophagic flux and late endosome function. Nat Cell Biol 17(3):300–310. https://doi.org/10.1038/ncb3112
127. Oeste CL, Pinar M, Schink KO, Martinez-Turrion J, Stenmark H, Penalva MA, Perez-Sala D (2014) An isoprenylation and palmitoylation motif promotes intraluminal vesicle delivery of proteins in cells from distant species. PLoS One 9(9):e107190. https://doi.org/10.1371/journal.pone.0107190
128. Villarroya-Beltri C, Baixauli F, Mittelbrunn M, Fernandez-Delgado I, Torralba D, Moreno-Gonzalo O, Baldanta S, Enrich C, Guerra S, Sanchez-Madrid F (2016) ISGylation controls exosome secretion by promoting lysosomal degradation of MVB proteins. Nat Commun 7:13588. https://doi.org/10.1038/ncomms13588
129. Li Z, Zhuang M, Zhang L, Zheng X, Yang P, Li Z (2016) Acetylation modification regulates GRP78 secretion in colon cancer cells. Sci Rep 6:30406. https://doi.org/10.1038/srep30406
130. Gasecka A, Boing AN, Filipiak KJ, Nieuwland R (2017) Platelet extracellular vesicles as biomarkers for arterial thrombosis. Platelets 28(3):228–234. https://doi.org/10.1080/09537104.2016.1254174
131. Nawaz M, Camussi G, Valadi H, Nazarenko I, Ekstrom K, Wang X, Principe S, Shah N, Ashraf NM, Fatima F, Neder L, Kislinger T (2014) The emerging role of extracellular vesicles as biomarkers for urogenital cancers. Nat Rev Urol 11(12):688–701. https://doi.org/10.1038/nrurol.2014.301
132. Perez-Hernandez J, Cortes R (2015) Extracellular vesicles as biomarkers of systemic lupus erythematosus. Dis Markers 2015:613536. https://doi.org/10.1155/2015/613536
133. Sadovska L, Eglitis J, Line A (2015) Extracellular vesicles as biomarkers and therapeutic targets in breast cancer. Anticancer Res 35(12):6379–6390
134. Nolte-'t Hoen E, Cremer T, Gallo RC, Margolis LB (2016) Extracellular vesicles and viruses: are they close relatives? Proc Natl Acad Sci USA 113(33):9155–9161. https://doi.org/10.1073/pnas.1605146113
135. Martin-Jaular L, Nakayasu ES, Ferrer M, Almeida IC, Del Portillo HA (2011) Exosomes from *Plasmodium yoelii*-infected reticulocytes protect mice from lethal infections. PLoS One 6(10):e26588. https://doi.org/10.1371/journal.pone.0026588
136. Smith VL, Jackson L, Schorey JS (2015) Ubiquitination as a mechanism to transport soluble mycobacterial and eukaryotic proteins to exosomes. J Immunol 195(6):2722–2730. https://doi.org/10.4049/jimmunol.1403186
137. Cheng Y, Schorey JS (2016) Targeting soluble proteins to exosomes using a ubiquitin tag. Biotechnol Bioeng 113(6):1315–1324. https://doi.org/10.1002/bit.25884
138. Gyorgy B, Hung ME, Breakefield XO, Leonard JN (2015) Therapeutic applications of extracellular vesicles: clinical promise and open questions. Annu Rev Pharmacol Toxicol 55:439–464. https://doi.org/10.1146/annurev-pharmtox-010814-124630
139. Sterzenbach U, Putz U, Low LH, Silke J, Tan SS, Howitt J (2017) Engineered exosomes as vehicles for biologically active proteins. Mol Ther 25(6):1269–1278. https://doi.org/10.1016/j.ymthe.2017.03.030
140. Soria FN, Pampliega O, Bourdenx M, Meissner WG, Bezard E, Dehay B (2017) Exosomes, an unmasked culprit in neurodegenerative diseases. Front Neurosci 11:26. https://doi.org/10.3389/fnins.2017.00026
141. Alvarez-Erviti L, Seow Y, Yin H, Betts C, Lakhal S, Wood MJ (2011) Delivery of siRNA to the mouse brain by systemic injection of targeted exosomes. Nat Biotechnol 29(4):341–345. https://doi.org/10.1038/nbt.1807
142. Hung ME, Leonard JN (2015) Stabilization of exosome-targeting peptides via engineered glycosylation. J Biol Chem 290(13):8166–8172. https://doi.org/10.1074/jbc.M114.621383
143. Sola RJ, Griebenow K (2010) Glycosylation of therapeutic proteins: an effective strategy to optimize efficacy. BioDrugs 24(1):9–21. https://doi.org/10.2165/11530550-000000000-00000
144. Ahmed SF, Das N, Sarkar M, Chatterjee U, Chatterjee S, Ghosh MK (2015) Exosome-mediated delivery of the intrinsic C-terminus domain of PTEN protects it from proteasomal degradation and ablates tumorigenesis. Mol Ther 23(2):255–269. https://doi.org/10.1038/mt.2014.202
145. Kooijmans SA, Aleza CG, Roffler SR, van Solinge WW, Vader P, Schiffelers RM (2016) Display of GPI-anchored anti-EGFR nanobodies on extracellular vesicles promotes tumour cell targeting. J Extracell Vesicles 5:31053. https://doi.org/10.3402/jev.v5.31053
146. Heider S, Dangerfield JA, Metzner C (2016) Biomedical applications of glycosylphosphatidylinositol-anchored proteins. J Lipid Res 57(10):1778–1788. https://doi.org/10.1194/jlr.R070201
147. Komander D (2009) The emerging complexity of protein ubiquitination. Biochem Soc Trans 37(Pt 5):937–953. https://doi.org/10.1042/BST0370937
148. Peng J, Schwartz D, Elias JE, Thoreen CC, Cheng D, Marsischky G, Roelofs J, Finley D, Gygi SP (2003) A proteomics approach to understanding protein ubiquitination. Nat Biotechnol 21(8):921–926. https://doi.org/10.1038/nbt849
149. Hendriks IA, Vertegaal AC (2016) A high-yield double-purification proteomics strategy for the identification of SUMO sites. Nat Protoc 11(9):1630–1649. https://doi.org/10.1038/nprot.2016.082
150. Pocsfalvi G, Stanly C, Fiume I, Vekey K (2016) Chromatography and its hyphenation to mass spectrometry for extracellular vesicle analysis. J Chromatogr A 1439:26–41. https://doi.org/10.1016/j.chroma.2016.01.017
151. Pocsfalvi G, Stanly C, Vilasi A, Fiume I, Capasso G, Turiak L, Buzas EI, Vekey K (2016) Mass spectrometry of extracellular vesicles. Mass Spectrom Rev 35(1):3–21. https://doi.org/10.1002/mas.21457
152. Dorayappan KD, Wallbillich JJ, Cohn DE, Selvendiran K (2016) The biological significance and clinical applications of exosomes in ovarian cancer. Gynecol Oncol 142(1):199–205. https://doi.org/10.1016/j.ygyno.2016.03.036

153. Santangelo L, Battistelli C, Montaldo C, Citarella F, Strippoli R, Cicchini C (2017) Functional roles and therapeutic applications of exosomes in hepatocellular carcinoma. Biomed Res Int 2017:2931813. https://doi.org/10.1155/2017/2931813
154. Cloutier N, Tan S, Boudreau LH, Cramb C, Subbaiah R, Lahey L, Albert A, Shnayder R, Gobezie R, Nigrovic PA, Farndale RW, Robinson WH, Brisson A, Lee DM, Boilard E (2013) The exposure of autoantigens by microparticles underlies the formation of potent inflammatory components: the microparticle-associated immune complexes. EMBO Mol Med 5(2):235–249. https://doi.org/10.1002/emmm.201201846
155. Ubersax JA, Ferrell JE Jr (2007) Mechanisms of specificity in protein phosphorylation. Nat Rev Mol Cell Biol 8(7):530–541. https://doi.org/10.1038/nrm2203
156. Choudhary C, Weinert BT, Nishida Y, Verdin E, Mann M (2014) The growing landscape of lysine acetylation links metabolism and cell signalling. Nat Rev Mol Cell Biol 15(8):536–550. https://doi.org/10.1038/nrm3841
157. Drazic A, Myklebust LM, Ree R, Arnesen T (2016) The world of protein acetylation. Biochim Biophys Acta 1864(10):1372–1401. https://doi.org/10.1016/j.bbapap.2016.06.007
158. Bedford MT (2006) Methylation of proteins. Encyclopedic reference of genomics and proteomics in molecular medicine. Springer, Berlin. https://doi.org/10.1007/3-540-29623-9_2780
159. Lanouette S, Mongeon V, Figeys D, Couture JF (2014) The functional diversity of protein lysine methylation. Mol Syst Biol 10:724. https://doi.org/10.1002/msb.134974
160. Schubert HL, Blumenthal RM, Cheng X (2003) Many paths to methyltransfer: a chronicle of convergence. Trends Biochem Sci 28(6):329–335. https://doi.org/10.1016/S0968-0004(03)00090-2
161. Schöneich C, Barrón LB (2006) Posttranslational oxidative modifications of proteins. Encycl Anal Chem. https://doi.org/10.1002/9780470027318.a1626
162. Anzenbacher P, Anzenbacherova E (2001) Cytochromes P450 and metabolism of xenobiotics. Cell Mol Life Sci 58(5–6):737–747
163. Beckman JS (1996) Oxidative damage and tyrosine nitration from peroxynitrite. Chem Res Toxicol 9(5):836–844. https://doi.org/10.1021/tx9501445
164. Nakamura T, Lipton SA (2011) Redox modulation by S-nitrosylation contributes to protein misfolding, mitochondrial dynamics, and neuronal synaptic damage in neurodegenerative diseases. Cell Death Differ 18(9):1478–1486. https://doi.org/10.1038/cdd.2011.65
165. Yang YS, Wang CC, Chen BH, Hou YH, Hung KS, Mao YC (2015) Tyrosine sulfation as a protein post-translational modification. Molecules 20(2):2138–2164. https://doi.org/10.3390/molecules20022138
166. Eipper BA, Stoffers DA, Mains RE (1992) The biosynthesis of neuropeptides: peptide alpha-amidation. Annu Rev Neurosci 15:57–85. https://doi.org/10.1146/annurev.ne.15.030192.000421
167. Clark BF, Marcker KA (1966) The role of N-formyl-methionyl-sRNA in protein biosynthesis. J Mol Biol 17(2):394–406
168. Wisniewski JR, Zougman A, Mann M (2008) Nepsilon-formylation of lysine is a widespread post-translational modification of nuclear proteins occurring at residues involved in regulation of chromatin function. Nucleic Acids Res 36(2):570–577. https://doi.org/10.1093/nar/gkm1057
169. Zhang Z, Tan M, Xie Z, Dai L, Chen Y, Zhao Y (2011) Identification of lysine succinylation as a new post-translational modification. Nat Chem Biol 7(1):58–63. https://doi.org/10.1038/nchembio.495
170. Peng C, Lu Z, Xie Z, Cheng Z, Chen Y, Tan M, Luo H, Zhang Y, He W, Yang K, Zwaans BM, Tishkoff D, Ho L, Lombard D, He TC, Dai J, Verdin E, Ye Y, Zhao Y (2011) The first identification of lysine malonylation substrates and its regulatory enzyme. Mol Cell Proteom 10(12):M111 012658. https://doi.org/10.1074/mcp.M111.012658
171. Moremen KW, Tiemeyer M, Nairn AV (2012) Vertebrate protein glycosylation: diversity, synthesis and function. Nat Rev Mol Cell Biol 13(7):448–462. https://doi.org/10.1038/nrm3383
172. Nothaft H, Szymanski CM (2010) Protein glycosylation in bacteria: sweeter than ever. Nat Rev Microbiol 8(11):765–778. https://doi.org/10.1038/nrmicro2383
173. Schwarz F, Aebi M (2011) Mechanisms and principles of N-linked protein glycosylation. Curr Opin Struct Biol 21(5):576–582. https://doi.org/10.1016/j.sbi.2011.08.005
174. Spiro RG (2002) Protein glycosylation: nature, distribution, enzymatic formation, and disease implications of glycopeptide bonds. Glycobiology 12(4):43R–56R
175. Van den Steen P, Rudd PM, Dwek RA, Opdenakker G (1998) Concepts and principles of O-linked glycosylation. Crit Rev Biochem Mol Biol 33(3):151–208. https://doi.org/10.1080/10409239891204198
176. Galian C, Bjorkholm P, Bulleid N, von Heijne G (2012) Efficient glycosylphosphatidylinositol (GPI) modification of membrane proteins requires a C-terminal anchoring signal of marginal hydrophobicity. J Biol Chem 287(20):16399–16409. https://doi.org/10.1074/jbc.M112.350009
177. Ikezawa H (2002) Glycosylphosphatidylinositol (GPI)-anchored proteins. Biol Pharm Bull 25(4):409–417
178. Mayor S, Riezman H (2004) Sorting GPI-anchored proteins. Nat Rev Mol Cell Biol 5(2):110–120. https://doi.org/10.1038/nrm1309
179. Nadolski MJ, Linder ME (2007) Protein lipidation. FEBS J 274(20):5202–5210. https://doi.org/10.1111/j.1742-4658.2007.06056.x
180. Resh MD (1999) Fatty acylation of proteins: new insights into membrane targeting of myristoylated and palmitoylated proteins. Biochim Biophys Acta 1451(1):1–16
181. Triola G (2011) The protein lipidation and its analysis. J Glycom Lipidom S 2:001. https://doi.org/10.4172/2153-0637.S2-001
182. Roskoski R Jr (2003) Protein prenylation: a pivotal posttranslational process. Biochem Biophys Res Commun 303(1):1–7
183. van Dijk J, Miro J, Strub JM, Lacroix B, van Dorsselaer A, Edde B, Janke C (2008) Polyglutamylation is a post-translational modification with a broad range of substrates. J Biol Chem 283(7):3915–3922. https://doi.org/10.1074/jbc.M705813200
184. Bre MH, Redeker V, Vinh J, Rossier J, Levilliers N (1998) Tubulin polyglycylation: differential posttranslational modification of dynamic cytoplasmic and stable axonemal microtubules in paramecium. Mol Biol Cell 9(9):2655–2665
185. Xia L, Hai B, Gao Y, Burnette D, Thazhath R, Duan J, Bre MH, Levilliers N, Gorovsky MA, Gaertig J (2000) Polyglycylation of tubulin is essential and affects cell motility and division in *Tetrahymena thermophila*. J Cell Biol 149(5):1097–1106
186. Baka Z, Gyorgy B, Geher P, Buzas EI, Falus A, Nagy G (2012) Citrullination under physiological and pathological conditions. Jt Bone Spine 79(5):431–436. https://doi.org/10.1016/j.jbspin.2012.01.008
187. Gyorgy B, Toth E, Tarcsa E, Falus A, Buzas EI (2006) Citrullination: a posttranslational modification in health and disease. Int J Biochem Cell Biol 38(10):1662–1677. https://doi.org/10.1016/j.biocel.2006.03.008
188. Johnson ES (2004) Protein modification by SUMO. Annu Rev Biochem 73:355–382. https://doi.org/10.1146/annurev.biochem.73.011303.074118

189. Zhang D, Zhang DE (2011) Interferon-stimulated gene 15 and the protein ISGylation system. J Interferon Cytokine Res 31(1):119–130. https://doi.org/10.1089/jir.2010.0110
190. Corda D, Di Girolamo M (2003) Functional aspects of protein mono-ADP-ribosylation. EMBO J 22(9):1953–1958. https://doi.org/10.1093/emboj/cdg209
191. Liu C, Yu X (2015) ADP-ribosyltransferases and poly ADP-ribosylation. Curr Protein Pept Sci 16(6):491–501

frontiers in
IMMUNOLOGY

MINI REVIEW ARTICLE
published: 11 August 2014
doi: 10.3389/fimmu.2014.00383

Post-translational modifications of exosomal proteins

Olga Moreno-Gonzalo[1,2], *Carolina Villarroya-Beltri*[1,2] *and Francisco Sánchez-Madrid*[1,2]*

[1] Vascular Biology and Inflammation Department, Centro Nacional de Investigaciones Cardiovasculares, Madrid, Spain
[2] Servicio de Inmunología, Hospital de la Princesa, Instituto de Investigación Sanitaria de la Princesa, Universidad Autónoma de Madrid, Madrid, Spain

Edited by:
Ana Maria Merino, Bellvitge Biomedical Research institute (IDIBELL), Spain

Reviewed by:
Raquel Santiago-Mora, Spain
Julia Carracedo, IMIBIC, Spain

***Correspondence:**
Francisco Sánchez-Madrid, Servicio de Inmunoogía, Hospital de la Princesa, Instituto de Investigación Sanitaria de la Princesa, Universidad Autónoma de Madrid, Madrid 28006, Spain
e-mail: fsmadrid@salud.madrid.org

Exosomes mediate intercellular communication and participate in many cell processes such as cancer progression, immune activation or evasion, and the spread of infection. Exosomes are small vesicles secreted to the extracellular environment through the release of intraluminal vesicles contained in multivesicular bodies (MVBs) upon the fusion of these MVBs with the plasma membrane. The composition of exosomes is not random, suggesting that the incorporation of cargo into them is a regulated process. However, the mechanisms that control the sorting of protein cargo into exosomes are currently elusive. Here, we review the post-translational modifications detected in exosomal proteins, and discuss their possible role in their specific sorting into exosomes.

Keywords: post-translational modifications, exosomes, ubiquitination, sorting, multivesicular bodies

INTRODUCTION

Post-translational modifications (PTMs) of proteins are biochemical changes generated after the synthesis of polypeptides on ribosomes. PTMs include changes to the chemical nature of aminoacid residues and also structural modifications that affect the interactive ability of proteins, and consequently their stability, subcellular localization, and activation state (1, 2). There are many types of PTM that can be classified according to the nature of the materials added: (1) a chemical group (phosphate, acetate, etc.), (2) carbohydrates, (3) lipids, (4) aminoacids, (5) other polypeptides, and (6) an isoprenyl group (**Table 1**). A protein can undergo many PTMs, changing its properties and broadening its capacity to adapt to cellular needs (2). Some modifications are reversible and are strictly regulated by the enzymes responsible for their addition or removal, acting as a dynamic switch that allows the cell to adjust protein functions according to requirements. Dysregulation of PTMs or mutation of modified residues are linked to disease, including cancer, neurodegenerative disorders such as Alzheimer, and cardiovascular disease, highlighting the importance of these protein modifications (3–7).

A specific pattern of PTMs is detected in exosomes, 50–200 nm diameter vesicles secreted by most cells to the extracellular environment. Once released, exosomes can adhere to or be internalized by recipient cells, and in this way mediate cell-to-cell communication in a variety of contexts. Exosomes form through the invagination of the limiting membrane of specific endosomic compartments called multivesicular bodies (MVBs) (22). The resulting intraluminal vesicles (ILVs) are released as exosomes upon fusion of MVBs with the plasma membrane. Alternatively, MVBs can fuse with lysosomes, leading to degradation of their content. Exosomes have a specific composition of lipids, proteins, and RNAs; however, the mechanisms that control the sorting of molecules into these exosomal-proteins vesicles remain elusive. Here, we review the PTMs detected in exosomal proteins, and discuss their possible role in their specific sorting into exosomes.

UBIQUITINATION AND SUMOylation

Post-translational modifications increase the versatility of proteins by influencing their activation state, stability, subcellular localization, and ability to interact with other proteins. A particularly effective means of increasing protein versatility is the addition of ubiquitin, which can be attached to a target protein at a number of positions and in a variety of ways. The C-terminal glycine of ubiquitin usually forms an isopeptide bond with the ε-amino group of a lysine residue present in the target protein, resulting in mono-ubiquitination. In some cases, E4 ubiquitin ligases can add a poly-ubiquitin chain to a mono-ubiquitinated site (23). The equation becomes even more complicated considering that ubiquitin has seven lysines, and the fate of the target protein is determined by which lysine forms the link in the poly-ubiquitin chain: chains linked through lysine-48 (Ub-K48) label target proteins for degradation in the proteasome; Ub-K63 chains seem to be important for the DNA-damage response, endocytosis, autophagy, and signal transduction; Ub-K11 chains are implicated in endoplasmic-reticulum-associated degradation (ERAD); and Ub-K29 chains are involved in lysosomal degradation (24–33). Moreover, in some cases, ubiquitin can be linked through residues other than lysine, such as the N-terminal through the free amino group or the sulfhydryl group of cysteine residues (34).Ubiquitination can also compete with other PTMs, such as sumoylation or acetylation, and can enhance others such as phosphorylation (35–37).

Ubiquination, thus denotes a complex network of PTMs, and its role in the sorting of proteins into exosomes is far from understood. There seems to be consensus that ubiquitination is necessary for sorting proteins into ILVs destined for degradation through the fusion of the encompassing MVB with lysosomes. This process is mediated by the endosomal sorting complex required for transport machinery (ESCRT complex) and affects proteins such as epithelial growth factor receptor (EGFR) (38) (**Figure 1**). This machinery recognizes ubiquitinated cargoes and catalyzes the abscission of endosomal invaginations, forming ILVs that contain the sorted

Table 1 | Post-translational modification of eukaryotic proteins.

Groups of PTMs	Modification	Added group	Modified residues of target proteins	PTM in exosomal proteins	Biological relevance conferred by the PTMs	Reference
POST-TRANSLATIONAL MODIFICATIONS OF EUKARYOTIC PROTEINS						
Addition of a chemical group	Phosphorylation	Phosphate group	Tyr, Thr, Ser, His	FasL; AnnexinA2; tau; γ-synuclein	Sorting into exosomes; incorporation into exosomal membrane; spreading of toxic aggregates through exosomes; spreading of toxic aggregates through exosomes	(8–11)
	Acetylation	Acetyl group	Lys	–	–	–
	Methylation	Methyl group	Lys, Arg	–	–	–
	Oxidation	Different oxygen species	All amino acids, but preferentially Tyr, Phe, Trp, His, Met, Cys	γ-Synuclein	Spreading of toxic aggregates through exosomes	(11)
	Nitrosylation	Nitric oxide (NO)	Cys, Met	–	–	–
Addition of carbohydrates or glycosylation	N-linked glycosylation	Glycosyl group	Asn, Arg, and N-terminus	Several glycoproteins	Sorting of particular glycoproteins into exosomes (?)	(12–14)
	O-linked glycosylation	Glycosyl group	Ser, Thr, and amino acids in close proximity to Tyr phosphorylation sites	Several glycoproteins	Sorting of particular glycoproteins into exosomes (?)	(12–14)
	C-linked mannosylation and glypiation [glycosylphosphatidylinositol (GPI)anchor]	Glycosylpho sphatidylinositol (GPI) group	Carbon on a tryptophan side-chain and C-terminus, respectively	Several glycoproteins	Sorting of particular glycoproteins into exosomes (?)	(12, 13)
Addition of lipids (lipidation)	Palmitoylation	Palmitic acid	Cys	–	–	–
	N-myristoylation	Myristoyl group	N-terminal glycine residue	Artificial conjugation of TyA protein to myristoyl group	Sorting of TyA into shedding vesicles	(15)
Addition of amino acids	Polyglutamylation	Glutamic acid	Gly	–	–	–

(Continued)

Table 1 | Continued

Groups of PTMs	Modification	Added group	Modified residues of target proteins	PTM in exosomal proteins	Biological relevance conferred by the PTMs	Reference
Addition of other polypeptides	Ubiquitination	Ubiquitin protein	Lys, N-terminus, non-lysine residues (Cys, Thr, Ser)	Several proteins, some examples: LMP2A; PTEN; SIMPLE; HSP70; ARRDC1	Exosomal LMP2A loading; Sorting of PTEN into exosomes; Unknown function; Unknown function; Secretion into shedding vesicles	(16–20)
	SUMOylation (Small ubiquitin-related modifier addition)	SUMO1-4 proteins	Tetrapeptide consensus motif Ψ-K-x-D/E (Ψ: hydrophobic residue, K: lysine conjugated to SUMO, x: any amino acid, D or E: acidic residue)	hnRNPA2B1	Regulate the binding of miRNAs to hnRNPA2B1	(21)
	NEDDylation (neural-precursor-cell-expressed developmentally down-regulated 8 addition)	NEDD8 protein	Lys	–	–	–
	ISGylatyon (Interferon-stimulated gene 15 addition)	ISG15 protein	Lys	–	–	–
Isoprenylation	Farnesylation	Farnesyl group	Cys and sequence motifs CAAX, CC, or CAC at C-terminus (C: Cys, A: alanine, X: any amino acid)	–	–	–
	Geranylgeranylation	Geranylgeranyl isoprene unit	Cys and sequence motifs CAAX, CC or CAC at C-terminus (C: Cys, A: alanine, X: any amino acid)	–	–	–

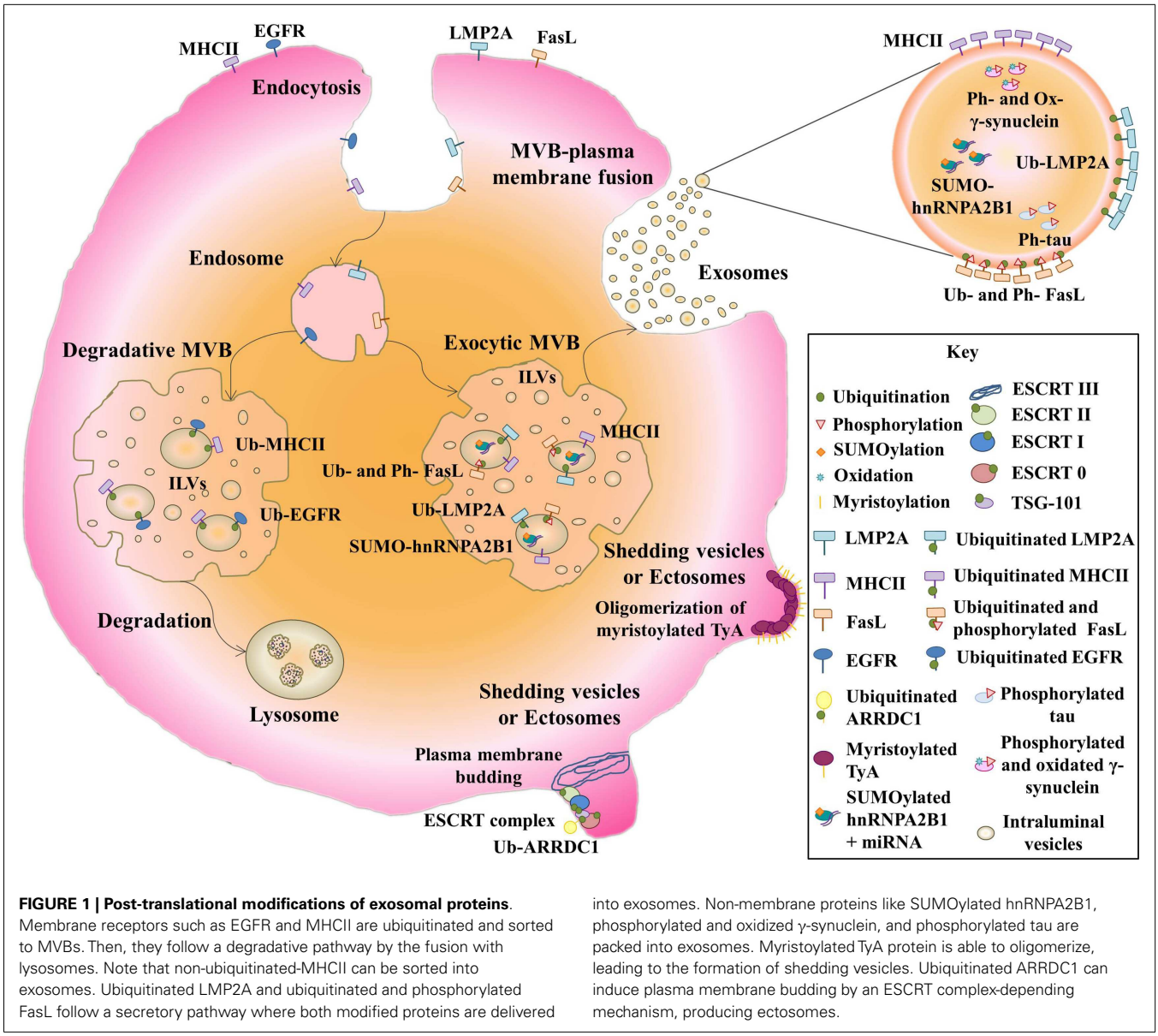

FIGURE 1 | Post-translational modifications of exosomal proteins. Membrane receptors such as EGFR and MHCII are ubiquitinated and sorted to MVBs. Then, they follow a degradative pathway by the fusion with lysosomes. Note that non-ubiquitinated-MHCII can be sorted into exosomes. Ubiquitinated LMP2A and ubiquitinated and phosphorylated FasL follow a secretory pathway where both modified proteins are delivered into exosomes. Non-membrane proteins like SUMOylated hnRNPA2B1, phosphorylated and oxidized γ-synuclein, and phosphorylated tau are packed into exosomes. Myristoylated TyA protein is able to oligomerize, leading to the formation of shedding vesicles. Ubiquitinated ARRDC1 can induce plasma membrane budding by an ESCRT complex-depending mechanism, producing ectosomes.

cargo [reviewed in Raiborg and Stenmark (39)]. The ESCRT complex consists of four subcomplexes, ESCRT-0, -I, -II, and -III, and several accessory proteins. ESCRT-0, -I, and -II contain ubiquitin-binding subunits that interact directly with ubiquitinated cargo. The directional flow of cargo from ESCRT-0 to ESCRT-I and -II might be regulated by PTMs. In fact, the ESCRT-0 subunits are known to be phosphorylated and to be mono-ubiquitinated (40–42). The latter modification keeps these subunits in an inactive form owing to intramolecular interactions between their ubiquitin interacting motifs and the appended ubiquitin (43, 44). However, the role of ubiquitin and the ESCRT complex in the sorting of proteins into ILVs for exosome secretion is still unclear, and MVB biogenesis, exosome secretion, and exosomal-protein sorting have been reported in an ESCRT/ubiquitin-independent manner [reviewed at Villarroya-Beltri et al. (45)].

The Epstein-Barr virus (EBV) protein LMP2A (latent membrane protein 2A) is ubiquitinated in exosomal fractions (16). LMP2A contains two PXYY motifs, through which it associates with neural precursor cell expressed developmentally down-regulated protein 4 (Nedd4)-family ubiquitin ligases (16). Ubiquitination of LMP2A leads to endocytic transport of the protein from the plasma membrane to MVBs. Nedd4 E3 ubiquitin ligases are able to bind directly to target proteins though the PPXY motif, but proteins lacking this motif can bind Nedd4 through the adaptor Nedd4-family-interacting protein 1(Ndfip1), leading to their ubiquitination (46). Ndfip1 is involved not only in protein degradation, but also in protein traffic to exosomes (46). Ndfip1 overexpression increases the protein content of exosomes and enhances exosomal sorting of normally absent proteins, such as Nedd4, Nedd4-2, and Itch. These exosomal proteins moreover

appear to be highly ubiquitinated, suggesting that Ndfip1 transfers other ubiquitinated proteins to exosomes (46) (**Figure 1**). For example, the Ndfip1 adaptor function is required for exosomal export of phosphatase and tensin homolog deleted on chromosome 10 protein (PTEN) ubiquitinated on lysine 13 (17).

With other proteins, however, ubiquitination appears to be unimportant or inhibitory to exosomal export. Secretion into exosomes of small integral membrane protein of the lysosome/late endosome (SIMPLE) is enhanced by mutations in its PPXY motif, which mediates its binding to E3 ubiquitin ligases (18). Ubiquitination is also not required for the packaging of major histocompatibility complex II (MHC-II) into exosomes (47). The use of a chimeric-ubiquitinated-MHC-II molecule does not specifically lead these molecules into exosomes, and forcing MHC-II ubiquitination by expression of membrane-associated ring finger (C3HC4) 8 (MARCH) E3 ubiquitin ligase does not enrich MHC-II molecules in exosomes, though it does completely deplete them from the plasma membrane. Moreover, directed-mutagenesis of all MHC-II lysine residues does not impair the exosome sorting of these receptors (47). However, ubiquitination of the MHC-II cytoplasmic domain, required for recognition by the ESCRT complex, is important for sorting membrane MHC-II to MVBs for lysosomal degradation (48). The non-ubiquitination of MHC-II molecules present in exosomes suggests that this PTM is not involved in sorting to these vesicles. The two mechanisms for loading MHC-II into MVBs are engaged for different physiological functions. Thus, whereas ubiquitin-dependent sorting takes place in immature DCs, in which ubiquitinated receptors are degraded in lysosomes, in activated-DCs, non-ubiquitinated MHC-II-containing exosomes are efficiently delivered to interact with T cells, enhancing antigen specific MHC-II-mediated presentation (48) (**Figure 1**). Heat shock protein 70 (HSP70) also seems to be sorted into exosomes independently of its ubiquitination. Thus, although deletion of the deubiquitin domain of COP9 signalosome complex subunit 5 (CSN5) enhances packing of ubiquitinated HSP70 into exosomes, knockdown of the entire CSN5 protein increases the levels of both modified and non-modified HSP70 in exosomes (19).

Mass spectrometry analysis of PTMs in extracellular vesicles released by insulinoma cells identified multiple poly-ubiquitinated proteins (49). Enrichment of exosomes in poly-ubiquitinatied proteins was also demonstrated by an approach based on the use of FK1 antibody (which only binds poly-ubiquitinated proteins) and P4D1 (which labels poly- and mono-ubiquitinated proteins) (50). Other studies suggest that exosomal proteins are preferentially mono-ubiquitinated or de-ubiquitinated, based on western analysis showing discrete ubiquitinated protein bands rather than smeared bands (19).

Ubiquitination has been shown to be important for the secretion of a novel type of extracellular vesicle, distinct from exosomes, called arrestin-domain-containing protein 1(ARRDC1)-mediated microvesicles (ARMMs). ARMMs directly bud from the plasma membrane upon interaction of the tumor susceptibility gene 101 protein (TSG101) with a PSAP motif in ARRDC1, which is localized through its arrestin domain at the plasma membrane (20). ARRDC1 in vesicles is ubiquitinated by the E3 ligase WW domain-containing protein 2 (WWP2). Down-regulation of WWP2 decreases ARRDC1 protein level in vesicles, and a PPXY-mutant of ARRDC1 strongly inhibits ARMM secretion, suggesting that ARRDC1 ubiquitination promotes ARRDC1 sorting into vesicles and ARMM secretion (20) (**Figure 1**).

Another ubiquitin-like modifier called small ubiquitin-related modifier (SUMO) has been found to modify the exosomal-protein heterogeneous nuclear ribonucleoprotein A2B1 (hnRNPA2B1). This modification affects the ability of this protein to export micro ribonucleic acids (miRNAs) into exosomes, probably by affecting its binding to miRNAs (21). hnRNPA1 in exosomes was also found to be modified, increasing its molecular weight by about 12 kDa on gel electrophoresis (21) (**Figure 1**). This change in molecular weight of hnRNPA2B1 and other proteins has been shown before (49).

OTHER PTMs: PHOSPHORYLATION AND GLYCOSYLATION

Mass spectrometry analysis of extracellular vesicles also detects phosphorylated proteins (49). Phosphorylation and ubiquitination co-regulate sorting of Fas ligand (FasL) into secretory lysosomes by controlling its entry into MVBs (8). FasL contains a proline-rich domain (PRD) in the cytosolic tail to which tyrosine kinases, such as FGR, FYN, and LYN bind, and phosphorylation of tyrosine residues by these kinases enhances internalization to MVBs. The flanking regions of the PRD contain lysines, which are mono-ubiquitinated. Mutation of these lysines impairs the localization of FasL in MVBs, but mutation of the tyrosines does not affect mono-ubiquitination. Phosphorylation is thus not required for ubiquitination, but both PTMs are necessary for incorporation of FasL into to MVBs (8) (**Figure 1**).

Phosphorylation is also involved in incorporation of the $Ca2^{+}$-dependent phospholipid-binding protein Annexin A2 into exosomal membranes, through the action of raft-resident kinases, such as SRC or LYN on Tyr-23 (9). Aberrant phosphorylation of the protein tau on threonine-181 promotes its incorporation into exosomes, resulting in the spreading of this abnormally processed protein in Alzheimer disease patients (10).

The protein γ-synuclein is transported in exosomes in its modified form. This modification consists of oxidation of Met-38 and Tyr-39, which confers prion-like properties and causes the formation of toxic aggregates. The spreading of these aggregates is in part mediated by the exosomal transport of oxidated-γ-synuclein to glial cells (11) (**Figure 1**).

Carbohydrate modifications, involved in protein trafficking, cellular recognition, and communication of cells with their extracellular environment, have also been studied in extracellular vesicles (12, 13, 51). Vesicles of diverse cells types are enriched in proteins with high mannose, polylactosamine, α-2,6-sialic acid, and complex N-linked glycans adjuncts; in contrast, there is a comparative under-representation of specific glycan epitopes, such as terminal blood group A and B antigens (12, 13). Exosome glycan profiles of different cell sources, such as T-cells, melanoma and colon cancer cells, and biological fluids like breast milk, are very similar, although they conserve some features of their parent membranes (13). The carbohydrate fingerprint detected in exosomes is less diverse than that observed in parent cells, but correspond to a conserved fraction of the parent cellular membrane that display a particular glycan profile (13). The variability observed between

cellular and exosomal carbohydrate signatures has been suggested to indicate different membrane microdomain origins of these vesicles (13). It has been described that polyLacNac and high mannose modifications associated with galectins and VIP36 are responsible for the oligomerization of glycoproteins that mediate their sorting into Golgi-derived vesicles (12, 52–55). Galectins and galectin-associated proteins have also been detected in exosomes so it is possible that glycosylation may also play a role in the sorting cargo into extracellular vesicles (12, 13).

Membrane anchors have also been shown to be important for the budding of vesicles derived from the plasma membrane. An N-terminal acylation tag serves as a signal for the import of highly oligomeric cytoplasmic proteins, like the yeast protein TyA, into shedding vesicles (56). The membrane anchor that most effectively promotes TyA budding is myristoylation. However, targeting of TyA to the endosomal membrane by fusion to a Phosphatidylinositol-3-phosphate (PI3P) binding domain does not produce the same effect (15) (**Figure 1**).

CONCLUDING REMARKS

Post-translational modifications decorate proteins and drive their fate in cells by affecting multiple parameters including stability and localization. Different modifications can affect the same protein; sometimes competing with each other or being mutually exclusive, but in other cases can promote other modifications. Enzymes controlling PTMs additionally show very specific patterns of expression, activation, and subcellular localization, exponentially increasing the diversity and potentiality of cellular proteomes.

Different types of PTMs have been found in exosomal proteins; however, the role of these modifications in the localization of proteins into exosomes is not clear. The enigmatic role of ubiquitination, whose final consequences seem to differ depending on the target protein, is a particular case in point. The type of ubiquitination may also account for the fate of the modified protein, and could be a key determinant for its loading in exosomes. In some cases, ubiquitination seems to target the protein into MVBs destined for degradation, whereas sorting of proteins into MVBs that fuse with the plasma membrane to release exosomes seems to be ubiquitin-independent, clearly pointing to the existence of different types of MVB with different sorting mechanisms.

Specific protein modifications can reflect a particular pathological condition. The presence of modified proteins in exosomes can therefore make them invaluable tools for diagnosis, since modifications could be easily detected in exosomes obtained from body fluids without the need for invasive tissue biopsies.

ACKNOWLEDGMENTS

The authors thank Dr. S. Bartlett for assistance with English editing. This work was supported by SAF2011-25834 from the Spanish Ministry of Science and Innovation. INDISNET-S2011/BMD-2332 from the Comunidad de Madrid, Red Cardiovascular RD 12-0042-0056 from Instituto Salud Carlos III (ISCIII), ERC-2011-AdG 294340-GENTRIS, and COST-Action BN1202. Olga Moreno-Gonzalo and Carolina Villarroya-Beltri were supported by FPU program (Spanish Ministry of Education).

REFERENCES

1. Uy R, Wold F. Posttranslational covalent modification of proteins. *Science* (1977) **198**(4320):890–6. doi:10.1126/science.337487
2. Xin F, Radivojac P. Post-translational modifications induce significant yet not extreme changes to protein structure. *Bioinformatics* (2012) **28**(22):2905–13. doi:10.1093/bioinformatics/bts541bts541
3. Bode AM, Dong Z. Post-translational modification of p53 in tumorigenesis. *Nat Rev Cancer* (2004) **4**(10):793–805. doi:10.1038/nrc1455
4. Gong CX, Liu F, Grundke-Iqbal I, Iqbal K. Post-translational modifications of tau protein in Alzheimer's disease. *J Neural Transm* (2005) **112**(6):813–38. doi:10.1007/s00702-004-0221-0
5. Martin L, Latypova X, Terro F. Post-translational modifications of tau protein: implications for Alzheimer's disease. *Neurochem Int* (2011) **58**(4):458–71. doi:10.1016/j.neuint.2010.12.023S0197-0186(10)00401-8
6. Toh KL, Jones CR, He Y, Eide EJ, Hinz WA, Virshup DM, et al. An hPer2 phosphorylation site mutation in familial advanced sleep phase syndrome. *Science* (2001) **291**(5506):1040–3. doi:10.1126/science.1057499
7. Van Eyk JE. Overview: the maturing of proteomics in cardiovascular research. *Circ Res* (2011) **108**(4):490–8. doi:10.1161/CIRCRESAHA.110.226894108/4/490
8. Zuccato E, Blott EJ, Holt O, Sigismund S, Shaw M, Bossi G, et al. Sorting of Fas ligand to secretory lysosomes is regulated by mono-ubiquitylation and phosphorylation. *J Cell Sci* (2007) **120**(Pt 1):191–9. doi:10.1242/jcs.03315
9. Valapala M, Vishwanatha JK. Lipid raft endocytosis and exosomal transport facilitate extracellular trafficking of annexin A2. *J Biol Chem* (2011) **286**(35):30911–25. doi:10.1074/jbc.M111.271155
10. Saman S, Kim W, Raya M, Visnick Y, Miro S, Jackson B, et al. Exosome-associated tau is secreted in tauopathy models and is selectively phosphorylated in cerebrospinal fluid in early Alzheimer disease. *J Biol Chem* (2012) **287**(6):3842–9. doi:10.1074/jbc.M111.277061
11. Surgucheva I, Sharov VS, Surguchov A. Gamma-Synuclein: seeding of alpha-synuclein aggregation and transmission between cells. *Biochemistry* (2012) **51**(23):4743–54. doi:10.1021/bi300478w
12. Escrevente C, Grammel N, Kandzia S, Zeiser J, Tranfield EM, Conradt HS, et al. Sialoglycoproteins and N-glycans from secreted exosomes of ovarian carcinoma cells. *PLoS One* (2013) **8**(10):e78631. doi:10.1371/journal.pone.0078631
13. Batista BS, Eng WS, Pilobello KT, Hendricks-Munoz KD, Mahal LK. Identification of a conserved glycan signature for microvesicles. *J Proteome Res* (2011) **10**(10):4624–33. doi:10.1021/pr200434y
14. Marimpietri D, Petretto A, Raffaghello L, Pezzolo A, Gagliani C, Tacchetti C, et al. Proteome profiling of neuroblastoma-derived exosomes reveal the expression of proteins potentially involved in tumor progression. *PLoS One* (2013) **8**(9):e75054. doi:10.1371/journal.pone.0075054
15. Shen B, Wu N, Yang JM, Gould SJ. Protein targeting to exosomes/microvesicles by plasma membrane anchors. *J Biol Chem* (2011) **286**(16):14383–95. doi:10.1074/jbc.M110.208660
16. Ikeda M, Longnecker R. Cholesterol is critical for Epstein-Barr virus latent membrane protein 2A trafficking and protein stability. *Virology* (2007) **360**(2):461–8. doi:10.1016/j.virol.2006.10.046
17. Putz U, Howitt J, Doan A, Goh CP, Low LH, Silke J, et al. The tumor suppressor PTEN is exported in exosomes and has phosphatase activity in recipient cells. *Sci Signal* (2012) **5**(243):ra70. doi:10.1126/scisignal.2003084
18. Zhu H, Guariglia S, Yu RY, Li W, Brancho D, Peinado H, et al. Mutation of SIMPLE in Charcot-Marie-Tooth 1C alters production of exosomes. *Mol Biol Cell* (2013) **24**(11):1619–37. doi:10.1091/mbc.E12-07-0544
19. Liu Y, Shah SV, Xiang X, Wang J, Deng ZB, Liu C, et al. COP9-associated CSN5 regulates exosomal protein deubiquitination and sorting. *Am J Pathol* (2009) **174**(4):1415–25. doi:10.2353/ajpath.2009.080861
20. Nabhan JF, Hu R, Oh RS, Cohen SN, Lu Q. Formation and release of arrestin domain-containing protein 1-mediated microvesicles (ARMMs) at plasma membrane by recruitment of TSG101 protein. *Proc Natl Acad Sci U S A* (2012) **109**(11):4146–51. doi:10.1073/pnas.1200448109
21. Villarroya-Beltri C, Gutierrez-Vazquez C, Sanchez-Cabo F, Perez-Hernandez D, Vazquez J, Martin-Cofreces N, et al. Sumoylated hnRNPA2B1 controls the sorting of miRNAs into exosomes through binding to specific motifs. *Nat Commun* (2013) **4**:2980. doi:10.1038/ncomms3980
22. Thery C, Ostrowski M, Segura E. Membrane vesicles as conveyors of immune responses. *Nat Rev Immunol* (2009) **9**(8):581–93. doi:10.1038/nri2567nri2567

23. Tanno H, Komada M. The ubiquitin code and its decoding machinery in the endocytic pathway. *J Biochem* (2013) **153**(6):497–504. doi:10.1093/jb/mvt028mvt028
24. Peng DJ, Zeng M, Muromoto R, Matsuda T, Shimoda K, Subramaniam M, et al. Noncanonical K27-linked polyubiquitination of TIEG1 regulates Foxp3 expression and tumor growth. *J Immunol* (2011) **186**(10):5638–47. doi:10.4049/jimmunol.1003801
25. Arimoto K, Funami K, Saeki Y, Tanaka K, Okawa K, Takeuchi O, et al. Polyubiquitin conjugation to NEMO by triparite motif protein 23 (TRIM23) is critical in antiviral defense. *Proc Natl Acad Sci U S A* (2010) **107**(36):15856–61. doi:10.1073/pnas.1004621107
26. Chastagner P, Israel A, Brou C. Itch/AIP4 mediates Deltex degradation through the formation of K29-linked polyubiquitin chains. *EMBO Rep* (2006) **7**(11):1147–53. doi:10.1038/sj.embor.7400822
27. Wu-Baer F, Lagrazon K, Yuan W, Baer R. The BRCA1/BARD1 heterodimer assembles polyubiquitin chains through an unconventional linkage involving lysine residue K6 of ubiquitin. *J Biol Chem* (2003) **278**(37):34743–6. doi:10.1074/jbc.C300249200
28. Matsumoto ML, Wickliffe KE, Dong KC, Yu C, Bosanac I, Bustos D, et al. K11-linked polyubiquitination in cell cycle control revealed by a K11 linkage-specific antibody. *Mol Cell* (2010) **39**(3):477–84. doi:10.1016/j.molcel.2010.07.001
29. Huang H, Jeon MS, Liao L, Yang C, Elly C, Yates JR III, et al. K33-linked polyubiquitination of T cell receptor-zeta regulates proteolysis-independent T cell signaling. *Immunity* (2010) **33**(1):60–70. doi:10.1016/j.immuni.2010.07.002
30. Bagola K, von Delbruck M, Dittmar G, Scheffner M, Ziv I, Glickman MH, et al. Ubiquitin binding by a CUE domain regulates ubiquitin chain formation by ERAD E3 ligases. *Mol Cell* (2013) **50**(4):528–39. doi:10.1016/j.molcel.2013.04.005
31. Nathan JA, Kim HT, Ting L, Gygi SP, Goldberg AL. Why do cellular proteins linked to K63-polyubiquitin chains not associate with proteasomes? *EMBO J* (2013) **32**(4):552–65. doi:10.1038/emboj.2012.354
32. Ori D, Kato H, Sanjo H, Tartey S, Mino T, Akira S, et al. Essential roles of K63-linked polyubiquitin-binding proteins TAB2 and TAB3 in B cell activation via MAPKs. *J Immunol* (2013) **190**(8):4037–45. doi:10.4049/jimmunol.1300173
33. Erpapazoglou Z, Dhaoui M, Pantazopoulou M, Giordano F, Mari M, Leon S, et al. A dual role for K63-linked ubiquitin chains in multivesicular body biogenesis and cargo sorting. *Mol Biol Cell* (2012) **23**(11):2170–83. doi:10.1091/mbc.E11-10-0891
34. McDowell GS, Philpott A. Non-canonical ubiquitylation: mechanisms and consequences. *Int J Biochem Cell Biol* (2013) **45**(8):1833–42. doi:10.1016/j.biocel.2013.05.026
35. Li H, Wittwer T, Weber A, Schneider H, Moreno R, Maine GN, et al. Regulation of NF-kappaB activity by competition between RelA acetylation and ubiquitination. *Oncogene* (2012) **31**(5):611–23. doi:10.1038/onc.2011.253
36. Lang V, Janzen J, Fischer GZ, Soneji Y, Beinke S, Salmeron A, et al. betaTrCP-mediated proteolysis of NF-kappaB1 p105 requires phosphorylation of p105 serines 927 and 932. *Mol Cell Biol* (2003) **23**(1):402–13. doi:10.1128/MCB.23.1.402-413.2003
37. Bies J, Markus J, Wolff L. Covalent attachment of the SUMO-1 protein to the negative regulatory domain of the c-Myb transcription factor modifies its stability and transactivation capacity. *J Biol Chem* (2002) **277**(11):8999–9009. doi:10.1074/jbc.M110453200
38. Trajkovic K, Hsu C, Chiantia S, Rajendran L, Wenzel D, Wieland F, et al. Ceramide triggers budding of exosome vesicles into multivesicular endosomes. *Science* (2008) **319**(5867):1244–7. doi:10.1126/science.1153124319/5867/1244
39. Raiborg C, Stenmark H. The ESCRT machinery in endosomal sorting of ubiquitylated membrane proteins. *Nature* (2009) **458**(7237):445–52. doi:10.1038/nature07961
40. Komada M, Kitamura N. Growth factor-induced tyrosine phosphorylation of Hrs, a novel 115-kilodalton protein with a structurally conserved putative zinc finger domain. *Mol Cell Biol* (1995) **15**(11):6213–21.
41. Takeshita T, Arita T, Asao H, Tanaka N, Higuchi M, Kuroda H, et al. Cloning of a novel signal-transducing adaptor molecule containing an SH3 domain and ITAM. *Biochem Biophys Res Commun* (1996) **225**(3):1035–9. doi:10.1006/bbrc.1996.1290
42. Polo S, Sigismund S, Faretta M, Guidi M, Capua MR, Bossi G, et al. A single motif responsible for ubiquitin recognition and monoubiquitination in endocytic proteins. *Nature* (2002) **416**(6879):451–5. doi:10.1038/416451a
43. Hoeller D, Crosetto N, Blagoev B, Raiborg C, Tikkanen R, Wagner S, et al. Regulation of ubiquitin-binding proteins by monoubiquitination. *Nat Cell Biol* (2006) **8**(2):163–9. doi:10.1038/ncb1354
44. Kim BY, Olzmann JA, Barsh GS, Chin LS, Li L. Spongiform neurodegeneration-associated E3 ligase Mahogunin ubiquitylates TSG101 and regulates endosomal trafficking. *Mol Biol Cell* (2007) **18**(4):1129–42. doi:10.1091/mbc.E06-09-0787
45. Villarroya-Beltri C, Baixauli F, Gutierrez-Vazquez C, Sanchez-Madrid F, Mittelbrunn M. Sorting it out: regulation of exosome loading. *Semin Cancer Biol* (2014). doi:10.1016/j.semcancer.2014.04.009
46. Putz U, Howitt J, Lackovic J, Foot N, Kumar S, Silke J, et al. Nedd4 family-interacting protein 1 (Ndfip1) is required for the exosomal secretion of Nedd4 family proteins. *J Biol Chem* (2008) **283**(47):32621–7. doi:10.1074/jbc.M804120200
47. Gauvreau ME, Cote MH, Bourgeois-Daigneault MC, Rivard LD, Xiu F, Brunet A, et al. Sorting of MHC class II molecules into exosomes through a ubiquitin-independent pathway. *Traffic* (2009) **10**(10):1518–27. doi:10.1111/j.1600-0854.2009.00948.x
48. Buschow SI, Nolte-'t Hoen EN, van Niel G, Pols MS, ten Broeke T, Lauwen M, et al. MHC II in dendritic cells is targeted to lysosomes or T cell-induced exosomes via distinct multivesicular body pathways. *Traffic* (2009) **10**(10):1528–42. doi:10.1111/j.1600-0854.2009.00963.x
49. Lee HS, Jeong J, Lee KJ. Characterization of vesicles secreted from insulinoma NIT-1 cells. *J Proteome Res* (2009) **8**(6):2851–62. doi:10.1021/pr900009y
50. Buschow SI, Liefhebber JM, Wubbolts R, Stoorvogel W. Exosomes contain ubiquitinated proteins. *Blood Cells Mol Dis* (2005) **35**(3):398–403. doi:10.1016/j.bcmd.2005.08.005
51. Rapoport EM, Kurmyshkina OV, Bovin NV. Mammalian galectins: structure, carbohydrate specificity, and functions. *Biochemistry (Mosc)* (2008) **73**(4):393–405. doi:10.1134/S0006297908040032
52. Delacour D, Gouyer V, Zanetta JP, Drobecq H, Leteurtre E, Grard G, et al. Galectin-4 and sulfatides in apical membrane trafficking in enterocyte-like cells. *J Cell Biol* (2005) **169**(3):491–501. doi:10.1083/jcb.200407073
53. Delacour D, Cramm-Behrens CI, Drobecq H, Le Bivic A, Naim HY, Jacob R. Requirement for galectin-3 in apical protein sorting. *Curr Biol* (2006) **16**(4):408–14. doi:10.1016/j.cub.2005.12.046
54. Delacour D, Greb C, Koch A, Salomonsson E, Leffler H, Le Bivic A, et al. Apical sorting by galectin-3-dependent glycoprotein clustering. *Traffic* (2007) **8**(4):379–88. doi:10.1111/j.1600-0854.2007.00539.x
55. Mishra R, Grzybek M, Niki T, Hirashima M, Simons K. Galectin-9 trafficking regulates apical-basal polarity in Madin-Darby canine kidney epithelial cells. *Proc Natl Acad Sci U S A* (2010) **107**(41):17633–8. doi:10.1073/pnas.1012424107
56. Fang Y, Wu N, Gan X, Yan W, Morrell JC, Gould SJ. Higher-order oligomerization targets plasma membrane proteins and HIV gag to exosomes. *PLoS Biol* (2007) **5**(6):e158. doi:10.1371/journal.pbio.0050158

Conflict of Interest Statement: The authors declare that the research was conducted in the absence of any commercial or financial relationships that could be construed as a potential conflict of interest.

Received: 25 June 2014; paper pending published: 13 July 2014; accepted: 28 July 2014; published online: 11 August 2014.

*Citation: Moreno-Gonzalo O, Villarroya-Beltri C and Sánchez-Madrid F (2014) Post-translational modifications of exosomal proteins. Front. Immunol. **5**:383. doi: 10.3389/fimmu.2014.00383*

This article was submitted to Immunotherapies and Vaccines, a section of the journal Frontiers in Immunology.

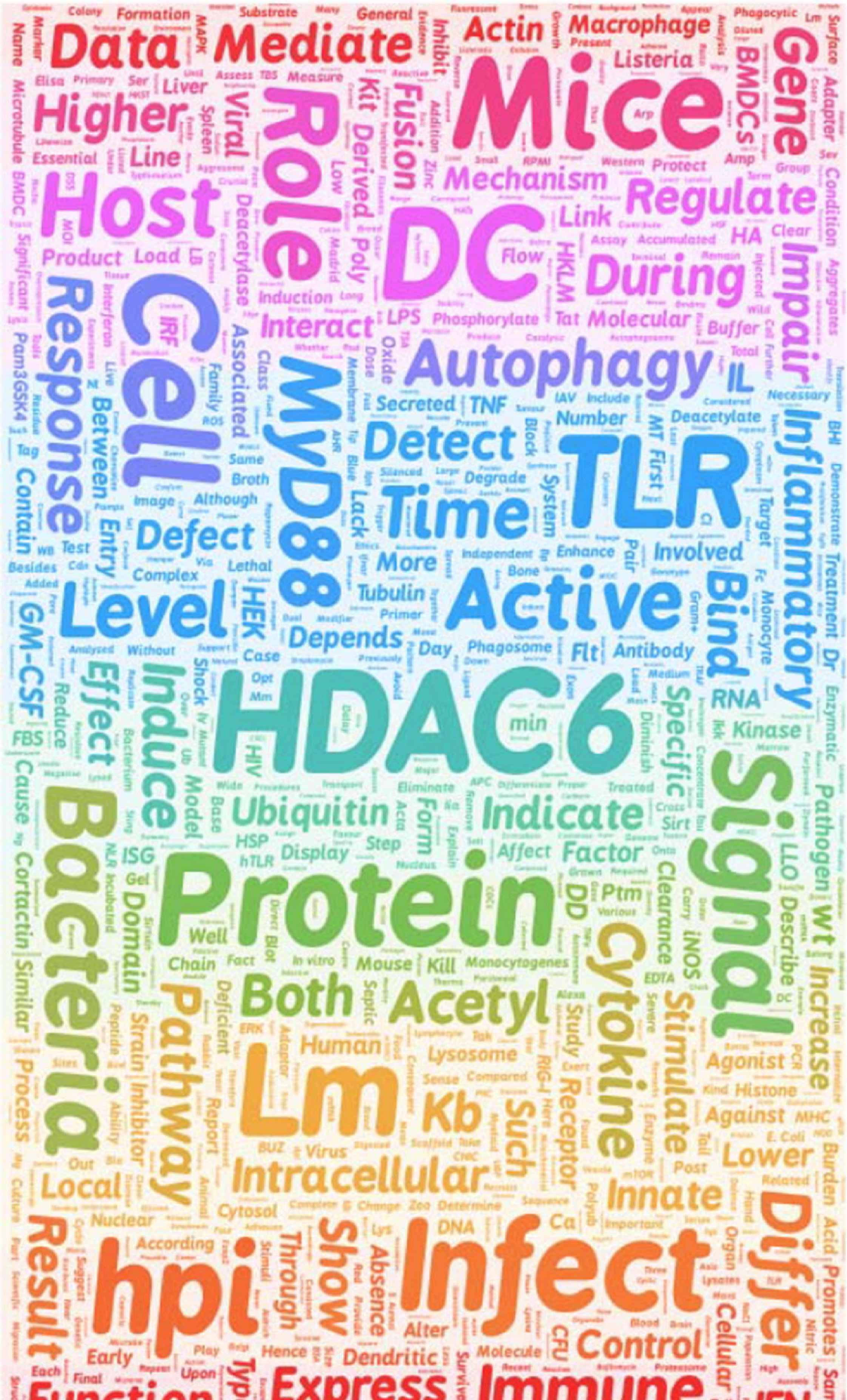
HDAC6
Protein
Mice
TLR
Infect
Cell
DC
Lm
hpi
Bacteria
Signal
MyD88
Role
Host
Data
Mediate
Response
Autophagy
Level
Active
Time
Detect
Cytokine
Pathway
Both
Acetyl
Immune
Function
Express
Result
Differ
Gene
Regulate
Impair
Inflammatory
Bind
Induce
Effect
Higher
During
Mechanism
Macrophage
Actin
Listeria
Ubiquitin
Indicate
Intracellular
Innate
Control
Show
Kb
Such
Stimulate
Receptor
Defect
Local
Lower
Agonist
Histone
Increase
Pathogen
Factor
Human
Lysosome
Dendritic
Molecule
IFN
Sample
Cellular
Absence
Through
Alter
Early
Upon
Type
Viral
Fusion
Kit
Derived
Deacetylase
Interact
Induction
LPS
Phosphorylate
Molecular
Buffer
Tat
HKLM
Link
Flow
Assay
Accumulated
HA
Clear
Product
Load
Interferon
IRF
Associated
Class
Oxide
Membrane
Secreted
TNF
IL
Number
Deacetylate
Target
Demonstrate
Treatment
Monocyte
Antibody
Depends
Day
Phagosome
Flt
Tubulin
Primer
More
Independent
Enhance
Involved
Bone
Complex
Lethal
HEK
Between
Entry
Contain
Test
Besides
GM-CSF
Cause
Reduce
FBS
Kinase
RNA
Enzymatic
Specific
Diminish
Concentrate
min
Eliminate
Treated
Form
Model
Base
Step
Display
Affect
HSP
hTLR
ISG
Gel
Domain
Strain
Inhibitor
Ability
Cortactin
Similar
Process
Chain
Well
Mouse
Kill
Monocytogenes
Clearance
Carry
iNOS
DD
Ptm
LLO
Describe
Wt
Deficient
Adaptor
Report
Septic
Study
Sense
Compared
Against
MHC
E. Coli
Burden
Acid
Promotes
Nitric
Virus
Scaffold
Post
Enzyme
Related
Cytosol
Nuclear
Determine
Ca
Important
Organ
According
Suggest
Stimuli
CFU
Hence
Blood
Toll
Each
Final
Survive
Moreover
PBS
Transcription
Seem
Mass
Heat
Titre
In vivo
Up
Nitrite
Modification
Quantification
Structure
Colony
Formation
Substrate
General
Inhibit
Growth
Phagocytic
Surface
Name
Marker
MAPK
Assess
Measure
Elisa
Primary
Liver
Spleen
Microtubule
Essential
Line
BMDC
BMDCs
Significant
Pam3CSK4
Tag
Western
Protect
Amp
Condition
Aggregates
Necessary
Present
Adapter
Group

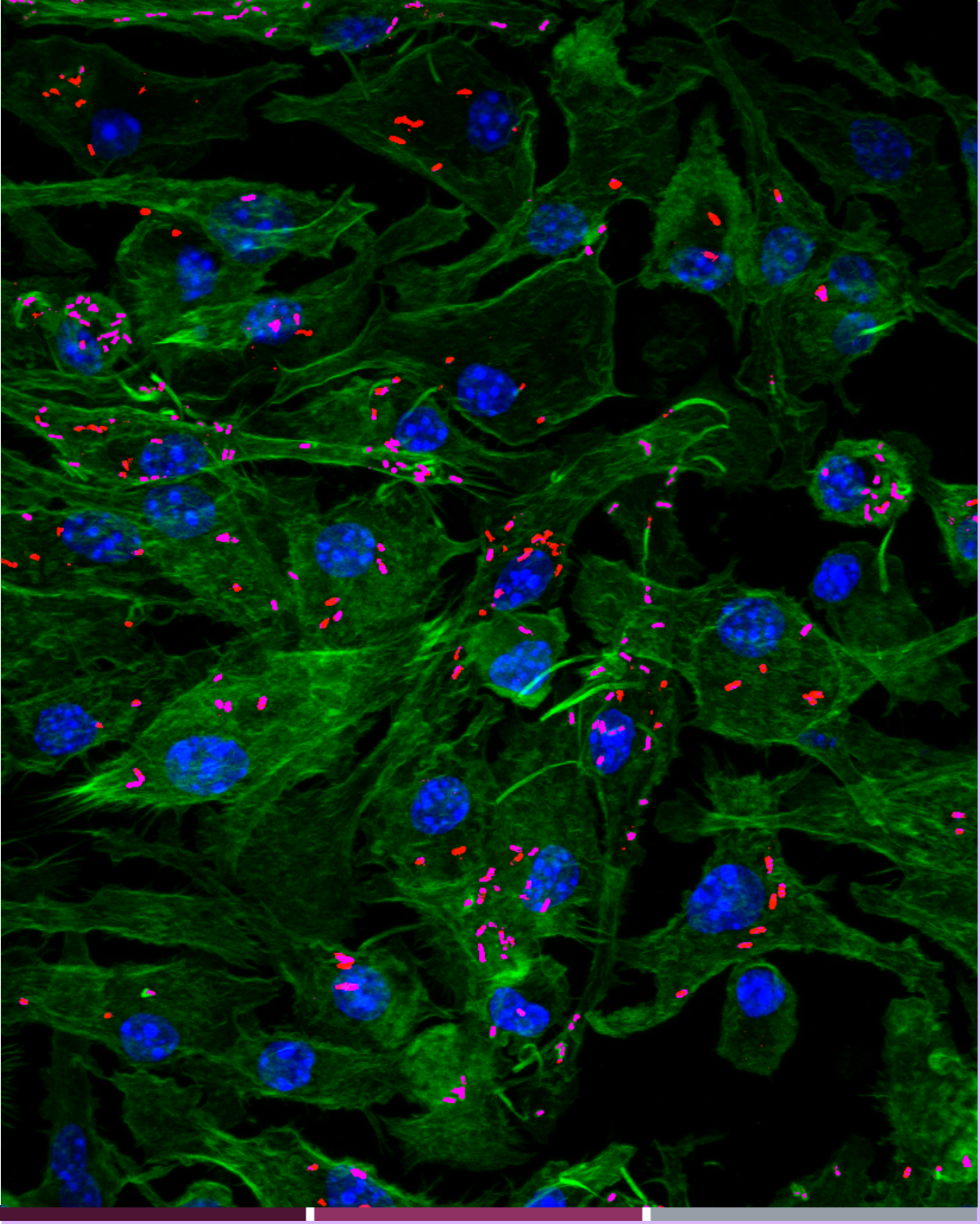

Universidad Autónoma de Madrid